Methods in Cell Biology • Volume 105

The Zebrafish: Disease Models and Chemical Screens

THIRD EDITION

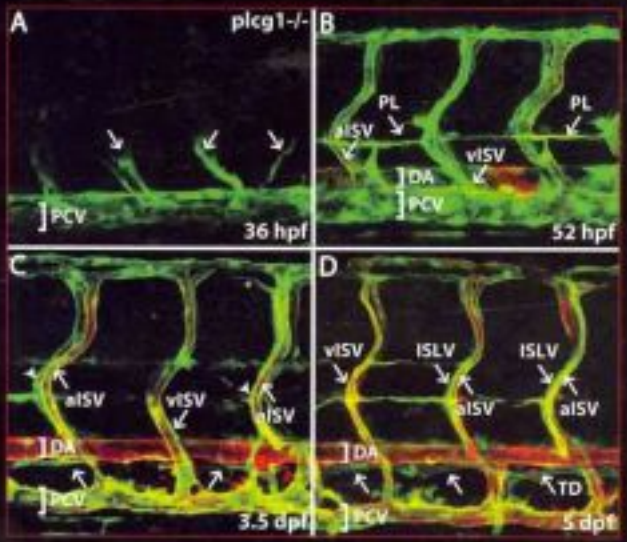

Edited by

H. William Detrich III, Monte Westerfield and Leonard I. Zon

Methods in Cell Biology • Volume 138

The Zebrafish: Disease Models and Chemical Screens

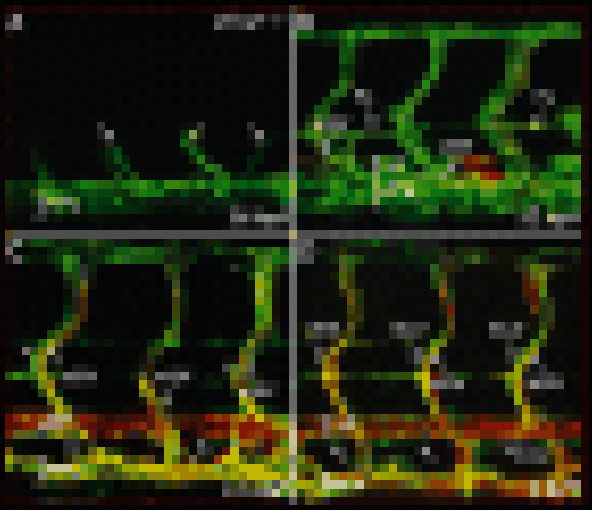

Edited by
H. William Detrich III, Monte Westerfield
and Leonard I. Zon

Methods in Cell Biology

VOLUME 105

The Zebrafish: Disease Models and Chemical Screens
3rd Edition

Series Editors

Leslie Wilson
Department of Molecular, Cellular and Developmental Biology
University of California
Santa Barbara, California

Paul Matsudaira
Department of Biological Sciences
National University of Singapore
Singapore

Methods in Cell Biology

VOLUME 105

The Zebrafish: Disease Models and Chemical Screens

3rd Edition

Edited by

H. William Detrich III

Department of Biology, Northeastern University, Boston, MA, USA

Monte Westerfield

Institute of Neuroscience, University of Oregon, Eugene, OR, USA

Leonard I. Zon

Division of Hematology/Oncology, Children's Hospital of Boson
Department of Pediatrics and Howard Hughes Medical Institute
Harvard Medical School, Boston, MA, USA

ELSEVIER

AMSTERDAM • BOSTON • HEIDELBERG • LONDON
NEW YORK • OXFORD • PARIS • SAN DIEGO
SAN FRANCISCO • SINGAPORE • SYDNEY • TOKYO

Academic Press is an imprint of Elsevier

Academic Press is an imprint of Elsevier
225 Wyman Street, Waltham, MA 02451, USA
525 B Street, Suite 1900, San Diego, CA 92101-4495, USA
32, Jamestown Road, London NW1 7BY, UK
Linacre House, Jordan Hill, Oxford OX2 8DP, UK

Third edition 2011

ISBN: 978-0-12-381320-6
ISSN: 0091-679X

Printed and bound in USA

11 12 13 14 10 9 8 7 6 5 4 3 2 1

DEDICATION

Dedication to Methods in Cell Biology – The Zebrafish, 3rd Edition

We dedicate the Third Edition of *Methods in Cell Biology: The Zebrafish* to Wolfgang Driever, Mark C. Fishman, Charles Kimmel, and Christiane Nüsslein-Volhard. Through their foresighted embrace of the zebrafish as a model vertebrate and their pursuit of genetic screens to illuminate vertebrate development, they fostered the emergence of the vibrant zebrafish research community.

CONTRIBUTORS

Numbers in parentheses indicate the pages on which the author's contributions begin.

James F. Amatruda (3), Department of Pediatrics, University of Texas Southwestern Medical Center, Dallas, Texas, USA; Department of Molecular Biology, University of Texas Southwestern Medical Center, Dallas, Texas, USA; Department of Internal Medicine, University of Texas Southwestern Medical Center, Dallas, Texas, USA

Alexander Apschner (239), Hubrecht Institute-KNAW & UMC Utrecht, Utrecht, The Netherlands

Erica L. Benard (273), Institute of Biology, Leiden University, Leiden, The Netherlands

Wilhelm Bloch (191), Institute of Cardiology and Sports Medicine, German Sport University Cologne, Cologne, Germany; Cologne Excellence Cluster on Cellular Stress Responses in Aging-Associated Diseases, University of Cologne, Cologne, Germany

Matthew G. Butler (137), Program in the Genomics of Differentiation, National Institute of Child Health and Development, National Institutes of Health, Bethesda, Maryland, USA

Jeremy R. Charette (87), Department of Molecular & Biomedical Sciences, University of Maine, Orono, Maine, USA

Eleanor Y. Chen (383), Molecular Pathology Unit, Massachusetts General Hospital, Charlestown, MA, USA; Department of Pathology, Brigham and Women's Hospital, Harvard Medical School, Boston, MA, USA

Chao Cui (273), Institute of Biology, Leiden University, Leiden, The Netherlands

Tim Czopka (25), Centre for Neuroregeneration, University of Edinburgh, Chancellor's Building, 49 Little France Crescent, Edinburgh, UK; Centre for Regenerative Medicine, University of Edinburgh, Edinburgh, UK; Centre for Multiple Sclerosis Research, University of Edinburgh, Edinburgh, UK

Vanessa Damoulis (3), Department of Pediatrics, University of Texas Southwestern Medical Center, Dallas, Texas, USA; Department of Molecular Biology, University of Texas Southwestern Medical Center, Dallas, Texas, USA

Fredericus van Eeden (163), MRC-CDBG/BMS, University of Sheffield, Western Bank, Sheffield, United Kingdom

Julia Etchin (309), Department of Pediatric Oncology, Dana-Farber Cancer Institute and Children's Hospital, Boston, Massachusetts, USA

Natália Martins Feitosa (191), Institute of Developmental Biology, University of Cologne, Cologne, Germany; Center for Molecular Medicine Cologne, University of Cologne, Cologne, Germany

Mark C. Fishman (525), Novartis Institutes for Biomedical Research, Cambridge, Massachusetts 02139, USA

Rachel Giles (163), Department of Nephrology, University Medical Center Utrecht, Universiteitsweg 100, 3584 CG, Utrecht, The Netherlands

Wolfram Goessling (117), Genetics Division, Brigham and Women's Hospital, Harvard Medical School, Boston, Massachusetts, USA; Harvard Stem Cell Institute, Cambridge, Massachusetts, USA

Aniket V. Gore (137), Program in the Genomics of Differentiation, National Institute of Child Health and Development, National Institutes of Health, Bethesda, Maryland, USA

Karen Guillemin (87), Institute of Molecular Biology, University of Oregon, Eugene, Oregon, USA

Matthias Hammerschmidt (191), Institute of Developmental Biology, University of Cologne, Cologne, Germany; Center for Molecular Medicine Cologne, University of Cologne, Cologne, Germany; Cologne Excellence Cluster on Cellular Stress Responses in Aging-Associated Diseases, University of Cologne, Cologne, Germany

Myron S. Ignatius (437), Molecular Pathology Unit, Massachusetts General Hospital, Charlestown, Massachusetts, USA; Center of Cancer Research, Massachusetts General Hospital Cancer Center, Charlestown, Massachusetts, USA; Harvard Stem Cell Institute, Boston, Massachusetts, USA

John P. Kanki (309), Department of Pediatric Oncology, Dana-Farber Cancer Institute and Children's Hospital, Boston, Massachusetts, USA

Zakia Kanwal (273), Institute of Biology, Leiden University, Leiden, The Netherlands

Terhi Karpanen (223), Hubrecht Institute - KNAW and University Medical Center Utrecht, Uppsalalaan 8, Utrecht, The Netherlands

Nicholas Katsanis (257), Center for Human Disease Modeling, Departments of Cell Biology and Pediatrics, Duke University Medical Center, Durham, North Carolina, USA

Carol H. Kim (87), Department of Molecular & Biomedical Sciences, University of Maine, Orono, Maine, USA; Graduate School of Biomedical Sciences, University of Maine, Orono, Maine, USA

David Kokel (517), Cardiovascular Research Center and Division of Cardiology, Department of Medicine, Massachusetts General Hospital, Harvard Medical School, Charlestown, Massachusetts, USA and Broad Institute, 7 Cambridge Center, Cambridge, Massachusetts, USA

D. Lai (419), Molecular, Cellular and Developmental Biology Group, School of Biological Sciences, University of Auckland, Auckland, New Zealand

C.-C. Lan (419), Molecular, Cellular and Developmental Biology Group, School of Biological Sciences, University of Auckland, Auckland, New Zealand

David M. Langenau (383, 437), Molecular Pathology Unit, Massachusetts General Hospital, Charlestown, MA, USA; Center of Cancer Research, Massachusetts General Hospital, Charlestown, MA, USA; Harvard Stem Cell Institute, Boston, MA, USA

Steven D. Leach (367), Department of Surgery and the McKusick-Nathans Institute of Genetic Medicine, Johns Hopkins University School of Medicine, Maryland, Baltimore

I.U.S. Leong (419), Molecular, Cellular and Developmental Biology Group, School of Biological Sciences, University of Auckland, Auckland, New Zealand; Diagnostic Genetics, LabPlus, Auckland City Hospital, Auckland, New Zealand

Pulin Li (403), Harvard Medical School, Howard Hughes Medical Institute, Harvard Stem Cell Institute, Children's Hospital Boston, Boston, Massachusetts, USA

Kate Lillard (3), Department of Pediatrics, University of Texas Southwestern Medical Center, Dallas, Texas, USA; Department of Molecular Biology, University of Texas Southwestern Medical Center, Dallas, Texas, USA

Shu Liu (367), Department of Surgery and the McKusick-Nathans Institute of Genetic Medicine, Johns Hopkins University School of Medicine, Maryland, Baltimore

Ive Logister (163), Department of Medical Oncology, University Medical Center, Universiteitsweg 100, Utrecht, The Netherlands; Hubrecht Institute for Developmental Biology and Stem Cell Research, KNAW and University Medical Center Utrecht, Uppsalalaan 8, Utrecht, The Netherlands

A. Thomas Look (309), Department of Pediatric Oncology, Dana-Farber Cancer Institute and Children's Hospital, Boston, Massachusetts, USA

D.R. Love (419), Molecular, Cellular and Developmental Biology Group, School of Biological Sciences, University of Auckland, Auckland, New Zealand; Diagnostic Genetics, LabPlus, Auckland City Hospital, Auckland, New Zealand

David A. Lyons (25), Centre for Neuroregeneration, University of Edinburgh, Chancellor's Building, 49 Little France Crescent, Edinburgh, UK; Centre for Multiple Sclerosis Research, University of Edinburgh, Edinburgh, UK

Marie E. Mathers (339), Department of Pathology, Western General Hospital, Edinburgh, EH4 2XU, Scotland, UK

Annemarie H. Meijer (273), Institute of Biology, Leiden University, Leiden, The Netherlands

Kathryn Milligan-Myhre (87), Institute of Molecular Biology, University of Oregon, Eugene, Oregon, USA

James E.N. Minchin (63), Department of Cell and Molecular Physiology, University of North Carolina at Chapel Hill, Chapel Hill, North Carolina, USA

Trista E. North (117), Harvard Stem Cell Institute, Cambridge, Massachusetts, USA; Department of Pathology, Beth Israel Deaconess Medical Center, Harvard Medical School, Boston, Massachusetts, USA

Joanie C. Neumann (3), Department of Pediatrics, University of Texas Southwestern Medical Center, Dallas, Texas, USA; Department of Molecular Biology, University of Texas Southwestern Medical Center, Dallas, Texas, USA

E. Elizabeth Patton (339), MRC Human Genetics Unit & Edinburgh Cancer Research Centre, The University of Edinburgh, Edinburgh, EH4 2XR, Scotland, UK

Randall T. Peterson (517, 525), Cardiovascular Research Center and Division of Cardiology, Department of Medicine, Massachusetts General Hospital, Harvard

Medical School, Charlestown, Massachusetts, USA and Broad Institute, 7 Cambridge Center, Cambridge, Massachusetts, USA

Ryan T. Phennicie (87), Department of Molecular & Biomedical Sciences, University of Maine, Orono, Maine, USA

John H. Postlethwait (461), University of Oregon, Institute of Neuroscience, Eugene, Oregon, USA

John F. Rawls (63, 87), Department of Cell and Molecular Physiology, University of North Carolina at Chapel Hill, Chapel Hill, North Carolina, USA; Department of Microbiology and Immunology, University of North Carolina at Chapel Hill, Chapel Hill, North Carolina, USA

Rebecca Richardson (191), Institute of Developmental Biology, University of Cologne, Cologne, Germany; Center for Molecular Medicine Cologne, University of Cologne, Cologne, Germany

Adriana Rodríguez-Marí (461), University of Oregon, Institute of Neuroscience, Eugene, Oregon, USA

Ellen van Rooijen (163), Department of Medical Oncology, University Medical Center, Universiteitsweg 100, Utrecht, The Netherlands; Hubrecht Institute for Developmental Biology and Stem Cell Research, KNAW and University Medical Center Utrecht, Uppsalalaan 8, Utrecht, The Netherlands; Present address: Children's Hospital Boston and Harvard Medical School, 1 Blackfan Circle, Boston, MA 02115, United States

Kirankumar Santhakumar (163), MRC-CDBG/BMS, University of Sheffield, Western Bank, Sheffield, United Kingdom

Manfred Schartl (339), University of Wuerzburg, Physiological Chemistry I, Biocenter, Am Hubland, Würzburg 97074, Germany

Stefan Schulte-Merker (163, 223, 239), Hubrecht Institute for Developmental Biology and Stem Cell Research, KNAW and University Medical Center Utrecht, Uppsalalaan 8, Utrecht, The Netherlands

Herman P. Spaink (273), Institute of Biology, Leiden University, Leiden, The Netherlands

Oliver W. Stockhammer (273), Institute of Biology, Leiden University, Leiden, The Netherlands

W. Zac Stephens (87), Institute of Molecular Biology, University of Oregon, Eugene, Oregon, USA

Justin L. Tan (493), Stem Cell Program and Division of Hematology and Oncology, Children's Hospital Boston, Dana-Farber Cancer Institute, Howard Hughes Medical Institute and Harvard Medical School, 1 Blackfan Circle, Boston, Massachusetts, USA

Michiel van der Vaart (273), Institute of Biology, Leiden University, Leiden, The Netherlands

Emile Voest (163), Department of Medical Oncology, University Medical Center, Universiteitsweg 100, Utrecht, The Netherlands

Brant M. Weinstein (137), Program in the Genomics of Differentiation, National Institute of Child Health and Development, National Institutes of Health, Bethesda, Maryland, USA

Richard M. White (403), Harvard Medical School, Howard Hughes Medical Institute, Harvard Stem Cell Institute, Children's Hospital Boston, Dana-Farber Cancer Institute, Boston, Massachusetts, USA

P. Eckhard Witten (239), Skretting Aquaculture Research Centre, Stavanger, Norway; Biology Department, Ghent University, Ghent, Belgium

Norann A. Zaghloul (257), Department of Medicine, Division of Endocrinology, Diabetes and Nutrition, University of Maryland School of Medicine, Baltimore, Maryland, USA

Anna Zakrzewska (273), Institute of Biology, Leiden University, Leiden, The Netherlands

Leonard I. Zon (403, 493), Stem Cell Program and Division of Hematology and Oncology, Children's Hospital Boston, Dana-Farber Cancer Institute, Howard Hughes Medical Institute and Harvard Medical School, 1 Blackfan Circle, Boston, Massachusetts, USA

PART I

Disease Models

CHAPTER 1

Zebrafish Models of Germ Cell Tumor

Joanie C. Neumann,[*,†] Kate Lillard,[*,†] Vanessa Damoulis[*,†] and James F. Amatruda[*,†,‡]

[*]Department of Pediatrics, University of Texas Southwestern Medical Center, Dallas, Texas, USA

[†]Department of Molecular Biology, University of Texas Southwestern Medical Center, Dallas, Texas, USA

[‡]Department of Internal Medicine, University of Texas Southwestern Medical Center, Dallas, Texas, USA

Abstract

Germ cell tumors are neoplasms arising from pluripotent germ cells. In humans, these tumors occur in infants, children and young adults. The tumors display a wide range of histologic differentiation states which exhibit different clinical behaviors. Information about the molecular basis of germ cell tumors, and representative animal models of these neoplasms, are lacking. Germline development in zebrafish and humans is broadly conserved, making the fish a useful model to probe the connections between germ cell development and tumorigenesis. Here, we provide

METHODS IN CELL BIOLOGY, VOL 105

0091-679X/10 $35.00
DOI 10.1016/B978-0-12-381320-6.00001-1

an overview of germline development and a brief review of germ cell tumor biology in humans and zebrafish. We also outline some methods for studying the zebrafish germline.

I. Overview

Germ cell tumors (GCTs) are cancers of the testis, ovary, or extragonadal sites that occur in infants, children, and adults. Although rare overall, they account for 15% of the cancers diagnosed in childhood and adolescence. Testicular GCT (TGCT) is the most common malignancy in young men aged 15–40, and the incidence of GCT around the world is rapidly increasing for unclear reasons (Frazier and Amatruda, 2009). Clinically, GCTs are treated with cisplatin-containing chemotherapy, surgery, and in some cases radiotherapy. While the results are overall excellent, patients undergoing these treatments often suffer long-term adverse effects, including cardiovascular disease, secondary malignancies, kidney dysfunction, and hearing loss. In addition, current regimens still fail to cure about 15–20% of patients (Frazier and Amatruda, 2009). Together, these problems indicate a pressing need for improved, targeted therapies for GCTs. However, the poor understanding of the molecular basis of GCTs, and the lack of suitable animal models, represents an impediment to the development of new therapies. The many advantages of zebrafish for genetic analysis and disease modeling suggest that fish models of GCTs could have great translational impact. Similar to Wilms tumor, neuroblastoma, and medulloblastoma, GCTs are "embryonal" tumors, in which misregulation of developmental signaling pathways is likely to play a critical role. Therefore, better understanding of GCT biology can potentially also reveal mechanisms of normal germline development.

II. Germline Development

The earliest cells of the germ cell lineage are the primordial germ cells (PGCs) (Kunwar *et al.*, 2006; Molyneaux *et al.*, 2001; Molyneaux and Wylie, 2004; Wylie, 2000). In most multicellular organisms, PGCs arise at distant sites and must migrate through the developing embryo to reach the site at which the gonad will develop. Throughout migration and development, PGCs are able to maintain their underlying pluripotency program while repressing somatic differentiation (van de Geijn *et al.*, 2009; Western, 2009). This specialized function enables PGCs to ultimately fulfill their role when, on fertilization, they reactivate their differentiation program to give rise to the next generation. Studies in *Drosophila melanogaster*, zebrafish, and mice have revealed conserved mechanisms of PGC specification, migration, and development (Kunwar *et al.*, 2006; Raz, 2003; Richardson and Lehmann, 2010; Williamson and Lehmann, 1996).

A. Specification of Primordial Germ Cells

PGC specification in most organisms requires two conserved molecular mechanisms: repression of the somatic differentiation program and reactivation of pluripotency-associated gene expression. In zebrafish, PGC specification is predetermined by the inheritance of maternal RNA and proteins located in the germ plasm (Houston and King, 2000; Raz, 2003; Saffman and Lasko, 1999; Williamson and Lehmann, 1996). In contrast to other organisms, zebrafish PGCs arise in four distinct random locations with respect to the developmental axis of the embryo (Raz, 2003; Weidinger *et al.*, 1999, 2002; Yoon *et al.*, 1997). The identification of *vasa* as a germline cell marker in zebrafish was an important discovery that facilitated the study of PGC/germline development (Olsen *et al.*, 1997; Yoon *et al.*, 1997). In zebrafish, *vasa* expression is first detected in four strips of electron-dense germ plasm along the first two cleavage planes in the embryo. By the 4K cell stage, the *vasa*-enriched germ plasm is distributed into the cytoplasm of four closely associated cells that then become PGCs. The four newly specified PGCs undergo multiple rounds of division to generate 25–50 PGCs that migrate to the genital ridges by the end of the first day (Braat *et al.*, 1999; Knaut *et al.*, 2000; Weidinger *et al.*, 1999; Yoon *et al.*, 1997).

Mice and other mammals lack germ plasm and require inductive signaling for PGC specification (Lawson *et al.*, 1999; Tam and Zhou, 1996; Ying *et al.*, 2001; Ying and Zhao, 2001). At E6.5, bone morphogenetic proteins 4, 8b, and 2 (BMP4/8b/2) and unidentified proteins signal from the extraembryonic ectoderm and visceral endoderm to pluripotent epiblast cells to induce *fragilis/Ifitm3* expression (Saitou *et al.*, 2002; Ying *et al.*, 2001; Ying and Zhao, 2001; Zhao and Garbers, 2002). *fragilis/Ifitm3* expression is required for the proximal epiblast cells to achieve competence to become PGC precursor cells (Lange *et al.*, 2003; Saitou *et al.*, 2002; Tanaka and Matsui, 2002; Tanaka *et al.*, 2004, 2005). BMP4, BMP2, and BMP8b null mice lack or have severely reduced numbers of PGCs due to the failure to generate PGC precursor cells (de Sousa Lopes *et al.*, 2004; Itman *et al.*, 2006; Lawson *et al.*, 1999; Ying *et al.*, 2001; Ying and Zhao, 2001; Zhao and Garbers, 2002).

An important molecular mechanism for PGC specification that is common to many organisms is the transcriptional silencing of somatic gene expression (Ohinata *et al.*, 2005; Saitou *et al.*, 2002; Yabuta *et al.*, 2006). The *fragilis/Ifitm*-positive proximal epiblast cells also express somatic mesodermal genes including *Hoxb1*, *Fgf8*, and *Snail* (Ancelin *et al.*, 2006; Hayashi *et al.*, 2007; Yabuta *et al.*, 2006). In these cells, B lymphocyte–induced maturation protein 1 (BLIMP1, also known as PRDM1), a transcriptional repressor, plays significant roles in the somatic gene repression as well as promoting upregulation of PGC-specific genes such as *stella* (Ohinata *et al.*, 2005; Saitou *et al.*, 2005; Vincent *et al.*, 2005). The loss of Blimp1 in mutant mice results in reduced somatic gene silencing, loss of founder PGCs, and lack of PGC migration (Kurimoto *et al.*, 2008; Yamaji *et al.*, 2008). By E7.25, there are approximately 40 Blimp1-positive, specified PGCs (Ohinata *et al.*, 2005). These

cells are characterized by their transcriptional silencing of somatic genes, the expression of PGC-specific genes, and maintenance or upregulation of pluripotency-associated genes such as Oct4, Sox2, and Nanog (Saitou *et al.*, 2002; Scholer *et al.*, 1990; Yabuta *et al.*, 2006; Yamaguchi *et al.*, 2005; Yeom *et al.*, 1996).

B. Primordial Germ Cell Migration

In most organisms, the PGCs arise in a location distal to the genital ridges where the PGCs will eventually reside. To arrive at the gonads, the PGCs must gain motility and migrate through the embryo to their final location. Similar to PGC specification, there are conserved mechanisms for migration among different organisms, but there are also important distinctions and modes of migration.

Zebrafish have four clusters of PGCs originating in dispersed locations in the embryo that must migrate to the genital ridges (Weidinger *et al.*, 1999, 2002, 2003; Yoon *et al.*, 1997). The PGCs use a "run" and "tumble" system in which they migrate "run" short distances to intermediate stops where they remain stationary "tumble" for a short period of time to realign themselves to attractant chemokine signals that are guiding them through the embryo (Raz and Reichman-Fried, 2006; Reichman-Fried *et al.*, 2004). The initiation of migration requires multiple steps in which the PGCs gain motility. Initially, zebrafish PGCs are morphologically indistinguishable from the surrounding somatic cells, exhibiting a smooth, round morphology. However, in the first 30 min after specification, the PGCs start to exhibit a ruffled edge appearance with the extension of short cellular protrusions in all directions. At this time, the PGCs have not gained the ability to migrate and these protrusions are eventually lost as the PGCs divide. This is followed by a 1-h transitional phase in which the PGCs become polarized and extend out broad pseudopodia for directional migration (Blaser *et al.*, 2005). An RNA-binding protein, dead end (Dnd), is critical for PGC polarization and extension of the broad directional protrusions (Weidinger *et al.*, 2003). The loss of Dnd in PGCs results in absence of PGC migration due to loss of polarization and protrusion extension, and ultimately in the death of the PGCs (Blaser *et al.*, 2005). After becoming motile, zebrafish PGCs start to actively migrate toward attractant signals provided by somatic cells. Stromal-derived factor-1 alpha (SDF-1a) has been identified as a critical component guiding the PGCs along the migratory pathway. SDF-1a binds to chemokine receptor, CXCR4b, which is expressed in PGCs. It was demonstrated that PGCs will migrate to ectopic locations in response to aberrant SDF-1a-secreting cells (Doitsidou *et al.*, 2002; Knaut *et al.*, 2003).

Mouse PGCs are initially located in the primitive streak and must follow a migratory path through the posterior embryonic endoderm, extraembryonic endoderm, and finally the allantois and hindgut to reach the genital ridges (Anderson *et al.*, 2000). Several molecules/pathways have been identified as important mediators of proper PGC migration. Similar to zebrafish PGCs, guidance is provided by the SDF1 chemokine and CXCR4 interaction (Ara *et al.*, 2003;

Molyneaux *et al.*, 2003). The c-kit receptor tyrosine kinase and its ligand *steel* were discovered to facilitate migration by regulating PGC motility (Gu *et al.*, 2009). In addition, E-cadherin and β-1 integrin are required for proper exiting from the hindgut and migration into the gonads (Anderson *et al.*, 1999a, 1999b; Bendel-Stenzel *et al.*, 2000).

C. Epigenetic Reprogramming of Primordial Germ Cells

Until the time of PGC migration, all cells in a developing embryo have a biparental pattern of genomic imprinting. Genomic imprinting is an epigenetic phenomenon in which DNA methylation controls expression of a limited number of genes that are dependent on parental origin (McLaren, 2003; Surani, 2001). Approximately 100–200 genes in the human genome are imprinted such that only one allele, either maternal or paternal, is expressed (Lucifero *et al.*, 2004; Paoloni-Giacobino and Chaillet, 2004). In PGCs, the biparental pattern of genomic imprinting must be erased, followed by the establishment of a uniparental pattern in order to ensure that proper sex-specific imprinting is passed on to the next generation. This process, called genome-wide epigenetic reprogramming, occurs in migratory and postmigratory PGCs in mammals. Zebrafish and *Xenopus*, however, do not exhibit imprinting and do not undergo paternal genome reprogramming (Macleod *et al.*, 1999; Reik *et al.*, 2001). Once the PGCs (now referred to as gonocytes) arrive at the gonads, they begin differentiating into either prospermatogonia or oogonia based on the signals they receive from the gonadal microenvironment and surrounding somatic cells, and, in mammals, on their chromosomal constitution (XY or XX). Then at the appropriate time, depending on the sex of the organism, the process of gametogenesis (spermatogenesis if male and oogenesis if female) is initiated to generate fully mature gametes that are capable of producing the next generation on fertilization. Oogenesis in zebrafish and medaka fish has been recently reviewed (Clelland and Peng, 2009; Lessman, 2009; Saito and Tanaka, 2009). In the next section, we review the process of spermatogenesis.

D. Spermatogenesis

Spermatogenesis is a dynamic process occurring in a series of highly organized steps that culminates in the production of fully mature spermatozoa. It is initiated during puberty and is maintained continuously throughout the life of most organisms. In most vertebrates, spermatogenesis occurs within seminiferous tubules that are composed of a basement membrane, basal compartment, and adluminal compartment. Blood vessels, Leydig cells, lymphatic epithelium, and macrophages surround each tubule in the interstitial space (as reviewed in Yoshida, 2008a). On the inside of the basement membrane reside the Sertoli cells. Representing the only somatic cell within the tubules, Sertoli cells support the germ cells by providing nourishment and growth factors, and function to organize the spermatogenic process

(Griswold, 1998). One distinguishing characteristic of spermatogenesis in lower vertebrates (also known as anamniotes) including fish is that in the seminiferous tubules, spermatogenesis occurs within cysts that are formed by Sertoli cell cytoplasmic extensions (Schulz *et al.*, 2010). In contrast to higher vertebrates (retiles, birds, and mammals) where one Sertoli cell is associated with several spermatogonial germ cells at different developmental stages, cystic spermatogenesis is represented by having one Sertoli cell associated with a single spermatogonial germ cell (Matta *et al.*, 2002; Schulz *et al.*, 2005).

The process of spermatogenesis is much conserved among different species including flies, fish, and mammals with relatively few minor distinctions. In the mouse, type A undifferentiated spermatogonia (A_{single}) are believed to be the stem cells of the testis and are closely associated with the basement membrane in the basal compartment (Chiarini-Garcia *et al.*, 2001; Chiarini-Garcia and Russell, 2001; Hess *et al.*, 2006; Oatley and Brinster, 2006; Ogawa *et al.*, 2005; Ryu *et al.*, 2006). The A_{single} spermatogonia are thought to undergo self-renewal as well as to give rise to specialized daughter cells that will divide and differentiate to ultimately become spermatozoa (Oatley and Brinster, 2006). A_{single} spermatogonia give rise to the undifferentiated type A spermatogonia (A_{undiff}), A_{paired} and $A_{aligned}$. These undifferentiated cells, including the A_{single} cells, are tightly clustered together and only account for 1% of testicular cells. The A_{undiff} cells will give rise to the next class of spermatogonia, the differentiated type A_1 spermatogonia. The differentiated type A_1 spermatogonia will undergo successive rounds of mitosis. The number of rounds is dependent on the organism. In rodents, there are typically six rounds of mitotic division that results in type $A_{2–4}$ differentiated spermatogonia, intermediate spermatogonia, type B spermatogonia, and finally the preleptotene primary spermatocytes (de Rooij and Russell, 2000). Zebrafish has a total of nine rounds of mitosis that is initiated by type A undifferentiated primary spermatogonia and results in three type A differentiated spermatogonia generations, five type B spermatogonia generations, and one generation of primary preleptotene spermatocytes (Leal *et al.*, 2009).

Still closely associated with the basement membrane, the preleptotene spermatocytes initiate meiosis. During a long prophase, the leptotene and zygotene spermatocytes will move away from the basement membrane and will enter the adluminal compartment through the tight junctions that are formed by the Sertoli cells. The exchange of genetic information occurs during the recombination event in pachytene spermatocytes, after which the completion of meiosis I results in 2*N* secondary spermatocytes. These will then undergo meiosis II to produce four haploid (1*N*) round spermatids (Hess and Renato de Franca, 2008; Schulz *et al.*, 2010; Yoshida, 2008b).

The round spermatids are transformed into elongated, highly condensed, mature spermatozoa through a process called spermiogenesis that includes four different stages: golgi, capping, acrosomal, and maturation (Hess and Renato de Franca, 2008). The mature spermatozoa are released into the lumen and on ejaculation exit the body through the rete testes, epididymis, and vas deferens. In zebrafish, mature spermatozoa are present in the lumen and are released through the efferent duct (Leal *et al.*, 2009).

III. Germ Cell Tumors

A. Human Germ Cell Tumors

In multicellular organisms, proper development of the germ cells is essential for the transmission of genetic information to the next generation, and ultimately for the survival of the species. For this reason, development of the germline is highly regulated to control germ cell proliferation, migration, differentiation, and survival (Chuva de Sousa Lopes and Roelen, 2010; Ewen and Koopman, 2009). Disruption of this regulation can lead to disorders such as infertility, chromosomal abnormalities, and GCTs. GCTs are malignant tumors of the germline that occur in neonates, infants, children, and adults (Frazier and Amatruda, 2009). They arise primarily in the testes and ovaries, though they also occur in extragonadal sites along the midline of the body and the brain. TGCT is the most common cancer in young men aged 15–40, and is increasing in incidence worldwide for unknown reasons. In humans, GCTs differ in clinical and histological presentation and are classified into five distinct groups based on differences in age of onset, histology, cell of origin, chromosomal constitution, and pattern of genomic imprinting (Oosterhuis and Looijenga, 2005). Type I GCTs consist of the teratomas (TE) and yolk sac tumors (YST) of neonates and young children. Type II GCTs encompass the seminomas (SE) and nonseminomas (NS) of adolescents and adults. Spermatocytic SE that affect men >50 years old make up the type III GCT. Finally, the ovarian dermoid cyst and uterine hydatidiform mole are classified as the type IV and type V GCTs, respectively.

1. Type I Germ Cell Tumors

Type I GCTs include TE and YST that affect neonates and children <5 years of age (Oosterhuis and Looijenga, 2005). They most commonly occur in the testes, ovaries, sacrococcygeal area, retroperitoneum, head and neck, and the hypophyseal region of the brain. The type I GCTs are relatively rare with an incidence of 0.12/100,000; sacral TE are the most commonly diagnosed type I GCT (Rescorla, 1999). Based on a partially erased biparental pattern of genomic imprinting, an early PGC is thought to be the cell of origin in type I GCTs (Bussey *et al.*, 2001; Schneider *et al.*, 2001). Typically, the type I TE are benign; however, ovarian TE can be malignant and TE that are incompletely surgically removed can progress to YST, which have the potential to be metastatic (Gobel *et al.*, 2000). Type I TE primarily have a normal chromosomal constitution while type I YST are characteristically aneuploid. Recurrent chromosomal abnormalities in YST include loss of 1p, 4, and 6q and gain of 1q, 12(p13), 20q, and 22 (Mostert *et al.*, 2000; Perlman *et al.*, 2000; Schneider *et al.*, 2001).

Type I animal models include various mouse models of TE. Spontaneous testicular TE arise in the inbred 129 strain of mice that closely resemble human type I TE (Noguchi and Noguchi, 1985; Stevens, 1973). Mutations in *Dead-end/Ter* in the 129-strain mice cause significant PGC loss and increased type I TGCT susceptibility

(Youngren *et al.*, 2005). Targeted deletion of *Pten* in mouse PGCs leads to greater risk for testicular TE, increased germ cell proliferation, and greater capacity to generate embryonic germ cells in culture, thus indicating an important role for *Pten* in regulating germ cell proliferation and differentiation (Kimura *et al.*, 2003).

2. Type II Germ Cell Tumors

Type II GCTs occur in adolescents and adults and TGCTs represent the most common malignancy found in men 20–40 years of age (McIntyre *et al.*, 2008). Type II GCTs largely occur in the testes and ovaries but also occur in extragonadal sites such as the mediastinum and in the brain (Oosterhuis and Looijenga, 2005). Although type II GCTs are often diagnosed in females, they predominantly affect males and are referred to as TGCTs. Type II GCTs are further divided into two subgroups based on histological and clinical variations: SE and NS (Fig. 1). SE are composed of primitive, undifferentiated germ cells that resemble PGCs/gonocytes and occur in the testes. They are also called dysgerminomas when present in the ovaries and germinomas when found extragonadally in the brain. NS include GCTs that are further along the differentiation program than SE such as embryonal carcinomas (EC), choriocarcinomas (CC), YST, and mature TE (Oosterhuis and Looijenga, 2005; van de Geijn *et al.*, 2009).

A fully erased pattern of biparental genomic imprinting suggests that type II GCTs arise from slightly later PGCs/gonocytes than the type I GCTs (Bussey *et al.*, 2001; Oosterhuis and Looijenga, 2005; Schneider *et al.*, 2001). Carcinoma *in situ* (CIS) is a noninvasive precursor lesion that gives rise to all type II TGCTs (Hoei-Hansen *et al.*, 2005; Rajpert-De Meyts *et al.*, 2003). It has an incidence rate similar to the type II GCTs and indicates that all CIS lesions will eventually progress to invasive TGCTs (Oosterhuis and Looijenga, 2005; van de Geijn *et al.*, 2009). CIS cells show phenotypic characteristics similar to PGCs such as morphology, pluripotent gene expression, and genomic imprinting. A confirmed marker for CIS is Oct3/4, a gene that is known for a role in maintaining pluripotency. Oct3/4 is expressed in all CIS, SE, and the EC component of NS that suggests that all SE and NS share similar pathogenesis pathways (Hoei-Hansen *et al.*, 2005; Rajpert-De Meyts *et al.*, 2003). Oct3/4 is expressed in normal PGCs during development but then decreases in the germ cells postnatally (Honecker *et al.*, 2004; Rajpert-De Meyts *et al.*, 2004; Stoop *et al.*, 2005).

SE exhibit an accumulation of undifferentiated PGC/gonocyte-like germ cells that share a similar morphology to CIS cells. NS can be composed of different histological components that represent the differentiation of a truly totipotent cell. EC consist of undifferentiated stem cells, and it is thought that ECs may arise from SE that have undergone reprogramming to activate underlying pluripotency to become ECs (Looijenga *et al.*, 1999; Oosterhuis *et al.*, 2003). ECs undergo differentiation to give rise to other NS components including CC and YST that are differentiated into extraembryonic components (trophoblast and yolk sac, respectively) and mature TE that have undergone somatic differentiation. Thus, the EC

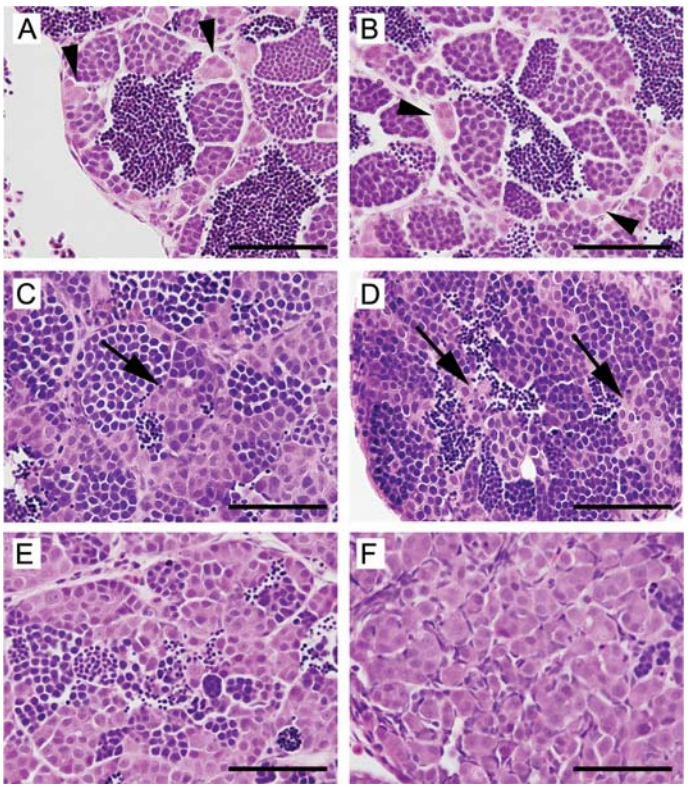

Fig. 1 Histology of zebrafish germ cell tumors. Hematoxylin and eosin-stained sections from formalin-fixed, paraffin-embedded zebrafish testes. (A and B) Normal testis. The testis consists of cysts or lobules of spermatogenic cells surrounded by a basement membrane and somatic cells. Small clusters of spermatogonia are seen adjacent to the basement membrane (arrowheads). Successive stages of differentiation are also evident, including primary and secondary spermatocytes, spermatids, and mature spermatozoa. (C–F) Testicular germ cell tumors. The images shown are from the *tgct* germ cell tumor mutant line; similar histology can be found in carcinogen-treated fish and in males of advanced age. Loss of orderly architecture and impaired differentiation. Ectopic clusters of spermatogonia are seen in the center of the lobule, distant from the basement membrane (arrows). In "E," a severe reduction in spermatogenesis is evident. (F) Complete loss of spermatocytic differentiation. The architecture of the lobule is overrun by a proliferation of primitive, spermatogonial-like cells. (Modified with permission from Neumann *et al.* (2009).) (For color version of this figure, the reader is referred to the web version of this book.)

represents the neoplastic counterpart to embryonic germ cells and the true cancer stem cell.

Type II TGCTs are typically aneuploid and show a consistent pattern of recurrent chromosomal abnormalities including the loss of chromosomes 4, 5, 11, 13, 18, and Y, and gain of chromosomes 7, 8, 12p, and X (Castedo *et al.*, 1989; Looijenga *et al.*, 2000; Oosterhuis and Looijenga, 2005; Ottesen *et al.*, 1997; Summersgill *et al.*,

1998). The gain of 12p is characteristic of all invasive type II TGCTs and interestingly is not consistently present in the preinvasive lesion, CIS (Looijenga *et al.*, 2000, 2007; Oosterhuis *et al.*, 1997; Summersgill *et al.*, 2001; van Echten *et al.*, 1995). This indicates that gain of 12p plays a significant role in the transformation of CIS into invasive TGCTs.

Very few mutations associated with TGCT development have been identified, primarily due to lack of large pedigrees for analysis and the lack of suitable animal models for type II TGCTs (Oosterhuis and Looijenga, 2005). However, activating mutations in c-Kit exon17, in particular at codon 816, are associated predominantly with bilateral TGCTs, which only account for up to 5% of TGCTs (Dieckmann *et al.*, 2007a, 2007b; Kemmer *et al.*, 2004; Looijenga *et al.*, 2003; Nakai *et al.*, 2005; Oosterhuis and Looijenga, 2005; Sakuma *et al.*, 2003; Tian *et al.*, 1999). Two recent genome-wide association studies implicated *KITLG* (the *kit* ligand), *DMRT1*, and *SPRY4* in familial testicular cancer (Kanetsky *et al.*, 2009; Rapley *et al.*, 2009; Turnbull *et al.*, 2010).

B. Germ Cell Tumors in Zebrafish

1. Carcinogenesis and Reverse Genetic Models of GCT

Previous studies have described the spontaneous development of gonadal neoplasms in male zebrafish >2 years of age. Moore *et al.* (2006) described the tumor spectrum at 30–34 months of age in wild-type zebrafish and in carriers of the *gin* genomic instability phenotype. Testicular hyperplasias (enlarged testes containing all stages of spermatogenesis) were found in 48% of wild types and 25% of *gin* heterozygotes. "Benign SE," which they defined as tumors of predominantly one cell type derived from an early stage in spermatogenesis, were seen in 17% of wild-type fish at 30–34 months of age; the incidence was 53% in *gin* carriers. In a survey of nearly 10,000 two-year-old zebrafish, Amsterdam *et al.* (2009) documented the tumor spectrum. Of 473 tumors found, approximately 40% were described as SE of the testis. The testis has also been identified as a target of carcinogens in multiple fish species, including rainbow trout, medaka, and zebrafish (Bailey *et al.*, 1984; Hawkins *et al.*, 1985; Neumann *et al.*, 2009). Spitsbergen *et al.* (2000a, 2000b) reported testicular neoplasms of 5 of 68 juvenile fish treated with the carcinogens MNNG, and in 1 of 99 juveniles treated with DMBA. Other teleosts, such as rainbow trout and medaka, are also susceptible to testicular carcinogenesis (Bailey *et al.*, 1984; Hawkins *et al.*, 1985). Recently, transgenic expression of large T antigen or the *scl* gene in the testis was found to result in GCTs by 36 months of age (Gill *et al.*, 2010).

2. Forward Genetic Screens for Gonadal Phenotypes and GCT

Forward genetic approaches have also been used to generate GCTs in zebrafish. Bauer and Goetz (2001) identified 11 mutations that caused gonadal phenotypes in either males or females during a mutational screen using *N*-ethyl *N*-nitrosourea. The

males had altered spermatogenesis in which the testes contained predominantly spermatogonia and/or spermatocytes, similar to the benign SE that were described by Moore *et al*. (Bauer and Goetz, 2001; Moore *et al.*, 2006). During a forward genetic screen to identify cancer susceptibility mutations, we identified a highly heritable *tgct* mutant (Neumann *et al.*, 2009). Homozygous and heterozygous adult male fish from this line develop bilateral TGCTs that can grow to occupy the entire abdominal cavity. The tumors are notable for impaired spermatocytic differentiation that leads to the accumulation of undifferentiated spermatogonial-like cells that disrupt normal testicular architecture (Fig. 1). Homozygous mutant females display an oocyte maturation defect that affects fertility and causes an increase of stage I and II immature oocytes and lack of fully mature stage Voocytes. We recently identified a mutation in the Type IB BMP receptor, alk6b, as the cause of the germ cell tumors in tgct mutants (Neumann *et al.*, 2011). In the *Medaka* fish mutant, *hotei*, a nonsense mutation in anti-Mullerian hormone receptor II (AMHRII) impairs gonadal development and results in a phenotype somewhat overlapping that of the zebrafish *tgct* mutant. *Hotei* (*hot*) mutant fish develop enlarged gonads; males exhibit hypertrophic testes with disorganized spermatogenesis, whereas females display arrested follicular development.

IV. Methods for Studying Zebrafish Germ Cells

Methods that can be used to study germline development and disease in zebrafish provide certain advantages over other model organisms. Techniques such as fusing GFP with *nanos* 3′ UTR, *in vitro* germ cell differentiation assays, and the use of germ cell–specific promoters (i.e., *ziwi*) allow studies of germ cell specification and migration, interactions with the microenvironment, and germ cell–specific gene expression. In this section, we provide protocols for several different methods to study germ cells in zebrafish.

A. Visualization of Primordial Germ Cells

Studies on germ cells in zebrafish are significantly enhanced by the ability to visualize germ cells both *in vitro* and *in vivo*. The identification of germ cell–specific genes such as *vasa* and *nanos* provided a means to visualize PGCs to examine germ cell specification, migration, and development (Koprunner *et al.*, 2001; Yoon *et al.*, 1997). *In situ* hybridization probes against *vasa* and *nanos* have frequently been used to look for germ cell–specific phenotypes. It was found that the 3′ UTR of *vasa* and *nanos* is essential to germ cell–specific gene expression. Constructs that fuse GFP to the *vasa* or *nanos* 3′ UTR allow visualization of PGCs in living embryos (Wolke *et al.*, 2002) (Fig. 2). These constructs not only can be used to conduct screens to identify genes required for germ cell development but can also be used to perform germ cell transplantation assays to study germ cell interactions with the

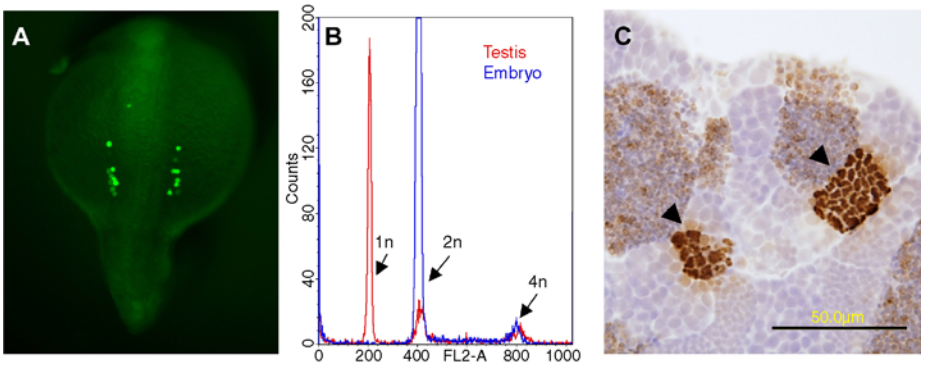

Fig. 2 Methods to visualize germ cells. (A) Embryo injected at the one-cell stage with GFP-nanos 3′ UTR mRNA (gift of Gilbert Weidinger). Bilateral clusters of PGCs are visible in this dorsal view of a 15-somite stage embryo. (B) FACS DNA content analysis of the testis. Red line indicates testis, with haploid (1*n*), diploid (2*n*), and mitotic (4*n*) cells. Blue line is a normal, diploid embryo DNA content profile for comparison. (C) Antiphosphohistone H3 immunohistochemistry of adult, wild-type testis. Clusters of synchronously dividing spermatocytes are seen (arrowheads). (See color plate.)

microenvironment. Recently, Leu and Draper (2010) achieved robust and specific expression of transgenes in the early cells of the testis and ovary using the *ziwi* promoter. Visualizing germ cells will undoubtedly remain critical to the study of germ cells and the identification of genes and pathways that are essential for proper germline development.

B. *In vitro* Culture of the Testis

Sakai (2002, 2006) published pioneering studies describing the *in vitro* culture of zebrafish testis. Unlike mammalian testis, zebrafish germ cells are capable of undergoing meiosis *in vitro* to produce functional sperm. Below, we present a protocol for culture of testicular germ cells (modified from Sakai, 2006). Note that variations of this protocol are possible, including the use of feeder cell layers (Sakai, 2006).

Sacrificing animals:

(1) Anesthetize fish in 0.2% tricaine solution for 2 min.
(2) Dip fish in 100% EtOH to disinfect the carcass.

Testis dissection:

(3) Decapitate the fish and use surgical scissors to open the ventral surface. Expose the testis by carefully removing the gut and swim bladder.
(4) Using fine-tipped tweezers, carefully remove the bilateral testis from the body cavity.

Note: It is recommended to use the testes from six to eight fish to obtain enough cells to set up primary cultures.

Primary culture from testis:
Note: All of these steps should be done in a sterile cell culture hood to avoid contamination of the primary cultures.

(5) Add dissected testis to a six-well plate with 2 mL 1× phosphate-buffered saline (PBS).
(6) Wash three times with sterile 1× PBS.
(7) Mince large pieces of the tissue with surgical scissors and pass through a pipette to break up the large pieces.
(8) Transfer the sample into a 15-mL conical tube and bring the volume up to 5 mL with sterile 1× PBS.
(9) Gently centrifuge the sample 5 min, 1000 rpm.
(10) Carefully remove the supernatant, being sure not to dislodge the cell pellet.
(11) Add 3 mL dispase to the cell pellet for enzymatic disaggregation of the sample.
(12) Incubate 37 °C for 30 min with gentle agitation to break up the tissue further.
(13) Once enzymatic digestion is completed, quench dispase with 12 mL DMEM/F12 Complete and shake well.
(14) Spin the sample 5 min, 1000 rpm.
(15) Remove the supernatant, leaving about 500 μL over the cell pellet.
(16) Resuspend the cell pellet gently with a pipette.
(17) Bring the volume up to 6 mL with DMEM/F12 Complete.
(18) Filter the sample through a nylon mesh cell strainer (40 μm) and into a 50-mL conical tube.
(19) Add 15 mL of DMEM/F12 Complete.
(20) Spin down the samples 5 min, 1000 rpm.
(21) Remove the supernatant, being careful not to disturb the small, loose cell pellet.
(22) Resuspend the pellet one last time in 4 mL DMEM/F12 Complete HI-TS, FBS.
(23) Add 1 mL sample to each of the 4 wells of a gelatin-coated 12-well plate.
Note: Adjust volume to plate about 2×10^5 cells per well.
(24) Incubate cells 28 °C/5% CO_2 overnight.
(25) Remove media and plate floating, nonadherent cells into a new gelatin-coated well to grow.
(26) Feed the cells new DMEM/F12 Complete HI-TS, FBS every ∼3 days, split cells 1:2 when 80–90% confluence is reached.

C. Profiling Testis DNA Content by FACS

DNA content profiling by fluorescence-activated cell sorting (FACS) is a rapid and convenient method to assess the capacity of zebrafish germ cells to differentiate to haploid spermatocytes and sperm (Fig. 2).

Sacrificing animals:

(1) Anesthetize fish in 0.2% tricaine solution for 2 min.
(2) Dip fish in 100% EtOH to disinfect the carcass.

Testis dissection:

(3) Decapitate the fish and use surgical scissors to open the ventral surface. Expose the testis by carefully removing the gut and swim bladder.
(4) Using fine-tipped tweezers, carefully remove the bilateral testis from the body cavity.

Preparation of samples for FACS sorting:

(5) Add dissected testis to 250 μL DMEM in a 1.5-mL tube.
(6) Using a pestle, grind the testis to disaggregate the tissue.
(7) Add 750 μL DMEM to bring the sample volume up to 1 mL.
(8) Disaggregate the sample further but pipetting up and down 5–10 times.
(9) Pass the sample through a piece of 40-μm mesh and into a new tube to remove any clumps of tissue left over.
(10) Gently spin down the sample for 4 min, 1200 rpm.
(11) Remove and discard the supernatant.
(12) Gently resuspend the cell pellet in 500 μL 1× PBS.
(13) Pass the sample through a new piece of 40-μm mesh and into a FACS culture tube to remove any cell clumps.
(14) Add 1.5 mL PI/Triton X-100 solution to the sample for a total volume of 2 mL.
(15) Add 4 μL DNase-free RNase to the sample and place on ice in the dark for 15–20 min.
(16) Samples are now ready to be analyzed.

Note: If performing FACS on cells from culture collect cells, gently pellet as in step 6 and continue protocol.

D. Detection of Cell Proliferation by Antiphosphohistone H3 Immunohistochemistry

Phosphorylation of Histone H3 on serine 10 is correlated with the onset of chromatin condensation, and therefore marks mitotic cells. Immunohistochemistry of the testis with this marker marks clusters of synchronously dividing spermatocytes (Fig. 2). The protocol can easily be adapted to detect other antigens.

Immunohistochemical staining of zebrafish testis:

(1) Deparaffinize slides in xylene, 2 × 10 min.
(2) Rehydrate slides by placing in decreasing amounts of EtOH:

- 100% EtOH, 2 × 3 min;
- 95% EtOH, 2 × 3 min;
- dH_2O, 2 × 3 min.

(3) Antigen retrieval: Incubate slides in Trilogy reagent (Cell Marque) in a pressure cooker for 15 min. For other antigens, conditions for antigen retrieval may need to be individually optimized.
(4) Cool slides in Trilogy reagent for 20 min.
(5) Peroxidase block: Place slides in 0.3% H_2O_2/H_2O for 30 min. Rinse in dH_2O for 1 min.
(6) Block in 2.5% horse serum (ImmPRESS; Vector Laboratories) for 30 min at room temperature. Do not let sections dry out at anytime during blocking or incubation with antibodies.
(7) Apply antiphosphohistone H3 (Santa Cruz Biotechnology) at 1:750 in horse serum for 2 h at room temperature or overnight at 4°.
(8) Rinse quickly in 1× phosphate-buffered saline plus 0.1% Tween-20 (PBST). Wash 4 × 5 min in 1× PBST.
(9) Apply ImmPRESS α-rabbit secondary antibody, enough to cover section. Incubate 30 min at room temperature.
(10) Rinse quickly in 1× PBST. Wash 4 × 5 min in 1× PBST.
(11) Apply 200 μL 1× DAB solution (1:10 DAB in DAB buffer; BD Pharmingen) until staining of sections is visible. Rinse quickly in 1× PBST before counterstaining.
(12) Counterstain in hematoxylin for 2 min. Run tap water over slides until hematoxylin stain is evident by acquisition of a blue tint; typically 7–11 min.
(13) Dehydrate slides by placing in increasing amounts of EtOH:

- 95% EtOH, 2 × 1 min;
- 100% EtOH, 2 × 1 min;
- Xylene, 2 × 1 min.

(14) Let slides air dry and then mount with DEPEX mounting solution.

E. Materials

PI/Triton X-100 solution:

- Dilute Triton X-100 1:10 (1 μL Triton X-100 into 9 μL PBS).
- Add 1 μL of 1:10 Triton X-100 to 5 mL propidium iodide (50 μg/mL in 0.1% sodium citrate).

2% gelatin-coated plates:

(1) Add 500 μL gelatin to necessary wells:

- Incubate 37 °C for 15 min.
- Remove excess liquid from top of wells before use.

DMEM/F12 Complete:

- 50% DMEM Media;
- 50% F12 Media;

- 1× Antibiotic-Antimycotic;
- 1× MEM vitamins;
- 1× MEM nonessential amino acids;
- 2 mM L-glutamine.

Note: Filter sterilize media before use.
DMEM/F12 Complete HI-TS, FBS:

- DMEM/F12 Complete;
- 5% fetal bovine serum;
- 5% heat-inactivated trout serum.

Note: Filter sterilize media before use.
Heat-inactivated trout serum:

(1) 10 mL trout serum.
(2) 10 mL DMEM/F12 Complete:

- Heat 55 °C for 30 min.
- Spin down.
- Collect supernatant.
- Filter sterilize before using.

Dispase: BD Biosciences #354235;
Trout serum ("SeaGrow"): East Coast Bio #JJ80;
2% gelatin: Sigma Aldrich #G1393;
DMEM/F12: Invitrogen #11039-047;
Antibiotic-Antimycotic: Invitrogen #15240-062;
MEM vitamin solution: Invitrogen #11120-052;
MEM nonessential amino acids: Invitrogen #11140-050;
200 mM L-glutamine: Invitrogen #25030-081.

References

Amsterdam, A., Lai, K., Komisarczuk, A. Z., Becker, T. S., Bronson, R. T., Hopkins, N., and Lees, J. A. (2009). Zebrafish hagoromo mutants up-regulate fgf8 postembryonically and develop neuroblastoma. *Mol. Cancer Res.* **7**, 841–850.

Ancelin, K., Lange, U. C., Hajkova, P., Schneider, R., Bannister, A. J., Kouzarides, T., and Surani, M. A. (2006). Blimp1 associates with Prmt5 and directs histone arginine methylation in mouse germ cells. *Nat. Cell Biol.* **8**, 623–630.

Anderson, R., Copeland, T. K., Scholer, H., Heasman, J., and Wylie, C. (2000). The onset of germ cell migration in the mouse embryo. *Mech. Dev.* **91**, 61–68.

Anderson, R., Fassler, R., Georges-Labouesse, E., Hynes, R. O., Bader, B. L., Kreidberg, J. A., Schaible, K., Heasman, J., and Wylie, C. (1999a). Mouse primordial germ cells lacking beta1 integrins enter the germline but fail to migrate normally to the gonads. *Development* **126**, 1655–1664.

Anderson, R., Schaible, K., Heasman, J., and Wylie, C. (1999b). Expression of the homophilic adhesion molecule, Ep-CAM, in the mammalian germ line. *J. Reprod. Fertil.* **116**, 379–384.

Ara, T., Nakamura, Y., Egawa, T., Sugiyama, T., Abe, K., Kishimoto, T., Matsui, Y., and Nagasawa, T. (2003). Impaired colonization of the gonads by primordial germ cells in mice lacking a chemokine, stromal cell-derived factor-1 (SDF-1). *Proc. Natl. Acad. Sci. U.S.A.* **100**, 5319–5323.

Bailey, G. S., Hendricks, J. D., Nixon, J. E., and Pawlowski, N. E. (1984). The sensitivity of rainbow trout and other fish to carcinogens. *Drug Metab. Rev.* **15**, 725–750.

Bauer, M. P., and Goetz, F. W. (2001). Isolation of gonadal mutations in adult zebrafish from a chemical mutagenesis screen. *Biol. Reprod.* **64**, 548–554.

Bendel-Stenzel, M. R., Gomperts, M., Anderson, R., Heasman, J., and Wylie, C. (2000). The role of cadherins during primordial germ cell migration and early gonad formation in the mouse. *Mech. Dev.* **91**, 143–152.

Blaser, H., Eisenbeiss, S., Neumann, M., Reichman-Fried, M., Thisse, B., Thisse, C., and Raz, E. (2005). Transition from non-motile behaviour to directed migration during early PGC development in zebrafish. *J. Cell Sci.* **118**, 4027–4038.

Braat, A. K., Zandbergen, T., van de Water, S., Goos, H. J., and Zivkovic, D. (1999). Characterization of zebrafish primordial germ cells: morphology and early distribution of vasa RNA. *Dev. Dyn.* **216**, 153–167.

Bussey, K. J., Lawce, H. J., Himoe, E., Shu, X. O., Heerema, N. A., Perlman, E. J., Olson, S. B., and Magenis, R. E. (2001). SNRPN methylation patterns in germ cell tumors as a reflection of primordial germ cell development. *Genes Chromosomes Cancer* **32**, 342–352.

Castedo, S. M., de Jong, B., Oosterhuis, J. W., Seruca, R., te Meerman, G. J., Dam, A., and Schraffordt Koops, H. (1989). Cytogenetic analysis of ten human seminomas. *Cancer Res.* **49**, 439–443.

Chiarini-Garcia, H., Hornick, J. R., Griswold, M. D., and Russell, L. D. (2001). Distribution of type A spermatogonia in the mouse is not random. *Biol. Reprod.* **65**, 1179–1185.

Chiarini-Garcia, H., and Russell, L. D. (2001). High-resolution light microscopic characterization of mouse spermatogonia. *Biol. Reprod.* **65**, 1170–1178.

Chuva de Sousa Lopes, S. M., and Roelen, B. A. (2010). On the formation of germ cells: the good, the bad and the ugly. *Differentiation* **79**, 131–140.

Clelland, E., and Peng, C. (2009). Endocrine/paracrine control of zebrafish ovarian development. *Mol. Cell. Endocrinol.* **312**, 42–52.

de Rooij, D. G., and Russell, L. D. (2000). All you wanted to know about spermatogonia but were afraid to ask. *J. Androl.* **21**, 776–798.

de Sousa Lopes, S. M., Roelen, B. A., Monteiro, R. M., Emmens, R., Lin, H. Y., Li, E., Lawson, K. A., and Mummery, C. L. (2004). BMP signaling mediated by ALK2 in the visceral endoderm is necessary for the generation of primordial germ cells in the mouse embryo. *Genes Dev.* **18**, 1838–1849.

Dieckmann, K. P., Kulejewski, M., Pichlmeier, U., and Loy, V. (2007 a). Diagnosis of contralateral testicular intraepithelial neoplasia (TIN) in patients with testicular germ cell cancer: systematic two-site biopsies are more sensitive than a single random biopsy. *Eur. Urol.* **51**, 175–183 discussion 183-185.

Dieckmann, K. P., Linke, J., Pichlmeier, U., Kulejewski, M., and Loy, V. (2007 b). Spermatogenesis in the contralateral testis of patients with testicular germ cell cancer: histological evaluation of testicular biopsies and a comparison with healthy males. *BJU Int.* **99**, 1079–1085.

Doitsidou, M., Reichman-Fried, M., Stebler, J., Koprunner, M., Dorries, J., Meyer, D., Esguerra, C. V., Leung, T., and Raz, E. (2002). Guidance of primordial germ cell migration by the chemokine SDF-1. *Cell* **111**, 647–659.

Ewen, K. A., and Koopman, P. (2009). Mouse germ cell development: from specification to sex determination. *Mol. Cell. Endocrinol.* **323**, 76–93.

Frazier, A. L., and Amatruda, J. F. (2009). Germ cell tumors. *In* "Nathan and Oski's Textbook of Pediatric Hematology–Oncology," (D. E. Fisher, D. Nathan, and A. T. Look, eds.), Elsevier, London.

Gill, J. A., Lowe, L., Nguyen, J., Liu, P. P., Blake, T., Venkatesh, B., and Aplan, P. D. (2010). Enforced expression of Simian virus 40 large T-antigen leads to testicular germ cell tumors in zebrafish. *Zebrafish* **7**, 333–341.

Gobel, U., Schneider, D. T., Calaminus, G., Haas, R. J., Schmidt, P., and Harms, D. (2000). Germ-cell tumors in childhood and adolescence. GPOH MAKEI and the MAHO study groups. *Ann. Oncol.* **11**, 263–271.

Griswold, M. D. (1998). The central role of Sertoli cells in spermatogenesis. *Semin. Cell Dev. Biol.* **9**, 411–416.

Gu, Y., Runyan, C., Shoemaker, A., Surani, A., and Wylie, C. (2009). Steel factor controls primordial germ cell survival and motility from the time of their specification in the allantois, and provides a continuous niche throughout their migration. *Development* **136**, 1295–1303.

Hawkins, W. E., Overstreet, R. M., Fournie, J. W., and Walker, W. W. (1985). Development of aquarium fish models for environmental carcinogenesis: tumor induction in seven species. *J. Appl. Toxicol.* **5**, 261–264.

Hayashi, K., de Sousa Lopes, S. M., and Surani, M. A. (2007). Germ cell specification in mice. *Science* **316**, 394–396.

Hess, R. A., Cooke, P. S., Hofmann, M. C., and Murphy, K. M. (2006). Mechanistic insights into the regulation of the spermatogonial stem cell niche. *Cell Cycle* **5**, 1164–1170.

Hess, R. A., and Renato de Franca, L. (2008). Spermatogenesis and cycle of the seminiferous epithelium. *Adv. Exp. Med. Biol.* **636**, 1–15.

Hoei-Hansen, C. E., Rajpert-De Meyts, E., Daugaard, G., and Skakkebaek, N. E. (2005). Carcinoma in situ testis, the progenitor of testicular germ cell tumours: a clinical review. *Ann. Oncol.* **16**, 863–868.

Honecker, F., Stoop, H., de Krijger, R. R., Chris Lau, Y. F., Bokemeyer, C., and Looijenga, L. H. (2004). Pathobiological implications of the expression of markers of testicular carcinoma in situ by fetal germ cells. *J. Pathol.* **203**, 849–857.

Houston, D. W., and King, M. L. (2000). Germ plasm and molecular determinants of germ cell fate. *Curr. Top. Dev. Biol.* **50**, 155–181.

Itman, C., Mendis, S., Barakat, B., and Loveland, K. L. (2006). All in the family: TGF-beta family action in testis development. *Reproduction* **132**, 233–246.

Kanetsky, P. A., Mitra, N., Vardhanabhuti, S., Li, M., Vaughn, D. J., Letrero, R., Ciosek, S. L., Doody, D. R., Smith, L. M., Weaver, J., Albano, A., Chen, C., Starr, J. R., Rader, D. J., Godwin, A. K., Reilly, M. P., Hakonarson, H., Schwartz, S. M., and Nathanson, K. L. (2009). Common variation in KITLG and at 5q31.3 predisposes to testicular germ cell cancer. *Nat. Genet.* **41**, 811–815.

Kemmer, K., Corless, C. L., Fletcher, J. A., McGreevey, L., Haley, A., Griffith, D., Cummings, O. W., Wait, C., Town, A., and Heinrich, M. C. (2004). KIT mutations are common in testicular seminomas. *Am. J. Pathol.* **164**, 305–313.

Kimura, T., Suzuki, A., Fujita, Y., Yomogida, K., Lomeli, H., Asada, N., Ikeuchi, M., Nagy, A., Mak, T. W., and Nakano, T. (2003). Conditional loss of PTEN leads to testicular teratoma and enhances embryonic germ cell production. *Development* **130**, 1691–1700.

Knaut, H., Pelegri, F., Bohmann, K., Schwarz, H., and Nusslein-Volhard, C. (2000). Zebrafish vasa RNA but not its protein is a component of the germ plasm and segregates asymmetrically before germline specification. *J. Cell Biol.* **149**, 875–888.

Knaut, H., Werz, C., Geisler, R., and Nusslein-Volhard, C. (2003). A zebrafish homologue of the chemokine receptor Cxcr4 is a germ-cell guidance receptor. *Nature* **421**, 279–282.

Koprunner, M., Thisse, C., Thisse, B., and Raz, E. (2001). A zebrafish nanos-related gene is essential for the development of primordial germ cells. *Genes Dev.* **15**, 2877–2885.

Kunwar, P. S., Siekhaus, D. E., and Lehmann, R. (2006). *In vivo* migration: a germ cell perspective. *Annu. Rev. Cell Dev. Biol.* **22**, 237–265.

Kurimoto, K., Yamaji, M., Seki, Y., and Saitou, M. (2008). Specification of the germ cell lineage in mice: a process orchestrated by the PR-domain proteins, Blimp1 and Prdm14. *Cell Cycle* **7**, 3514–3518.

Lange, U. C., Saitou, M., Western, P. S., Barton, S. C., and Surani, M. A. (2003). The fragilis interferon-inducible gene family of transmembrane proteins is associated with germ cell specification in mice. *BMC Dev. Biol.* **3**, 1.

Lawson, K. A., Dunn, N. R., Roelen, B. A., Zeinstra, L. M., Davis, A. M., Wright, C. V., Korving, J. P., and Hogan, B. L. (1999). Bmp4 is required for the generation of primordial germ cells in the mouse embryo. *Genes Dev.* **13**, 424–436.

Leal, M. C., Cardoso, E. R., Nobrega, R. H., Batlouni, S. R., Bogerd, J., Franca, L. R., and Schulz, R. W. (2009). Histological and stereological evaluation of zebrafish (*Danio rerio*) spermatogenesis with an emphasis on spermatogonial generations. *Biol. Reprod.* **81**, 177–187.

Lessman, C. A. (2009). Oocyte maturation: converting the zebrafish oocyte to the fertilizable egg. *Gen. Comp. Endocrinol.* **161**, 53–57.

Leu, D. H., and Draper, B. W. (2010). The ziwi promoter drives germline-specific gene expression in zebrafish. *Dev. Dyn.* **239**, 2714–2721.

Looijenga, L. H., de Leeuw, H., van Oorschot, M., van Gurp, R. J., Stoop, H., Gillis, A. J., de Gouveia Brazao, C. A., Weber, R. F., Kirkels, W. J., van Dijk, T., von Lindern, M., Valk, P., Lajos, G., Olah, E., Nesland, J. M., Fossa, S. D., and Oosterhuis, J. W. (2003). Stem cell factor receptor (c-KIT) codon 816 mutations predict development of bilateral testicular germ-cell tumors. *Cancer Res.* **63**, 7674–7678.

Looijenga, L. H., de Munnik, H., and Oosterhuis, J. W. (1999). A molecular model for the development of germ cell cancer. *Int. J. Cancer* **83**, 809–814.

Looijenga, L. H., Gillis, A. J., Stoop, H. J., Hersmus, R., and Oosterhuis, J. W. (2007). Chromosomes and expression in human testicular germ-cell tumors: insight into their cell of origin and pathogenesis. *Ann. N. Y. Acad. Sci.* **1120**, 187–214.

Looijenga, L. H., Rosenberg, C., van Gurp, R. J., Geelen, E., van Echten-Arends, J., de Jong, B., Mostert, M., and Wolter Oosterhuis, J. (2000). Comparative genomic hybridization of microdissected samples from different stages in the development of a seminoma and a non-seminoma. *J. Pathol.* **191**, 187–192.

Lucifero, D., Chaillet, J. R., and Trasler, J. M. (2004). Potential significance of genomic imprinting defects for reproduction and assisted reproductive technology. *Hum. Reprod. Update* **10**, 3–18.

Macleod, D., Clark, V. H., and Bird, A. (1999). Absence of genome-wide changes in DNA methylation during development of the zebrafish. *Nat. Genet.* **23**, 139–140.

Matta, S. L., Vilela, D. A., Godinho, H. P., and Franca, L. R. (2002). The goitrogen 6-*n*-propyl-2-thiouracil (PTU) given during testis development increases Sertoli and germ cell numbers per cyst in fish: the tilapia (*Oreochromis niloticus*) model. *Endocrinology* **143**, 970–978.

McIntyre, A., Gilbert, D., Goddard, N., Looijenga, L., and Shipley, J. (2008). Genes, chromosomes and the development of testicular germ cell tumors of adolescents and adults. *Genes Chromosomes Cancer* **47**, 547–557.

McLaren, A. (2003). Primordial germ cells in the mouse. *Dev. Biol.* **262**, 1–15.

Molyneaux, K. A., Stallock, J., Schaible, K., and Wylie, C. (2001). Time-lapse analysis of living mouse germ cell migration. *Dev. Biol.* **240**, 488–498.

Molyneaux, K., and Wylie, C. (2004). Primordial germ cell migration. *Int. J. Dev. Biol.* **48**, 537–544.

Molyneaux, K. A., Zinszner, H., Kunwar, P. S., Schaible, K., Stebler, J., Sunshine, M. J., O'Brien, W., Raz, E., Littman, D., Wylie, C., and Lehmann, R. (2003). The chemokine SDF1/CXCL12 and its receptor CXCR4 regulate mouse germ cell migration and survival. *Development* **130**, 4279–4286.

Moore, J. L., Rush, L. M., Breneman, C., Mohideen, M. A., and Cheng, K. C. (2006). Zebrafish genomic instability mutants and cancer susceptibility. *Genetics* **174**, 585–600.

Mostert, M., Rosenberg, C., Stoop, H., Schuyer, M., Timmer, A., Oosterhuis, W., and Looijenga, L. (2000). Comparative genomic and in situ hybridization of germ cell tumors of the infantile testis. *Lab. Invest.* **80**, 1055–1064.

Nakai, Y., Nonomura, N., Oka, D., Shiba, M., Arai, Y., Nakayama, M., Inoue, H., Nishimura, K., Aozasa, K., Mizutani, Y., Miki, T., and Okuyama, A. (2005). KIT (c-kit oncogene product) pathway is constitutively activated in human testicular germ cell tumors. *Biochem. Biophys. Res. Commun.* **337**, 289–296.

Neumann, J. C., Dovey, J. S., Chandler, G. L., Carbajal, L., and Amatruda, J. F. (2009). Identification of a heritable model of testicular germ cell tumor in the zebrafish. *Zebrafish* **6**, 319–327.

Neumann, J. C., Chandler, G. L., Damoulis, V. A., Fustino, N. J., Lillard, K., Looijenga, L., Margraf, L., Rakheja, D. and Amatruda, J. F. (2011). Mutation in the type IB bone morphogenetic protein receptor alk6b impairs germ-cell differentiation and causes germ-cell tumors in zebrafish. *Proc. Natl. Acad. Sci. USA.* Jul 20. [Epub ahead of print].

Noguchi, T., and Noguchi, M. (1985). A recessive mutation (ter) causing germ cell deficiency and a high incidence of congenital testicular teratomas in 129/Sv-ter mice. *J. Natl. Cancer Inst.* **75**, 385–392.

Oatley, J. M., and Brinster, R. L. (2006). Spermatogonial stem cells. *Methods Enzymol.* **419**, 259–282.

Ogawa, T., Ohmura, M., and Ohbo, K. (2005). The niche for spermatogonial stem cells in the mammalian testis. *Int. J. Hematol.* **82**, 381–388.

Ohinata, Y., Payer, B., O'Carroll, D., Ancelin, K., Ono, Y., Sano, M., Barton, S. C., Obukhanych, T., Nussenzweig, M., Tarakhovsky, A., Saitou, M., and Surani, M. A. (2005). Blimp1 is a critical determinant of the germ cell lineage in mice. *Nature* **436**, 207–213.

Olsen, L. C., Aasland, R., and Fjose, A. (1997). A vasa-like gene in zebrafish identifies putative primordial germ cells. *Mech. Dev.* **66**, 95–105.

Oosterhuis, J. W., Kersemaekers, A. M., Jacobsen, G. K., Timmer, A., Steyerberg, E. W., Molier, M., Van Weeren, P. C., Stoop, H., and Looijenga, L. H. (2003). Morphology of testicular parenchyma adjacent to germ cell tumours. An interim report. *APMIS* **111**, 32–40 discussion 41-42.

Oosterhuis, J. W., and Looijenga, L. H. (2005). Testicular germ-cell tumours in a broader perspective. *Nat. Rev. Cancer* **5**, 210–222.

Oosterhuis, J. W., Looijenga, L. H., van Echten, J., and de Jong, B. (1997). Chromosomal constitution and developmental potential of human germ cell tumors and teratomas. *Cancer Genet. Cytogenet.* **95**, 96–102.

Ottesen, A. M., Kirchhoff, M., De-Meyts, E. R., Maahr, J., Gerdes, T., Rose, H., Lundsteen, C., Petersen, P. M., Philip, J., and Skakkebaek, N. E. (1997). Detection of chromosomal aberrations in seminomatous germ cell tumours using comparative genomic hybridization. *Genes Chromosomes Cancer* **20**, 412–418.

Paoloni-Giacobino, A., and Chaillet, J. R. (2004). Genomic imprinting and assisted reproduction. *Reprod. Health.* **1**, 6.

Perlman, E. J., Hu, J., Ho, D., Cushing, B., Lauer, S., and Castleberry, R. P. (2000). Genetic analysis of childhood endodermal sinus tumors by comparative genomic hybridization. *J. Pediatr. Hematol. Oncol.* **22**, 100–105.

Rajpert-De Meyts, E., Bartkova, J., Samson, M., Hoei-Hansen, C. E., Frydelund-Larsen, L., Bartek, J., and Skakkebaek, N. E. (2003). The emerging phenotype of the testicular carcinoma in situ germ cell. *APMIS* **111**, 267–278 discussion 278-279.

Rajpert-De Meyts, E., Hanstein, R., Jorgensen, N., Graem, N., Vogt, P. H., and Skakkebaek, N. E. (2004). Developmental expression of POU5F1 (OCT-3/4) in normal and dysgenetic human gonads. *Hum. Reprod.* **19**, 1338–1344.

Rapley, E. A., Turnbull, C., Al Olama, A. A., Dermitzakis, E. T., Linger, R., Huddart, R. A., Renwick, A., Hughes, D., Hines, S., Seal, S., Morrison, J., Nsengimana, J., Deloukas, P., Rahman, N., Bishop, D. T., Easton, D. F., and Stratton, M. R. (2009). A genome-wide association study of testicular germ cell tumor. *Nat. Genet.* **41**, 807–810.

Raz, E. (2003). Primordial germ-cell development: the zebrafish perspective. *Nat. Rev. Genet.* **4**, 690–700.

Raz, E., and Reichman-Fried, M. (2006). Attraction rules: germ cell migration in zebrafish. *Curr. Opin. Genet. Dev.* **16**, 355-339.

Reichman-Fried, M., Minina, S., and Raz, E. (2004). Autonomous modes of behavior in primordial germ cell migration. *Dev. Cell* **6**, 589–596.

Reik, W., Dean, W., and Walter, J. (2001). Epigenetic reprogramming in mammalian development. *Science* **293**, 1089–1093.

Rescorla, F. J. (1999). Pediatric germ cell tumors. *Semin. Surg. Oncol.* **16**, 144–158.

Richardson, B. E., and Lehmann, R. (2010). Mechanisms guiding primordial germ cell migration: strategies from different organisms. *Nat. Rev. Mol. Cell Biol.* **11**, 37–49.

Ryu, B. Y., Orwig, K. E., Oatley, J. M., Avarbock, M. R., and Brinster, R. L. (2006). Effects of aging and niche microenvironment on spermatogonial stem cell self-renewal. *Stem Cells* **24**, 1505–1511.

Saffman, E. E., and Lasko, P. (1999). Germline development in vertebrates and invertebrates. *Cell. Mol. Life Sci.* **55**, 1141–1163.

Saito, D., and Tanaka, M. (2009). Comparative aspects of gonadal sex differentiation in medaka: a conserved role of developing oocytes in sexual canalization. *Sex Dev.* **3**, 99–107.

Saitou, M., Barton, S. C., and Surani, M. A. (2002). A molecular programme for the specification of germ cell fate in mice. *Nature* **418**, 293–300.

Saitou, M., Payer, B., O'Carroll, D., Ohinata, Y., and Surani, M. A. (2005). Blimp1 and the emergence of the germ line during development in the mouse. *Cell Cycle.* **4**, 1736–1740.

Sakai, N. (2002). Transmeiotic differentiation of zebrafish germ cells into functional sperm in culture. *Development* **129**, 3359–3365.

Sakai, N. (2006). *In vitro* male germ cell cultures of zebrafish. *Methods* **39**, 239–245.

Sakuma, Y., Sakurai, S., Oguni, S., Hironaka, M., and Saito, K. (2003). Alterations of the c-kit gene in testicular germ cell tumors. *Cancer Sci.* **94**, 486–491.

Schneider, D. T., Schuster, A. E., Fritsch, M. K., Hu, J., Olson, T., Lauer, S., Gobel, U., and Perlman, E. J. (2001). Multipoint imprinting analysis indicates a common precursor cell for gonadal and nongonadal pediatric germ cell tumors. *Cancer Res.* **61**, 7268–7276.

Scholer, H. R., Dressler, G. R., Balling, R., Rohdewohld, H., and Gruss, P. (1990). Oct-4: a germline-specific transcription factor mapping to the mouse t-complex. *EMBO J.* **9**, 2185–2195.

Schulz, R. W., de Franca, L. R., Lareyre, J. J., Le Gac, F., Chiarini-Garcia, H., Nobrega, R. H., and Miura, T. (2010). Spermatogenesis in fish. *Gen. Comp. Endocrinol.* **165**, 390–411.

Schulz, R. W., Menting, S., Bogerd, J., Franca, L. R., Vilela, D. A., and Godinho, H. P. (2005). Sertoli cell proliferation in the adult testis – evidence from two fish species belonging to different orders. *Biol. Reprod.* **73**, 891–898.

Spitsbergen, J. M., Tsai, H. W., Reddy, A., Miller, T., Arbogast, D., Hendricks, J. D., and Bailey, G. S. (2000a). Neoplasia in zebrafish (Danio rerio) treated with 7,12-dimethylbenz[a]anthracene by two exposure routes at different developmental stages. *Toxicol. Pathol.* **28**, 705–715.

Spitsbergen, J. M., Tsai, H. W., Reddy, A., Miller, T., Arbogast, D., Hendricks, J. D., and Bailey, G. S. (2000b). Neoplasia in zebrafish (Danio rerio) treated with N-methyl-N′-nitro-N-nitrosoguanidine by three exposure routes at different developmental stages. *Toxicol. Pathol* **28**, 716–725.

Stevens, L. C. (1973). A new inbred subline of mice (129-terSv) with a high incidence of spontaneous congenital testicular teratomas. *J. Natl. Cancer Inst.* **50**, 235–242.

Stoop, H., Honecker, F., Cools, M., de Krijger, R., Bokemeyer, C., and Looijenga, L. H. (2005). Differentiation and development of human female germ cells during prenatal gonadogenesis: an immunohistochemical study. *Hum. Reprod.* **20**, 1466–1476.

Summersgill, B., Goker, H., Weber-Hall, S., Huddart, R., Horwich, A., and Shipley, J. (1998). Molecular cytogenetic analysis of adult testicular germ cell tumours and identification of regions of consensus copy number change. *Br. J. Cancer* **77**, 305–313.

Summersgill, B., Osin, P., Lu, Y. J., Huddart, R., and Shipley, J. (2001). Chromosomal imbalances associated with carcinoma in situ and associated testicular germ cell tumours of adolescents and adults. *Br. J. Cancer* **85**, 213–220.

Surani, M. A. (2001). Reprogramming of genome function through epigenetic inheritance. *Nature* **414**, 122–128.

Tam, P. P., and Zhou, S. X. (1996). The allocation of epiblast cells to ectodermal and germ-line lineages is influenced by the position of the cells in the gastrulating mouse embryo. *Dev. Biol.* **178**, 124–132.

Tanaka, S. S., and Matsui, Y. (2002). Developmentally regulated expression of mil-1 and mil-2, mouse interferon-induced transmembrane protein like genes, during formation and differentiation of primordial germ cells. *Mech. Dev.* **119**(suppl. 1), S261–S267.

Tanaka, S. S., Nagamatsu, G., Tokitake, Y., Kasa, M., Tam, P. P., and Matsui, Y. (2004). Regulation of expression of mouse interferon-induced transmembrane protein like gene-3, Ifitm3 (mil-1, fragilis), in germ cells. *Dev. Dyn.* **230**, 651–659.

Tanaka, S. S., Yamaguchi, Y. L., Tsoi, B., Lickert, H., and Tam, P. P. (2005). IFITM/Mil/fragilis family proteins IFITM1 and IFITM3 play distinct roles in mouse primordial germ cell homing and repulsion. *Dev. Cell* **9**, 745–756.

Tian, Q., Frierson Jr., H. F., Krystal, G. W., and Moskaluk, C. A. (1999). Activating c-kit gene mutations in human germ cell tumors. *Am. J. Pathol.* **154**, 1643–1647.

Turnbull, C., Rapley, E. A., Seal, S., Pernet, D., Renwick, A., Hughes, D., Ricketts, M., Linger, R., Nsengimana, J., Deloukas, P., Huddart, R. A., Bishop, D. T., Easton, D. F., Stratton, M. R., and Rahman, N. (2010). Variants near DMRT1, TERT and ATF7IP are associated with testicular germ cell cancer. *Nat. Genet.* **42**, 604–607.

van de Geijn, G. J., Hersmus, R., and Looijenga, L. H. (2009). Recent developments in testicular germ cell tumor research. *Birth Defects Res. C Embryo Today* **87**, 96–113.

van Echten, J., van Gurp, R. J., Stoepker, M., Looijenga, L. H., de Jong, J., and Oosterhuis, W. (1995). Cytogenetic evidence that carcinoma in situ is the precursor lesion for invasive testicular germ cell tumors. *Cancer Genet. Cytogenet.* **85**, 133–137.

Vincent, S. D., Dunn, N. R., Sciammas, R., Shapiro-Shalef, M., Davis, M. M., Calame, K., Bikoff, E. K., and Robertson, E. J. (2005). The zinc finger transcriptional repressor Blimp1/Prdm1 is dispensable for early axis formation but is required for specification of primordial germ cells in the mouse. *Development* **132**, 1315–1325.

Weidinger, G., Stebler, J., Slanchev, K., Dumstrei, K., Wise, C., Lovell-Badge, R., Thisse, C., Thisse, B., and Raz, E. (2003). dead end, a novel vertebrate germ plasm component, is required for zebrafish primordial germ cell migration and survival. *Curr. Biol.* **13**, 1429–1434.

Weidinger, G., Wolke, U., Koprunner, M., Klinger, M., and Raz, E. (1999). Identification of tissues and patterning events required for distinct steps in early migration of zebrafish primordial germ cells. *Development* **126**, 5295–5307.

Weidinger, G., Wolke, U., Koprunner, M., Thisse, C., Thisse, B., and Raz, E. (2002). Regulation of zebrafish primordial germ cell migration by attraction towards an intermediate target. *Development* **129**, 25–36.

Western, P. (2009). Foetal germ cells: striking the balance between pluripotency and differentiation. *Int. J. Dev. Biol.* **53**, 393–409.

Williamson, A., and Lehmann, R. (1996). Germ cell development in *Drosophila*. *Annu. Rev. Cell Dev. Biol.* **12**, 365–391.

Wolke, U., Weidinger, G., Koprunner, M., and Raz, E. (2002). Multiple levels of posttranscriptional control lead to germ line-specific gene expression in the zebrafish. *Curr. Biol.* **12**, 289–294.

Wylie, C. (2000). Germ cells. *Curr. Opin. Genet. Dev.* **10**, 410–413.

Yabuta, Y., Kurimoto, K., Ohinata, Y., Seki, Y., and Saitou, M. (2006). Gene expression dynamics during germline specification in mice identified by quantitative single-cell gene expression profiling. *Biol. Reprod.* **75**, 705–716.

Yamaguchi, S., Kimura, H., Tada, M., Nakatsuji, N., and Tada, T. (2005). Nanog expression in mouse germ cell development. *Gene Expr. Patterns* **5**, 639–646.

Yamaji, M., Seki, Y., Kurimoto, K., Yabuta, Y., Yuasa, M., Shigeta, M., Yamanaka, K., Ohinata, Y., and Saitou, M. (2008). Critical function of Prdm14 for the establishment of the germ cell lineage in mice. *Nat. Genet.* **40**, 1016–1022.

Yeom, Y. I., Fuhrmann, G., Ovitt, C. E., Brehm, A., Ohbo, K., Gross, M., Hubner, K., and Scholer, H. R. (1996). Germline regulatory element of Oct-4 specific for the totipotent cycle of embryonal cells. *Development* **122**, 881–894.

Ying, Y., Qi, X., and Zhao, G. Q. (2001). Induction of primordial germ cells from murine epiblasts by synergistic action of BMP4 and BMP8B signaling pathways. *Proc. Natl. Acad. Sci. U. S. A.* **98**, 7858–7862.

Ying, Y., and Zhao, G. Q. (2001). Cooperation of endoderm-derived BMP2 and extraembryonic ectoderm-derived BMP4 in primordial germ cell generation in the mouse. *Dev. Biol.* **232**, 484–492.

Yoon, C., Kawakami, K., and Hopkins, N. (1997). Zebrafish vasa homologue RNA is localized to the cleavage planes of 2- and 4-cell-stage embryos and is expressed in the primordial germ cells. *Development* **124**, 3157–3165.

Yoshida, S. (2008 a). "Flexible" stem cell-niche system in mouse spermatogenesis. *Tanpakushitsu Kakusan Koso* **53**, 1125–1132.

Yoshida, S. (2008 b). Spermatogenic stem cell system in the mouse testis. *Cold Spring Harb. Symp. Quant. Biol.* **73**, 25–32.

Youngren, K. K., Coveney, D., Peng, X., Bhattacharya, C., Schmidt, L. S., Nickerson, M. L., Lamb, B. T., Deng, J. M., Behringer, R. R., Capel, B., Rubin, E. M., Nadeau, J. H., and Matin, A. (2005). The Ter mutation in the dead end gene causes germ cell loss and testicular germ cell tumours. *Nature* **435**, 360–364.

Zhao, G. Q., and Garbers, D. L. (2002). Male germ cell specification and differentiation. *Dev. Cell* **2**, 537–547.

CHAPTER 2

Dissecting Mechanisms of Myelinated Axon Formation Using Zebrafish

Tim Czopka[*,†,‡] **and David A. Lyons**[*,‡]

[*]Centre for Neuroregeneration, University of Edinburgh, Chancellor's Building, 49 Little France Crescent, Edinburgh, UK

[†]Centre for Regenerative Medicine, University of Edinburgh, Edinburgh, UK

[‡]Centre for Multiple Sclerosis Research, University of Edinburgh, Edinburgh, UK

METHODS IN CELL BIOLOGY, VOL 105

0091-679X/10 $35.00
DOI 10.1016/B978-0-12-381320-6.00002-3

Abstract

The myelin sheath is an essential component of the vertebrate nervous system, and its disruption causes numerous diseases, including multiple sclerosis (MS), and neurodegeneration. Although we understand a great deal about the early development of the glial cells that make myelin (Schwann cells in the peripheral nervous system and oligodendrocytes in the central nervous system), we know much less about the cellular and molecular mechanisms that regulate the later stages of differentiation that orchestrate myelin formation. Over the past decade, the zebrafish has been employed as a model with which to dissect the development of myelinated axons. Forward genetic screens have revealed new genes essential for myelination, as well as new roles for genes previously implicated in myelinated axon formation in other systems. High-resolution *in vivo* imaging in zebrafish has also begun to illuminate novel cell behaviors during myelinating glial cell development. Here we review the contribution of zebrafish research to our understanding of myelinated axon formation to date. We also describe and discuss many of the methodologies used in these studies and preview future endeavors that will ensure that the zebrafish remains at the cutting edge of this important area of research.

I. Introduction

The myelin sheath is a plasma membrane extension of specialized glial cells that is "wrapped" around axons. The glial cells that make myelin are called Schwann cells in the peripheral nervous system (PNS) and oligodendrocytes in the central nervous system (CNS) (Fig. 1) (Sherman and Brophy, 2005). A single segment of myelin is called an internode, and, as the name suggests, consecutive internodes are flanked on both sides by nodes (of Ranvier), which are short unmyelinated gaps along the length of the axon where voltage-gated sodium channels are clustered and where the saltatory action potential is propagated (Sherman and Brophy, 2005). The presence of myelin sheaths along axons facilitates rapid, energy-efficient transmission of electrical impulses over long distances, and the unique properties of the myelin sheath and myelinated axons have facilitated the evolution of large and complex nervous systems such as our own (Hartline and Colman, 2007). Disruption to the myelin sheath or myelinated axons, therefore, is extremely detrimental and contributes to numerous neurological disorders and human diseases including multiple sclerosis (MS) (Franklin and ffrench-Constant, 2008) and Charcot–Marie–Tooth neuropathies (Shy, 2004). Demyelinated axons are prone to defects in axonal transport and susceptible to axonal degeneration (Edgar and Nave, 2009), phenotypes that often precede cell death in debilitating neurodegenerative diseases such as motor neuron disease, Alzheimer's disease, and Parkinson's disease (De Vos *et al.*, 2008). There is also increasing evidence that the potentially lifelong regulation of myelination through differential neuronal activity might represent an understudied but important form of nervous system functional plasticity (Fields, 2005).

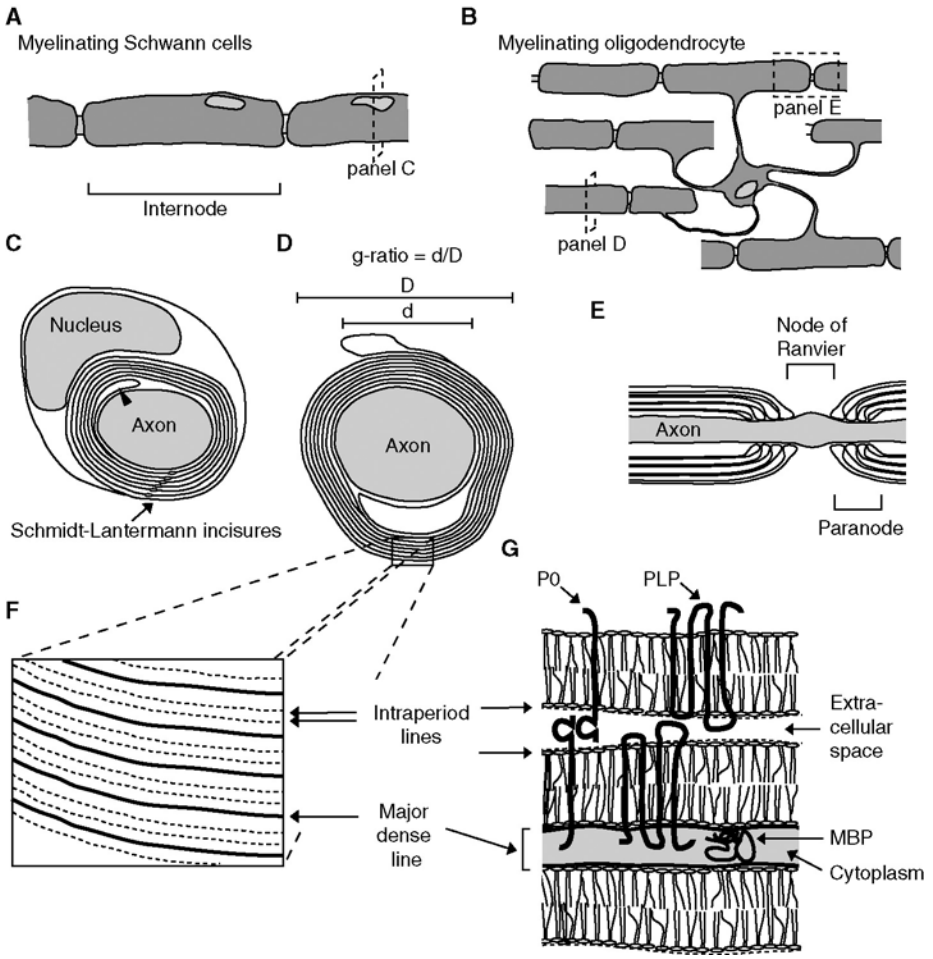

Fig. 1 Myelinating glia and the myelin sheath. (A) Individual Schwann cells form a single segment of myelin, called an internode, along myelinated axons of the peripheral nervous system (PNS). (B) Oligodendrocytes can form many internodes on multiple myelinated axons of the central nervous system (CNS). (C) Cross-section through a myelinated axon in the PNS. The "inner loop" of Schwann cell cytoplasm (arrowhead) is thought to iteratively wrap around the axon to generate the multilamellar myelin sheath (Bunge *et al.*, 1989). Schmidt-Lanterman incisures are cytoplasmic channels within the myelin sheath that connect the inner loop of Schwann cell cytoplasm with cytoplasm in the Schwann cell body. (D) Cross-section through a myelinated axon in the CNS. An inner loop of oligodendrocyte cytoplasm contacts the axon; how this generates the myelin sheath and how this cytoplasm connects to the proximal oligodendrocyte process through the myelin sheath remain unclear. The g-ratio is used as a measure of the extent of myelination and is defined as the ratio of the diameter of the axon (*d*) divided by the diameter of the myelinated axon (*D*). To quantify the extent of myelination of noncircular axons, it may be better to measure the relative perimeters of the outermost layer of myelin and of the axon, or the relative area occupied by myelin compared to the axon. (E) Longitudinal section through a myelinated axon. Unmyelinated gaps between consecutive internodes are called nodes of Ranvier and are the sites of action potential propagation along myelinated axons. The regions that flank the node of Ranvier, called paranodes, are sites of tight axon–glial contact that, among numerous functions, restrict proteins such as voltage-gated sodium channels to the nodes. (F) Features of the compact myelin sheath that can be visualized by electron microscopy include

The stereotypical myelinated axon with nodes of Ranvier is a vertebrate-specific adaptation. The fact that invertebrate model organisms such as *Caenorhabditis elegans* and *Drosophila melanogaster* do not possess myelinated axons means that the zebrafish is the simplest model for discovery and functional analysis of genes required for this process. Since the turn of the 21st century, the contribution of zebrafish to this field has become significant, and it now serves as an excellent complement to analyses in higher vertebrate models. This chapter is intended to give an overview of the development of myelinated axons in zebrafish and to review the reagents and techniques currently available for their study.

A. Origin of Myelinating Glia: Schwann Cells

Schwann cells derive from the neural crest (Jessen *et al.*, 2008), which is specified at the transition between neural ectoderm and nonneural ectoderm during neurulation (Le Douarin and Dupin, 2003; Woodhoo and Sommer, 2008). Once specified, neural crest cells delaminate and migrate throughout the body to generate a multitude of cell types (Le Douarin and Dupin, 2003). A subset of neural crest cells associates with axons during their migration and begins to express markers of the immature Schwann cell precursor stage (Jessen *et al.*, 2008). Fig. 2 illustrates the steps of Schwann cell development. The transcription factor Sox10 is expressed in immature Schwann cells and is required for the transition from the neural crest to immature Schwann cell precursor state (Gilmour *et al.*, 2002). Sox10 is also required for the specification of additional nonectomesenchymal neural crest cell fates, including melanocytes (Dutton *et al.*, 2001). Previous studies of peripheral nerve development in zebrafish have shown that axonal growth cones migrate just ahead of Schwann cells and can direct their migration (Gilmour *et al.*, 2002). In mutants with aberrantly projecting peripheral axons, Schwann cells follow the inappropriate route taken by axons (Gilmour *et al.*, 2002). In a forward genetic screen that aimed to identify mutations that disrupted myelinated axon formation (Pogoda *et al.*, 2006), mutations in the genes that encode the heterodimeric tyrosine kinase receptors ErbB2 and ErbB3 were isolated (Lyons *et al.*, 2005). Documentation of *erbb3* expression in Schwann cells, characterization of *erbb2* and *erbb3* mutant phenotypes, and conditional inactivation of ErbB signaling via a small molecule inhibitor revealed that ErbB signaling is essential for Schwann cell comigration along axons in zebrafish in addition to early proliferation and survival (Lyons *et al.*, 2005). These

Fig. 1(*Cont.*) the major dense line, thought to reflect the site of compaction of the intracellular membranes of the myelinating process, and the intraperiod lines, which are thought to represent the region where extracellular proteins of consecutive "wraps" of the myelin sheath come into close apposition. (G) Schematic model of the molecular constitution of the compact myelin sheath. MBP localized to the major dense line is thought to actively compact apposing intracellular plasma membranes. P0 and PLP/DM20 are transmembrane proteins that function during compaction of extracellular myelinating membranes.

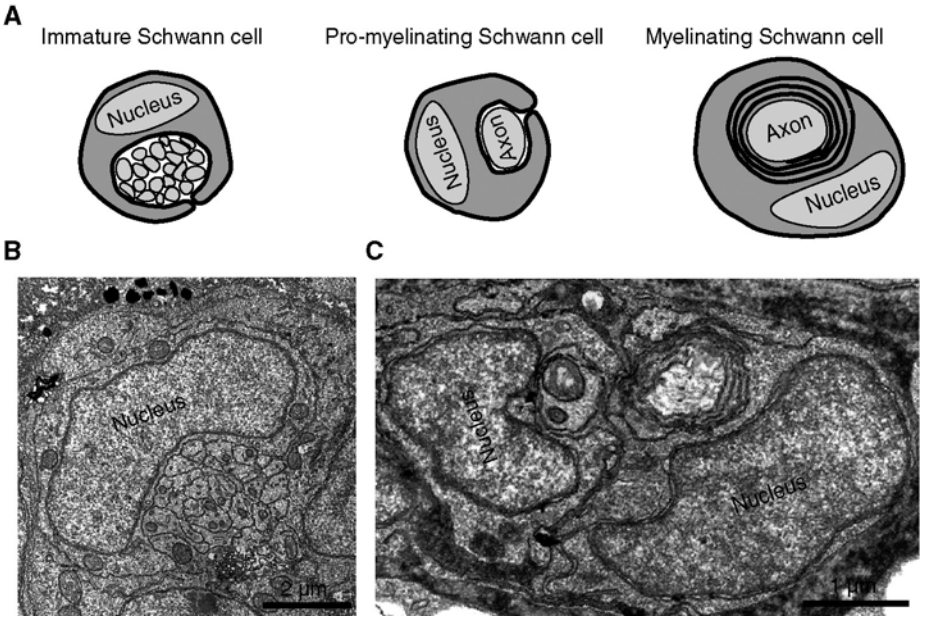

Fig. 2 Stages of Schwann cell development. (A) Cross-sections through Schwann cells at different stages of myelination. Immature Schwann cells associate with bundles of axons, but prior to the onset of myelination, some Schwann cells extend processes into the axonal bundle and come to associate with a single axon in an event called radial sorting. Once radial sorting is complete, these Schwann cells differentiate and go on to generate the multilamellar myelin sheath. (B and C) Electron microscope images of sections through posterior lateral line nerves showing an immature Schwann cell (B), a cell that is undergoing radial sorting (left cell, C), and one that has initiated myelination (right cell, C).

results are in keeping with knockout studies in mice, where disruption of either *erbb2* or *erbb3* leads to peripheral nerves that lack Schwann cells (Garratt *et al.*, 2000; Riethmacher *et al.*, 1997).

After the completion of migration, Schwann cells undergo proliferation to regulate their number with respect to axons, which is also regulated by ErbB signaling (Lyons *et al.*, 2005). During this time, individual Schwann cells extend processes into axon bundles and associate with just one axon (Fig. 2) (Jessen *et al.*, 2008). This process, called radial sorting, has been extensively studied in mammals (Chan, 2007), and studies in zebrafish show that both proliferation and ErbB signaling are essential for its completion (Raphael *et al.*, 2011). After radial sorting is complete, Schwann cells initiate myelination. The onset and extent of myelination in the PNS is related to axonal thickness (caliber), such that axons that have a cross-sectional area greater than $\sim 1\ \mu m^2$ tend to be myelinated and the amount of myelin surrounding an axon correlates positively with caliber (Jessen *et al.*, 2008; Nave and Salzer, 2006; Sherman and Brophy, 2005). Studies in mammals have shown that large caliber myelinated axons tend to express high levels of the growth factor

neuregulin 1 type III (Nrg1-III) (Taveggia *et al.*, 2005), an ErbB receptor ligand (Nave and Salzer, 2006), whereas smaller axons that are normally not myelinated express less Nrg1-III (Taveggia *et al.*, 2005). Remarkably, overexpression of Nrg1-III in small-caliber axons that are not normally myelinated is sufficient to induce myelination, which suggests that Nrg1-III is a key regulator of the decision to myelinate (Taveggia *et al.*, 2005). Conditional abrogation of ErbB receptor signaling in zebrafish after Schwann cell migration is complete shows that this pathway is also required for myelination in zebrafish (Lyons *et al.*, 2005), although the requirement for Nrg1-III remains to be demonstrated.

The expression and function of key transcription factors during the development of Schwann cells in zebrafish also reflects that of mammals. The transcription factors *oct6* and *krox20* are expressed in zebrafish Schwann cells (Levavasseur *et al.*, 1998; Pogoda *et al.*, 2006) just prior to the onset of myelination, as in mammals (Blanchard *et al.*, 1996; Ghazvini *et al.*, 2002; Jaegle *et al.*, 2003; Murphy *et al.*, 1996; Topilko *et al.*, 1994; Zorick *et al.*, 1996). The stage when Schwann cells have completed radial sorting but not yet initiated myelination is called the promyelinating stage (Fig. 2). *krox20* mutant zebrafish are arrested at the promyelinating stage (Monk *et al.*, 2009), as are *krox20* knockout mice (Zorick *et al.*, 1996). Following a forward genetic screen (Pogoda *et al.*, 2006), Monk *et al.* (2009) identified a novel key regulator of PNS myelination, a member of the adhesion family of G protein–coupled receptors, Gpr126. In *gpr126* mutants, Schwann cells do not progress through the promyelinating stage and therefore fail to express myelin-specific genes, such as myelin basic protein (MBP), and fail to initiate myelination. Further characterization showed that *gpr126* acts in Schwann cells, upstream of both *oct6* and *krox20* transcription factors, and that mutant phenotypes can be rescued by forskolin, which elevates cyclic AMP levels, placing *gpr126* upstream of the cAMP cascade (Monk *et al.*, 2009). It will be very interesting to identify the Gpr126 ligand and to determine its cellular locus of activity. Following the initiation of myelination, a small number of molecules have been implicated in controlling the extent of myelination including interactions between dDiscs large homolog 1 (Dlg1) and PTEN (Cotter *et al.*, 2010), and Nrg1-III signaling (Michailov *et al.*, 2004).

B. Origin of Myelinating Glia: Oligodendrocytes

Oligodendrocytes, in contrast to Schwann cells, are neuroectodermal in origin. The first oligodendrocyte precursor cells (OPCs) arise from the motor neuron progenitor (pMN) domains of the ventral CNS, but at later stages additional sources of oligodendrocytes emerge in both the dorsal spinal cord and forebrain (Richardson *et al.*, 2006). The transcriptional control of oligodendrocyte development has been very well characterized in mammals and has been reviewed extensively elsewhere (Li *et al.*, 2009). In general, the roles of known transcription factors during zebrafish oligodendrocyte development appear well conserved with mammals. The basic helix–loop–helix transcription factor Olig2, for example, is expressed from the early oligodendrocyte progenitor cell stage through migration, differentiation, and myelination, and is

essential for the generation of oligodendrocytes in both mammals and zebrafish (Park *et al.*, 2002; Zhou and Anderson, 2002; Zhou *et al.*, 2001). The related transcription factor Olig1 is expressed in cells of the oligodendrocyte lineage at a slightly later stage of differentiation (Schebesta and Serluca, 2009; Zhou and Anderson, 2002) and acts, together with Sox10, to activate the *mbp* promoter in both fish and mammals (Li *et al.*, 2007). Sox10 mutant mice do not express MBP or myelinate CNS axons (Stolt *et al.*, 2002), and studies in zebrafish suggest that this may be due to induction cell death shortly after the onset of axon–glial contact (Takada *et al.*, 2010). Some differences between fish and mammalian oligodendrocytes do exist, such as the apparent absence of Olig2 binding to Sox10 in fish oligodendrocytes (Li *et al.*, 2007). Furthermore, the major myelin protein, myelin protein zero (MPZ or P0), is expressed in myelinating oligodendrocytes in fish (Brosamle and Halpern, 2002) but not in mammals. The bases of such differences are not yet clear.

In vivo time-lapse microscopy in zebrafish has revealed that OPCs extend dynamic growth cone-like processes during migration. Fig. 3 summarizes the steps of oligodendrocyte differentiation following completion of cellular migration.

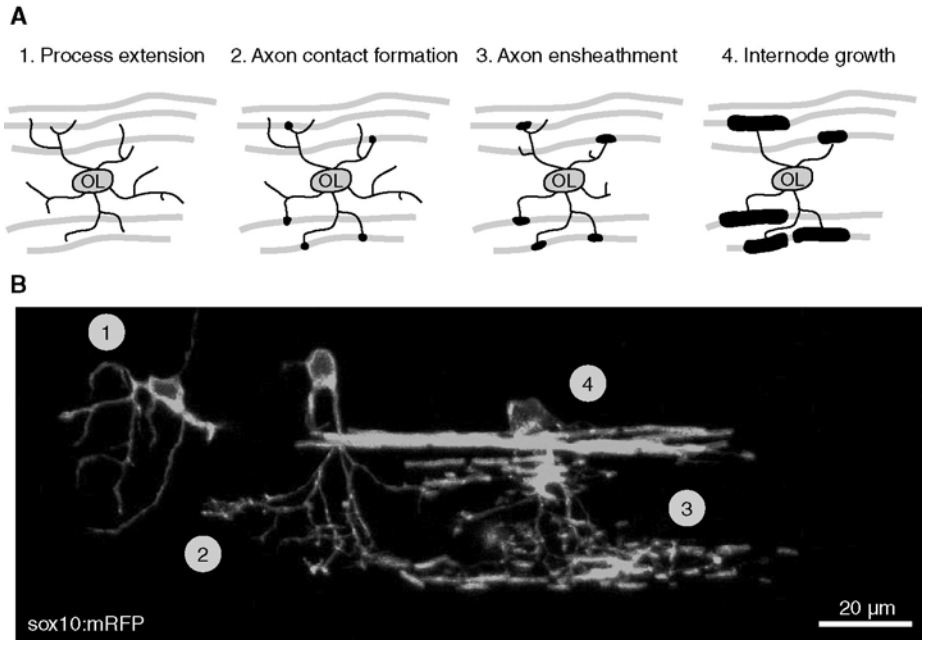

Fig. 3 Stages of oligodendrocyte development. (A) Following completion of migration, oligodendrocyte lineage cells bear multiple dynamic processes (1), which initiate contact with axons (2) to begin the process of ensheathment (3). Premyelinating oligodendrocytes then differentiate, begin to express myelin-specific markers, and format their myelin sheaths (4). (B) Confocal image of the spinal cord of a living zebrafish shows four sox10:mRFP-expressing cells, each of which is at one of the stages of oligodendrocyte development outlined in "A.".

Toward the end of migration, cells of the oligodendrocyte lineage withdraw their processes when they contact one another (Kirby *et al.*, 2006), which suggests that repulsive cell–cell interactions might regulate the spacing of oligodendrocytes along axons. Interestingly, when individual cells were ablated, their neighbors moved into the vacant territory until they came into contact with one another, whereupon they again exhibited mutually repulsive behaviors to establish their positions (Kirby *et al.*, 2006). The cellular behavior during the subsequent initiation of myelination, however, remains unclear, as do the molecular bases of axon–oligodendrocyte interactions that might control CNS myelination. Nrg1-III ErbB signaling, for instance, plays a negligible role in CNS myelination (Brinkmann *et al.*, 2008; Taveggia *et al.*, 2008), and Gpr126 also appears superfluous for CNS myelination (Monk *et al.*, 2009). Further molecular analyses in zebrafish are likely to help reveal the genetic basis of CNS myelination.

C. Cell Biology of Myelination

The compaction of the myelin sheath is mediated by the coordinated expression of myelin-specific proteins and their localization to specific regions in the myelin membrane. Major myelin proteins that are essential for membrane compaction in the PNS and/or CNS include MBP, the proteolipid protein (PLP) and its splice variant DM20 (Baumann and Pham-Dinh, 2001), and MPZ or P0 (Hartline and Colman, 2007) (see Fig. 1). MBP is a small and strongly cationic protein that localizes to the cytoplasmic side of the myelin membrane and is implicated in bringing the intracellular membranes into tight apposition (Boggs, 2006). The *shiverer* mouse, a naturally occurring mutant in *mbp*, almost completely lacks compact CNS myelin (Popko *et al.*, 1987; Readhead *et al.*, 1987). The differential targeting of *mbp* mRNA to distal processes of myelinating glia was documented nearly 30 years ago (Colman *et al.*, 1982), but how or why this occurs remained unknown. Using zebrafish with a mutation in the gene encoding the zebrafish kinesin motor Kif1b, it was found that this motor was required autonomously in oligodendrocytes for the normal localization of *mbp* mRNA to myelinating oligodendrocyte processes (Lyons *et al.*, 2009). Ultrastructural analyses of myelinated axons in *kif1b* mutant zebrafish revealed a striking phenotype, namely, the ectopic appearance of myelin-like membrane along part of oligodendrocyte processes not wrapping axons (Lyons *et al.*, 2009). This observation suggested the hypothesis that specific localization of mRNAs (including those that encode MBP) prevents deleterious effects of their protein products elsewhere in the cell. Zebrafish with disruption of the *tubulin alpha 8-like 3a* gene also exhibit mislocalization of *mbp* mRNA in oligodendrocytes (Larson *et al.*, 2010), which suggests that this microtubule subunit may be a component of the glial cytoskeleton that mediates the transport of myelin constituents. Further cell-type-specific analyses remain to be carried out to document that this factor functions autonomously in oligodendrocytes during mRNA localization.

The trafficking of essential components of the myelin sheath *in vivo* is not well characterized, but the zebrafish is poised to make a significant contribution in this area given its amenability to live cell imaging.

D. Node of Ranvier Formation

The identification of factors required for the correct localization of essential proteins to the node of Ranvier (e.g., voltage-gated sodium channels) has been successfully pursued in mammals (Rosenbluth, 2009; Salzer *et al.*, 2008). Genetic analyses using zebrafish, have, however, also contributed to this important area of research. For example, zebrafish with mutations in the gene encoding *N*-ethylmaleimide-sensitive factor (NSF, a protein essential for membrane fusion at synaptic termini; Kawasaki *et al.*, 1998; Tolar and Pallanck, 1998) completely fail to cluster voltage-gated sodium channels at nodes of Ranvier (Woods *et al.*, 2006), which suggests that NSF may be required for the fusion of vesicles containing node components to the axonal membrane. Testing this hypothesis would, in part, require the visualization of nodal components in live axons, which should be possible in zebrafish. Another protein with a newly defined role in the formation of normal nodes is the cytoskeletal-associated protein alpha II spectrin (Voas *et al.*, 2007). Alpha II spectrin is expressed at the node and paranodal domains during myelinated axon development (Voas *et al.*, 2007), where it likely interacts with either beta II or beta IV spectrin, as suggested by the localization of these factors in myelinated axons (Susuki and Rasband, 2008; Voas *et al.*, 2007).

To determine the role of Schwann cells in the clustering of nodal components, Voas and colleagues made use of *sox10* and *erbb* mutants that lack Schwann cells along peripheral nerves. Surprisingly, they found that numerous components of mature nodes were capable of coclustering in the complete absence of Schwann cells (Voas *et al.*, 2009). However, *gpr126* mutants, which have Schwann cells in association with axons but fail to initiate myelination, also fail to cluster proteins at putative nodes. *gpr126* mutants treated with an inhibitor of ErbB signaling to block Schwann cell development can, however, cluster components to the node, which shows that Grp126 is not required for clustering of nodal proteins *per se*. This suggests that immature Schwann cells disrupt the early formation and clustering of nodal components at inappropriate positions (Voas *et al.*, 2009). These data also suggest that the initiation of myelination is essential for node of Ranvier formation in the PNS.

E. Zebrafish Models of Disruption to Myelinated Axons in Humans

In the postgenomic era, the genetic bases of numerous human diseases are being elucidated. For example, an intronic SNP in the gene encoding human KIF1B has been associated with susceptibility for MS (Aulchenko *et al.*, 2008), which raised the possibility that analysis of Kif1b function in zebrafish may reveal aspects of disease susceptibility or progression. However, the association reported in the initial genome-wide association study (GWAS) has been called into question (Booth *et al.*, 2010). MS results from a multitude of genetic and environmental factors, each of which is likely to contribute in varying degrees to disease susceptibility (Handel *et al.*, 2010; Oksenberg *et al.*, 2008; Sawcer, 2008). Therefore, mutant zebrafish that disrupt individual genes implicated in MS susceptibility will,

most likely, be informative with respect to the basic biological function of the gene but will not serve as general models for such a complex, multifactorial disease. In other cases, where the genetic bases of diseases are purely Mendelian such as in Charcot-Marie-Tooth neuropathies and Leukodystrophies (Shy, 2004; Boespflug-Tanguy *et al.*, 2008), zebrafish models are potentially much more informative. For example, a mutation in the gene encoding zebrafish kinesin-binding protein (KBP; Lyons *et al.*, 2008) may serve as a useful model for certain aspects of the rare human neurological disorder, Goldberg-Shprintzen syndrome, caused by homozygous null mutations in human *kbp* (Brooks *et al.*, 2005; Murphy *et al.*, 2006).

In conclusion, zebrafish have contributed significantly to our growing understanding of the basis of formation of myelinated axons. In the rest of this chapter, we review some of the available reagents, techniques, and protocols that have facilitated such studies. We also preview new technologies that will ensure that the zebrafish remains a major contributor to future advances in the study of myelin formation, its disruption, and repair.

II. Methods and Materials

A. Raising Animals for Analysis of Myelinated Axons

Numerous factors are important to consider when raising animals for analysis at postembryonic stages (Parichy *et al.*, 2009). The chemical PTU is often used to prevent pigment formation during embryonic development (Wang *et al.*, 2004), but previous studies have found that it can cause developmental defects (Elsalini and Rohr, 2003). As an alternative to PTU, one can instead use mutant zebrafish lines in which pigment formation is disrupted, such as *golden*, which disrupts a cation exchanger slc24A5, also implicated in human pigmentation (Lamason *et al.*, 2005), *nacre*, which disrupts zebrafish *mitfa* (Lister *et al.*, 1999), and *casper* (White *et al.*, 2008), which is a cross between the *nacre* mutant and the *roy orbison* mutant. The genetic basis of *roy orbison* has not yet been identified and so it is possible that this mutation might affect myelination, due to the neural crest origin of both pigment cells and Schwann cells. As the zebrafish field incorporates higher-resolution analyses of nervous system formation and function, better genotypic and phenotypic characterization of distinct wild-type lines will also be required.

B. Markers of Myelinating Glia and Myelinated Axons

Numerous reagents have already been developed to study myelinated axon formation using zebrafish. In Tables I and II, we provide a list of published *in situ* hybridization probes and primary antibodies (Table I) as well as transgenic lines (Table II) that have been used to visualize myelinated axons in zebrafish. (See also Figs. 3B and 4A and B.) There are, however, many gaps in our ability to visualize important cell types and subcellular structures relevant to myelinated axon formation.

Table I
In situ hybridization and antibody markers

gene/Protein	Cell type/area of expression	Primary zebrafish references
36k	Myelinating OLs	Morris *et al.* (2004)
36K	Myelinating OLs	Morris *et al.* (2004)
Alpha II spectrin	Node of Ranvier and paranode-early Paranode only-late	Voas *et al.* (2007)
Ank3b (ankyrin G)	Node of Ranvier	Voas *et al.* (2009)
claudinK	Myelinating OLs and myelinating SCs	Takada and Appel (2010)
ctnnd2	Myelinating OLs and myelinating SCs	Takada and Appel (2010)
erbb3	Immature SCs through myelinating SCs, various PNS and CNS cell types (not completely defined)	Lyons *et al.* (2005)
FIGQY	L1 family of CAMs. Thought to label neurofascin at zebrafish nodes of Ranvier	Woods *et al.* (2006)
foxd3	Immature SCs through myelinating SCs, various PNS and CNS cell types (not completely defined)	Gilmour *et al.* (2002)
gpr126	SCs	Monk *et al.* (2009)
krox20	Promyelinating SCs	Lyons *et al.* (2005)
mbp	Myelinating OLs and myelinating SCs	Brosamle and Halpern (2002) and Lyons *et al.* (2005)
MBP	Myelinating OLs and myelinating SCs	Buckley *et al.* (2010a) and Lyons *et al.* (2005)
mid1ip1b	Myelinating OLs and myelinating SCs	Takada and Appel (2010)
Neurofascin (NfExtra)	Node of Ranvier	Voas *et al.* (2009)
nkx2.2a	Subset of OPCs, multiple nonrelated cell types	Kirby *et al.* (2006)
oct6	Promyelinating SCs and additional CNS cell types	Levavasseur *et al.* (1998)
olig1	OPCs and myelinating OLs	Li *et al.* (2007) and Schebesta and Serluca (2009)
olig2	OPCs and myelinating OLs, MN progenitors and MNs, plus additional CNS cell types	Park *et al.* (2002)
p0	Myelinating OLs	Brosamle and Halpern (2002)
PanNaVCh	Concentrated at nodes of Ranvier	Woods *et al.* (2006)
plcl1	Myelinating OLs and myelinating SCs	Takada and Appel (2010)
plp1a	Myelinating OLs	Brosamle and Halpern (2002)
plp1b	Myelinating OLs	Thisse *et al.* (2004)
ppp1r14a	Myelinating OLs	Takada and Appel (2010)
sh2d3cb	Myelinating OLs	Takada and Appel (2010)
sox10	OPCs, OLs, immature SCs through myelinating SCs, other neural crest derivatives and CNS cell types	Dutton *et al.* (2001)
Sox10	OPCs, OLs, immature SCs through myelinating SCs, other neural crest derivatives and CNS cell types	Park *et al.* (2005)
swap-70	Myelinating OLs	Takada and Appel (2010)
tlcd1	Myelinating OLs	Takada and Appel (2010)
Zwilling-A and *-B*	Myelinating OLs and myelinating SCs	Schaefer and Brosamle (2009)

We do not have specific markers for immature Schwann cells (available markers also detect at least one other neural crest derivative), definitive markers for nonmyelinating Schwann cells (whose role is to ensheath small-caliber axons in so-called Remak bundles; Jessen and Mirsky, 2005), or markers for the specific neurons that have

Table II
Transgenic fluorescent reporter lines

gene	Cell type of expression	Reference
foxd3	Immature SCs through myelinating SCs, various PNS and CNS cell types (not completely defined)	Gilmour *et al.* (2002)
mbp	Myelinating OLs	Jung *et al.* (2010)
nkx2.2a	Subset of OPCs, multiple nonrelated cell types	Kirby *et al.* (2006) and Ng *et al.* (2005)
olig1	OPCs and myelinating OLs	Schebesta and Serluca (2009) and Li *et al.* (2007)
olig2	OPCs and myelinating OLs, MN progenitors and MNs, plus additional CNS cell types	Park *et al.* (2007) and Shin *et al.* (2003)
p0	Myelinating OLs	Yoshida and Macklin (2005)
plp (mammalian promoter)	OPCs and myelinating OLs	Yoshida and Macklin (2005)
sox10	OPCs, OLs, immature SCs through myelinating SCs, other neural crest derivatives and CNS cell types	Kirby *et al.* (2006)

myelinated axons (although some proteins, such as the neurofilament associated proteins recognized by the 3A10 antibody (Furley *et al.*, 1990), are enriched in large myelinated axons). Stellate astrocytes, which fulfill a myriad of functions in the mammalian brain (Barres, 2008) including regulation of myelination (Watkins *et al.*,

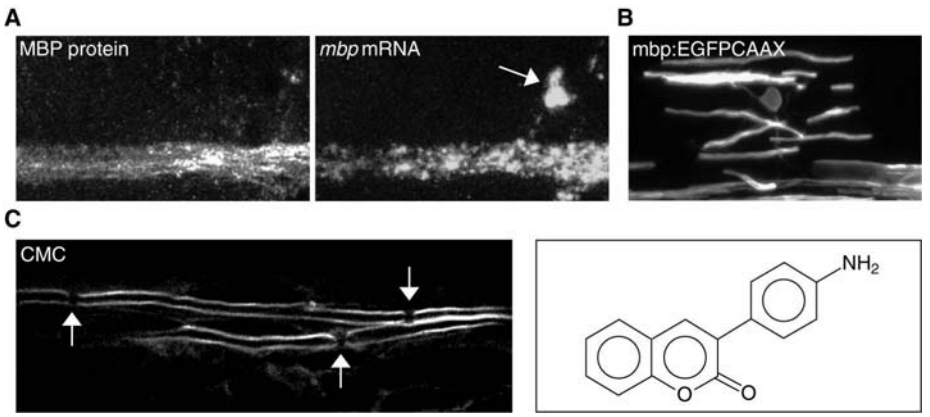

Fig. 4 Methods of visualizing myelinating glia and their constituents. (A) Confocal image of a single zebrafish larva stained by immunohistochemistry to reveal MBP protein localization and by *in situ* hybridization to reveal *mbp* mRNA expression. MBP protein is localized along the length of myelinating processes, whereas *mbp* mRNA is found in the oligodendrocyte cell body (arrow) as well as along myelinating processes. See Brend and Holley (2009) for fluorescent *in situ* hybridization protocol. (B) Live imaging of a myelinating oligodendrocyte in transgenic zebrafish expressing EGFPCAAX (a membrane-tethered EGFP) under the control of the *mbp* promoter. (C) Confocal image of Schwann cell myelin in the lateral line nerve of a live zebrafish labeled with the small molecule 3-(4-aminophenyl)-2H-chromen-2-one (also called case myelin compound (CMC); structure shown in right-hand panel; Wang *et al.*, 2010). Note the clear unmyelinated gaps between consecutive internodes, which represent the positions of the nodes of Ranvier (arrows).

2008), have not been identified in zebrafish (Grupp *et al.*, 2010). Heterogeneity within the oligodendrocyte lineage has received only a little attention in zebrafish (Kucenas *et al.*, 2008) but is the subject of intense investigation in mammals (see reviews by Staugaitis and Trapp, 2009; Trotter *et al.*, 2010).

In addition to the generation of *in situ*, antibody, and transgenic-based reagents, systematic approaches to identify factors expressed in both neurons and glia are helpful. The Appel lab has performed a microarray screen to identify factors expressed in myelinating glia in zebrafish (Takada and Appel, 2010), and the Barres lab has performed a large-scale screen to identify genes expressed in a variety of cells at different stages of CNS development in mammals (Cahoy *et al.*, 2008). Such approaches also identify important gene candidates whose function can be investigated through reverse genetic targeting.

C. Brief Practical Notes on Whole-Mount Immunochemistry

Whole-mount immunochemistry of zebrafish from ~2 dpf onwards (when myelinated axons start to form) necessitates permeabilization of the specimen, or even "skinning," prior to antibody incubation (Wilson *et al.*, 1990). We have found that short fixation times enhance whole-mount immunolabeling of myelinated axons. As fixatives, we use either 4% formaldehyde in PBS or a mixture of 2% formaldehyde/1% trichloroacetic acid in PBS. We heat EM grade paraformaldehyde in solution to 60 °C to generate formaldehyde monomers and then allow the fixative to cool to room temperature prior to use.

We fix animals for 30 min at room temperature with 4% formaldehyde, or for 12 min at room temperature with the 2% formaldehyde/1% trichloroacetic mix. Two- to 3-day incubations in primary antibody solution can also enhance staining. In some cases, antibodies raised against zebrafish proteins or peptides can be far superior to those generated against antigens of other species (see side-by-side comparison of anti-MBP antibodies in Buckley *et al.*, 2010a).

D. Visualization of Myelinated Axons: Transgenesis and Chemical Biology

As outlined in Table II, gene-specific regulatory sequences have been used to visualize myelinated axons in zebrafish. Numerous studies have used fluorescent fusion proteins to visualize subcellular protein localization (e.g., Tawk *et al.*, 2007) and subcellular structures in the zebrafish nervous system (Meyer and Smith, 2006), but these techniques have not yet been used to study myelinated axon formation. One important caveat is that the use of fusion proteins may disrupt protein function *in vivo*. For instance, overexpression of a construct composed of a myc (10 amino acids) tag fused to the extracellular domain of the major myelin protein P0 caused a demyelination phenotype in rodents (Previtali *et al.*, 2000). Nonetheless, cell-specific drivers and fluorescent reporters remain a powerful method to help dissect many aspects of myelination. Transgenesis of zebrafish is now straightforward due

to the creation of the Tol2kit (Kwan *et al.*, 2007), which combines modular transgene design aided by Gateway cloning and enhanced germline transgenesis mediated by the Tol2 transposase. This system has been described and reviewed extensively elsewhere (Asakawa and Kawakami, 2009; Halpern *et al.*, 2008; Kwan *et al.*, 2007; Suster *et al.*, 2009).

In addition to regulatory sequences that can directly drive genes of interest, one can employ binary amplification systems, such as Gal4 UAS (Brand and Perrimon, 1993), to regulate gene expression (e.g., to amplify expression from weak promoters). The adaptation of this technology for use in zebrafish has been described and reviewed by others (Asakawa and Kawakami, 2008; Distel *et al.*, 2009; Goll *et al.*, 2009; Halpern *et al.*, 2008; Koster and Fraser, 2001; Ogura *et al.*, 2009; Scheer *et al.*, 2002). We have generated specific Gal4 drivers using *sox10* and *mbp* upstream regulatory sequences to study myelinating glial cell formation. These driver lines successfully transactivate reporters specifically in oligodendrocytes, but some disturbances to myelination in individual founder fish have been observed. The causes of these disruptions may reside in position-dependent effects at the sites of transgene integration or in levels of gene expression (Asakawa *et al.*, 2008; Flanagan-Steet *et al.*, 2005).

Such observations highlight the necessity to carefully study individual transgenic founders. Several labs have already optimized the Gal4-based systems (Asakawa and Kawakami, 2008; Distel *et al.*, 2009; Halpern *et al.*, 2008), but the use of additional methods (e.g., split Gal4 s; Pfeiffer *et al.*, 2010) might improve the specificity of stage-specific expression. One could, for example, drive split components using *sox10* and *olig2* regulatory sequences to specifically identify OPCs. Enhancer trap screens have also generated zebrafish lines that define specific cell types and populations and allow their manipulation (Asakawa and Kawakami, 2008, 2009; Kawakami *et al.*, 2010; Scott and Baier, 2009; Scott *et al.*, 2007; Urasaki and Kawakami, 2009). With respect to myelination, a high priority should be assigned to identification of a *cis*-regulatory element for manipulation of genes only in those neurons with myelinated axons.

Since fusion proteins can potentially disrupt myelination, alternative approaches to label myelin (e.g., by small molecules (MW $<$800 Da)) should be pursued. One obvious advantage of small molecule compounds is their potential to readily cross the blood–brain barrier. The small molecule called case myelin compound (CMC) has been used to stain myelin in mammals (Wang *et al.*, 2010), and we have adapted it for use in zebrafish (Fig. 4C). Small molecule reagents may also serve as specific biomarkers to visualize myelinated axons in humans (e.g., as PET ligands or tethered to gadolinium in MRI).

E. Visualization of Myelinated Axons: Single Cell Analysis

Using the Tol2kit (Kwan *et al.*, 2007), we have generated constructs whereby membrane-tethered EGFP is driven by *mbp* regulatory sequence. Mosaic expression in embryos following DNA injection (Stuart *et al.*, 1990) has allowed us to visualize myelinating oligodendrocyte morphology at the single cell level *in vivo* (Fig. 4B).

The activity of different regulatory sequences can, of course, vary over time; for example, the *nkx2.2a* promoter has been used to activate fluorescent protein expression transiently in premyelinating oligodendrocytes, but expression diminishes as oligodendrocytes start to myelinate. To generate long-term fluorescent protein expression, positive feed-forward methodologies using Gal4-UAS-based technology have been used (Collins *et al.*, 2010; Distel *et al.*, 2009). The gold standard for long-term gene manipulation in mammals is the Cre-Lox system (Wang, 2009), which has now been exploited in zebrafish field to study cells over extended periods (Hans *et al.*, 2009; Sato *et al.*, 2007; Thummel *et al.*, 2005).

One can also directly label single cells in zebrafish by iontophoresis (Clarke, 2008; Lyons *et al.*, 2003) or single cell electroporation (Concha *et al.*, 2003; Tawk *et al.*, 2009). Iontophoresis has been used primarily for the introduction of charged molecules, such as fluorescent dyes, into cells for lineage tracing and characterization of cell morphology. Focal electroporation represents a more versatile system because larger microelectrodes can be used to deliver large charged molecules (e.g., plasmid DNA, RNA, or morpholino oligonucleotides) into single cells or small groups of cells *in vivo*.

F. Visualization of Myelinated Axons: Live Imaging

Common options for live imaging cells and molecules of the zebrafish nervous system include confocal (Fig. 5) and multiphoton microscopy (Meyer and Smith, 2006). Additional options, however, include selective plane illumination microscopy (deep tissue imaging) (Huisken and Stainier, 2007; Swoger *et al.*, 2011), laser-based spinning disk imaging (increased speed and reduced photodamage) (Lecaudey *et al.*, 2008), aperture correlation microscopy (increased speed, no laser requirement; Czopka, Soetaert, and Lyons, unpublished), and noninvasive, high-harmonic imaging (myelin has a natural third harmonic–generating structure) (Hsieh *et al.*, 2008; Huff and Cheng, 2007; Sun *et al.*, 2004). In addition, newly developed, so-called super-resolution options such as stimulated emission depletion (STED) and

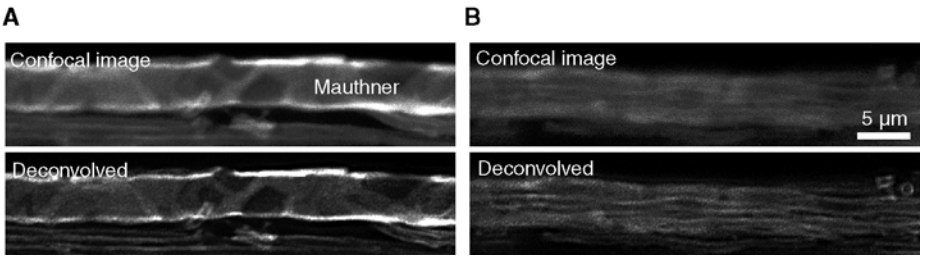

Fig. 5 Deconvolution of confocal images. Maximum-intensity projections of a subset of confocal sections at the surface of the large myelinated Mauthner axon (A) and deeper within the *z*-axis of the same stack (B) show that the deconvolution of confocal images can reveal myelinated axon profiles obscured in the original unprocessed images.

structured illumination microscopy (SIM) (Schermelleh *et al.*, 2010) may soon be adapted for live cell imaging in whole animals.

G. Visualization of Myelinated Axons: Electron Microscopy

Visualization of the fine structure of the myelin sheath has historically been the domain of electron microscopy (EM). The preparation of tissue for the analysis of myelinated axons by electron microscopy is difficult and thus warrants special attention in this chapter.

1. Microwave-Assisted Embryonic and Larval Zebrafish Tissue Processing for Electron Microscopy

For best results, tissue that will be processed for electron microscopy must be fixed uniformly as fast as possible, and for this reason we have adapted microwave stimulation techniques (Feirabend *et al.*, 1994, 1998; Wild *et al.*, 1989) to accelerate tissue processing for EM (Lyons *et al.*, 2008, 2009). In these protocols, it is critical to use a microwave with true power control. Standard microwaves alter their power output over time by pulsing full power at discrete intervals. Options for true variable wattage include the Pelco laboratory microwave processor (Ted Pella, Mountain Lakes, CA) or Panasonic microwaves with inverter technology. Use power outputs similar to those described below.

During each of the steps of the protocol, keep tissue at about 15–18 °C to prevent heating of samples beyond room temperature. The Pelco Biowave system allows one to directly regulate temperature throughout the protocol. If using another system, check the temperature of your water bath and adjust accordingly (e.g., with ice) to maintain relatively constant specimen temperature throughout each step. The biophysical basis of microwave-stimulated processing is not clear.

Primary Fixation

Two percent glutaraldehyde + 4% (para)formaldehyde, 0.1 M sodium cacodylate buffer, pH 7.4.

Use EM grade reagents throughout. To generate a solution of formaldehyde (rather than paraformaldehyde polymer), heat the solution to 60 °C before use; cool to room temperature before combining with other ingredients of fixative.

Volumes of solution per animal: If using 0.5-mL strip tubes, place one embryo or larva per tube in ~200 μL of solution. When using a 1.5-mL Eppendorf tube, up to five larvae can be placed in ~500 μL of solution.

Microwave specimens as soon as possible after adding fixative:

1. 100 W for 1 min, OFF for 1 min, 100 W for 1 min, and OFF for 1 min.
2. 450 W for 20 s and OFF for 20 s. Repeat five times.
3. Continue to fix for at least 2 h at room temperature.

If you are planning to section near the hindbrain, in the vicinity of the ears, it is important to remove the otoliths at this stage, as these can damage diamond knives. Dissect in fume hood.

Rinse

Rinse in 0.1 M sodium cacodylate buffer, 3 × 10 min at room temperature.

Secondary Fixation

Two percent osmium tetroxide, 0.1 M sodium cacodylate, 0.1 M imidazole, pH 7.5. If the pH of the secondary fixation solution is incorrect, the osmium will precipitate out of solution. This will result in poor secondary fixation.
Microwave stimulation:

1. 100 W for 1 min, OFF for 1 min, 100 W for 1 min, and OFF for 1 min.
2. 450 W for 20 s and OFF for 20 s. Repeat five times.
3. Continue to fix for at least 1 h at room temperature.

Rinse

Rinse specimens well in distilled water until solution is clear. Three × 10 min washes. The specimen should be a dark golden brown color throughout.

En Bloc Stain

Saturated uranyl acetate (∼8%, w/v, in water).
Microwave stimulation: 450 W for 1 min, OFF for 1 min, and 450 W for 1 min.
Samples in uranyl acetate can be left overnight at 4 °C, or one can directly proceed to dehydration steps.

Dehydration

Make up an ethanol:water series: 50:50, 70:30, 95:5, and 100:0.
Use EM grade ethanol.
For each wash (50% EtOH, 70% EtOH, and 95% EtOH), microwave at 250 W for 45 s followed by incubation at room temperature for 10 min.
Change solution to 100% EtOH and microwave at 250 W for 1 min, OFF for 1 min, and then 250 W for 1 min; then incubate at room temperature for 10 min.
Replace with 100% EtOH.
Microwave again; 250 W for 1 min, OFF for 1 min, and 250 W for 1 min; then incubate at room temperature for 10 min.

Acetone Dehydration: 100% EM Grade Acetone

Microwave at 250 W for 1 min, OFF for 1 min, and 250 W for 1 min. Incubate at room temperature for 10 min.
Change solution (i.e., fresh 100% acetone). Repeat three times.

EMBED: Acetone

1:1, EMBED: 100% acetone.
Remove EMBED (see the section "Recipes") from freezer about 30 min before use, so that it reaches room temperature and becomes fluid. When the EMBED becomes too viscous to be taken up easily using a plastic Pasteur pipette, it has started to polymerize during storage, and it should not be used anymore.
Remove 100% acetone solution.
Add the EMBED: acetone mix, 1:1.
Infiltrate specimens at room temperature overnight. Gentle agitation may be used.
Wrap any disposable materials that were used with the EMBED in foil and bake at 65 °C to cure before disposal.

EMBED Preinfiltration

Remove EMBED:acetone mix.
Add 100% EMBED at room temperature.
Leave tubes upright in fume hood with lids open for at least 6 h. The open lids will help residual acetone to evaporate.

Embedding

Transfer the samples in 100% EMBED to the appropriate wells of embedding molds using a glass Pasteur pipette. Add additional EMBED to fill each well. With the aid of a dissecting microscope, carefully orient the samples so that they are properly aligned for sectioning.
To assess processing, break a redundant specimen with forceps. The specimen should be quite hard and "crunch" under the pressure. If the specimen has not hardened, then some aspect of the processing was not optimal. When the samples are properly aligned, place them in an oven set at 60–65 °C. Always check the temperature and stability of the oven. Do not let the oven go higher than 65 °C. Allow blocks to polymerize in the oven for at least 24 h.
Trim and section blocks as required.
We cut silver sections (about 80 nm) and mount them on naked grids with 300 hexagonal grid holes.

Staining of Sections Mounted on Grids

1. Stain sections with 1:1 saturated uranyl acetate (~8%):absolute ethanol (or acetone) for 5 min per grid.
2. Wash grid with 50% ethanol for 1 min by continuous streaming of solution over both sides of grid.
3. Blot grid dry on a piece of Whatman filter paper.
4. Place two or three NaOH pellets on the perimeter of a Petri dish to absorb CO_2. Place grid in a 100- to 200-μL drop of Sato lead stain (see the section "Recipes") in the center of the Petri dish. Cover dish and stain for 5 min.
5. Wash grid for 1 min with pure water by continuous streaming of solution over both sides of grid.
6. Blot dry grid with Whatman filter paper and store before imaging.

Recipes

EMBED solution

We use Embed-812 kit (ingredients listed in step 1) with benzyldimethylamine (BDMA) (Electron Microscopy Sciences) to make resin:

1. Heat the following to 65 °C in an oven:
   - 100 mL EMBED;
   - 45 mL dodecenyl succinic anhydride (DDSA);
   - 60 mL methyl-5-norbornene-2,3-dicarboxylic anhydride (NMA).
2. Mix the above ingredients in a disposable plastic beaker in the hood.
3. Place on stir plate in hood and stir for 1 h while ingredients cool. Try to minimize bubbles.
4. Add 6.15 mL BDMA; stir until EMBED solution is uniform (no Schlieren lines).
5. Aliquot as appropriate and store at −20 °C.

Sato's lead stain

Boil filtered reverse osmosis water, and then cool to room temperature. Cap the bottle as soon as safe to do so. This treatment reduces CO_2 in the stain that would otherwise speed precipitation of the lead:

1. Make a small stock of 5 M NaOH from some of the boiled water.
2. Rinse stir bar, beaker, and six 10-mL syringes with 100 mL water containing three drops of 5 M NaOH.
3. Rinse beaker, stirbar, and syringes with water; shake off excess.
4. Heat 0.2 g lead citrate powder in a glass Petri dish or foil weigh boat on a hot plate in the hood for 5–10 min until it turns a very light tan color.
5. Put 48.2 mL of the boiled and cooled water in the beaker. While stirbar is turning, add 0.2 g lead citrate, 0.15 g lead nitrate, 0.15 g lead acetate, and 1 g sodium citrate.

6. Add 1.8 mL of 5 M NaOH while stirring. Solution should be clear.
7. Quickly filter solution through filter top bottle. Withhold any residue that may be in the bottom of the beaker.
8. Quickly backload 8 mL of lead stain into a capped syringe barrel. Insert plunger, invert, uncap, and push plunger until all air is gone. Cap and wrap cap in Parafilm. Repeat with remaining syringes.

2. Analysis of Electron Microscopy Images

Although considerable effort has been devoted to optimizing the protocol above, preservation of myelinated axons is not always optimal.

Here we provide a checklist to help assess the quality of preparations:

1. Analyze 0.5- to 1-μm sections stained with toluidine blue prior to cutting ultrathin sections. Make sure there are no translucent gaps in the tissue. Myelinated axon ultrastructure is unlikely to be satisfactory if gross defects are observed in the 0.5- to 1-μm sections.
2. Analyze myelinated axon ultrastructure in electron micrographs:
   - Well-preserved axons will have clearly delineated, continuously labeled external membranes.
   - Circular microtubule profiles (24 nm) should also be obvious in well-preserved axons cut in cross-section. Fixation at low temperatures should be avoided because microtubules may depolymerize. Circular microtubule profiles provide an unbiased indication that axons have been cut well in cross-section.
   - Large-caliber myelinated axons also have abundant neurofilaments (10 nm), which are electron dense.
   - The integrity of axonal mitochondria also provides a clear indication of specimen preservation. One should aim to visualize the inner and outer membrane bilayer structures of mitochondria. Swollen mitochondria can indicate poor tissue preservation.
   - The myelin sheath: The myelin sheath itself is difficult to preserve perfectly. One hallmark of poor preservation is the appearance of apparently "loose" wraps of myelin. Only myelinated axons that have concentrically compact myelin sheaths surrounding circular axonal profiles can be reliably quantified by the g-ratio method. It can therefore also be helpful to count the number of "wraps" of myelin (Fig. 6D) when quantifying myelination.
   - Fixation artifacts: The most serious artifact that occurs in electron microscopic analysis of myelinated axons involves poorly fixed specimens that yield images with structures that resemble myelin sheaths, which are not necessarily myelin sheaths. Fig. 6A shows a poorly preserved lateral line nerve (30 hpf) with a structure that could be mistaken for a myelinated axon. Fig. 6B shows a well-preserved nerve at the same time, a stage when immature Schwann cells are still migrating along axons and myelination has not yet commenced. We

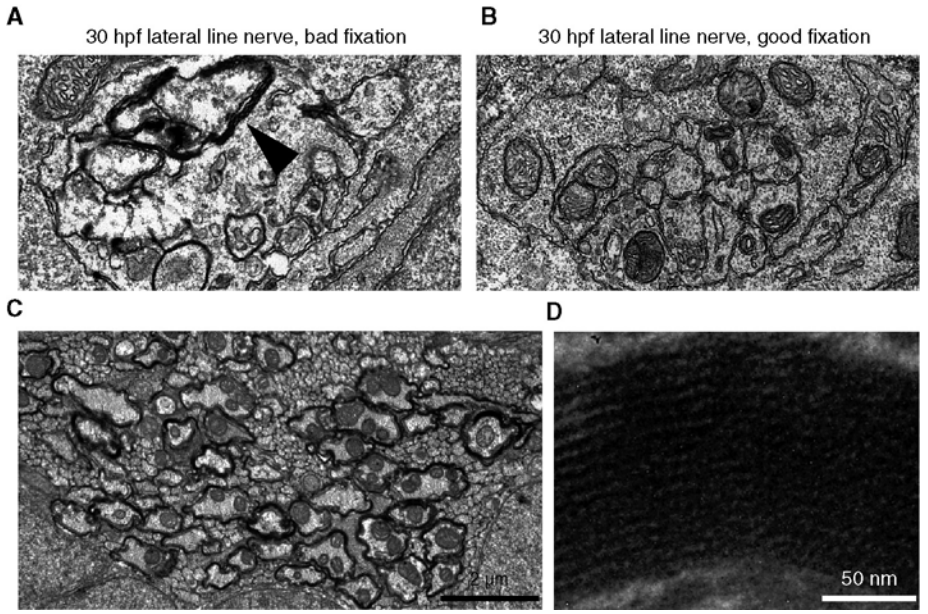

Fig. 6 Variability in zebrafish tissue preparation for electron microscopy. (A) Electron micrograph shows electron-dense structures (arrowhead) that resemble myelin sheaths, but which are, in fact, fixation artifacts. Lateral line axons in well-preserved tissue (B) are never myelinated at this early stage. (C) Electron micrograph shows myelinated axons in well-preserved central nervous system tissue. (D) High-magnification electron micrograph shows a myelin sheath where the number of individual wraps of myelin membrane can be counted.

can readily conclude therefore that the apparent myelinated axon in Fig. 6A must be erroneous. Skepticism should also be exercised during examination of myelinated axons at later stages until one is certain that the presence of artifacts can be ruled out.

3. New Frontiers in Electron Microscopy

New advances in high-pressure freezing technology are beginning to greatly enhance tissue preservation prior to EM analyses (Spiegelhalter *et al.*, 2010), and these methods should be useful for the preparation of zebrafish tissues in the future. Furthermore, electron-based imaging is also providing insight into structures that may long remain beyond the resolution of light microscopy. Recent cryo-electron microscopy studies have, for example, allowed the direct visualization of the secondary structures of filamentous actin (Fujii *et al.*, 2010). Three-dimensional reconstruction of components of the nervous system is also being performed using

electron microscopy. Two of the most exciting of these are focused ion beam scanning electron microscopy (FIB-SEM) (Merchan-Perez *et al.*, 2009) and the serial block face-trimming technique pioneered by the Denk lab (Jurrus *et al.*, 2009). A third important imaging option is correlative light and electron microscopy, in which images taken by light microscopy can be directly correlated with electron micrographs (Brown *et al.*, 2009; Mobius, 2009; Spiegelhalter *et al.*, 2010). Among the most versatile of the correlative techniques is array tomography, which has been developed by Stephen Smith's laboratory at Stanford University (Micheva and Smith, 2007).

H. Behavioral and Physiological Analyses of Myelinated Axon Function in Zebrafish

A complete analysis of myelinated axons will ultimately include assessment of their physiological properties and consequent effects on behavior. Using high-speed camera imaging, specific disruptions of sensory and motor responses to a defined stimulus were observed in *erbb3* mutant larvae (Pogoda *et al.*, 2006). Although these behavioral defects were not correlated with disruption to specific myelinated axons or circuits, the zebrafish is readily amenable to such analyses (Baier and Scott, 2009; McLean and Fetcho, 2011; Portugues and Engert, 2009). Transgenic lines are available that define the morphology and projections of neurons known to be important in early behaviors (Flanagan-Steet *et al.*, 2005; Sato *et al.*, 2006; Satou *et al.*, 2009), which include neurons that have some of the first axons myelinated in zebrafish. The zebrafish also has numerous advantages for assessing the physiological status of neurons *in vivo*. Electrophysiological recordings have been made of the giant myelinated Mauthner neuron in both larval (Drapeau *et al.*, 1999) and adult zebrafish (Hatta and Korn, 1998) and of individual motor neurons at embryonic stages of development when the very first behaviors are emerging (Saint-Amant and Drapeau, 2000). *In vivo* multiphoton Ca^{2+} imaging of neuronal activity has been carried out both at the population level (Orger *et al.*, 2008) and with respect to individual localized synapses (Dreosti *et al.*, 2009). Individual action potentials have been decoded using *in vivo* Ca^{2+} imaging in zebrafish (Yaksi and Friedrich, 2006). Optogenetic methods have also been used to directly manipulate and record neural activity in zebrafish, for example (Douglass *et al.*, 2008). Further detailed characterization of neuronal circuitry at the single cell level will ultimately enable high-resolution physiological analyses of myelinated axons *in vivo*.

I. Forward Genetic Manipulation

In 1996, an issue of *Development* was dedicated to reporting the first large-scale, ENU-based forward genetic screens carried out in zebrafish, one completed in Christiane Nüsslein-Volhard's laboratory in Tübingen, Germany (Haffter *et al.*, 1996), and the other in Wolfgang Driever's laboratory in Boston, USA (Driever *et al.*, 1996). These screens identified mutants that disrupted early

developmental events as detected by abnormal morphological phenotypes. Subsequent analyses of many of these mutants helped establish the zebrafish as the preeminent vertebrate model organism for forward genetics. Here we will focus on the design of screens to identify new genes with essential functions in myelinated axons.

Myelination is a late event in nervous system development that occurs after neuronal differentiation. Therefore, disruption to genes that function during earlier stages of development may indirectly cause defects in myelin formation. The ideal screen would identify genes specifically required for myelination and discard irrelevant mutants while retaining those with specific effects. However, some genes function during early development *and* during myelination and for this reason, Kazakova *et al.* (2006) performed a shelf screen of available, early acting mutants for aberrant expression of *mbp*. They identified several mutants that displayed both early morphological phenotypes and disruption of *mbp* expression (Kazakova *et al.*, 2006).

In William Talbot's laboratory at Stanford University, we analyzed *mbp* mRNA expression in 1860 clutches of F3 larvae generated from newly mutagenized males (Pogoda *et al.*, 2006). Thirteen mutations in 10 different genes that affected many aspects of myelinated axon formation were identified. Arguably the most interesting mutants isolated in this screen were the *st49* and *st63* alleles, which lacked *mbp* expression in the PNS but had almost completely normal axons as well as premyelinating Schwann cells. In-depth characterization of these mutations showed that they disrupted the novel protein, Gpr126 (see above), and that Gpr126 is essential for the initiation of myelination by Schwann cells. The identification of the role for this gene in myelination highlights the power of forward genetic screens in the zebrafish.

To date, screens for myelination mutants have yet to reach saturation, as shown by the number of genes that are represented by single mutant alleles. Further forward genetic screens therefore promise to reveal new facets of myelination.

J. Reverse Genetic Manipulation

Until forward genetic screens in zebrafish began to identify genes required for myelination, reverse genetic manipulation using mice was the primary experimental tool used to dissect the molecular basis of myelination. Numerous reverse genetic options are available to study myelinated axons in zebrafish, although they are not yet as sophisticated as those available to regulate gene expression in rodents.

1. Morpholino Antisense Oligonucleotides

Numerous studies have used morpholino antisense oligonucleotides (MOs) to assess gene function by blocking translation or inhibiting normal mRNA splicing

in zebrafish (Bill *et al.*, 2009; Eisen and Smith, 2008; Nasevicius and Ekker, 2000). MOs also have disadvantages, including incomplete knockdown and occasional off-target nonspecific deleterious effects. Although relatively stable, MOs become diluted in the animal over time, which means that their efficacy diminishes at later stages. As myelination is often analyzed at larval stages, it is important to assess the degree of protein knockdown by antibody-based immunolabeling or Western blotting, or of mRNA mis-splicing by RT-PCR. Depending on the nature of the target, however, Morpholinos can be effective long into larval development (Wyatt *et al.*, 2010). To control for potential off-target effects, one should aim to rescue MO phenotypes by overexpressing synthetic mRNA encoding the target molecule. Unfortunately, synthetic mRNA often degrades in the animal by 3–4 days of development, when analysis of myelination typically begins.

There are, however, effective methodologies to introduce MOs into tissues at later stages, such as using focal electroporation to introduce MOs into small groups of cells (Concha *et al.*, 2003). However, quantification of the amounts of MO introduced can be problematic. The use of caged MOs also represents a promising approach to engineer conditional gene knockdown in zebrafish (Deiters *et al.*, 2010; Ouyang *et al.*, 2009) at the later stages when myelination occurs.

2. TILLING

In addition to MOs, there are other reverse genetic approaches available to the zebrafish community. These usually require a greater initial investment than the MO strategy, but in the examples described here, the outcome is a definitive, stable genetic alteration, which can be maintained indefinitely. Targeted Induced Local Lesions in Genomes (TILLING) is a strategy that identifies lesions in target genes within libraries of heavily mutagenized genomes by PCR and restriction digest or sequencing-based means (Moens *et al.*, 2008). The mutagenized genomes are usually maintained as cryopreserved sperm, from which founder mutant fish can be derived. Individual mutagenized genomes will, of course, contain multiple mutations in addition to that found in a gene of interest. Genetic outcrossing is therefore required before being able to unambiguously link genotype to a phenotype. Two community-wide initiatives are generating mutant lines of zebrafish by TILLING, one located at the Sanger Centre in the United Kingdom (http://www.sanger.ac.uk/Projects/D_rerio/mutres/) and the second a consortium comprising groups at the Fred Hutchison Cancer Research centre (Seattle), Vanderbilt University (Nashville, TN), and the University of Oregon (http://www.zfishtilling.org/zfish/). The long-term goal of TILLING initiatives is to generate function-disrupting mutations in all essential zebrafish genes. With the generation of new libraries of mutagenized genomes and next-generation sequencing technologies (Metzker, 2010), this goal could be realized within the next decade.

3. Zinc Finger Nuclease Engineering

Zinc finger nuclease (ZFN) technology has recently been introduced to the zebrafish system as a complementary reverse genetic strategy to induce targeted mutations. ZFNs are artificial restriction enzymes that cause double-stranded breaks at defined points within the genome. If breakage is followed by nonhomologous end joining repair, a frameshift mutation is typically introduced at the cut site (Foley *et al.*, 2009a, 2009b; Gupta *et al.*, 2011; Meng *et al.*, 2008; Urnov *et al.*, 2010). In addition to targeting individual genes, ZFN technology also allows one to target exons that may be specific to individual, alternatively spliced mRNA isoforms. Many genes involved in myelinated axon formation are expressed as multiple isoforms, including neuregulin 1 (Birchmeier and Nave, 2008; Nave and Salzer, 2006) and neurofascin (Basak *et al.*, 2007; Thaxton *et al.*, 2010; Voas *et al.*, 2009; Zonta *et al.*, 2008). ZFN targeting of specific alleles also creates the opportunity to generate disease-specific alleles, where conserved amino acid residues that are disrupted in a particular human disease can be targeted directly in zebrafish. For example, many Charcot–Marie–Tooth neuropathies and Leukodystrophies that disrupt myelinated axons (Shy, 2004; Boespflug-Tanguy *et al.*, 2008) have known genetic lesions that could possibly be recapitulated and analyzed using zebrafish.

K. Generation of Genetic Chimeras

Myelination is a multicellular event, involving interactions between axons and the glial cells that myelinate them. It is also affected by other cell types, such as astrocytes (Watkins *et al.*, 2008), NG2 cells (De Biase *et al.*, 2010; Trotter *et al.*, 2010), and immune cells (Gandhi *et al.*, 2010). Conditional ablation of gene function in specific cells by Cre/loxP conditional knockout has taught us much of what we know about myelin formation (Emery *et al.*, 2009; Wang, 2009; Zonta *et al.*, 2008). Drug-inducible forms of Cre also permit the timing of recombination to be regulated (Danielian *et al.*, 1998). Generation of conditional disruption of endogenous alleles requires ES cell technology (Wang, 2009), which has not yet been successfully applied to zebrafish, but this goal is under active pursuit (Fan *et al.*, 2008).

1. Generation of Genetic Chimeras by Cell Transplantation

Cell transplantation is a relatively simple, common, and versatile technique employed by many zebrafish laboratories since its inception (Ho and Kane, 1990), and detailed protocols have been described elsewhere (e.g., Kemp *et al.*, 2009). Cell transplantation can be used to visualize either dye-labeled or transgenically labeled cells that are transplanted from donor embryos into unlabeled hosts. Heterotopic and heterochronic transplantation can be used to test cell fate and potential, for example

(Eisen, 1991a, 1991b; Houart *et al.*, 1998), and cell transplantation has even been used to demonstrate the morphogenetic properties of molecules *in vivo* following the transplantation of donor cells overexpressing a particular mRNA into a host embryo (Chen and Schier, 2001). Here, however, we will focus on isochronic transplants of genetically distinct cells that test whether genes function by cell-autonomous or cell-nonautonomous mechanisms during myelinated axon formation.

Timing of Chimera Generation

We typically transplant cells from isochronic donor embryos to host embryos at the 1000-cell stage through ~50% epiboly. The donor cells will behave according to the host environment because the neural lineage has not yet been restricted (Woo and Fraser, 1998). The distribution of transplanted cells can be quite variable within the host, but existing fate maps provide an indication of transplant residency in older embryos (Kimmel *et al.*, 1990).

Cell Mosaicism of Individual Chimeras

The mosaicisim of clones in chimeras is an important issue to consider. We label donor embryos with fluorescent dextrans (MW 3000 Da) to monitor transplanted cells in the host. In some cases, it can be useful to transplant cells from a dextran-labeled donor that also expresses a transgenic marker to help visualize specific structures (e.g., axonal processes; Lyons *et al.*, 2008; Sato *et al.*, 2006). An alternative to dye labeling is use of a ubiquitous transgenic reporter line as a source of donor cells, but one must ascertain that the promoter will not be silenced in specific cell types or over time.

Cell transplantation has been used to show that the kinesin motor protein Kif1b functions autonomously in oligodendrocytes during *mbp mRNA* localization. In this study, five chimeras in which individual wild-type oligodendrocytes had normal *mbp* mRNA localization in an otherwise *kif1b* mutant background were identified (Lyons *et al.*, 2009). These chimeras did not contain wild-type neurons that could have indirectly rescued mRNA localization in a cell-nonautonomous way. Identification of chimeras that contain wild-type oligodendrocytes but no wild-type neurons is unusual, due to the fact that neurons greatly outnumber oligodendrocytes at embryonic and early larval stages (Lyons *et al.*, 2003) and derive from shared progenitor pools (Shin *et al.*, 2007; Zannino and Appel, 2009). To conclude unambiguously that Kif1b functioned autonomously in oligodendrocytes, it was important to ensure that wild-type neurons that associated with myelinating oligodendrocytes failed to rescue *mbp* mRNA localization in mutant oligodendrocytes. Few CNS chimeras contain such neurons because the number of myelinated axons is very low compared to total axon number (Brosamle and Halpern, 2002; Lyons *et al.*, 2009). The situation for cell-type-specific analyses in the PNS is more straightforward, as there are numerous nerves where the

embryonic origins of neurons and glia are distinct (e.g., Gilmour *et al.*, 2002; Sarrazin *et al.*, 2010) and the relative numbers of neurons and glia are more closely matched. In the PNS, one can routinely identify chimeras where large populations of genetically distinct neurons and glia are in close proximity (Grant *et al.*, 2005; Lyons *et al.*, 2008, 2009; Raphael *et al.*, 2010).

2. Transgenic Generation of Genetic Chimeras

To generate cell-type-specific genetic chimeras, one can also use specific regulatory sequences to directly drive expression of genes of interest in neurons and/or myelinating glia. One can, for instance, express the wild-type version of a mutated gene in a specific cell type(s) in a mutant background to assess gene function. One can also express dominant negative, truncated or mutant variants of specific proteins in wild-type or genetically modified backgrounds.

It is, however, important to consider how transgene-driven expression compares to physiological levels, and that the function of transgenic protein variants may not always reflect the role of the endogenous protein.

L. Chemical Biology

The suitability of embryonic and larval zebrafish for chemical biological screens and analyses is now well documented (Choi *et al.*, 2007; Hong, 2009; Kaufman *et al.*, 2009; Khersonsky *et al.*, 2003; Kitambi *et al.*, 2009; Murphey *et al.*, 2006; Peterson *et al.*, 2004; Rihel *et al.*, 2010). Buckley *et al.* performed a drug reprofiling screen to identify molecules that could enhance myelination and potentially aid myelin repair. They found that ~2% of over 1000 compounds screened from available libraries affected the development of oligodendrocytes as assessed by examining the transgenic line olig2:GFP (Buckley *et al.*, 2010b; Shin *et al.*, 2003). Secondary and tertiary screens revealed interesting phenotypic effects of these compounds on myelination. Other chemical genetic screens in zebrafish have used libraries of molecules to reverse the effects of mutations in important genes (Peterson *et al.*, 2004). Although it may be difficult to develop simple assays for complex conditions, such as MS, there are numerous inherited neuropathies and Leukodystrophies that could potentially be modeled in zebrafish. One might use these models to search for drugs that could reverse the debilitating phenotypes of these diseases.

It is clear that chemical biological approaches in zebrafish will also aid many aspects of basic biological investigation. These include conditional analyses of molecular function *in vivo* (Lyons *et al.*, 2005), identifying new proteins involved in biological processes (Ahn and Chang, 2007; Khersonsky *et al.*, 2003), visualizing specific structures and molecules (Wang *et al.*, 2010), and allowing pharmacological manipulation of physiology and behavior (Woods *et al.*, 2006), all of which are relevant to the study of myelinated axons.

III. Summary

The study of myelinated axons in zebrafish is a growing field. To date the most significant contributions from zebrafish research have arisen from two of the main strengths of the system, namely, high-resolution imaging of cell behavior *in vivo* and forward genetic screens. Given current advances in microscopy and the growing number of reagents to visualize cells, subcellular structures, and molecules *in vivo*, we expect live imaging in zebrafish to be at the forefront of efforts to better understand the morphogenetic basis of myelination. Future forward genetic screens will continue to identify genes required for specific aspects of myelinated axon formation. We also anticipate that the number of new mutants generated through TILLING- and ZFN-based enterprises will increase dramatically and that additional future advances will allow the conditional manipulation of endogenous genes. Continued elucidation of the genetic bases of human conditions of the nervous system may also allow the reverse genetic generation of robust zebrafish models of disease. By incorporating such zebrafish models into chemical genetic screens, it may even be possible to identify factors that ameliorate symptoms of disease. In summary, the zebrafish promises to serve as an important model organism for understanding the development, disruption, and potential for repair of myelinated axons.

Acknowledgments

We would like to acknowledge the work of Drs. Kelly Monk, Matt Voas, and Joann Buchanan, who contributed to the development of the protocol that allows visualization of zebrafish myelin by TEM. We thank Dr. Robert Hartley and Theo Hirst for deconvolving confocal images. We would like to acknowledge Prof. Charles ffrench-Constant for support, and we are grateful to the Euan MacDonald Centre for Motor Neurone Disease Research and Crerar Hotels for providing free access to a Zeiss LSM 710 confocal microscope.

D.A.L. is a BBSRC David Phillips Fellow. Work in the Lyons lab is funded by BBSRC, the European Commission, and the UK Multiple Sclerosis Society.

References

Ahn, Y. H., and Chang, Y. T. (2007). Tagged small molecule library approach for facilitated chemical genetics. *Acc. Chem. Res.* **40**, 1025–1033.

Asakawa, K., and Kawakami, K. (2008). Targeted gene expression by the Gal4-UAS system in zebrafish. *Dev Growth Differ.* **50**, 391–399.

Asakawa, K., and Kawakami, K. (2009). The Tol2-mediated Gal4-UAS method for gene and enhancer trapping in zebrafish. *Methods* **49**, 275–281.

Asakawa, K., Suster, M. L., Mizusawa, K., Nagayoshi, S., Kotani, T., Urasaki, A., Kishimoto, Y., Hibi, M., and Kawakami, K. (2008). Genetic dissection of neural circuits by Tol2 transposon-mediated Gal4 gene and enhancer trapping in zebrafish. *Proc. Natl. Acad. Sci. U. S. A.* **105**, 1255–1260.

Aulchenko, Y. S., Hoppenbrouwers, I. A., Ramagopalan, S. V., Broer, L., Jafari, N., Hillert, J., Link, J., Lundstrom, W., Greiner, E., Dessa Sadovnick, A., Goossens, D., Van Broeckhoven, C., Del-Favero, J., Ebers, G. C., Oostra, B. A., van Duijn, C. M., and Hintzen, R. Q. (2008). Genetic variation in the KIF1B locus influences susceptibility to multiple sclerosis. *Nat. Genet.* **40**, 1402–1403.

Baier, H., and Scott, E. K. (2009). Genetic and optical targeting of neural circuits and behavior – zebrafish in the spotlight. *Curr. Opin. Neurobiol.* **19**, 553–560.

Barres, B. A. (2008). The mystery and magic of glia: a perspective on their roles in health and disease. *Neuron* **60**, 430–440.

Basak, S., Raju, K., Babiarz, J., Kane-Goldsmith, N., Koticha, D., and Grumet, M. (2007). Differential expression and functions of neuronal and glial neurofascin isoforms and splice variants during PNS development. *Dev. Biol.* **311**, 408–422.

Baumann, N., and Pham-Dinh, D. (2001). Biology of oligodendrocyte and myelin in the mammalian central nervous system. *Physiol. Rev.* **81**, 871–927.

Bill, B. R., Petzold, A. M., Clark, K. J., Schimmenti, L. A., and Ekker, S. C. (2009). A primer for morpholino use in zebrafish. *Zebrafish* **6**, 69–77.

Birchmeier, C., and Nave, K. A. (2008). Neuregulin-1, a key axonal signal that drives Schwann cell growth and differentiation. *Glia* **56**, 1491–1497.

Blanchard, A. D., Sinanan, A., Parmantier, E., Zwart, R., Broos, L., Meijer, D., Meier, C., Jessen, K. R., and Mirsky, R. (1996). Oct-6 (SCIP/Tst-1) is expressed in Schwann cell precursors, embryonic Schwann cells, and postnatal myelinating Schwann cells: comparison with Oct-1, Krox-20, and Pax-3. *J. Neurosci. Res.* **46**, 630–640.

Boespflug-Tanguy, O., *et al*. (2008). Genes involved in leukodystrophies: a glance at glial functions. *Curr Neurol Neurosci Rep.* **8**, 217–229.

Boggs, J. M. (2006). Myelin basic protein: a multifunctional protein. *Cell. Mol. Life Sci.* **63**, 1945–1961.

Booth, D. R., Heard, R. N., Stewart, G. J., Cox, M., Scott, R. J., Lechner-Scott, J., Goris, A., Dobosi, R., Dubois, B., Saarela, J., Leppa, V., Peltonen, L., Pirttila, T., Cournu-Rebeix, I., Fontaine, B., Bergamaschi, L., D'Alfonso, S., Leone, M., Lorentzen, A. R., Harbo, H. F., Celius, E. G., Spurkland, A., Link, J., Kockum, I., Olsson, T., Hillert, J., Ban, M., Baker, A., Kemppinen, A., Sawcer, S., Compston, A., Robertson, N. P., De Jager, P. L., Hafler, D. A., Barcellos, L. F., Ivinson, A. J., McCauley, J. L., Pericak-Vance, M. A., Oksenberg, J. R., Hauser, S. L., Sexton, D., and Haines, J. (2010). Lack of support for association between the KIF1B rs10492972[C] variant and multiple sclerosis. *Nat. Genet.* **42**, 469–470 author reply 470-471.

Brand, A. H., and Perrimon, N. (1993). Targeted gene expression as a means of altering cell fates and generating dominant phenotypes. *Development* **118**, 401–415.

Brend, T., and Holley, S. A. (2009). Zebrafish whole mount high-resolution double fluorescent in situ hybridization. *J. Vis. Exp.* **25**, http://www.jove.com/details.php?id=1229, doi: 10.3791/1229.

Brinkmann, B. G., Agarwal, A., Sereda, M. W., Garratt, A. N., Muller, T., Wende, H., Stassart, R. M., Nawaz, S., Humml, C., Velanac, V., Radyushkin, K., Goebbels, S., Fischer, T. M., Franklin, R. J., Lai, C., Ehrenreich, H., Birchmeier, C., Schwab, M. H., and Nave, K. A. (2008). Neuregulin-1/ErbB signaling serves distinct functions in myelination of the peripheral and central nervous system. *Neuron* **59**, 581–595.

Brooks, A. S., Bertoli-Avella, A. M., Burzynski, G. M., Breedveld, G. J., Osinga, J., Boven, L. G., Hurst, J. A., Mancini, G. M., Lequin, M. H., de Coo, R. F., Matera, I., de Graaff, E., Meijers, C., Willems, P. J., Tibboel, D., Oostra, B. A., and Hofstra, R. M. (2005). Homozygous nonsense mutations in KIAA1279 are associated with malformations of the central and enteric nervous systems. *Am. J. Hum. Genet.* **77**, 120–126.

Brosamle, C., and Halpern, M. E. (2002). Characterization of myelination in the developing zebrafish. *Glia* **39**, 47–57.

Brown, E., Mantell, J., Carter, D., Tilly, G., and Verkade, P. (2009). Studying intracellular transport using high-pressure freezing and correlative light electron microscopy. *Semin. Cell Dev. Biol.* **20**, 910–919.

Buckley, C. E., Marguerie, A., Alderton, W. K., and Franklin, R. J. (2010 a). Temporal dynamics of myelination in the zebrafish spinal cord. *Glia* **58**, 802–812.

Buckley, C. E., Marguerie, A., Roach, A. G., Goldsmith, P., Fleming, A., Alderton, W. K., and Franklin, R. J. (2010 b). Drug reprofiling using zebrafish identifies novel compounds with potential pro-myelination effects. *Neuropharmacology* **59**, 149–159.

Bunge, R. P., Bunge, M. B., and Bates, M. (1989). Movements of the Schwann cell nucleus implicate progression of the inner (axon-related) Schwann cell process during myelination. *J. Cell Biol.* **109**, 273–284.

Cahoy, J. D., Emery, B., Kaushal, A., Foo, L. C., Zamanian, J. L., Christopherson, K. S., Xing, Y., Lubischer, J. L., Krieg, P. A., Krupenko, S. A., Thompson, W. J., and Barres, B. A. (2008). A transcriptome database for astrocytes, neurons, and oligodendrocytes: a new resource for understanding brain development and function. *J. Neurosci.* **28**, 264–278.

Chan, J. R. (2007). Myelination: all about Rac 'n' roll. *J. Cell Biol.* **177**, 953–955.

Chen, Y., and Schier, A. F. (2001). The zebrafish Nodal signal Squint functions as a morphogen. *Nature* **411**, 607–610.

Choi, T. Y., Kim, J. H., Ko, D. H., Kim, C. H., Hwang, J. S., Ahn, S., Kim, S. Y., Kim, C. D., Lee, J. H., and Yoon, T. J. (2007). Zebrafish as a new model for phenotype-based screening of melanogenic regulatory compounds. *Pigment Cell Res.* **20**, 120–127.

Clarke, J. D. (2008). Using fluorescent dyes for fate mapping, lineage analysis, and axon tracing in the chick embryo. *Methods Mol. Biol.* **461**, 351–361.

Collins, R. T., Linker, C., and Lewis, J. (2010). MAZe: a tool for mosaic analysis of gene function in zebrafish. *Nat. Methods* **7**, 219–223.

Colman, D. R., Kreibich, G., Frey, A. B., and Sabatini, D. D. (1982). Synthesis and incorporation of myelin polypeptides into CNS myelin. *J. Cell Biol.* **95**, 598–608.

Concha, M. L., Russell, C., Regan, J. C., Tawk, M., Sidi, S., Gilmour, D. T., Kapsimali, M., Sumoy, L., Goldstone, K., Amaya, E., Kimelman, D., Nicolson, T., Grunder, S., Gomperts, M., Clarke, J. D., and Wilson, S. W. (2003). Local tissue interactions across the dorsal midline of the forebrain establish CNS laterality. *Neuron* **39**, 423–438.

Cotter, L., Ozcelik, M., Jacob, C., Pereira, J. A., Locher, V., Baumann, R., Relvas, J. B., Suter, U., and Tricaud, N. (2010). Dlg1–PTEN interaction regulates myelin thickness to prevent damaging peripheral nerve overmyelination. *Science* **328**, 1415–1418.

Danielian, P. S., Muccino, D., Rowitch, D. H., Michael, S. K., and McMahon, A. P. (1998). Modification of gene activity in mouse embryos in utero by a tamoxifen-inducible form of Cre recombinase. *Curr. Biol.* **8**, 1323–1326.

De Biase, L. M., Nishiyama, A., and Bergles, D. E. (2010). Excitability and synaptic communication within the oligodendrocyte lineage. *J. Neurosci.* **30**, 3600–3611.

De Vos, K. J., Grierson, A. J., Ackerley, S., and Miller, C. C. (2008). Role of axonal transport in neurodegenerative diseases. *Annu. Rev. Neurosci.* **31**, 151–173.

Deiters, A., Garner, R. A., Lusic, H., Govan, J. M., Dush, M., Nascone-Yoder, N. M., and Yoder, J. A. (2010). Photocaged morpholino oligomers for the light-regulation of gene function in zebrafish and *Xenopus* embryos. *J. Am. Chem. Soc.* **132**, 15644–15650.

Distel, M., Wullimann, M. F., and Koster, R. W. (2009). Optimized Gal4 genetics for permanent gene expression mapping in zebrafish. *Proc. Natl. Acad. Sci. U. S. A.* **106**, 13365–13370.

Douglass, A. D., Kraves, S., Deisseroth, K., Schier, A. F., and Engert, F. (2008). Escape behavior elicited by single, channelrhodopsin-2-evoked spikes in zebrafish somatosensory neurons. *Curr. Biol.* **18**, 1133–1137.

Drapeau, P., Ali, D. W., Buss, R. R., and Saint-Amant, L. (1999). In vivo recording from identifiable neurons of the locomotor network in the developing zebrafish. *J. Neurosci. Methods* **88**, 1–13.

Dreosti, E., Odermatt, B., Dorostkar, M. M., and Lagnado, L. (2009). A genetically encoded reporter of synaptic activity in vivo. *Nat. Methods* **6**, 883–889.

Driever, W., Solnica-Krezel, L., Schier, A. F., Neuhauss, S. C., Malicki, J., Stemple, D. L., Stainier, D. Y., Zwartkruis, F., Abdelilah, S., Rangini, Z., Belak, J., and Boggs, C. (1996). A genetic screen for mutations affecting embryogenesis in zebrafish. *Development* **123**, 37–46.

Dutton, K. A., Pauliny, A., Lopes, S. S., Elworthy, S., Carney, T. J., Rauch, J., Geisler, R., Haffter, P., and Kelsh, R. N. (2001). Zebrafish colourless encodes sox10 and specifies non-ectomesenchymal neural crest fates. *Development* **128**, 4113–4125.

Edgar, J. M., and Nave, K. A. (2009). The role of CNS glia in preserving axon function. *Curr. Opin. Neurobiol.* **19**, 498–504.

Eisen, J. S. (1991a). Determination of primary motoneuron identity in developing zebrafish embryos. *Science* **252**, 569–572.

Eisen, J. S. (1991b). Motoneuronal development in the embryonic zebrafish. *Development* **113**(Suppl. 2), 141–147.

Eisen, J. S., and Smith, J. C. (2008). Controlling morpholino experiments: don't stop making antisense. *Development* **135**, 1735–1743.

Elsalini, O. A., and Rohr, K. B. (2003). Phenylthiourea disrupts thyroid function in developing zebrafish. *Dev. Genes Evol.* **212**, 593–598.

Emery, B., Agalliu, D., Cahoy, J. D., Watkins, T. A., Dugas, J. C., Mulinyawe, S. B., Ibrahim, A., Ligon, K. L., Rowitch, D. H., and Barres, B. A. (2009). Myelin gene regulatory factor is a critical transcriptional regulator required for CNS myelination. *Cell* **138**, 172–185.

Fan, L., Moon, J., Wong, T. T., Crodian, J., and Collodi, P. (2008). Zebrafish primordial germ cell cultures derived from vasa: RFP transgenic embryos. *Stem Cells Dev.* **17**, 585–597.

Feirabend, H. K., Choufoer, H., and Ploeger, S. (1998). Preservation and staining of myelinated nerve fibers. *Methods* **15**, 123–131.

Feirabend, H. K., Kok, P., Choufoer, H., and Ploeger, S. (1994). Preservation of myelinated fibers for electron microscopy: a qualitative comparison of aldehyde fixation, microwave stabilisation and other procedures all completed by osmication. *J. Neurosci. Methods* **55**, 137–153.

Fields, R. D. (2005). Myelination: an overlooked mechanism of synaptic plasticity? *Neuroscientist* **11**, 528–531.

Flanagan-Steet, H., Fox, M. A., Meyer, D., and Sanes, J. R. (2005). Neuromuscular synapses can form in vivo by incorporation of initially aneural postsynaptic specializations. *Development* **132**, 4471–4481.

Foley, J. E., Maeder, M. L., Pearlberg, J., Joung, J. K., Peterson, R. T., and Yeh, J. R. (2009 a). Targeted mutagenesis in zebrafish using customized zinc-finger nucleases. *Nat. Protoc.* **4**, 1855–1867.

Foley, J. E., Yeh, J. R., Maeder, M. L., Reyon, D., Sander, J. D., Peterson, R. T., and Joung, J. K. (2009 b). Rapid mutation of endogenous zebrafish genes using zinc finger nucleases made by oligomerized pool engineering (OPEN). *PLoS One* **4**, e4348.

Franklin, R. J., and ffrench-Constant, C. (2008). Remyelination in the CNS: from biology to therapy. *Nat. Rev. Neurosci.* **9**, 839–855.

Fujii, T., Iwane, A. H., Yanagida, T., and Namba, K. (2010). Direct visualization of secondary structures of F-actin by electron cryomicroscopy. *Nature* **467**, 724–728.

Furley, A. J., Morton, S. B., Manalo, D., Karagogeos, D., Dodd, J., and Jessell, T. M. (1990). The axonal glycoprotein TAG-1 is an immunoglobulin superfamily member with neurite outgrowth-promoting activity. *Cell* **61**, 157–170.

Gandhi, R., Laroni, A., and Weiner, H. L. (2010). Role of the innate immune system in the pathogenesis of multiple sclerosis. *J. Neuroimmunol.* **221**, 7–14.

Garratt, A. N., Voiculescu, O., Topilko, P., Charnay, P., and Birchmeier, C. (2000). A dual role of erbB2 in myelination and in expansion of the Schwann cell precursor pool. *J. Cell Biol.* **148**, 1035–1046.

Ghazvini, M., Mandemakers, W., Jaegle, M., Piirsoo, M., Driegen, S., Koutsourakis, M., Smit, X., Grosveld, F., and Meijer, D. (2002). A cell type-specific allele of the POU gene Oct-6 reveals Schwann cell autonomous function in nerve development and regeneration. *EMBO J.* **21**, 4612–4620.

Gilmour, D. T., Maischein, H. M., and Nusslein-Volhard, C. (2002). Migration and function of a glial subtype in the vertebrate peripheral nervous system. *Neuron* **34**, 577–588.

Goll, M. G., Anderson, R., Stainier, D. Y., Spradling, A. C., and Halpern, M. E. (2009). Transcriptional silencing and reactivation in transgenic zebrafish. *Genetics* **182**, 747–755.

Grant, K. A., Raible, D. W., and Piotrowski, T. (2005). Regulation of latent sensory hair cell precursors by glia in the zebrafish lateral line. *Neuron* **45**, 69–80.

Grupp, L., Wolburg, H., and Mack, A. F. (2010). Astroglial structures in the zebrafish brain. *J. Comp. Neurol.* **518**, 4277–4287.

Gupta, A., Meng, X., Zhu, L. J., Lawson, N. D., and Wolfe, S. A. (2011). Zinc finger protein-dependent and -independent contributions to the in vivo off-target activity of zinc finger nucleases. *Nucleic Acids Res.* **39**, 381–392.

Haffter, P., Granato, M., Brand, M., Mullins, M. C., Hammerschmidt, M., Kane, D. A., Odenthal, J., van Eeden, F. J., Jiang, Y. J., Heisenberg, C. P., Kelsh, R. N., Furutani-Seiki, M., Vogelsang, E., Beuchle, D.,

Schach, U., Fabian, C., and Nusslein-Volhard, C. (1996). The identification of genes with unique and essential functions in the development of the zebrafish. *Danio rerio. Development* **123**, 1–36.

Halpern, M. E., Rhee, J., Goll, M. G., Akitake, C. M., Parsons, M., and Leach, S. D. (2008). Gal4/UAS transgenic tools and their application to zebrafish. *Zebrafish* **5**, 97–110.

Handel, A. E., Giovannoni, G., Ebers, G. C., and Ramagopalan, S. V. (2010). Environmental factors and their timing in adult-onset multiple sclerosis. *Nat. Rev. Neurol.* **6**, 156–166.

Hans, S., Kaslin, J., Freudenreich, D., and Brand, M. (2009). Temporally-controlled site-specific recombination in zebrafish. *PLoS One* **4**, e4640.

Hartline, D. K., and Colman, D. R. (2007). Rapid conduction and the evolution of giant axons and myelinated fibers. *Curr. Biol.* **17**, R29–R35.

Hatta, K., and Korn, H. (1998). Physiological properties of the Mauthner system in the adult zebrafish. *J. Comp. Neurol.* **395**, 493–509.

Ho, R. K., and Kane, D. A. (1990). Cell-autonomous action of zebrafish spt-1 mutation in specific mesodermal precursors. *Nature* **348**, 728–730.

Hong, C. C. (2009). Large-scale small-molecule screen using zebrafish embryos. *Methods Mol. Biol.* **486**, 43–55.

Houart, C., Westerfield, M., and Wilson, S. W. (1998). A small population of anterior cells patterns the forebrain during zebrafish gastrulation. *Nature* **391**, 788–792.

Hsieh, C. S., Ko, C. Y., Chen, S. Y., Liu, T. M., Wu, J. S., Hu, C. H., and Sun, C. K. (2008). In vivo long-term continuous observation of gene expression in zebrafish embryo nerve systems by using harmonic generation microscopy and morphant technology. *J. Biomed. Opt.* **13**, 064041.

Huff, T. B., and Cheng, J. X. (2007). In vivo coherent anti-Stokes Raman scattering imaging of sciatic nerve tissue. *J. Microsc.* **225**, 175–182.

Huisken, J., and Stainier, D. Y. (2007). Even fluorescence excitation by multidirectional selective plane illumination microscopy (mSPIM). *Opt. Lett.* **32**, 2608–2610.

Jaegle, M., Ghazvini, M., Mandemakers, W., Piirsoo, M., Driegen, S., Levavasseur, F., Raghoenath, S., Grosveld, F., and Meijer, D. (2003). The POU proteins Brn-2 and Oct-6 share important functions in Schwann cell development. *Genes Dev.* **17**, 1380–1391.

Jessen, K. R., and Mirsky, R. (2005). The origin and development of glial cells in peripheral nerves. *Nat. Rev. Neurosci.* **6**, 671–682.

Jessen, K. R., Mirsky, R., and Salzer, J. (2008). Introduction. Schwann cell biology. *Glia* **56**, 1479–1480.

Jung, S. H., Kim, S., Chung, A. Y., Kim, H. T., So, J. H., Ryu, J., Park, H. C., and Kim, C. H. (2010). Visualization of myelination in GFP-transgenic zebrafish. *Dev. Dyn.* **239**, 592–597.

Jurrus, E., Hardy, M., Tasdizen, T., Fletcher, P. T., Koshevoy, P., Chien, C. B., Denk, W., and Whitaker, R. (2009). Axon tracking in serial block-face scanning electron microscopy. *Med. Image Anal.* **13**, 180–188.

Kaufman, C. K., White, R. M., and Zon, L. (2009). Chemical genetic screening in the zebrafish embryo. *Nat. Protoc.* **4**, 1422–1432.

Kawakami, K., Abe, G., Asada, T., Asakawa, K., Fukuda, R., Ito, A., Lal, P., Mouri, N., Muto, A., Suster, M. L., Takakubo, H., Urasaki, A., Wada, H., and Yoshida, M. (2010). zTrap: zebrafish gene trap and enhancer trap database. *BMC Dev. Biol.* **10**, 105.

Kawasaki, F., Mattiuz, A. M., and Ordway, R. W. (1998). Synaptic physiology and ultrastructure in comatose mutants define an in vivo role for NSF in neurotransmitter release. *J. Neurosci.* **18**, 10241–10249.

Kazakova, N., Li, H., Mora, A., Jessen, K. R., Mirsky, R., Richardson, W. D., and Smith, H. K. (2006). A screen for mutations in zebrafish that affect myelin gene expression in Schwann cells and oligodendrocytes. *Dev. Biol.* **297**, 1–13.

Kemp, H. A., Carmany-Rampey, A., and Moens, C. (2009). Generating chimeric zebrafish embryos by transplantation. *J. Vis. Exp.* **29**, http://www.jove.com/details.php?id=1394, doi: 10.3791/1394.

Khersonsky, S. M., Jung, D. W., Kang, T. W., Walsh, D. P., Moon, H. S., Jo, H., Jacobson, E. M., Shetty, V., Neubert, T. A., and Chang, Y. T. (2003). Facilitated forward chemical genetics using a tagged triazine library and zebrafish embryo screening. *J. Am. Chem. Soc.* **125**, 11804–11805.

Kimmel, C. B., Warga, R. M., and Schilling, T. F. (1990). Origin and organization of the zebrafish fate map. *Development* **108**, 581–594.

Kirby, B. B., Takada, N., Latimer, A. J., Shin, J., Carney, T. J., Kelsh, R. N., and Appel, B. (2006). In vivo time-lapse imaging shows dynamic oligodendrocyte progenitor behavior during zebrafish development. *Nat. Neurosci.* **9**, 1506–1511.

Kitambi, S. S., McCulloch, K. J., Peterson, R. T., and Malicki, J. J. (2009). Small molecule screen for compounds that affect vascular development in the zebrafish retina. *Mech. Dev.* **126**, 464–477.

Koster, R. W., and Fraser, S. E. (2001). Tracing transgene expression in living zebrafish embryos. *Dev. Biol.* **233**, 329–346.

Kucenas, S., Snell, H., and Appel, B. (2008). nkx2.2a promotes specification and differentiation of a myelinating subset of oligodendrocyte lineage cells in zebrafish. *Neuron Glia Biol.* **4**, 71–81.

Kwan, K. M., Fujimoto, E., Grabher, C., Mangum, B. D., Hardy, M. E., Campbell, D. S., Parant, J. M., Yost, H. J., Kanki, J. P., and Chien, C. B. (2007). The Tol2kit: a multisite gateway-based construction kit for Tol2 transposon transgenesis constructs. *Dev. Dyn.* **236**, 3088–3099.

Lamason, R. L., Mohideen, M. A., Mest, J. R., Wong, A. C., Norton, H. L., Aros, M. C., Jurynec, M. J., Mao, X., Humphreville, V. R., Humbert, J. E., Sinha, S., Moore, J. L., Jagadeeswaran, P., Zhao, W., Ning, G., Makalowska, I., McKeigue, P. M., O'Donnell, D., Kittles, R., Parra, E. J., Mangini, N. J., Grunwald, D. J., Shriver, M. D., Canfield, V. A., and Cheng, K. C. (2005). SLC24A5, a putative cation exchanger, affects pigmentation in zebrafish and humans. *Science* **310**, 1782–1786.

Larson, T. A., Gordon, T. N., Lau, H. E., and Parichy, D. M. (2010). Defective adult oligodendrocyte and Schwann cell development, pigment pattern, and craniofacial morphology in puma mutant zebrafish having an alpha tubulin mutation. *Dev. Biol.* **346**, 296–309.

Le Douarin, N. M., and Dupin, E. (2003). Multipotentiality of the neural crest. *Curr. Opin. Genet. Dev.* **13**, 529–536.

Lecaudey, V., Cakan-Akdogan, G., Norton, W. H., and Gilmour, D. (2008). Dynamic Fgf signaling couples morphogenesis and migration in the zebrafish lateral line primordium. *Development* **135**, 2695–2705.

Levavasseur, F., Mandemakers, W., Visser, P., Broos, L., Grosveld, F., Zivkovic, D., and Meijer, D. (1998). Comparison of sequence and function of the Oct-6 genes in zebrafish, chicken and mouse. *Mech. Dev.* **74**, 89–98.

Li, H., He, Y., Richardson, W. D., and Casaccia, P. (2009). Two-tier transcriptional control of oligodendrocyte differentiation. *Curr. Opin. Neurobiol.* **19**, 479–485.

Li, H., Lu, Y., Smith, H. K., and Richardson, W. D. (2007). Olig1 and Sox10 interact synergistically to drive myelin basic protein transcription in oligodendrocytes. *J. Neurosci.* **27**, 14375–14382.

Lister, J. A., Robertson, C. P., Lepage, T., Johnson, S. L., and Raible, D. W. (1999). nacre encodes a zebrafish microphthalmia-related protein that regulates neural-crest-derived pigment cell fate. *Development* **126**, 3757–3767.

Lyons, D. A., Guy, A. T., and Clarke, J. D. (2003). Monitoring neural progenitor fate through multiple rounds of division in an intact vertebrate brain. *Development* **130**, 3427–3436.

Lyons, D. A., Naylor, S. G., Mercurio, S., Dominguez, C., and Talbot, W. S. (2008). KBP is essential for axonal structure, outgrowth and maintenance in zebrafish, providing insight into the cellular basis of Goldberg-Shprintzen syndrome. *Development* **135**, 599–608.

Lyons, D. A., Naylor, S. G., Scholze, A., and Talbot, W. S. (2009). Kif1b is essential for mRNA localization in oligodendrocytes and development of myelinated axons. *Nat. Genet.* **41**, 854–858.

Lyons, D. A., Pogoda, H. M., Voas, M. G., Woods, I. G., Diamond, B., Nix, R., Arana, N., Jacobs, J., and Talbot, W. S. (2005). erbb3 and erbb2 are essential for Schwann cell migration and myelination in zebrafish. *Curr. Biol.* **15**, 513–524.

McLean, D. L., and Fetcho, J. R. (2011). Movement, technology and discovery in the zebrafish. *Curr. Opin. Neurobiol* **21**, 110–115.

Meng, X., Noyes, M. B., Zhu, L. J., Lawson, N. D., and Wolfe, S. A. (2008). Targeted gene inactivation in zebrafish using engineered zinc-finger nucleases. *Nat. Biotechnol.* **26**, 695–701.

Merchan-Perez, A., Rodriguez, J. R., Alonso-Nanclares, L., Schertel, A., and Defelipe, J. (2009). Counting synapses using FIB/SEM microscopy: a true revolution for ultrastructural volume reconstruction. *Front. Neuroanat.* **3**, 18.

Metzker, M. L. (2010). Sequencing technologies – the next generation. *Nat. Rev. Genet.* **11**, 31–46.

Meyer, M. P., and Smith, S. J. (2006). Evidence from in vivo imaging that synaptogenesis guides the growth and branching of axonal arbors by two distinct mechanisms. *J. Neurosci.* **26**, 3604–3614.

Michailov, G. V., Sereda, M. W., Brinkmann, B. G., Fischer, T. M., Haug, B., Birchmeier, C., Role, L., Lai, C., Schwab, M. H., and Nave, K. A. (2004). Axonal neuregulin-1 regulates myelin sheath thickness. *Science* **304**, 700–703.

Micheva, K. D., and Smith, S. J. (2007). Array tomography: a new tool for imaging the molecular architecture and ultrastructure of neural circuits. *Neuron* **55**, 25–36.

Mobius, W. (2009). Cryopreparation of biological specimens for immunoelectron microscopy. *Ann. Anat.* **191**, 231–247.

Moens, C. B., Donn, T. M., Wolf-Saxon, E. R., and Ma, T. P. (2008). Reverse genetics in zebrafish by TILLING. *Brief Funct. Genomic Proteomic* **7**, 454–459.

Monk, K. R., Naylor, S. G., Glenn, T. D., Mercurio, S., Perlin, J. R., Dominguez, C., Moens, C. B., and Talbot, W. S. (2009). A G protein-coupled receptor is essential for Schwann cells to initiate myelination. *Science* **325**, 1402–1405.

Morris, J. K., Willard, B. B., Yin, X., Jeserich, G., Kinter, M., and Trapp, B. D. (2004). The 36K protein of zebrafish CNS myelin is a short-chain dehydrogenase. *Glia* **45**, 378–391.

Murphey, R. D., Stern, H. M., Straub, C. T., and Zon, L. I. (2006). A chemical genetic screen for cell cycle inhibitors in zebrafish embryos. *Chem. Biol. Drug Des.* **68**, 213–219.

Murphy, H. R., Carver, M. J., Brooks, A. S., Kenny, S. E., and Ellis, I. H. (2006). Two brothers with Goldberg-Shprintzen syndrome. *Clin. Dysmorphol.* **15**, 165–169.

Murphy, P., Topilko, P., Schneider-Maunoury, S., Seitanidou, T., Baron-Van Evercooren, A., and Charnay, P. (1996). The regulation of Krox-20 expression reveals important steps in the control of peripheral glial cell development. *Development* **122**, 2847–2857.

Nasevicius, A., and Ekker, S. C. (2000). Effective targeted gene 'knockdown' in zebrafish. *Nat. Genet.* **26**, 216–220.

Nave, K. A., and Salzer, J. L. (2006). Axonal regulation of myelination by neuregulin 1. *Curr. Opin. Neurobiol.* **16**, 492–500.

Ng, A. N., de Jong-Curtain, T. A., Mawdsley, D. J., White, S. J., Shin, J., Appel, B., Dong, P. D., Stainier, D. Y., and Heath, J. K. (2005). Formation of the digestive system in zebrafish: III. Intestinal epithelium morphogenesis. *Dev. Biol.* **286**, 114–135.

Ogura, E., Okuda, Y., Kondoh, H., and Kamachi, Y. (2009). Adaptation of GAL4 activators for GAL4 enhancer trapping in zebrafish. *Dev. Dyn.* **238**, 641–655.

Oksenberg, J. R., Baranzini, S. E., Sawcer, S., and Hauser, S. L. (2008). The genetics of multiple sclerosis: SNPs to pathways to pathogenesis. *Nat. Rev. Genet.* **9**, 516–526.

Orger, M. B., Kampff, A. R., Severi, K. E., Bollmann, J. H., and Engert, F. (2008). Control of visually guided behavior by distinct populations of spinal projection neurons. *Nat. Neurosci.* **11**, 327–333.

Ouyang, X., Shestopalov, I. A., Sinha, S., Zheng, G., Pitt, C. L., Li, W. H., Olson, A. J., and Chen, J. K. (2009). Versatile synthesis and rational design of caged morpholinos. *J. Am. Chem. Soc.* **131**, 13255–13269.

Parichy, D. M., Elizondo, M. R., Mills, M. G., Gordon, T. N., and Engeszer, R. E. (2009). Normal table of postembryonic zebrafish development: staging by externally visible anatomy of the living fish. *Dev. Dyn.* **238**, 2975–3015.

Park, H. C., Boyce, J., Shin, J., and Appel, B. (2005). Oligodendrocyte specification in zebrafish requires notch-regulated cyclin-dependent kinase inhibitor function. *J. Neurosci.* **25**, 6836–6844.

Park, H. C., Mehta, A., Richardson, J. S., and Appel, B. (2002). olig2 is required for zebrafish primary motor neuron and oligodendrocyte development. *Dev. Biol.* **248**, 356–368.

Park, H. C., Shin, J., Roberts, R. K., and Appel, B. (2007). An olig2 reporter gene marks oligodendrocyte precursors in the postembryonic spinal cord of zebrafish. *Dev. Dyn.* **236**, 3402–3407.

Peterson, R. T., Shaw, S. Y., Peterson, T. A., Milan, D. J., Zhong, T. P., Schreiber, S. L., MacRae, C. A., and Fishman, M. C. (2004). Chemical suppression of a genetic mutation in a zebrafish model of aortic coarctation. *Nat. Biotechnol.* **22**, 595–599.

Pfeiffer, B. D., Ngo, T. T., Hibbard, K. L., Murphy, C., Jenett, A., Truman, J. W., and Rubin, G. M. (2010). Refinement of tools for targeted gene expression in *Drosophila*. *Genetics* **186**, 735–755.

Pogoda, H. M., Sternheim, N., Lyons, D. A., Diamond, B., Hawkins, T. A., Woods, I. G., Bhatt, D. H., Franzini-Armstrong, C., Dominguez, C., Arana, N., Jacobs, J., Nix, R., Fetcho, J. R., and Talbot, W. S. (2006). A genetic screen identifies genes essential for development of myelinated axons in zebrafish. *Dev. Biol.* **298**, 118–131.

Popko, B., Puckett, C., Lai, E., Shine, H. D., Readhead, C., Takahashi, N., Hunt 3rd, S. W., Sidman, R. L., and Hood, L. (1987). Myelin deficient mice: expression of myelin basic protein and generation of mice with varying levels of myelin. *Cell* **48**, 713–721.

Portugues, R., and Engert, F. (2009). The neural basis of visual behaviors in the larval zebrafish. *Curr. Opin. Neurobiol.* **19**, 644–647.

Previtali, S. C., Quattrini, A., Fasolini, M., Panzeri, M. C., Villa, A., Filbin, M. T., Li, W., Chiu, S. Y., Messing, A., Wrabetz, L., and Feltri, M. L. (2000). Epitope-tagged P(0) glycoprotein causes Charcot–Marie–Tooth-like neuropathy in transgenic mice. *J. Cell Biol.* **151**, 1035–1046.

Raphael, A. R., Perlin, J. R., and Talbot, W. S. (2010). Schwann cells reposition a peripheral nerve to isolate it from postembryonic remodeling of its targets. *Development* **137**, 3643–3649.

Raphael, A. R., *et al*. (2011). ErbB signaling has a role in radial sorting independent of Schwann cell number. *Glia.* **59**, 1047–1055.

Readhead, C., Popko, B., Takahashi, N., Shine, H. D., Saavedra, R. A., Sidman, R. L., and Hood, L. (1987). Expression of a myelin basic protein gene in transgenic shiverer mice: correction of the dysmyelinating phenotype. *Cell* **48**, 703–712.

Richardson, W. D., Kessaris, N., and Pringle, N. (2006). Oligodendrocyte wars. *Nat. Rev. Neurosci.* **7**, 11–18.

Riethmacher, D., Sonnenberg-Riethmacher, E., Brinkmann, V., Yamaai, T., Lewin, G. R., and Birchmeier, C. (1997). Severe neuropathies in mice with targeted mutations in the ErbB3 receptor. *Nature* **389**, 725–730.

Rihel, J., Prober, D. A., Arvanites, A., Lam, K., Zimmerman, S., Jang, S., Haggarty, S. J., Kokel, D., Rubin, L. L., Peterson, R. T., and Schier, A. F. (2010). Zebrafish behavioral profiling links drugs to biological targets and rest/wake regulation. *Science* **327**, 348–351.

Rosenbluth, J. (2009). Multiple functions of the paranodal junction of myelinated nerve fibers. *J. Neurosci. Res.* **87**, 3250–3258.

Saint-Amant, L., and Drapeau, P. (2000). Motoneuron activity patterns related to the earliest behavior of the zebrafish embryo. *J. Neurosci.* **20**, 3964–3972.

Salzer, J. L., Brophy, P. J., and Peles, E. (2008). Molecular domains of myelinated axons in the peripheral nervous system. *Glia* **56**, 1532–1540.

Sarrazin, A. F., Nunez, V. A., Sapede, D., Tassin, V., Dambly-Chaudiere, C., and Ghysen, A. (2010). Origin and early development of the posterior lateral line system of zebrafish. *J. Neurosci.* **30**, 8234–8244.

Sato, T., Hamaoka, T., Aizawa, H., Hosoya, T., and Okamoto, H. (2007). Genetic single-cell mosaic analysis implicates ephrinB2 reverse signaling in projections from the posterior tectum to the hindbrain in zebrafish. *J. Neurosci.* **27**, 5271–5279.

Sato, T., Takahoko, M., and Okamoto, H. (2006). HuC:Kaede, a useful tool to label neural morphologies in networks in vivo. *Genesis* **44**, 136–142.

Satou, C., Kimura, Y., Kohashi, T., Horikawa, K., Takeda, H., Oda, Y., and Higashijima, S. (2009). Functional role of a specialized class of spinal commissural inhibitory neurons during fast escapes in zebrafish. *J. Neurosci.* **29**, 6780–6793.

Sawcer, S. (2008). The complex genetics of multiple sclerosis: pitfalls and prospects. *Brain* **131**, 3118–3131.

Schaefer, K., and Brosamle, C. (2009). Zwilling-A and -B, two related myelin proteins of teleosts, which originate from a single bicistronic transcript. *Mol. Biol. Evol.* **26**, 495–499.

Schebesta, M., and Serluca, F. C. (2009). olig1 expression identifies developing oligodendrocytes in zebrafish and requires hedgehog and notch signaling. *Dev. Dyn.* **238**, 887–898.

Scheer, N., Riedl, I., Warren, J. T., Kuwada, J. Y., and Campos-Ortega, J. A. (2002). A quantitative analysis of the kinetics of Gal4 activator and effector gene expression in the zebrafish. *Mech. Dev.* **112**, 9–14.

Schermelleh, L., Heintzmann, R., and Leonhardt, H. (2010). A guide to super-resolution fluorescence microscopy. *J. Cell Biol.* **190**, 165–175.

Scott, E. K., and Baier, H. (2009). The cellular architecture of the larval zebrafish tectum, as revealed by gal4 enhancer trap lines. *Front. Neural Circuits* **3**, 13.

Scott, E. K., Mason, L., Arrenberg, A. B., Ziv, L., Gosse, N. J., Xiao, T., Chi, N. C., Asakawa, K., Kawakami, K., and Baier, H. (2007). Targeting neural circuitry in zebrafish using GAL4 enhancer trapping. *Nat. Methods* **4**, 323–326.

Sherman, D. L., and Brophy, P. J. (2005). Mechanisms of axon ensheathment and myelin growth. *Nat. Rev. Neurosci.* **6**, 683–690.

Shin, J., Park, H. C., Topczewska, J. M., Mawdsley, D. J., and Appel, B. (2003). Neural cell fate analysis in zebrafish using olig2 BAC transgenics. *Methods Cell Sci.* **25**, 7–14.

Shin, J., Poling, J., Park, H. C., and Appel, B. (2007). Notch signaling regulates neural precursor allocation and binary neuronal fate decisions in zebrafish. *Development* **134**, 1911–1920.

Shy, M. E. (2004). Charcot–Marie–Tooth disease: an update. *Curr. Opin. Neurol.* **17**, 579–585.

Spiegelhalter, C., Tosch, V., Hentsch, D., Koch, M., Kessler, P., Schwab, Y., and Laporte, J. (2010). From dynamic live cell imaging to 3D ultrastructure: novel integrated methods for high pressure freezing and correlative light-electron microscopy. *PLoS One* **5**, e9014.

Staugaitis, S. M., and Trapp, B. D. (2009). NG2-positive glia in the human central nervous system. *Neuron Glia Biol.* **5**, 35–44.

Stolt, C. C., Rehberg, S., Ader, M., Lommes, P., Riethmacher, D., Schachner, M., Bartsch, U., and Wegner, M. (2002). Terminal differentiation of myelin-forming oligodendrocytes depends on the transcription factor Sox10. *Genes Dev.* **16**, 165–170.

Stuart, G. W., Vielkind, J. R., McMurray, J. V., and Westerfield, M. (1990). Stable lines of transgenic zebrafish exhibit reproducible patterns of transgene expression. *Development* **109**, 577–584.

Sun, C. K., Chu, S. W., Chen, S. Y., Tsai, T. H., Liu, T. M., Lin, C. Y., and Tsai, H. J. (2004). Higher harmonic generation microscopy for developmental biology. *J. Struct. Biol.* **147**, 19–30.

Suster, M. L., Kikuta, H., Urasaki, A., Asakawa, K., and Kawakami, K. (2009). Transgenesis in zebrafish with the tol2 transposon system. *Methods Mol. Biol.* **561**, 41–63.

Susuki, K., and Rasband, M. N. (2008). Molecular mechanisms of node of Ranvier formation. *Curr. Opin. Cell Biol.* **20**, 616–623.

Swoger, J., Muzzopappa, M., Lopez-Schier, H., and Sharpe, J. (2011). 4D retrospective lineage tracing using SPIM for zebrafish organogenesis studies. *J. Biophotonics* **4**, 122–134.

Takada, N., and Appel, B. (2010). Identification of genes expressed by zebrafish oligodendrocytes using a differential microarray screen. *Dev. Dyn.* **239**, 2041–2047.

Takada, N., Kucenas, S., and Appel, B. (2010). Sox10 is necessary for oligodendrocyte survival following axon wrapping. *Glia* **58**, 996–1006.

Taveggia, C., Thaker, P., Petrylak, A., Caporaso, G. L., Toews, A., Falls, D. L., Einheber, S., and Salzer, J. L. (2008). Type III neuregulin-1 promotes oligodendrocyte myelination. *Glia* **56**, 284–293.

Taveggia, C., Zanazzi, G., Petrylak, A., Yano, H., Rosenbluth, J., Einheber, S., Xu, X., Esper, R. M., Loeb, J. A., Shrager, P., Chao, M. V., Falls, D. L., Role, L., and Salzer, J. L. (2005). Neuregulin-1 type III determines the ensheathment fate of axons. *Neuron* **47**, 681–694.

Tawk, M., Araya, C., Lyons, D. A., Reugels, A. M., Girdler, G. C., Bayley, P. R., Hyde, D. R., Tada, M., and Clarke, J. D. (2007). A mirror-symmetric cell division that orchestrates neuroepithelial morphogenesis. *Nature* **446**, 797–800.

Tawk, M., Bianco, I. H., and Clarke, J. D. (2009). Focal electroporation in zebrafish embryos and larvae. *Methods Mol. Biol.* **546**, 145–151.

Thaxton, C., Pillai, A. M., Pribisko, A. L., Labasque, M., Dupree, J. L., Faivre-Sarrailh, C., and Bhat, M. A. (2010). In vivo deletion of immunoglobulin domains 5 and 6 in neurofascin (Nfasc) reveals domain-specific requirements in myelinated axons. *J. Neurosci.* **30**, 4868–4876.

Thisse, B., Heyer, V., Lux, A., Alunni, V., Degrave, A., Seiliez, I., Kirchner, J., Parkhill, J. P., and Thisse, C. (2004). Spatial and temporal expression of the zebrafish genome by large-scale in situ hybridization screening. *Methods Cell Biol.* **77**, 505–519.

Thummel, R., Burket, C. T., Brewer, J. L., Sarras Jr, M. P., Li, L., Perry, M., McDermott, J. P., Sauer, B., Hyde, D. R., and Godwin, A. R. (2005). Cre-mediated site-specific recombination in zebrafish embryos. *Dev. Dyn.* **233**, 1366–1377.

Tolar, L. A., and Pallanck, L. (1998). NSF function in neurotransmitter release involves rearrangement of the SNARE complex downstream of synaptic vesicle docking. *J. Neurosci.* **18**, 10250–10256.

Topilko, P., Schneider-Maunoury, S., Levi, G., Baron-Van Evercooren, A., Chennoufi, A. B., Seitanidou, T., Babinet, C., and Charnay, P. (1994). Krox-20 controls myelination in the peripheral nervous system. *Nature* **371**, 796–799.

Trotter, J., Karram, K., and Nishiyama, A. (2010). NG2 cells: properties, progeny and origin. *Brain Res. Rev.* **63**, 72–82.

Urasaki, A., and Kawakami, K. (2009). Analysis of genes and genome by the tol2-mediated gene and enhancer trap methods. *Methods Mol. Biol.* **546**, 85–102.

Urnov, F. D., Rebar, E. J., Holmes, M. C., Zhang, H. S., and Gregory, P. D. (2010). Genome editing with engineered zinc finger nucleases. *Nat. Rev. Genet.* **11**, 636–646.

Voas, M. G., Glenn, T. D., Raphael, A. R., and Talbot, W. S. (2009). Schwann cells inhibit ectopic clustering of axonal sodium channels. *J. Neurosci.* **29**, 14408–14414.

Voas, M. G., Lyons, D. A., Naylor, S. G., Arana, N., Rasband, M. N., and Talbot, W. S. (2007). alphaII-Spectrin is essential for assembly of the nodes of Ranvier in myelinated axons. *Curr. Biol.* **17**, 562–568.

Wang, X. (2009). Cre transgenic mouse lines. *Methods Mol. Biol.* **561**, 265–273.

Wang, C., Popescu, D. C., Wu, C., Zhu, J., Macklin, W., and Wang, Y. (2010). In situ fluorescence imaging of myelination. *J. Histochem. Cytochem.* **58**, 611–621.

Wang, W. D., Wang, Y., Wen, H. J., Buhler, D. R., and Hu, C. H. (2004). Phenylthiourea as a weak activator of aryl hydrocarbon receptor inhibiting 2,3,7,8-tetrachlorodibenzo-*p*-dioxin-induced CYP1A1 transcription in zebrafish embryo. *Biochem. Pharmacol.* **68**, 63–71.

Watkins, T. A., Emery, B., Mulinyawe, S., and Barres, B. A. (2008). Distinct stages of myelination regulated by gamma-secretase and astrocytes in a rapidly myelinating CNS coculture system. *Neuron* **60**, 555–569.

White, R. M., Sessa, A., Burke, C., Bowman, T., LeBlanc, J., Ceol, C., Bourque, C., Dovey, M., Goessling, W., Burns, C. E., and Zon, L. I. (2008). Transparent adult zebrafish as a tool for in vivo transplantation analysis. *Cell Stem Cell* **2**, 183–189.

Wild, P., Krahenbuhl, M., and Schraner, E. M. (1989). Potency of microwave irradiation during fixation for electron microscopy. *Histochemistry* **91**, 213–220.

Wilson, S. W., Ross, L. S., Parrett, T., and Easter Jr., S. S. (1990). The development of a simple scaffold of axon tracts in the brain of the embryonic zebrafish. *Brachydanio rerio. Development* **108**, 121–145.

Woo, K., and Fraser, S. E. (1998). Specification of the hindbrain fate in the zebrafish. *Dev. Biol.* **197**, 283–296.

Woodhoo, A., and Sommer, L. (2008). Development of the Schwann cell lineage: from the neural crest to the myelinated nerve. *Glia* **56**, 1481–1490.

Woods, I. G., Lyons, D. A., Voas, M. G., Pogoda, H. M., and Talbot, W. S. (2006). nsf is essential for organization of myelinated axons in zebrafish. *Curr. Biol.* **16**, 636–648.

Wyatt, C., Ebert, A., Reimer, M. M., Rasband, K., Hardy, M., Chien, C. B., Becker, T., and Becker, C. G. (2010). Analysis of the astray/robo2 zebrafish mutant reveals that degenerating tracts do not provide strong guidance cues for regenerating optic axons. *J. Neurosci.* **30**, 13838–13849.

Yaksi, E., and Friedrich, R. W. (2006). Reconstruction of firing rate changes across neuronal populations by temporally deconvolved Ca2+ imaging. *Nat. Methods* **3**, 377–383.

Yoshida, M., and Macklin, W. B. (2005). Oligodendrocyte development and myelination in GFP-transgenic zebrafish. *J. Neurosci. Res.* **81**, 1–8.

Zannino, D. A., and Appel, B. (2009). Olig2+ precursors produce abducens motor neurons and oligodendrocytes in the zebrafish hindbrain. *J. Neurosci.* **29**, 2322–2333.

Zhou, Q., and Anderson, D. J. (2002). The bHLH transcription factors OLIG2 and OLIG1 couple neuronal and glial subtype specification. *Cell* **109**, 61–73.

Zhou, Q., Choi, G., and Anderson, D. J. (2001). The bHLH transcription factor Olig2 promotes oligodendrocyte differentiation in collaboration with Nkx2.2. *Neuron* **31**, 791–807.

Zonta, B., Tait, S., Melrose, S., Anderson, H., Harroch, S., Higginson, J., Sherman, D. L., and Brophy, P. J. (2008). Glial and neuronal isoforms of neurofascin have distinct roles in the assembly of nodes of Ranvier in the central nervous system. *J. Cell Biol.* **181**, 1169–1177.

Zorick, T. S., Syroid, D. E., Arroyo, E., Scherer, S. S., and Lemke, G. (1996). The transcription factors SCIP and Krox-20 mark distinct stages and cell fates in Schwann cell differentiation. *Mol. Cell. Neurosci.* **8**, 129–145.

CHAPTER 3

In vivo Analysis of White Adipose Tissue in Zebrafish

James E.N. Minchin[*] and John F. Rawls[*,†]

[*]Department of Cell and Molecular Physiology, University of North Carolina at Chapel Hill, Chapel Hill, North Carolina, USA

[†]Department of Microbiology and Immunology, University of North Carolina at Chapel Hill, Chapel Hill, North Carolina, USA

Abstract

White adipose tissue (WAT) is the major site of energy storage in bony vertebrates, and also serves central roles in the endocrine regulation of energy balance. The cellular and molecular mechanisms underlying WAT development and physiology are not well understood. This is due in part to difficulties associated with imaging adipose tissues in mammalian model systems, especially during early life stages.

METHODS IN CELL BIOLOGY, VOL 105

0091-679X/10 $35.00
DOI 10.1016/B978-0-12-381320-6.00003-5

The zebrafish (*Danio rerio*) has recently emerged as a new model system for adipose tissue research, in which WAT can be imaged in a transparent living vertebrate at all life stages. Here we present detailed methods for labeling adipocytes in live zebrafish using fluorescent lipophilic dyes, and for *in vivo* microscopy of zebrafish WAT.

I. Introduction

A. Biomedical Relevance of Adipose Tissue

The prevalence of obesity has reached epidemic proportions in developed as well as developing countries (Yach *et al.*, 2006). Furthermore, adult obesity is recognized as a major risk factor for the development of metabolic disease including insulin resistance, type II diabetes, and nonalcoholic fatty liver disease (Morse *et al.*, 2010). New methods for primary prevention and treatment of obesity are therefore urgently required to address this global public health crisis. Obesity develops when energy intake exceeds energy expenditure, resulting in increased storage of excess energy in adipose tissues (Rosen and Spiegelman, 2006). Adipose tissues also serve active roles in endocrine control of energy balance and thermogenic energy expenditure (Cypess and Kahn, 2010; Poulos *et al.*, 2010). Therefore, manipulation of adipose tissue structure and function is an attractive strategy to alleviate obesity and its associated morbidities. In this chapter, we discuss zebrafish as a novel model system in adipose tissue research, with emphasis on methods for fluorescent labeling and *in vivo* imaging of zebrafish adipose tissues.

B. Cellularity of White Adipose Tissue

The major constituent of adipose tissue, adipocytes, can be of two distinct lineages: white and brown. Brown adipocytes are thermogenic and help regulate body temperature by converting energy to heat through the action of the mitochondrial anion transporter uncoupling protein 1 (UCP1) (Cypess and Kahn, 2010). Although UCP1 homologs have been identified in zebrafish and other poikilothermic vertebrates (Hughes and Criscuolo, 2008; Jastroch *et al.*, 2005), zebrafish are not considered to possess brown adipose tissue; therefore, brown adipocytes will not be discussed further in this chapter. White adipocytes, within white adipose tissue (WAT), store surplus energy in the form of triacylglyceride (TG), and hydrolyze accumulated TG for use as a fuel source during times of nutrient deprivation (Redinger, 2009). They are present in bony vertebrates (e.g., fish, amphibians, reptiles, birds, and mammals), and WAT is considered the primary site of energy storage in these vertebrate taxa (Gesta *et al.*, 2007). Stored TG within mature white adipocytes (hereafter referred to as "adipocytes") is contained in a single, large (up to $\sim$100 μm in diameter) lipid droplet (LD) (Farese and Walther, 2009). Manipulation of WAT metabolism can induce whole-animal insulin resistance (Abel *et al.*, 2001), whereas removal of WAT can improve insulin sensitivity (Barzilai *et al.*, 1999; Carvalho *et al.*, 2005; Gabriely *et al.*, 2002). Therefore,

modification of WAT form and function may represent viable strategies for primary prevention of obesity and mitigation of associated metabolic disease.

Mammalian animal and cell culture systems have contributed the majority of our current information on WAT cell biology. However, the importance of WAT to commercial aquaculture and the increasing use of zebrafish as a biomedical model system have provided a rapidly expanding knowledge base on WAT in teleost fish (the largest subclass of Actinopterygii or ray-finned fish). All teleost species analyzed accumulate lipid within WAT (Figs. 1 and 2) (Flynn *et al.*, 2009; Imrie and Sadler, 2010; Sheridan, 1988; Song and Cone, 2007). Deposition and mobilization of lipid within teleost WAT is altered in response to nutritional manipulation (Fig. 2), suggesting the energy storage functions of WAT have been conserved between teleosts and mammals (Albalat *et al.*, 2007; Bellardi *et al.*, 1995; Company *et al.*, 1999; Flynn *et al.*, 2009; Imrie and Sadler, 2010; Om *et al.*, 2001). Furthermore, histological analysis reveals evolutionarily conserved morphological features of teleost adipocytes, including large cytoplasmic LDs, caveolae, and close association with capillaries (Flynn *et al.*, 2009; Imrie and Sadler, 2010). In addition, teleost adipocytes express genes associated with adipocyte differentiation (*fatty acid–binding protein 11a*, *fabp11a*; *peroxisome proliferator–activated receptor gamma*, *pparg*; and *CCAAT/enhancer-binding protein alpha*, *cebpa*) (Fig. 3) (Flynn *et al.*, 2009; Ibabe *et al.*, 2005; Imrie and Sadler, 2010; Oku and Umino, 2008; Vegusdal *et al.*, 2003), adipocyte lipolysis (*lipoprotein lipase*, *lpl*) (Oku *et al.*, 2006), and adipocyte endocrine function (*leptin*, *lep*; *adiponectin b, adipoql/acrp30*; and *adipsin*, *cfd*) (Imrie and Sadler, 2010; Vegusdal *et al.*, 2003; Nishio *et al.*, 2008). Like mammals, fish WAT also possesses a stromal–vascular fraction (SVF, defined as a heterogeneous population of stromal cells isolated by enzymatic digestion of WAT), which contains adipocyte progenitors (Rodeheffer *et al.*, 2008; Tang *et al.*, 2008; Todorcevic *et al.*, 2010; Vegusdal *et al.*, 2003). Gene expression studies on unfractionated zebrafish WAT suggest shared pathophysiologic pathways with mammalian WATs (Nishio *et al.*, 2008; Oka *et al.*, 2010). Together, the considerable functional, morphological, and molecular homology between teleost and mammalian WAT suggests new insights into WAT biology gained in the zebrafish system will be directly translatable to humans and other vertebrates.

Adipose tissue is not a single homogeneous tissue in mammals and fishes, but rather is distributed at specific anatomical locations throughout the body. In humans, the largest sites of WAT deposition are either subcutaneous (defined as between muscle and skin) or intra-abdominal (within the abdominal cavity) (Gesta *et al.*, 2007; Shen and Chen, 2008). Anatomically distinct depots display different molecular and physiological characteristics (Gesta *et al.*, 2006; Peinado *et al.*, 2010; Vidal, 2001; Vohl *et al.*, 2004), and have different risk associations for obesity-related disorders (Kissebah and Krakower, 1994). In particular, visceral adipose tissue (VAT, intra-abdominal WAT surrounding internal organs) is associated with more adverse risk factors than subcutaneous WAT (Despres, 1998; Fox *et al.*, 2007). Teleost WAT is also deposited in both subcutaneous and intra-abdominal positions, including VAT locations (Figs. 1 and 2A), raising the possibility that developmental programs responsible for WAT anatomy have been maintained during vertebrate evolution (Flynn *et al.*, 2009; Imrie and Sadler, 2010; Umino *et al.*, 1996; Weil *et al.*,

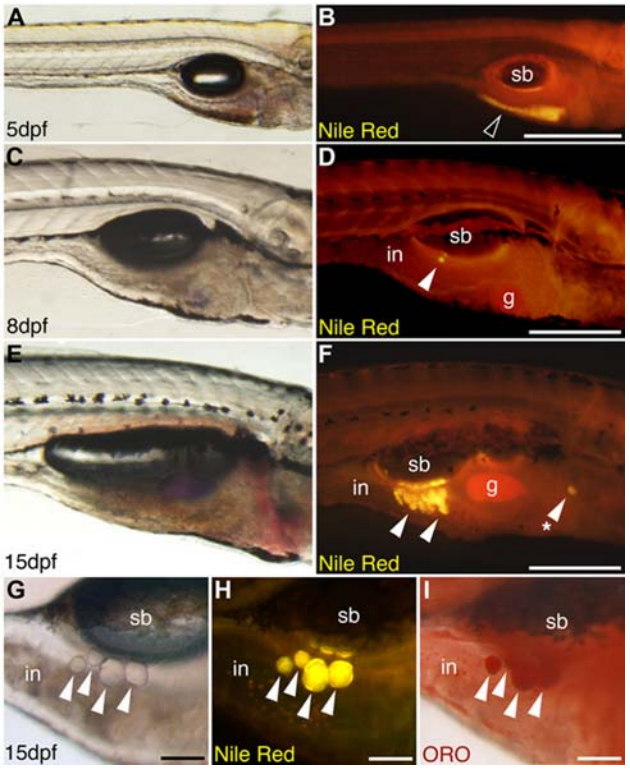

Fig. 1 Fluorescent lipophilic dyes reveal lipid droplet accumulation in live zebrafish. Live zebrafish at 5 dpf (3.6 ± 0.1 mm SL), 8 dpf (4.3 ± 0.1 mm SL), or 15 dpf (5.3 ± 0.1 mm SL) were stained with the fluorescent lipophilic dye Nile Red, and imaged on a fluorescence stereomicroscope using a GFP longpass emission filter set. Bright field (A, C, E, G) and corresponding fluorescence images (B, D, F, H) are shown. Nile Red fluorescence emission maxima are shifted to shorter wavelengths when incorporated into neutral lipid, so neutral lipid depots in yolk (black arrowhead in B) and adipocytes (white arrowheads in D, F, H) appear yellow-orange. (A and B) The yolk is the major neutral lipid depot in 5 dpf larvae. (C and D) After yolk resorption, the first adipocyte neutral lipid droplets form in the right viscera by 8 dpf in association with the pancreas. (E and F) By 15 dpf, adipocyte lipid droplets have increased in number within the viscera, and also appear in other locations (asterisk in F). An individual 15 dpf zebrafish stained with Nile Red (G and H) then stained with Oil Red O (ORO; I) reveals colocalization of Nile Red and ORO staining in neutral lipid droplets of visceral adipocytes (white arrowheads). Swim bladder (sb), gall bladder (g), and intestine (in) are indicated. Anterior is to the right, and dorsal to the top in all images. Scale bars: 400 μm (A and B), 300 μm (C–F), and 100 μm (G–I). This research was originally published in Journal of Lipid Research. Flynn et al. Ontogeny and nutritional control of adipogenesis in zebrafish (Danio rerio). J. Lipid Res. (2009) 50 (8):1641–1652. © The American Society for Biochemistry and Molecular Biology. (See color plate.)

2009). Recent work from our lab and others has provided a provisional nomenclature for zebrafish adipose depots (Fig. 2A) (Flynn *et al.*, 2009; Imrie and Sadler, 2010), but an expanded evaluation of adipose depot anatomy and heterogeneity is needed to comprehensively enumerate and categorize zebrafish adipose depots. Both

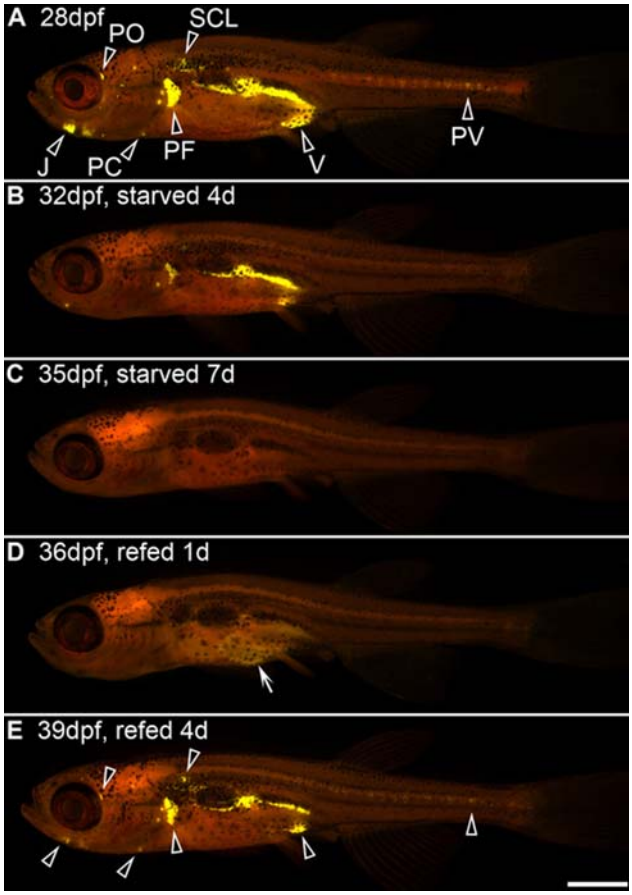

Fig. 2 Longitudinal analysis of zebrafish adipose depots can be used to visualize fat mobilization in response to starvation, and fat deposition in response to refeeding. Zebrafish were starved for 7 days beginning at 28 dpf (9.6 ± 0.4 mm SL) and then refed for 4 days. Individual zebrafish were stained with Nile Red and imaged daily using a fluorescence stereomicroscope with a GFP longpass emission filter set to monitor neutral lipid deposits (black arrowheads in A and E). Panels A–E depict an individual representative animal. (A) Zebrafish fed normally through 28 dpf store neutral lipid in multiple salient adipose depots, including visceral (V), pectoral fin plate (PF), pericardial (PC), jaw (J), perivertebral (PV), periorbital (PO), and subcutaneous lateral (SCL) depots. Note that zebrafish begin depositing fat in additional adipose depots [e.g., subcutaneous dorsal (SCD), subcutaneous ventral (SCV), and at the base of fins] at subsequent developmental stages (Imrie and Sadler, 2010; J. Minchin, unpublished). (B) When starved for 4 days, neutral lipid depots were reduced in all locations, although the larger visceral and pectoral fin plate depots were the last to be exhausted. (C) After 7 days of starvation, all neutral lipid depots were depleted. (D) Refeeding for 1 day was sufficient to form transient neutral lipid deposits in the intestine (white arrow in D), and refeeding for 4 days was sufficient to reestablish neutral lipid depots in the same locations as before starvation (black arrowheads in E and A). Anterior is to the left, and dorsal to the top in all images. Scale bar: 1 mm. This research was originally published in Journal of Lipid Research. Flynn et al. Ontogeny and nutritional control of adipogenesis in zebrafish (Danio rerio). J. Lipid Res. (2009) 50(8):1641–1652. © The American Society for Biochemistry and Molecular Biology. (For interpretation of the references to color in this figure legend, the reader is referred to the web version of this book.)

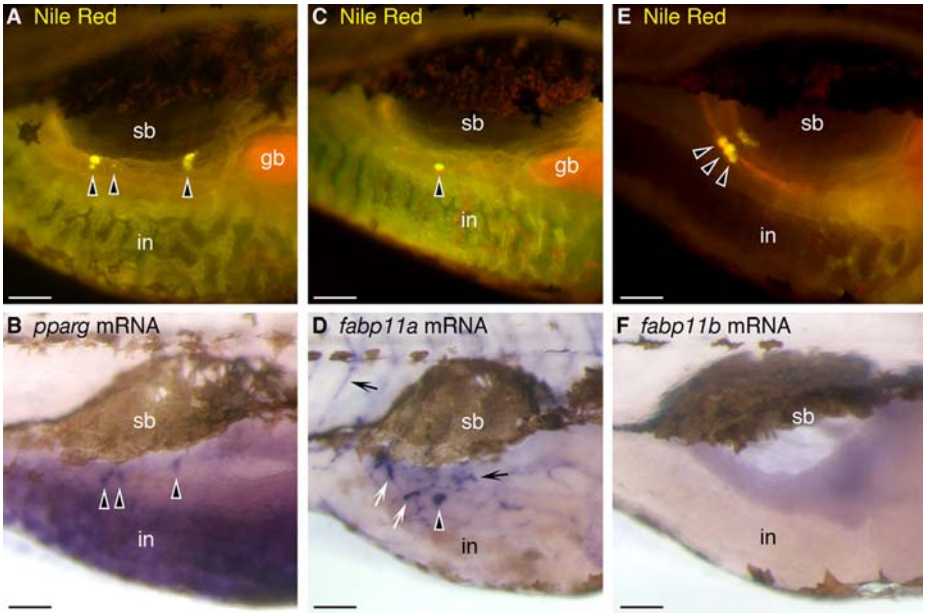

Fig. 3 Coupling of fluorescent lipophilic dyes with *in situ* hybridization reveals expression of *pparg* and *fabp11a* mRNA in zebrafish visceral adipocytes. Individual zebrafish were stained with Nile Red at 15 dpf (5.3 ± 0.1 mm SL), imaged using a fluorescence stereomicroscope with a GFP longpass emission filter set, and then processed for whole-mount *in situ* hybridization (WISH) using riboprobes directed against zebrafish *pparg*, *fabp11a*, or *fabp11b* mRNA. Cells labeled by WISH stain purple, in contrast to the brown melanin pigment contained within melanophores. Nile Red and WISH staining patterns were compared to detect colocalization. Whole-mount images from the trunk of the same individuals are shown. Both *fabp11a* and *pparg* mRNA colocalize with visceral neutral lipid droplets associated with the pancreas (black arrowheads). *fabp11a* mRNA is also observed in nearby cells lacking neutral lipid droplets (white arrows in D) and blood vessels (black arrows in D), while *pparg* mRNA is also found in the intestinal epithelium (B). In contrast, visceral adipocytes did not express *fabp11b* (F). Swim bladder (sb), gall bladder (gb), and intestine (in) are indicated. Dorsal is to the top and anterior is to the right in all images. Scale bars: 100 μm. This research was originally published in Journal of Lipid Research. Flynn et al. Ontogeny and nutritional control of adipogenesis in zebrafish (Danio rerio). J. Lipid Res. (2009) 50(8):1641–1652. © The American Society for Biochemistry and Molecular Biology. (See color plate.)

terminally differentiated adipocytes and the SVF within distinct WAT locations contribute to the diverse physiologies of WAT (Peinado *et al.*, 2010; Wajchenberg, 2000), although the molecular and cellular basis for disease risk associations based on WAT anatomic location is unclear. Therefore, it is apparent that investigation of multiple sites of WAT deposition within whole animals is desperately needed.

II. Rationale

Current analysis of WAT is predominantly conducted after fixation and histological sectioning of adipose tissues. This often results in incomplete preservation of

WAT architecture and limited information on cellular interactions and dynamics (Xue *et al.*, 2010). In addition, imaging of whole-animal WAT deposition in mammals is technically challenging, is typically restricted to low-resolution views, and has only been undertaken on a limited scale (Shen and Chen, 2008). Moreover, most of our knowledge of mammalian adipose tissues is derived from adult stages, due in part to the difficulty of accessing adipose tissues during the gestational stages when they initially develop (Ailhaud *et al.*, 1992). As a consequence, outstanding questions regarding the spatial and temporal dynamics of *in vivo* adipose tissue formation and growth remain understudied. Innovative approaches have been developed to address these gaps in our knowledge, such as high-resolution imaging of resected adipose tissue cultured *in vitro* (Nishimura *et al.*, 2007), and *in vivo* imaging of adipocyte precursors introduced into mice fitted with an implanted coverslip (Nishimura *et al.*, 2008). However, these approaches do not permit imaging of adipose tissues within the intact physiological context of a living organism. Mathematical modeling has also been used to predict *in vivo* mechanisms of adipose tissue growth, but these models remain largely untested due to a paucity of suitable *in vivo* model systems (Jo *et al.*, 2009). There is, therefore, a pressing need for new experimental platforms for image analysis of WAT formation and function in live animals.

The features of the zebrafish system are especially well suited to meet these needs. Zebrafish develop externally and are optically transparent from fertilization to the onset of adulthood, permitting *in vivo* imaging of dynamic cellular events during adipose tissue formation and growth. This provides new opportunities to investigate the earliest stages of WAT morphogenesis (Fig. 1), a process poorly understood in mammals with potentially high relevance for obesity and metabolic disease. The small size of the zebrafish also facilitates whole-animal imaging of multiple adipose depots (Fig. 2), unlike mammalian systems in which specific adipose depots are difficult to access. Real-time imaging of living adipose tissues is also possible in the zebrafish, enabling observation of molecular and cellular events over short time scales. Furthermore, the amenability of the zebrafish to *in vivo* imaging permits longitudinal imaging of WAT in individual animals, which can be used to mitigate complications from interindividual variation in adiposity (Fig. 2). As described above, the identification of extensive conserved homologies between teleost and mammalian adipose tissue suggests that insights gained in the zebrafish system could be applicable to humans and other vertebrates.

These diverse imaging strategies require robust methods for labeling the cellular constituents of WAT in live animals. In this chapter, we present methods for labeling adipocytes in zebrafish using fluorescent lipophilic dyes that specifically incorporate into adipocyte LDs, and for imaging adipose tissues in live zebrafish using stereomicroscopy and confocal microscopy. These methods can be used in combination with transgenic zebrafish expressing fluorescent proteins (FP) in specific WAT cell types to reveal the dynamic cellular interactions underlying WAT formation and function.

III. Materials

- Adult zebrafish. Any strain of adult zebrafish can be used for this protocol. Zebrafish lines may be obtained from the Zebrafish International Resource Center (ZIRC, http://zebrafish.org/zirc). All experiments should be performed in accordance with protocols approved by the user's Institutional Animal Care and Use Committee.
- Large nets (Aquatic Eco-Systems, cat. no. AN8).
- Zebrafish aquarium (system) water.
- Breeding tanks (Laboratory Product Sales, cat. no. T233792).
- Plastic tea strainer, 7 cm (Comet Plastics, cat. no. strainer 0).
- Scienceware pipette pump (Fisher Scientific, cat. no. 13-683C).
- Wide-bore Pasteur pipettes (Kimble Chase, cat. no. 63A53WT).
- 100 × 15 mm Petri dishes (Fisher Scientific, cat. no. 0875712).
- Methylene blue stock solution (0.01%) (Sigma, cat. no. M9140). Dissolve 50 mg methylene blue in 500 mL distilled water (dH_2O). Dilute this stock solution 1:200 in fresh zebrafish aquarium system water to prevent growth of bacteria and mold during embryonic development.
- dH_2O.
- Fluorescence stereomicroscope (e.g., Leica MZ 16F or M205 FA) equipped with an eyepiece graticule and the following Leica emission filter sets: GFP2 (510LP) for the green fluorescent lipophilic dyes (i.e., BODIPY 505/515, 500/510, NBD-Cholesterol, BODIPY FL C5, and the yellow-orange dye, Nile Red); YFP (535-630BP) for the yellow, orange, and orange-red dyes (i.e., BODIPY 530/550, 558/568, and Cholesteryl BODIPY 576/589); and Texas Red (610LP) for HCS LipidTOX Red/Deep Red. See Table I for a full description of fluorescent lipophilic dyes. Equivalent fluorescence stereomicroscopes and filter sets can be used from alternative manufacturers.
- Air incubator set at 28.5 °C (Powers Scientific Inc., cat. no. IS33SD).
- Two-liter fish tanks (Marine Biotech, cat. no. 10198-00A).
- Assorted mesh drainage plugs for 2-L fish tanks (Marine Biotech, 425 μm, cat. no. 10222-01A; 600 μm, cat. no. 10222-02A; 1600 μm, cat. no. 10222-03A; 4000 μm, cat. no. 10222-04A).
- Brine shrimp (*Artemia franciscana*) cysts (Utah strain; Aquafauna Bio-Marine Inc., cat. no. ABMGSL-TIN90). Detailed brine shrimp hatchery methods are included in *The Zebrafish Book* (Westerfield, 2000). Briefly, 80 mL of brine shrimp cysts is momentarily immersed in bleach before rinsing with system water. After rinsing, the cysts are added to 12 L of system water supplemented with 10 g sodium bicarbonate and 155 g sodium chloride. The cysts are aerated vigorously for 24 h, under continuous light. The hatched brine shrimp are filtered through a 105-μm mesh sieve and diluted in 2 L of system water. Although brine shrimp hatching rates can vary, we typically find this procedure generates $\sim 4 \times 10^7$ brine shrimp per 24 h.

Table I
Lipophilic fluorescent dyes for staining lipid droplets in zebrafish

Color	Name	IUPAC name	Cat. no.[a]	Solvent	Stock concentration	Working concentration[b]	Absorption/emission maxima (nm)[c]	Additional notes[d]
Green	BODIPY 500/510	4,4-Difluoro-5-methyl-4-bora-3a,4a-diaza-*s*-indacene-3-dodecanoic acid	D3823	Chloroform: MeOH	1 mg/mL	0.5 μg/mL (2,000×)	500/510 (use filter sets appropriate for Alexa Fluor 488)	Very bright LD stain, weak gall bladder stain
Green	BODIPY 505/515	4,4-Difluoro-1,3,5,7-tetramethyl-4-bora-3a,4a-diaza-*s*-indacene	D3921	DMSO	1 mg/mL	1 μg/mL (1,000×)	505/515 (use filter sets appropriate for Alexa Fluor 488)	Very bright LD stain, bright gall bladder stain, bright intestine stain, stains blood plasma, significant fluorescence emission in red channel after 488 nm laser excitation
Green	BODIPY FL C5	4,4-Difluoro-5,7-dimethyl-4-bora-3a,4a-diaza-*s*-indacene-3-pentanoic acid	D3834	Chloroform: MeOH	0.5 μg/mL	0.25 ng/mL (2,000×)	503/512 (use filter sets appropriate for Alexa Fluor 488)	Weak LD stain, bright gall gladder stain, bright intestine stain
Green	NBD-Cholesterol	22-(*N*-(7-Nitrobenz-2-oxa-1,3-diazol-4-yl)amino)-23,24-bisnor-5-cholen-3β-ol	N1148	Chloroform: MeOH	5 μg/mL	0.5 ng/mL (10,000×)	Absorption/emission maxima are dependent on solvent and environment. However, we use filter sets appropriate for Alexa Fluor 488	Bright LD stain, weak gall bladder stain
Yellow	BODIPY 530/550	4,4-Difluoro-5,7-diphenyl-4-bora-3a,4a-diaza-*s*-indacene-3-dodecanoic acid	D3832	Chloroform: MeOH	1 mg/mL	10 μg/mL (100×)	530/550 (use filter sets appropriate for Alexa Fluor 532)	Very weak LD stain, high non-LD background
Yellow-orange	Nile Red	9-Diethylamino-5H-benzo [alpha]phenoxazine-5-one	N1142	Acetone	1.25 mg/mL	0.5 μg/mL	510/580 (excite with argon 514 nm laser, collect emission with a longpass 530 filter)[e]	Very bright LD stain, red phospholipid background stain
Orange	BODIPY 558/568	4,4-Difluoro-5-(2-thienyl)-4-bora-3a,4a-diaza-*s*-indacene-3-dodecanoic acid	D3835	Chloroform: MeOH	1 mg/mL	2 μg/mL (500×)	558/568 (use filter sets appropriate for Alexa Fluor 546)	Very bright LD stain, very bright non-LD background

(Continued)

Table I *(Continued)*

Color	Name	IUPAC name	Cat. no.[a]	Solvent	Stock concentration	Working concentration[b]	Absorption/emission maxima (nm)[c]	Additional notes[d]
Red-orange	Cholesteryl BODIPY 576/589	Cholesteryl 4,4-difluoro-5-(2-pyrrolyl)-4-bora-3a,4a-diaza-*s*-indacene-3-undecanoate	C12681	Chloroform: MeOH	1 mg/mL	10 μg/mL (100×)	576/589 (use filter sets appropriate for Alexa Fluor 568)	Weak LD stain
Red	HCS LipidTOX RED	–	H34476	DMSO	–	(5000×)	577/609 (use filter sets appropriate for Alexa Fluor 594 or Texas Red)	Very bright LD stain, bright gall bladder stain, stains blood plasma
Far-red	HCS LipidTOX Deep Red	–	H34477	DMSO	–	(5,000×)	637/655 (use filter sets appropriate for Alexa Fluor 647 or Cy5 dye)	Very bright LD stain, bright gall bladder stain, stains blood plasma

[a] All catalog numbers (cat. no.) are from Invitrogen.
[b] Dilution of stock solution to achieve working concentration is in parentheses.
[c] Alexa Fluor dyes are from Invitrogen.
[d] Staining patterns correspond to wild-type fish raised under the husbandry protocols described here. These staining patterns could potentially be altered as a function of fish genotype, dietary status, and other exposures.
[e] Nile Red bound to phospholipid bilayer has absorption/emission maxima of ~550/640 nm.

- Sodium bicarbonate (Aquatic Eco-Systems, cat. no. SC12).
- Sodium chloride (Fisher Scientific, cat. no. S96860).
- Brine shrimp net (Aquatic Eco-Systems, cat. no. BSN1).
- Fifteen-milliliter conical tubes (polystyrene or polypropylene) (Becton Dickinson, cat. no. 35-2099).
- Plastic transfer pipettes (Samco Scientific, cat. no. 225).
- Fluorescent lipophilic dyes (see Table I for details). Chloroform:methanol (MeOH) (2:1) is typically used as a solvent when making stock solutions of lipophilic dyes. However, chloroform:MeOH cannot be added directly to system water containing zebrafish. Therefore, the desired quantity of chloroform:MeOH stock solution containing lipophilic dye is air dried in a 1.6-mL microcentrifuge tube for ~10 min before being resuspended in 10 μL of 100% ethanol (EtOH). The EtOH/dye solution can be added directly to system water containing zebrafish. Alternatively, dimethyl sulfoxide (DMSO) or acetone can be used as solvents when making stock solutions, and can be added directly to system water containing zebrafish. However, use of DMSO and acetone as solvents is not advised as the resulting stock solution is less stable over long periods of storage. Stock solutions of fluorescent lipophilic dyes are kept in the dark at −20 °C.
- Chloroform (Fisher Scientific, cat. no. BP1145-1).
- MeOH (VWR, cat. no. BDH1135-4LP).
- EtOH (Decon Labs, Inc., cat. no. 2716).
- DMSO (Fisher Scientific, cat. no. D128-1).
- Acetone (Mallinckrodt Chemicals, cat. no. 2440-02).
- Ethyl 3-aminobenzoate methanesulfonate salt (tricaine or MS222) stock solution (24×) (Sigma, cat. no. A5040-110G). Combine 0.8 g of tricaine, 4.2 mL of 1 M Tris (pH 9.0), and 195.8 mL of dH_2O. Adjust pH to between 7.0 and 7.5, and store at 4 °C. Anesthetizing concentration is 1×, and euthanizing concentration is 5×.
- Methyl cellulose (4%) (Sigma, cat. no. MO387-100G). Dissolve 4 g methyl cellulose in 100 mL dH_2O. Make 1-mL aliquots in 1.6-mL microcentrifuge tubes and freeze at −20 °C.
- Low-melting-point (LMP) agarose (1%) (Fisher Scientific, cat. no. BP165-25). Dissolve 1 g LMP agarose in 100 mL of 1× phosphate buffered saline (PBS). Make 1-mL aliquots in 1.6-mL microcentrifuge tubes and freeze at −20 °C.
- 1.6-mL microcentrifuge tubes (Genesee Scientific, cat. no. 22-282A).
- Heat blocks set at 65 and 42 °C (Denville Scientific, Inc., D1100).
- Twenty-four-well plastic culture plates (Greiner Bio-One, cat. no. 662160).
- Metal dissection probe (Fine Science Tools, cat. no. 10140-01).
- Thirty-five-millimeter Petri dish with glass coverslip as base (MatTek Corp., cat. no. P35G-1.5-10-C).
- Thirty-five-millimeter Petri dish (Becton Dickinson, cat. no. 351008).
- Epinephrine stock solution (100 mg/mL) (Sigma, cat. no. E4375-5G). Dissolve 1 g epinephrine powder in 10 mL of dH_2O. Store at 4 °C in the dark. Add 3 mL of stock solution to 30 mL system water (10 mg/mL final concentration) containing fish for 5 min to contract melanosomes (Rawls and Johnson, 2003).

- Paraformaldehyde (PFA) stock solution (4%) (Acros, cat. no. 30525-89-4). Dissolve 4 g PFA powder in 99 mL prewarmed 1× PBS. Once cooled, add 1 mL of DMSO.
- PBS stock solution (25×). Dissolve 200 g sodium chloride, 5 g potassium chloride, 36 g sodium dihydrogen phosphate, and 6 g monopotassium phosphate in 1 L dH_2O and autoclave.
- Tween-20 (Fisher Scientific, cat. no. BP337-500).
- Laser scanning confocal microscope (e.g., Zeiss LSM 510), equipped with argon 488 nm, HeNe1 543 nm, and HeNe2 633 nm excitation lasers. Other platforms, such as spinning disk confocal and multiphoton fluorescence microscopes, can also be used.

IV. Methods

A. Obtaining Zebrafish Embryos

1. *Day* 1, duration ∼60 min. The day before embryos are required, use a large net to place suitable breeding pairs of adult zebrafish in specialized breeding tanks filled with fresh system water. Adults remain in breeding tanks overnight and typically spawn once the aquarium lights turn on the following morning. Be sure to label each breeding tank with the genotype and stock number(s) of the respective breeding pair.

   Optional: Specific fluorescent lipid probes can be used in conjunction with transgenic zebrafish lines expressing FP to facilitate cell localization studies (see Table I for excitation/emission properties of lipid probes). If required, obtain transgenic zebrafish from ZIRC (see Section III).

2. *Day* 2, duration ∼60 min. To collect fertilized embryos, remove adult zebrafish to a different tank. Maintain labeling system of adult fish to track parentage of embryos. Collect embryos by pouring through a tea strainer. Clean embryos by rinsing multiple times in fresh system water, and dispense groups of 20–40 embryos into each 100-mm Petri dish filled with 30 mL of fresh system water. View embryos on a light stereomicroscope and remove unfertilized embryos using a wide-bore Pasteur pipette and pipette pump. Place fertilized embryos within an air incubator at 28.5 °C.

   Optional: If natural breeding is unsuccessful, embryos can alternatively be generated by *in vitro* fertilization (or "squeezing") using established protocols (Westerfield, 2000).
   Optional: Methylene blue stock solution can be added to system water (0.01% final concentration) to inhibit fungal and bacterial growth during zebrafish development.
   Optional: If using FP-expressing transgenic zebrafish, use a fluorescence stereomicroscope to screen for fluorescent embryos at a suitable developmental stage when FP expression is known to be observed. This procedure is

preferentially done during embryonic stages to minimize rearing and feeding of unnecessary nontransgenic fish.

B. Rearing Zebrafish to Postembryonic Stages in Preparation for Fluorescent Lipid Staining

1. *Days* 2–6; duration 15–30 min/day. Continue to raise embryos/larvae at 28.5 °C in 100-mm Petri dishes until 5 days postfertilization (dpf). During these first 5 days of development, check daily for, and remove, dead embryos using a wide-bore Pasteur pipette and pipette pump (dead embryos are typically white in appearance). In addition, replace ∼50% of water with fresh system water once every 2–3 days using a plastic transfer pipette. Zebrafish do not need exogenous nutrition until 5 dpf; therefore, do not feed during this period.
2. *Day* 6; static tank stage; duration ∼15 min. At 5 dpf, transfer ∼40 larvae to 1 L of fresh system water contained within a clean 2-L tank and fitted with 425-μm mesh drainage plugs.
3. *Day* 6 onwards; duration ∼15 min/day. From 5 dpf, and once larvae are transferred to 2-L tanks, feeding can commence. It is routine procedure for laboratory zebrafish facilities to feed young larvae (typically 5–10 dpf) either a *Paramecium multimicronucleatum* diet (http://zfin.org/zf_info/zfbook/chapt3/3.3.html) or commercial powdered food (reviewed in Lawrence, 2007). Although these diets can support adipogenesis in developing zebrafish, we observe increased larval survival rate and improved water quality with a diet consisting exclusively of live brine shrimp from 5 dpf (see Section IV). We feed each 2-L tank containing 20–40 fish with 0.5 mL of ∼1000 brine shrimp/mL concentration once per day. Dead brine shrimp and debris collecting at the bottom of the tank should be removed every few days with a plastic transfer pipette.
4. *Day* 9; duration ∼15 min. At 8 dpf, add 1 L of fresh system water to the existing 1 L containing larvae in each 2-L tank.
5. *Day* 12; low-flow tank stage; duration ∼15 min/day. At 12 dpf, the 2-L tanks are placed on slow running system water with fine mesh (600 μm) drainage plugs. It is important to clean the drainage plugs every day to ensure unobstructed water flow. Continue feeding each tank with 0.5 mL of ∼1000 brine shrimp/mL concentration once per day.
6. *Day* 16; duration 15 min/day. Increase strength of water flow from 15 dpf. It is important to continue swapping mesh drainage plugs for ones with a larger mesh (typically 1600 and 4000 μm can be used) concomitant with growth of larvae/juveniles. Continue feeding each tank with 0.5 mL of ∼1000 brine shrimp/mL concentration once per day.
7. Zebrafish that are fed using this protocol begin storing neutral lipid in adipocytes from ∼10 to 15 dpf (Fig. 1). However, once independent feeding initiates (5 dpf), subsequent larval and juvenile growth rates vary considerably. Physical measurements such as standard length (SL; defined as distance from snout tip to caudal peduncle) provide more accurate metrics of postembryonic zebrafish development and growth (Parichy *et al.*, 2009). Adipose tissue development in wild-type

zebrafish is robustly correlated with SL (Imrie and Sadler, 2010; J. Minchin, unpublished). SL can be measured directly on live larvae/juveniles using a stereomicroscope equipped with an eyepiece graticule. Alternatively, the specimen can be imaged on a stereomicroscope using known magnification, and subsequently measured using suitable image analysis software (e.g., ImageJ or Adobe Photoshop).

8. *Day* 16 onwards; duration 5 min. To undertake a lipid stain at a selected time point, larvae/juveniles must be transferred to a smaller vessel such as a 15-mL conical tube. Larval and juvenile zebrafish are very delicate; therefore, during this step, it is essential to handle them with care. To transfer larvae/juveniles from 2-L tanks to a suitable vessel, fill a clean 2-L tank with system water. Then place a brine shrimp net into the freshly prepared tank of system water, and gently pour your larvae/juvenile sample into the net partially submerged within the freshly prepared tank. Pour carefully so larvae are not buffeted by water, as vigorous pouring will damage the fish. Individually remove each larvae/juvenile from the net while partially submerged in the tank of system water using a plastic transfer pipette, and place in a 15-mL conical tube filled with an appropriate volume of fresh system water.

C. Staining Live Zebrafish Larvae/Juveniles with Fluorescent Lipophilic Dyes

A distinguishing feature of white adipocytes in fish as well as mammals is the presence of large cytoplasmic neutral LDs that consist largely of TG (Tobias and Farese, 2009). As described below, these characteristic adipocyte organelles can be unambiguously labeled in live zebrafish using any of several commercially available fluorescent lipophilic probes (see Table I).

1. Duration 5 min. Wash unanesthetized larvae/juveniles in fresh system water three times at room temperature. This is accomplished by removing 80% of the system water from the 15-mL conical tube with a transfer pipette before adding fresh system water. This step removes debris included with larvae. After the final wash, adjust volume of each 15-mL conical tube containing zebrafish to 5 mL with fresh system water.
2. Duration 5 min. Add lipid probe, at appropriate concentration (see Table I), to 5 mL fresh system water containing larvae/juveniles. Lipid probe dissolved in DMSO can be added directly to system water. However, lipid probe dissolved in chloroform:MeOH must first be dried by chloroform:MeOH evaporation, and then resuspended in 100% EtOH (see Section IV). It is important to minimize the volume of 100% EtOH added to system water containing specimen; therefore, we typically add 10 μL to 5 mL system water containing fish.
3. The experimental procedure for zebrafish LD staining varies depending on the lipid probe used. Based on fluorescent lipophilic dyes that we have used for staining LDs in zebrafish (see Table I), we have devised two main protocols (see Fig. 4 for details). Protocol 1 should be followed for BODIPY dyes (both nonpolar and fatty acid/cholesteryl conjugates) as these require extensive wash steps

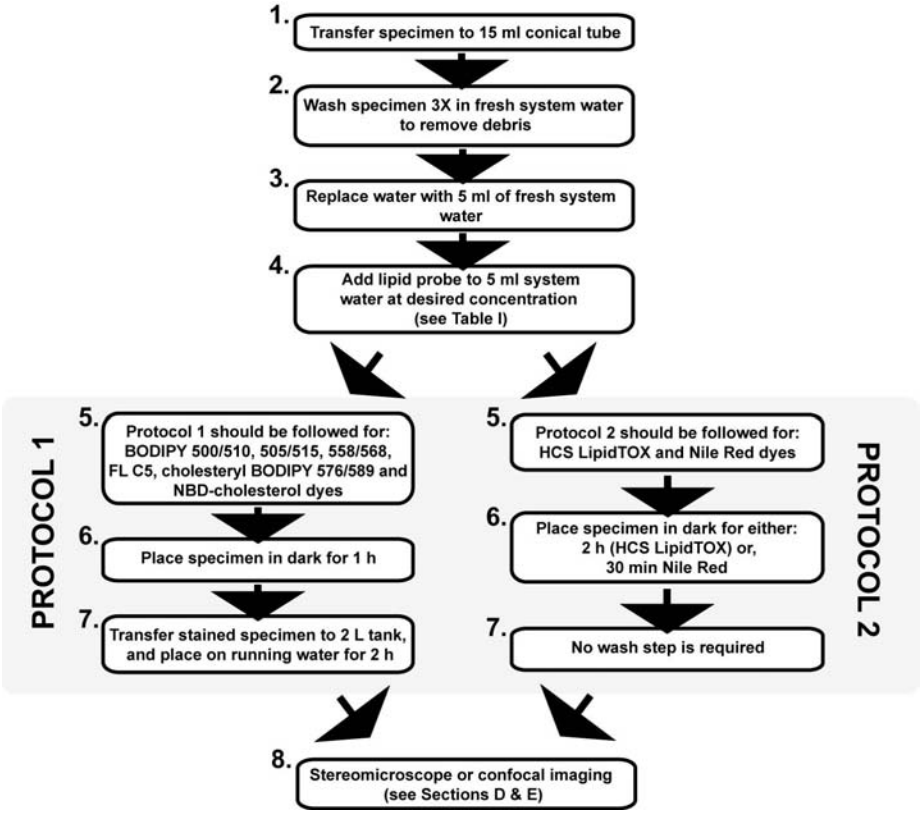

Fig. 4 Flow diagram depicting protocols for staining zebrafish with fluorescent lipophilic dyes. Protocol 1 includes wash steps and should be used for BODIPY dyes. Protocol 2 does not contain wash steps and should be used for HCS LipidTOX and Nile Red dyes. See Table I for information on lipophilic dyes.

to reduce background staining. Protocol 2 should be followed for Nile Red and HCS LipidTOX stains as these dyes do not require a wash step. Subsequent to the lipid staining protocol, all specimens are imaged using standard techniques regardless of protocol followed (see Sections D and E).

Optional: It is common for ingested food and bile within the intestine to autofluoresce. In order to reduce these unwanted fluorescence signals, fish can be starved overnight to "clear" the intestine of food before beginning the lipid stain.

D. *In vivo* Imaging of Neutral Lipid on a Fluorescence Stereomicroscope

Imaging fluorescently labeled neutral lipid on a stereomicroscope allows for relatively high-throughput analysis of whole-animal fat deposition (Figs. 1 and 2).

Using the following imaging procedure, it is possible to acquire multiple images of distinct adipose depots in an individual fish within 5 min. Therefore, stereoscopic imaging of fluorescently stained zebrafish adipose tissues is suitably quick for use as a viable phenotyping assay during chemical or genetic screens for factors that influence lipid storage in adipose tissues.

To image and measure stained zebrafish, 1× tricaine is used as a standard anesthetic in zebrafish research. Embryonic and larval zebrafish are particularly amenable to dosing with 1× tricaine, and recovery after 72 h of anesthesia is commonplace. However, older larval (larger than ~7 mm SL), juvenile, and adult zebrafish have more difficulty recovering after tricaine anesthesia. Presumably this is due to an increasing requirement for gill respiration as the zebrafish grows due to increased body size and epidermal thickness, combined with the absence of active gill respiration while under tricaine anesthesia. The consequence of increased sensitivity to tricaine anesthesia is higher rates of death. We try to minimize exposure to tricaine by imaging as quickly as possible, and we increase animal number to compensate for any death that might occur.

1. Fill a 100-mm Petri dish with 30 mL of fresh system water and add 1.25 mL of 24× tricaine.
2. Place a 3 × 3 mm drop of 4% methyl cellulose at the center of a 100-mm Petri dish lid. Cover the 4% methylcellulose drop with system water containing 1× tricaine.
3. Transfer stained unanesthetized fish from 15-mL conical tube to fish water containing tricaine. Allow fish to sit in tricaine-containing system water for ~5 min, or until fish has symptoms of being under anesthesia (i.e., belly up swimming, reduced gill ventilation). Do not keep fish in tricaine for longer than required as this may impede recovery from anesthesia.
4. Immediately transfer anesthetized fish to Petri dish lid containing 4% methyl cellulose droplet. Gently position tail of larvae/juvenile in the methyl cellulose and orientate appropriately using a metal dissection probe. Do not completely embed specimen in 4% methyl cellulose as this increases likelihood of damaging fish when subsequently releasing it. In zebrafish, neutral lipid within adipocytes is first deposited in association with the pancreas at ~5 mm SL, which is asymmetrically located on the right-hand side of the visceral cavity of larvae/juveniles (Fig. 1) (Flynn *et al.*, 2009). Therefore, it is usually important to orient the specimen so the right-hand side is observable by the microscope objective.
5. Once the fish is positioned correctly, measure SL using an eyepiece graticule.

Optional: The zebrafish pigment pattern can obscure imaging of adipose depots. Before imaging, the confounding effects of the zebrafish pigment pattern can by reduced by treating animals with 10 mg/mL epinephrine for 5 min to contract the melanosomes into the center of the cell (Rawls and Johnson, 2003). This step is not optimal as epinephrine is known to stimulate lipolysis in adipocytes (Fain and Garcija-Sainz, 1983); however, our imaging procedure is sufficiently brief to prevent any salient effect on fat storage. Furthermore, for imaging visceral/pancreatic

adipose tissue, melanin is usually not a problem during larval and early juvenile stages (i.e., through ~8 mm SL). Alternative solutions include using zebrafish mutants that fail to develop pigment cells, but the potential effects of these mutations on adipose development and function have not been explored. Although inhibition of melanin synthesis during zebrafish development can be achieved by treatment with phenylthiourea (PTU), this is not practical for fish kept in tanks maintained on flowing recirculating water.

E. *In vivo* Imaging of Neutral Lipid on a Confocal Microscope

Although considerably more time consuming than stereomicroscopic analysis, imaging fluorescently stained neutral lipid by confocal microscopy provides much greater resolution. Furthermore, if FP transgenic lines are used, exact colocalization of adipocyte LDs with fluorescent cell types of interest is achievable (Fig. 5). The following protocol takes ~35 min per zebrafish imaged (based on a 15-min Z-stack); however, exact timing will vary depending on length of confocal scan taken:

1. Anesthetize fish in tricaine (see Section D).
2. Measure SL of each fish to be imaged (see Section B7).
3. Thaw 1% LMP agarose aliquots by placing 1-mL aliquot at 65 °C until completely melted. Cool LMP agarose to 42 °C using a heat block or water bath for 1 h until needed.

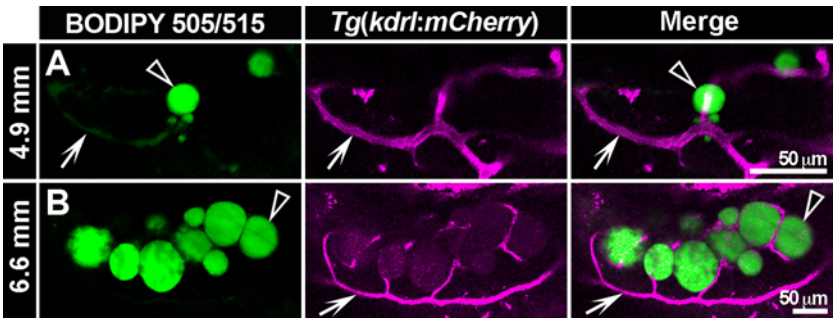

Fig. 5 Confocal imaging of live zebrafish stained with BODIPY 505/515 fluorescent lipophilic dye reveals close interplay between lipid droplets and the vascular system in visceral adipose tissue. *Tg(kdrl:mCherry)* transgenic zebrafish express mCherry fluorescent protein specifically in endothelial cells of the vasculature (Jin *et al.*, 2005). Live *Tg(kdrl:mCherry)* transgenic zebrafish were stained with BODIPY 505/515 according to protocol 1 (see Fig. 4) at 4.9 mm SL (~14 dpf) and 6.6 mm SL (~18 dpf). Stained zebrafish were imaged on a Zeiss LSM510 confocal microscope using filter settings for mCherry and BODIPY 505/515 (see Table I). Individual optical sections from a Z-stack are presented in this figure. At 4.9 mm, LDs (arrowheads) are small and loosely associated with vasculature (arrows, A). At 6.6 mm, LDs (arrowheads) are larger and interspersed with mCherry^{+} vasculature (arrows, B). *Note*: BODIPY 505/515 has weak fluorescence in the red channel (B), and also labels lipid in vasculature (A). Scale bars: 50 µm. (For interpretation of the references to color in this figure legend, the reader is referred to the web version of this book.)

Note: For confocal imaging, there are multiple methods for stably mounting zebrafish in 1% LMP agarose during imaging. Depending on microscope design (inverted or upright) and the type of objective to be used (air, immersion, or dipping), we have found the following methods for mounting to be most successful (see Fig. 6):

Upright confocal microscopes. It is preferential to use a water dipping objective. First, deposit a 3 × 3 mm droplet of 4% methyl cellulose in the center of a 35-mm Petri dish. Anesthetize larvae/juveniles in 1× tricaine (see Section D), transfer to methyl cellulose droplet, and roughly orientate. Remove excess system water with plastic transfer pipette and replace with 1% LMP agarose cooled to 42 °C. Using a stereoscope, quickly orientate sample into correct position with a metal dissecting probe. Continuously observe specimen as LMP solidifies to ensure correct positioning. It is important for specimen to be only lightly covered by LMP agarose. If too much LMP is added, it will prevent focusing the objective to regions deep within zebrafish adipose tissue. Once the LMP agarose has solidified, add ∼2 mL of 1× tricaine diluted in system water to the Petri dish in order to keep fish anesthetized.

Inverted confocal microscopes. It is common to use either air or immersion objectives. We mount the specimen in a 35-mm Petri dish with a glass coverslip as base. When using this method, it is important to orientate specimen as close as possible to the coverslip. Anesthetize zebrafish in 1× tricaine (see Section D) and place the specimen on the glass coverslip within the 35-mm Petri dish. Remove excess system water carried over from transfer of specimen. Quickly add 1% LMP agarose cooled to 42 °C to cover the fish, and orient into correct position using a metal dissection probe. Continuously observe orientation of the fish as LMP solidifies to ensure correct positioning. Once LMP agarose is solidified, add ∼2 mL of 1% tricaine diluted in system water to the Petri dish.

4. Table I contains excitation and emission information for each fluorescent lipid stain used to visualize neutral lipid. Due to the size of late larvae/juveniles, best results are obtained using 10× or 20× objectives that have large working distances but a numerical aperture (NA) of ∼1.

F. Recovery of Sample After Imaging of Fluorescent Neutral Lipid

1. Zebrafish are amenable to longitudinal analyses of fat storage within individual fish (Fig. 2) (Flynn *et al.*, 2009). Therefore, once imaging has been completed, it is often necessary to recover larvae and allow development to proceed. Under a dissecting microscope, gently cut LMP agarose away from tail of larvae with a metal dissection probe. We find it is easier to recover fish from 1% LMP agarose if it is first immersed in fresh system water. Once tail is free, it may be possible to release larvae by gently squeezing clean system water over the specimen with a plastic transfer pipette. If necessary, carefully remove more of LMP agarose from anterior regions until larvae are released.

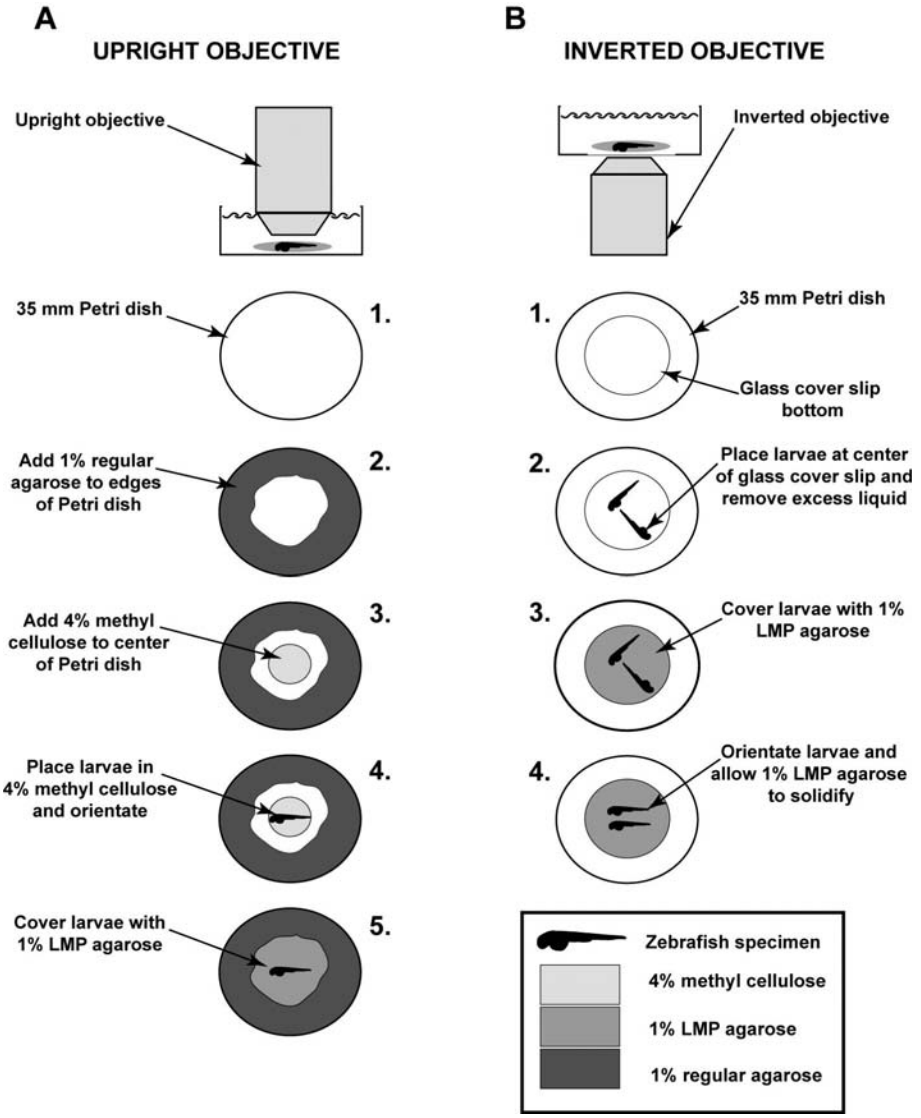

Fig. 6 Schematic illustrating stable mounting procedures for regular and inverted microscopes. (A) When imaging using an upright objective, a 60-mm Petri dish is used (step 1), and 1% regular agarose is used to fill in around the edges of the Petri dish (step 2). Four percent methyl cellulose is then placed in center of Petri dish (step 3), before the anesthetized animal is placed in 4% methyl cellulose and oriented (step 4). Once specimen is correctly oriented, it is covered with 1% LMP agarose and allowed to solidify (step 5). (B) For imaging using an inverted objective, a 60-mm Petri dish with a fitted glass coverslip as a base is used (step 1). Anesthetized zebrafish are place onto the glass coverslip base (step 2) and excess liquid is removed. The specimen is then covered with 1% LMP agarose (step 3) and quickly oriented while agarose is solidifying (step 4). For both methods, 2 mL of system water, containing 1× tricaine, is added to specimen. When undertaking imaging using the upright objective method, be sure to use a water dipping objective.

2. Once larvae are free and recovered from anesthesia, house each fish individually in a well of a 24-well plate filled with 2 mL system water to keep record of subsequent larvae/juvenile growth during longitudinal analysis. It is necessary to change 80% of system water within each well daily and to feed ~30 live brine shrimp per well per day.

G. Methods for Analyzing Fixed Zebrafish Adipose Tissues

Zebrafish adipose tissues can be analyzed in fixed specimens using the HCS LipidTOX series of fluorescent stains (J. Minchin, unpublished). Furthermore, HCS LipidTOX can be utilized after histological sectioning of zebrafish (Stoletov *et al.*, 2009), which indicates that equivalent analytical techniques undertaken in mammalian adipose tissue research can be attempted in zebrafish. *In vivo* imaging of zebrafish adipocyte LDs can also be coupled with subsequent *in situ* hybridization analysis to assess gene expression in adipocytes and other WAT cell types (Fig. 3) (Flynn *et al.*, 2009). Moreover, analysis of zebrafish adipose tissues within fixed specimens permits testing of the extensive range of antibodies used in mammalian adipose tissue research (Ibabe *et al.*, 2005). Thus, when used in conjunction with *in vivo* observation of cell dynamics, analysis of fixed zebrafish adipose tissues offers several useful opportunities:

1. Zebrafish larvae/juveniles of an appropriate SL are transferred to a suitable vessel, such as a 15-mL conical tube. Specimen is washed 3× in fresh system water to remove any debris. System water is removed and freshly prepared 4% PFA/1% DMSO in PBS is added to the conical tube. Larvae/juveniles are fixed, while gently shaking, overnight at 4 °C.
2. Prior to staining, fixed specimen is washed 5× in 1× PBS/0.1% Tween-20 at room temperature.
3. A 200× dilution of HCS LipidTOX (in 1× PBS/0.1% Tween-20) is added to the specimen and incubated, in the dark, at room temperature for 2 h.
4. Specimen can be imaged immediately using techniques described in Sections D and E. No wash step is required.
5. In addition to the fluorescent HCS LipidTOX staining of fixed zebrafish LDs described above, numerous additional methods of analyzing fixed zebrafish WAT can be employed. These methods include, but are not limited to, *in situ* hybridization on whole (Flynn *et al.*, 2009) and sectioned zebrafish (Imrie and Sadler, 2010), histological analysis of adipose tissues by hemotoxylin and eosin staining of paraffin sections (Imrie and Sadler, 2010; Song and Cone, 2007), immunohistochemical analysis (Ibabe *et al.*, 2005), extraction and analysis of lipid from zebrafish tissues (Flynn *et al.*, 2009; Song and Cone, 2007), and oil red O (ORO) staining of lipid within adipose tissues in whole (Flynn *et al.*, 2009; Li *et al.*, 2010) and sectioned zebrafish (Imrie and Sadler, 2010). Although ORO staining of LDs within adipocytes is usually unambiguous and can be confidently identified (Flynn *et al.*, 2009; Imrie and Sadler, 2010), it should be noted that ORO readily

stains nonadipogenic cells (Kinkel *et al.*, 2004) and should thus be used with caution. A detailed description of these methods is beyond the scope of this chapter. However, coupled with fluorescent analysis of live and fixed zebrafish, these methods complement available tools for investigating zebrafish adipose tissues.

V. Summary

Investigation of WATs has only recently been initiated in the zebrafish, and consequently we have a relatively limited knowledge of adipose tissue development and physiology in this important vertebrate model system. However, the amenability of the zebrafish to high-resolution *in vivo* imaging presents exciting opportunities to address longstanding questions about WAT formation and function that have been difficult to resolve using available mammalian models. Moreover, systematic genetic and chemical tests in the zebrafish model could be used to identify novel factors regulating distinct aspects of adipose tissue biology.

Here we have provided detailed methods for *in vivo* imaging of zebrafish WATs in order to support the use of the zebrafish as a model for adipose tissue research. We anticipate that the fluorescence stereomicroscopy methods presented here will be useful for rapid phenotypic assessments required for genetic and chemical screens, while the confocal microscopy methods will facilitate high-resolution analysis of cellular and molecular events within adipose tissues. Furthermore, we expect that these methods will also be generally applicable to *in vivo* imaging of adipose tissues in other fish species. Deployment of these methods in the zebrafish system will be enriched by the use of existing and forthcoming zebrafish lines expressing FP and other transgenes in adipocyte lineages and other cellular constituents of adipose tissues. Use of zebrafish as a model for adipose tissue biology will also be enhanced by identification of genetic alterations, dietary and environmental manipulations, and chemicals that modify zebrafish adipose tissue formation and function.

Acknowledgments

We are grateful to Dru Imrie and Kirsten Sadler for sharing data prior to publication, and to Edward Flynn for valuable technical support. This work was supported by NIH grant DK056350 to the University of North Carolina at Chapel Hill's Nutrition Obesity Research Center, as well as NIH grants DK081426 and DK073695, a Pilot Research Project Award from the UNC University Cancer Research Fund, and a Pew Scholars Program in the Biomedical Sciences Award to J.F.R.

References

Abel, E. D., *et al*. (2001). Adipose-selective targeting of the GLUT4 gene impairs insulin action in muscle and liver. *Nature* **409**, 729–733.

Ailhaud, G., *et al*. (1992). Cellular and molecular aspects of adipose tissue development. *Annu. Rev. Nutr.* **12**, 207–233.

Albalat, A., *et al*. (2007). Insulin regulation of lipoprotein lipase (LPL) activity and expression in gilthead sea bream (*Sparus aurata*). *Comp. Biochem. Physiol. B Biochem. Mol. Biol.* **148**, 151–159.

Barzilai, N., *et al*. (1999). Surgical removal of visceral fat reverses hepatic insulin resistance. *Diabetes* **48**, 94–98.

Bellardi, S., *et al*. (1995). Effect of feeding schedule and feeding rate on size and number of adipocytes in rainbow trout *Oncorhynchus mykiss*. *J. World Aquacult. Soc.* **26**, 80–83.

Carvalho, E., *et al*. (2005). Adipose-specific overexpression of GLUT4 reverses insulin resistance and diabetes in mice lacking GLUT4 selectively in muscle. *Am. J. Physiol. Endocrinol. Metab.* **289**, E551–E561.

Company, R., *et al*. (1999). Growth performance and adiposity in gilthead seabream (*Sparus aurata*): risks and benefits of the high energy diets. *Aquacult. Res.* **171**, 279–292.

Cypess, A. M., and Kahn, C. R. (2010). Brown fat as a therapy for obesity and diabetes. *Curr. Opin. Endocrinol. Diabetes Obes.* **17**, 143–149.

Despres, J. P. (1998). The insulin resistance-dyslipidemic syndrome of visceral obesity: effect on patients' risk. *Obes. Res.* **6**(suppl. 1), 8S–17S.

Fain, J. N., and Garcija-Sainz, J. A. (1983). Adrenergic regulation of adipocyte metabolism. *J. Lipid Res.* **24**, 945–966.

Farese Jr., R. V., and Walther, T. C. (2009). Lipid droplets finally get a little R-E-S-P-E-C-T. *Cell* **139**, 855–860.

Flynn 3rd, E. J., Trent, C. M., and Rawls, J. F. (2009). Ontogeny and nutritional control of adipogenesis in zebrafish (Danio rerio). *J. Lipid Res.* **50**(8), 1641–1652.

Fox, C. S., *et al*. (2007). Abdominal visceral and subcutaneous adipose tissue compartments: association with metabolic risk factors in the Framingham Heart Study. *Circulation* **116**, 39–48.

Gabriely, I., *et al*. (2002). Removal of visceral fat prevents insulin resistance and glucose intolerance of aging: an adipokine-mediated process? *Diabetes* **51**, 2951–2958.

Gesta, S., *et al*. (2006). Evidence for a role of developmental genes in the origin of obesity and body fat distribution. *Proc. Natl. Acad. Sci. U. S. A.* **103**, 6676–6681.

Gesta, S., *et al*. (2007). Developmental origin of fat: tracking obesity to its source. *Cell* **131**, 242–256.

Hughes, J., and Criscuolo, F. (2008). Evolutionary history of the UCP gene family: gene duplication and selection. *BMC Evol. Biol.* **8**, 306.

Ibabe, A., *et al*. (2005). Expression of peroxisome proliferator-activated receptors in zebrafish (*Danio rerio*) depending on gender and developmental stage. *Histochem. Cell Biol.* **123**, 75–87.

Imrie, D., and Sadler, K. (2010). White adipose tissue development in zebrafish is regulated by both developmental time and fish size. *Dev. Dyn.* **239**, 3013–3023.

Jastroch, M., *et al*. (2005). Uncoupling protein 1 in fish uncovers an ancient evolutionary history of mammalian nonshivering thermogenesis. *Physiol. Genomics* **22**, 150–156.

Jin, S. W., *et al*. (2005). Cellular and molecular analyses of vascular tube and lumen formation in zebrafish. *Development* **132**, 5199–5209.

Jo, J., *et al*. (2009). Hypertrophy and/or hyperplasia: dynamics of adipose tissue growth. *PLoS Comput. Biol.* **5**, e1000324.

Kinkel, A. D., *et al*. (2004). Oil red-O stains non-adipogenic cells: a precautionary note. *Cytotechnology* **46**, 49–56.

Kissebah, A. H., and Krakower, G. R. (1994). Regional adiposity and morbidity. *Physiol Rev.* **74**, 761–811.

Lawrence, C. (2007). The husbandry of zebrafish (*Danio rerio*): a review. *Aquaculture* **269**, 1–20.

Li, N., *et al*. (2010). Regulation of neural crest cell fate by the retinoic acid and Pparg signalling pathways. *Development* **137**, 389–394.

Morse, S. A., *et al*. (2010). The obesity paradox and cardiovascular disease. *Curr. Hypertens. Rep.* **12**, 120–126.

Nishimura, S., *et al*. (2007). Adipogenesis in obesity requires close interplay between differentiating adipocytes, stromal cells, and blood vessels. *Diabetes* **56**, 1517–1526.

Nishimura, S., *et al*. (2008). *In vivo* imaging in mice reveals local cell dynamics and inflammation in obese adipose tissue. *J. Clin. Invest.* **118**, 710–721.

Nishio, S. -I., *et al*. (2008). Adiponectin and adiponectin receptor genes are coexpressed during zebrafish embryogenesis and regulated by food deprivation. *Dev. Dyn.* **237**, 1682–1690.

Oka, T., *et al*. (2010). Diet-induced obesity in zebrafish shares common pathophysiological pathways with mammalian obesity. *BMC Physiol* **10**, 21.

Oku, H., *et al*. (2006). Effects of insulin, triiodothyronine and fat soluble vitamins on adipocyte differentiation and LPL gene expression in the stromal–vascular cells of red sea bream. *Pagrus major. Comp. Biochem. Physiol. B Biochem. Mol. Biol.* **144**, 326–333.

Oku, H., and Umino, T. (2008). Molecular characterization of peroxisome proliferator-activated receptors (PPARs) and their gene expression in the differentiating adipocytes of red sea bream *Pagrus major. Comp. Biochem. Physiol. B Biochem. Mol. Biol.* **151**, 268–277.

Om, A. D., *et al*. (2001). The effects of dietary EPA and DHA fortification on lipolysis activity and physiological function in juvenile black sea bream *Acanthopagrus schlegeli* (Bleeker). *Aquacult. Res.* **32**, 255–262.

Parichy, D. M., *et al*. (2009). Normal table of postembryonic zebrafish development: staging by externally visible anatomy of the living fish. *Dev. Dyn.* **238**, 2975–3015.

Peinado, J. R., *et al*. (2010). The stromal–vascular fraction of adipose tissue contributes to major differences between subcutaneous and visceral fat depots. *Proteomics* **10**, 3356–3366.

Poulos, S. P., *et al*. (2010). The development and endocrine functions of adipose tissue. *Mol. Cell. Endocrinol.* **323**, 20–34.

Rawls, J. F., and Johnson, S. L. (2003). Temporal and molecular separation of the kit receptor tyrosine kinase's roles in zebrafish melanocyte migration and survival. *Dev. Biol.* **262**, 152–161.

Redinger, R. N. (2009). Fat storage and the biology of energy expenditure. *Transl. Res.* **154**, 52–60.

Rodeheffer, M. S., *et al*. (2008). Identification of white adipocyte progenitor cells *in vivo*. *Cell* **135**, 240–249.

Rosen, E. D., and Spiegelman, B. M. (2006). Adipocytes as regulators of energy balance and glucose homeostasis. *Nature* **444**, 847–853.

Shen, W., and Chen, J. (2008). Application of imaging and other noninvasive techniques in determining adipose tissue mass. *Methods Mol. Biol.* **456**, 39–54.

Sheridan, M. A. (1988). Lipid dynamics in fish: aspects of absorption, transportation, deposition and mobilization. *Comp. Biochem. Physiol. B* **90**, 679–690.

Song, Y., and Cone, R. D. (2007). Creation of a genetic model of obesity in a teleost. *FASEB J.* **21**, 2042–2049.

Stoletov, K., *et al*. (2009). Vascular lipid accumulation, lipoprotein oxidation, and macrophage lipid uptake in hypercholesterolemic zebrafish. *Circ. Res.* **104**, 952–960.

Tang, W., *et al*. (2008). White fat progenitor cells reside in the adipose vasculature. *Science* **322**, 583–586.

Tobias, C. W., and Farese Jr, R. V. (2009). The life of lipid droplets. *Biochim Biophys. Acta* **1791**, 459–466.

Todorcevic, M., *et al*. (2010). Gene expression profiles in Atlantic salmon adipose-derived stromovascular fraction during differentiation into adipocytes. *BMC Genomics* **11**, 39.

Umino, T., *et al*. (1996). Development of adipose tissue in juvenile red sea bream. *Fisheries Sci.* **62**, 520–523.

Vegusdal, A., *et al*. (2003). An *in vitro* method for studying the proliferation and differentiation of Atlantic salmon preadipocytes. *Lipids* **38**, 289–296.

Vidal, H. (2001). Gene expression in visceral and subcutaneous adipose tissues. *Ann. Med.* **33**, 547–555.

Vohl, M. C., *et al*. (2004). A survey of genes differentially expressed in subcutaneous and visceral adipose tissue in men. *Obes. Res.* **12**, 1217–1222.

Wajchenberg, B. L. (2000). Subcutaneous and visceral adipose tissue: their relation to the metabolic syndrome. *Endocr. Rev.* **21**, 697–738.

Weil, C., *et al*. (2009). Differentially expressed proteins in rainbow trout adipocytes isolated from visceral and subcutaneous tissues. *Comp. Biochem. Physiol. D Genomics Proteomics.* **4**, 235–241.

Westerfield, M. (2000). *The Zebrafish Book – A Guide for the Laboratory Use of Zebrafish (Danio rerio).* University of Oregon Press, Eugene, OR.

Xue, Y., *et al*. (2010). Adipose angiogenesis: quantitative methods to study microvessel growth, regression and remodeling *in vivo*. *Nat. Protoc.* **5**, 912–920.

Yach, D., *et al*. (2006). Epidemiologic and economic consequences of the global epidemics of obesity and diabetes. *Nat. Med.* **12**, 62–66.

CHAPTER 4

Study of Host–Microbe Interactions in Zebrafish

Kathryn Milligan-Myhre[*], Jeremy R. Charette[†], Ryan T. Phennicie[†], W. Zac Stephens[*], John F. Rawls[‡,§], Karen Guillemin[*] and Carol H. Kim[†,]**

[*]Institute of Molecular Biology, University of Oregon, Eugene, Oregon, USA

[†]Department of Molecular & Biomedical Sciences, University of Maine, Orono, Maine, USA

[‡]Department of Cell and Molecular Physiology, University of North Carolina at Chapel Hill, Chapel Hill, North Carolina, USA

[§]Department of Microbiology and Immunology, University of North Carolina at Chapel Hill, Chapel Hill, North Carolina, USA

[**]Graduate School of Biomedical Sciences, University of Maine, Orono, Maine, USA

Abstract

All animals are ecosystems, home to diverse microbial populations.

Animal-associated microbes play important roles in the normal development and physiology of their hosts, but can also be agents of infectious disease. Traditionally, mice have been used to study pathogenic and beneficial associations between microbes and vertebrate animals. The zebrafish is emerging as a valuable new model system for host-microbe interaction studies, affording researchers with the opportunity to survey

METHODS IN CELL BIOLOGY, VOL 105

0091-679X/10 $35.00
DOI 10.1016/B978-0-12-381320-6.00004-7

large populations of hosts and to visualize microbe-host associations at a cellular level in living animals. This chapter provides detailed protocols for the analysis of zebrafish-associated microbial communities, the derivation and husbandry of germ-free zebrafish, and the modeling of infectious disease in different stages of zebrafish development via different routes of inoculation. These protocols offer a starting point for researchers to address a multitude of questions about animals' coexistence with microorganisms.

I. Introduction

No animal is ever truly alone, but instead each lives in constant association with single-celled microorganisms. Bacteria, Archaea, fungi, single-celled eukaryotes, and viruses are present both in and on the body from birth to death. These organisms have a spectrum of interactions with their hosts, ranging from beneficial contributions to host development and physiology to harmful infections. For example, beneficial microbes contribute unique enzymatic activities required to break down ingested food and make the caloric content accessible to the host. Additionally, mutualistic microbes promote the development of the digestive tract and the immune system. On the other hand, pathogenic microbes cause harm to the body, sometimes through the active release of toxins or through invasion and expansion in host tissue from which they are normally excluded. It is often tricky to define a host-associated microbe as a strict mutualist or a pathogen because the outcome of any host–microbe interaction can depend on the context of the association, including such factors as the microbial ecology and the immune status of the host.

As a framework to begin to define the functional consequences of a particular microbial interaction with a host, and in particular to ascribe the disease-causing capacity of a potential pathogen, the eminent founding father of microbiology, Robert Koch, defined a set of postulates in 1890 to determine whether a microorganism is the cause of a disease. These rules stipulated that:

1. The microorganism must be found in abundance in all organisms suffering from the disease, but should not be found in healthy organisms.
2. The microorganism must be isolated from a diseased organism and grown in pure culture.
3. The cultured microorganism should cause disease when introduced into a healthy organism.
4. The microorganism must be reisolated from the inoculated, diseased experimental host and identified as being identical to the original specific causative agent.

Over a century later, these postulates still provide a useful experimental approach for infectious disease researchers to establish causation between infection with a microbe and symptoms in a host, and have been extended to "molecular Koch's postulates" to establish causation between specific microbial factors and host responses (Falkow, 1988). Such an experimental framework is relevant because infectious diseases

continue to play a major role in the human condition worldwide. Since the discovery of microorganisms as the cause of infectious diseases, our ability to control and treat these diseases has advanced enormously with the development of sterile practices, vaccines, antibiotic drugs, and intervention strategies. However, microbial adaptation and environmental changes continue to trigger the emergence of new pathogens, fueling the need for alternative methods for studying infectious diseases.

A prerequisite for fulfilling Koch's postulates is the existence of an animal model that can be infected with a microorganism. Traditionally mice have been the workhorse model for infectious disease researchers. An emerging model system in this field is the zebrafish, *Danio rerio*. The zebrafish model system offers numerous advantages, including external fertilization, large clutches, optical clarity during development, and the rapid development of organ primordia (within 5 days postfertilization [dpf]). These advantages first made zebrafish attractive to embryologists and developmental geneticists, but the model has since been adopted by other fields, including toxicology, immunology, and infectious diseases. The model continues to evolve as an effective tool within the field of biomedicine as researchers learn to exploit its unique advantages to address their specific questions. Today large collections of transgenic zebrafish lines and molecularly defined mutants are available; molecular, forward, and reverse genetics techniques have been developed; the zebrafish genome project is nearly complete; and compelling human disease models have been created. In particular, the zebrafish model is now being used to answer questions about infectious disease and immunity (reviewed in Traver *et al.*, 2003; Trede *et al.*, 2004). Zebrafish rely solely on the innate immune response for approximately the first 30 days of development to protect against pathogen infection (Lam *et al.*, 2004). This temporal segregation of innate versus adaptive immune response renders the zebrafish an excellent model for the study of infectious diseases. Table I, adapted from Kanther and Rawls (2010), provides a summary of the infection models that have been established to date in the zebrafish.

A. Host–Pathogen Interactions

A number of factors must be taken into account when considering the zebrafish as an infection model. The zebrafish supports the growth and replication of a number of fish and human pathogens (Table I), but no animal model is suitable for propagation of all animal pathogens. When developing an infection model in the zebrafish, a researcher should consider questions such as: Can the pathogen be transmitted through the water or must it be injected? Is mimicking the natural route of infection essential for the infection model? What is the optimal temperature for the pathogen? Does the replication temperature of the pathogen match the maintenance temperature of the zebrafish? The maintenance temperature of the zebrafish may be varied to accommodate infection by a pathogen with a growth temperature range that is either higher or lower than 28 °C. If infection studies are initiated to study immune function of the host, the effects of varying the maintenance temperature outside of the host's normal range should be carefully considered. Altering the temperature

Table I
Bacterial and viral infection models in zebrafish

Pathogen	Infection method	Embryos/adults	Reference(s)
		Bacteria	
Aeromonas hydrophila	Injection, static immersion	Larvae, adult	Rawls *et al.* (2004, 2006), Rodriguez *et al.* (2008)
Aeromonas salmonicida	Static immersion	Adult	Lin *et al.* (2007)
Aeromonas veronii	Static immersion	Larvae	Bates *et al.* (2006)
Bacillus subtilus	Injection	Embryo	Herbomel *et al.* (1999)
Burkholderia cenocepacia	Injection	Embryo, adult	Deng *et al.* (2009), Vergunst *et al.* (2010)
Edwardsiella ictaluri	Injection	Adult	Petrie-Hanson *et al.* (2007)
Edwardsiella tarda	Injection, static immersion	Embryo, larvae, adult	Nayak *et al.* (2007), Phelan *et al.* (2005a), Pressley *et al.* (2005)
Escherichia coli MG1655	Static immersion	Larvae	Rawls *et al.* (2006, 2007)
E. coli O157:H7	Static immersion	Larvae	Szabady *et al.* (2009)
Flavobacterium columnare	Injection, static immersion	Adult	Moyer and Hunnicutt (2007)
Flavobacterium johnsoniae	Injection, static immersion	Adult	Moyer and Hunnicutt (2007)
Francisella spp.	Injection	Adult	Vojtech *et al.* (2009)
Leptospira interrogansa	Injection	Embryo	Davis and Ramakrishnan (2009), PMID 19547748
Listeria monocytogenes	Injection	Embryo, adult	Levraud *et al.* (2009), Menudier *et al.* (1996)
Listeria spp.	Injection	Adult	Menudier *et al.* (1996)
Listonella anguillaruma	Injection, static immersion	Adult	Rojo *et al.* (2007)
Mycobacterium haemophiluma	Injection	Adult	Whipps *et al.* (2007)
Mycobacterium marinum	Injection, static immersion	Embryo, larvae, adult	Adams *et al.* (2011), Carvalho *et al.* (2011), Clay *et al.* (2007, 2008), Davis *et al.* (2002), Davis *et al.* (2009), Gao *et al.* (2006), Harriff *et al.* (2007), Meijer *et al.* (2005), Stoop *et al.* (2011), Volkman *et al.* (2010)
Mycobacterium peregrinum	Static immersion	Adult	Harriff *et al.* (2007)
Pseudomonas aeruginosa	Injection, static immersion	Embryo, larvae	Brannon *et al.* (2009), Clatworthy *et al.* (2009), Llamas *et al.* (2009), Phennicie *et al.* (2010), Rawls *et al.* (2004, 2006, 2007), Singer *et al.* (2010), Vasil *et al.* (2009)
Pseudomonas fluorescens	Static immersion	Larvae	Bates *et al.* (2006)
Salmonella arizonae	Injection	Embryo	Davis *et al.* (2002)
Salmonella typhimurium	Injection	Embryo, larvae	Ordas *et al.* (2010), Stockhammer *et al.* (2009), van der Sar *et al.* (2003, 2006)

Staphylococcus aureus	Injection	Embryo, adult	Lin *et al.* (2007), Prajsnar *et al.* (2008)
Streptococcus iniae	Injection	Adult	Lowe *et al.* (2007), Miller and Neely (2005), Neely *et al.* (2002)
Streptococcus pyogenes	Injection	Adult	Bates *et al.* (2005), Cho and Caparon (2005), Kizy and Neely (2009), Montanez *et al.* (2005), Neely *et al.* (2002)
Vibrio anguillarum	Static immersion	Larvae	O'Toole *et al.* (2004)
		Virus	
Herpes simplex virus type 1 (HSV-1)	Injection	Adult	Burgos *et al.* (2008)
Infectious hematopoietic necrosis virus (IHNV)	Injection	Adult	LaPatra *et al.* (2000), Ludwig *et al.* (2011), Wang *et al.* (2006)
Infectious pancreatic necrosis virus (IPNV)	Injection	Adult	Garner *et al.* (2003), LaPatra *et al.* (2000)
Infectious spleen and kidney necrosis virus (ISKNV)	Injection	Embryo, adult	Wang *et al.* (2008), Xiong *et al.* (2011), Xu *et al.* (2008)
Nervous necrosis virus (NNV)	Injection	Larvae, adult	Lu *et al.* (2008)
Snakehead rhabdovirus (SHRV)	Injection, static immersion	Embryo, larvae, adult	Alonso *et al.* (2004), Altmann *et al.* (2003, 2004), Hermann and Kim (2005), Nayak *et al.* (2007), Phelan *et al.* (2005a, 2005b)
Spring viremia of carp virus (SVCV)	Injection, static immersion	Adult	Sanders *et al.* (2003), Wang *et al.* (2006)
Viral hemorrhagic septicemia virus (VHSV)	Injection	Adult	Encinas *et al.* (2010), Novoa *et al.* (2006)

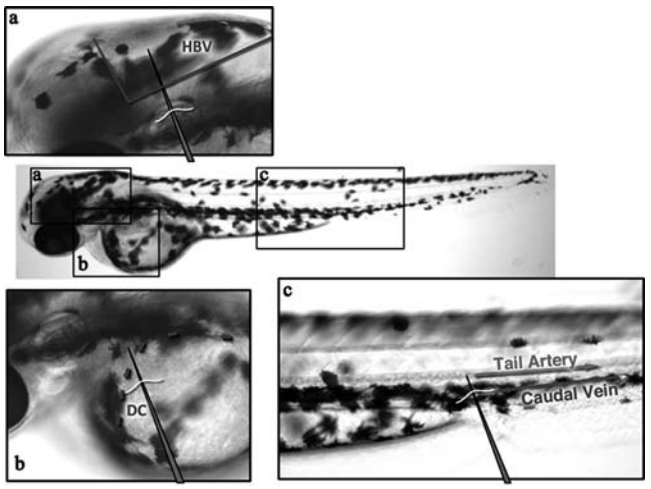

Fig. 1 Microinjection sites of zebrafish embryos. Three methods are commonly used for microinjection of pathogens into zebrafish embryos. The figure demonstrates microinjection into the (a) hindbrain ventricle (HBV), (b) duct of Cuvier (DC), and (c) tail artery of a 48 hpf zebrafish embryo.

beyond the optimal range for the host may permit infection with a pathogen, but will not necessarily reflect the typical homeostasis between host and pathogen. A researcher should consider whether the temperature will change the host's ability to resist or be susceptible to infection and whether the immune response to this infection will reflect a normal outcome.

Infection protocols presented here were developed to investigate host–pathogen interactions via a number of infection routes. With some pathogens, infections can be achieved by static emersion of embryos, larvae, or adults, but for many nonindigenous pathogens passive exposure does not result in acceptable rates of infection. Systemic infections with bacteria and virus can be established by injection of the pathogen into the duct of Cuvier or tail artery (Fig. 1b and c). Such models are useful for studying global responses to infection, such as cytokine profiles and activation of immune pathways as assayed by quantitative RT-PCR, luciferase assays, and respiratory burst assays (Hermann *et al.*, 2004; Nayak *et al.*, 2007; Sullivan *et al.*, 2007, 2009). Pathogen injection into the hindbrain ventricle (Fig. 1a) typically leads to a contained infection. Localized infection models are useful for tracking the movement of neutrophils or macrophages to a site of infection (Davis *et al.*, 2002; Phennicie *et al.*; Prajsnar *et al.*, 2008).

Several genetic tools are available to aid in the study of the immune reaction to infections in zebrafish. A number of transgenic zebrafish reporter lines are useful for *in vivo* studies of infections, including those with fluorescent protein–labeled macrophages and neutrophils (Ellett *et al.*, 2011; Gray *et al.*, 2011; Lawson and Weinstein, 2002; Mathias *et al.*, 2006; Renshaw *et al.*, 2006). Zebrafish lines with immune deficiencies also exist, including loss-of-function alleles of *csf1ra* and *rag1* (Parichy

et al., 2000; Wienholds *et al.*, 2002), which lack macrophage and mature lymphocytes, respectively. Antisense morpholinos are frequently used to knock down specific immune-related genes transiently, to discern their relevance and significance during infection. For example, *spic*-morpholinos inhibit myeloid development for the first 5 dpf and prevent macrophage and neutrophil development (Rhodes *et al.*, 2005; Su *et al.*, 2007). Injection of morpholinos that target *myd88* significantly impairs clearance of *Salmonella enterica* (van der Sar *et al.*, 2006). Several IFN-related genes such as *crfb1–8*, *crfb12–17*, *ifnph1*, *ifng1*, and *infg2* can be targeted for knockdown and observed during viral and bacterial infections (Aggad *et al.*, 2009, 2010). By taking advantage of the optical clarity of the embryo, these transgenic or mutant lines can be used in conjunction with fluorescent protein–labeled pathogens to assist in the characterization of host–pathogen interactions.

Several of the protocols outlined in this chapter were developed for infection of zebrafish with specific pathogens, including snakehead rhabdovirus, *Edwardsiella tarda*, or *Pseudomonas aeruginosa*. Adaptation of these protocols to other pathogens will be governed by the specific organism under investigation.

B. Host–Microbiota Interactions

As noted previously, Koch's postulates are useful for establishing causation between a putative pathogen or virulence determinant and a disease, but the same logic can be applied to investigations into mutualisms between microbes and animals. There are several beautiful examples of animal mutualisms in which the presence of a single microbe profoundly shapes the development or physiology of an animal host, such as the gut endosymbionts of insects and the bioluminescent symbionts of squid (Fraune and Bosch, 2010). Vertebrates, however, are typically associated with complex microbial communities (microbiota) that are difficult to characterize and often recalcitrant to culture in the lab. With a loosening of the requirement for the growth of the microorganism in pure culture, Koch's postulates can be applied to understanding the effects of these complex microbial communities on their hosts. The collective effect of the microbial community can be evaluated by the comparison of developmental, physiological, and immune markers between conventionally colonized and "germ-free" animals (which lack the microbial community). Alternatively, the effects of individual or subsets of culturable microbes can be evaluated in monoassociated animals, in which a single microbe is introduced into an otherwise germ-free animal, or animals with simple, defined microbial communities. Finally the microbiota's collective effects can be approximated by transplantation of microbial communities harvested from one donor host into a germ-free recipient host. All together, these experiments can provide powerful evidence for the roles of microbial associations in normal animal development and physiology.

The mouse has been the traditional animal used in the field of gnotobiology (Greek for "known life"), in which the microbial associates of animals are entirely defined. Recently, the zebrafish has emerged as a powerful new gnotobiotic model. The *ex utero* development of the zebrafish allows for easy surface sterilization of the

embryo's chorion, facilitating the derivation of thousands of germ-free animals at a time. Although we have not yet established methods to rear germ-free zebrafish to adulthood, as is possible for germ-free mice, recent husbandry advances have resulted in maintenance of germ-free fish through a month of age, potentially to the onset of adaptive immunity. Studies of germ-free mice and zebrafish have revealed a number of common differences from their conventionally reared counterparts, indicating a conserved vertebrate program of responses to their microbiota. These responses are listed in Table II.

This chapter provides the tools for the zebrafish researcher to fulfill Koch's postulates to establish a functional connection between the presence of a microorganism and an effect on the host. We will begin by addressing the first postulate of characterizing the microbial associates of the zebrafish. We provide protocols for culture-dependent and -independent enumeration of associated bacteria from the intestine, but these can be extended to other anatomical sites and classes of microorganisms. We then provide protocols for the derivation and rearing of germ-free zebrafish, and methods for the generation of zebrafish with defined microbial associates. Finally we provide a series of protocols for infecting zebrafish at different ages and via different routes with different classes of infectious agents. These protocols are designed to provide researchers with the starting point for a diversity of experiments. We leave the final analysis of the experiments – the particular methodologies of 16S rRNA gene sequence analysis and the endpoint analyses of gnotobiotic and infection experiments, including microbiological measurements, pathological assessments, and molecular measures of host responses – to the experimenter.

Table II
Germ-free traits shared between zebrafish and rodents

Germ-free trait	Zebrafish	Rodents
Reduced cell proliferation (as measured by incorporation of nucleotide analogues)	Cheesman *et al.* (2011), Rawls *et al.* (2004, 2006)	Savage *et al.* (1981)
Reduced numbers of goblet cells	Bates *et al.* (2006)	Kandori *et al.* (1996)
Altered expression of genes involved in metabolism (e.g., *fasting-induced adipose factor*)	Kanther *et al.* (2011), Rawls *et al.* (2004, 2006)	Hooper *et al.* (2001)
Reduced expression of genes involved in innate immunity (e.g., *serum amyloid A1*)	Kanther *et al.* (2011), Rawls *et al.* (2004, 2006)	Hooper *et al.* (2001)
Reduced numbers of intestinal associated immune cells	Bates *et al.* (2007) (fewer intestinal neutrophils)	Bouskra *et al.* (2008), Cebra *et al.* (1998) (fewer lamina propria cells and lymphoid follicles)
Differences in glycan expression	Bates *et al.* (2006)	Bry *et al.* (1996)
Altered gut motility	Bates *et al.* (2006) (increased in germ-free)	Husebye *et al.* (1994) (decreased in germ-free)

II. Laboratory Protocols

A. Characterization of Microbial Communities in the Gut

Bacterial communities that reside in the vertebrate guts are not homogenous, but include a wide taxonomic diversity of organisms. Not all of the organisms are cultivable outside of the zebrafish gut, but a good representation of the bacteria present in the gut can be inferred from culturing. The choice of media used to culture the bacteria will depend on what organisms are targeted for culturing. For a broad idea of what is present, aerobic growth of intestinal material on tryptic soy agar (TSA) is sufficient. For isolation of anaerobic bacteria, anaerobe plates made with Oxoid Wilkins-Chalgren anaerobe agar and enriched with equine blood should be incubated in anaerobic chambers. However, some bacteria are present in low numbers, are outcompeted by other organisms due to slow growth rates, or selectively grow on media higher in some nutrients. For example, to isolate Fusobacteria, intestinal material should be plated on Fusobacteria-selective agar, which contains low levels of drugs that will inhibit growth of most Gram-positive and Gram-negative anaerobes, and incubated in an anaerobic chamber to enrich for those bacteria. (See Buller (2004) for lists of different media used to isolate specific strains.)

1. Gut Dissections

Materials

- Insect pins and holders (Fine Science Tools, cat. no. 26002-15, 26018-17)
- 3-5% methylcellulose (viscosity is a matter of preference)
- Glass slides
- 0.4% tricaine in embryonic medium
- 0.4% tricaine (AKA Tricaine-S; tricaine methanesulfonate; MS-222; 3-aminobenzoic acid ethyl ester (Western Chemical, Inc.)):
  - 400 mg tricaine
  - 97.9 mL H_2O
  - 2.1 mL Tris 1 M (pH 9.0)
- Adjust to pH 7.0; filter sterilize with 0.22 μm filter
- This can be made ahead of time and stored for long periods at 20°C or for up to 2 weeks at 4°C
- Sterile embryonic medium (EM, sterilized through 0.22 μm filter; Westerfield, 2000)
- 200 μL aliquots of sterile EM in 1.5-mL tubes (one per sample)
- Motor and pestle (Pellet Pestle® Motor, Kontes; Pellet Pestle®, Kimble Chase Kontes)

(1) Immediately before dissections, anesthetize fish with 2.1 mL 0.4% tricaine.
(2) Briefly rinse fish by transferring to a clean Petri dish with sterile EM containing tricaine.
(3) On a clean slide, spread a thin layer of 3–5% methylcellulose using a sterile glass pipette or sterile wooden stick.

(4) Transfer fish from the rinse medium onto the methylcellulose, minimizing the amount of EM carried over. Remove remaining EM from the methylcellulose.
(5) Gently press the fish into the methylcellulose to immobilize it during dissection.
(6) Dissections:

   (a) Insert one pin into the head of the fish and another through the mouth, as shown in Fig. 2a. Begin by pulling the lower jaw away from the head.
   (b) Repeat the process further posterior. Insert one pin into the medial trunk of the animal, and the second pin immediately dorsal to the intestine. Pull the intestine ventrally with the second pin. At this point, the rest of the intestine will often begin to slide out of the animal's body cavity fully intact.
   (c) As needed, make additional cuts with the pins to separate the intestine from the rest of the body without puncturing the intestine. Pull the rest of the intestine out, taking care not to stretch it to the point of breaking.
   (d) Depending on downstream application, remove liver from the anterior intestine, and remove mouth and esophagus anterior to intestinal junction (Fig. 2b).
   (e) Use an insect pin to transfer intestines into a 1.5 mL tube containing 200 μL sterile EM, PBS, or other solution depending on downstream application.

(7) Homogenize intestines with motorized pestle and continue with sample preparation depending on experiment. This homogenate can be used to prepare genomic DNA for 16S rRNA gene sequencing, or can be plated to phenotypically characterize bacterial colonies or determine the colony-forming units (CFU) of known bacteria in the gut.

2. Plating Gut Microbiota

Materials

- Insect pins and holders (Fine Science Tools, cat. no. 26002-15, 26018-17)
- 3-5% methylcellulose (viscosity is a matter of preference)

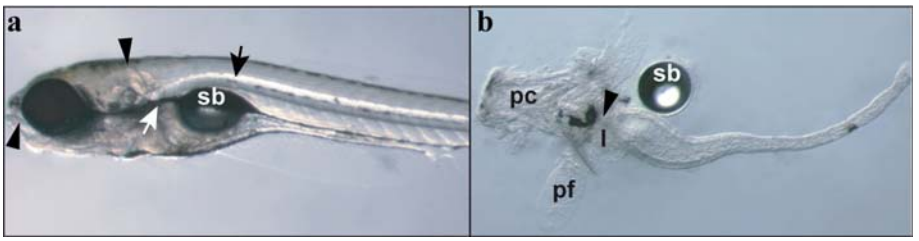

Fig. 2 Dissection of zebrafish larval intestine. (a) Lateral view of 7 dpf larvae indicating initial (arrowheads) and subsequent (arrows) placement of pins for intestine dissection. (b) Seven dpf dissected intestine illustrating anatomical structures that are often pulled out with the intestine and are generally removed prior to analysis. The arrowhead indicates the esophageal–intestinal junction; sb, swim bladder; pc, pharyngeal cartilage; pf, pectoral fin; l, liver. (For color version of this figure, the reader is referred to the web version of this book.)

- Glass slides
- 0.4% tricaine
- 200 μL aliquots of sterile EM in 1.5-mL tubes (one per sample)
- Mortar and pestle (Pellet Pestle® Motor, Kontes; Pellet Pestle®, Kimble Chase Kontes)
- Filter-sterilized EM
- Sterilize 1.5 mL snap top tubes
- TSA plates
- Beads

(1) Dissect guts and homogenize with pestles as described above in 200 μL of filter-sterilized EM in 1.5 mL snap top tube.
(2) Bring volume in tube up to 1 mL with filter-sterilized EM. Vortex to distribute bacterial cells evenly.
(3) Dilute homogenized, vortexed guts in filter-sterilized EM in sterile 1.5 mL snap top tubes. Most bacteria can be detected on plates diluted between 10^{-1} and 10^{-4}.
(4) Plate bacteria diluted between 10^{-1} and 10^{-4} on medium of choice.
(5) Incubate plates at 28 °C between 24 and 48 h aerobically or anaerobically before counting.

3. Bacterial gDNA Extractions from Fish Intestines for 16S rRNA Gene Sequencing

The methods described here are for larval zebrafish intestines. The same techniques can be employed for adult intestines, although the elution volumes should be increased. The genomic DNA isolated using this protocol can be used for a variety of downstream applications including sequencing of 16S rRNA gene amplicons or the whole metagenome. Indeed, similar methods have already been successfully used to define the membership and structure of bacterial communities in the zebrafish intestine using 16S rRNA gene sequencing (Bates *et al.*, 2006; Brugman *et al.*, 2009; Rawls *et al.*, 2004, 2006; Roeselers *et al.*, 2011).

Column-based DNA isolation methods (such as Qiagen's DNeasy columns) are often sufficient for isolating bacterial DNA from fish intestines and generally yield the highest quality DNA for downstream enzymatic reactions, including PCR. However, these methods rely on enzymatic digestion to lyse bacterial cells and may bias the final DNA composition toward certain species with membranes and/or cell walls that are more susceptible to digestion by these enzymes (Morgan *et al.*, 2010). DNA extraction that includes physical disruption of bacterial cells by bead beating appears to be less biased, but tends to yield more variable downstream results. The purification method should be determined based on the purpose of the experiment. The Qiagen DNeasy blood and tissue kits, with the accompanying modification for Gram-positive bacteria, yield consistent 16S rRNA gene PCR amplicons from single 7 dpf zebrafish intestines. This is particularly useful if the intestines harbor a known community of bacteria. If the aim of the study is to describe an unknown community, the bead-beating protocol below may be a more suitable choice.

Materials

- 0.1 mm sterile zirconia/silica beads (Biospec Products, cat. no. 11079105z)
- 120 mM sodium phosphate buffer, pH 8.0, filter sterilized
- SDS lysis buffer (10% SDS, 0.5 M Tris–Cl, pH 8.0, 0.1 M NaCl), filter sterilized
- 100 mg/mL lysozyme in sterile PBS. Make fresh each time
- 7.5 M ammonium acetate
- 95% EtOH
- 2 mL sterile screw cap tubes
- Bead beater (Biospec Products, Inc.)
- TE (pH 8.0) or Qiagen buffer EB, filter sterilized
- 1.5 ml sterile tube Isopropanol

(1) Combine in 2-mL screw top tubes:

   (a) Fish intestines
   (b) 0.5 mL beads
   (c) 0.4 mL 120 mM sodium phosphate buffer
   (d) 0.2 mL SDS lysis buffer

(2) Bead beat on high 2 min for adult or 1 min for larval intestines.
(3) Remove supernatant to fresh tube and add lysozyme to 10 mg/mL final concentration.
(4) Incubate tubes for 45 min at 37 °C.
(5) Add 2 volumes 7.5 M ammonium acetate to 5 volumes lysis/DNA solution.
(6) Centrifuge at 13,000 × *g* for 5 min to precipitate protein.
(7) Transfer supernatant to new 1.5-mL tube.
(8) Add 0.7 volumes room temperature isopropanol and mix.
(9) Centrifuge at 13,000 × *g* for 30 min at 4 °C.
(10) Remove supernatant and wash pellet with ice-cold 95% EtOH. (*Note*: Single larval intestines do not generally yield enough DNA to generate a visible pellet.)
(11) Centrifuge at 13,000 × *g* for 5 min.
(12) Carefully remove supernatant from pellet and air dry pellet.
(13) Resuspend DNA pellet in TE (pH 8.0) or Qiagen buffer EB (10 mM Tris–Cl, pH 8.5).

4. Fluorescent *in situ* Hybridization for the Detection of Bacteria

Fluorescent *in situ* hybridization (FISH) with short, fluorophore-conjugated oligonucleotide probes targeting unique sequences in the bacterial 16S rRNA gene is commonly used to examine localization and abundance of known bacteria in a mixed community, such as the intestinal microbiota. Several databases exist that curate known probes (probeBase.org) and facilitate the design of novel probes (Greengenes, the Ribosomal Database Project, and SILVA). New probes must be optimized for specificity and hybridization conditions (particularly the percent of formamide). Here we describe a basic FISH protocol that works well on zebrafish paraffin sections (Bates *et al.*, 2006).

Materials

- 4% Paraformaldehyde (PFA)
- Hybridization buffer:
  - 20 mM Tris-HCl, pH 7.4
  - 0.9 M NaCl
  - 0.1% SDS
  - 35% (v/v) formamide
- Probe (short, fluorophore-conjugated oligo-nucleotides resuspended in nuclease free water)
- 70°C heat block or water bath
- Hybridization chambers (Corning #2551)
- 48°C water bath
- PBS, filter sterilized
- PBSt (0.05% Triton X-100 in filter-sterilized PBS)
- Vectashield (Vector labs) or another mounting medium

(1) Fix 7 dpf larval fish in 4% PFA overnight with shaking. Adult fish should be gavaged with fixative, the head removed behind the gills and the tail removed behind the vent, incisions made on both flanks of the fish above the intestine but below and parallel to the spine, and fixed overnight in 4% PFA with shaking. Section the fish and paraffin fix the sections to slides.
(2) Deparaffin slides and rehydrate through decreasing EtOH concentrations into sterile ddH_2O.
(3) Prewarm 200 μL hybridization buffer per slide at 70 °C.
(4) Dilute probes (final concentration is dependent on type of probe) in hybridization buffer and heat to 70 °C for 5 min.
(5) To equilibrate slide, add 200 μL prewarmed hybridization buffer without probes to each slide; let sit for 1 min, and then wick off excess with paper towel.
(6) Add 150 μL prewarmed, diluted probes to each slide.
(7) Add glass coverslips and place in hybridization chambers with 10 μL hybridization buffer in wells.
(8) Incubate at 48 °C overnight in the dark.
(9) Heat sterile PBS in 48 °C water bath.
(10) Remove slides from hybridization chambers and soak in Coplin jars with PBS at 48 °C for 10 min, or until coverslips fall off when slides are lifted out of Coplin jars.
(11) Rinse twice more, 10 min each, with PBS prewarmed to 48 °C; allow second rinse to come to room temperature.
(12) Rinse briefly with PBSt and mount with glycerol-based mounting media such as Vectashield.

B. Rearing Germ-Free or Gnotobiotic Zebrafish to 30 dpf

There are several different ways to fertilize eggs for the derivation of germ-free fish, each with advantages and disadvantages. Fertilized eggs may be obtained by surgical removal of gametes from adults, squeezing the eggs and sperm from the fish, and fertilizing the eggs in a sterile Petri dish, or by natural breeding. High success in generating bacteria-free zebrafish is achieved using the *in vitro* fertilization method. However, surgical removal of the gametes is not ideal as the adults must be euthanized, and the process of squeezing the gametes from live adult results in a shortened reproductive life and can only be performed every 2 weeks due to the stress on the fish. On the other hand, if a limited number of females are available for generating eggs, a conventional cross is sufficient and can be performed weekly, but usually results in higher contamination rates. Further discussion of these different fertilization methods can be found in Pham *et al.* (2008). Following the fertilization of the eggs, the sorting and cleaning of the eggs is the same for both methods, as outlined in Fig. 3. The protocol has been optimized to generate the cleanest eggs with the highest survival rate and lowest rate of abnormal development.

Zebrafish may be reared for up to 30 days in a sterile environment (Rawls *et al.*, 2006). The choice of housing for the fish will depend on the length of the experiment, number of fish involved, and equipment available. For experiments with fewer than 300 fish and lasting less than 2 weeks, fish may be reared in sterile flasks with changes of EM and feeding occurring in a tissue culture hood. For larger experiments (we typically start with up to 1200 fish) and longer time commitments (up to 30 dpf), fish should be reared in a gnotobiotic isolator. The gnotobiotic isolator requires special equipment and more time to prepare for the experiment, but once the equipment is set up, the EM changes and feeding will be less time consuming. There is also a reduced risk of contamination in a gnotobiotic isolator, because the reagents and fish are maintained in a sterile environment from the start to the end of the experiment. Further discussion of gnotobiotic isolator husbandry and associated protocols can be found in Pham *et al.* (2008).

Sterility of the EM and zebrafish can be monitored in many ways. For daily monitoring, EM can be spotted onto TSA plates and incubated aerobically overnight at 28 °C. Many microbes cannot be cultured on TSA or may require anaerobic

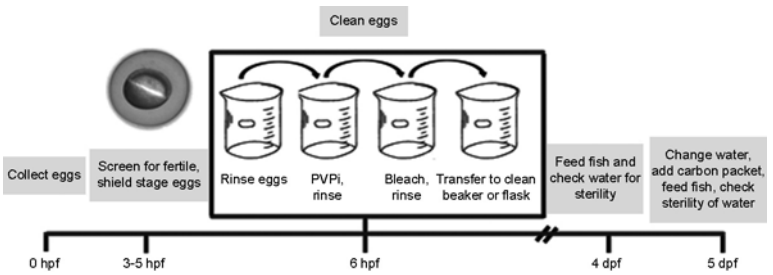

Fig. 3 Timeline for generation and maintenance of germ-free zebrafish.

conditions for growth resulting in false-negative results; however, we have found that for daily monitoring of sterility, this method is sufficient because many common contaminants are aerobic. Alternatively, 16S rRNA genes may be amplified from the EM by PCR and run on an agarose gel for visualization. PCR may result in false-positives due to amplification of DNA from dead organisms or contaminating DNA. For final analysis of the sterility of the water and fish at the end of an experiment, a combination of culturing the water in several liquid media – including TSA, BHI, or nutrient media – 16S rRNA gene PCR amplification, and *in situ* hybridization with 16S rRNA gene-specific probes is sufficient for determining the sterility of the environment.

If experiments are to be carried out to 8 dpf or earlier, zebrafish do not need to be fed. However, zebrafish housed for more than 8 dpf will require a food source because the yolk will be depleted by then. Zebrafish can be fed dry powder diets sterilized either (i) by combining with water to create a slurry that can be sterilized by autoclaving or (ii) by γ-irradiation. However, in our experience, sterile powder diets are not sufficient to support growth and maturation of germ-free zebrafish through metamorphosis (Pham *et al.*, 2008). We are therefore currently exploring the possibility of culturing live germ-free paramecia and brine shrimp to facilitate growth of germ-free zebrafish through metamorphosis toward reproductive maturity.

1. Derivation of Germ-Free Zebrafish

Materials

- Flasks (75 cm^2, 200 mL, sterile, with vented screw tops; for smaller, shorter experiments; 50 zebrafish per flask) or beakers (200–400 mL, autoclaved with foil covers; for use in the gnotobiotic isolator; 50 zebrafish per 50 mL EM in 200-mL beakers or 100 zebrafish per 100 mL EM in 400-mL beakers)
- 40 to 50-mL beakers (bleached, rinsed, and autoclaved with foil covers)
- Sterile, individually wrapped pediatric gradient 3.0-mL pipettes
- 25 or 50-mL graduated pipettes, sterile
- Large beaker (1–2 L) to collect waste
- 70% ethanol in spray bottle
- 6% bleach (sodium hyperchlorite solution, Fisher S5290-1, stored at 4 °C)
- 10% PVP-I stock (polyvinylpyrrolidone–iodine 0.01% free iodine; Western Chemical, Inc.)
- Filter-sterilized EM
- Clidox-S activator and base (if using a gnotobiotic isolator; Pharmacal Research Laboratories, cat. no. 95120F and 96120F)
- Drug stocks (all stored at −20 °C):
  - 100 mg/mL ampicillin
  - 50 mg/mL kanamycin
  - 8 mg/mL amphotericin B

Additional items required for feeding and changing water for sterile fish:

- Sterile food in 1- to 4-mL aliquots
- Filter-sterilized EM (enough to change 70% of water per day)
- 10 µL sterile loops
- TSA plates for plating water
- Beads to spread bacteria on TSA plates, or p20 pipette to plate 10 µL of water
- Ammo-Carb (Aquarium Pharmaceuticals, Inc., PA), rinsed, dried, placed in mesh packets or cotton muslin tea bags, and autoclaved

Solutions (Make the Same Day as Use)

Antibiotic EM:

- 150 µL ampicillin 100 mg/mL (100 µg/mL final)
- 25 µL kanamycin 50 mg/mL (5 µg/mL final)
- 7.8 µL amphotericin B 8 mg/mL (250 ng/mL final)
- 250 µL EM
- Filter sterilize with 0.22 µm filter

0.003% bleach solution:

- 125 µL 6.0% bleach solution
- 250 mL EM
- Filter sterilize with 0.22 µm filter

0.1% PVP-I solution (polyvinylpyrrolidone–iodine [0.01% free iodine] Western Chemical, Inc.):

- 2.5 mL 10% PVP-I stock (5 g PVP-I in 50 mL nanopure water)
- 247.5 mL EM
- Filter sterilize with 0.22 µm filter

0.4% tricaine (3-aminobenzoic acid ethyl ester):

- 400 mg tricaine
- 97.9 mL H_2O
- 2.1 mL Tris 1 M (pH 9.0)
- Adjust to pH 7.0; filter sterilize with 0.22 µm filter
- This can be made ahead of time and stored for long periods at −20 °C or for up to 2 weeks at 4 °C

(1) Collect embryos in antibiotic EM.
(2) Incubate embryos at 28–30 °C between 4 and 6 h.
(3) Collect viable embryos in 50 mL antibiotic EM in beakers.
    (a) For embryos grown at 30 °C, collect embryos at about 5 hours postfertilization (hpf); for embryos kept at 28 °C, wait until 6–7 hpf.
    (b) Wear gloves.

(c) Transfer up to 300 embryos in 50% epiboly, germ ring or shield stage into sterile, autoclaved 50-mL beaker containing ~40 mL filter-sterilized EM.

(4) Clean the following with 70% ethanol; transfer into the hood and UV treat for up to 10 min (per 300 embryos cleaned):

(a) 3 sterile 50-mL beakers with foil tops
(b) Individually wrapped, sterile transfer pipettes
(c) 1 L filter-sterilized EM
(d) 0.003% bleach
(e) 0.1% PVP-I
(f) Sterile flasks – 75 cm^2 with vented screw topped caps (in hood, add 48 mL sterile EM to each flask prior to adding embryos)
(g) 15 or 50 mL pipettes, sterile, individually wrapped
(h) Pipette aid
(i) Large 1- to 2-L beaker for collecting waste

(5) Transfer embryos to clean beaker.

(a) Pour off all but ~10 mL EM into waste container.
(b) Transfer remaining 10 mL EM with eggs into clean 50-mL beaker.
(c) Add ~20 mL sterile EM to first beaker to get remaining eggs.
(d) Transfer remaining eggs to beaker.
(e) Bring volume in second beaker up to 50 mL with sterile EM.

(6) Rinse embryos 3× with 50 mL filter-sterilized EM.
(7) Immerse embryos in ~50 mL 0.1% PVP-I solution for exactly 2 min.
(8) Rinse embryos with sterile EM 1×.
(9) Transfer embryos to fresh beaker as in step 5.
(10) Rinse embryos in sterile EM an additional 2×.
(11) Immerse embryos in 0.003% bleach for 10 min. Do not bleach more than 30 min as this will result in embryo mortality.
(12) Rinse embryos in sterile EM 1×.
(13) Transfer embryos to fresh beaker as in step 5.
(14) Rinse embryos additional 2× in sterile EM (if using gnotobiotic isolator, transfer embryos to sterile 15-mL conical tube and clean outside of tube with Clidox for at least 20 min).
(15) Transfer 40–50 embryos to flasks containing sterile EM using sterile, individually wrapped pipettes (gnotobiotic isolator: transfer embryos to beakers containing sterile EM).
(16) Incubate embryos at 28.5 °C.
(17) Feed fish if maintained longer than 8 dpf, starting at 4 dpf.
(18) Feeding: spray the following with 70% EtOH and place into a sterile hood (gnotobiotic isolator should already contain these items):

(a) Large flask for liquid waste
(b) 10 to 25- and 1- to 50-mL pipettes, sterile and individually wrapped

(c) 1 L filter-sterilized EM
(d) Sterile 10-μL loops
(e) Aliquot of sterile food

(19) Use a 25-mL pipette to remove 70% of the EM and most of the debris from the flask, including any dead zebrafish, undeveloped eggs, and empty chorions.
(20) Plate 10–100 μL of flask EM on TSA; incubate plate at 28.5 °C to screen for contaminants.
(21) Replace the EM with an equal volume of filter-sterilized EM.
(22) Place a loop full of food into the flask.
(23) Return flasks to 28.5 °C.
(24) At 5 dpf, add rinsed, autoclaved ammo-carb packets or cotton muslin tea bags to flasks or beakers during water change and feeding:

(a) Rinse ammo-carb with distilled water until water is clear.
(b) Dry rinse ammo-carb in fume hood overnight.
(c) Place about 5 g ammo-carb into mesh packets (should fit through neck of 75-cm^2 flask; for beakers use cotton muslin tea bags) and seal.
(d) Autoclave ammo-carb packets in aluminum foil.
(e) Store at room temperature.
(f) When changing water and feeding on 5 dpf, remove sterile ammo-carb packet from foil and gently place into flask.

2. Bacterial Association of Germ-Free Zebrafish

At 3 dpf, the anterior alimentary tract is patent and the intestine may be colonized by bacteria from the medium. The bacterial inoculums should be determined empirically for each species used. For many bacteria, 10^4 CFU/mL EM suffices for full colonization of the intestine and minimal toxicity to the fish. Prior to inoculation of the EM with bacteria, dead larvae in the flask should be removed as this will often result in increased bacterial growth, which can ultimately be fatal to the remaining larvae. The method below is used for several Proteobacteria strains in our laboratory. Please note that any experiments involving exposure of zebrafish to commensal microorganisms must be approved in advance by the appropriate Institutional Animal Care and Use Committee.
Materials:

- Spectrophotometer, 600 nm
- 75cm^2 flask
- Tryptic Soy Agar (TSA) plates

(1) Incubate bacteria for 16 h in 50 mL of growth medium in 250-mL flask at 28–30 °C, 200 rpm.
(2) Measure the optical density at 600 nm (OD_{600}) of the culture.

(3) Calculate the original culture density, assuming 1 $OD_{600} = 10^9$ CFU/mL.
(4) Dilute culture to predetermined concentration as needed in filter-sterilized EM and inoculate flask in tissue culture hood.
(5) Plate dilutions of the original bacterial culture in order to verify the CFU/mL of the inoculum.

C. Infection of Zebrafish with Pathogens

1. Infections of Embryos and Larvae by Static Immersion with Bacterial Pathogens

The factors discussed above should be taken into account when designing the parameters for infection of zebrafish with a bacterial pathogen. For example, as we developed the *E. tarda* infection model, we considered the fact that *E. tarda* is a fish pathogen and likely could be used in a static immersion infection. Interestingly, *E. tarda* and the related pathogen *Edwardsiella ictaluri* were recently found to be members of the normal intestinal microbiota in wild yellow catfish and wild-caught zebrafish, respectively (Roeselers *et al.*, 2011). The following section outlines the protocols for infecting zebrafish embryos by immersion using *E. tarda* as an example (Pressley *et al.*, 2005). Please note that any experiments involving exposure or infection of zebrafish to pathogenic microorganisms must be approved in advance by the appropriate Institutional Animal Care and Use Committee.

Materials

- Spectrophotometer, 600nm
- 1.5 ml tubes
- Cuvettes for 600nm readings
- Dumont watchmaker forceps #5
- 35 × 10 mm disposable polystyrene Petri dishes (USA Scientific, no. 5662-7161)
- Extra deep 100 × 20 mm polystyrene Petri dishes (Fisher Scientific, no. 08-757-11Z)
- Transfer pipettes
- 0.5% methylene blue
- Spectrophotometer
- 15 ml conical tubes
- Cuvettes
- Dumont Watchmaker's forceps no. 5

Solutions

- *Egg water:*
  - 60 mg Instant Ocean® sea salts
  - Bring to 1 L with dH_2O
  - Autoclave
  - Prewarm to 28 °C

- *E. ictaluri medium* (EIM, described by Shotts and Waltman, 1990):
  - 40 g/L TSA
  - 10 g/L yeast extract
  - 0.03 g/L Bromthymol Blue
  - 1.0 g/L bile salts and 3.5 g/L mannitol
  - 1.0 mg/L colistin B
  - Bring to 1 L with ddH_2O; autoclave to sterilize
- *Luria broth:*
  - 10 g/L casein peptone
  - 5 g/L yeast extract
  - 5 g/L NaCl
  - Bring to 1 L with ddH_2O; autoclave to sterilize

(1) Prepare bacterial culture:

(a) Streak *E. tarda* from a freezer stock on an EIM plate. Incubate at 28 °C overnight.
(b) Twelve hours prior to infection, prepare two cultures of *E. tarda* in Luria broth by aseptically picking a colony from an EIM agar plate and inoculating 4 mL LB in a 15-mL conical tube.
(c) Shake cultures overnight (12 h) at 250 rpm in a 28 °C incubator.

(2) Prepare and quantify the bacterial culture for infection:

(a) Subculture *E. tarda* by adding 1 mL of the overnight culture into 3 mL of fresh media.
(b) Measure the OD_{600} of the subculture after 1–1.5 h by diluting the culture 1:10 (100 μL into 0.9 mL PBS), transferring the dilution to a cuvette and measuring the OD_{600} in a spectrophotometer.
(c) Dilute the bacterial cultures with sterile egg water in a final volume of 2 mL.

(3) Collect embryos:

(a) Separate embryos into no more than 100 per dish.
(b) Remove most of the water from the dish using a transfer pipette.
(c) Add 60 mL of egg water to each dish and supplement with 20 μL of 0.5% methylene blue on the first day only, as methylene blue may inhibit infection with pathogen. Add 60 mL of egg water every day following.

(4) Prepare embryos for infection:

(a) Remove most of the water and dead embryos with a transfer pipette and add 60 mL of fresh egg water (with no methylene blue) to each dish.
(b) Manually dechorionate all embryos with Dumont Watchmaker's forceps no. 5 in each dish and move the embryos into new dishes, approximately 100 per dish, with 60 mL of fresh egg water.

(5) Infect 24 hpf embryos by immersion:

(a) Transfer the manually dechorionated 24 hpf embryos to a 35-mm Petri dish and remove as much of the egg water as possible.
(b) Add the egg water containing the bacterial culture at the appropriate concentration to the dish of embryos.
(c) Incubate the embryos in the bacterial suspension for 5 h at 28 °C.
(d) After 5 h, carefully transfer the embryos to a wash dish containing 60 mL of sterile egg water.
(e) Carefully transfer all the embryos from this dish into a new dish of fresh egg water and hold at 28 °C.
(f) Dishes of embryos should be monitored daily, dead embryos removed, and fresh egg water added.

2. Infections of Embryos and Larva by Injection with Bacterial or Viral Pathogens

In contrast to the natural fish pathogen *E. tarda*, *P. aeruginosa*, a ubiquitous microbe that is isolated in fresh water environments, is not likely to cause infection in an aquatic species through immersion unless the host is immune-compromised. We found that it was necessary to inject *P. aeruginosa* to establish infection. The following protocol outlines the methods for infecting zebrafish embryos by microinjection using *P. aeruginosa* as an example (Phennicie *et al.*, 2010). A similar injection technique is used when infecting embryos or larva with virus. Preparation of virus should be carried out as outlined in sectino 3.

Materials

- Extra deep 100 × 20 mm polystyrene Petri dishes (Fisher Scientific, no. 08-757-11Z)
- 100 × 15 mm disposable polystyrene Petri dishes (Fisher Scientific, no. 08-757-13) that have been filled half with 3% agarose in deionized water
- 1 × 0.01 mm stage micrometer for droplet calibration (Fisher, cat. no. 12-561-SM1)
- Halocarbon oil, series 27 (Sigma, cat. no. H8773)
- MPPI-2 pressure injection system (Applied Scientific Instrumentation, Eugene, OR) mounted on an Olympus SZ61 stereo microscope
- Microinjection needles drawn from 1.2 mm OD, 0.69 mm ID borosilicate glass micropipette tubes (Sutter, no. BF120-69-10) using a P97 Flaming/Brown micropipette puller (Sutter, no. P97) or similar equipment
- Dumont Watchmaker's forcep no.5
- 0.5% methylene blue
- PBS

Solutions

- *Egg water*:
  - 60 mg Instant Ocean® sea salts
  - Bring to 1 L with dH_2O

- Autoclave
- Prewarm to 28 °C

- *Luria broth:*
  - 10 g/L casein peptone
  - 5 g/L yeast extract
  - 5 g/L NaCl
  - Bring to 1 L with ddH_2O; autoclave to sterilize
- Tricaine (Western Chemical, Inc.) at 200 μg/mL in sterile egg water. Note: Extended periods of time in the tricaine solution should be avoided. A stock solution of 4 mg/mL tricaine in Tris-buffered egg water can be prepared in advance and stored at −20 °C for about a month
- *Cetrimide agar* (Neogen, no. 7222A)

(1) Embryo collection:

(a) Separate embryos into no more than 100 per dish.
(b) Remove most of the water from the dish using a transfer pipette.
(c) Add 60 mL of egg water to each dish and supplement with 20 μL of 0.5% methylene blue.
(d) Remove dead embryos from each dish and place viable embryos in 60 mL of fresh egg water every 24 h.

(2) Prepare bacterial culture:

(a) Prepare an isolation streak of *P. aeruginosa* from a freezer stock on a cetrimide agar plate. Place the plate in a 37 °C incubator overnight.
(b) Twelve hours prior to infection, prepare two cultures of *P. aeruginosa* in Luria broth by aseptically picking a colony from a cetrimide agar plate and inoculate 5 mL of Luria broth in a 20-mL test tube. Shake overnight at 250 rpm in a 37 °C incubator.
(c) Wash the overnight culture twice by centrifuging at 4000 rpm for 15 min at 4 °C and resuspend in 5 mL of PBS.
(d) Determine the relationship between OD_{600} and viable cell density in the growing culture. Use OD_{600} to determine the bacterial cell density.
(e) Dilute washed culture in PBS to the desired inoculum size.

(3) Prepare zebrafish embryos for injection:

(a) Manually dechorionate all fish using Dumont Watchmaker's forceps no. 5.
(b) Remove dead fish and most of the egg water with transfer pipette and add 60 mL of fresh egg water to each dish.
(c) Thaw a frozen 2-mL aliquot of the 4 mg/mL tricaine stock solution.

(4) Infect 48 hpf zebrafish embryos by microinjection:

(a) Load the culture dilution into the needle and clip the end of the microinjection needle so that the droplet is equal to 5 nL.

i. Clean the calibration micrometer ruler slide with ethanol and on it place a single drop of halocarbon oil.
ii. Inject a single droplet of liquid into the oil and measure the diameter of the spherical droplet.
iii. Adjust the injection volume accordingly.

(b) Prepare 45 mL of egg water with 2 mL of tricaine to a final concentration of 200 μg/mL and move the embryos for injection into this dish for no more than 5 min.
(c) Transfer the embryos from the tricaine to the surface of a Petri dish that has been filled half with 3% agarose (this provides a semisolid substrate to align the sedated embryos), leaving as little water on the surface of the agarose as possible and aligning the fish in the same direction on the plate.
(d) Inject 5 nL of the bacterial suspension into the duct of Cuvier of each embryo as shown in Fig. 1.
(e) Carefully rinse and transfer the embryos from the injection plate into a new dish containing 60 mL of fresh egg water and maintain the embryos at 28 °C.
(f) Dishes of embryos should be monitored daily, dead embryos removed, and fresh egg water added.

3. Infections of Embryos and Larva by Static Immersion with Viral Pathogens

The following section outlines the protocols for infecting zebrafish embryos by immersion, using snakehead rhabdovirus as an example (Phelan *et al.*, 2005b). The titer of the virus should be determined and a range of doses tested. Factors to consider include the infectious dose that will cause 50% mortality and whether or not infection is dose dependent.

Materials

- 100 × 20 and 35 × 10 mm Petri dishes
- Dumont Watchmaker's forceps no. 5
- Transfer pipettes
- *Egg water*:
  - 60 mg Instant Ocean® sea salts
  - Bring to 1 L with dH_2O
  - Autoclave and prewarm to 28 °C
  - Perosan (1.5 mL/L)
- PBS
- Perosan (1.5 mL/L).

Methods

(1) Embryo collection:

(a) Separate embryos into no more than 100 per 100 × 20 mm Petri dish.
(b) Remove most of the water from the dish using a transfer pipette.
(c) Add 60 mL of egg water to each dish.
(d) At 4–6 hpf, disinfect embryos by rinsing in Perosan (1.5 mL/L) for 1 min.

(2) Prepare embryos for infection:

(a) Remove most of the water and dead embryos with a transfer pipette and add 60 mL of fresh egg water to each dish.
(b) At 3 dpf, manually dechorionate all embryos using Dumont Watchmaker's forceps no. 5 and transfer the embryos into new dishes, approximately 100 per dish, with 60 mL of fresh egg water.

(3) Infect 3 dpf embryos by static immersion:

(a) Transfer the manually dechorionated 3 dpf embryos to a 35 × 10 mm Petri dish and remove as much of the egg water as possible.
(b) Expose the embryos to 10^6 $TCID_{50}$ of SHRV/mL in 3 mL of egg water. Control embryos should be exposed to an equal volume of PBS in 3 mL of egg water.
(c) Immerse the embryos for 5 h at 28 °C.
(d) After 5 h, carefully transfer the embryos to a wash dish containing 60 mL of sterile egg water.
(e) Carefully transfer all of the embryos from this dish into a new dish of fresh egg water and hold at 28 °C.
(f) Dishes of embryos should be monitored daily, dead embryos removed, and fresh egg water added.

4. Infections of Adults by Intraperitoneal Injection with Viral or Bacterial Pathogens

The following section outlines the protocols for infecting zebrafish adults by intraperitoneal injection using snakehead rhabdovirus as an example (Phelan *et al.*, 2005b). The injection technique is similar when infecting adults with bacteria that have been prepared as outlined above.

An alternative method for infecting adult zebrafish involves abrading the skin of the fish and infecting by static immersion (Nayak *et al.*, 2007; Neely *et al.*, 2002; Phelan *et al.*, 2005b; Pressley *et al.*, 2005). In nature, fish are often rendered more susceptible to infection under crowded conditions, for instance, during spawning, when fish rub and bump into one another repeatedly. Minor injuries and surface abrasion provide entryways for pathogens to penetrate and infect the host. In the laboratory, a hypodermic needle can be used to scrape and remove a small area of scales and skin from the zebrafish. The host can then be exposed to pathogen by static immersion as described above.

Materials

- Repeating pipetter
- 0.5-mL syringe tip (VWR, no. 80085-980)
- 30-gauge needles
- Small strips of Parafilm to attach needle to syringe tip
- Nets
- 500 mL beaker/tub for anesthetization
- PBS
- Tricaine (0.4 mg/100 mL)

Methods

(1) Prepare adults for infection:

   (a) All adult fish (>3 months old) used in infection experiments should be placed in an isolated flow-through system, maintained at 28 °C with a flow rate of 150 L/min, and acclimated for several days before infection.
   (b) Prepare anesthetization solution by adding 20 mL of Tricaine to 480 mL of system water. Anesthetize as many fish as can be injected in 5 min. Ensure the fish have stopped gill movements before injection to ensure adequate anesthesia.

(2) Infect adult zebrafish by intraperitoneal injection:

   (a) Virus or bacterial dilutions should be prepared in PBS. Control uninfected fish should be injected with PBS alone, and should be injected before preparing the virus to prevent any virus contamination.
   (b) Install a 0.5-mL syringe tip onto the repeating pipettor. Place a 30-gauge needle on the tip of the 0.5-mL syringe tip and hold in place by wrapping Parafilm around the base of the needle and end of the syringe tip.
   (c) Place the fish in a supine position. With the needle parallel to the spine, insert it into the midline of the abdomen just posterior to the pectoral fins pointing to the anterior section of the fish. The needle should penetrate only 1–2 mm.
   (d) Inject 10 μL into each fish. Place injected fish into a tank of system water and allow them to recuperate before placing back into the flow-through system.
   (e) Fish should be monitored and fed daily.

References

Adams, K. N., Takaki, K., Connolly, L. E., Wiedenhoft, H., Winglee, K., Humbert, O., Edelstein, P. H., Cosma, C. L., and Ramakrishnan, L. (2011). Drug tolerance in replicating mycobacteria mediated by a macrophage-induced efflux mechanism. *Cell* **145**, 39–53.

Aggad, D., Mazel, M., Boudinot, P., Mogensen, K. E., Hamming, O. J., Hartmann, R., Kotenko, S., Herbomel, P., Lutfalla, G., and Levraud, J. P. (2009). The two groups of zebrafish virus-induced interferons signal via distinct receptors with specific and shared chains. *J. Immunol.* **183**, 3924–3931.

Aggad, D., Stein, C., Sieger, D., Mazel, M., Boudinot, P., Herbomel, P., Levraud, J. P., Lutfalla, G., and Leptin, M. (2010). In vivo analysis of Ifn-gamma1 and Ifn-gamma2 signaling in zebrafish. *J. Immunol.* **185**, 6774–6782.

Alonso, M., Kim, C. H., Johnson, M. C., Pressley, M., and Leong, J. A. (2004). The NV gene of snakehead rhabdovirus (SHRV) is not required for pathogenesis, and a heterologous glycoprotein can be incorporated into the SHRV envelope. *J. Virol.* **78**, 5875–5882.

Altmann, S. M., Mellon, M. T., Distel, D. L., and Kim, C. H. (2003). Molecular and functional analysis of an interferon gene from the zebrafish. *Danio rerio. J. Virol.* **77**, 1992–2002.

Altmann, S. M., Mellon, M. T., Johnson, M. C., Paw, B. H., Trede, N. S., Zon, L. I., and Kim, C. H. (2004). Cloning and characterization of an Mx gene and its corresponding promoter from the zebrafish. *Danio rerio. Dev. Comp. Immunol.* **28**, 295–306.

Bates, J. M., Akerlund, J., Mittge, E., and Guillemin, K. (2007). Intestinal alkaline phosphatase detoxifies lipopolysaccharide and prevents inflammation in zebrafish in response to the gut microbiota. *Cell Host Microbe* **2**, 371–382.

Bates, J. M., Mittge, E., Kuhlman, J., Baden, K. N., Cheesman, S. E., and Guillemin, K. (2006). Distinct signals from the microbiota promote different aspects of zebrafish gut differentiation. *Dev. Biol.* **297**, 374–386.

Bates, C. S., Toukoki, C., Neely, M. N., and Eichenbaum, Z. (2005). Characterization of MtsR, a new metal regulator in group A streptococcus, involved in iron acquisition and virulence. *Infect. Immun.* **73**, 5743–5753.

Bouskra, D., Brezillon, C., Berard, M., Werts, C., Varona, R., Boneca, I. G., and Eberl, G. (2008). Lymphoid tissue genesis induced by commensals through NOD1 regulates intestinal homeostasis. *Nature* **456**, 507–510.

Brannon, M. K., Davis, J. M., Mathias, J. R., Hall, C. J., Emerson, J. C., Crosier, P. S., Huttenlocher, A., Ramakrishnan, L., and Moskowitz, S. M. (2009). *Pseudomonas aeruginosa* type III secretion system interacts with phagocytes to modulate systemic infection of zebrafish embryos. *Cell. Microbiol.* **11**, 755–768.

Brugman, S., Liu, K. Y., Lindenbergh-Kortleve, D., Samsom, J. N., Furuta, G. T., Renshaw, S. A., Willemsen, R., and Nieuwenhuis, E. E. (2009). Oxazolone-induced enterocolitis in zebrafish depends on the composition of the intestinal microbiota. *Gastroenterology* **137**, 1757–17670.

Bry, L., Falk, P. G., Midtvedt, T., and Gordon, J. I. (1996). A model of host–microbial interactions in an open mammalian ecosystem. *Science* **273**, 1380–1383.

Buller, N. B. (2004). *Bacteria from Fish and Other Aquatic Animals: A Practical Identification Manual.* CABI Publishing, Wallingford, UK.

Burgos, J. S., Ripoll-Gomez, J., Alfaro, J. M., Sastre, I., and Valdivieso, F. (2008). Zebrafish as a new model for herpes simplex virus type 1 infection. *Zebrafish* **5**, 323–333.

Carvalho, R., de Sonneville, J., Stockhammer, O. W., Savage, N. D., Veneman, W. J., Ottenhoff, T. H., Dirks, R. P., Meijer, A. H., and Spaink, H. P. (2011). A high-throughput screen for tuberculosis progression. *PLoS One* **6**, e16779.

Cebra, J. J., Periwal, S. B., Lee, G., Lee, F., and Shroff, K. E. (1998). Development and maintenance of the gut-associated lymphoid tissue (GALT): the roles of enteric bacteria and viruses. *Dev. Immunol.* **6**, 13–18.

Cheesman, S. E., Neal, J. T., Mittge, E., Seredick, B. M., and Guillemin, K. (2011). Epithelial cell proliferation in the developing zebrafish intestine is regulated by the Wnt pathway and microbial signaling via Myd88. *Proc. Natl. Acad. Sci. U. S. A.* **108**(suppl. 1), 4570–4577.

Cho, K. H., and Caparon, M. G. (2005). Patterns of virulence gene expression differ between biofilm and tissue communities of *Streptococcus pyogenes*. *Mol. Microbiol.* **57**, 1545–1556.

Clatworthy, A. E., Lee, J. S., Leibman, M., Kostun, Z., Davidson, A. J., and Hung, D. T. (2009). *Pseudomonas aeruginosa* infection of zebrafish involves both host and pathogen determinants. *Infect. Immun.* **77**, 1293–1303.

Clay, H., Davis, J. M., Beery, D., Huttenlocher, A., Lyons, S. E., and Ramakrishnan, L. (2007). Dichotomous role of the macrophage in early *Mycobacterium marinum* infection of the zebrafish. *Cell Host Microbe* **2**, 29–39.

Clay, H., Volkman, H. E., and Ramakrishnan, L. (2008). Tumor necrosis factor signaling mediates resistance to mycobacteria by inhibiting bacterial growth and macrophage death. *Immunity* **29**, 283–294.

Davis, J. M., Clay, H., Lewis, J. L., Ghori, N., Herbomel, P., and Ramakrishnan, L. (2002). Real-time visualization of mycobacterium-macrophage interactions leading to initiation of granuloma formation in zebrafish embryos. *Immunity* **17**, 693–702.

Davis, J. M., Haake, D. A., and Ramakrishnan, L. (2009). *Leptospira interrogans* stably infects zebrafish embryos, altering phagocyte behavior and homing to specific tissues. *PLoS Negl. Trop. Dis.* **3**, e463.

Davis, J. M., and Ramakrishnan, L. (2009). The role of the granuloma in expansion and dissemination of early tuberculous infection. *Cell* **136**, 37–49.

Deng, Y., Boon, C., Eberl, L., and Zhang, L. H. (2009). Differential modulation of *Burkholderia cenocepacia* virulence and energy metabolism by the quorum-sensing signal BDSF and its synthase. *J. Bacteriol.* **191**, 7270–7278.

Ellett, F., Pase, L., Hayman, J. W., Andrianopoulos, A., and Lieschke, G. J. (2011). mpeg1 promoter transgenes direct macrophage-lineage expression in zebrafish. *Blood* **117**, e49–e56.

Encinas, P., Rodriguez-Milla, M. A., Novoa, B., Estepa, A., Figueras, A., and Coll, J. (2010). Zebrafish fin immune responses during high mortality infections with viral haemorrhagic septicemia rhabdovirus. A proteomic and transcriptomic approach. *BMC Genomics* **11**, 518.

Falkow, S. (1988). Molecular Koch's postulates applied to microbial pathogenicity. *Rev. Infect. Dis.* **10** (suppl. 2), S274–S276.

Fraune, S., and Bosch, T. C. (2010). Why bacteria matter in animal development and evolution. *Bioessays* **32**, 571–580.

Gao, L. Y., Pak, M., Kish, R., Kajihara, K., and Brown, E. J. (2006). A mycobacterial operon essential for virulence in vivo and invasion and intracellular persistence in macrophages. *Infect. Immun.* **74**, 1757–1767.

Garner, J. N., Joshi, B., and Jagus, R. (2003). Characterization of rainbow trout and zebrafish eukaryotic initiation factor 2alpha and its response to endoplasmic reticulum stress and IPNV infection. *Dev. Comp. Immunol.* **27**, 217–231.

Gray, C., Loynes, C. A., Whyte, M. K., Crossman, D. C., Renshaw, S. A., and Chico, T. J. (2011). Simultaneous intravital imaging of macrophage and neutrophil behaviour during inflammation using a novel transgenic zebrafish. *Thromb. Haemost.* **105**, 811–819.

Harriff, M. J., Bermudez, L. E., and Kent, M. L. (2007). Experimental exposure of zebrafish, Danio rerio (Hamilton), to Mycobacterium marinum and Mycobacterium peregrinum reveals the gastrointestinal tract as the primary route of infection: a potential model for environmental mycobacterial infection. *J. Fish Dis.* **30**, 587–600.

Herbomel, P., Thisse, B., and Thisse, C. (1999). Ontogeny and behaviour of early macrophages in the zebrafish embryo. *Development* **126**, 3735–3745.

Hermann, A. C., and Kim, C. H. (2005). Effects of arsenic on zebrafish innate immune system. *Mar. Biotechnol. (NY)* **7**, 494–505.

Hermann, A. C., Millard, P. J., Blake, S. L., and Kim, C. H. (2004). Development of a respiratory burst assay using zebrafish kidneys and embryos. *J. Immunol. Methods* **292**, 119–129.

Hooper, L. V., Wong, M. H., Thelin, A., Hansson, L., Falk, P. G., and Gordon, J. I. (2001). Molecular analysis of commensal host–microbial relationships in the intestine. *Science* **291**, 881–884.

Husebye, E., Hellstrom, P. M., and Midtvedt, T. (1994). Intestinal microflora stimulates myoelectric activity of rat small intestine by promoting cyclic initiation and aboral propagation of migrating myoelectric complex. *Dig. Dis. Sci.* **39**, 946–956.

Kandori, H., Hirayama, K., Takeda, M., and Doi, K. (1996). Histochemical, lectin-histochemical and morphometrical characteristics of intestinal goblet cells of germfree and conventional mice. *Exp. Anim.* **45**, 155–160.

Kanther, M., and Rawls, J. F. (2010). Host–microbe interactions in the developing zebrafish. *Curr. Opin. Immunol.* **22**, 10–19.

Kanther, M., Sun, X., Muhlbauer, M., Mackey, L. C., Flynn 3rd, E. J., Bagnat, M., Jobin, C., and Rawls, J. F. (2011). Microbial colonization induces dynamic temporal and spatial patterns of NF-kappaB activation in the zebrafish digestive tract. *Gastroenterology* **146**, 197–207.

Kizy, A. E., and Neely, M. N. (2009). First *Streptococcus pyogenes* signature-tagged mutagenesis screen identifies novel virulence determinants. *Infect. Immun.* **77**, 1854–1865.

Lam, S. H., Chua, H. L., Gong, Z., Lam, T. J., and Sin, Y. M. (2004). Development and maturation of the immune system in zebrafish, Danio rerio: a gene expression profiling, in situ hybridization and immunological study. *Dev. Comp. Immunol.* **28**, 9–28.

LaPatra, S. E., Barone, L., Jones, G. R., and Zon, L. I. (2000). Effects of infectious hematopoietic necrosis virus and infectious pancreatic necrosis virus infection on hematopoietic precursors of the zebrafish. *Blood Cells Mol. Dis.* **26**, 445–452.

Lawson, N. D., and Weinstein, B. M. (2002). In vivo imaging of embryonic vascular development using transgenic zebrafish. *Dev. Biol.* **248**, 307–318.

Levraud, J. P., Disson, O., Kissa, K., Bonne, I., Cossart, P., Herbomel, P., and Lecuit, M. (2009). Real-time observation of *Listeria* monocytogenes-phagocyte interactions in living zebrafish larvae. *Infect. Immun.* **77**, 3651–3660.

Lin, B., Chen, S., Cao, Z., Lin, Y., Mo, D., Zhang, H., Gu, J., Dong, M., Liu, Z., and Xu, A. (2007). Acute phase response in zebrafish upon *Aeromonas salmonicida* and *Staphylococcus aureus* infection: striking similarities and obvious differences with mammals. *Mol. Immunol.* **44**, 295–301.

Llamas, M. A., van der Sar, A., Chu, B. C., Sparrius, M., Vogel, H. J., and Bitter, W. (2009). A novel extracytoplasmic function (ECF) sigma factor regulates virulence in *Pseudomonas aeruginosa*. *PLoS Pathog.* **5**, e1000572.

Lowe, B. A., Miller, J. D., and Neely, M. N. (2007). Analysis of the polysaccharide capsule of the systemic pathogen *Streptococcus iniae* and its implications in virulence. *Infect. Immun.* **75**, 1255–1264.

Lu, M. W., Chao, Y. M., Guo, T. C., Santi, N., Evensen, O., Kasani, S. K., Hong, J. R., and Wu, J. L. (2008). The interferon response is involved in nervous necrosis virus acute and persistent infection in zebrafish infection model. *Mol. Immunol.* **45**, 1146–1152.

Ludwig, M., Palha, N., Torhy, C., Briolat, V., Colucci-Guyon, E., Bremont, M., Herbomel, P., Boudinot, P., and Levraud, J. P. (2011). Whole-body analysis of a viral infection: vascular endothelium is a primary target of infectious hematopoietic necrosis virus in zebrafish larvae. *PLoS Pathog.* **7**, e1001269.

Mathias, J. R., Perrin, B. J., Liu, T. X., Kanki, J., Look, A. T., and Huttenlocher, A. (2006). Resolution of inflammation by retrograde chemotaxis of neutrophils in transgenic zebrafish. *J. Leukoc. Biol.* **80**, 1281–1288.

Meijer, A. H., Verbeek, F. J., Salas-Vidal, E., Corredor-Adamez, M., Bussman, J., van der Sar, A. M., Otto, G. W., Geisler, R., and Spaink, H. P. (2005). Transcriptome profiling of adult zebrafish at the late stage of chronic tuberculosis due to *Mycobacterium marinum* infection. *Mol. Immunol.* **42**, 1185–1203.

Menudier, A., Rougier, F. P., and Bosgiraud, C. (1996). Comparative virulence between different strains of *Listeria* in zebrafish (*Brachydanio rerio*) and mice. *Pathol. Biol. (Paris)* **44**, 783–789.

Miller, J. D., and Neely, M. N. (2005). Large-scale screen highlights the importance of capsule for virulence in the zoonotic pathogen *Streptococcus iniae*. *Infect. Immun.* **73**, 921–934.

Montanez, G. E., Neely, M. N., and Eichenbaum, Z. (2005). The streptococcal iron uptake (Siu) transporter is required for iron uptake and virulence in a zebrafish infection model. *Microbiology* **151**, 3749–3757.

Morgan, J. L., Darling, A. E., and Eisen, J. A. (2010). Metagenomic sequencing of an in vitro-simulated microbial community. *PLoS One* **5**, e10209.

Moyer, T. R., and Hunnicutt, D. W. (2007). Susceptibility of zebra fish *Danio rerio* to infection by *Flavobacterium columnare* and *F. johnsoniae*. *Dis. Aquat. Organ.* **76**, 39–44.

Nayak, A. S., Lage, C. R., and Kim, C. H. (2007). Effects of low concentrations of arsenic on the innate immune system of the zebrafish (*Danio rerio*). *Toxicol. Sci.* **98**, 118–124.

Neely, M. N., Pfeifer, J. D., and Caparon, M. (2002). Streptococcus-zebrafish model of bacterial pathogenesis. *Infect. Immun.* **70**, 3904–3914.

Novoa, B., Romero, A., Mulero, V., Rodriguez, I., Fernandez, I., and Figueras, A. (2006). Zebrafish (*Danio rerio*) as a model for the study of vaccination against viral haemorrhagic septicemia virus (VHSV). *Vaccine* **24**, 5806–5816.

O'Toole, R., Von Hofsten, J., Rosqvist, R., Olsson, P. E., and Wolf-Watz, H. (2004). Visualisation of zebrafish infection by GFP-labelled *Vibrio anguillarum*. *Microb. Pathog.* **37**, 41–46.

Ordas, A., Hegedus, Z., Henkel, C. V., Stockhammer, O. W., Butler, D., Jansen, H. J., Racz, P., Mink, M., Spaink, H. P., and Meijer, A. H. (2010). Deep sequencing of the innate immune transcriptomic response

of zebrafish embryos to *Salmonella* infection. *Fish Shellfish Immunol* (Epub ahead of print) 2010 Sep 8. PMID: 20816807.

Parichy, D. M., Ransom, D. G., Paw, B., Zon, L. I., and Johnson, S. L. (2000). An orthologue of the kit-related gene fms is required for development of neural crest-derived xanthophores and a subpopulation of adult melanocytes in the zebrafish, Danio rerio. *Development* **127**, 3031–3044.

Petrie-Hanson, L., Romano, C. L., Mackey, R. B., Khosravi, P., Hohn, C. M., and Boyle, C. R. (2007). Evaluation of zebrafish *Danio rerio* as a model for enteric septicemia of catfish (ESC). *J. Aquat. Anim. Health* **19**, 151–158.

Pham, L. N., Kanther, M., Semova, I., and Rawls, J. F. (2008). Methods for generating and colonizing gnotobiotic zebrafish. *Nat. Protoc.* **3**, 1862–1875.

Phelan, P. E., Mellon, M. T., and Kim, C. H. (2005a). Functional characterization of full-length TLR3, IRAK-4, and TRAF6 in zebrafish (Danio rerio). *Mol. Immunol.* **42**, 1057–1071.

Phelan, P. E., Pressley, M. E., Witten, P. E., Mellon, M. T., Blake, S., and Kim, C. H. (2005b). Characterization of snakehead rhabdovirus infection in zebrafish (Danio rerio). *J. Virol.* **79**, 1842–1852.

Phennicie, R. T., Sullivan, M. J., Singer, J. T., Yoder, J. A., and Kim, C. H. (2010). Specific resistance to *Pseudomonas aeruginosa* infection in zebrafish is mediated by the cystic fibrosis transmembrane conductance regulator. *Infect. Immun.* **78**, 4542–4550.

Prajsnar, T. K., Cunliffe, V. T., Foster, S. J., and Renshaw, S. A. (2008). A novel vertebrate model of *Staphylococcus aureus* infection reveals phagocyte-dependent resistance of zebrafish to non-host specialized pathogens. *Cell. Microbiol.* **10**, 2312–2325.

Pressley, M. E., Phelan 3rd, P. E., Witten, P. E., Mellon, M. T., and Kim, C. H. (2005). Pathogenesis and inflammatory response to *Edwardsiella tarda* infection in the zebrafish. *Dev. Comp. Immunol.* **29**, 501–513.

Rawls, J. F., Mahowald, M. A., Goodman, A. L., Trent, C. M., and Gordon, J. I. (2007). In vivo imaging and genetic analysis link bacterial motility and symbiosis in the zebrafish gut. *Proc. Natl. Acad. Sci. U. S. A.* **104**, 7622–7627.

Rawls, J. F., Mahowald, M. A., Ley, R. E., and Gordon, J. I. (2006). Reciprocal gut microbiota transplants from zebrafish and mice to germ-free recipients reveal host habitat selection. *Cell* **127**, 423–433.

Rawls, J. F., Samuel, B. S., and Gordon, J. I. (2004). Gnotobiotic zebrafish reveal evolutionarily conserved responses to the gut microbiota. *Proc. Natl. Acad. Sci. U. S. A.* **101**, 4596–4601.

Renshaw, S. A., Loynes, C. A., Trushell, D. M., Elworthy, S., Ingham, P. W., and Whyte, M. K. (2006). A transgenic zebrafish model of neutrophilic inflammation. *Blood* **108**, 3976–3978.

Rhodes, J., Hagen, A., Hsu, K., Deng, M., Liu, T. X., Look, A. T., and Kanki, J. P. (2005). Interplay of pu.1 and gata1 determines myelo-erythroid progenitor cell fate in zebrafish. *Dev. Cell* **8**, 97–108.

Rodriguez, I., Novoa, B., and Figueras, A. (2008). Immune response of zebrafish (*Danio rerio*) against a newly isolated bacterial pathogen *Aeromonas hydrophila*. *Fish Shellfish Immunol.* **25**, 239–249.

Roeselers, G., Mittge, E., Parichy, D., Cavanaugh, C. M., Guillemin, K., and Rawls, J. F. (2011). Evidence for a core gut microbiota in the zebrafish. *ISME J.* (Epub ahead of print) 2011 Apr 7. PMID: 21472014.

Rojo, I., de Ilarduya, O. M., Estonba, A., and Pardo, M. A. (2007). Innate immune gene expression in individual zebrafish after *Listonella anguillarum* inoculation. *Fish Shellfish Immunol.* **23**, 1285–1293.

Sanders, G. E., Batts, W. N., and Winton, J. R. (2003). Susceptibility of zebrafish (*Danio rerio*) to a model pathogen, spring viremia of carp virus. *Comp. Med.* **53**, 514–521.

Savage, D. C., Siegel, J. E., Snellen, J. E., and Whitt, D. D. (1981). Transit time of epithelial cells in the small intestines of germfree mice and ex-germfree mice associated with indigenous microorganisms. *Appl. Environ. Microbiol.* **42**, 996–1001.

Shotts, E. B., and Waltman 2nd, W. D. (1990). A medium for the selective isolation of *Edwardsiella ictaluri*. *J. Wildl. Dis.* **26**, 214–218.

Singer, J. T., Phennicie, R. T., Sullivan, M. J., Porter, L. A., Shaffer, V. J., and Kim, C. H. (2010). Broad-host-range plasmids for red fluorescent protein labeling of gram-negative bacteria for use in the zebrafish model system. *Appl. Environ. Microbiol.* **76**, 3467–3474.

Stockhammer, O. W., Zakrzewska, A., Hegedus, Z., Spaink, H. P., and Meijer, A. H. (2009). Transcriptome profiling and functional analyses of the zebrafish embryonic innate immune response to *Salmonella* infection. *J. Immunol.* **182**, 5641–5653.

Stoop, E. J., Schipper, T., Rosendahl Huber, S. K., Nezhinsky, A. E., Verbeek, F. J., Gurcha, S. S., Besra, G. S., Vandenbroucke-Grauls, C. M., Bitter, W., and van der Sar, A. M. (2011). Zebrafish embryo screen for mycobacterial genes involved in the initiation of granuloma formation reveals a newly identified ESX-1 component. *Dis. Model Mech* **4**, 526–536.

Su, F., Juarez, M. A., Cooke, C. L., Lapointe, L., Shavit, J. A., Yamaoka, J. S., and Lyons, S. E. (2007). Differential regulation of primitive myelopoiesis in the zebrafish by Spi-1/Pu.1 and C/ebp1. *Zebrafish* **4**, 187–199.

Sullivan, C., Charette, J., Catchen, J., Lage, C. R., Giasson, G., Postlethwait, J. H., Millard, P. J., and Kim, C. H. (2009). The gene history of zebrafish tlr4a and tlr4b is predictive of their divergent functions. *J. Immunol.* **183**, 5896–5908.

Sullivan, C., Postlethwait, J. H., Lage, C. R., Millard, P. J., and Kim, C. H. (2007). Evidence for evolving Toll-IL-1 receptor-containing adaptor molecule function in vertebrates. *J. Immunol.* **178**, 4517–4527.

Szabady, R. L., Lokuta, M. A., Walters, K. B., Huttenlocher, A., and Welch, R. A. (2009). Modulation of neutrophil function by a secreted mucinase of *Escherichia coli* O157:H7. *PLoS Pathog.* **5**, e1000320.

Traver, D., Herbomel, P., Patton, E. E., Murphey, R. D., Yoder, J. A., Litman, G. W., Catic, A., Amemiya, C. T., Zon, L. I., and Trede, N. S. (2003). The zebrafish as a model organism to study development of the immune system. *Adv. Immunol.* **81**, 253–330.

Trede, N. S., Langenau, D. M., Traver, D., Look, A. T., and Zon, L. I. (2004). The use of zebrafish to understand immunity. *Immunity* **20**, 367–379.

van der Sar, A. M., Musters, R. J., van Eeden, F. J., Appelmelk, B. J., Vandenbroucke-Grauls, C. M., and Bitter, W. (2003). Zebrafish embryos as a model host for the real time analysis of *Salmonella typhimurium* infections. *Cell. Microbiol.* **5**, 601–611.

van der Sar, A. M., Stockhammer, O. W., van der Laan, C., Spaink, H. P., Bitter, W., and Meijer, A. H. (2006). MyD88 innate immune function in a zebrafish embryo infection model. *Infect. Immun.* **74**, 2436–2441.

Vasil, M. L., Stonehouse, M. J., Vasil, A. I., Wadsworth, S. J., Goldfine, H., Bolcome 3rd, R. E., and Chan, J. (2009). A complex extracellular sphingomyelinase of *Pseudomonas aeruginosa* inhibits angiogenesis by selective cytotoxicity to endothelial cells. *PLoS Pathog.* **5**, e1000420.

Vergunst, A. C., Meijer, A. H., Renshaw, S. A., and O'Callaghan, D. (2010). *Burkholderia cenocepacia* creates an intramacrophage replication niche in zebrafish embryos, followed by bacterial dissemination and establishment of systemic infection. *Infect. Immun.* **78**, 1495–1508.

Vojtech, L. N., Sanders, G. E., Conway, C., Ostland, V., and Hansen, J. D. (2009). Host immune response and acute disease in a zebrafish model of *Francisella* pathogenesis. *Infect. Immun.* **77**, 914–925.

Volkman, H. E., Pozos, T. C., Zheng, J., Davis, J. M., Rawls, J. F., and Ramakrishnan, L. (2010). Tuberculous granuloma induction via interaction of a bacterial secreted protein with host epithelium. *Science* **327**, 466–469.

Wang, Z. L., Xu, X. P., He, B. L., Weng, S. P., Xiao, J., Wang, L., Lin, T., Liu, X., Wang, Q., and Yu, X. Q., *et al*. (2008). Infectious spleen and kidney necrosis virus ORF48R functions as a new viral vascular endothelial growth factor. *J. Virol.* **82**, 4371–4383.

Wang, L., Zhang, H. X., Zhang, J. H., Chen, W. H., Ruan, X. F., and Xia, C. (2006). In vitro effects of recombinant zebrafish IFN on spring viremia of carp virus and infectious hematopoietic necrosis virus. *J. Interferon Cytokine Res.* **26**, 256–259.

Westerfield, M. (2000). *The Zebrafish Book.* University of Oregon Press, Eugene, OR.

Whipps, C. M., Dougan, S. T., and Kent, M. L. (2007). *Mycobacterium haemophilum* infections of zebrafish (*Danio rerio*) in research facilities. *FEMS Microbiol. Lett.* **270**, 21–26.

Wienholds, E., Schulte-Merker, S., Walderich, B., and Plasterk, R. H. (2002). Target-selected inactivation of the zebrafish rag1 gene. *Science* **297**, 99–102.

Xiong, X. P., Dong, C. F., Xu, X., Weng, S. P., Liu, Z. Y., and He, J. G. (2011). Proteomic analysis of zebrafish (*Danio rerio*) infected with infectious spleen and kidney necrosis virus. *Dev. Comp. Immunol.* **35**, 431–440.

Xu, X., Zhang, L., Weng, S., Huang, Z., Lu, J., Lan, D., Zhong, X., Yu, X., Xu, A., and He, J. (2008). A zebrafish (*Danio rerio*) model of infectious spleen and kidney necrosis virus (ISKNV) infection. *Virology* **376**, 1–12.

CHAPTER 5

Hematopoietic Stem Cell Development: Using the Zebrafish to Identify the Signaling Networks and Physical Forces Regulating Hematopoiesis

Wolfram Goessling[*,†] **and Trista E. North**[†,‡]

[*]Genetics Division, Brigham and Women's Hospital, Harvard Medical School, Boston, Massachusetts, USA

[†]Harvard Stem Cell Institute, Cambridge, Massachusetts, USA

[‡]Department of Pathology, Beth Israel Deaconess Medical Center, Harvard Medical School, Boston, Massachusetts, USA

METHODS IN CELL BIOLOGY, VOL 105

0091-679X/10 $35.00
DOI 10.1016/B978-0-12-381320-6.00005-9

Abstract

Hematopoietic stem cells (HSC) form the basis of the hematopoietic hierarchy, giving rise to each of the blood lineages found throughout the lifetime of the organism. The genetic programs regulating HSC development are highly conserved between vertebrate species. The zebrafish has proven to be an excellent model for discovering and characterizing the signaling networks and physical forces regulating vertebrate hematopoietic development.

I. Developmental Hematopoiesis

There are several phases of blood cell formation, referred to as waves, which occur throughout vertebrate development (Fig. 1). The first wave of hematopoiesis, termed primitive, occurs in the zebrafish in the intermediate cell mass (ICM); it is the functional equivalent of the early blood islands in the mammalian yolk sac (at murine embryonic days e7.5–e9.5) (Detrich *et al.*, 1995) and gives rise primarily to erythrocytes. In the second, or definitive, wave, multipotent progenitors are produced; intriguingly, in studies of fish, chick, and murine embryos, this ability to contribute

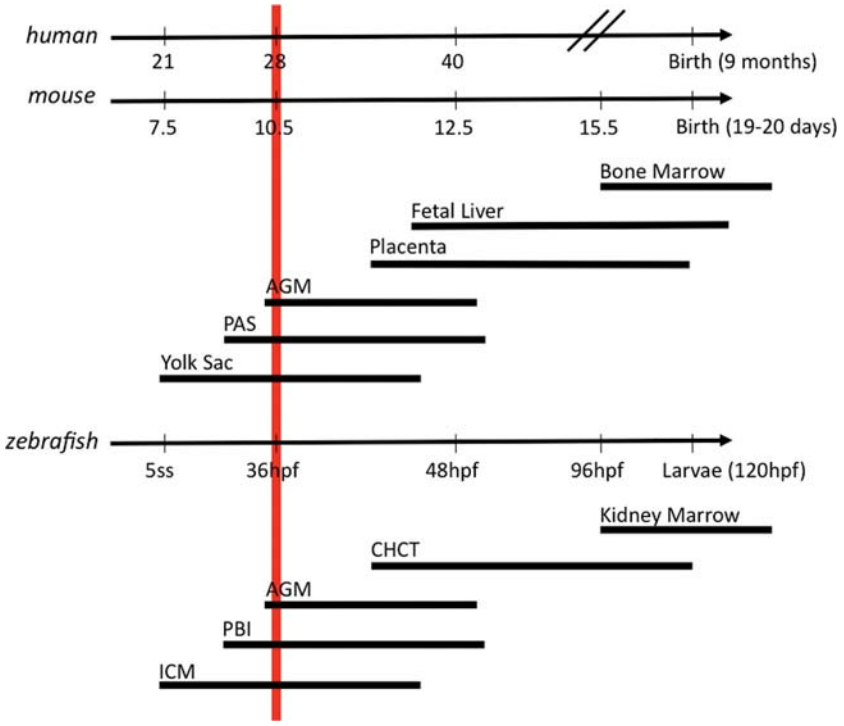

Fig. 1 Comparison of conserved spatiotemporal regulation of hematopoiesis across vertebrate species. (For color version of this figure, the reader is referred to the web version of this book.)

to multiple lineages appears to be acquired in reverse. In the mouse, for example, erythromyeloid progenitors (EMP) are formed in the primitive blood islands first, and then later, HSCs emerge from the ventral wall of the dorsal aorta in the aorta–gonad–mesonephros (AGM) region. As in other vertebrates, more recent analysis has demonstrated that this sequence is maintained in the zebrafish: EMPs, non-self-renewing progenitors with limited multilineage differentiation potential, are formed prior to the generation of HSCs (Bertrand *et al.*, 2007). HSCs are believed to be produced *de novo* at several different anatomical locations in the developing vertebrate: in the zebrafish, it is unclear if multiple sites can produce HSCs; however, they do migrate to seed different tissues for the purpose of proliferation and differentiation as in mammals. HSCs initially emerge in the AGM region of the dorsal aorta between 30 and 36 hours postfertilization (hpf). Subsequently, they appear in the distal region of the tail, termed the caudal hematopoietic tissue (CHT), before seeding the kidney marrow and thymus, where adult hematopoiesis continues.

II. Review of the Literature

A. Patterning of the Ventral Mesoderm

Fate-mapping experiments of the zebrafish blastula demonstrate that blood and endothelial cells as well as posterior somites derive from the ventral mesoderm. The dorsal mesoderm gives rise to the prechordal plate and notochord, whereas the more lateral mesoderm develops into anterior somites, kidney, and heart (Kimmel *et al.*, 1990; Warga and Nusslein-Volhard, 1999). Cell fate is specified by signaling pathways such as the nodal, fibroblast growth factor (fgf), and bone morphogenetic protein (bmp) families during the late blastula stage. Nodal signaling is required for the induction of both the mesoderm and endoderm; mutations in the *nodal-related 1* and *2* genes in *squint* and *cyclops* result in the lack of all mesodermal and endodermal structures, except for the tail somites (Feldman *et al.*, 1998). The ventral mesoderm is further specified by members of the bmp family during early gastrulation: mutants in *bmp2b* (*swirl*) (Kishimoto *et al.*, 1997) have radialized trunk somites, reduced blood, vasculature and pronephros, and no tail tissue. The *bmp7* mutant, *snailhouse*, which is characterized by a dorsalized (slightly less severe) phenotype without ventral structures (Dick *et al.*, 2000), further demonstrates the importance of this pathway in the formation of the ventral mesoderm. Several genes function cooperatively to either induce or maintain ventral mesodermal fate in conjunction with *bmp2*: *wnt8* coregulates the homeobox genes *vox* and *vent*, which act redundantly to prevent expression of dorsal genes in the ventral mesendoderm (Imai *et al.*, 2001; Melby *et al.*, 2000; Ramel *et al.*, 2005).

B. Hemangioblast Formation

During early somitogenesis, the ventral lateral mesoderm is specified into hematopoietic, endothelial, and kidney progenitors. Within this region, the anterior

portion of the lateral plate mesoderm (ALM) gives rise to primitive myeloid cells, and the posterior portion (PLM) produces primarily erythrocytes, in addition to some cells of the myeloid lineage. Endothelial and hematopoietic precursors are initially colocalized in the lateral plate mesoderm and coexpress transcription factor genes such as stem cell leukemia (*scl*), *lmo2*, *fli1a*, *gata2*, and *etsrp*, indicative of either blood or endothelial fate. These findings support the existence of a common precursor for blood and vessels during the primitive wave of hematopoiesis, which has been termed the hemangioblast. The "hemangioblast" concept was initially postulated in the early 1920 s based on studies in the chick embryo (Sabin, 1920). The hemangioblasts are believed to have a transient existence and are regulated by signals that are antagonistic to cardiac development (Gering *et al.*, 2003; Schoenebeck *et al.*, 2007); however, some reports have postulated that a similar cell type exists in the adult vertebrate marrow (Schatteman, 2004). Further evidence for the existence of a common hematopoietic and endothelial precursor comes from the *cloche* (*clo*) mutant, which lacks both blood and blood vessels, but demonstrates no other defect in mesodermal organ formation (Stainier *et al.*, 1995). In a recent study, Vogeli *et al.* (2006) used a fate-mapping approach to demonstrate that a cell population, identified during gastrulation, can develop into both endothelial precursors and HSCs, but no other mesodermal structures, providing *in vivo* evidence for the existence of a hemangioblast. Murine studies in *Flk1* knockout mice have further argued for the existence of the hemangioblast, because these mice do not develop blood islands, yolk sac endothelial cells, and only very rare hematopoietic progenitors (Shalaby *et al.*, 1995, 1997). In contrast, blastocyst transplantation studies suggest that the parallel development of blood and blood vessels from hemangioblast precursors is at best a very rare event, arguing against the functional importance of a hemangioblast (Ueno and Weissman, 2006). Further studies are needed to fully elucidate the importance and relative contribution of hemangioblast cells to both vasculogenesis and hematopoiesis.

C. Primitive Hematopoiesis

During mid-somitogenesis, cells in both the ALM and PLM begin to express genes of myeloid differentiation, such as *spi1* (also known as *pu.1*) and *l-plastin* (Bennett *et al.*, 2001), whereas *gata1*-positive erythroid progenitors are mainly formed in the PLM. The hematopoietic cells in the PLM, together with their endothelial counterparts, converge to the midline and subsequently form the ICM region, the main site of primitive hematopoiesis. Several genes are involved in these early steps of blood formation. The zinc finger transcription factor *gata1* is expressed in the PLM and is considered the principal regulator of erythropoiesis, as evident in the *gata1* mutant *vlad tepes* (vlt^{m651}), which has few circulating red blood cells, but normal to enhanced production of myeloid cell types (Lyons *et al.*, 2002). Recent knockdown studies have shown that *pbx* and *meis1* act upstream of *gata1* to affect primitive erythropoiesis (Pillay *et al.*, 2010). spi1 is a central regulator of myeloid fate during the primitive wave (Hsu *et al.*, 2004; Lieschke *et al.*, 2002; Ward *et al.*, 2003). Together gata1 and spi1 function in a mutually antagonistic manner,

providing reciprocal regulation in specifying mesodermal development, such that lack of *gata1* overexpression leads to a conversion to myeloid fate (Galloway *et al.*, 2005), while *spi1* knockdown causes ectopic *gata1* expression (Rhodes *et al.*, 2005).

D. Definitive Hematopoiesis

The definitive wave of hematopoiesis produces multipotent progenitors, including the HSCs that can give rise to all hematopoietic lineages for the lifetime of the organism. The anatomical locations and genes involved in HSC development during embryogenesis are highly conserved among vertebrate species. Definitive hematopoiesis begins at ~24 hpf with the production of EMPs in the posterior blood island (Bertrand *et al.*, 2007; Jin *et al.*, 2007). The first HSCs arise shortly thereafter in the ventral aspect of the dorsal aorta, termed the AGM for its mammalian equivalent, and are characterized by the expression of transcription factor genes proven essential for the genesis and function of HSCs: *runx1*, *cmyb*, and *itga2b* (previously called *CD41*). As in the mouse and chick embryo, there appear to be successive anatomical sites that can support definitive hematopoietic development following the initial occurrence of HSCs in the AGM. At ~44 hpf, *cmyb*-positive cells appear further distally in the tail, in the CHT, where they are also marked by expression of the surface marker integrin 2b (*itga2b*, *CD41*); it has been argued that the CHT may represent the equivalent of the mammalian fetal liver (Murayama *et al.*, 2006), and supports expansion of HSCs rather than *de novo* production. Eventually, HSCs seed the pronephros, either directly from the AGM or via the CHT (Bertrand *et al.*, 2008), and will continue to be localized primarily in the kidney marrow (mammalian bone marrow equivalent) for the lifetime of the adult zebrafish.

As indicated above, several genes considered essential for definitive hematopoiesis are well-characterized markers of definitive HSC maturation. Runx1 (also known as AML1 and core-binding factor a2) is a member of the runt-domain-containing family of transcription factors, which are highly evolutionarily conserved. Runt family members are involved in multiple developmental processes and often play a role in carcinogenesis. *Runx1* is involved as a fusion gene partner in a significant fraction of cases of acute myelogenous and lymphoblastic leukemia (Gilliland *et al.*, 2004). *Runx1* is expressed in hematopoietic clusters within the ventral endothelial layer of the mouse dorsal aorta (North *et al.*, 1999), and knockout studies revealed its requirement for definitive hematopoiesis (Okuda *et al.*, 1996; Wang *et al.*, 1996). In the zebrafish, *runx1* is similarly detected in the AGM region of the dorsal aorta in HSCs and the ventral endothelium (Burns *et al.*, 2002; Crosier *et al.*, 2002). Paralleling *Runx1* loss in mice, *runx1* knockdown in zebrafish does not significantly alter primitive erythropoiesis, indicating that it is not required for the first wave of hematopoiesis, but completely impairs HSC formation and multilineage differentiation (Burns *et al.*, 2002; Kalev-Zylinska *et al.*, 2002). Interestingly, recent data in zebrafish using a *runx1* truncation mutant (*runx1*^{w84x}) reveal that some homozygous fish can overcome the initial bloodless phase; *itga2b:GFP*+ cells were found to emerge in the AGM and then migrate to the kidney at a later time point in

development (Sood *et al.*, 2010). These data suggest that HSCs formed during the larval stages are *runx1*-independent, and may be produced via a "salvage" method that does not require *runx1* function, recently reported to be essential for the process of budding from the endothelial layer itself in both mice (Chen *et al.*, 2009) and fish (Kissa and Herbomel, 2010). In the zebrafish, *cmyb* is coexpressed with *runx1* in the AGM at 36 hpf and labels the HSC population; its expression is dependent on Runx1, suggesting a transcriptional hierarchy. Cmyb belongs to a proto-oncogene family of transcription factors and in the mouse, its absence leads to embryonic death due to lack of hepatic erythropoiesis (Mucenski *et al.*, 1991), indicating its primary role in definitive (formerly called fetal liver) hematopoiesis; it is also essential for myeloid differentiation (Sakamoto *et al.*, 2006). *cmyb:GFP* reporter fish (in combination with lmo2) have been used to identify and quantify effects on HSCs *in vivo* (North *et al.*, 2007). The recent characterization of a *cmyb* mutant zebrafish ($cmyb^{t25127}$) demonstrated the high degree of evolutionary conservation in definitive HSC production; *cmyb* mutant embryos have no discernible defects in the primitive wave of hematopoiesis, but by 20 dpf they exhibit defects in all hematopoietic lineages, with stunted growth and premature death at 2–3 months (Soza-Ried *et al.*, 2010). HSC maturation, including the ability to migrate and home to the niche, is indicated by the expression of *itga2b* (Bertrand *et al.*, 2008; Lin *et al.*, 2005), first shown to be required for HSC function in the mouse (Mikkola *et al.*, 2003). Similarly, the pan-leukocyte marker Ptprc (previously called CD45) can be accurately utilized in the zebrafish, as in all vertebrates, to denote all cells of the hematopoietic lineage, with the exception of erythrocytes, as they differentiate from the HSC population.

III. Use of Zebrafish to Investigate HSC Biology

A. Zebrafish Mutants

Zebrafish mutants have enabled the detailed analysis of the steps leading up to the formation and differentiation of HSCs. These involve the early steps of mesoderm patterning, hemangioblast formation, and differentiation and maintenance of HSCs. An array of hematopoietic mutants has arisen as the result of spontaneous mutations, ENU mutagenesis screens, and targeted deletions, as well as induced transgenesis. Representative examples of mutants described for each step in hematopoietic maturation are described below; a more exhaustive list, particularly for primitive hematopoiesis, can be found in the review by de Jong and Zon (2005).

1. Mesoderm Mutants

Kugelig and spadetail

The *kugelig (kgg)* mutant is defective in *cdx4* and has a characteristic round morphology with a shortened tail. It shows low expression of *gata1* and T-cell acute

lymphocytic leukemia 1 (*tal1*) (previously called *scl*) during early somitogenesis as well as reduced *runx1* expression at 36 hpf. *cdx4* acts through the hox genes *hoxa9a* and *hoxb7a*, which when overexpressed can rescue the *kgg* mutants. These findings demonstrate a role for *cdx4* during both primitive and definitive hematopoiesis; however, other mesodermal tissues such as the blood vessels and the pronephros are largely normal. Subsequent work revealed *β-arrestin 1* as an epigenetic upstream regulator of *cdx4*, because its knockdown leads to a failure of hematopoiesis that can be rescued by *cdx4* addition (Yue *et al.*, 2009). Recent studies further defined this pathway, identifying retinoic acid signaling as downstream of *cdx4*, and functioning to block primitive hematopoiesis through inhibition of *tal1* (de Jong *et al.*, 2010). The T-box transcription factor, *tbx16*, is mutated in *spadetail* (*spt*), resulting in defects in several mesodermal organs, including the blood with decreased expression of *tal1*, *gata1*, *gata2*, *lmo2*, and *fli1a*. Recent data suggest that *tbx16* may regulate both wnt and retinoic acid signaling to affect mesoderm formation and primitive hematopoiesis (Mueller *et al.*, 2010).

2. Hemangioblast Mutants

Scl/tal1

A mutant in scl/tal1 was found through a genetic screen to identify embryos with abnormal vascular development (Habeck *et al.*, 2002), revealing a severe reduction in endothelial alkaline phosphatase activity at 4 dpf. In addition, the mutant embryos exhibit an absence of the primitive erythroid (*gata1*) and myeloid (*spi1*) lineages as well as the formation of HSCs (*runx1*) (Bussmann *et al.*, 2007). These fish also display defects in endocardial precursor migration and subsequent failure of endocardial development. These findings provide further support for the existence of a common vascular–hematopoietic precursor cell.

Cloche

The mutant *clo* is characterized by gross cardiac edema and an enlarged atrium due to endocardial loss, giving it its name, which is French for "bell." It has not been conclusively cloned in the 16 years since the publication of its initial description due to the mutation's telomeric location on chromosome 13; however, part of the *clo* mutant phenotype appears to be phenocopied by a mutation in *lycat1*, which is located in the region of the deletion (Xiong *et al.*, 2008). *clo* mutants exhibit disrupted differentiation of both endothelial and hematopoietic structures, with almost complete loss of expression of *tal1*, *lmo2*, *gata1*, *mpx*, *l-plastin*, and *kdrl* (*also known as flk1*) (Liao *et al.*, 1997; Stainier *et al.*, 1995). The effect of *clo* was shown to have both cell-autonomous and non-cell-autonomous features in blastula transplantation studies (Parker and Stainier, 1999). In contrast, other mesodermal organs do not show any defects, further indicating that *clo* might play a role in hemangioblast formation.

3. Primitive Hematopoietic Mutants

Bloodless

The *bloodless (bls)* mutant was identified as a spontaneous mutation. *bls* embryos exhibit a failure of the initial wave of primitive erythropoiesis, demonstrating no erythrocytes until 5 dpf. However, they can survive via passive diffusion of oxygen into all tissues due to *ex vivo* aqueous development and subsequently produce (definitive) erythrocytes (Liao *et al.*, 2002). In *bls* mutants, *tal1* expression initiated in the PLM disappears by 23 hpf, and *gata1* expression is absent; in contrast, ALM myelopoiesis is not affected, indicating that this mutation specifically affects the primitive wave. The gene affected in the *bls* mutant has not yet been cloned.

Vlad tepes

The *vlt* mutant carries a mutation in the gata1a transcription factor (Lyons *et al.*, 2002; Weinstein *et al.*, 1996). Although the mutants initiate expression of erythroid genes such as *gata1a* and *α-globin* during somitogenesis, they are no longer expressed after 26 hpf; the loss of binding and function of gata1a at the regulatory regions of erythroid target genes presumably causes mesodermal cells to lose the ability to maintain erythropoiesis and switch to a myeloid fate (Galloway *et al.*, 2005). The mutants eventually die between 8 and 15 dpf, although rare adults of small size have been reported when maintained under high tank aeration.

Moonshine

The *moonshine* (*mon*) mutant was initially classified as having abnormal pigmentation (Kelsh *et al.*, 1996). However, it also exhibits defects in both primitive and definitive erythropoiesis, while showing normal myelopoiesis (Ransom *et al.*, 1996). As with many primitive hematopoietic mutants, expressions of *gata1* and *tal1* are initiated normally, but are subsequently lost due to apoptosis and are no longer detectable by 22 hpf (Ransom *et al.*, 2004). Moonshine is a mutation in the chromatin remodeling factor *transcriptional intermediate factor 1 g* (*trim33*, formerly *tif1 g*) (Ransom *et al.*, 2004). It was recently found that *trim33* controls transcriptional elongation specifically in the hematopoietic lineage by interacting physically with Tal1 and the positive elongation factors p-TEFb and FACT, highlighting a novel mechanism for regulating hematopoiesis (Bai *et al.*, 2010).

4. Definitive Hematopoietic Mutants

Runx1

Runx has been shown to be universally required for HSC formation from the hemogenic endothelial layer during the definitive wave of hematopoiesis. A recent

report by Sood *et al.* (2010) characterizes a *runx1* truncation mutation (*runx1*^{w48x}) that exhibits lack of *runx1* expression between 36 and 120 hpf. However, a fraction (~20%) of homozygous embryos was noted to regain circulating itga2b+ blood cells at 15–21 dpf, allowing them to develop into adulthood; this finding has led the authors to postulate the existence of a secondary or "rescue" mechanism by which HSCs can be generated if runx1 is not present; however, at this time, the factor(s) controlling this process have not been identified.

Mindbomb

The characterization of the hematopoietic defects in the *mindbomb* (*mib*) mutant confirmed the role of notch in HSC formation (Burns *et al.*, 2005), initially described in the mouse (Kumano *et al.*, 2003). The *mib* mutant was, as the name implies, first described for its neural defects. It carries a defect in the gene for ubiquitin E3 ligase, which is required for the processing of the notch ligands delta and jagged. *mib* mutants have normal primitive erythropoiesis, but exhibit defects in definitive hematopoiesis with significantly reduced *runx1* and *cmyb* expression in the ventral wall of the dorsal aorta. Recent data investigating the formation of EMP as a hematopoietic wave preceding HSC development found no notch receptors on *gata3* expressing EMPs and no defect in this cell population in *mib* mutants. In addition, *mib* mutants have macrophages and neutrophils, suggesting a direct descent from the primitive ALM myeloid wave or bipotential EMPs (Bertrand *et al.*, 2010b).

Rumba and samba

The recently identified *rumba* and *samba* mutants are the first to be found to exhibit specific defects in the formation and proliferation of HSCs in the CHT (Du *et al.*, 2011). These mutants encode for a novel C2H2 zinc finger factor with unknown function and a protein homologous to the human augmin complex subunit 3 (HAUS3), respectively. Both are characterized by normal *cmyb* expression at 30 hpf, but progressive loss of HSC markers and myeloid cell types at 3–5 dpf, with *rumba* affecting the early phase of CHT population at 3 days, and *samba* modifying the subsequent expansion phase. Both mutants display a loss of cell cycle progression and are cell autonomously required to maintain the HSC pool in the CHT.

B. Chemical Screens

In recent years, chemical screening approaches have also yielded great insight into the biology of hematopoietic development. Chemical screening strategies are particularly useful in that, unlike mutation, knockdown, or overexpression analysis, the timing and duration of exposure can be altered to directly impact the population of interest during hematopoietic development (Fig. 2). Screening can be conducted on wild-type fish and scored for alterations in developmental expression patterns or

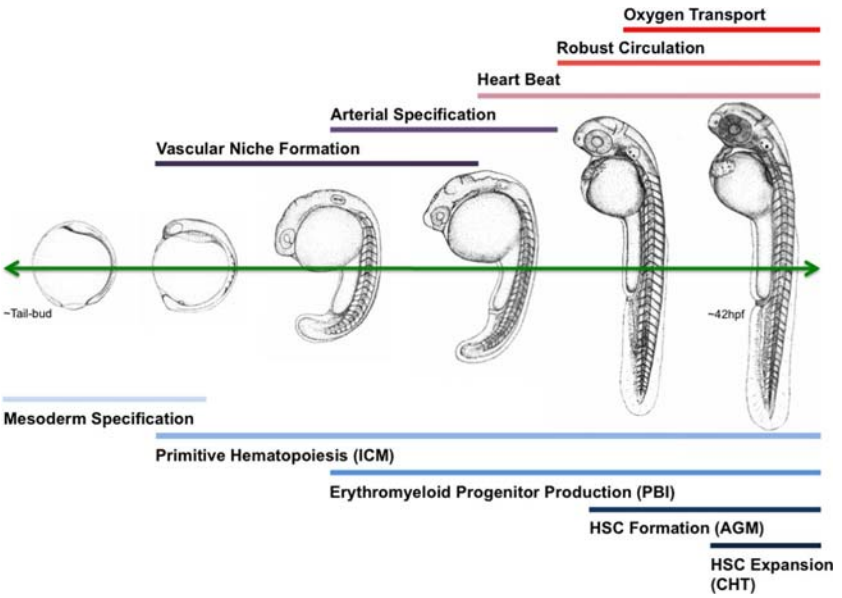

Fig. 2 Depiction of developmental milestones for determination of exposure windows during chemical screens to impact hematopoiesis. (For color version of this figure, the reader is referred to the web version of this book.)

lineage-specific hematopoietic reporters, or it can be used to modify or rescue alterations in the hematopoietic program caused by mutation or transgenesis.

1. PGE2 and wnt

The initial hematopoietic regulatory pathway discovered by this approach is that of prostaglandin E2 (PGE2). In a chemical genetic screen in zebrafish embryos for modulators of the expression of HSC markers runx1 and cmyb, both agonists and antagonists of prostaglandin signaling were identified as regulators of HSC formation. In particular, exposure to exogenous PGE2, the most ubiquitous prostanoid produced during development (Grosser *et al.*, 2002), significantly enhanced HSC formation; in contrast, inhibitors of the synthesizing enzymes cyclooxygenase 1 and 2, as well as MO knockdown of these enzymes or the G protein–coupled receptors *ptger2a* and *ptger4a*, resulted in greatly reduced HSC number (North *et al.*, 2007). The effects of PGE2 were conserved in adult zebrafish recovering from kidney marrow irradiation injury as well as in murine bone marrow transplants. In a separate study, a role for PGE2 signaling was also identified specifically in lymphoid development (Villablanca *et al.*, 2007). In subsequent studies, through the use of multiple inducible transgenic fish to modify wnt signaling, PGE2 was found to affect HSC formation by modulating wnt activity via cAMP-mediated activation of PKA. This action results in direct phosphorylation of the central mediator of wnt activity,

β-catenin, and GSK3β to inhibit degradation and allow transactivation in the nucleus (Goessling *et al.*, 2009). These findings and subsequent preclinical studies (Goessling *et al.*, 2011) have led to the first FDA-approved clinical trial originated from a chemical screen in the zebrafish, evaluating the use of PGE2 in patients undergoing HSC transplants with cord blood (http://clinicaltrials.gov/ct2/show/results/NCT00890500).

2. Nitric Oxide and Blood Flow

This chemical screening approach also resulted in the identification of several groups of compounds that had the common ability to regulate blood flow by affecting heart rate, contractility, or vascular diameter of the developing embryo (North *et al.*, 2009). The chemicals included agents acting on α- and β-adrenergic receptors, and those affecting calcium flux and angiotensin-converting enzyme signaling; however, the action of each was dependent on the presence of blood flow. The only compounds able to affect HSC formation before the onset of a heart beat and subsequent blood flow at 24 hpf were those modulating nitric oxide (NO) signaling. NO donors, such as *S*-nitroso-*N*-acetylpenicillamine (SNAP), enhanced the population of *runx1*- and *cmyb*-positive HSCs in the AGM at 36 hpf, whereas the NO synthesis inhibitor *N*-nitro-L-arginine methyl ester (L-NAME) diminished HSC formation. The cardiac mutant *silent heart* (*sih*), which lacks heart beat and blood flow due to a mutation in *troponin T2a* (*tnnt2a*), exhibits diminished HSC formation, indicating the importance of blood flow for HSC formation. However, NO donors could rescue the HSC defect in *sih* mutant embryos, indicating that NO signaling is the downstream signal linking blood flow to HSC development in the AGM. These studies indicate that chemical screens can not only identify chemical targets that modulate developmental processes but also – by their physiological effects – uncover physical forces required for initiating HSC induction in the AGM.

3. Rescue Screens

Recent chemical screens in the zebrafish have since been completed that do not focus on the modulation of the induction process normally occurring *in vivo* but the rescue of a mutant phenotype or a transgenically induced alteration. Paik *et al.* (2010) recently used a bioactive library to identify chemicals that rescue *gata1* expression in *kgg* embryos. Two psoralens, bergapten and 8-methoxypsoralen, that rescued the *cdx4* mutant defect were identified. In separate studies, Yeh *et al.* (2008) sought to isolate modulators of the hematopoietic differentiation defect induced by the leukemogenic transgenic fusion construct *runx1–mtg8* (also known as *aml1-eto*). The transgenic fish typically have an arrest in erythropoietic differentiation; the screen revealed the cyclooxygenase 2 inhibitor nimesulide as capable of preventing this block, further documenting the importance of prostaglandin signaling in hematopoietic regulation (Yeh *et al.*, 2009).

C. Visualization of HSC Emergence

Using the optical clarity of the developing zebrafish and innovative transgenic constructs, several groups have recently visualized the emergence and migration of HSCs and hematopoietic progenitors *in vivo* (Fig. 3). Bertrand *et al.* (2008) used *itga2b:GFP* transgenic fish to visualize colonization of the pronephros with HSCs. To demonstrate the direct formation of HSCs from vascular precursors, the same group used *cmyb:EGFP; kdrl:mCherry* double transgenic animals and confocal time lapse imaging of the zebrafish AGM region to perform lineage tracing experiments (Bertrand *et al.*, 2010a). They found that *cmyb:EGFP*+ cells developed directly from *kdrl:memCherry*+ cells in the ventral wall of the dorsal aorta, forming buds extending into the vascular lumen. Similarly, Kissa and Herbomel (2010) used a *kdr:GFP* transgenic line to observe the interaction and movements of endothelial cells in the dorsal aorta, including the emergence and release of HSCs from the vessel wall and demonstrate the effects of a lack of runx1. Using the recently established *runx1P2:GFP* transgenic line, Lam *et al.* (2010) also visualized the direct maturation and emergence of HSCs from kdr+ endothelial cells and confirmed the conserved use of the distal *runx1* promoter for HSC regulation. These studies demonstrate the utility of the zebrafish model for characterizing complex and essential developmental processes *in vivo* in real time in the developing vertebrate.

D. Transgenic Lines, Hematopoietic Cell Culture, FACS Analysis, and Transplantation

The biological advantages of the zebrafish model have been successfully employed to extend our knowledge of vertebrate hematopoietic development. In recent years, great effort has been made to enhance the ability to characterize and quantify the effects of genetic (or chemical) hematopoietic regulation in the zebrafish. The use of transgenic reporters is now widespread and offers unprecedented ability for *in vivo* characterization; these lines can be further used to quantify effects of interest by FACS analysis, as is standard in mammalian systems, or to enrich populations for genomic or functional analysis. Both FACS-based analysis (Traver *et al.*, 2003) and functional approaches, such as transplantation studies (Traver *et al.*, 2003) and *in vitro* culture (Stachura *et al.*, 2009), were modified from

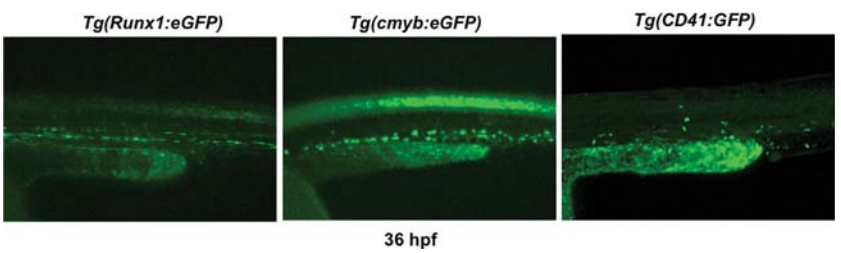

Fig. 3 Representative examples of available HSC reporter zebrafish lines at 36 hpf. (See color plate.)

the murine system and are now available in the zebrafish; much of the work to date has been focused on the adult (de Jong *et al.*, 2011); however, current protocols are being adapted to study hematopoietic development as well (Bertrand *et al.*, 2010a; Lam *et al.*, 2010; North *et al.*, 2007).

IV. Zebrafish Tools and Protocols

A. Tools – Transgenic Reporter Lines

In recent years, the production of transgenic reporter lines (Table I) to highlight organs and cell types of interest has substantially increased thanks to the development of enhanced transgenesis, such as using transposons, as well as the use of recombination-based strategies for fate mapping. These reporter lines have been used to highlight developmental cell populations and processes *in vivo*, to isolate cell populations for gene expression studies, and for cell transplantation experiments.

B. Protocol – Chemical Screen for HSC Formation

In addition to its advantages for forward genetics in mutagenesis screens, zebrafish are uniquely amenable to chemical interrogation of developmental processes. In our experience, the zebrafish is best used in this context for a global assessment of *in vivo* processes, using chemical libraries of well-characterized compounds that serve as indicators of signaling pathways of interest. Although recent advances have enabled enhanced throughput, such as *in situ* robots or automated fluorescence imaging, high content screening approaches may provide the biggest advantage

Table I
Compilation of currently published reporter zebrafish lines to highlight blood and vessel development

Transgenic line	Target cell population
Tg(kdrl:mCherry)is5, *Tg(kdrl:RFP)la4*, *Tg(kdrl:GRCFP)zn10*, *Tg(kdrl:GFP)la116*	Vasculature
Tg(fli1a:EGFP)y5, *Tg(fli1a.ep:DsRedEx)um13*, *Tg(fli1a:nEGFP)y7*	Vasculature
Tg(lmo2:DsRed)zf73, *Tg(lmo2:EGFP)zf71*	Vasculature, HSC
Tg(gata1a:GFP)la781, *Tg(-8.1gata1:gata1-EGFP)zf100*, *Tg(gata1:DsRed)sd2*	Erythrocytes
Tg(ptprc:DsRed)sd3	Myeloid cells
Tg(mpx:GFP)i114, *Tg(-8mpx:Dendra2)uwm4*, *Tg(-8mpx:mCherry)uwm5*	Neutrophils, monocytes
Tg(-6.0itga2b:EGFP)la2	Thrombocytes, HSC, EMP
Tg(rag2:GFP)la6	Lymphoid precursors
Tg(lck:lck-EGFP)cz2	T cells
Tg(cmyb:EGFP)zf169	HSC
Tg(runx1P2:EGFP)zf188, *Tg(runx1P1:EGFP)zf187*	HSC
Tg(-5.0tal1:EGFP)sq1	HSC

due to their ability to assess phenotypic changes in the context of whole-organism modifications.

1. Harvest and pool stage-matched embryos; about 250–500 embryos are required for each 48-well plate.
2. Slow embryo development in the incubator at 22 °C until the 5-somite stage.
3. Prepare multiwell plates: fill each well with 1 mL E3 embryo buffer. *Note*: We have found that 48-well plates (such as Greiner) allow better embryo survival (and the ability to remove dead embryos) than 96-well plates when filled with 5–10 embryos.
4. Prepare chemical compounds from library. Most premade libraries will have stocks of 10–20 mM compounds, dissolved in DMSO. Transfer 1 μL of each compound into each well. *Important*: In our experience, combinatorial exposure to two or more *bioactive* compounds at the same time results in excessive toxicity.
5. Using a small spatula, aliquot 5–10 embryos per well, minimizing transfer of additional water. *Note*: This can be achieved most easily by removing excess embryo buffer from the embryo plate before aliquoting the embryos via the "Caviar" method (pick up relatively dry embryos with spatula and flick against the top side wall of each well).
6. Incubate embryos in drug at 28.5 °C until 36 hpf for HSC screening. *Note*: Use phenotypic markers in the *control* to assess the stopping point; do not wait for delayed embryos to catch up and fix separately.
7. Process for *in situ* hybridization. We found the combination of runx1 and cmyb to be more robust as HSC markers than either one alone for screening purposes. *Alteration*: If using HSC reporters, skip to #8; we recommend fixing embryos to confirm phenotype if using fluorescent reporters for analysis.
8. Score embryos for HSC alterations, using untreated and/or DMSO-treated embryos from the same clutch as reference. *Note*: In early stages of the screen, it is helpful to seed each plate with a positive and/or negative control in addition to the untreated well.
9. Identify compound wells that affect organ formation and correlate with chemical library; group-related hits according to mechanism of action and/or biological function.
10. Retest "hits" to confirm phenotype. *Note*: For known bioactives, you do *not* need to use the exact compound from the screen in all cases if prototypical or classically used related compounds are more readily available.

C. Protocol – Confocal Microscopy for Analysis of HSC Formation and Blood Flow

The advent of an array of transgenic reporter fish enables the *in vivo* documentation of developmental processes in real time. As previously noted, this approach has recently allowed the direct visualization of HSC emergence from the hemogenic endothelium in the AGM (Bertrand *et al.*, 2010a; Kissa and Herbomel,

2010; Lam *et al.*, 2010). We have previously demonstrated that HSCs can be visualized and enumerated (within a selected field) for the purpose of quantifying an effect of your pathway of interest by double labeling in *cmyb:GFP* and *lmo2-DsRed* transgenic reporters.

1. Harvest appropriate transgenic embryos.
2. Expose embryos to chemicals from 5-somite stage until 36 hpf.
3. Using fluorescence stereomicroscopy, identify transgenic embryos.
4. Anesthetize embryos in tricaine solution.
5. Embed embryos in 1% low-melting agarose (in E3 embryo water) using glass bottom optical dishes.
6. Cover agarose with cover glass.
7. For HSC imaging, confocal microscopy using lasers with appropriate wavelength for the most commonly used fluorophores is performed focused on the tail region; we use a 40× long-distance lens for high-resolution imaging. *Alteration*: To assess blood flow, a spinning disc confocal microscope, such as the PerkinElmer UltraVIEW VoX, with kymograph analysis can be utilized.
8. Following image acquisition and processing with confocal software, HSCs can be enumerated in a fixed 3D field; several embryos should be imaged and counted to produce statistically meaningful data. *Note*: We use the end of the yolk sac extension in each embryo as a fixed point of interest to center the image for counting.

D. Protocol – Use of Fluorescence-Activated Cell Sorting to Demonstrate Cellular Processes During HSC Formation

The availability of a vast array of antibodies has greatly facilitated the characterization of hematopoietic cell types in humans and in the mouse. In contrast, this resource is largely absent in the blood cells of the zebrafish; however, fluorescence-activated cell sorting can be used to analyze the zebrafish hematopoietic system by taking advantage of the transgenic reporter lines. The FACS-based approach to identify hematopoietic cell types in the adult kidney marrow was pioneered by Traver *et al.* in 2003. Here we describe the procedure for characterizing and quantifying changes in embryonic hematopoietic cell types by FACS in mutant and compound-treated embryos.

1. Use appropriate transgenic reporter fish as highlighted in Table I; it is necessary to cross lines to highlight your cell type of interest if each labels multiple populations (e.g., *cmyb:GFP x lmo2:DsRed* to mark HSCs). *Alteration*: Crossing reporters can also help you identify modifications of multiple lineages or stages of differentiation in single embryos (e.g., itga2b x ptprc); care must be taken to ensure each embryo expresses all reporter constructs prior to analysis for accurate comparison.
2. Perform appropriate manipulations and treatments to analyze embryos at desired time point.

3. Separate nonfluorescent and fluorescent embryos under the microscope; nonfluorescent embryos (of a given color) will serve as gating controls.
4. Pool equal numbers of control (as above) or fluorescent embryos into separate 1.5-mL microfuge tubes. *Note*: Typically, 5–10 embryos are sufficient for detection, depending on age, but single-embryo analysis is also possible.
5. Remove all excess fish water by pipet.
6. Add 50 μL 0.9× Dulbecco's buffer.
7. Homogenize embryos using a tight-fitting pestle with twirl and lift motion. Grind embryos against sides of walls until they appear macroscopically well homogenized. *Note*: Overly aggressive homogenization may result in cell shearing and death.
8. Wash remaining cells off pestle into microfuge tube using 150 μL of 0.9× Dulbecco's buffer.
9. Strain homogenate through Falcon FACS tubes with 40 μm filter top and perform FACS analysis for reporter lines of interest.
10. Examine FACS data using available software (such as FloJo) and calculate alterations in cell number across biological replicates.

References

Bai, X., Kim, J., Yang, Z., Jurynec, M. J., Akie, T. E., Lee, J., LeBlanc, J., Sessa, A., Jiang, H., and DiBiase, A., *et al*. (2010). TIF1gamma controls erythroid cell fate by regulating transcription elongation. *Cell* **142**, 133–143.

Bennett, C. M., Kanki, J. P., Rhodes, J., Liu, T. X., Paw, B. H., Kieran, M. W., Langenau, D. M., Delahaye-Brown, A., Zon, L. I., and Fleming, M. D., *et al*. (2001). Myelopoiesis in the zebrafish. *Danio rerio. Blood* **98**, 643–651.

Bertrand, J. Y., Chi, N. C., Santoso, B., Teng, S., Stainier, D. Y., and Traver, D. (2010a). Haematopoietic stem cells derive directly from aortic endothelium during development. *Nature* **464**, 108–111.

Bertrand, J. Y., Cisson, J. L., Stachura, D. L., and Traver, D. (2010b). Notch signaling distinguishes 2 waves of definitive hematopoiesis in the zebrafish embryo. *Blood* **115**, 2777–2783.

Bertrand, J. Y., Kim, A. D., Teng, S., and Traver, D. (2008). CD41+ cmyb+ precursors colonize the zebrafish pronephros by a novel migration route to initiate adult hematopoiesis. *Development* **135**, 1853–1862.

Bertrand, J. Y., Kim, A. D., Violette, E. P., Stachura, D. L., Cisson, J. L., and Traver, D. (2007). Definitive hematopoiesis initiates through a committed erythromyeloid progenitor in the zebrafish embryo. *Development* **134**, 4147–4156.

Burns, C. E., DeBlasio, T., Zhou, Y., Zhang, J., Zon, L., and Nimer, S. D. (2002). Isolation and characterization of runxa and runxb, zebrafish members of the runt family of transcriptional regulators. *Exp. Hematol* **30**, 1381–1389.

Burns, C. E., Traver, D., Mayhall, E., Shepard, J. L., and Zon, L. I. (2005). Hematopoietic stem cell fate is established by the Notch-Runx pathway. *Genes Dev* **19**, 2331–2342.

Bussmann, J., Bakkers, J., and Schulte-Merker, S. (2007). Early endocardial morphogenesis requires Scl/Tal1. *PLoS Genet* **3**, e140.

Chen, M. J., Yokomizo, T., Zeigler, B. M., Dzierzak, E., and Speck, N. A. (2009). Runx1 is required for the endothelial to haematopoietic cell transition but not thereafter. *Nature* **457**, 887–891.

Crosier, P. S., Kalev-Zylinska, M. L., Hall, C. J., Flores, M. V., Horsfield, J. A., and Crosier, K. E. (2002). Pathways in blood and vessel development revealed through zebrafish genetics. *Int. J. Dev. Biol* **46**, 493–502.

de Jong, J. L., Burns, C. E., Chen, A. T., Pugach, E., Mayhall, E. A., Smith, A. C., Feldman, H. A., Zhou, Y., and Zon, L. I. (2011). Characterization of immune-matched hematopoietic transplantation in zebrafish. *Blood* **117**, 4234–4242.

de Jong, J. L., Davidson, A. J., Wang, Y., Palis, J., Opara, P., Pugach, E., Daley, G. Q., and Zon, L. I. (2010). Interaction of retinoic acid and scl controls primitive blood development. *Blood* **116**, 201–209.

de Jong, J. L., and Zon, L. I. (2005). Use of the zebrafish system to study primitive and definitive hematopoiesis. *Annu. Rev. Genet* **39**, 481–501.

Detrich 3rd, H. W., Kieran, M. W., Chan, F. Y., Barone, L. M., Yee, K., Rundstadler, J. A., Pratt, S., Ransom, D., and Zon, L. I. (1995). Intraembryonic hematopoietic cell migration during vertebrate development. *Proc. Natl. Acad. Sci. U. S. A* **92**, 10713–10717.

Dick, A., Hild, M., Bauer, H., Imai, Y., Maifeld, H., Schier, A. F., Talbot, W. S., Bouwmeester, T., and Hammerschmidt, M. (2000). Essential role of Bmp7 (snailhouse) and its prodomain in dorsoventral patterning of the zebrafish embryo. *Development* **127**, 343–354.

Du, L., Xu, J., Li, X., Ma, N., Liu, Y., Peng, J., Osato, M., Zhang, W., and Wen, Z. (2011). Rumba and Haus3 are essential factors for the maintenance of hematopoietic stem/progenitor cells during zebrafish hematopoiesis. *Development* **138**, 619–629.

Feldman, B., Gates, M. A., Egan, E. S., Dougan, S. T., Rennebeck, G., Sirotkin, H. I., Schier, A. F., and Talbot, W. S. (1998). Zebrafish organizer development and germ-layer formation require nodal-related signals. *Nature* **395**, 181–185.

Galloway, J. L., Wingert, R. A., Thisse, C., Thisse, B., and Zon, L. I. (2005). Loss of gata1 but not gata2 converts erythropoiesis to myelopoiesis in zebrafish embryos. *Dev. Cell* **8**, 109–116.

Gering, M., Yamada, Y., Rabbitts, T. H., and Patient, R. K. (2003). Lmo2 and Scl/Tal1 convert non-axial mesoderm into haemangioblasts which differentiate into endothelial cells in the absence of Gata1. *Development* **130**, 6187–6199.

Gilliland, D. G., Jordan, C. T., and Felix, C. A. (2004). The molecular basis of leukemia. *Hematology (Am. Soc. Hematol. Educ. Program)* 80–97.

Goessling, W., Allen, R. S., Guan, X., Jin, P., Uchida, N., Dovey, M., Harris, J. H., Metzger, M. E., Bonifacino, A. C., and Stroncek, D., *et al*. (2011). Prostaglandin E2 enhances engraftment of human umbilical cord blood stem cells and is safe for use in preclinical primate and xenotransplantation models. *Cell. Stem. Cell.* **8**, 445–458.

Goessling, W., North, T. E., Loewer, S., Lord, A. M., Lee, S., Stoick-Cooper, C. L., Weidinger, G., Puder, M., Daley, G. Q., and Moon, R. T., *et al*. (2009). Genetic interaction of PGE2 and Wnt signaling regulates developmental specification of stem cells and regeneration. *Cell* **136**, 1136–1147.

Grosser, T., Yusuff, S., Cheskis, E., Pack, M. A., and FitzGerald, G. A. (2002). Developmental expression of functional cyclooxygenases in zebrafish. *Proc. Natl. Acad. Sci. U. S. A* **99**, 8418–8423.

Habeck, H., Odenthal, J., Walderich, B., Maischein, H., and Schulte-Merker, S. (2002). Analysis of a zebrafish VEGF receptor mutant reveals specific disruption of angiogenesis. *Curr. Biol* **12**, 1405–1412.

Hsu, K., Traver, D., Kutok, J. L., Hagen, A., Liu, T. X., Paw, B. H., Rhodes, J., Berman, J. N., Zon, L. I., and Kanki, J. P., *et al*. (2004). The pu.1 promoter drives myeloid gene expression in zebrafish. *Blood* **104**, 1291–1297.

Imai, Y., Gates, M. A., Melby, A. E., Kimelman, D., Schier, A. F., and Talbot, W. S. (2001). The homeobox genes vox and vent are redundant repressors of dorsal fates in zebrafish. *Development* **128**, 2407–2420.

Jin, H., Xu, J., and Wen, Z. (2007). Migratory path of definitive hematopoietic stem/progenitor cells during zebrafish development. *Blood* **109**, 5208–5214.

Kalev-Zylinska, M. L., Horsfield, J. A., Flores, M. V., Postlethwait, J. H., Vitas, M. R., Baas, A. M., Crosier, P. S., and Crosier, K. E. (2002). Runx1 is required for zebrafish blood and vessel development and expression of a human RUNX1-CBF2T1 transgene advances a model for studies of leukemogenesis. *Development* **129**, 2015–2030.

Kelsh, R. N., Brand, M., Jiang, Y. J., Heisenberg, C. P., Lin, S., Haffter, P., Odenthal, J., Mullins, M. C., van Eeden, F. J., and Furutani-Seiki, M., *et al*. (1996). Zebrafish pigmentation mutations and the processes of neural crest development. *Development* **123**, 369–389.

Kimmel, C. B., Warga, R. M., and Schilling, T. F. (1990). Origin and organization of the zebrafish fate map. *Development* **108**, 581–594.

Kishimoto, Y., Lee, K. H., Zon, L., Hammerschmidt, M., and Schulte-Merker, S. (1997). The molecular nature of zebrafish swirl: BMP2 function is essential during early dorsoventral patterning. *Development* **124**, 4457–4466.

Kissa, K., and Herbomel, P. (2010). Blood stem cells emerge from aortic endothelium by a novel type of cell transition. *Nature* **464**, 112–115.

Kumano, K., Chiba, S., Kunisato, A., Sata, M., Saito, T., Nakagami-Yamaguchi, E., Yamaguchi, T., Masuda, S., Shimizu, K., and Takahashi, T., *et al*. (2003). Notch1 but not Notch2 is essential for generating hematopoietic stem cells from endothelial cells. *Immunity* **18**, 699–711.

Lam, E. Y., Hall, C. J., Crosier, P. S., Crosier, K. E., and Flores, M. V. (2010). Live imaging of Runx1 expression in the dorsal aorta tracks the emergence of blood progenitors from endothelial cells. *Blood* **116**, 909–914.

Liao, W., Bisgrove, B. W., Sawyer, H., Hug, B., Bell, B., Peters, K., Grunwald, D. J., and Stainier, D. Y. (1997). The zebrafish gene cloche acts upstream of a flk-1 homologue to regulate endothelial cell differentiation. *Development* **124**, 381–389.

Liao, E. C., Trede, N. S., Ransom, D., Zapata, A., Kieran, M., and Zon, L. I. (2002). Non-cell autonomous requirement for the bloodless gene in primitive hematopoiesis of zebrafish. *Development* **129**, 649–659.

Lieschke, G. J., Oates, A. C., Paw, B. H., Thompson, M. A., Hall, N. E., Ward, A. C., Ho, R. K., Zon, L. I., and Layton, J. E. (2002). Zebrafish SPI-1 (PU.1) marks a site of myeloid development independent of primitive erythropoiesis: implications for axial patterning. *Dev. Biol* **246**, 274–295.

Lin, H. F., Traver, D., Zhu, H., Dooley, K., Paw, B. H., Zon, L. I., and Handin, R. I. (2005). Analysis of thrombocyte development in CD41-GFP transgenic zebrafish. *Blood* **106**, 3803–3810.

Lyons, S. E., Lawson, N. D., Lei, L., Bennett, P. E., Weinstein, B. M., and Liu, P. P. (2002). A nonsense mutation in zebrafish gata1 causes the bloodless phenotype in vlad tepes. *Proc. Natl. Acad. Sci. U. S. A* **99**, 5454–5459.

Melby, A. E., Beach, C., Mullins, M., and Kimelman, D. (2000). Patterning the early zebrafish by the opposing actions of bozozok and vox/vent. *Dev. Biol* **224**, 275–285.

Mikkola, H. K., Fujiwara, Y., Schlaeger, T. M., Traver, D., and Orkin, S. H. (2003). Expression of CD41 marks the initiation of definitive hematopoiesis in the mouse embryo. *Blood* **101**, 508–516.

Mucenski, M. L., McLain, K., Kier, A. B., Swerdlow, S. H., Schreiner, C. M., Miller, T. A., Pietryga, D. W., Scott Jr., W. J., and Potter, S. S. (1991). A functional c-myb gene is required for normal murine fetal hepatic hematopoiesis. *Cell* **65**, 677–689.

Mueller, R. L., Huang, C., and Ho, R. K. (2010). Spatio-temporal regulation of Wnt and retinoic acid signaling by tbx16/spadetail during zebrafish mesoderm differentiation. *BMC Genomics* **11**, 492.

Murayama, E., Kissa, K., Zapata, A., Mordelet, E., Briolat, V., Lin, H. F., Handin, R. I., and Herbomel, P. (2006). Tracing hematopoietic precursor migration to successive hematopoietic organs during zebrafish development. *Immunity* **25**, 963–975.

North, T. E., Goessling, W., Peeters, M., Li, P., Ceol, C., Lord, A. M., Weber, G. J., Harris, J., Cutting, C. C., and Huang, P., *et al*. (2009). Hematopoietic stem cell development is dependent on blood flow. *Cell* **137**, 736–748.

North, T. E., Goessling, W., Walkley, C. R., Lengerke, C., Kopani, K. R., Lord, A. M., Weber, G. J., Bowman, T. V., Jang, I. H., and Grosser, T., *et al*. (2007). Prostaglandin E2 regulates vertebrate haematopoietic stem cell homeostasis. *Nature* **447**, 1007–1011.

North, T., Gu, T. L., Stacy, T., Wang, Q., Howard, L., Binder, M., Marin-Padilla, M., and Speck, N. A. (1999). Cbfa2 is required for the formation of intra-aortic hematopoietic clusters. *Development* **126**, 2563–2575.

Okuda, T., van Deursen, J., Hiebert, S. W., Grosveld, G., and Downing, J. R. (1996). AML1, the target of multiple chromosomal translocations in human leukemia, is essential for normal fetal liver hematopoiesis. *Cell* **84**, 321–330.

Paik, E. J., de Jong, J. L., Pugach, E., Opara, P., and Zon, L. I. (2010). A chemical genetic screen in zebrafish for pathways interacting with cdx4 in primitive hematopoiesis. *Zebrafish* **7**, 61–68.

Parker, L., and Stainier, D. Y. (1999). Cell-autonomous and non-autonomous requirements for the zebrafish gene cloche in hematopoiesis. *Development* **126**, 2643–2651.

Pillay, L. M., Forrester, A. M., Erickson, T., Berman, J. N., and Waskiewicz, A. J. (2010). The Hox cofactors Meis1 and Pbx act upstream of gata1 to regulate primitive hematopoiesis. *Dev. Biol* **340**, 306–317.

Ramel, M. C., Buckles, G. R., Baker, K. D., and Lekven, A. C. (2005). WNT8 and BMP2B co-regulate non-axial mesoderm patterning during zebrafish gastrulation. *Dev. Biol* **287**, 237–248.

Ransom, D. G., Bahary, N., Niss, K., Traver, D., Burns, C., Trede, N. S., Paffett-Lugassy, N., Saganic, W. J., Lim, C. A., and Hersey, C., *et al*. (2004). The zebrafish moonshine gene encodes transcriptional intermediary factor 1gamma, an essential regulator of hematopoiesis. *PLoS Biol* **2**, E237.

Ransom, D. G., Haffter, P., Odenthal, J., Brownlie, A., Vogelsang, E., Kelsh, R. N., Brand, M., van Eeden, F. J., Furutani-Seiki, M., and Granato, M., *et al*. (1996). Characterization of zebrafish mutants with defects in embryonic hematopoiesis. *Development* **123**, 311–319.

Rhodes, J., Hagen, A., Hsu, K., Deng, M., Liu, T. X., Look, A. T., and Kanki, J. P. (2005). Interplay of pu.1 and gata1 determines myelo-erythroid progenitor cell fate in zebrafish. *Dev. Cell* **8**, 97–108.

Sabin, F. (1920). Studies on the origin of blood vessels and of red corpuscles as seen in the living blastoderm of the chick during the second day of incubation. *Beiträge zuer Embryologie* **9**, 213–262.

Sakamoto, H., Dai, G., Tsujino, K., Hashimoto, K., Huang, X., Fujimoto, T., Mucenski, M., Frampton, J., and Ogawa, M. (2006). Proper levels of c-Myb are discretely defined at distinct steps of hematopoietic cell development. *Blood* **108**, 896–903.

Schatteman, G. C. (2004). Adult bone marrow-derived hemangioblasts, endothelial cell progenitors, and EPCs. *Curr. Top. Dev. Biol* **64**, 141–180.

Schoenebeck, J. J., Keegan, B. R., and Yelon, D. (2007). Vessel and blood specification override cardiac potential in anterior mesoderm. *Dev. Cell* **13**, 254–267.

Shalaby, F., Ho, J., Stanford, W. L., Fischer, K. D., Schuh, A. C., Schwartz, L., Bernstein, A., and Rossant, J. (1997). A requirement for Flk1 in primitive and definitive hematopoiesis and vasculogenesis. *Cell* **89**, 981–990.

Shalaby, F., Rossant, J., Yamaguchi, T. P., Gertsenstein, M., Wu, X. F., Breitman, M. L., and Schuh, A. C. (1995). Failure of blood-island formation and vasculogenesis in Flk-1-deficient mice. *Nature* **376**, 62–66.

Sood, R., English, M. A., Belele, C. L., Jin, H., Bishop, K., Haskins, R., McKinney, M. C., Chahal, J., Weinstein, B. M., and Wen, Z., *et al*. (2010). Development of multilineage adult hematopoiesis in the zebrafish with a runx1 truncation mutation. *Blood* **115**, 2806–2809.

Soza-Ried, C., Hess, I., Netuschil, N., Schorpp, M., and Boehm, T. (2010). Essential role of c-myb in definitive hematopoiesis is evolutionarily conserved. *Proc. Natl. Acad. Sci. U. S. A* **107**, 17304–17308.

Stachura, D. L., Reyes, J. R., Bartunek, P., Paw, B. H., Zon, L. I., and Traver, D. (2009). Zebrafish kidney stromal cell lines support multilineage hematopoiesis. *Blood* **114**, 279–289.

Stainier, D. Y., Weinstein, B. M., Detrich 3rd, H. W., Zon, L. I., and Fishman, M. C. (1995). Cloche, an early acting zebrafish gene, is required by both the endothelial and hematopoietic lineages. *Development* **121**, 3141–3150.

Traver, D., Paw, B. H., Poss, K. D., Penberthy, W. T., Lin, S., and Zon, L. I. (2003). Transplantation and *in vivo* imaging of multilineage engraftment in zebrafish bloodless mutants. *Nat. Immunol* **4**, 1238–1246.

Ueno, H., and Weissman, I. L. (2006). Clonal analysis of mouse development reveals a polyclonal origin for yolk sac blood islands. *Dev. Cell* **11**, 519–533.

Villablanca, E. J., Pistocchi, A., Court, F. A., Cotelli, F., Bordignon, C., Allende, M. L., Traversari, C., and Russo, V. (2007). Abrogation of prostaglandin E2/EP4 signaling impairs the development of rag1+ lymphoid precursors in the thymus of zebrafish embryos. *J. Immunol* **179**, 357–364.

Vogeli, K. M., Jin, S. W., Martin, G. R., and Stainier, D. Y. (2006). A common progenitor for haematopoietic and endothelial lineages in the zebrafish gastrula. *Nature* **443**, 337–339.

Wang, Q., Stacy, T., Binder, M., Marin-Padilla, M., Sharpe, A. H., and Speck, N. A. (1996). Disruption of the Cbfa2 gene causes necrosis and hemorrhaging in the central nervous system and blocks definitive hematopoiesis. *Proc. Natl. Acad. Sci. U. S. A* **93**, 3444–3449.

Ward, A. C., McPhee, D. O., Condron, M. M., Varma, S., Cody, S. H., Onnebo, S. M., Paw, B. H., Zon, L. I., and Lieschke, G. J. (2003). The zebrafish spi1 promoter drives myeloid-specific expression in stable transgenic fish. *Blood* **102**, 3238–3240.

Warga, R. M., and Nusslein-Volhard, C. (1999). Origin and development of the zebrafish endoderm. *Development* **126**, 827–838.

Weinstein, B. M., Schier, A. F., Abdelilah, S., Malicki, J., Solnica-Krezel, L., Stemple, D. L., Stainier, D. Y., Zwartkruis, F., Driever, W., and Fishman, M. C. (1996). Hematopoietic mutations in the zebrafish. *Development* **123**, 303–309.

Xiong, J. W., Yu, Q., Zhang, J., and Mably, J. D. (2008). An acyltransferase controls the generation of hematopoietic and endothelial lineages in zebrafish. *Circ. Res* **102**, 1057–1064.

Yeh, J. R., Munson, K. M., Chao, Y. L., Peterson, Q. P., Macrae, C. A., and Peterson, R. T. (2008). AML1-ETO reprograms hematopoietic cell fate by downregulating scl expression. *Development* **135**, 401–410.

Yeh, J. R., Munson, K. M., Elagib, K. E., Goldfarb, A. N., Sweetser, D. A., and Peterson, R. T. (2009). Discovering chemical modifiers of oncogene-regulated hematopoietic differentiation. *Nat. Chem. Biol* **5**, 236–243.

Yue, R., Kang, J., Zhao, C., Hu, W., Tang, Y., Liu, X., and Pei, G. (2009). Beta-arrestin1 regulates zebrafish hematopoiesis through binding to YY1 and relieving polycomb group repression. *Cell* **139**, 535–546.

CHAPTER 6

Zebrafish as a Model for Hemorrhagic Stroke

Matthew G. Butler, Aniket V. Gore and Brant M. Weinstein

Program in the Genomics of Differentiation, National Institute of Child Health and Development, National Institutes of Health, Bethesda, Maryland, USA

Abstract

Blood vessels perform the fundamental role of providing conduits for the circulation of oxygen and nutrients and the removal of waste products throughout the body. Disruption of tissue perfusion by ischemia or hemorrhage of blood vessels has a range of devastating consequences including stroke. Stroke is a complex trait that includes both genetic and environmental risk factors. The zebrafish is an attractive model for the study of hemorrhagic stroke due to the conservation of the molecular mechanisms of blood vascular development among vertebrates and the experimental advantages that can be applied to zebrafish embryos and larva. This chapter will focus on the maintenance of vascular integrity and some of the seminal experimentation carried out in the zebrafish.

I. Introduction and Basic Concepts

All cells must maintain homeostasis by respiration, metabolism, and excretion of waste products. During the course of evolution, the emergence of complex multicellular organisms led to the development of a system dedicated to supplying oxygen

0091-679X/10 $35.00
DOI 10.1016/B978-0-12-381320-6.00006-0

and nutrients to all cells and removing waste products and carbon dioxide from them (Strilic *et al.*, 2010). In vertebrates, the cardiovascular system performs these critical functions. Blood is pumped to and from the heart in a continuous loop, carrying oxygenated blood and nutrients to all tissues and removing wastes from them through a hierarchy of tubular blood vessels. It exits from the heart into large arteries, dividing into ever smaller arterioles before reaching the fine capillary beds. Blood is then returned through venules of ever increasing caliber that merge and join together into large veins before returning to the heart. In air-breathing organisms, a second pulmonary circulatory loop is superimposed on the primary circulatory loop, bringing blood from the heart to the lungs to be oxygenated and returning it once again to the heart.

Blood vessels are composed of two major cell types. Endothelial cells (ECs) form a single cell thick epithelium that lines the inner surface of all blood vessels and provides a permeability barrier preventing excessive leakage of fluid, macromolecules, and cells in the blood plasma. In contrast, pericytes and smooth muscle cells adhere to the outside of smaller caliber vessels or form a muscular wall around larger caliber vessels, respectively. Smooth muscle and pericytes provide trophic and physical support to the endothelium and regulate vascular stability and vascular tone. Larger arterial and venous vessels have a similar gross anatomical structure (Fig. 1). The vessel wall consists of three distinct layers: the *tunica intima* (an inner layer of continuous ECs), with a basal lamina at the abluminal surface, the *tunica*

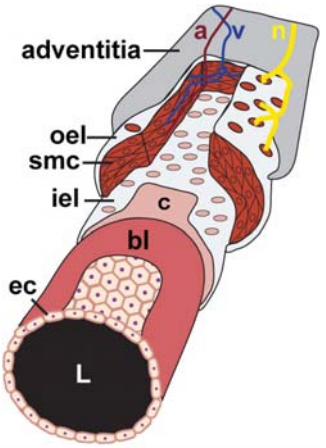

Fig. 1 Diagram of the basic structure of an elastic artery. The innermost *tunica intima* is composed of a continuous monolayer of endothelial cells (ec) surrounding the open vessel lumen (L). This endothelial lining is progressively covered by the basal lamina (bl), a collagenous matrix (c), and the fenestrated internal elastic lamina (iel). The medial layer of the vessel wall is the *tunica media*, mainly composed of a thick layer of smooth muscle cells (smc) covered by the outer elastic lamina (oel). The outermost *tunica adventitia* consists of fibroblasts, collagen, and elastic fibers. In the walls of large vessels the tunica media and tunica adventitia can be themselves innervated by nerves (n) and by smaller arteries (a) and veins (v). (For color version of this figure, the reader is referred to the web version of this book.)

media (circumferential layers of smooth muscle cells and connective tissue), and the *tunica adventitia* (mainly connective tissue with some smooth muscle cells as well as other cell types). Each of these layers is separated by an elastic lamina. In arteries, the size and composition of each of the layers varies depending on the location and flow characteristics of a particular vessel segment. Smaller caliber arterioles have a thinner SMC layer, which is also innervated to control blood flow. From the arterioles, blood enters into capillaries, which are composed only of a single layer of endothelium and a basal membrane (continuous, fenestrated, and discontinuous) that can vary to regulate its inherent permeability (Fig. 2). A limited number of pericytes are associated with capillaries, providing trophic support, but they do not form a continuous wall (although generally most ECs have at least minimal contact with one pericyte cell) and are not required for physical support of these smaller caliber vessels. After exiting the capillary bed, blood is returned to the heart through veins with similar organization to large arteries except that the veins have a thinner *tunica media* than comparably sized arteries, and larger veins frequently have valvular structures preventing backflow of blood through these relatively lower pressure vessels.

As discussed in greater detail below, the proper functioning of the vasculature relies critically on the integrity of the permeability barrier provided by the single cell layer thick endothelial epithelium. Passage of solute, ions, macromolecules, etc., across the endothelium occurs via two major mechanisms, the "paracellular" and "transcellular" pathways (Komarova and Malik, 2010). Paracellular transit occurs between ECs, and is regulated by the dynamic regulation of endothelial junctions (Dejana *et al.*, 2008). Transcellular transit occurs across individual ECs, and depends on vesicular transport systems, fenestrae, and biochemical transporters (Dvorak *et al.*, 1996). Since vascular fragility and disruption of the endothelium leading to hemorrhage depends primarily on defects in endothelial cell–cell junctions, we focus here on junctions – their role in maintaining vascular integrity, their involvement in pathological conditions in humans, and how the zebrafish is helping us to understand more about both of these.

The architecture and molecular composition of endothelial cell–cell junctions have been discussed comprehensively elsewhere, and we will only briefly review them here. Junctions in the endothelium include many of the same types of structures found in other epithelia (Fig. 3). Adherens junctions (AJ) initiate cell–cell contacts between ECs, promote the maturation and maintenance of these cell–cell contacts, and are important for physical stability of the endothelial epithelium. Tight junctions (TJ) are primarily responsible for maintenance of the endothelial permeability barrier, regulating the passage of ions and solutes between cells via the paracellular pathway. They are also important for maintaining distinct apical and basolateral membrane compartments, acting as a membrane "fence" to limit the free movement of lipids and proteins between the two surfaces. Although gap junctions are also present and important for endothelial function, they have not been reported to play a role in endothelial permeability and integrity and will not be further discussed here. AJ and TJ have a distinct molecular composition but share some characteristics

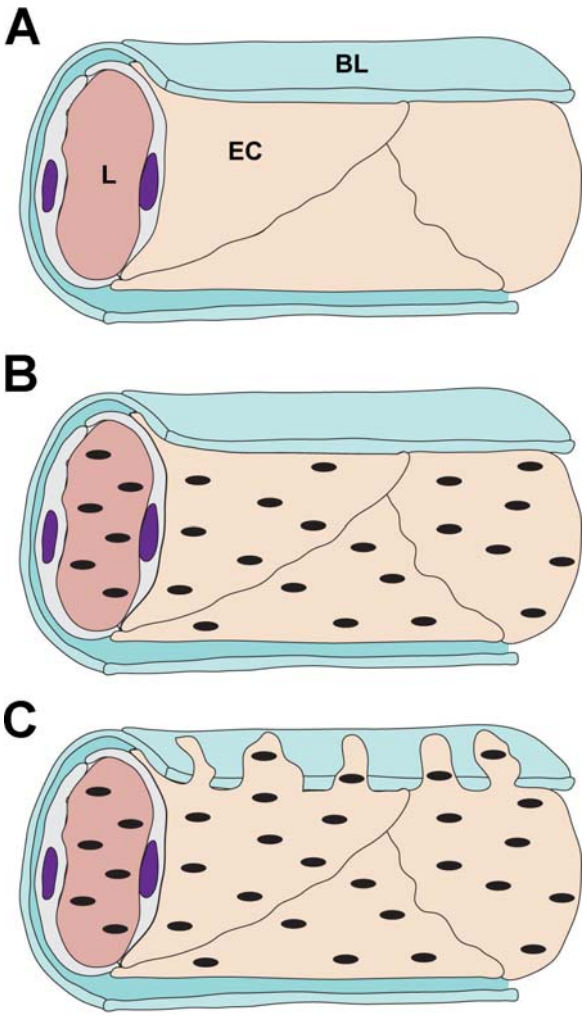

Fig. 2 Diagram illustrating the differential properties of capillaries. Capillaries are formed by a continuous endothelial cell monolayer (EC) surrounding the open lumen (L), covered by a basal lamina (BL). Capillaries lack a smooth muscle invested vascular wall, although pericytes make contact with most endothelial cells, providing trophic support. Continuous capillaries (A), such as those found in the brain, lack fenestrae and have an uninterrupted basal lamina, providing for a relatively "tight" barrier. Fenestrated capillaries (B) contain small passages between the lumenal and abluminal surfaces of the endothelium, but generally have a continuous basal lamina. Discontinuous capillaries (C), as, for example, found in the lungs, consist of fenestrated endothelium with an incomplete basal lamina to further facilitate transport and transit across the endothelium, making them the most "leaky." (For color version of this figure, the reader is referred to the web version of this book.)

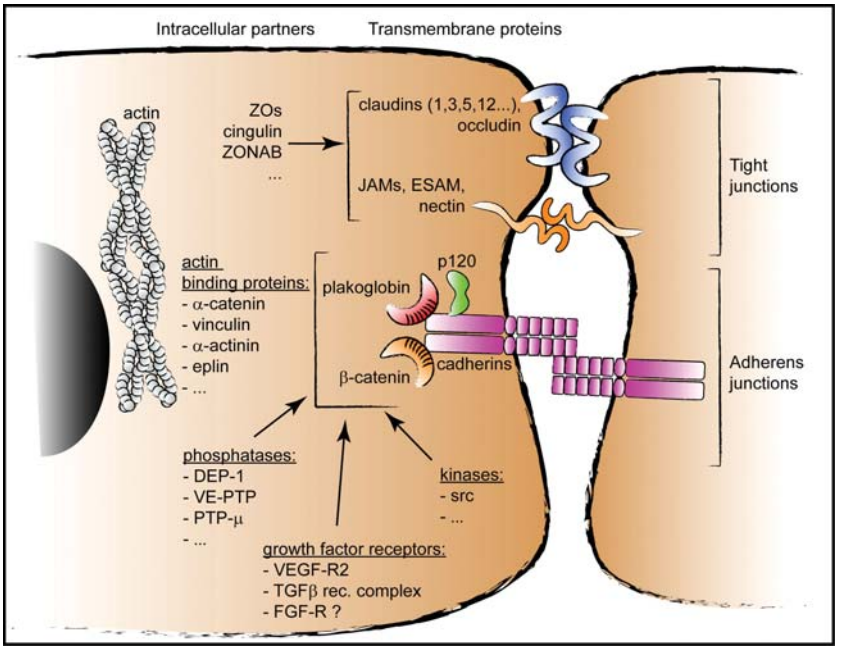

Fig. 3 Schematic illustration of the molecular components of endothelial tight junctions and adherens junctions. Adhesion at tight junctions is mediated by claudins, occludin, members of the JAM family, and ESAM. The cytoplasmic components of tight junctions include ZO proteins, cingulin, ZONAB, and others. At adherens junctions, adhesion is promoted by cadherins (Vecad and N-cadherin) that directly bind to p120, β-catenin, and plakoglobin. Nectin participates in the organization of both tight and adherens junctions. Numerous actin-binding proteins are associated with adherens junctions, including α-catenin, vinculin, α-actinin, eplin, and others. In addition, phosphatases (DEP-1, VE-PTP, PTPμ, etc.) and kinases (src, etc.) are directly or indirectly associated with adherens junction components. Interaction between the VEcdn complex and VEGFR2 or TGF-β receptor complexes results in modulation of both receptor signaling and functional complex activity and localization. See text for additional discussion, and Dejana *et al.* (2008) for comprehensive review. Illustration is from Dejana *et al.* (2009) (See color plate.).

(Fig. 3). Both types of junction mediate adhesion through endothelial-specific transmembrane proteins that promote homophilic interactions and form a pericellular zipper-like structure along the cell border through their lateral aggregation in *trans* and *cis* (for review, see Bazzoni and Dejana, 2004; Gonzalez-Mariscal *et al.*, 2008; Wallez and Huber, 2008). Vascular endothelial cadherin vecad and Claudin-5 are key transmembrane adhesion proteins found in AJ and TJ, respectively. The restricted cell specificity of these components suggests that they modulate selective cell–cell recognition and/or specific functional properties of ECs. The cytoplasmic tails of adhesion proteins interact with a variety of additional proteins including cytoskeletal, signaling, and adaptor proteins that permit junctions to both respond to and promote intracellular signaling, as discussed further below.

The organization of TJs and AJs varies throughout the vasculature depending on the functional needs of particular vessels. For example, TJ are particularly abundant and complex in the brain where there is a need to strictly control permeability, whereas junctions are relatively poorly organized in postcapillary venules where there is extensive exchange between blood and tissues (Dejana, 2004; Engelhardt, 2003). However, preserving an effective circulation perfusing all parts of the body requires maintaining the integrity of all of these vessels, and preventing their rupture and/or blockage. In the next section, we discuss the molecular regulation of endothelial barrier function, and some of the pathological consequences of failure of vascular integrity.

II. Maintaining the Barrier Function of Blood Vessels

The permeability of the endothelial barrier varies throughout the blood vasculature based on the requirements of a particular organ system. Organs like the lung have endothelium with relatively high levels of permeability, whereas others like the brain endothelium have comparatively low levels. As noted above, fluid and macromolecules move across the endothelial barrier by either the paracellular or transcytosis pathway (Komarova and Malik, 2010). Paracellular transport is the size-selective diffusion of molecules from the plasma within the vessel lumen to the interstitium at interendothelial cell–cell junctions. Transcytosis is the bidirectional transport of molecules within membrane-bound caveolae into and/or across ECs (Simionescu *et al.*, 2009). We are mainly focusing here on paracellular transport and endothelial epithelial integrity, controlled by dynamic endothelial AJ and TJ (Dejana *et al.*, 2009). AJ are primarily involved in the formation and maintenance of cell–cell contacts while TJ control the paracellular transport of ions and solutes. Endothelial AJ are composed of the integral membrane protein vascular endothelial cadherin (vecad; aka cadherin 5 (cdh5)), which binds to β-catenin, p120, and plakoglobin through its cytoplasmic tail (Breviario *et al.*, 1995; Lampugnani *et al.*, 1995). Endothelial TJ are also composed of integral membrane proteins including members of the claudin family (mainly Claudin-3 and -5) and occludin (mainly restricted to the brain) (Furuse *et al.*, 1993). Like AJ, the cytoplasmic portions of endothelial TJ also bind to cytosolic partners such as the zonula occludens proteins ZO-1 and ZO-2, which are members of the membrane-associated guanylate kinase family (MAGUK) (Gonzalez-Mariscal *et al.*, 2000). The ZOs interact with claudins and occludin to tether TJ to the actin cytoskeleton and act as a scaffold for kinases, phosphatases, G proteins, and transcription factors (Gonzalez-Mariscal *et al.*, 2008). Additional accessory transmembrane glycoproteins including junctional adhesion molecules (Jams-A, B, C) and EC-selective adhesion molecule (Esam) associate with TJ, but mouse models suggest each is unnecessary for vascular development (Weber *et al.*, 2007; Wegmann *et al.*, 2006). Some TJ components have been shown to play a role in regulating vascular integrity of ECs. In particular, the loss of Claudin-5, a member of the claudin family

specifically expressed in ECs, causes lethality in mice due to vascular leak of the blood–brain barrier (Morita *et al.*, 1999; Nitta *et al.*, 2003).

Within AJ, vecad plays a central role in determining endothelial permeability. Vecad forms zipper-like aggregations between adjacent ECs through homophilic interactions (Bazzoni and Dejana, 2004). Vascular permeability is generally increased by Vecad phosphorylation, internalization, or cleavage (Dejana *et al.*, 2009). Phosphorylation of Vecad at residues Y658 and Y731 prevents the binding of p120 and β-catenin to Vecad to increase permeability (Potter *et al.*, 2005). Vascular endothelial growth factor (Vegf) is a potent activator of EC permeability and destabilizes Vecad in multiple ways. Vegf signaling induces phosphorylation of Vecad in an Src kinase–dependent manner (Adam *et al.*, 2010). It also induces the recruitment of the protein tyrosine phosphatase Shp2 to Vecad and dissociates the C-terminal Src kinase (Csk) from Y685 of Vecad leading to Src activation (Ha *et al.*, 2008). Src activation leads to the activation of eNOS, a potent inducer of EC permeability (Ha *et al.*, 2008). Vegf-induced Src kinase phosphorylation can also lead to Vecad internalization by initiating a Vav2–Rac1–Pak1 cascade leading to the phosphorylation of Y668 and ultimately β-arrestin 2 endocytosis (Gavard and Gutkind, 2006). The stabilization of Vecad is enhanced by the dephosphorylation of plakoglobin by the protein tyrosine phosphatase VE-PTP (Nottebaum *et al.*, 2008). Conversely, Vecad can interact with Vegfr2 to limit its internalization and decrease its signaling capacity (Lampugnani *et al.*, 2006). In addition to phosphorylation, proteolytic cleavage of Vecad can increase the permeability of ECs. The zinc-dependent transmembrane disintegrin metalloproteinase Adam10 has been shown to cleave Vecad in response to thrombin (Schulz *et al.*, 2008). The actual expression levels of *vecad* within ECs can also contribute to the level of EC permeability. The ETS transcription factor Erg as well as the basic helix–loop–helix transcription factor Tal1, required for EC tube formation *in vitro*, binds to the *vecad* promoter and activates its transcription (Birdsey *et al.*, 2008; Deleuze *et al.*, 2007). More recently, the flow-sensitive Krüppel-like factor 4 (Klf4) transcription factor has been shown to bind to the *vecad* promoter and increase levels of *Vecad* expression especially in response to wnt signaling (Cowan *et al.*, 2010). The *in vivo* role of *vecad* has also been studied in the zebrafish (Mitchell *et al.*, 2010; Montero-Balaguer *et al.*, 2009). Low-dose *vecad* knockdown causes hemorrhage and leaky vessels leading to poor circulation in zebrafish embryos, confirming that full expression of vecad is required for vascular stability in the zebrafish as well (Mitchell *et al.*, 2010; Montero-Balaguer *et al.*, 2009).

III. Vascular Integrity and Stroke

As noted above, the integrity of the vasculature depends on maintenance of an intact continuous layer of ECs lining the luminal side of all blood vessels, although other cell types, especially pericytes and smooth muscle cells, also play critical roles in maintaining vascular integrity. Loss of integrity of the vascular endothelium can

result in the rupture of vessels and hemorrhage of blood into interstitial spaces. If this occurs within the arteries that supply or are located within the brain, stroke (loss of circulation to and eventual death of nervous tissue in portions of the brain) ensues.

Stroke is the third leading cause of death and the leading cause of disability in adults in the United States. The genetic and environmental risk factors for susceptibility to hemorrhagic stroke are complex and still poorly understood, although hypertension, hypercholesterolemia, smoking, diabetes mellitus, hormone replacement therapy, oral contraceptive, alcohol consumption, physical inactivity, and obesity are all known to be associated with higher incidence of stroke (Leys *et al.*, 2002). The majority of stroke cases (80–85%) are caused by ischemia in which arteries supplying blood to the brain become occluded preventing perfusion of parts of the brain. The remaining stroke cases are caused by hemorrhage of arteries supplying blood to the brain, and can be further classified into two subtypes: intracerebral hemorrhage (ICH; arteries penetrating into the brain parenchyma) and subarachnoid hemorrhage (arteries along the surface of the brain). Although ICH accounts for a smaller percentage of total strokes, they have the highest rate of mortality of any stroke subtype (Qureshi *et al.*, 2001). ICH is often associated with vascular anomalies of the cerebral vasculature. Two prominent examples of this include cerebral cavernous malformations (CCMs) and hereditary hemorrhagic telangiectasia (HHT). HHT is a vascular dysplasia characterized by the presence of arterial–venous malformations and telangiectasias of the dermal and mucosal membranes caused by autosomal dominant mutations in the TGFβ superfamily receptors endoglin (*ENG*) and activin-like receptor kinase (*ACVRL1*/*ALK1*), respectively. Zebrafish studies exploring the functional roles of these genes in the vasculature are discussed further below. CCM is a vascular disease resulting in the formation of clusters of grossly enlarged, fragile, hemorrhage-prone vessels that lack smooth muscle support. CCM lesions have multiple enlarged vessels adjacent to each other without intervening brain parenchyma, in contrast to single enlarged vessels found in other disorders such as HHT. Sporadic CCM is not uncommon, occurring approximately in 1 in 200–250 individuals in the general population (Otten *et al.*, 1989; Robinson *et al.*, 1991). Most CCM cases present as cerebral hemorrhages and/or seizures. A variety of immune cells are found in CCM lesions (Shi *et al.*, 2009) and inflammatory responses appear to be important in the pathology of CCM. However, recent evidence suggests that these inflammatory responses may be a secondary reaction to antigens exposed by the defective blood–brain barrier of a CCM (Clatterbuck *et al.*, 2001), since vascular malformations occur in murine and zebrafish CCM models without an apparent inflammatory contribution, at least initially (see below).

Positional cloning of the defective genes from familial CCM syndromes has led to the identification of three loci, *CCM1* (*KRIT1*), *CCM2* (*OSM*, *MGC4607*), and *CCM3* (*PCD10*) (Bergametti *et al.*, 2005; Denier *et al.*, 2004; Laberge-le Couteulx *et al.*, 1999; Liquori *et al.*, 2003; Sahoo *et al.*, 1999). *CCM1*, *CCM2*, and *CCM3* account for the vast majority of familial CCM cases, but at least one report suggests that 5% of familial CCMs are caused by an unidentified *CCM* locus

or an as yet to be described mechanism to disrupt *CCM1*, *CCM2*, or *CCM3* (Denier *et al.*, 2006). Each of the CCM genes encodes a scaffold protein that physically interacts with other CCM proteins and a myriad of additional proteins (*CCM1–CCM2*; *CCM2–CCM3*) in a multiprotein complex (Stahl *et al.*, 2008; Voss *et al.*, 2007; Zawistowski *et al.*, 2005; Zhang *et al.*, 2007). CCM1 (KRIT1) is a scaffold protein containing FERM, PTB, and NPXY/F protein–protein interaction domains that was first identified in a yeast two-hybrid screen as a partner of the small G-protein Krev-1/Rap1. CCM2 (OSM) was also identified in a two-hybrid screen, using mitogen-activated protein kinase kinase 3 (MEKK3) as bait to identify proteins involved in the cell response to hyperosmotic shock (hence *Osmosensing Scaffold for MEKK3*). CCM3 (PDCD10) is a small (25 kDa) protein with no known homology domains whose expression is increased in apoptotic fibroblasts (hence *Programmed Cell Death-10*). The interactions and functions of this multiprotein complex in CCM pathology have been reviewed extensively elsewhere (Faurobert and Albiges-Rizo, 2010), and we will only briefly discuss them below, mainly in the context of relevant zebrafish studies.

Familial CCM disorders have an autosomal dominant inheritance pattern, and the vast majority of CCM mutations cause premature termination and are putative null alleles (Riant *et al.*, 2010). In addition to germline mutations, somatic mutations have been found in ECs of CCM lesions, providing support for a Knudson "two-hit" mechanism for CCM lesion pathogenesis (Gault *et al.*, 2005, 2009). Somatic mutations for each CCM locus have now been demonstrated, suggesting that loss of one of the CCM proteins may be required for lesion formation (Akers *et al.*, 2009). The second somatic hit can be mosaic among ECs within CCM lesions, (Akers *et al.*, 2009; Pagenstecher *et al.*, 2009), suggesting heterozygous ECs may also be able to participate in lesion formation. The highly variable penetrance and expressivity (number of lesions and age of onset) of familial CCM suggests that additional genetic and/or environmental factors in addition to loss of heterozygosity at the primary disease locus are likely influencing lesion formation and progression. As discussed further below, zebrafish studies suggest that minor, individually subphenotypic defects in CCM proteins and/or their interacting partners can synergize to promote the formation or increase the severity of CCM lesions.

In addition to identification of the "trigger(s)" for lesion formation, another important issue is which specific target tissue is responsible for initiating lesion pathogenesis. Expression studies performed using *in situ* hybridization, immunohistochemistry, or analysis of knock-in alleles have shown that all three CCM genes are expressed in both neurons and blood vessels in the brains of mice and zebrafish (Gore *et al.*, 2008; Hogan *et al.*, 2008; Mably *et al.*, 2006; Petit *et al.*, 2006; Plummer *et al.*, 2006; Tanriover *et al.*, 2008). The strong expression of the CCM genes in neural tissue and the neural involvement in lesion formation in CCM patients have led to suggestions that cavernous malformations may be the result of a primary defect in surrounding neural cells rather than blood vessel ECs, with vascular defects occurring secondarily (Plummer *et al.*, 2006). As discussed below, however, studies in mice and zebrafish have shown clearly that despite their strong expression in

neuronal tissue, it is the endothelial function of these genes that is critical for maintaining vascular integrity.

IV. Zebrafish as a Model for Studying Hemorrhage and Stroke

The zebrafish already enjoys a reputation as the preeminent vertebrate model organism for large-scale, phenotype-based forward genetic (Patton and Zon, 2001) or chemical (Peal *et al.*, 2010) screening to uncover novel genes and biologically active compounds relevant to processes of interest. As discussed above, genetic and environmental risk factors for susceptibility to hemorrhagic stroke are complex and still largely unknown, and it would be highly advantageous to be able to uncover and study susceptibility factors using an accessible animal model. One of the most advantageous features of the zebrafish as an animal model for hemorrhagic stroke is the ability to easily and directly observe ICH using only a conventional inverted light microscope (Fig. 4). This makes it possible to rapidly screen very large numbers of mutagenized or compound-treated animals for hemorrhage defects. Traditional F_3 screens have already been used extensively to identify a range of cardiovascular mutants, including a large number isolated in the first large-scale zebrafish genetic screens carried out in Boston and Tübingen (Chen *et al.*, 1996; Stainier *et al.*, 1996). Mutants with vascular integrity defects were not a major focus of these original screens, but a handful of mutants with phenotypes of this sort were identified and subsequently studied further, including the *mush for brains*, *bubblehead* (*bbh*), *leaky heart*, *gridlock*, and *migraine* mutants (Stainier *et al.*, 1996). The *gridlock* mutation causes malformation of the dorsal aorta, with vascular rupture and hemorrhage occurring at the point where the paired rostral lateral dorsal aortae normally fuse into a single midline aorta before continuing caudally (Weinstein *et al.*, 1995). The *mush for brains* mutation causes extensive cranial hemorrhage closely followed by extensive death of central nervous system tissues (Stainier *et al.*, 1996). However, many of the mutants exhibit cranial hemorrhage without other obvious defects, suggesting they cause more specific defects in maintenance of vascular integrity.

The *redhead* (*rdh*) mutant was discovered serendipitously in a screen for genes involved in neuron development and axonogenesis (Buchner *et al.*, 2007; Gulati-Leekha and Goldman, 2006). *Rdh* mutants develop cerebral hemorrhages between 2 and 3 days postfertilization (Buchner *et al.*, 2007). Positional cloning showed that the mutant phenotype is caused by a splice mutation in *pak2a* (*p21 protein (Cdc42/Rac)-activated kinase 2a*). The zebrafish genome also contains a *pak2a* paralog (designated *pak2b*) that is insufficient to rescue *rdh* mutants by mRNA injection, but that exacerbates the severity of *rdh* mutants when simultaneously knocked down, suggesting a partially redundant role. Microinjection of red quantum dots does not demonstrate vascular leakage prior to hemorrhage, suggesting that an increase in vascular permeability of cerebral vasculature is not necessary for the catastrophic loss of junctional integrity in *rdh* mutants. *Rdh* mutants do not exhibit any obvious

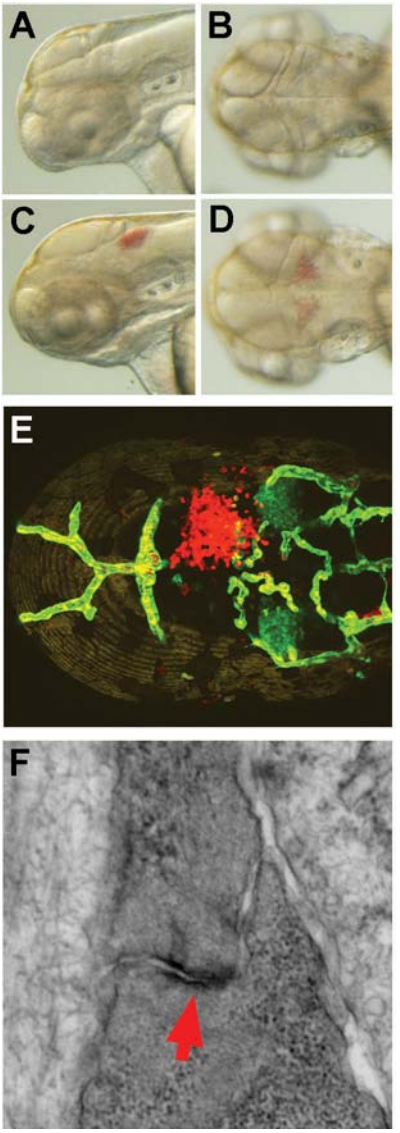

Fig. 4 Intracranial hemorrhage and endothelial junctions in the zebrafish. Intracranial hemorrhage is easily visualized in the zebrafish. Lateral (A and C) and dorsal (B and D) transmitted light images of normal (A and B) and hemorrhaging *rap1b*-deficient (C and D) zebrafish embryos at approximately 2 days postfertilization. Intracranial hemorrhage can also be visualized by fluorescence using transgenic lines. Gata-DsRed-positive hemorrhaged blood cells are seen adjacent to Fli1a-EGFP-positive blood vessels in a dorsal view confocal micrograph of a double-transgenic zebrafish at 2.5 days postfertilization (E). Typical endothelial cell–cell junctions are seen using ultrastructural analysis of zebrafish blood vessels. Transmission electron micrograph of a typical endothelial cell–cell junctional structure in normal 2.5-day-old zebrafish (F). The electron-dense material at the membrane interface between the two endothelial cells (red arrow) is typical of junctional structures seen by ultrastructural analysis in other vertebrates. (See color plate.)

cerebral vascular patterning abnormalities that might be responsible for hemorrhage, leaving the molecular mechanism downstream of pak2a to be determined.

Another mutant, *bbh*, has nonstereotypic cerebral hemorrhage with cranial (ventricular) edema that appears between 36 and 52 hpf (Liu *et al.*, 2007). Positional cloning of the *bbh* identified β-*pix* (*pak-interacting exchange factor* β), a guanine nucleotide exchange factor, as a novel ICH locus (Liu *et al.*, 2007). A splice mutation in *bbh* mutants causes a premature stop codon that leads to a truncated polypeptide sequence. Morpholino experiments demonstrated that the loss of β-pix B isoform, containing an N-terminal calponin homology domain, induced ICH. Microinjection of a constitutively active *pak2a* rescued ICH in *bbh* mutants suggesting that pak2a may function downstream from or together with β-pix. Cranial angiogenesis and cell/extracellular matrix organization surrounding cranial ECs were disorganized, but the responsible molecular mechanism(s) remain to be elucidated.

As discussed in more detail below, both β-*pix* and *pak2a* have been implicated in the CCM pathway, and analysis of these mutants and other genetic and experimental models in the zebrafish has begun to yield new insights into both the etiology of CCM pathology and the maintenance of vascular integrity in general.

V. Studying Vascular Integrity in the Zebrafish

Studying the human genetic disorders caused by defects in CCM, HHT, and other ICH-associated genes has begun to yield new insights into the mechanisms regulating endothelial junctional stability and integrity of the vasculature. However, *in vivo* experimental analysis of disease etiology is not possible in human patients, and naturally occurring disease lesions are identified and characterized too late to determine the nature of the original defect that gave rise to these lesions. The zebrafish has recently been shown to be a useful model for dissecting the *in vivo* functions of CCM genes and their interacting partners, and their roles in maintaining vascular integrity.

Zebrafish possess orthologs of all three of the human CCM genes, and genetic and experimental studies have suggested that all three function together, as in humans. Mutations in some of the CCM genes and genes encoding proteins that function in the CCM complex were identified in a large-scale chemical mutagenesis screens conducted to isolate cardiovascular mutants (Stainier *et al.*, 1996). The *santa*, *valentine*, and *heart of glass* (*heg*) mutants were first identified as recessive lethal mutants exhibiting similar dilated heart phenotypes (Mably *et al.*, 2003, 2006). Zebrafish embryos homozygous for *santa* or *valentine* mutations have highly enlarged heart chambers with thin, monolayered myocardium lining the (endothelial) endocardium (Fig. 5). Although the myocardium does not thicken, it does contain the proper number of cells. Positional cloning of *santa* and *valentine* identified mutations in zebrafish *ccm1* (*krit1*) and *ccm2*, respectively, with both genes showing expression in both endothelium and other tissues (Mably *et al.*, 2006). Analysis of independently isolated mutants in zebrafish

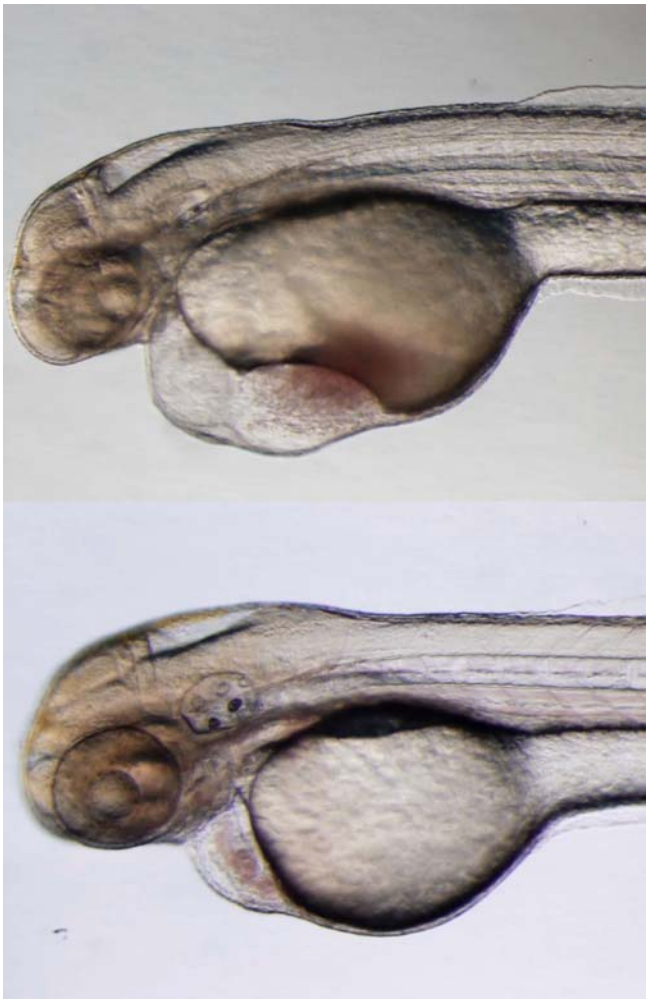

Fig. 5 Enlarged heart phenotype in *santa* mutant zebrafish. Transmitted light images of a 24 hpf *santa* mutant zebrafish (top) showing a highly enlarged heart compared to one of its 24 hpf wild-type siblings (bottom).

ccm1 and *ccm2* by another group showed that in addition to heart dilation, both mutants exhibit defects in vascular morphogenesis with progressively enlarged and dilated blood vessels, although vascular patterning is reasonably normal and endothelial junctions are noted on ultrastructural analysis (Hogan *et al.*, 2008). As for mutant myocardium and endocardium, the number of ECs in vessels is not increased, and markers of arterial–venous identity indicate normal differentiation. Blastomere transplantation experiments with *ccm1* mutants suggest that ccm1

function is required cell-autonomously in the endothelium for proper vascular morphogenesis (Hogan *et al.*, 2008). Although lumenization occurs in primary vasculogenic vessels such as the dorsal aorta and cardinal vein, a recent study using morpholinos to knock down ccm1 in the zebrafish suggests that lumen formation in the angiogenic microvasculature is defective, with impaired intraendothelial vacuole formation and fusion (Liu *et al.*, 2011). However, it is not clear whether these later defects in the microvasculature might be secondary to disruption of circulatory flow.

In addition to orthologous *ccm1* and *ccm2* genes, zebrafish possess two duplicate orthologs of human *CCM3*, *ccm3a* and *ccm3b*, and several recent reports have also examined the roles of the proteins encoded by these genes and their functional interactions with other CCM complex proteins (Voss *et al.*, 2009; Zheng *et al.*, 2010). Although individual knockdown of either *ccm3a* or *ccm3b* does not cause a phenotype, simultaneous inactivation of both *ccm3* genes by morpholino knockdown results in a cardiovascular phenotype indistinguishable from that of *ccm1* or *ccm2* mutants. These phenotypes are also recapitulated by expression of mutant forms of the protein known to cause CCMs in human patients that lack domains for interaction with downstream effector proteins, as discussed further below (Zheng *et al.*, 2010). The cardiovascular dilations are also reproduced by morpholino-induced in-frame skipping of the exon encoding this same interaction domain in *ccm3a* if *ccm3b* is repressed in parallel (Voss *et al.*, 2009). Together, the conserved primary structure and symmetrical functions in vascular morphogenesis and lumenization suggest that the zebrafish *ccm* genes act together to carry out similar functional roles to their mammalian counterparts. Thus, the zebrafish provides a highly useful experimental animal model for dissection of the functional defects present in human CCM disorders.

In addition to studying the functions of the three CCM disease genes, the zebrafish has proven useful for uncovering interactions between the CCM gene products and additional proteins, and/or dissecting the functional roles of some of these interacting partners. Zebrafish genetic screens have identified novel CCM interacting proteins. Like the *santa* and *valentine* mutants, *heg* mutants display highly enlarged hearts with a thin, single-cell-layered myocardium (Mably *et al.*, 2003). Positional cloning of *heg* revealed a defect in a novel gene encoding a protein of previously unknown function. The *heg* gene is expressed in the endocardium but not in myocardial cells, showing that it plays a nonautonomous role in morphogenesis of the myocardium. Three distinct isoforms of *heg* are generated by alternative splicing, one of which is predicted to be transmembrane and the other two secreted. The transmembrane isoform was found to be functionally important by selectively knocking down this isoform using splice-blocking morpholinos. Although humans have an orthologous *HEG* gene, mutations in human *HEG* have not been found in any hereditary or sporadic case of CCM, unlike the *CCM* genes. However, combinatorial low-dose morpholino knockdown of *heg* synergizes strongly with either *ccm1* or *ccm2* to phenocopy the dilated heart phenotype in zebrafish, suggesting that their gene products interact (Mably *et al.*, 2006). Indeed, mammalian *HEG* was recently

shown to physically interact with *CCM1* in cultured cells (Kleaveland *et al.*, 2009), and *Heg1*$^{-/-}$ mice display defective integrity of the heart, blood vessels, and lymphatic vessels, with more severe failure of proper vascular assembly seen in combination with *Ccm2*$^{lacZ/+}$ or *Ccm2*$^{lacZ/lacZ}$. Mice lacking Heg1 also show defects in EC junction formation similar to those observed in human CCMs (Kleaveland *et al.*, 2009). Thus, zebrafish mutagenesis studies led to the identification of a previously unknown member of the mammalian CCM complex.

The question of whether lesion formation in CCM disorders reflects a requirement for CCM gene function in endothelium, neural tissue, or both has recently been examined in both zebrafish and mice, with clear evidence that the endothelial and not neural function is critical in the pathobiology of CCM. As discussed earlier, the CCM genes and HEG are all expressed in both vascular and neural tissues, and the strong neural expression led to the idea that the brain vascular defects in CCM were secondary to primary defects in the neural parenchyma (Plummer *et al.*, 2006). However, blastomere transplantation shows that wild-type ECs can adopt a "wild-type" morphology when they integrated into vessels in *ccm1* mutant animals, indicating that ccm1 is required cell-autonomously for regulation of EC shape (Hogan *et al.*, 2008). Furthermore, EC-autonomous expression of CCM1 interacting proteins rap1b or pak2a rescues the cranial vascular hemorrhage caused by antisense morpholino-mediated knockdown of each of these genes (Buchner *et al.*, 2007; Gore *et al.*, 2008). Recent work in the mouse has provided what is probably the most conclusive evidence to date that the primary defects in CCM are endothelial-specific (Boulday *et al.*, 2009). Ubiquitous, endothelial-, or neural-specific *Ccm2* knockout mice were generated using cre-lox technology and examined for homozygous phenotypes. Mice homozygous for a ubiquitous deletion of *Ccm2* die during early embryogenesis, like *Ccm1* knockouts. However, despite the high level of expression of this gene in the neuroepithelium, targeting of *Ccm2* in neuroglial precursor cells does not lead to cerebrovascular defects. In contrast, endothelial-specific knockout of *Ccm2* severely affects angiogenesis and leads to major heart and arterial and venous morphogenesis defects and embryonic lethality at midgestation. Thus, while further analysis will be required to verify a specific functional requirement for the other CCM genes in endothelium versus neuroepithelium, it appears that the proximal defect in CCM is probably initiated within the endothelium.

Zebrafish has been useful for studying the interactions between CCM proteins and other interacting partners. Several recent studies have examined the signaling pathways downstream from *ccm3* in the zebrafish (Voss *et al.*, 2009; Zheng *et al.*, 2010). Ccm3 contains a domain for interaction with serine/threonine protein kinase MST4, sterile 20-like serine/threonine kinase 24 (STK24), and STK25, and deletion of this domain in human CCM3 is known to cause CCM in humans. Expression of ccm3 proteins lacking this interaction domain in the zebrafish results in similar cardiovascular defects to loss-of-CCM phenotypes. Morpholino knockdown of some of these STKs, or STKs and *ccm3* together, also causes analogous cardiovascular defects. Low-dose morpholino-mediated knockdown of *stk24*, *stk25a*, and *stk25b* together produced the dilated heart phenotype (Zheng *et al.*, 2010). CCM3 and

STK25 regulate barrier function in ECs *in vitro* in a manner similar to CCM2, with STKs negatively regulating Rho by directly activating moesin (Zheng *et al.*, 2010). These studies identify STKs as essential downstream effectors of CCM signaling in development and disease that may regulate both endothelial and epithelial cell junctions.

As described above, the hemorrhage phenotypes in *bbh* (Liu *et al.*, 2007) and *rdh* (Buchner *et al.*, 2007) mutants result from defects in *beta-pix* and *pak2a*, respectively, and some previous evidence suggests that these genes might function together in a complex with the CCM genes (Faurobert and Albiges-Rizo, 2010). The small GTPase Rap1 is also known to bind to CCM1/KRIT1 and facilitate its localization to cell–cell junctions. Recent work has probed the *in vivo* functional interaction between these proteins and provided new insights into the factors influencing the etiology of CCM. As noted above, the incidence of lesion formation is highly variable within affected CCM families, and the factors that trigger ICH in either inherited or sporadic forms of the disease are not understood. Not all individuals harboring defective CCM genes develop ICH, reflecting incomplete penetrance of these mutations and/or involvement of additional genetic modifiers predisposing to lesion formation (Lucas *et al.*, 2003). As also noted above, there is ample evidence that CCM genes act together in common intracellular complexes and/or signaling pathways, suggesting that minor functional perturbations of different genes in these complexes or pathways might act together to predispose to or even precipitate ICH. However, demonstrating this sort of multigene association is not possible in the available small human CCM pedigrees. By injecting morpholinos into zebrafish embryos, the authors of a recent study simultaneously inhibited the expression of multiple CCM pathway genes in various combinations (Gore *et al.*, 2008). Subtle decreases in the expression of each of these genes alone caused little or no effect independently, but when combined this resulted in very high frequencies of ICH. Thus, small, individually silent defects in the CCM pathway can strongly synergize to increase susceptibility to ICH. These findings have important implications. Single heterozygous mutations in CCM proteins may not be enough to induce stroke, but may require accompanying subtle secondary mutations to "trigger" lesion formation. Mutations in CCM pathway effectors may contribute to the highly variable penetrance of familial CCM disorders. Subtle genetic second hits in individuals that are outwardly normal but "sensitized" by minor deficits in CCM pathway genes could also lead to sporadic forms of hemorrhagic stroke.

A variety of other genes and pathways have been shown to modulate vascular integrity in the zebrafish. Several zebrafish studies have shown that microRNAs (miRs), small noncoding RNAs that regulate mRNA turnover, regulate vascular integrity (Fish *et al.*, 2008; Zou *et al.*, 2011). A number of miRs have been identified with vascular-enriched expression in the zebrafish, including miR-126a and miR-126b. Knockdown of either or both of the miR-126 genes causes cranial hemorrhage (Fish *et al.*, 2008; Zou *et al.*, 2011). One study (Fish *et al.*, 2008) showed that miR-126a represses negative regulators of the VEGF pathway, including the Sprouty-related protein SPRED1 and phosphoinositol-3 kinase regulatory subunit 2

(PIK3R2/p85-beta), with increased expression of Spred1 or inhibition of VEGF signaling in zebrafish resulting in defects similar to miR-126a knockdown. A later study (Zou *et al.*, 2011) reported the existence of not one but two highly similar (differing by only a single nucleotide) miR-126 genes in zebrafish and identified p21-activated kinase1 (*pak1*) as a novel target of miR-126a/b, showing that the *pak1* 3′-untranslated region is differentially regulated by the two miR-126 s. Pak1 levels are reduced when miR-126a/b is overexpressed *in vivo*, and *pak1* expression is increased in ECs *in vitro* when miR-126a/b were knocked down. Overexpression of the active form of human pak1 caused cranial hemorrhage in zebrafish, and pak1 morpholino knockdown rescued the hemorrhage caused by inhibiting miR-126a/b, confirming the importance of pak1 downstream from miR-126. Additional studies should help to determine the relative importance and specific functional roles of these and other miR-126 targets in vascular integrity and morphogenesis. EC survival and homeostasis are also important for maintaining proper vascular integrity. Zebrafish genetic screening identified a mutant in *birc2* with severe hemorrhage and vascular regression due to EC integrity defects and apoptosis (Santoro *et al.*, 2007). Birc2 regulates the formation of the TNF receptor complex I in ECs, promoting NF-κB activation and maintaining vessel integrity and stabilization. In the absence of Birc2, a caspase-8-dependent apoptotic program takes place that leads to vessel regression.

As mentioned earlier, the endothelium of arteries and veins is covered by mural cells, which include vascular smooth muscle cells (vSMC) and pericytes. These cells provide physical and trophic support to the endothelium, and, as also noted above, are likewise important for maintaining vascular integrity. Little is known regarding the investment of endothelial tubes with vSMCs and pericytes in the zebrafish model. One study examined the stages of development of the vascular wall of the dorsal aorta, the major trunk artery, in the zebrafish (Miano *et al.*, 2006). Perivascular mural cells are seen in close proximity to the dorsal aorta in 7 dpf free-swimming larval zebrafish, but these cells lack the hallmarks of differentiated vSMC, indicating that the vascular wall of the zebrafish aorta forms somewhat later by comparison to comparable developmental stages of mammals such as the mouse. By 1 month postfertilization, however, a mature aortic wall has formed that closely resembles those found in major arteries of other vertebrates, including EC, vSMC, and adventitial fibroblasts (Miano *et al.*, 2006). Thus, the zebrafish provides a useful model for studying the development of the vascular wall and mural cell investment. Although morphologically obvious smooth muscle differentiation occurs relatively late, molecular evidence of mural cell differentiation can be detected at somewhat earlier stages of development. Expression analysis of vSMC markers commonly used in mammals shows that *transgelin* (*tagln*; aka sm22alpha-b) and *actin alpha 2* (*acta2*) are expressed in presumptive vSMC at 72 and 96 hpf (Santoro *et al.*, 2009). Immunohistochemistry also reveals a small population of *tagln*$^{+}$ vSMC ventral to the rostral bifurcation of the dorsal aorta into paired lateral dorsal aortae in 80 hpf zebrafish larvae (Santoro *et al.*, 2009). The *tagln*$^{+}$ vSMC appear to originate from the lateral plate mesoderm since they are absent in *hands off* mutants (defective

lateral plate mesoderm development), but remain unchanged in *cloche* mutants (devoid of endothelia) (Santoro *et al.*, 2009; Stainier *et al.*, 1995; Yelon *et al.*, 2000). A recently developed *Tg*(*tgln-eGFP*) transgenic line shows GFP expression along the dorsal aorta and weakly in the posterior cardinal vein (Seiler *et al.*, 2010). Unlike the aorta, the posterior cardinal vein is covered by a thin layer of vascular smooth muscle (Santoro *et al.*, 2009).

Identification of mutants that cause ICH has also been useful for uncovering additional genes required for vascular integrity, some of which also functionally interact with the CCM pathway. In addition to their U-shaped somites, zebrafish *iguana* mutants have reduced dorsal aortae and defects in perivascular mural cell recruitment, and develop hemorrhage (Lamont *et al.*, 2010). The causative mutation is in *daz-interacting protein 1* (*dzip1*), a gene encoding a zinc-finger protein involved in modulating hedgehog signaling (Sekimizu *et al.*, 2004; Wolff *et al.*, 2004). Transmission electron microscopy showed a general dysmorphology of the tissue surrounding the endothelium of the lateral dorsal aortae in *iguana* mutants compared to controls (Lamont *et al.*, 2010). Angiopoietin–Tie2 receptor signaling has been shown to be important for stabilization and maturation of blood vessels, and angiopoietin 1 (*angptn1*), previously shown to be induced by hedgehog signaling in cultured fibroblasts, is diminished in the perivascular mesenchyme of *iguana* mutants compared to control siblings (Lamont *et al.*, 2010; Lee *et al.*, 2007; Pola *et al.*, 2001). The vascular integrity defects in iguana mutants appear to be nonautonomous due to loss of *angpt1* expression since they can be rescued by either overexpression of *angpt1* or partial downregulation of the endogenous *angpt1* antagonist *angpt2* (Lamont *et al.*, 2010). Ubiquitous misexpression of *angptn2* also causes cranial hemorrhage in wild-type embryos, confirming the *in vivo* link between hedgehog signaling and the vascular stabilization via angiopoietin-induced perivascular cell recruitment. Recent reports suggest that Dzip function is required for primary cilia formation, since the primary cilia in *igu* mutants fail to form ciliary pits and axonemes (Tay *et al.*, 2010). Published studies have documented primary cilia in ECs from a variety of vertebrates including fish and humans (Collin and Barry Collin, 2004; Egorova *et al.*, 2011; Iomini *et al.*, 2004), but exactly what these primary cilia might be sensing (blood flow?) and how this is important for maintenance of vascular integrity remains to be determined. Surprisingly, unlike mice with targeted disruption of Tie-2, the main receptor tyrosine kinase for *angptn1* (Sato *et al.*, 1995), zebrafish with a truncated *tie2* protein lacking the kinase domain do not display vascular or other phenotypes, although reduction of both Tie-2 and related Tie-1 receptor function causes a cardiac phenotype (Gjini *et al.*, 2011). Paradoxically, *tie2* mutant zebrafish show significantly reduced hemorrhage following treatment with atorvastatin and simvastatin, drugs that cause bleeding in wild-type zebrafish larvae. The protective effect of loss of *tie2* on statin-induced vascular integrity defects contradicts the results of the zebrafish angiopoietin study and other published data suggesting that Tie2 signaling is important for vessel stabilization and maturation. This discrepancy may reflect context-dependent effects of Tie2 signaling in mature versus developing vessels, in pathological contexts, or following drug challenge.

Thrombosis plays an important role in many cases of occlusive and hemorrhagic stroke. The coagulation cascade has a well-documented critical role in hemostasis and maintenance of vascular integrity, and recent reports suggest that the zebrafish may also be a useful model for genetic and experimental dissection and identification of novel genes involved in hemostasis and thrombosis (for recent review, see Jagadeeswaran *et al.*, 2005; Lang *et al.*, 2010). Since comprehensive treatment of zebrafish research work in this area would require a chapter of its own, we will only briefly touch on a few recent findings. Zebrafish have been shown to have functionally analogous thrombocytes and possess the entire coagulation cascade. Importantly, a variety of novel methods and tools have been brought to bear on the study of thrombosis in the zebrafish. Taking advantage of the optical clarity of the fish embryo, a laser can be used to induce thrombosis in a specifically targeted area of the zebrafish vasculature, permitting rapid screening for fish with abnormal hemostasis due to experimental manipulation or genetic mutation (Jagadeeswaran *et al.*, 2006). Also taking advantage of the favorable optical properties of the fish, a number of transgenic lines have been isolated that permit direct visualization of thrombocyte development, aggregation, and thrombosis in real time in living animals (Jagadeeswaran *et al.*, 2010; Lin *et al.*, 2005). These and other features make the fish a very valuable model for studying thrombosis. Zebrafish genetic and knockdown studies have already permitted the identification and/or functional validation of a number of factors important for thrombocyte development and function and thrombosis, including Mlck1a (Tournoij *et al.*, 2010), Fli1 (Jagadeeswaran *et al.*, 2010), LRRFIP1 (Goodall *et al.*, 2010), vWF (Carrillo *et al.*, 2010), BAMBI, LRRC32, DCBLD2, and ESAM (O'Connor *et al.*, 2009).

VI. Concluding Remarks

ICH is a complex, heterogeneous phenotype involving significant hereditary and environmental risk factors. The consequences of ICH are often a debilitating stroke or death; therefore, a detailed understanding of these risk factors is essential. The hereditary components contributing to hemorrhagic stroke are only beginning to be elucidated in various model organisms. In this chapter, we have highlighted the experimental advantages of the zebrafish for experimental and genetic analysis of the factors underlying ICH and stroke, and some recent research findings resulting from the use of this model organism. Genetic screens and morpholino knockdown experiments in the fish have been particularly useful for identifying novel stroke susceptibility genes and studying their functional roles. For example, zebrafish studies have been particularly successful in functional the dissection of the molecular pathways underlying *CCM*. Coupled with the conservation of many of the molecular mechanisms of vascular development among vertebrates, it seems likely that discoveries resulting from work in the zebrafish will ultimately lead to new breakthroughs in the clinic.

References

Adam, A. P., Sharenko, A. L., Pumiglia, K., and Vincent, P. A. (2010). Src-induced tyrosine phosphorylation of VE-cadherin is not sufficient to decrease barrier function of endothelial monolayers. *J. Biol. Chem.* **285**, 7045–7055.

Akers, A. L., Johnson, E., Steinberg, G. K., Zabramski, J. M., and Marchuk, D. A. (2009). Biallelic somatic and germline mutations in cerebral cavernous malformations (CCMs): evidence for a two-hit mechanism of CCM pathogenesis. *Hum. Mol. Genet.* **18**, 919–930.

Bazzoni, G., and Dejana, E. (2004). Endothelial cell-to-cell junctions: molecular organization and role in vascular homeostasis. *Physiol. Rev.* **84**, 869–901.

Bergametti, F., Denier, C., Labauge, P., Arnoult, M., Boetto, S., Clanet, M., Coubes, P., Echenne, B., Ibrahim, R., and Irthum, B., *et al*. (2005). Mutations within the programmed cell death 10 gene cause cerebral cavernous malformations. *Am. J. Hum. Genet.* **76**, 42–51.

Birdsey, G. M., Dryden, N. H., Amsellem, V., Gebhardt, F., Sahnan, K., Haskard, D. O., Dejana, E., Mason, J. C., and Randi, A. M. (2008). Transcription factor Erg regulates angiogenesis and endothelial apoptosis through VE-cadherin. *Blood* **111**, 3498–3506.

Boulday, G., Blecon, A., Petit, N., Chareyre, F., Garcia, L. A., Niwa-Kawakita, M., Giovannini, M., and Tournier-Lasserve, E. (2009). Tissue-specific conditional CCM2 knockout mice establish the essential role of endothelial CCM2 in angiogenesis: implications for human cerebral cavernous malformations. *Dis. Model Mech.* **2**, 168–177.

Breviario, F., Caveda, L., Corada, M., Martin-Padura, I., Navarro, P., Golay, J., Introna, M., Gulino, D., Lampugnani, M. G., and Dejana, E. (1995). Functional properties of human vascular endothelial cadherin (7B4/cadherin-5), an endothelium-specific cadherin. *Arterioscler. Thromb. Vasc. Biol.* **15**, 1229–1239.

Buchner, D. A., Su, F., Yamaoka, J. S., Kamei, M., Shavit, J. A., Barthel, L. K., McGee, B., Amigo, J. D., Kim, S., and Hanosh, A. W., *et al*. (2007). pak2a mutations cause cerebral hemorrhage in redhead zebrafish. *Proc. Natl. Acad. Sci. U. S. A.* **104**, 13996–14001.

Carrillo, M., Kim, S., Rajpurohit, S. K., Kulkarni, V., and Jagadeeswaran, P. (2010). Zebrafish von Willebrand factor. *Blood Cells Mol. Dis.* **45**, 326–333.

Chen, J. N., Haffter, P., Odenthal, J., Vogelsang, E., Brand, M., van Eeden, F. J., Furutani-Seiki, M., Granato, M., Hammerschmidt, M., and Heisenberg, C. P., *et al*. (1996). Mutations affecting the cardiovascular system and other internal organs in zebrafish. *Development* **123**, 293–302.

Clatterbuck, R. E., Eberhart, C. G., Crain, B. J., and Rigamonti, D. (2001). Ultrastructural and immunocytochemical evidence that an incompetent blood–brain barrier is related to the pathophysiology of cavernous malformations. *J. Neurol. Neurosurg. Psychiatry* **71**, 188–192.

Collin, S. P., and Barry Collin, H. (2004). Primary cilia in vertebrate corneal endothelial cells. *Cell Biol. Int.* **28**, 125–130.

Cowan, C. E., Kohler, E. E., Dugan, T. A., Mirza, M. K., Malik, A. B., and Wary, K. K. (2010). Kruppel-like factor-4 transcriptionally regulates VE-cadherin expression and endothelial barrier function. *Circ. Res.* **107**, 959–966.

Dejana, E. (2004). Endothelial cell–cell junctions: happy together. *Nat. Rev. Mol. Cell Biol.* **5**, 261–270.

Dejana, E., Orsenigo, F., and Lampugnani, M. G. (2008). The role of adherens junctions and VE-cadherin in the control of vascular permeability. *J. Cell Sci.* **121**, 2115–2122.

Dejana, E., Tournier-Lasserve, E., and Weinstein, B. M. (2009). The control of vascular integrity by endothelial cell junctions: molecular basis and pathological implications. *Dev. Cell* **16**, 209–221.

Deleuze, V., Chalhoub, E., El-Hajj, R., Dohet, C., Le Clech, M., Couraud, P. O., Huber, P., and Mathieu, D. (2007). TAL-1/SCL and its partners E47 and LMO2 up-regulate VE-cadherin expression in endothelial cells. *Mol. Cell. Biol.* **27**, 2687–2697.

Denier, C., Goutagny, S., Labauge, P., Krivosic, V., Arnoult, M., Cousin, A., Benabid, A. L., Comoy, J., Frerebeau, P., and Gilbert, B., *et al*. (2004). Mutations within the MGC4607 gene cause cerebral cavernous malformations. *Am. J. Hum. Genet.* **74**, 326–337.

Denier, C., Labauge, P., Bergametti, F., Marchelli, F., Riant, F., Arnoult, M., Maciazek, J., Vicaut, E., Brunereau, L., and Tournier-Lasserve, E. (2006). Genotype–phenotype correlations in cerebral cavernous malformations patients. *Ann. Neurol.* **60**, 550–556.

Dvorak, A. M., Kohn, S., Morgan, E. S., Fox, P., Nagy, J. A., and Dvorak, H. F. (1996). The vesiculo-vacuolar organelle (VVO): a distinct endothelial cell structure that provides a transcellular pathway for macromolecular extravasation. *J. Leukoc. Biol.* **59**, 100–115.

Egorova, A. D., Khedoe, P. P., Goumans, M. J., Yoder, B. K., Nauli, S. M., Ten Dijke, P., Poelmann, R. E., and Hierck, B. P. (2011). Lack of primary cilia primes shear-induced endothelial-to-mesenchymal transition. *Circ. Res.* **108**, 1093–1101.

Engelhardt, B. (2003). Development of the blood–brain barrier. *Cell Tissue Res.* **314**, 119–129.

Faurobert, E., and Albiges-Rizo, C. (2010). Recent insights into cerebral cavernous malformations: a complex jigsaw puzzle under construction. *FEBS J.* **277**, 1084–1096.

Fish, J. E., Santoro, M. M., Morton, S. U., Yu, S., Yeh, R. F., Wythe, J. D., Ivey, K. N., Bruneau, B. G., Stainier, D. Y., and Srivastava, D. (2008). miR-126 regulates angiogenic signaling and vascular integrity. *Dev. Cell* **15**, 272–284.

Furuse, M., Hirase, T., Itoh, M., Nagafuchi, A., Yonemura, S., Tsukita, S., and Tsukita, S. (1993). Occludin: a novel integral membrane protein localizing at tight junctions. *J. Cell Biol.* **123**, 1777–1788.

Gault, J., Awad, I. A., Recksiek, P., Shenkar, R., Breeze, R., Handler, M., and Kleinschmidt-DeMasters, B. K. (2009). Cerebral cavernous malformations: somatic mutations in vascular endothelial cells. *Neurosurgery* **65**, 138–144 discussion 138-145.

Gault, J., Shenkar, R., Recksiek, P., and Awad, I. A. (2005). Biallelic somatic and germ line CCM1 truncating mutations in a cerebral cavernous malformation lesion. *Stroke* **36**, 872–874.

Gavard, J., and Gutkind, J. S. (2006). VEGF controls endothelial-cell permeability by promoting the beta-arrestin-dependent endocytosis of VE-cadherin. *Nat. Cell Biol.* **8**, 1223–1234.

Gjini, E., Hekking, L. H., Kuchler, A., Saharinen, P., Wienholds, E., Post, J. A., Alitalo, K., and Schulte-Merker, S. (2011). Zebrafish Tie-2 shares a redundant role with Tie-1 in heart development and regulates vessel integrity. *Dis. Model Mech.* **4**, 57–66.

Gonzalez-Mariscal, L., Betanzos, A., and Avila-Flores, A. (2000). MAGUK proteins: structure and role in the tight junction. *Semin. Cell Dev. Biol.* **11**, 315–324.

Gonzalez-Mariscal, L., Tapia, R., and Chamorro, D. (2008). Crosstalk of tight junction components with signaling pathways. *Biochim. Biophys. Acta* **1778**, 729–756.

Goodall, A. H., Burns, P., Salles, I., Macaulay, I. C., Jones, C. I., Ardissino, D., de Bono, B., Bray, S. L., Deckmyn, H., and Dudbridge, F., *et al*. (2010). Transcription profiling in human platelets reveals LRRFIP1 as a novel protein regulating platelet function. *Blood* **116**, 4646–4656.

Gore, A. V., Lampugnani, M. G., Dye, L., Dejana, E., and Weinstein, B. M. (2008). Combinatorial interaction between CCM pathway genes precipitates hemorrhagic stroke. *Dis. Model Mech.* **1**, 275–281.

Gulati-Leekha, A., and Goldman, D. (2006). A reporter-assisted mutagenesis screen using alpha 1-tubulin-GFP transgenic zebrafish uncovers missteps during neuronal development and axonogenesis. *Dev. Biol.* **296**, 29–47.

Ha, C. H., Bennett, A. M., and Jin, Z. G. (2008). A novel role of vascular endothelial cadherin in modulating c-Src activation and downstream signaling of vascular endothelial growth factor. *J. Biol. Chem.* **283**, 7261–7270.

Hogan, B. M., Bussmann, J., Wolburg, H., and Schulte-Merker, S. (2008). ccm1 cell autonomously regulates endothelial cellular morphogenesis and vascular tubulogenesis in zebrafish. *Hum. Mol. Genet.* **17**, 2424–2432.

Iomini, C., Tejada, K., Mo, W., Vaananen, H., and Piperno, G. (2004). Primary cilia of human endothelial cells disassemble under laminar shear stress. *J. Cell Biol.* **164**, 811–817.

Jagadeeswaran, P., Gregory, M., Day, K., Cykowski, M., and Thattaliyath, B. (2005). Zebrafish: a genetic model for hemostasis and thrombosis. *J. Thromb. Haemost.* **3**, 46–53.

Jagadeeswaran, P., Lin, S., Weinstein, B., Hutson, A., and Kim, S. (2010). Loss of GATA1 and gain of FLI1 expression during thrombocyte maturation. *Blood Cells Mol. Dis.* **44**, 175–180.

Jagadeeswaran, P., Paris, R., and Rao, P. (2006). Laser-induced thrombosis in zebrafish larvae: a novel genetic screening method for thrombosis. *Methods Mol. Med.* **129**, 187–195.

Kleaveland, B., Zheng, X., Liu, J. J., Blum, Y., Tung, J. J., Zou, Z., Sweeney, S. M., Chen, M., Guo, L., and Lu, M. M., *et al*. (2009). Regulation of cardiovascular development and integrity by the heart of glass-cerebral cavernous malformation protein pathway. *Nat. Med.* **15**, 169–176.

Komarova, Y., and Malik, A. B. (2010). Regulation of endothelial permeability via paracellular and transcellular transport pathways. *Annu. Rev. Physiol.* **72**, 463–493.

Laberge-le Couteulx, S., Jung, H. H., Labauge, P., Houtteville, J. P., Lescoat, C., Cecillon, M., Marechal, E., Joutel, A., Bach, J. F., and Tournier-Lasserve, E. (1999). Truncating mutations in CCM1, encoding KRIT1, cause hereditary cavernous angiomas. *Nat. Genet.* **23**, 189–193.

Lamont, R. E., Vu, W., Carter, A. D., Serluca, F. C., MacRae, C. A., and Childs, S. J. (2010). Hedgehog signaling via angiopoietin1 is required for developmental vascular stability. *Mech. Dev.* **127**, 159–168.

Lampugnani, M. G., Corada, M., Caveda, L., Breviario, F., Ayalon, O., Geiger, B., and Dejana, E. (1995). The molecular organization of endothelial cell to cell junctions: differential association of plakoglobin, beta-catenin, and alpha-catenin with vascular endothelial cadherin (VE-cadherin). *J. Cell Biol.* **129**, 203–217.

Lampugnani, M. G., Orsenigo, F., Gagliani, M. C., Tacchetti, C., and Dejana, E. (2006). Vascular endothelial cadherin controls VEGFR-2 internalization and signaling from intracellular compartments. *J. Cell Biol.* **174**, 593–604.

Lang, M. R., Gihr, G., Gawaz, M. P., and Muller, I. I. (2010). Hemostasis in *Danio rerio*: is the zebrafish a useful model for platelet research? *J. Thromb. Haemost.* **8**, 1159–1169.

Lee, S. W., Moskowitz, M. A., and Sims, J. R. (2007). Sonic hedgehog inversely regulates the expression of angiopoietin-1 and angiopoietin-2 in fibroblasts. *Int. J. Mol. Med.* **19**, 445–451.

Leys, D., Deplanque, D., Mounier-Vehier, C., Mackowiak-Cordoliani, M. A., Lucas, C., and Bordet, R. (2002). Stroke prevention: management of modifiable vascular risk factors. *J. Neurol.* **249**, 507–517.

Lin, H. F., Traver, D., Zhu, H., Dooley, K., Paw, B. H., Zon, L. I., and Handin, R. I. (2005). Analysis of thrombocyte development in CD41-GFP transgenic zebrafish. *Blood* **106**, 3803–3810.

Liquori, C. L., Berg, M. J., Siegel, A. M., Huang, E., Zawistowski, J. S., Stoffer, T., Verlaan, D., Balogun, F., Hughes, L., and Leedom, T. P., *et al*. (2003). Mutations in a gene encoding a novel protein containing a phosphotyrosine-binding domain cause type 2 cerebral cavernous malformations. *Am. J. Hum. Genet.* **73**, 1459–1464.

Liu, J., Fraser, S. D., Faloon, P. W., Rollins, E. L., Vom Berg, J., Starovic-Subota, O., Laliberte, A. L., Chen, J. N., Serluca, F. C., and Childs, S. J. (2007). A betaPix Pak2a signaling pathway regulates cerebral vascular stability in zebrafish. *Proc. Natl. Acad. Sci. U. S. A.* **104**, 13990–13995.

Liu, H., Rigamonti, D., Badr, A., and Zhang, J. (2011). Ccm1 regulates microvascular morphogenesis during angiogenesis. *J. Vasc. Res.* **48**, 130–140.

Lucas, M., Costa, A. F., Garcia-Moreno, J. M., Solano, F., Gamero, M. A., and Izquierdo, G. (2003). Variable expression of cerebral cavernous malformations in carriers of a premature termination codon in exon 17 of the Krit1 gene. *BMC Neurol.* **3**, 5.

Mably, J. D., Chuang, L. P., Serluca, F. C., Mohideen, M. A., Chen, J. N., and Fishman, M. C. (2006). santa and valentine pattern concentric growth of cardiac myocardium in the zebrafish. *Development* **133**, 3139–3146.

Mably, J. D., Mohideen, M. A., Burns, C. G., Chen, J. N., and Fishman, M. C. (2003). Heart of glass regulates the concentric growth of the heart in zebrafish. *Curr. Biol.* **13**, 2138–2147.

Miano, J. M., Georger, M. A., Rich, A., and De Mesy Bentley, K. L. (2006). Ultrastructure of zebrafish dorsal aortic cells. *Zebrafish* **3**, 455–463.

Mitchell, I. C., Brown, T. S., Terada, L. S., Amatruda, J. F., and Nwariaku, F. E. (2010). Effect of vascular cadherin knockdown on zebrafish vasculature during development. *PloS One* **5**, e8807.

Montero-Balaguer, M., Swirsding, K., Orsenigo, F., Cotelli, F., Mione, M., and Dejana, E. (2009). Stable vascular connections and remodeling require full expression of VE-cadherin in zebrafish embryos. *PloS One* **4**, e5772.

Morita, K., Sasaki, H., Furuse, M., and Tsukita, S. (1999). Endothelial claudin: claudin-5/TMVCF constitutes tight junction strands in endothelial cells. *J. Cell Biol.* **147**, 185–194.

Nitta, T., Hata, M., Gotoh, S., Seo, Y., Sasaki, H., Hashimoto, N., Furuse, M., and Tsukita, S. (2003). Size-selective loosening of the blood–brain barrier in claudin-5-deficient mice. *J. Cell Biol.* **161**, 653–660.

Nottebaum, A. F., Cagna, G., Winderlich, M., Gamp, A. C., Linnepe, R., Polaschegg, C., Filippova, K., Lyck, R., Engelhardt, B., and Kamenyeva, O., *et al*. (2008). VE-PTP maintains the endothelial barrier via plakoglobin and becomes dissociated from VE-cadherin by leukocytes and by VEGF. *J. Exp. Med.* **205**, 2929–2945.

O'Connor, M. N., Salles, I. I., Cvejic, A., Watkins, N. A., Walker, A., Garner, S. F., Jones, C. I., Macaulay, I. C., Steward, M., and Zwaginga, J. J., *et al*. (2009). Functional genomics in zebrafish permits rapid characterization of novel platelet membrane proteins. *Blood* **113**, 4754–4762.

Otten, P., Pizzolato, G. P., Rilliet, B., and Berney, J. (1989). 131 cases of cavernous angioma (cavernomas) of the CNS, discovered by retrospective analysis of 24,535 autopsies. *Neurochirurgie* **35**, 82–83 128-131.

Pagenstecher, A., Stahl, S., Sure, U., and Felbor, U. (2009). A two-hit mechanism causes cerebral cavernous malformations: complete inactivation of CCM1, CCM2 or CCM3 in affected endothelial cells. *Hum. Mol. Genet.* **18**, 911–918.

Patton, E. E., and Zon, L. I. (2001). The art and design of genetic screens: zebrafish. *Nat. Rev. Genet.* **2**, 956–966.

Peal, D. S., Peterson, R. T., and Milan, D. (2010). Small molecule screening in zebrafish. *J. Cardiovasc. Transl. Res.* **3**, 454–460.

Petit, N., Blecon, A., Denier, C., and Tournier-Lasserve, E. (2006). Patterns of expression of the three cerebral cavernous malformation (CCM) genes during embryonic and postnatal brain development. *Gene Expr. Patterns* **6**, 495–503.

Plummer, N. W., Squire, T. L., Srinivasan, S., Huang, E., Zawistowski, J. S., Matsunami, H., Hale, L. P., and Marchuk, D. A. (2006). Neuronal expression of the Ccm2 gene in a new mouse model of cerebral cavernous malformations. *Mamm. Genome* **17**, 119–128.

Pola, R., Ling, L. E., Silver, M., Corbley, M. J., Kearney, M., Blake Pepinsky, R., Shapiro, R., Taylor, F. R., Baker, D. P., and Asahara, T., *et al*. (2001). The morphogen Sonic hedgehog is an indirect angiogenic agent upregulating two families of angiogenic growth factors. *Nat. Med.* **7**, 706–711.

Potter, M. D., Barbero, S., and Cheresh, D. A. (2005). Tyrosine phosphorylation of VE-cadherin prevents binding of p120- and beta-catenin and maintains the cellular mesenchymal state. *J. Biol. Chem.* **280**, 31906–31912.

Qureshi, A. I., Tuhrim, S., Broderick, J. P., Batjer, H. H., Hondo, H., and Hanley, D. F. (2001). Spontaneous intracerebral hemorrhage. *N. Engl. J. Med.* **344**, 1450–1460.

Riant, F., Bergametti, F., Ayrignac, X., Boulday, G., and Tournier-Lasserve, E. (2010). Recent insights into cerebral cavernous malformations: the molecular genetics of CCM. *FEBS J.* **277**, 1070–1075.

Robinson, J. R., Awad, I. A., and Little, J. R. (1991). Natural history of the cavernous angioma. *J. Neurosurg.* **75**, 709–714.

Sahoo, T., Johnson, E. W., Thomas, J. W., Kuehl, P. M., Jones, T. L., Dokken, C. G., Touchman, J. W., Gallione, C. J., Lee-Lin, S. Q., and Kosofsky, B., *et al*. (1999). Mutations in the gene encoding KRIT1, a Krev-1/rap1a binding protein, cause cerebral cavernous malformations (CCM1). *Hum. Mol. Genet.* **8**, 2325–2333.

Santoro, M. M., Pesce, G., and Stainier, D. Y. (2009). Characterization of vascular mural cells during zebrafish development. *Mech. Dev.* **126**, 638–649.

Santoro, M. M., Samuel, T., Mitchell, T., Reed, J. C., and Stainier, D. Y. (2007). Birc2 (cIap1) regulates endothelial cell integrity and blood vessel homeostasis. *Nat. Genet.* **39**, 1397–1402.

Sato, T. N., Tozawa, Y., Deutsch, U., Wolburg-Buchholz, K., Fujiwara, Y., Gendron-Maguire, M., Gridley, T., Wolburg, H., Risau, W., and Qin, Y. (1995). Distinct roles of the receptor tyrosine kinases Tie-1 and Tie-2 in blood vessel formation. *Nature* **376**, 70–74.

Schulz, B., Pruessmeyer, J., Maretzky, T., Ludwig, A., Blobel, C. P., Saftig, P., and Reiss, K. (2008). ADAM10 regulates endothelial permeability and T-cell transmigration by proteolysis of vascular endothelial cadherin. *Circ. Res.* **102**, 1192–1201.

Seiler, C., Abrams, J., and Pack, M. (2010). Characterization of zebrafish intestinal smooth muscle development using a novel sm22alpha-b promoter. *Dev. Dyn.* **239**, 2806–2812.

Sekimizu, K., Nishioka, N., Sasaki, H., Takeda, H., Karlstrom, R. O., and Kawakami, A. (2004). The zebrafish iguana locus encodes Dzip1, a novel zinc-finger protein required for proper regulation of Hedgehog signaling. *Development* **131**, 2521–2532.

Shi, C., Shenkar, R., Du, H., Duckworth, E., Raja, H., Batjer, H. H., and Awad, I. A. (2009). Immune response in human cerebral cavernous malformations. *Stroke* **40**, 1659–1665.

Simionescu, M., Popov, D., and Sima, A. (2009). Endothelial transcytosis in health and disease. *Cell Tissue Res.* **335**, 27–40.

Stahl, S., Gaetzner, S., Voss, K., Brackertz, B., Schleider, E., Surucu, O., Kunze, E., Netzer, C., Korenke, C., and Finckh, U., *et al*. (2008). Novel CCM1, CCM2, and CCM3 mutations in patients with cerebral cavernous malformations: in-frame deletion in CCM2 prevents formation of a CCM1/CCM2/CCM3 protein complex. *Hum. Mutat.* **29**, 709–717.

Stainier, D. Y., Fouquet, B., Chen, J. N., Warren, K. S., Weinstein, B. M., Meiler, S. E., Mohideen, M. A., Neuhauss, S. C., Solnica-Krezel, L., and Schier, A. F., *et al*. (1996). Mutations affecting the formation and function of the cardiovascular system in the zebrafish embryo. *Development* **123**, 285–292.

Stainier, D. Y., Weinstein, B. M., Detrich 3rd, H. W., Zon, L. I., and Fishman, M. C. (1995). Cloche, an early acting zebrafish gene, is required by both the endothelial and hematopoietic lineages. *Development* **121**, 3141–3150.

Strilic, B., Kucera, T., and Lammert, E. (2010). Formation of cardiovascular tubes in invertebrates and vertebrates. *Cell. Mol. Life Sci.* **67**, 3209–3218.

Tanriover, G., Boylan, A. J., Diluna, M. L., Pricola, K. L., Louvi, A., and Gunel, M. (2008). PDCD10, the gene mutated in cerebral cavernous malformation 3, is expressed in the neurovascular unit. *Neurosurgery* **62**, 930–938 discussion 938.

Tay, S. Y., Yu, X., Wong, K. N., Panse, P., Ng, C. P., and Roy, S. (2010). The iguana/DZIP1 protein is a novel component of the ciliogenic pathway essential for axonemal biogenesis. *Dev. Dyn.* **239**, 527–534.

Tournoij, E., Weber, G. J., Akkerman, J. W., de Groot, P. G., Zon, L. I., Moll, F. L., and Schulte-Merker, S. (2010). Mlck1a is expressed in zebrafish thrombocytes and is an essential component of thrombus formation. *J. Thromb. Haemost.* **8**, 588–595.

Voss, K., Stahl, S., Hogan, B. M., Reinders, J., Schleider, E., Schulte-Merker, S., and Felbor, U. (2009). Functional analyses of human and zebrafish 18-amino acid in-frame deletion pave the way for domain mapping of the cerebral cavernous malformation 3 protein. *Hum. Mutat.* **30**, 1003–1011.

Voss, K., Stahl, S., Schleider, E., Ullrich, S., Nickel, J., Mueller, T. D., and Felbor, U. (2007). CCM3 interacts with CCM2 indicating common pathogenesis for cerebral cavernous malformations. *Neurogenetics* **8**, 249–256.

Wallez, Y., and Huber, P. (2008). Endothelial adherens and tight junctions in vascular homeostasis, inflammation and angiogenesis. *Biochim. Biophys. Acta* **1778**, 794–809.

Weber, C., Fraemohs, L., and Dejana, E. (2007). The role of junctional adhesion molecules in vascular inflammation. *Nat. Rev.* **7**, 467–477.

Wegmann, F., Petri, B., Khandoga, A. G., Moser, C., Khandoga, A., Volkery, S., Li, H., Nasdala, I., Brandau, O., and Fassler, R., *et al*. (2006). ESAM supports neutrophil extravasation, activation of Rho, and VEGF-induced vascular permeability. *J. Exp. Med.* **203**, 1671–1677.

Weinstein, B. M., Stemple, D. L., Driever, W., and Fishman, M. C. (1995). Gridlock, a localized heritable vascular patterning defect in the zebrafish. *Nat. Med.* **1**, 1143–1147.

Wolff, C., Roy, S., Lewis, K. E., Schauerte, H., Joerg-Rauch, G., Kirn, A., Weiler, C., Geisler, R., Haffter, P., and Ingham, P. W. (2004). iguana encodes a novel zinc-finger protein with coiled-coil domains essential for Hedgehog signal transduction in the zebrafish embryo. *Genes Dev.* **18**, 1565–1576.

Yelon, D., Ticho, B., Halpern, M. E., Ruvinsky, I., Ho, R. K., Silver, L. M., and Stainier, D. Y. (2000). The bHLH transcription factor hand2 plays parallel roles in zebrafish heart and pectoral fin development. *Development* **127**, 2573–2582.

Zawistowski, J. S., Stalheim, L., Uhlik, M. T., Abell, A. N., Ancrile, B. B., Johnson, G. L., and Marchuk, D. A. (2005). CCM1 and CCM2 protein interactions in cell signaling: implications for cerebral cavernous malformations pathogenesis. *Hum. Mol. Genet.* **14**, 2521–2531.

Zhang, J., Rigamonti, D., Dietz, H. C., and Clatterbuck, R. E. (2007). Interaction between krit1 and malcavernin: implications for the pathogenesis of cerebral cavernous malformations. *Neurosurgery* **60**, 353–359 discussion 359.

Zheng, X., Xu, C., Di Lorenzo, A., Kleaveland, B., Zou, Z., Seiler, C., Chen, M., Cheng, L., Xiao, J., and He, J., *et al*. (2010). CCM3 signaling through sterile 20-like kinases plays an essential role during zebrafish cardiovascular development and cerebral cavernous malformations. *J. Clin. Invest.* **120**, 2795–2804.

Zou, J., Li, W. Q., Li, Q., Li, X. Q., Zhang, J. T., Liu, G. Q., Chen, J., Qiu, X. X., Tian, F. J., and Wang, Z. Z., *et al*. (2011). Two functional microRNA-126s repress a novel target gene p21-activated kinase 1 to regulate vascular integrity in zebrafish. *Circ. Res.* **108**, 201–209.

CHAPTER 7

A Zebrafish Model for VHL and Hypoxia Signaling

Ellen van Rooijen[*,†,¶], Kirankumar Santhakumar[**], Ive Logister[*,†], Emile Voest[*], Stefan Schulte-Merker[†], Rachel Giles[‡] and Fredericus van Eeden[**]

[*]Department of Medical Oncology, University Medical Center, Universiteitsweg 100, Utrecht, The Netherlands

[†]Hubrecht Institute for Developmental Biology and Stem Cell Research, KNAW and University Medical Center Utrecht, Uppsalalaan 8, Utrecht, The Netherlands

[**]MRC-CDBG/BMS, University of Sheffield, Western Bank, Sheffield, United Kingdom

[‡]Department of Nephrology, University Medical Center Utrecht, Universiteitsweg 100, 3584 CG, Utrecht, The Netherlands

[¶]Present address: Children's Hospital Boston and Harvard Medical School, 1 Blackfan Circle, Boston, MA 02115, United States

METHODS IN CELL BIOLOGY, VOL 105

0091-679X/10 $35.00
DOI 10.1016/B978-0-12-381320-6.00007-2

Abstract

The von Hippel–Lindau (*VHL*) tumor suppressor gene encodes an adaptor protein that regulates an array of transcription-dependent and -independent cellular and physiological processes. Mutations in this gene cause VHL disease, congenital polycythemia, and several sporadic tumor types. The last 15 years of fundamental and clinical research have helped define the phenotypic spectrum of VHL-associated diseases and have introduced new cellular functions for pVHL. Here, we review the current knowledge of VHL function, and the different animal models for VHL disease, with a particular focus on the zebrafish. Zebrafish *vhl* mutants develop key aspects of the human disease condition, including activation of the hypoxia-inducible factor (HIF) signaling pathway, polycythemia, excessive neovascularization, macular edema, and pronephric abnormalities. The zebrafish *vhl* model offers a platform for the identification of genetic pathways, modifiers, and interactors involved in the development of VHL-associated neoplasms. *Vhl* mutants represent a unique and clinically relevant *in vivo* model for studying genotype–phenotype correlations and the identification of prognostic biomarkers. The amenability of zebrafish for chemical genetic screens will not only be helpful to identify novel therapeutic agents but may also reveal novel processes that require regulation by VHL.

I. VHL Disease

Humans heterozygous for mutations in the von Hippel–Lindau (VHL) tumor suppressor are at high risk of developing the autosomal dominant syndrome VHL disease, affecting 1 in 36,000 live births (Lonser *et al.*, 2003). Consistent with Knudson's (1971) two-hit hypothesis of tumorigenesis, inactivation of the remaining allele in somatic cells predisposes VHL patients to the development of highly vascularized benign and malignant tumors and cysts (Lonser *et al.*, 2003; Maher *et al.*, 1990, 1991; Van Poppel *et al.*, 2000). The most common cause of morbidity in VHL patients is the development of vascularized hemangioblastomas in the retina and central nervous system (CNS) (Lonser *et al.*, 2003). While hemangioblastomas are rarely malignant, enlargement of these masses within the eye can lead to retinal detachment and vision loss, and neurological damage in the CNS. VHL disease can also induce the development of pancreatic tumors and cysts, epididymal and broad ligament cystadenomas, and renal pheochromocytomas and cysts (Lonser *et al.*, 2003; Maher *et al.*, 1990, 1991; Van Poppel *et al.*, 2000).

Moreover, *VHL* mutations can cause clear cell renal cell carcinoma (ccRCC), the most common type of renal cancer (Kim and Kaelin, 2004). In VHL patients, mortality is mainly due to ccRCC metastases (Van Poppel *et al.*, 2000). Importantly, somatic inactivating *VHL* mutations occur in $\pm$75% of all sporadic ccRCCs (Kaelin, 2007; Kim and Kaelin, 2004; Lonser *et al.*, 2003). It was long thought that ccRCC develops from cells lining premalignant renal tubular cysts;

however, not all cysts develop ccRCC, and not all cases of ccRCC are preceded by cysts (Maher *et al.*, 1990; Mandriota *et al.*, 2002; Walther *et al.*, 1995). While biallelic inactivation of *VHL* is required – as restoration of wild-type pVHL in $VHL^{-/-}$ renal carcinoma cells suppressed their tumorigenicity in nude mice (Iliopoulos *et al.*, 1995) – it is not sufficient for VHL disease progression.

II. Chuvash Polycythemia

Congenital polycythemias are autosomal recessive disorders, often associated with homozygous mutations in *VHL* (Gordeuk *et al.*, 2005). The Chuvash form of polycythemia (CP) results from an Arg200Trp (R200W) substitution at the C-terminus of pVHL, impairing normoxic ubiquitination and degradation of hypoxia-inducible factor (HIF) and resulting in upregulation of its target genes including glucose transporter member 1 (GLUT1), vascular endothelial growth factor (VEGF), and erythropoietin (EPO) (Ang *et al.*, 2002). CP is further characterized by high hemoglobin and hematocrit levels. Patients have abnormalities in respiratory and pulmonary vascular regulation and responses to acute hypoxia are increased (Smith *et al.*, 2006). Premature mortality is observed as a result of cerebral vascular events or peripheral thrombosis (Gordeuk *et al.*, 2004).

CP is distinct from VHL disease, which is associated with heterozygous inactivating germline mutations in *VHL* (Kaelin, 2005). Although patients with VHL disease can develop secondary polycythemias in response to EPO production from their tumors (prevalence of around 5–20%) (Motzer *et al.*, 1996; Richard *et al.*, 2000), CP patients, however, are not predisposed to cancer (Gordeuk *et al.*, 2004).

III. VHL Regulates HIF Signaling

The *VHL* tumor suppressor gene was identified by positional cloning in the 1990s (Latif *et al.*, 1993). *VHL* is located on the short arm of chromosome 3 (3p23–26) (Seizinger *et al.*, 1988), and consists of three exons encoding a 213-amino-acid protein. In humans, two VHL isoforms (collectively named pVHL) exist: a 30-kDa protein (pVHL30) and a 19-kDa protein (pVHL19) that is generated by translation from the second methionine at residue 54 (Iliopoulos *et al.*, 1998; Schoenfeld *et al.*, 1998). However, both suppress tumor formation in nude mice, and regulate hypoxia-inducible factor-α (HIF-α). The best understood function of pVHL is its negative regulation of HIFs (Fig. 1).

The hypoxia-induced transcription factor HIF is a heterodimer composed of a hypoxia-regulated α subunit (HIF-1α, HIF-2α, and HIF-3α) and a stable HIF-1β subunit (Semenza, 2001). Under normoxic conditions, HIF-α is hydroxylated on either of two prolyl residues (Pro402, Pro564) (Jaakkola *et al.*, 2001) by a family of prolyl hydroxylases (PHD1–3) (Bruick and McKnight, 2001; Epstein *et al.*, 2001; Ivan *et al.*, 2001). Hydroxylated HIF-α is targeted for proteasomal degradation via

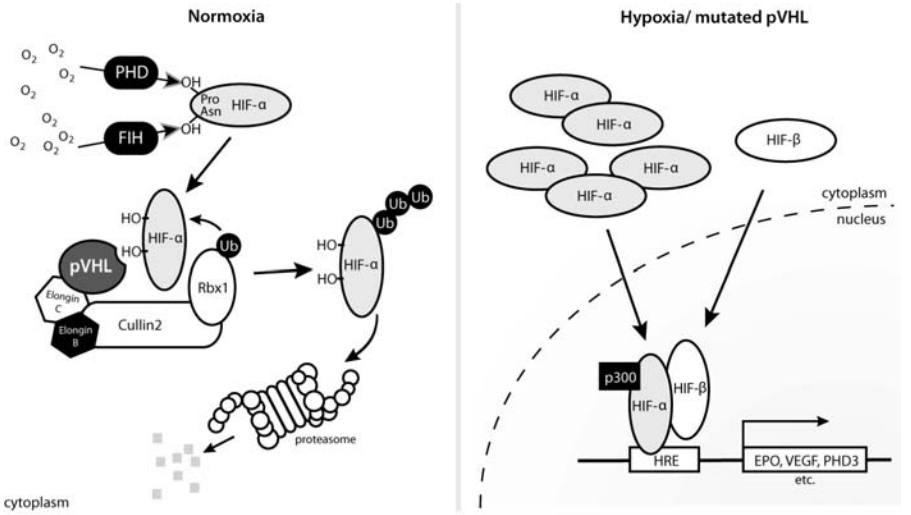

Fig. 1 Schematic representation of hypoxic signaling. Under normoxic conditions, HIF-α is hydroxylated on either of two prolyl residues, and targeted for rapid proteasomal degradation by a multisubunit Skp1/Cullin/F-box protein (SCF)–like E3 ubiquitin ligase complex, containing the von Hippel–Lindau (VHL) protein as substrate recognition component, Elongin B, Elongin C, Ring-box 1 (Rbx1), and Cullin 2 (Cul2). Additionally, HIF-α is hydroxylated on asparagine residue 803 by factor-inhibiting HIF (FIH), which prevents recruitment of the transcriptional coactivators p300/CBP. In the absence of oxygen or functional pVHL, HIF-α protein is stabilized and translocated to the nucleus where it partners with HIF-β to form a functional transcription factor HIF, binding to hypoxia response elements (HRE) and initiating transcription of target genes.

polyubiquitination by an E3 ubiquitin ligase complex, containing pVHL as substrate recognition component, Elongin B (Kibel *et al.*, 1995), Elongin C (Kibel *et al.*, 1995), Ring-box 1 (Rbx1) (Kamura *et al.*, 1999), and Cullin 2 (Cul2) (Duan *et al.*, 1995; Kibel *et al.*, 1995; Pause *et al.*, 1997). Additionally, HIF-α is hydroxylated on asparagine 803 by factor-inhibiting HIF (FIH) (Koivunen *et al.*, 2004), which prevents recruitment of the transcriptional coactivators p300/CBP (Mahon *et al.*, 2001).

In the absence of oxygen or functional pVHL, HIF-α is stabilized and translocated to the nucleus where it partners with HIF-β to form functional HIF (Maxwell *et al.*, 1999). HIF is a master regulator of a wide array of hypoxia-inducible genes, globally regulating oxygen sensing and transport (PHD1–3, EPO, GATA1), angiogenesis (VEGF, PAI-1), anaerobic energy metabolism (GLUT-1, LDHA), and cell growth and survival (cyclin D1, TGF-α, c-MYC) (for reviews, see Kaelin, 2005; Ruas and Poellinger, 2005; Wenger, 2002).

Overproduction of hypoxia-inducible mRNAs, such as VEGF, is a hallmark of the vascularized neoplasms associated with inactivation of *VHL* (Lonser *et al.*, 2003; Maher *et al.*, 1991; Maher and Kaelin, 1997; Van Poppel *et al.*, 2000); however, the

ability of different *VHL* disease alleles to regulate HIF levels differs greatly. Suggestive genotype–phenotype correlations have been found with respect to the absence or presence of pheochromocytomas (VHL disease type 1 or 2, respectively), and the development of hemangioblastomas, pancreatic tumors, and ccRCC (Lonser *et al.*, 2003; Neumann and Wiestler, 1991; Zbar *et al.*, 1996). Alleles linked to type 1 and type 2a/b VHL disease encode proteins that are at least partially defective with respect to HIF-α regulation. However, CP patients carrying homozygous germline *VHL* mutations display upregulated HIF-α levels, yet are not predisposed to cancer (Gordeuk *et al.*, 2004). Thus, upregulation of HIF-α alone does not appear to be oncogenic in humans. Furthermore, while products of type 2c *VHL* alleles regulate HIF normally, patients exclusively develop pheochromocytoma (Clifford *et al.*, 2001; Hoffman *et al.*, 2001). This indicates that VHL has various functions that differentially contribute to tumorigenesis in patients.

IV. HIF-Independent Functions of pVHL

Several HIF-independent functions of pVHL have been identified, showing that pVHL acts as a multipurpose adaptor protein regulating a wide variety of transcription-dependent and -independent cellular processes (Frew and Krek, 2008) (Table I). The direct regulation of the extracellular matrix (ECM) and the microtubule (MT) cytoskeleton appears to be an important aspect of the "alternative" functions of pVHL.

pVHL is involved in the correct formation and turnover of the ECM (Bishop *et al.*, 2004; Kurban *et al.*, 2006) by interacting with collagen IV (Kurban *et al.*, 2008), fibronectin (Hoffman *et al.*, 2001; Ohh *et al.*, 1998; Stickle *et al.*, 2004), and integrin processing (Esteban-Barragan *et al.*, 2002). Activity of matrix metalloproteinases is also increased in a HIF-dependent manner (Koochekpour *et al.*, 1999). Thus, pVHL inactivation causes both HIF-independent and -dependent defects in the ECM that may promote angiogenesis, invasion, and metastasis of tumor cells (Kurban *et al.*, 2006; Ohh *et al.*, 1998; Tang *et al.*, 2006).

The MT cytoskeleton regulates many cellular processes, including mitosis, cell migration, and ciliogenesis. pVHL localizes to the mitotic spindle in mammalian cells and its inactivation provokes spindle defects and chromosomal instability (Thoma *et al.*, 2009). Ciliary dysfunction can cause proliferative kidney cysts (Eley *et al.*, 2005), a hallmark feature of VHL disease. Interestingly, pVHL localizes to the primary cilium and functions in its formation or maintenance (Esteban *et al.*, 2006; Lolkema *et al.*, 2008; Lutz and Burk, 2006; Schermer *et al.*, 2006; Thoma *et al.*, 2007). pVHL might function in intraflagellar transport, since pVHL binds the polarity protein Par3–Par6–aPKC complex that is targeted to the cilium by kinesin-2 (Fan *et al.*, 2004; Frew and Krek, 2008; Schermer *et al.*, 2006). Alternatively, pVHL might act as an adaptor for the transport of MT-stabilizing factors, or organelles such as the centrosome (Kuehn *et al.*, 2007), to the plus ends of MTs (Frew and Krek,

Table I
Adaptor functions of VHL

Complex	Target	Action	References
EloB, EloC, Cul2, Rbx1	HIF-α	VHL destabilizes HIF. HIF promotes switch to anaerobic glycolysis, angiogenesis, blood vessel enlargement, EPO, and blood cell production. Affects polarization/cilia formation, differentiation	Semenza (2009)
	Rbp1	Stress-induced transcription; increased RNAPII activity	Mikhaylova *et al.* (2008)
Fibronectin Rho GAP?	ECM Actin stress fiber formation	Promote assembly, VHL loss reduces activation of RhoA, activation of RhoGAP	Ohh *et al.* (1998), Feijoo-Cuaresma *et al.* (2008)
ColIV	ColIV	Promote colIV network remodeling/assembly	Kurban *et al.* (2008), Grosfeld *et al.* (2007)
Kinesin 2	Microtubules Mad2	Mediates microtubule binding Stabilizes microtubules Spindle orientation Maintenance of kidney primary cilia	Lolkema *et al.* (2007), Hergovich *et al.* (2003), Thoma *et al.* (2007, 2009)
Par3, Par6, aPKC	Microtubules	Orienting microtubules, ciliogenesis	Schermer *et al.* (2006)
aPKC	junB	VHL loss increases levels of junB, prevents apoptosis	Lee *et al.* (2005)
ND	Skp2 expression P400	Block p27 accumulation, possibly by increasing skp2 Rb and p400 levels, thus reducing senescence in fibroblasts	Young *et al.* (2008), Welford *et al.* (2010)
p53 ATM p300/pCAF	Mdm2, others	pVHL stabilizes and enhances p53 transcriptional activity, prevents MDM2-mediated ubiquitination	Roe *et al.* (2006)
CARD9 CK2	NF-κB	Promote CARD9 phosphorylation, decrease NF-κB signaling	Yang *et al.* (2007)
Awd/NM23	Awd	Promotes Awd stability and activity. May stabilize rab5 and promote endocytosis	Hsouna *et al.* (2010), Hsu *et al.* (2006)
Jade-1	Jade-1	Promotes stability; Jade-1 may promote apoptosis/reduce growth via Wnt inhibition	Chitalia *et al.* (2008)

2008). pVHL also mediates MT-based endocytosis (Champion *et al.*, 2008; Hsouna *et al.*, 2010; Hsu *et al.*, 2006; Koochekpour *et al.*, 1999; Wang *et al.*, 2009).

V. VHL Animal Models

A multitude of animal models have been generated to study pVHL *in vivo* (Table II). In vertebrates, numerous mouse models have elucidated the importance of VHL in several physiological processes, although their ability to model the disease has been limited.

Vhlh$^{-/-}$ knockout mice die *in utero* between E9 and E12.5 due to hemorrhagic lesions and reduced placental vascularization (Gnarra *et al.*, 1997; Haase *et al.*, 2001; Kleymenova *et al.*, 2004). *Drosophila* morphants/mutants in *d-VHL* display ectopic and excessive branching and looping of the smaller tracheal branches and breakage of dorsal tracheal tubes (Adryan *et al.*, 2000; Hsouna *et al.*, 2010). Defects in branching morphogenesis and tube fusion may underlie the defects in both organisms (Adryan *et al.*, 2000).

Numerous *Vhlh* conditional knockout mice exist (Table II). Even though retinal and CNS hemangioblastomas and ccRCC are prevalent VHL symptoms in humans, they were not observed in any of these models. Mice harboring a deletion of *Vhlh* in endothelial cells (Tang *et al.*, 2006) are lethal due to hemorrhagic lesions and vascular abnormalities in the placenta, similar to complete *Vhlh* knockouts. Deletion of *Vhlh* in the epidermis (Boutin *et al.*, 2008) and liver (Haase *et al.*, 2001; Rankin *et al.*, 2005) resulted in increased angiogenesis in the targeted organs, and *Vhlh*$^{+/-}$ mice, or mice with mosaic *Vhlh* inactivation (Ma *et al.*, 2003), often developed hepatic cavernous hemangiomas, a rare VHL symptom (McGrath *et al.*, 1992; Rojiani *et al.*, 1991). Tumor formation in *Vhlh*-deficient livers is entirely dependent on HIF (Rankin *et al.*, 2005). However, genetic background determined variable frequency in different studies (Gnarra *et al.*, 1997; Haase *et al.*, 2001; Kleymenova *et al.*, 2004; Ma *et al.*, 2003).

VHL is critical for the development of ccRCC; restoration of VHL function in *VHL*$^{-/-}$ renal carcinoma cells suppresses tumorigenicity in nude mice (Iliopoulos *et al.*, 1995). However, renal pathology was not observed in mice in which *Vhlh* was inactivated in a systemic mosaic pattern (Ma *et al.*, 2003), or in *Vhlh*$^{+/-}$ mice (Haase *et al.*, 2001; Kleymenova *et al.*, 2004). Conversely, mutations in *Vhlh* have not generally been detected during sequencing of rat/mouse renal neoplasms (Kikuchi *et al.*, 1995; Kleymenova *et al.*, 2004; Shiao *et al.*, 1997; Walker *et al.*, 1996). Renal cysts were only found at a low frequency in *Vhlh* heterozygotes ($\pm$1/30; Haase *et al.*, 2001; Kleymenova *et al.*, 2004). Conditional deletion of *Vhlh* in renal tissues resulted in a low incidence of glomerular and tubular cysts but not in neoplasms (Frew *et al.*, 2008b; Rankin *et al.*, 2006). Therefore, additional VHL-independent events may be required that activate other cancer signaling pathways.

Table II
VHL animal models

Animal	Type	Method of inactivation	Reference	Cell type targeted	Phenotype
Drosophila	Transient	RNAi	Adryan *et al.* (2000)	Systemic	Excessive branching and looping of the smaller tracheal branches, breakage of dorsal trunks (tracheal tubes). Lethal (L): stage 12–17
	Knockout	Δ243 bp removing first two AUGs	Hsouna *et al.* (2010)	Systemic	Tracheal defects. Class 1: misdirected tubules, ectopic branching, and disruption of the dorsal trunk. Class 2: enlarged lumina, torturous tracheal tubes. Impaired endocytosis resulting in tracheal surface accumulation of FGFR. L: first to second instar larva
C. elegans	Knockout	Deletion	Epstein *et al.* (2001), Bishop *et al.* (2004), Pocock and Hobert (2008), Treinin *et al.* (2003), Shen *et al.* (2005)	Systemic	Viable, slow growth, reduced brood size, activation of *Ce*HIF-1 targets, PVQ axon-pathfinding defects. Link to ECM function
Zebrafish	Knockout	ENU-mutagenesis Q23X or C31X	van Rooijen *et al.* (2009, 2010)	Sytemic	$vhl^{-/-}$ constitutive hypoxic signaling, hyperventilation response, polycythemia, cardiomegaly, increased cardiac output, general neovascularization, pronephros defects. $vhl^{+/-}$ adults have no phenotype. L: 8–11 dpf
Mouse	Knockout	Neomycin selection cassette replacing *Vhlh* gene	Gnarra *et al.* (1997)	Systemic (C57Bl/6-129 background)	$Vhlh^{-/-}$ E9.5 defective vasculogenesis in placental labyrinth, hemorrhage. $Vhlh^{+/-}$ no phenotype. L: E11.5–E12.5
			Kleymenova *et al.* (2004)	Systemic (C57Bl/6-129 background)	$Vhlh^{-/-}$: embryonic lethal. $Vhlh^{+/-}$ 14–18 months: hepatic vascular lesions (21%), vascular lesions of the uterus, ovary, spleen, and heart (5–28%)
			Haase *et al.* (2001)	Systemic (BALB/c-129 background)	$Vhlh^{-/-}$: lethal at E9–E11 $Vhlh^{+/-}$ 3–17 months: cavernous liver hemangiomas (88%)
	Missense	Neomycin selection cassette R116W	Hickey *et al.* (2007, 2010)	Systemic	"Chuvash mutation" 10–14 weeks: polycythemia
	Knockout	Mosaic β-actin-Cre	Ma *et al.* (2003)	Mosaic	Hepatic vascular tumors, angiectasis in heart, liver, pancreas, lung, kidney. Abnormal spermatogenesis. Visible at 3 months L: 6–12 months
	Inducible knockout	Tamoxifen-inducible ER-Cre, floxed VHL exon 2 and 3	Hong *et al.* (2006)		E14.5: small, pale embryos, hemorrhage, vascular defects, and liver damage (induced VHL inactivation at E10.5) L:E14.5–E15

Conditional knockout	PEPCK-Cre	Rankin *et al.* (2006)	Renal proximal tubule, hepatocytes	Renal cysts (~30%), liver hemangiomas, and polycythemia. Polycythemia from 2 months, cysts >12 months
	Ksp1.3-Cre	Frew *et al.* (2008b)	Renal epithelium; epithelia of the genital tracts	2–3 months: *Vhlh*$^{-/-}$ hydronephrosis, no kidney abnormalities. No genital tract abnormalities 6–8 weeks: *Vhlh*$^{-/-}$/*Pten*$^{-/-}$: kidney – proliferative renal cysts; genital tracts – epididymal cystadenomas
	Podocin-Cre	Ding *et al.* (2006)	Podocytes	3–4 weeks: glomerulonephritis, hematuria, proteinuria, renal insufficiency. Increased proliferation of podocytes and *de novo* expression of CXCR4. L:7 weeks
		Brukamp *et al.* (2007)	Podocytes (BALB/c, 129Sv/J, C57BL/6J mixed background)	8 weeks: glomerulomegaly, increased Bowman space, glomerulosclerosis, no significant proteinuria. Increased podocyte apoptosis *in vitro*
	Tie2-Cre	Tang *et al.* (2006)	Endothelial cells	E9.5–E11.5: defective vasculogenesis in placental labyrinth, collapsed endocardium, impaired vessel network patterning, hemorrhages, diminished vascular fibronectin L:E12.5
	MLC2v-Cre	Lei *et al.* (2008)	Cardiomyocytes	3–5 months: progressive heart failure. Lipid accumulation, myofibril rarefaction, altered nuclear morphology, myocyte loss, fibrosis, malignant cardiac tumors. L:5–12 months
	LysM-Cre	Cramer *et al.* (2003)	Myeloid cells	No phenotype under sterile barrier conditions. *Vhlh/Hif-1α* inactivation results in increased inflammatory response
	Lck-Cre	Biju *et al.* (2004), Neumann *et al.* (2005)	Thymocytes	Biju *et al.*: small, highly vascularized thymi, increased caspase-8-dependent apoptosis in $CD4^+/CD8^+$ cells Neumann *et al.*: Diminished Ca^{2+} response on T-cell receptor cross-linking, accelerated removal of cytoplasmic Ca^{2+} into intracellular compartments, overexpression of SERCA2
	Albumin-Cre	Haase *et al.* (2001), Rankin *et al.* (2005)	Hepatocytes	2 weeks: angiectasis, hemangiomas, endothelial cell proliferation, hepatic steatosis, polycythemia. L:6–12 weeks
		Peyssonnaux *et al.* (2007)		3 weeks: alopecia, reduced weight, hepatomegaly, splenomegaly, iron deficiency, poikilocytosis, microcytosis, decreased total iron, ferritin, and hepcidin levels. L:5–7 weeks
	Rip2-Cre	Zehetner *et al.* (2008)	Pancreatic β-cells	26–52 weeks: impaired glucose tolerance, abnormal insulin secretion

(Continued)

Table II *(Continued)*

Animal	Type	Method of inactivation	Reference	Cell type targeted	Phenotype
		Fabp-Cre	Karhausen *et al.* (2004)	Colonic epithelial cells	8–16 weeks: increased expression of HIF-regulated barrier-protective factors, glycogen accumulation. Protection from inflammatory bowel disease
		K14-Cre	Boutin *et al.* (2008)	Epidermis	10 weeks: increased dermal vasculature, higher metabolic rate, low weight, polycythemia. Early death
		Osteocalcin-Cre	Wang *et al.* (2007)	Osteoblasts	7 days: increased bone modeling. Dense, heavily vascularized long bones, increasing vessel numbers, reduced trabecular separation
		ColII-Cre	Pfander *et al.* (2004)	Growth plate, chondrocytes	E14.5: dwarfism, decreased chondrocyte proliferation, increased ECM deposition

In primary renal proximal epithelial cells, it was shown that only the combined inactivation of pVHL and glycogen synthase kinase beta (GSK3β) resulted in the loss of primary cilia, likely via Akt activation (Thoma *et al.*, 2007). This was supported *in vivo*, where only the combined deletion of *Vhlh* and *Pten* (a negative regulator of Akt) resulted in the robust formation of renal cysts with reduced cilia numbers (Frew *et al.*, 2008b). Notably, renal cysts of human VHL patients frequently display PI3K pathway activation (Frew and Krek, 2008; Frew *et al.*, 2008a). Therefore, tumor formation in VHL patients may result from pVHL loss of function concomitant with activation of additional pathways supporting malignant progression (Frew and Krek, 2007).

While mouse models have contributed greatly to our understanding of pVHL function, their use is limited for modeling VHL-associated pathologies (including hemangioblastomas and ccRCC) (Haase, 2005). Additional vertebrate *VHL* models might help to elucidate these functions. To study the diverse and complex regulatory functions of pVHL in development and disease, we developed a novel VHL animal model system in zebrafish.

VI. Zebrafish as a New Model for VHL

Zebrafish have become a valuable model for vertebrate biology and human disease (Feitsma and Cuppen, 2008; Lieschke and Currie, 2007). They provide large numbers of externally developing embryos with excellent optical properties. Thus, processes can be followed noninvasively and in great detail. The availability of target-selected mutagenesis (Wienholds *et al.*, 2003) and zinc finger nuclease technology (Doyon *et al.*, 2008; Meng *et al.*, 2008) allows the generation of mutants in a gene of choice. Importantly, the HIF pathway (Carradice and Lieschke, 2008; de Jong and Zon, 2005; Song *et al.*, 2004) is conserved and the zebrafish vascular (Covassin *et al.*, 2006; Herpers *et al.*, 2008; Vogel and Weinstein, 2000) and hematopoietic (Ma *et al.*, 2007; Paffett-Lugassy *et al.*, 2007) systems show a remarkable functional conservation with humans.

Zebrafish *vhl* maps to chromosome 6, near 44.0 Mb on the Zv8 Ensembl genome assembly. This region is syntenic with human chromosome band 3p25.3 containing *VHL*. *vhl* encodes a 175-amino-acid protein that is 52% identical and 70% similar to human pVHL, with highly conserved Elongin C and HIF-binding domains (Fig. 2). Vhl lacks the N-terminal acidic domain, found in VHLp30. However, this domain is not conserved through evolution; it is absent in invertebrates, and reduced in rodents. During zebrafish development, *vhl* is ubiquitously expressed (van Rooijen *et al.*, 2009).

A more distant relative exists in zebrafish and other fish species in the form of *vhl-like* (*vll*) (van Rooijen *et al.*, 2009) Interestingly, Vll contains several amino acid changes that were identified in VHL patients, suggesting that Vll cannot exert the tumor-suppressive function of human VHL efficiently (probably suppressing HIF signaling; Fig. 2). It differs from VLP, a dominant negative VHL-like gene in humans (Qi *et al.*, 2004). We have isolated several zebrafish mutants in *vll*, and preliminary analysis reveals that *vll* null mutants are viable. However, when both *vhl* and *vll* are

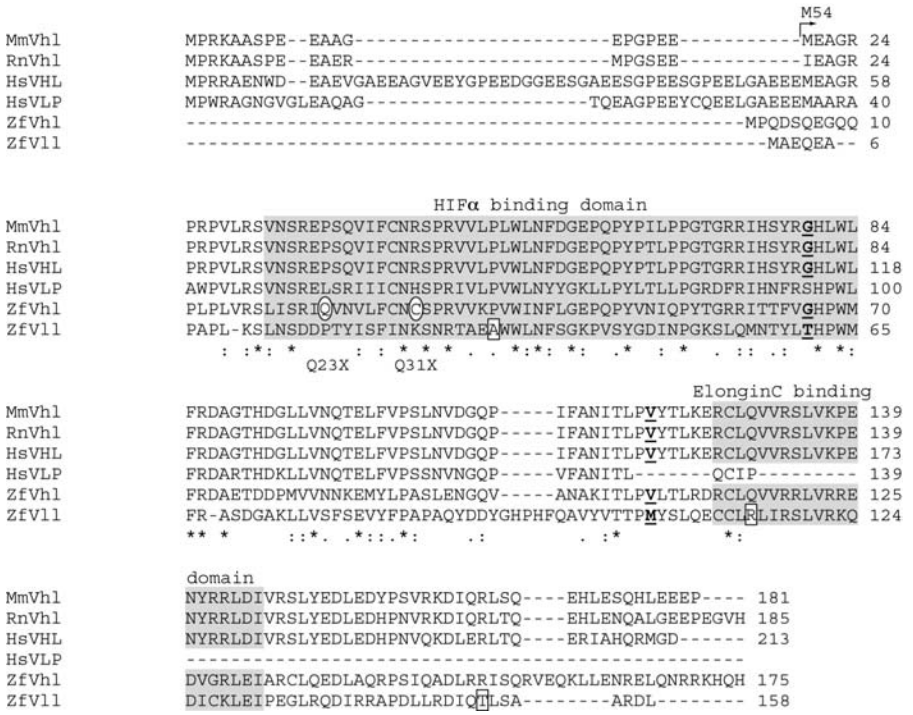

Fig. 2 ClustalW comparison of mouse (Mm), rat (Rn) human (Hs), and zebrafish (Zf) Vhl, Vll, and VLP. Highlighted in gray are the HIF-α and Elongin C–binding domains, VLP lacks the latter domain. Amino acids encoded at exon–exon junctions are bold underlined, and show that exon boundaries in VHL, Vhl, and Vll are conserved. M54 is the alternative start codon in human VHL. The encircled amino acids are mutated to stop codons in *vhl*^{hu20117} and *vhl*^{hu2081}, respectively. In Vll, two amino acids are boxed that were identical to VHL mutations that were detected in VHL patients (Chen *et al.*, 1995). The third boxed change may be similar to the human R200W Chuvash mutation. (See color plate.)

absent, the *vhl* phenotype is enhanced (Kirankumar Santhakumar and Ellen van Rooijen, unpublished).

Target-selected mutagenesis generated two *vhl* alleles: *vhl*^{hu2117}(C/T, Q23X) and *vhl*^{hu2081}(C/A, C31X). Both lines carry early nonsense mutations in the HIF-binding domain of Vhl, and no protein could be detected in 6.5 days postfertilization (dpf) *vhl* mutants, indicating a complete loss-of-function situation. While hypoxia-induced genes are upregulated even during early somitogenesis (e.g., *phd3*), *vhl* mutants are morphologically indistinguishable from siblings before 2 dpf. Contrary to the early embryonic lethal mouse knockout, the zebrafish *vhl* mutants do not display early patterning defects, indicating Vhl is not involved, or that a maternal contribution relieves early zygotic requirements. Early morphological markers for identification of *vhl* mutants are given in Fig. 3. During the course of development, *vhl*$^{-/-}$ mutants develop key aspects of the human disease condition, including CP (van Rooijen *et al.*, 2009), severe neovascularization defects predominantly in tissues with high *vegf*

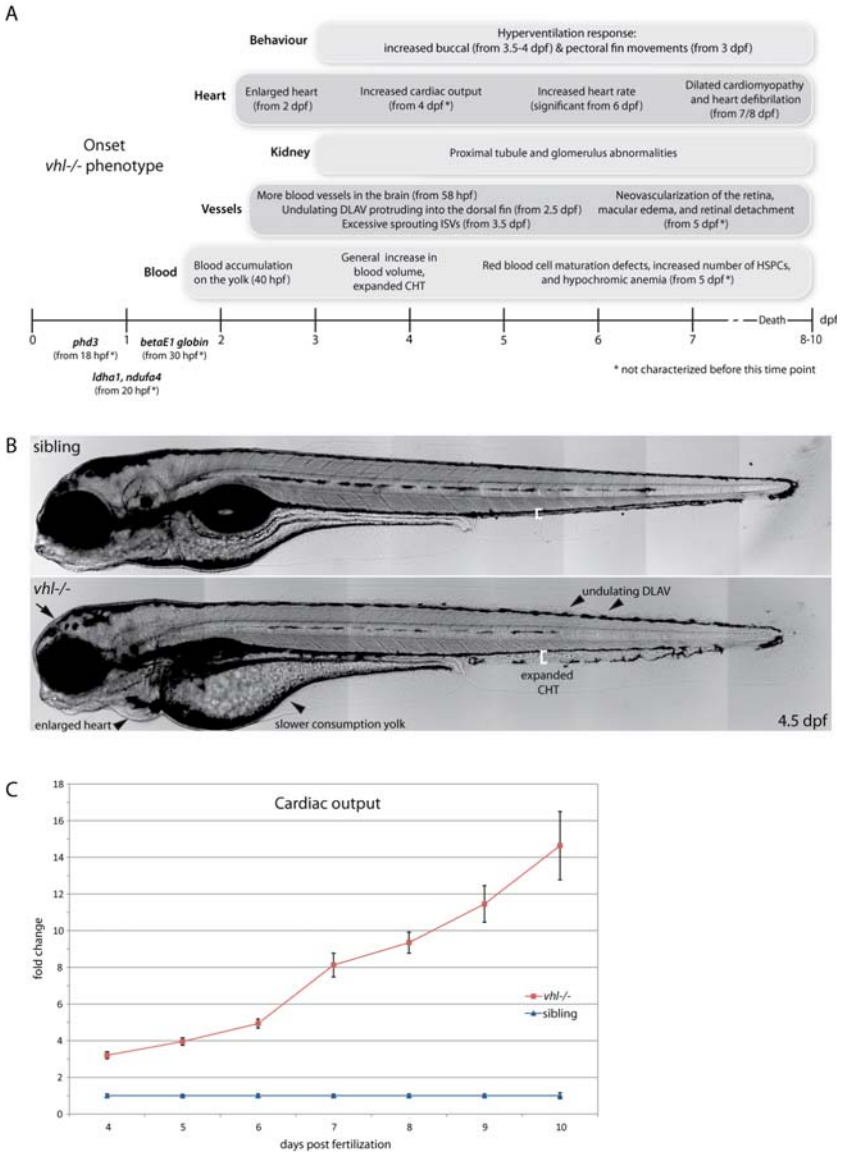

Fig. 3 (A) Time course representation of the onset of the various $vhl^{-/-}$ phenotypes. Earliest *in situ* hybridization markers are indicated. (B) Wild-type sibling and *vhl* mutant embryo at 4.5 dpf. In *vhl* mutants, the dorsal longitudinal anastomotic vessel (DLAV) undulates far above the dorsal pigment stripe, protruding into the tailfin (black arrowheads). The $vhl^{-/-}$ caudal hematopoietic tissue (CHT) is expanded, indicated by a wider separation of the two pigment stripes (white brackets). The yolk is less consumed at 4.5 dpf (black arrowhead) than in the age-matched sibling. *vhl* mutants have a smaller rounder head (arrow) and an enlarged heart. (C) Relative to wild-type siblings, *vhl* mutants have an increased cardiac output (up to 15-fold). dpf, days postfertilization; hpf, hours postfertilization; HSPC, hematopoietic stem/progenitor cell; ISV, intersomitic vessel. (For color version of this figure, the reader is referred to the web version of this book.)

mRNA expression such as the brain and retina (van Rooijen *et al.*, 2010), and pronephros abnormalities (unpublished results). These data indicate that Vhl function is conserved in zebrafish. Zebrafish *vhl* mutants complete embryogenesis and survive to late larval stages (8–10 dpf). Therefore, they represent a unique vertebrate model in which VHL functions can be addressed until postembryonic stages.

VII. Loss of Vhl Leads to a Systemic Hypoxic Response in Zebrafish

pVHL is essential for the adaptive cellular response to hypoxia through the negative regulation of HIFs. Zebrafish mutant embryos display a general systemic hypoxic response, including the upregulation of hypoxia-induced genes by 1 dpf and a severe hyperventilation and cardiophysiological response.

From 4 to 5 dpf, mutants show a strong increase in buccal and pectoral fin movements, thereby increasing ventilation of the gills. This is a known adaptation to a hypoxic environment (Jonz and Nurse, 2005). Interestingly, despite the increased ventilation, the oxygen consumption is lower in *vhl* mutants (Yaqoob and Schwerte, 2010). This is likely due to a switch toward anaerobic glycolysis, as suggested by our microarrays (see below). The perceived hypoxia also induces changes in cardiac physiology as both stroke volume and heart rate are increased. Over the course of development, cardiac output increases up to 15-fold compared to wild type (Fig. 3). Both the atrium and ventricle become enlarged and their walls are thinned, reminiscent of dilated cardiomyopathy. This ultimately leads to cardiac insufficiency, edema, and circulation arrest. While most *vhl* mutants likely die from cardiac and renal failure around 8 dpf, some mutants survive slightly longer. We have tried feeding these $vhl^{-/-}$ larvae using fry food, glucose, or fluorescent beads; however, they fail to take up food. It is conceivable that the ventilation response may inhibit a normal larval feeding reflex.

Molecularly, *vhl* mutants display an early and general hypoxic response. Microarray and qPCR experiments comparing 7 dpf wild-type and mutant larvae showed that many known HIF targets are upregulated. These include (1) genes in the HIF pathway itself, acting as negative feedback regulators (e.g., the *phd* and *fih* genes), (2) genes that facilitate a switch to an anaerobic metabolism, such as *lactate dehydrogenase* (Semenza *et al.*, 1994), *pfkfb3* (Minchenko *et al.*, 2002), and *glut1* (Ebert *et al.*, 1995), and (3) classical HIF targets, such as genes in the VEGF and Epo pathway (Fig. 4), and several others such as *redd1/ddit4* (Brugarolas *et al.*, 2004) and *lysyl oxidase* (Erler *et al.*, 2006).

VIII. *vhl* Mutants Develop Chuvash Polycythemia and Blood Cell Maturation Defects

vhl mutants show an increased number of red blood cells (RBCs), which becomes apparent around 2 dpf as an increase of blood accumulation on the yolk. Later,

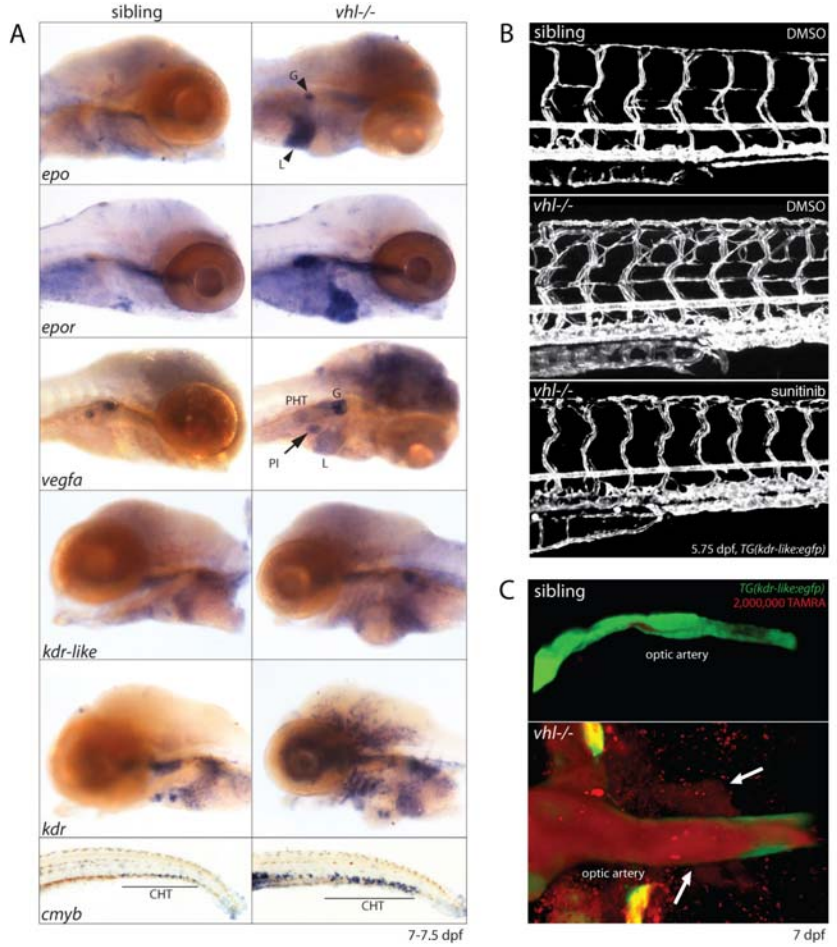

Fig. 4 (A) *vhl* mutants display elevated mRNA expression levels of *epo* and its receptor *epoR*, *vegfa* and its receptors *kdr* and *kdr-like*, and the HSPC marker *cmyb*, compared to wild-type siblings. (B) Confocal analysis of the trunk vasculature in TG (*kdr-like:egfp*) embryos at 5.75 dpf. Vegf receptor tyrosine kinase inhibition (0.2 μM sunitinib) blocks the excessive angiogenesis normally observed in *vhl* mutants. (C) 3D confocal reconstruction of the optic artery, 20–25 h after rhodamine-dextran (TAMRA) injection. *vhl* mutants display severe vascular leakage through the vessel wall into the surrounding tissue (arrows). Reproduced with permission from van Rooijen *et al.* (2009, 2010); http://dmm.biologists.org. (See color plate.)

increased amounts of RBCs can be seen in the widened blood vessels and in the heart. Epo signaling is an important regulator of RBC development and is at the basis of many polycythemias. Epo signals via the EpoR/Jak2a/STAT5 pathway (Yoshimura and Misawa, 1998). Indeed, increased Epo expression and increased Jak/STAT signaling were observed in *vhl* mutants. Surprisingly, also white hematopoietic lineages are increased, as marked by *l-plastin*, *lck*, and *mpo* expression. These markers are

unresponsive to *epo* mRNA overexpression (Paffett-Lugassy *et al.*, 2007). The number of circulating erythrocyte precursors was increased eightfold in *vhl* mutants, but RBCs remained immature, retaining *scl*, *gata1*, and *ikaros* expression. Furthermore, elevated levels of HSC markers such as *cd41 scl* and *cmyb* (Fig. 4) suggest a general increase in the number of HSCs and their resulting lineages.

vhl mutants manifest hypochromic anemia. This is due to depletion of iron stores in the embryo; iron-dextran injection can rescue this phenotype. This parallels effects seen in CP patients where venesection can lower iron levels and cause secondary anemia (Smith *et al.*, 2006). Our microarray also indicates iron deficiency, showing increased *transferrin a*, *transferrin receptor1b*, and *ferroportin* as well as decreased *hepcidin* levels.

The R200W Chuvash knock-in mouse mutant develops polycythemia by 10–14 weeks of age, and has pulmonary hypertension and an increased breathing rate (Hickey *et al.*, 2007, 2010). The white blood cell number was slightly increased albeit just below significant levels. Overall, we observe more severe defects in blood, cardiac, and the baseline ventilation phenotypes in $vhl^{-/-}$ fish larvae than in either Chuvash patients or Chuvash R200W knock-in mice. We conclude that the R200W mutation still allows for partial pVHL function.

IX. Zebrafish *vhl* Mutants Develop Angiogenesis Defects

Angiogenesis increases the oxygen supply to hypoxic areas. Indeed, VEGF is a classical target of the VHL/HIF pathway (Forsythe *et al.*, 1996). Likewise, zebrafish *vhl* mutants have increased Vegf signaling, reflected by upregulation of *vegfa*, *vegfab*, *vegfb*. Interestingly, Vegf receptors Kdr and Kdrl-like (Bussmann *et al.*, 2008) (Fig. 4) also show increased vascular expression. This suggests that endothelial cells become sensitized to VEGF in hypoxia, aiding in targeting angiogenesis to regions where oxygen levels are the lowest.

While vasculogenesis appears normal, from 58 hours postfertilization (hpf) onwards *vhl* mutants display an increased number of blood vessels particularly in regions where *vegf* is strongly upregulated, including the head and eyes. Furthermore, vessels appear dilated, likely due to the increased blood volume. From 3.5 dpf, aberrant angiogenic sprouts also form in regions where there is no detectable *vegf* expression, for example, from the intersomitic vessels (Bahary *et al.*, 2007). Clinical VEGF inhibitors designed to block human VEGF (such as sunitinib) rescue the angiogenic phenotype in these fish, demonstrating the conservation of this pathway and also the value of this model for understanding tumor angiogenesis (Fig. 4).

A striking neovascularization is observed in the $vhl^{-/-}$ eye. The zebrafish eye receives its blood supply from networks of choroidal and hyaloid vessels that initially connect to the back of the lens (Alvarez *et al.*, 2007). Both types of vessels are radically enhanced in the *vhl* larvae. Normally vessels cannot be detected within the retina itself. However, in 7.5 dpf, *vhl* larvae vessels were observed in the inner plexiform layer. Comparable to VHL-associated retinal neoplasms, rhodamine-dextran angiographies

show that vascular abnormalities in the *vhl*$^{-/-}$ retina lead to vascular leakage, macular edema, and retinal detachment (Fig. 4).

Although hemangioblastomas were not observed in *vhl*$^{-/-}$ embryos or in heterozygous adult fish, the observed retinal neovascularization appears to be more similar to a new class of ocular VHL disease similar to diabetic retinal neovascularization (Chew, 2005). Hemangioblastomas are made up by stromal cells and endothelial cells, where the former are considered the true neoplastic cells and are thought to be related to endothelial cells/embryonic hemangioblast progenitors (Glasker *et al.*, 2006; Lach *et al.*, 1999). It is interesting to note that RCC metastases preferentially develop in hemangioblastomas, suggesting they provide a permissive environment for tumor growth (Jarrell *et al.*, 2006).

The chemokine receptor CXCR4 and its ligand SDF1 are expressed in stromal hemangioblastoma cells and in ccRCC. Interestingly, both were also upregulated in endothelial cells of hemangioblastomas (Staller *et al.*, 2003; Zagzag *et al.*, 2005). CXCR4a acts in conjunction with VEGF in vascular patterning (Kryczek *et al.*, 2005; Siekmann *et al.*, 2009). We found that CXCR4a is upregulated in a subset of newly forming retinal and brain vessels in *vhl* mutants but not elsewhere. Intriguingly, the most severe neovascularization phenotypes in *vhl* mutants (brain and eye) correspond to areas where hemangiomas develop in VHL patients. We speculate that brain and eye provide a special environment (competence to express high levels of VEGF) that promotes tumorigenesis.

The dramatic angiogenesis that we observe in *vhl* mutants is a unique feature of our model and different from *Vhlh*$^{-/-}$ mice. Knockout of murine Vhlh in the entire embryo leads to reduced complexity of the placental vascular network. The difference in phenotype between fish and mice may be explained by timing; in mice an early placental requirement could obscure a later angiogenic phenotype in the embryo, and placental hypoxic signaling is unusual with respect to inducing angiogenesis/VEGF (Gnarra *et al.*, 1997).

Interestingly, endothelial-specific mouse knockouts also have a reduced vessel complexity in the body; yet this phenotype is not seen in fish. However, the endothelial cells in such mice will not be exposed to VEGF produced by other VHL-deficient tissues; thus, a comparison is difficult. The endothelial phenotype of these mice was reported to be independent of HIF (Tang *et al.*, 2004, 2006), and defective fibronectin deposition was suggested as a cause. We have not analyzed fibronectin in the *vhl* larvae but the widened diameter and increased permeability of blood vessels in *vhl*$^{-/-}$ fish and mouse endothelial *Vhlh* knockout could support a parallel.

X. Zebrafish *vhl* Mutants Develop Pronephros Abnormalities

VHL is accepted to hold a gatekeeper function in renal cell function, with loss of *VHL* causing renal disease and cancer. Our results agree with mouse and human data, indicating that loss of pVHL alone is insufficient to cause cysts (Frew *et al.*, 2008b; Mandriota *et al.*, 2002) or ccRCC (Frew *et al.*, 2008b; Rankin *et al.*, 2006). We find

that *vhl* is required to maintain pronephric tubule and glomerulus integrity in zebrafish embryos. While we did not observe pronephric cysts, the cells of the pronephric tubule appear enlarged. We are currently investigating the exact nature of these defects.

Normal renal tissue in VHL patients contains several $VHL^{-/-}$ single cells that express HIF-target carbonic anhydrase IX (Mandriota *et al.*, 2002). Interestingly, both hemangioblastomas (Shively *et al.*, 2008) and epididymal tumors (Mehta *et al.*, 2008) from VHL patients originate from developmentally arrested embryonic *VHL*-deficient cells. These data suggest that the second inactivating hit in *VHL* occurs during embryonic development, which would suggest VHL might be a developmental disease. Since $vhl^{-/-}$ zebrafish are the only systemic embryonic viable animal model for VHL that display proximal tubule abnormalities, further characterization of these cells may contribute to the understanding of the initiating events that lead to renal disease progression in human patients. The high conservation of *VHL* between zebrafish and humans furthermore allows $vhl^{-/-}$ zebrafish to be used as a clinically relevant model to study genotype/phenotype correlations, identify new biomarkers, and test pharmacological agents.

XI. Translation from Fish to Humans

A. Dissection of Genotype/Phenotype Correlations

Over 700 unique familial and sporadic *VHL* mutations have been identified (Nordstrom-O'Brien *et al.*, 2010). Attempts have been made to identify patients at risk for certain tumor types based on their particular *VHL* mutation. Despite this progress, the postulated genotype–phenotype correlations have not been particularly helpful for the patient.

We showed that human *pVHL30* mRNA rescues the zebrafish $vhl^{-/-}$ polycythemia phenotype when injected into zygotes, whereas *VHL R200W* mRNA did not (van Rooijen *et al.*, 2009). These experiments demonstrate conservation of pVHL function between mammals and zebrafish to the amino acid level, indicating *vhl* mutants are a powerful new tool to study genotype–phenotype correlations in human disease.

We are now testing several other VHL mutations, examining their effect on hematopoiesis, angiogenesis, kidney morphology, hypoxia, and metabolism. This developmental model will provide the first (nonhuman) *in vivo* data interrogating genotype–phenotype correlations in VHL disease. If successful, our tool will help to individualize treatment and screening procedures. The flexibility and speed of our system may allow modeling novel or rare mutations, suggesting the spectrum of the disease that might be anticipated in the patient.

B. Translation from Fish to Humans – Identification of Biomarkers

In addition to the standard suite of hypoxia-related genes and known *vhl* targets, microarray analysis of 7 dpf *vhl* mutants and siblings has revealed several surprising

differentially expressed genes. We have begun to validate these in human cell lines and tissue microarrays. This approach has resulted in the identification of a novel clinical marker *E2F1*, and analysis of its expression in 138 RCCs predicts overall survival in both VHL patients and sporadic RCC patients (D. Mans *et al.*, submitted).

C. Translation from Fish to Humans – Screening for Novel Agents and Combination Therapies

Proangiogenic factors such as VEGF, VEGF receptors, and members of the HIF signaling pathway are potential targets for drugs against cancer and the treatment of angiogenesis-related disorders. However, the current *in vitro* and (invasive) *in vivo* models for angiogenesis to evaluate potential targeting agents are incapable of reflecting the complexity of angiogenesis and its microenvironment, or allowing *in vivo* functional evaluations (reviewed by Taraboletti and Giavazzi, 2004).

Vhl$^{-/-}$ zebrafish display excessive blood vessel formation, which can be halted by treatment with VEGF inhibitors. Therefore, *vhl* mutants expressing a *fli1-a::egfp* transgene, for example, represent a powerful tool for functional screening of anti-angiogenic therapies in an *in vivo* model prior to clinical trials. Furthermore, other *vhl*$^{-/-}$ phenotypes, such as the kidney, could serve as a readout for the identification of compounds specifically targeting certain disease aspects. Zebrafish model systems allow screening at medium throughput for compounds that modify disease-relevant phenotypes (Tan *et al.*, this issue). Additionally, larval screens are a powerful way to test hundreds of primary hits from *in vitro* chemical screens, or derivatives of a lead compound. We predict that zebrafish will become an important tool in directing drug design.

XII. Concluding Remarks

Unlike *Vhlh* knockout mice, which die during early embryogenesis, zebrafish *vhl* mutants survive up to late larval stages. Therefore, *vhl*$^{-/-}$ zebrafish represent a unique vertebrate model in which VHL can be studied during both embryonic and postembryonic stages. Our results demonstrate that this novel genetic zebrafish *vhl* model may provide further insights into VHL function in the context of oxygen homeostasis, hematopoiesis, angiogenesis, and renal pathology. Although which VHL function(s) contribute to its role in renal homeostasis is unknown, the zebrafish pronephros may provide a simple and valuable model for identifying disease mechanisms (Drummond, 2005; Wingert and Davidson, 2008).

The zebrafish *vhl* model offers an excellent platform for the identification of genetic/chemical modifiers involved in the development of VHL-associated neoplasms. Crossing *vhl* mutants into tumor suppressor zebrafish lines (e.g., *Apc*, *PTEN*, or *p53*) may allow insights into the contributions of candidate pathways driving early processes involved in VHL-associated disease progression. The amenability of

zebrafish for chemical and genetic screens might not only be valuable for the identification of therapeutic leads but also aid in identifying unexpected pathways influenced by VHL.

Acknowledgments

This work was supported by the Dutch Cancer Association (UU-2006-3565). KS and FvE were supported by CRUK grant C23207/A8066 and MRC Centre grant G0700091. RG is supported by the Netherlands Organization for Scientific Research (NWO VIDI 917.66.354) and the European Community's Seventh Framework Programme FP7/2009 under grant agreement no. 241955, SYSCILIA.

References

Adryan, B., Decker, H. J., Papas, T. S., and Hsu, T. (2000). Tracheal development and the von Hippel–Lindau tumor suppressor homolog in *Drosophila*. *Oncogene* **19**, 2803–2811.

Alvarez, Y., Cederlund, M. L., Cottell, D. C., Bill, B. R., Ekker, S. C., Torres-Vazquez, J., Weinstein, B. M., Hyde, D. R., Vihtelic, T. S., and Kennedy, B. N. (2007). Genetic determinants of hyaloid and retinal vasculature in zebrafish. *BMC Dev. Biol* **7**, 114.

Ang, S. O., Chen, H., Hirota, K., Gordeuk, V. R., Jelinek, J., Guan, Y., Liu, E., Sergueeva, A. I., Miasnikova, G. Y., Mole, D., Maxwell, P. H., Stockton, D. W., Semenza, G. L., and Prchal, J. T. (2002). Disruption of oxygen homeostasis underlies congenital Chuvash polycythemia. *Nat. Genet* **32**, 614–621.

Bahary, N., Goishi, K., Stuckenholz, C., Weber, G., Leblanc, J., Schafer, C. A., Berman, S. S., Klagsbrun, M., and Zon, L. I. (2007). Duplicate VegfA genes and orthologues of the KDR receptor tyrosine kinase family mediate vascular development in the zebrafish. *Blood* **110**, 3627–3636.

Biju, M. P., Neumann, A. K., Bensinger, S. J., Johnson, R. S., Turka, L. A., and Haase, V. H. (2004). Vhlh gene deletion induces Hif-1-mediated cell death in thymocytes. *Mol. Cell. Biol* **24**, 9038–9047.

Bishop, T., Lau, K. W., Epstein, A. C., Kim, S. K., Jiang, M., O'Rourke, D., Pugh, C. W., Gleadle, J. M., Taylor, M. S., Hodgkin, J., and Ratcliffe, P. J. (2004). Genetic analysis of pathways regulated by the von Hippel–Lindau tumor suppressor in *Caenorhabditis elegans*. *PLoS Biol* **2**, e289.

Boutin, A. T., Weidemann, A., Fu, Z., Mesropian, L., Gradin, K., Jamora, C., Wiesener, M., Eckardt, K. U., Koch, C. J., Ellies, L. G., Haddad, G., Haase, V. H., Simon, M. C., Poellinger, L., Powell, F. L., and Johnson, R. S. (2008). Epidermal sensing of oxygen is essential for systemic hypoxic response. *Cell* **133**, 223–234.

Brugarolas, J., Lei, K., Hurley, R. L., Manning, B. D., Reiling, J. H., Hafen, E., Witters, L. A., Ellisen, L. W., and Kaelin Jr., W. G. (2004). Regulation of mTOR function in response to hypoxia by REDD1 and the TSC1/TSC2 tumor suppressor complex. *Genes Dev* **18**, 2893–2904.

Bruick, R. K., and McKnight, S. L. (2001). A conserved family of prolyl-4-hydroxylases that modify HIF. *Science* **294**, 1337–1340.

Brukamp, K., Jim, B., Moeller, M. J., and Haase, V. H. (2007). Hypoxia and podocyte-specific Vhlh deletion confer risk of glomerular disease. *Am. J. Physiol. Renal Physiol* **293**, F1397–F1407.

Bussmann, J., Lawson, N., Zon, L., and Schulte-Merker, S. (2008). Zebrafish VEGF receptors: a guideline to nomenclature. *PLoS Genet* **4**, e1000064.

Carradice, D., and Lieschke, G. J. (2008). Zebrafish in hematology: sushi or science? *Blood* **111**, 3331–3342.

Champion, K. J., Guinea, M., Dammai, V., and Hsu, T. (2008). Endothelial function of von Hippel–Lindau tumor suppressor gene: control of fibroblast growth factor receptor signaling. *Cancer Res* **68**, 4649–4657.

Chen, F., Kishida, T., Yao, M., Hustad, T., Glavac, D., Dean, M., Gnarra, J. R., Orcutt, M. L., Duh, F. M., and Glenn, G., *et al*. (1995). Germline mutations in the von Hippel–Lindau disease tumor suppressor gene: correlations with phenotype. *Hum. Mutat* **5**, 66–75.

Chew, E. Y. (2005). Ocular manifestations of von Hippel–Lindau disease: clinical and genetic investigations. *Trans. Am. Ophthalmol. Soc* **103**, 495–511.

Chitalia, V. C., Foy, R. L., Bachschmid, M. M., Zeng, L., Panchenko, M. V., Zhou, M. I., Bharti, A., Seldin, D. C., Lecker, S. H., Dominguez, I., and Cohen, H. T. (2008). Jade-1 inhibits Wnt signalling by ubiquitylating beta-catenin and mediates Wnt pathway inhibition by pVHL. *Nat. Cell Biol* **10**, 1208–1216.

Clifford, S. C., Cockman, M. E., Smallwood, A. C., Mole, D. R., Woodward, E. R., Maxwell, P. H., Ratcliffe, P. J., and Maher, E. R. (2001). Contrasting effects on HIF-1alpha regulation by disease-causing pVHL mutations correlate with patterns of tumourigenesis in von Hippel–Lindau disease. *Hum. Mol. Genet* **10**, 1029–1038.

Covassin, L. D., Villefranc, J. A., Kacergis, M. C., Weinstein, B. M., and Lawson, N. D. (2006). Distinct genetic interactions between multiple Vegf receptors are required for development of different blood vessel types in zebrafish. *Proc. Natl. Acad. Sci. U. S. A* **103**, 6554–6559.

Cramer, T., Yamanishi, Y., Clausen, B. E., Forster, I., Pawlinski, R., Mackman, N., Haase, V. H., Jaenisch, R., Corr, M., Nizet, V., Firestein, G. S., Gerber, H. P., Ferrara, N., and Johnson, R. S. (2003). HIF-1alpha is essential for myeloid cell-mediated inflammation. *Cell* **112**, 645–657.

de Jong, J. L., and Zon, L. I. (2005). Use of the zebrafish system to study primitive and definitive hematopoiesis. *Annu. Rev. Genet* **39**, 481–501.

Ding, M., Cui, S., Li, C., Jothy, S., Haase, V., Steer, B. M., Marsden, P. A., Pippin, J., Shankland, S., Rastaldi, M. P., Cohen, C. D., Kretzler, M., and Quaggin, S. E. (2006). Loss of the tumor suppressor Vhlh leads to upregulation of Cxcr4 and rapidly progressive glomerulonephritis in mice. *Nat. Med* **12**, 1081–1087.

Doyon, Y., McCammon, J. M., Miller, J. C., Faraji, F., Ngo, C., Katibah, G. E., Amora, R., Hocking, T. D., Zhang, L., Rebar, E. J., Gregory, P. D., Urnov, F. D., and Amacher, S. L. (2008). Heritable targeted gene disruption in zebrafish using designed zinc-finger nucleases. *Nat. Biotechnol* **26**, 702–708.

Drummond, I. A. (2005). Kidney development and disease in the zebrafish. *J. Am. Soc. Nephrol* **16**, 299–304.

Duan, D. R., Pause, A., Burgess, W. H., Aso, T., Chen, D. Y., Garrett, K. P., Conaway, R. C., Conaway, J. W., Linehan, W. M., and Klausner, R. D. (1995). Inhibition of transcription elongation by the VHL tumor suppressor protein. *Science* **269**, 1402–1406.

Ebert, B. L., Firth, J. D., and Ratcliffe, P. J. (1995). Hypoxia and mitochondrial inhibitors regulate expression of glucose transporter-1 via distinct Cis-acting sequences. *J. Biol. Chem* **270**, 29083–29089.

Eley, L., Yates, L. M., and Goodship, J. A. (2005). Cilia and disease. *Curr. Opin. Genet. Dev* **15**, 308–314.

Epstein, A. C., Gleadle, J. M., McNeill, L. A., Hewitson, K. S., O'Rourke, J., Mole, D. R., Mukherji, M., Metzen, E., Wilson, M. I., Dhanda, A., Tian, Y. M., Masson, N., Hamilton, D. L., Jaakkola, P., Barstead, R., Hodgkin, J., Maxwell, P. H., Pugh, C. W., Schofield, C. J., and Ratcliffe, P. J. (2001). *C. elegans* EGL-9 and mammalian homologs define a family of dioxygenases that regulate HIF by prolyl hydroxylation. *Cell* **107**, 43–54.

Erler, J. T., Bennewith, K. L., Nicolau, M., Dornhofer, N., Kong, C., Le, Q. T., Chi, J. T., Jeffrey, S. S., and Giaccia, A. J. (2006). Lysyl oxidase is essential for hypoxia-induced metastasis. *Nature* **440**, 1222–1226.

Esteban, M. A., Harten, S. K., Tran, M. G., and Maxwell, P. H. (2006). Formation of primary cilia in the renal epithelium is regulated by the von Hippel–Lindau tumor suppressor protein. *J. Am. Soc. Nephrol* **17**, 1801–1806.

Esteban-Barragan, M. A., Avila, P., Alvarez-Tejado, M., Gutierrez, M. D., Garcia-Pardo, A., Sanchez-Madrid, F., and Landazuri, M. O. (2002). Role of the von Hippel–Lindau tumor suppressor gene in the formation of beta1-integrin fibrillar adhesions. *Cancer Res* **62**, 2929–2936.

Fan, S., Hurd, T. W., Liu, C. J., Straight, S. W., Weimbs, T., Hurd, E. A., Domino, S. E., and Margolis, B. (2004). Polarity proteins control ciliogenesis via kinesin motor interactions. *Curr. Biol* **14**, 1451–1461.

Feijoo-Cuaresma, M., Mendez, F., Maqueda, A., Esteban, M. A., Naranjo-Suarez, S., Castellanos, M. C., del Cerro, M. H., Vazquez, S. N., Garcia-Pardo, A., Landazuri, M. O., and Calzada, M. J. (2008). Inadequate activation of the GTPase RhoA contributes to the lack of fibronectin matrix assembly in von Hippel–Lindau protein-defective renal cancer cells. *J. Biol. Chem* **283**, 24982–24990.

Feitsma, H., and Cuppen, E. (2008). Zebrafish as a cancer model. *Mol. Cancer Res* **6**, 685–694.

Forsythe, J. A., Jiang, B. H., Iyer, N. V., Agani, F., Leung, S. W., Koos, R. D., and Semenza, G. L. (1996). Activation of vascular endothelial growth factor gene transcription by hypoxia-inducible factor 1. *Mol. Cell. Biol* **16**, 4604–4613.

Frew, I. J., and Krek, W. (2007). Multitasking by pVHL in tumour suppression. *Curr. Opin. Cell Biol* **19**, 685–690.

Frew, I. J., and Krek, W. (2008). pVHL: a multipurpose adaptor protein. *Sci. Signal* **1**, pe30.

Frew, I. J., Minola, A., Georgiev, S., Hitz, M., Moch, H., Richard, S., Vortmeyer, A. O., and Krek, W. (2008a). Combined VHLH and PTEN mutation causes genital tract cystadenoma and squamous metaplasia. *Mol. Cell. Biol* **28**, 4536–4548.

Frew, I. J., Thoma, C. R., Georgiev, S., Minola, A., Hitz, M., Montani, M., Moch, H., and Krek, W. (2008b). pVHL and PTEN tumour suppressor proteins cooperatively suppress kidney cyst formation. *EMBO J* **27**, 1747–1757.

Glasker, S., Li, J., Xia, J. B., Okamoto, H., Zeng, W., Lonser, R. R., Zhuang, Z., Oldfield, E. H., and Vortmeyer, A. O. (2006). Hemangioblastomas share protein expression with embryonal hemangioblast progenitor cell. *Cancer Res* **66**, 4167–4172.

Gnarra, J. R., Ward, J. M., Porter, F. D., Wagner, J. R., Devor, D. E., Grinberg, A., Emmert-Buck, M. R., Westphal, H., Klausner, R. D., and Linehan, W. M. (1997). Defective placental vasculogenesis causes embryonic lethality in VHL-deficient mice. *Proc. Natl. Acad. Sci. U. S. A* **94**, 9102–9107.

Gordeuk, V. R., Sergueeva, A. I., Miasnikova, G. Y., Okhotin, D., Voloshin, Y., Choyke, P. L., Butman, J. A., Jedlickova, K., Prchal, J. T., and Polyakova, L. A. (2004). Congenital disorder of oxygen sensing: association of the homozygous Chuvash polycythemia VHL mutation with thrombosis and vascular abnormalities but not tumors. *Blood* **103**, 3924–3932.

Gordeuk, V. R., Stockton, D. W., and Prchal, J. T. (2005). Congenital polycythemias/erythrocytoses. *Haematologica* **90**, 109–116.

Grosfeld, A., Stolze, I. P., Cockman, M. E., Pugh, C. W., Edelmann, M., Kessler, B., Bullock, A. N., Ratcliffe, P. J., and Masson, N. (2007). Interaction of hydroxylated collagen IV with the von Hippel–Lindau tumor suppressor. *J. Biol. Chem* **282**, 13264–13269.

Haase, V. H. (2005). The VHL tumor suppressor in development and disease: functional studies in mice by conditional gene targeting. *Semin. Cell Dev. Biol* **16**, 564–574.

Haase, V. H., Glickman, J. N., Socolovsky, M., and Jaenisch, R. (2001). Vascular tumors in livers with targeted inactivation of the von Hippel–Lindau tumor suppressor. *Proc. Natl. Acad. Sci. U. S. A* **98**, 1583–1588.

Hergovich, A., Lisztwan, J., Barry, R., Ballschmieter, P., and Krek, W. (2003). Regulation of microtubule stability by the von Hippel–Lindau tumour suppressor protein pVHL. *Nat. Cell Biol* **5**, 64–70.

Herpers, R., van de Kamp, E., Duckers, H. J., and Schulte-Merker, S. (2008). Redundant roles for sox7 and sox18 in arteriovenous specification in zebrafish. *Circ. Res* **102**, 12–15.

Hickey, M. M., Lam, J. C., Bezman, N. A., Rathmell, W. K., and Simon, M. C. (2007). von Hippel–Lindau mutation in mice recapitulates Chuvash polycythemia via hypoxia-inducible factor-2alpha signaling and splenic erythropoiesis. *J. Clin. Invest* **117**, 3879–3889.

Hickey, M. M., Richardson, T., Wang, T., Mosqueira, M., Arguiri, E., Yu, H., Yu, Q. C., Solomides, C. C., Morrisey, E. E., Khurana, T. S., Christofidou-Solomidou, M., and Simon, M. C. (2010). The von Hippel–Lindau Chuvash mutation promotes pulmonary hypertension and fibrosis in mice. *J. Clin. Invest* **120**, 827–839.

Hoffman, M. A., Ohh, M., Yang, H., Klco, J. M., Ivan, M., and Kaelin Jr., W. G. (2001). von Hippel–Lindau protein mutants linked to type 2C VHL disease preserve the ability to downregulate HIF. *Hum. Mol. Genet* **10**, 1019–1027.

Hong, S. B., Furihata, M., Baba, M., Zbar, B., and Schmidt, L. S. (2006). Vascular defects and liver damage by the acute inactivation of the VHL gene during mouse embryogenesis. *Lab. Invest* **86**, 664–675.

Hsouna, A., Nallamothu, G., Kose, N., Guinea, M., Dammai, V., and Hsu, T. (2010). *Drosophila* von Hippel–Lindau tumor suppressor gene function in epithelial tubule morphogenesis. *Mol. Cell. Biol* **30**, 3779–3794.

Hsu, T., Adereth, Y., Kose, N., and Dammai, V. (2006). Endocytic function of von Hippel–Lindau tumor suppressor protein regulates surface localization of fibroblast growth factor receptor 1 and cell motility. *J. Biol. Chem* **281**, 12069–12080.

Iliopoulos, O., Kibel, A., Gray, S., and Kaelin Jr., W. G. (1995). Tumour suppression by the human von Hippel–Lindau gene product. *Nat. Med* **1**, 822–826.

Iliopoulos, O., Ohh, M., and Kaelin Jr., W. G. (1998). pVHL19 is a biologically active product of the von Hippel–Lindau gene arising from internal translation initiation. *Proc. Natl. Acad. Sci. U. S. A* **95**, 11661–11666.

Ivan, M., Kondo, K., Yang, H., Kim, W., Valiando, J., Ohh, M., Salic, A., Asara, J. M., Lane, W. S., and Kaelin Jr., W. G. (2001). HIFalpha targeted for VHL-mediated destruction by proline hydroxylation: implications for O2 sensing. *Science* **292**, 464–468.

Jaakkola, P., Mole, D. R., Tian, Y. M., Wilson, M. I., Gielbert, J., Gaskell, S. J., Kriegsheim, A., Hebestreit, H. F., Mukherji, M., Schofield, C. J., Maxwell, P. H., Pugh, C. W., and Ratcliffe, P. J. (2001). Targeting of HIF-alpha to the von Hippel–Lindau ubiquitylation complex by O2-regulated prolyl hydroxylation. *Science* **292**, 468–472.

Jarrell, S. T., Vortmeyer, A. O., Linehan, W. M., Oldfield, E. H., and Lonser, R. R. (2006). Metastases to hemangioblastomas in von Hippel–Lindau disease. *J. Neurosurg* **105**, 256–263.

Jonz, M. G., and Nurse, C. A. (2005). Development of oxygen sensing in the gills of zebrafish. *J. Exp. Biol* **208**, 1537–1549.

Kaelin, W. G. (2005). The von Hippel–Lindau tumor suppressor protein: roles in cancer and oxygen sensing. *Cold Spring Harb. Symp. Quant. Biol* **70**, 159–166.

Kaelin Jr., W. G. (2007). The von Hippel–Lindau tumor suppressor protein and clear cell renal carcinoma. *Clin. Cancer Res* **13**, 680s–684s.

Kamura, T., Koepp, D. M., Conrad, M. N., Skowyra, D., Moreland, R. J., Iliopoulos, O., Lane, W. S., Kaelin Jr., W. G., Elledge, S. J., Conaway, R. C., Harper, J. W., and Conaway, J. W. (1999). Rbx1, a component of the VHL tumor suppressor complex and SCF ubiquitin ligase. *Science* **284**, 657–661.

Karhausen, J., Furuta, G. T., Tomaszewski, J. E., Johnson, R. S., Colgan, S. P., and Haase, V. H. (2004). Epithelial hypoxia-inducible factor-1 is protective in murine experimental colitis. *J. Clin. Invest* **114**, 1098–1106.

Kibel, A., Iliopoulos, O., DeCaprio, J. A., and Kaelin Jr., W. G. (1995). Binding of the von Hippel–Lindau tumor suppressor protein to Elongin B and C. *Science* **269**, 1444–1446.

Kikuchi, Y., Kobayashi, E., Nishizawa, M., Hamazaki, S., Okada, S., and Hino, O. (1995). Cloning of the rat homologue of the von Hippel–Lindau tumor suppressor gene and its non-somatic mutation in rat renal cell carcinomas. *Jpn. J. Cancer Res* **86**, 905–909.

Kim, W. Y., and Kaelin, W. G. (2004). Role of VHL gene mutation in human cancer. *J. Clin. Oncol* **22**, 4991–5004.

Kleymenova, E., Everitt, J. I., Pluta, L., Portis, M., Gnarra, J. R., and Walker, C. L. (2004). Susceptibility to vascular neoplasms but no increased susceptibility to renal carcinogenesis in Vhl knockout mice. *Carcinogenesis* **25**, 309–315.

Knudson Jr, A. G. (1971). Mutation and cancer: statistical study of retinoblastoma. *Proc. Natl. Acad. Sci. U. S. A* **68**, 820–823.

Koivunen, P., Hirsila, M., Gunzler, V., Kivirikko, K. I., and Myllyharju, J. (2004). Catalytic properties of the asparaginyl hydroxylase (FIH) in the oxygen sensing pathway are distinct from those of its prolyl 4-hydroxylases. *J. Biol. Chem* **279**, 9899–9904.

Koochekpour, S., Jeffers, M., Wang, P. H., Gong, C., Taylor, G. A., Roessler, L. M., Stearman, R., Vasselli, J. R., Stetler-Stevenson, W. G., Kaelin Jr., W. G., Linehan, W. M., Klausner, R. D., Gnarra, J. R., and Vande Woude, G. F. (1999). The von Hippel–Lindau tumor suppressor gene inhibits hepatocyte growth factor/scatter factor-induced invasion and branching morphogenesis in renal carcinoma cells. *Mol. Cell. Biol* **19**, 5902–5912.

Kryczek, I., Lange, A., Mottram, P., Alvarez, X., Cheng, P., Hogan, M., Moons, L., Wei, S., Zou, L., Machelon, V., Emilie, D., Terrassa, M., Lackner, A., Curiel, T. J., Carmeliet, P., and Zou, W. (2005). CXCL12 and vascular endothelial growth factor synergistically induce neoangiogenesis in human ovarian cancers. *Cancer Res* **65**, 465–472.

Kuehn, E. W., Walz, G., and Benzing, T. (2007). von Hippel–Lindau: a tumor suppressor links microtubules to ciliogenesis and cancer development. *Cancer Res* **67**, 4537–4540.

Kurban, G., Duplan, E., Ramlal, N., Hudon, V., Sado, Y., Ninomiya, Y., and Pause, A. (2008). Collagen matrix assembly is driven by the interaction of von Hippel–Lindau tumor suppressor protein with hydroxylated collagen IV alpha 2. *Oncogene* **27**, 1004–1012.

Kurban, G., Hudon, V., Duplan, E., Ohh, M., and Pause, A. (2006). Characterization of a von Hippel Lindau pathway involved in extracellular matrix remodeling, cell invasion, and angiogenesis. *Cancer Res* **66**, 1313–1319.

Lach, B., Gregor, A., Rippstein, P., and Omulecka, A. (1999). Angiogenic histogenesis of stromal cells in hemangioblastoma: ultrastructural and immunohistochemical study. *Ultrastruct. Pathol* **23**, 299–310.

Latif, F., Tory, K., Gnarra, J., Yao, M., Duh, F. M., Orcutt, M. L., Stackhouse, T., Kuzmin, I., Modi, W., and Geil, L., *et al*. (1993). Identification of the von Hippel–Lindau disease tumor suppressor gene. *Science* **260**, 1317–1320.

Lee, S., Nakamura, E., Yang, H., Wei, W., Linggi, M. S., Sajan, M. P., Farese, R. V., Freeman, R. S., Carter, B. D., Kaelin Jr., W. G., and Schlisio, S. (2005). Neuronal apoptosis linked to EglN3 prolyl hydroxylase and familial pheochromocytoma genes: developmental culling and cancer. *Cancer Cell* **8**, 155–167.

Lei, L., Mason, S., Liu, D., Huang, Y., Marks, C., Hickey, R., Jovin, I. S., Pypaert, M., Johnson, R. S., and Giordano, F. J. (2008). Hypoxia-inducible factor-dependent degeneration, failure, and malignant transformation of the heart in the absence of the von Hippel–Lindau protein. *Mol. Cell. Biol* **28**, 3790–3803.

Lieschke, G. J., and Currie, P. D. (2007). Animal models of human disease: zebrafish swim into view. *Nat. Rev. Genet* **8**, 353–367.

Lolkema, M. P., Mans, D. A., Snijckers, C. M., van Noort, M., van Beest, M., Voest, E. E., and Giles, R. H. (2007). The von Hippel–Lindau tumour suppressor interacts with microtubules through kinesin-2. *FEBS Lett.* **581**, 4571–4576.

Lolkema, M. P., Mans, D. A., Ulfman, L. H., Volpi, S., Voest, E. E., and Giles, R. H. (2008). Allele-specific regulation of primary cilia function by the von Hippel–Lindau tumor suppressor. *Eur. J. Hum. Genet* **16**, 73–78.

Lonser, R. R., Glenn, G. M., Walther, M., Chew, E. Y., Libutti, S. K., Linehan, W. M., and Oldfield, E. H. (2003). von Hippel–Lindau disease. *Lancet* **361**, 2059–2067.

Lutz, M. S., and Burk, R. D. (2006). Primary cilium formation requires von Hippel–Lindau gene function in renal-derived cells. *Cancer Res* **66**, 6903–6907.

Ma, W., Tessarollo, L., Hong, S. B., Baba, M., Southon, E., Back, T. C., Spence, S., Lobe, C. G., Sharma, N., Maher, G. W., Pack, S., Vortmeyer, A. O., Guo, C., Zbar, B., and Schmidt, L. S. (2003). Hepatic vascular tumors, angiectasis in multiple organs, and impaired spermatogenesis in mice with conditional inactivation of the VHL gene. *Cancer Res* **63**, 5320–5328.

Ma, A. C., Ward, A. C., Liang, R., and Leung, A. Y. (2007). The role of jak2a in zebrafish hematopoiesis. *Blood* **110**, 1824–1830.

Maher, E. R., Iselius, L., Yates, J. R., Littler, M., Benjamin, C., Harris, R., Sampson, J., Williams, A., Ferguson-Smith, M. A., and Morton, N. (1991). von Hippel–Lindau disease: a genetic study. *J. Med. Genet* **28**, 443–447.

Maher, E. R., and Kaelin Jr., W. G. (1997). von Hippel–Lindau disease. *Medicine (Baltimore)* **76**, 381–391.

Maher, E. R., Yates, J. R., Harries, R., Benjamin, C., Harris, R., Moore, A. T., and Ferguson-Smith, M. A. (1990). Clinical features and natural history of von Hippel–Lindau disease. *Q. J. Med* **77**, 1151–1163.

Mahon, P. C., Hirota, K., and Semenza, G. L. (2001). FIH-1: a novel protein that interacts with HIF-1alpha and VHL to mediate repression of HIF-1 transcriptional activity. *Genes Dev* **15**, 2675–2686.

Mandriota, S. J., Turner, K. J., Davies, D. R., Murray, P. G., Morgan, N. V., Sowter, H. M., Wykoff, C. C., Maher, E. R., Harris, A. L., Ratcliffe, P. J., and Maxwell, P. H. (2002). HIF activation identifies early lesions in VHL kidneys: evidence for site-specific tumor suppressor function in the nephron. *Cancer Cell* **1**, 459–468.

Maxwell, P. H., Wiesener, M. S., Chang, G. W., Clifford, S. C., Vaux, E. C., Cockman, M. E., Wykoff, C. C., Pugh, C. W., Maher, E. R., and Ratcliffe, P. J. (1999). The tumour suppressor protein VHL targets hypoxia-inducible factors for oxygen-dependent proteolysis. *Nature* **399**, 271–275.

McGrath, F. P., Gibney, R. G., Morris, D. C., Owen, D. A., and Erb, S. R. (1992). Case report: multiple hepatic and pulmonary haemangioblastomas – a new manifestation of von Hippel–Lindau disease. *Clin. Radiol* **45**, 37–39.

Mehta, G. U., Shively, S. B., Duong, H., Tran, M. G., Moncrief, T. J., Smith, J. H., Li, J., Edwards, N. A., Lonser, R. R., Zhuang, Z., Merrill, M. J., Raffeld, M., Maxwell, P. H., Oldfield, E. H., and Vortmeyer, A. O. (2008). Progression of epididymal maldevelopment into hamartoma-like neoplasia in VHL disease. *Neoplasia* **10**, 1146–1153.

Meng, X., Noyes, M. B., Zhu, L. J., Lawson, N. D., and Wolfe, S. A. (2008). Targeted gene inactivation in zebrafish using engineered zinc-finger nucleases. *Nat. Biotechnol* **26**, 695–701.

Mikhaylova, O., Ignacak, M. L., Barankiewicz, T. J., Harbaugh, S. V., Yi, Y., Maxwell, P. H., Schneider, M., Van Geyte, K., Carmeliet, P., Revelo, M. P., Wyder, M., Greis, K. D., Meller, J., and Czyzyk-Krzeska, M. F. (2008). The von Hippel–Lindau tumor suppressor protein and Egl-9-type proline hydroxylases regulate the large subunit of RNA polymerase II in response to oxidative stress. *Mol. Cell. Biol* **28**, 2701–2717.

Minchenko, A., Leshchinsky, I., Opentanova, I., Sang, N., Srinivas, V., Armstead, V., and Caro, J. (2002). Hypoxia-inducible factor-1-mediated expression of the 6-phosphofructo-2-kinase/fructose-2,6-bisphosphatase-3 (PFKFB3) gene. Its possible role in the Warburg effect. *J. Biol. Chem* **277**, 6183–6187.

Motzer, R. J., Bander, N. H., and Nanus, D. M. (1996). Renal-cell carcinoma. *N. Engl. J. Med* **335**, 865–875.

Neumann, H. P., and Wiestler, O. D. (1991). Clustering of features of von Hippel–Lindau syndrome: evidence for a complex genetic locus. *Lancet* **337**, 1052–1054.

Neumann, A. K., Yang, J., Biju, M. P., Joseph, S. K., Johnson, R. S., Haase, V. H., Freedman, B. D., and Turka, L. A. (2005). Hypoxia inducible factor 1 alpha regulates T cell receptor signal transduction. *Proc. Natl. Acad. Sci. U. S. A* **102**, 17071–17076.

Nordstrom-O'Brien, M., van der Luijt, R. B., van Rooijen, E., van den Ouweland, A. M., Majoor-Krakauer, D. F., Lolkema, M. P., van Brussel, A., Voest, E. E., and Giles, R. H. (2010). Genetic analysis of von Hippel–Lindau disease. *Hum. Mutat* **31**, 521–537.

Ohh, M., Yauch, R. L., Lonergan, K. M., Whaley, J. M., Stemmer-Rachamimov, A. O., Louis, D. N., Gavin, B. J., Kley, N., Kaelin Jr., W. G., and Iliopoulos, O. (1998). The von Hippel–Lindau tumor suppressor protein is required for proper assembly of an extracellular fibronectin matrix. *Mol. Cell* **1**, 959–968.

Paffett-Lugassy, N., Hsia, N., Fraenkel, P. G., Paw, B., Leshinsky, I., Barut, B., Bahary, N., Caro, J., Handin, R., and Zon, L. I. (2007). Functional conservation of erythropoietin signaling in zebrafish. *Blood* **110**, 2718–2726.

Pause, A., Lee, S., Worrell, R. A., Chen, D. Y., Burgess, W. H., Linehan, W. M., and Klausner, R. D. (1997). The von Hippel–Lindau tumor-suppressor gene product forms a stable complex with human CUL-2, a member of the Cdc53 family of proteins. *Proc. Natl. Acad. Sci. U. S. A* **94**, 2156–2161.

Peyssonnaux, C., Zinkernagel, A. S., Schuepbach, R. A., Rankin, E., Vaulont, S., Haase, V. H., Nizet, V., and Johnson, R. S. (2007). Regulation of iron homeostasis by the hypoxia-inducible transcription factors (HIFs). *J. Clin. Invest* **117**, 1926–1932.

Pfander, D., Kobayashi, T., Knight, M. C., Zelzer, E., Chan, D. A., Olsen, B. R., Giaccia, A. J., Johnson, R. S., Haase, V. H., and Schipani, E. (2004). Deletion of Vhlh in chondrocytes reduces cell proliferation and increases matrix deposition during growth plate development. *Development* **131**, 2497–2508.

Pocock, R., and Hobert, O. (2008). Oxygen levels affect axon guidance and neuronal migration in *Caenorhabditis elegans*. *Nat. Neurosci* **11**, 894–900.

Qi, H., Gervais, M. L., Li, W., DeCaprio, J. A., Challis, J. R., and Ohh, M. (2004). Molecular cloning and characterization of the von Hippel–Lindau-like protein. *Mol. Cancer Res* **2**, 43–52.

Rankin, E. B., Higgins, D. F., Walisser, J. A., Johnson, R. S., Bradfield, C. A., and Haase, V. H. (2005). Inactivation of the arylhydrocarbon receptor nuclear translocator (Arnt) suppresses von Hippel–Lindau disease-associated vascular tumors in mice. *Mol. Cell. Biol* **25**, 3163–3172.

Rankin, E. B., Tomaszewski, J. E., and Haase, V. H. (2006). Renal cyst development in mice with conditional inactivation of the von Hippel–Lindau tumor suppressor. *Cancer Res* **66**, 2576–2583.

Richard, S., David, P., Marsot-Dupuch, K., Giraud, S., Beroud, C., and Resche, F. (2000). Central nervous system hemangioblastomas, endolymphatic sac tumors, and von Hippel–Lindau disease. *Neurosurg. Rev* **23**, 1–22 (discussion 23-24).

Roe, J. S., Kim, H., Lee, S. M., Kim, S. T., Cho, E. J., and Youn, H. D. (2006). p53 stabilization and transactivation by a von Hippel–Lindau protein. *Mol. Cell* **22**, 395–405.

Rojiani, A. M., Owen, D. A., Berry, K., Woodhurst, B., Anderson, F. H., Scudamore, C. H., and Erb, S. (1991). Hepatic hemangioblastoma. An unusual presentation in a patient with von Hippel–Lindau disease. *Am. J. Surg. Pathol* **15**, 81–86.

Ruas, J. L., and Poellinger, L. (2005). Hypoxia-dependent activation of HIF into a transcriptional regulator. *Semin. Cell Dev. Biol* **16**, 514–522.

Schermer, B., Ghenoiu, C., Bartram, M., Muller, R. U., Kotsis, F., Hohne, M., Kuhn, W., Rapka, M., Nitschke, R., Zentgraf, H., Fliegauf, M., Omran, H., Walz, G., and Benzing, T. (2006). The von Hippel–Lindau tumor suppressor protein controls ciliogenesis by orienting microtubule growth. *J. Cell Biol* **175**, 547–554.

Schoenfeld, A., Davidowitz, E. J., and Burk, R. D. (1998). A second major native von Hippel–Lindau gene product, initiated from an internal translation start site, functions as a tumor suppressor. *Proc. Natl. Acad. Sci. U. S. A* **95**, 8817–8822.

Seizinger, B. R., Rouleau, G. A., Ozelius, L. J., Lane, A. H., Farmer, G. E., Lamiell, J. M., Haines, J., Yuen, J. W., Collins, D., and Majoor-Krakauer, D., *et al*. (1988). von Hippel–Lindau disease maps to the region of chromosome 3 associated with renal cell carcinoma. *Nature* **332**, 268–269.

Semenza, G. L. (2001). HIF-1, O(2), and the 3 PHDs: how animal cells signal hypoxia to the nucleus. *Cell* **107**, 1–3.

Semenza, G. L. (2009). Regulation of vascularization by hypoxia-inducible factor 1. *Ann. N. Y. Acad. Sci* **1177**, 2–8.

Semenza, G. L., Roth, P. H., Fang, H. M., and Wang, G. L. (1994). Transcriptional regulation of genes encoding glycolytic enzymes by hypoxia-inducible factor 1. *J. Biol. Chem* **269**, 23757–23763.

Shen, C., Nettleton, D., Jiang, M., Kim, S. K., and Powell-Coffman, J. A. (2005). Roles of the HIF-1 hypoxia-inducible factor during hypoxia response in *Caenorhabditis elegans*. *J. Biol. Chem* **280**, 20580–20588.

Shiao, Y. H., Diwan, B. A., Perantoni, A. O., Calvert, R. J., Zbar, B., Lerman, M. I., and Rice, J. M. (1997). Polymerase chain reaction-single-strand conformation polymorphism analysis for the VHL gene in chemically induced kidney tumors of rats using intron-derived primers. *Mol. Carcinog* **19**, 230–235.

Shively, S., Beltaifa, S., Gehrs, B., Duong, H., Smith, J., Edwards, N., Lonser, R., Raffeld, M., and Vortmeyer, A. (2008). Protracted haemangioblastic proliferation and differentiation in von Hippel–Lindau disease. *J. Pathol* **216**, 514–520.

Siekmann, A. F., Standley, C., Fogarty, K. E., Wolfe, S. A., and Lawson, N. D. (2009). Chemokine signaling guides regional patterning of the first embryonic artery. *Genes Dev* **23**, 2272–2277.

Smith, T. G., Brooks, J. T., Balanos, G. M., Lappin, T. R., Layton, D. M., Leedham, D. L., Liu, C., Maxwell, P. H., McMullin, M. F., McNamara, C. J., Percy, M. J., Pugh, C. W., Ratcliffe, P. J., Talbot, N. P., Treacy, M., and Robbins, P. A. (2006). Mutation of von Hippel–Lindau tumour suppressor and human cardiopulmonary physiology. *PLoS Med* **3**, e290.

Song, H. D., Sun, X. J., Deng, M., Zhang, G. W., Zhou, Y., Wu, X. Y., Sheng, Y., Chen, Y., Ruan, Z., Jiang, C. L., Fan, H. Y., Zon, L. I., Kanki, J. P., Liu, T. X., Look, A. T., and Chen, Z. (2004). Hematopoietic gene expression profile in zebrafish kidney marrow. *Proc. Natl. Acad. Sci. U. S. A* **101**, 16240–16245.

Staller, P., Sulitkova, J., Lisztwan, J., Moch, H., Oakeley, E. J., and Krek, W. (2003). Chemokine receptor CXCR4 downregulated by von Hippel–Lindau tumour suppressor pVHL. *Nature* **425**, 307–311.

Stickle, N. H., Chung, J., Klco, J. M., Hill, R. P., Kaelin Jr., W. G., and Ohh, M. (2004). pVHL modification by NEDD8 is required for fibronectin matrix assembly and suppression of tumor development. *Mol. Cell. Biol* **24**, 3251–3261.

Tang, N., Mack, F., Haase, V. H., Simon, M. C., and Johnson, R. S. (2006). pVHL function is essential for endothelial extracellular matrix deposition. *Mol. Cell. Biol* **26**, 2519–2530.

Tang, N., Wang, L., Esko, J., Giordano, F. J., Huang, Y., Gerber, H. P., Ferrara, N., and Johnson, R. S. (2004). Loss of HIF-1alpha in endothelial cells disrupts a hypoxia-driven VEGF autocrine loop necessary for tumorigenesis. *Cancer Cell* **6**, 485–495.

Taraboletti, G., and Giavazzi, R. (2004). Modelling approaches for angiogenesis. *Eur. J. Cancer* **40**, 881–889.

Thoma, C. R., Frew, I. J., Hoerner, C. R., Montani, M., Moch, H., and Krek, W. (2007). pVHL and GSK3beta are components of a primary cilium-maintenance signalling network. *Nat. Cell Biol* **9**, 588–595.

Thoma, C. R., Toso, A., Gutbrodt, K. L., Reggi, S. P., Frew, I. J., Schraml, P., Hergovich, A., Moch, H., Meraldi, P., and Krek, W. (2009). VHL loss causes spindle misorientation and chromosome instability. *Nat. Cell Biol* **11**, 994–1001.

Treinin, M., Shliar, J., Jiang, H., Powell-Coffman, J. A., Bromberg, Z., and Horowitz, M. (2003). HIF-1 is required for heat acclimation in the nematode *Caenorhabditis elegans*. *Physiol. Genomics* **14**, 17–24.

Van Poppel, H., Nilsson, S., Algaba, F., Bergerheim, U., Dal Cin, P., Fleming, S., Hellsten, S., Kirkali, Z., Klotz, L., Lindblad, P., Ljungberg, B., Mulders, P., Roskams, T., Ross, R. K., Walker, C., and Wersall, P. (2000). Precancerous lesions in the kidney. *Scand. J. Urol. Nephrol. Suppl* 136–165.

van Rooijen, E., Voest, E. E., Logister, I., Bussmann, J., Korving, J., van Eeden, F. J., Giles, R. H., and Schulte-Merker, S. (2010). von Hippel–Lindau tumor suppressor mutants faithfully model pathological hypoxia-driven angiogenesis and vascular retinopathies in zebrafish. *Dis. Model Mech* **3**, 343–353.

van Rooijen, E., Voest, E. E., Logister, I., Korving, J., Schwerte, T., Schulte-Merker, S., Giles, R. H., and van Eeden, F. J. (2009). Zebrafish mutants in the von Hippel–Lindau tumor suppressor display a hypoxic response and recapitulate key aspects of Chuvash polycythemia. *Blood* **113**, 6449–6460.

Vogel, A. M., and Weinstein, B. M. (2000). Studying vascular development in the zebrafish. *Trends Cardiovasc. Med* **10**, 352–360.

Walker, C., Ahn, Y. T., Everitt, J., and Yuan, X. (1996). Renal cell carcinoma development in the rat independent of alterations at the VHL gene locus. *Mol. Carcinog* **15**, 154–161.

Walther, M. M., Lubensky, I. A., Venzon, D., Zbar, B., and Linehan, W. M. (1995). Prevalence of microscopic lesions in grossly normal renal parenchyma from patients with von Hippel–Lindau disease, sporadic renal cell carcinoma and no renal disease: clinical implications. *J. Urol* **154**, 2010–2014 (discussion 2014–2015).

Wang, Y., Roche, O., Yan, M. S., Finak, G., Evans, A. J., Metcalf, J. L., Hast, B. E., Hanna, S. C., Wondergem, B., Furge, K. A., Irwin, M. S., Kim, W. Y., Teh, B. T., Grinstein, S., Park, M., Marsden, P. A., and Ohh, M. (2009). Regulation of endocytosis via the oxygen-sensing pathway. *Nat. Med* **15**, 319–324.

Wang, Y., Wan, C., Deng, L., Liu, X., Cao, X., Gilbert, S. R., Bouxsein, M. L., Faugere, M. C., Guldberg, R. E., Gerstenfeld, L. C., Haase, V. H., Johnson, R. S., Schipani, E., and Clemens, T. L. (2007). The hypoxia-inducible factor alpha pathway couples angiogenesis to osteogenesis during skeletal development. *J. Clin. Invest* **117**, 1616–1626.

Welford, S. M., Dorie, M. J., Li, X., Haase, V. H., and Giaccia, A. J. (2010). Renal oxygenation suppresses VHL-loss-induced senescence that is caused by increased sensitivity to oxidative stress. *Mol. Cell. Biol.* **30**, 4595–4603.

Wenger, R. H. (2002). Cellular adaptation to hypoxia: O2-sensing protein hydroxylases, hypoxia-inducible transcription factors, and O2-regulated gene expression. *FASEB J* **16**, 1151–1162.

Wienholds, E., van Eeden, F., Kosters, M., Mudde, J., Plasterk, R. H., and Cuppen, E. (2003). Efficient target-selected mutagenesis in zebrafish. *Genome Res* **13**, 2700–2707.

Wingert, R. A., and Davidson, A. J. (2008). The zebrafish pronephros: a model to study nephron segmentation. *Kidney Int* **73**, 1120–1127.

Yang, H., Minamishima, Y. A., Yan, Q., Schlisio, S., Ebert, B. L., Zhang, X., Zhang, L., Kim, W. Y., Olumi, A. F., and Kaelin Jr., W. G. (2007). pVHL acts as an adaptor to promote the inhibitory phosphorylation of the NF-kappaB agonist Card9 by CK2. *Mol. Cell* **28**, 15–27.

Yaqoob, N., and Schwerte, T. (2010). Cardiovascular and respiratory developmental plasticity under oxygen depleted environment and in genetically hypoxic zebrafish (*Danio rerio*). *Comp. Biochem. Physiol. A Mol. Integr. Physiol.* **156**, 475–484.

Yoshimura, A., and Misawa, H. (1998). Physiology and function of the erythropoietin receptor. *Curr. Opin. Hematol* **5**, 171–176.

Young, A. P., Schlisio, S., Minamishima, Y. A., Zhang, Q., Li, L., Grisanzio, C., Signoretti, S., and Kaelin Jr., W. G. (2008). VHL loss actuates a HIF-independent senescence programme mediated by Rb and p400. *Nat. Cell Biol* **10**, 361–369.

Zagzag, D., Krishnamachary, B., Yee, H., Okuyama, H., Chiriboga, L., Ali, M. A., Melamed, J., and Semenza, G. L. (2005). Stromal cell-derived factor-1alpha and CXCR4 expression in hemangioblastoma and clear cell-renal cell carcinoma: von Hippel–Lindau loss-of-function induces expression of a ligand and its receptor. *Cancer Res* **65**, 6178–6188.

Zbar, B., Kishida, T., Chen, F., Schmidt, L., Maher, E. R., Richards, F. M., Crossey, P. A., Webster, A. R., Affara, N. A., Ferguson-Smith, M. A., Brauch, H., Glavac, D., Neumann, H. P., Tisherman, S., Mulvihill, J. J., Gross, D. J., Shuin, T., Whaley, J., Seizinger, B., Kley, N., Olschwang, S., Boisson, C., Richard, S., Lips, C. H., and Lerman, M., *et al*. (1996). Germline mutations in the von Hippel–Lindau disease (VHL) gene in families from North America. *Europe, and Japan. Hum. Mutat* **8**, 348–357.

Zehetner, J., Danzer, C., Collins, S., Eckhardt, K., Gerber, P. A., Ballschmieter, P., Galvanovskis, J., Shimomura, K., Ashcroft, F. M., Thorens, B., Rorsman, P., and Krek, W. (2008). PVHL is a regulator of glucose metabolism and insulin secretion in pancreatic beta cells. *Genes Dev* **22**, 3135–3146.

CHAPTER 8

Basement Membrane Diseases in Zebrafish

Natália Martins Feitosa,[*,†] Rebecca Richardson,[*,†] Wilhelm Bloch[‡,§] and Matthias Hammerschmidt[*,†,§]

[*]Institute of Developmental Biology, University of Cologne, Cologne, Germany

[†]Center for Molecular Medicine Cologne, University of Cologne, Cologne, Germany

[‡]Institute of Cardiology and Sports Medicine, German Sport University Cologne, Cologne, Germany

[§]Cologne Excellence Cluster on Cellular Stress Responses in Aging-Associated Diseases, University of Cologne, Cologne, Germany

Abstract

Basement membranes (BMs) are a complex, sheet-like network of specialized extracellular matrix that underlies epithelial cells and surrounds muscle cells. They provide adherence between neighboring tissues, permit some flexibility of these adherent structures, and can act as a store for growth factors and as a guide for cell

METHODS IN CELL BIOLOGY, VOL 105

0091-679X/10 $35.00
DOI 10.1016/B978-0-12-381320-6.00008-4

migration. The BM is not just a static structure; its deposition and remodeling are important for many processes including embryonic development, immune response, and wound healing. To date, dysfunction in BM deposition or remodeling has been linked to many human congenital disorders and diseases, affecting many different tissues in the body, including malformations, dystrophies, and cancer. However, many questions remain to be answered on the role BM proteins, and their mutations, play in the pathogenesis of human disease. In recent years, the zebrafish (*Danio rerio*) has emerged as a powerful animal model for human development and disease. In the first part of this chapter, we provide an overview of described defects caused by BM dysfunction in zebrafish, including development and function of notochord, muscle, central nervous system, skin, cardiovascular system, and kidney. In the second part, we will describe details of methods used to visualize and assess the structure of the BM in zebrafish, and to functionally analyze its different components.

I. Introduction

Basement membranes (BMs) are dense, acellular, 60- to 300-nm thick specialized, sheet-like extracellular matrix structures that underlie all epithelia, and in higher organisms BMs also underlie endothelial cells and surround muscle cells, nerve-supporting cells, and adipocytes (Kalluri, 2003; Paulsson, 1992; Yurchenco *et al.*, 2004). Many vertebrate extracellular matrix (ECM) genes evolved rather recently within the deuterostome lineage, involving an expansion and elaboration of pre-existing families (e.g. laminins and collagens), as well as the invention of novel proteins (e.g. fibronectin and tenascins). This most likely is a reflection of the versatile roles of the ECM in different species and biological processes (Hynes, 2009). In contrast the core BM components are much more ancient and found in most metazoa, suggesting that BMs were crucial for metazoan evolution (Hynes, 2009; Whittaker *et al.*, 2006). This ancient BM "toolkit" includes collagen IV, laminin, nidogen, the heparin sulfate proteoglycan (HSPG) perlecan, and type XV/XVIII collagen (Figure 1A). Laminins are heterotrimers composed of one α, one β, and one γ chain. In mammals, at least 18 isoforms isoforms have been identified, which are composed of 11 different subunits (α1–5, β1–3, γ1–3) (Colognato and Yurchenco, 2000; Durbeej, 2010). Collagen subunits are also made up of three polypeptide strands that form a triple helix and self-associate to form a cooperative quaternary structure stabilized by numerous hydrogen bonds. So far, 28 types of collagen have been identified and described (I–XXVIII), which are present at many sites throughout the body (Ricard-Blum, 2011). Each collagen is encoded either by a single or by multiple genes. Mammalian type IV collagen, the major component of BMs, is encoded by six different genes, *COL4A1–COL4A6* (Hudson *et al.*, 1993, 2003). Of these six different chains, α1 and α2 are present in all mammalian BMs, whereas the remaining chains show distinct tissue-specific expression patterns (Hudson *et al.*, 2003; Kleppel *et al.*, 1989; Nakano *et al.*, 1999, 2001; Ninomiya *et al.*, 1995). Both laminins and collagen IV contribute to proper mechanical stability within the BM. In

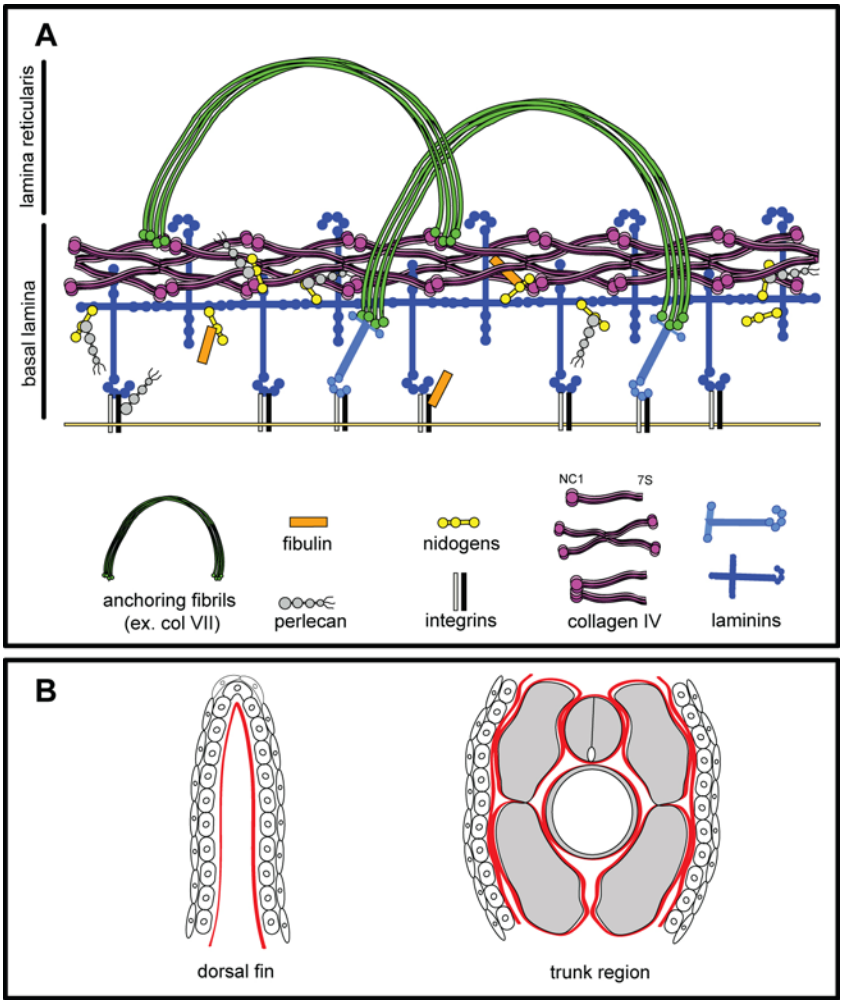

Fig. 1 (A) Simplified basement membrane (BM) diagram composed of basal lamina and lamina reticularis. This diagram contains the major components of the BM: type IV collagen, laminin, HSPGs (perlecan), and nidogen; two examples of minor components: type VII collagen and fibulins; and integrins as examples of cell adhesion molecules that bind directly to BM proteins. The localization of the molecules in the BM represents their binding partners; however, not all interactions are shown, such as type IV collagen binding to dimers of integrins. Two types of laminin are shown: the "classical" laminin structure (dark blue) and laminin5 (light blue) that has truncations of all three short arms. Type IV collagen is shown as a protomer (a trimer of α-chains) that can associate via its carboxy-terminal NC1 domain to form dimers, or via its glycosylated amino-terminal 7S region to form tetramers (diagram based on Cheng *et al.*, 1997; Kalluri, 2003; Masunaga, 2006; Yurchenco *et al.*, 2004). (B) Diagrams showing the BM of the fin and trunk of a zebrafish embryo. At this stage, the epidermis consists of two layers: the inner basal layer and the outer periderm. The BM is shown as a red line on the basal surface of the epidermis. The dermis at this time point is acellular. Adjacent BMs are connected via cross-fibers (not shown here). In the trunk of the embryo, the BM surrounds the main structures: epidermis, somites, notochord, and spinal cord. The skin is also composed of one layer of epidermis and one layer of periderm. At this stage, the BM of the epidermis is in very close proximity to the BM of the somites. (See color plate.)

addition, they can mediate attachment to adjacent epithelial cells by binding to transmembrane receptors such as integrins or dystroglycan (Fig. 1A; see also below for more details). Minor BM components include SPARC, fibulins, agrin, and type VII, XV, and XVIII collagens (Fig. 1A) (Kalluri, 2003; Yurchenco *et al.*, 2004; Yurchenco and Schittny, 1990). The BM has many vital functions including to both connect and separate epithelia and their neighboring connective tissue, as a substrate for cell migration, storage, and presentation of growth factors and as a nonimpenetrable barrier to cell invasion (Aviezer *et al.*, 1994; Gohring *et al.*, 1998; Iozzo, 2005; Kramer, 2005; Marinkovich, 2007; Rowe and Weiss, 2008; Sherwood, 2006).

Although the major BM molecules are always present, the composition of the BM can vary depending on where it is assembled, as demonstrated by tissue-specific expression patterns for several different BM component isoforms (Aumailley and Krieg, 1996; Hallmann *et al.*, 2005; Maatta *et al.*, 2004). It has also, more recently, been suggested that the expression patterns of BM components and, therefore, BM composition can not only be spatially but also temporally regulated during development (Hudson *et al.*, 2003; Saito *et al.*, 2010).

To date, much of the work performed on the composition and distribution of BM components has been performed on human tissue samples or mammalian animal models; nevertheless, zebrafish BM structure and the components of this structure are highly similar to those found in humans and mammalian models that, along with the plethora of other advantages of a lower vertebrate model, makes the zebrafish a wonderful system to study BM homeostasis, formation, and disease. Indeed, in the last few years, aided by powerful techniques of genetic manipulation and transplantation, zebrafish researchers have made crucial contributions to BM research, most of which are also relevant for human diseases, ranging from the developmental multisystem disorder Fraser syndrome (Carney *et al.*, 2010) to muscular dystrophies (Jacoby *et al.*, 2009; Thornhill *et al.*, 2008) and diabetic retinopathies (Alvarez *et al.*, 2010). Here, we will first review current zebrafish literature dealing with different developmental processes and pathologies involving BM function and dysfunction, followed by a detailed description of methods used to study BM composition and function in zebrafish.

II. Basement Membrane-Related Zebrafish Pathologies

The zebrafish BM represents a powerful biological tool for the study of the adherent properties and dynamic regulation of this specialized extracellular matrix structure as well as providing valuable insight into the pathogenesis of BM-related human disease. Forward genetic screening (see below; Driever *et al.*, 1996; Haffter *et al.*, 1996), for which zebrafish has become the predominant vertebrate model system, has identified multiple BM mutants that are related to human disease (see below). Like in other vertebrates, the homeostasis of the BM is important to maintain the flexibility and stability of a tissue. Any disruption to the connection between epithelial cells and the BM or between the BM and the underlying connective tissue

can lead to blistering, dysfunction, and even degeneration of the tissue (Carney *et al.*, 2010; Masunaga, 2006; Olasz and Yancey, 2008). In addition, basic morphogenetic processes of development can be affected, such as cell migratory processes that require the BM as a substrate or guiding structure. An overview of known zebrafish mutants with defects of BM formation, stability, or function is presented in Table I. These mutants and their phenotypes will be discussed in more detail below, together with the phenotypes of morphants, in which genes encoding BM components, binding partners, or modifiers have been knocked down via antisense morpholino oligonucleotides.

As in other vertebrates, including mammals, BMs or BM-like ECM structures are present at multiple sites of the developing zebrafish embryo, around the notochord, the somites, and the neural tube, on the basal side of endothelial cells in the walls of blood vessels, and on the basal side of the basal epidermal layer of the skin, separating it from the underlying dermis (Fig. 1B). For all of these sites, zebrafish mutants or morphants have been described.

A. Notochord

The notochord is a transient rod-like structure located at the developing midline, ventral to the neural tube and dorsal to the dorsal aorta. It is composed of a single column of large vacuolated cells surrounded by a thick BM. Studies of zebrafish mutants showed that this BM plays a fundamental role in notochord development

Table I
Zebrafish mutants in basement membrane components

Mutant	Gene	Affected structures	References
bashful	*laminin α1*	Notochord, intersegmental blood vessels, somatic muscle	Pollard *et al.* (2006)
candyfloss	*laminin α2*	Notochord, intersegmental blood vessels, somatic muscle	Hall *et al.* (2007)
fransen	*laminin α5*	Fin skin (epidermis–BM junction)	Carney *et al.* (2010), Webb *et al.* (2007)
grumpy	*laminin β1a*	Notochord, intersegmental blood vessels, somitic muscle	Parsons *et al.* (2002b), Snow *et al.* (2008)
softy	*laminin β2*	Somitic muscle	Jacoby *et al.* (2009)
sleepy	*laminin γ1*	Notochord, intersegmental blood vessels, somitic muscle	Parsons *et al.* (2002b), Snow *et al.* (2008)
gulliver	*collagen 8α1a*	Notochord	Gansner and Gitlin (2008a)
dragnet	*collagen 4α5*	Retinotectal axonal targeting	Xiao and Baier (2007)
pinfin	*fras1*	Fin skin (BM–dermis junction)	Carney *et al.* (2010)
blasen	*frem2a*	Fin skin (BM–dermis junction)	Carney *et al.* (2010)
rafels	*frem1a*	Fin skin (BM–dermis junction)	Carney *et al.* (2010)
nagel	*hmcn1*	Fin skin (BM–dermis junction)	Carney *et al.* (2010)
puff daddy	*fibrillin2b*	Notochord, blood vessels, fin skin (BM–dermis junction)	Xiao and Baier (2007)

and function (see for review Scott and Stemple, 2005). Transmission electron microscopy (TEM) reveals that the notochordal BM is composed of at least three layers of organized fibers: an inner layer that most likely contains laminins, a thicker intermediate layer with dense collagen fibers, and an outer layer with perpendicular collagen fibers that run in parallel to the notochord (Parsons *et al.*, 2002b; Scott and Stemple, 2005; Stemple, 2005). In *grumpy* and *sleepy* mutants, which carry loss-of-function mutations in the laminin β1 and γ1 chain genes *lamb1a* and *lamc1*, respectively, all three layers are disorganized, accompanied by failed notochordal differentiation and subsequent death of chordamesodermal cells (Parsons *et al.*, 2002b). This indicates that signaling by BM components to the chordamesoderm is required for notochordal differentiation and survival, although the receptors on chordamesodermal cells mediating these effects are unknown so far (Scott and Stemple, 2005). During early vertebrate development, the notochord serves both structural and signaling functions (Stemple, 2005). It is important for the elongation of the embryonic axis. As the notochord cells become vacuolated, the notochord stiffens and elongates. Accordingly, it has been proposed that the perinotochordal BM has to withstand high hydrostatic pressures, and is therefore comparable to the glomerular basement membrane (GBM) of the mammalian kidney (see below) (Parsons *et al.*, 2002b). In *lamb1a* and *lamc1* mutants, notochordal cells fail to differentiate and vacuoles do not inflate, resulting in a severe shortening of the embryonic axis. In addition, the notochord plays a critical function in muscle development during the first stages of somitogenesis (approximately 10 hours postfertilization (hpf)), when notochord-derived Hedgehog (Hh) proteins induce medial paraxial mesoderm, also known as adaxial cells, to become muscle pioneer and slow-twitch muscle fibers (Wolff *et al.*, 2003). *lamb1a* and *lamc1* mutants lack these specific muscle cell types, although expression of the *hh* genes in chordamesodermal cells is unaltered or even upregulated (Parsons *et al.*, 2002b; Stemple *et al.*, 1996), suggesting that laminins are crucial for proper lateral transport of the signaling proteins.

A similar, although weaker, phenotype is present in *lama1* (*bashful*) mutants (Pollard *et al.*, 2006). The α1, β1, and γ1 chains are essential components of Laminin111 (formerly called Laminin1; Aumailley *et al.*, 2005). The weaker defects of the *lama1* mutants are most likely due to functional redundancy between the α1 and other laminin α chains. Thus, phenotypes as strong as in *lamb1a* and *lamc1* mutants were obtained when *lama1* mutants were injected with antisense morpholinos against *lama4* or *lama5*, which, in association with laminin β1 and laminin γ1, form laminin 411 (formerly called laminin 8) and laminin 511 (formerly called laminin 10) (Pollard *et al.*, 2006).

In addition to laminins, essential roles for zebrafish notochord development have been demonstrated for collagen VIII (Gansner and Gitlin, 2008a), collagen XV (Pagnon-Minot *et al.*, 2008), collagen-modifying lysyl oxidases (Gansner *et al.*, 2007), and Fibrillin 2 (Gansner *et al.*, 2008b), a member of a family of extracellular matrix proteins that form 10-nm-diameter microfibrils and can bind to integrins and growth factors such as bone morphogenetic proteins (BMPs) (Hubmacher *et al.*, 2006). Like the laminins, all of these ECM proteins are made by notochordal cells.

fibrillin 2b (*puff daddy*) mutants display rather late and moderate notochord deficiencies, with a specific disorganization of the outer layer of the perinotochordal BM, whereas the medial and inner layers appear normal (Gansner *et al.*, 2008b). Morpholino-mediated knockdown of *col15a1a* causes a disorganization of all perinotochordal BM layers, defective notochordal differentiation, and alterations in somitic muscle patterning. Although the notochord and BM defects are similar to those in the laminin mutants, the somite defects appear different. In contrast to the laminin mutants, *col15a1a* morphants had unaltered numbers of muscle pioneer cells, whereas the number of fast-twitch muscle fibers, which also depend on Hh signals (Wolff *et al.*, 2003), was substantially increased, suggesting that collagen XV might normally hinder, rather than facilitate, the transport of Hh proteins (Pagnon-Minot *et al.*, 2008). Comparable later and weaker notochordal and BM defects were observed in mutants (*gulliver*) and morphants in *col8a1a*. Here, only the medial layer of the BM seems affected, with disorganized collagen fibrils, and notochordal cells form inflated vacuoles and survive, with an undulated shape of the notochord (Gansner and Gitlin, 2008a). A similar phenotype was obtained on morpholino-based knockdown of the lysyl oxidase *lox* (Reynaud *et al.*, 2008), on dual knockdown of *loxl1* and *loxl5a*, two lysyl oxidase-like genes expressed in the developing zebrafish notochord (Gansner *et al.*, 2007), and on genetically or chemically induced copper deficiency (Mendelsohn *et al.*, 2006). Lysyl oxidases are copper-dependent enzymes involved in the cross-linking of collagen subunits that strengthens collagen fibers. Together, these findings provide an interesting link between copper metabolism, BM organization, and developmental defects caused by nutritional deficiencies and the inherited human copper metabolism disorders, Menke's disease, and Wilson's disease (Mendelsohn *et al.*, 2006). In addition, the integrity of the different layers of the zebrafish perinotochordal BM seems to be dependent on different proteins, which confer different functional properties on the structure.

B. Somites and Muscle

In skeletal muscle, the BM surrounds each myofiber and provides the elasticity that enables the sarcolemma to withstand the mechanical stress of repeated contraction, as well as allows proper attachment between adjacent muscle fibers (myomuscular junctions) and between muscle fibers and tendons (myotendinous junctions (MTJ)). In young zebrafish embryos, MTJ-like junctions are formed between somatic fast muscle fibers and the myosepta, BM-like structures of the ECM surrounding the somites. Zebrafish mutations in *lamb1a* (*grumpy*) and *lamc1* (*sleepy*) display compromised anchoring of the ends of somatic muscle fibers to the myosepta, a process called boundary capture, which in turn stops muscle fiber elongation (Snow *et al.*, 2008). Genetic mosaic experiments in laminin-deficient embryos further revealed that boundary capture is a cell-autonomous phenomenon, indicating that individual muscle cells are sufficient to condition properly their respective attachment sites (Snow *et al.*, 2008). Similar, but comparably later, essential roles

for proper MTJ formation, skeletal muscle integrity, and the prevention of muscle dystrophies have been revealed for zebrafish laminin α2, laminin α4, and laminin β2 in *lama2* (*candyfloss*) mutants (Hall *et al.*, 2007), *lama4* morphants (Postel *et al.*, 2008), and *lamb2* (*softy*) mutants (Jacoby *et al.*, 2009), respectively, for lysyl oxidases, which are involved in collagen stabilization (see above) (Reynaud *et al.*, 2008), and for the HSPG perlecan (Zoeller *et al.*, 2008), a major structural constituent of BMs (see Fig. 1A) and key regulator of several growth factor signaling pathways. All of these laminins, as well as collagens and perlecan, are components of the myosepta. Muscle cells bind to these BM components via plasma membrane receptors such as integrin $\alpha7\beta1$ (laminins and collagens) and dystroglycan (laminins). Integrins and dystroglycan, in turn, are associated with muscular actin cytoskeleton binding partners and intracellular signaling pathway components such as integrin-linked kinase (Ilk) and dystrophin. Accordingly, zebrafish morphants in *itga7* (Postel *et al.*, 2008), *dystroglycan* (Parsons *et al.*, 2002a), or *fukutin-related protein* (*fkrp*), an O-linked glycosyltransferase involved in the glycosylation of dystroglycan (Thornhill *et al.*, 2008), as well as mutants in *ilk* (*lost-contact*) (Postel *et al.*, 2008) or *dystrophin* (*sapje*) (Bassett *et al.*, 2003), display compromised MTJ formation, reduced mechanical stability of skeletal muscles, and muscle dystrophies of various strengths. The zebrafish *dystrophin* gene mutated in *sapje* mutants is the orthologue of the X-linked human Duchenne muscular dystrophy (DMD) gene, mutations in which cause Duchenne or Becker muscular dystrophies (Bassett *et al.*, 2003). In addition, human mutations in *FKRP* or genes encoding other known or putative O-linked glycosyltransferases have been shown to cause severe forms of congenital muscular dystrophy associated with structural brain defects and variable eye involvement such as Fukuyama congenital muscular dystrophy, muscle–eye–brain disease, and Walker–Warburg syndrome (Thornhill *et al.*, 2008). Furthermore, laminins have been implicated in muscle dystrophy in mammals, mediating the attachment between muscle cells and tendons (Snow *et al.*, 2008). Together, this makes the zebrafish a powerful model to elucidate further the molecular and cellular basis of human muscle dystrophies, possibly even providing the basis for new therapeutic strategies to inhibit myofiber loss (Jacoby *et al.*, 2009).

C. Blood Vessels

In addition to the notochord defects and muscle dystrophy described above, zebrafish mutants in *lama1* (*bashful*), *lamb1a* (*grumpy*), and *lamc1* (*sleepy*) also display failed migration of sprouts of intersegmental blood vessels along intersegmental, normally laminin-rich myoseptal regions (Parsons *et al.*, 2002b; Pollard *et al.*, 2006). As described above for the notochord phenotype, the intersegmental vessel defects of *lama1* mutants are weaker than those of *lamb1a* and *lamc1* mutants, because laminin 111 (formerly called laminin 1) acts in partial redundancy with laminin 411 (formerly called laminin 8) and laminin 511 (formerly called laminin 10), all of which share the same β and γ chains, but have different α chains

(Pollard *et al.*, 2006). These defects are most likely due to compromised formation of myoseptal BMs, which serve as a substrate for endothelial cells at the tip of the vessel sprouts. Essential functions during zebrafish angiogenesis have also been described for the integrin α2 subunit (San Antonio *et al.*, 2009), and for perlecan (Zoeller *et al.*, 2008, 2009), the major HSPG of BMs. *itga2* as well as *perlecan* morphants display compromised sprouting of intersegmental vessels and other vessel systems (San Antonio *et al.*, 2009; Zoeller *et al.*, 2008). In *perlecan* morphants, these defects are caused by an inappropriate localization of the vascular endothelial growth factor VEGF-A, providing an attractive mechanism by which BM components could direct endothelial migrations underlying angiogenesis (Zoeller *et al.*, 2009). Itga2 might in turn be involved in the same processes by assisting VEGFR signaling in migratory endothelial cells, consistent with similar results obtained for integrin $\alpha 2\beta 1$ in mammalian systems (Senger *et al.*, 1997).

In addition to these roles during blood vessel morphogenesis, other reports have demonstrated roles of BM components during blood vessel function. Laminin 8 and laminin 10 are the two major endothelial BM laminins in mammals. In mouse, *Lama4* mutants display weakened capillary BMs, leading to rupturing of microvascular walls and widespread hemorrhaging during embryonic and neonatal periods, whereas later, these vascular defects disappear, most likely due to the onset of laminin 10 expression (Thyboll *et al.*, 2002). Similar cardiovascular defects, characterized by blood vessel dilation and ruptures due to thinning of the endothelial wall, together with severe hemorrhaging, were observed in zebrafish *lama4* morphants (Knöll *et al.*, 2007), pointing to an essential role of laminin 411 in endothelial BMs of the zebrafish. A similar role was also revealed for integrin-linked kinase, a likely intracellular mediator of laminin-integrin signaling (see above) (Knöll *et al.*, 2007). Interestingly, the same study reports mutations in the human LAMA4 and ILK orthologues to be associated with, and most likely causative of, endothelial-based dilated cardiomyopathies (Knöll *et al.*, 2007). Furthermore, potentially conserved functions during blood vessel development in zebrafish and human could be revealed for Fibrillin 1 and Fibrillin 2, major components of microfibrils that are present in the extracellular matrix of the vessel walls, possibly attached to the endothelial BM, lending elasticity to the tissue. In humans, mutations in *FBN1* cause Marfan syndrome, characterized by dilation or dissection of the aorta and mutations in *FBN2* cause congenital contractural arachnodactyly, a rare disease with autosomal inheritance characterized by joint contractions, arachnodactyly, kyphoscoliosis, and vascular abnormalities. Consistently, zebrafish *fbn2b* (*puff daddy*) mutants (Gansner *et al.*, 2008b) and morphants in *fbn1* or the microfibril-associated glycoprotein *MAGP1* (Chen *et al.*, 2006) display reduced branching and dilation of various blood vessels. The exact molecular mechanisms underlying these defects are unclear; however, they may involve reduced integrin–matrix interaction (Chen *et al.*, 2006) and altered growth factor signaling to endothelial cells (Gansner *et al.*, 2008b). Finally, recent work has shown that the transcription factor Foxc1 is required for proper BM integrity in diverse blood vessels (De Val *et al.*, 2008), including vessels of the developing eye, which could underlie the glaucoma

(optic nerve degeneration) and anterior chamber eye defects caused by *FOXC1* alterations in humans (Skarie and Link, 2009). Concomitant morpholino injection experiments further revealed a genetic interaction between zebrafish *foxc1a* and *lama1*, shedding first light onto possible mechanisms of Foxc1 function during BM biology, and suggesting that Foxc1 might be involved in the transcriptional regulation of *laminin* genes (Skarie and Link, 2009). Together, these results underline the value of the zebrafish model to elucidate human diseases, in this case related to endothelial BMs and associated ECM components.

D. Kidney

The physiological functions of the zebrafish pronephros are blood plasma filtration and osmoregulation. Vascularization of the glomerulus involves the intimate association between podocytes and endothelial cells and the formation of an intervening GBM. In the zebrafish mutant *cloche*, where endothelial cell development is blocked at an early stage, glomerular epithelial cells initially differentiate into podocytes and form a GBM; however, the integrity of this GBM is not maintained, suggesting that the mature glomerular filtration barrier requires the presence of endothelial cells (Majumdar and Drummond, 1999). As in mammals, proper filtration in the zebrafish pronephros requires the formation of so-called slit diaphragms, consisting of specialized cell junctions between podocyte foot processes on one side and fenestrated endothelial cells on the other side of the GBM. These slit diaphragms normally form between 3 and 4 days postfertilization (dpf). Their formation and selective glomerular filtration are compromised on morpholino-mediated inactivation of the podocyte-specific *nphs1l* and *nphs2* transcripts, disease genes implicated in congenital nephropathies and proteinuria in humans (Kramer-Zucker *et al.*, 2005). Elegant *in vivo* imaging studies further revealed an instrumental role of the GBM during nephron morphogenesis that could underlie tubule segment dysfunctions found in several human kidney pathologies including Fanconi syndrome, renal tubular acidosis, and renal tubular dysgenesis (Vasilyev *et al.*, 2009). Similar to intersegmental vasculogenesis described above, the pronephric tubule BM serves as a substrate for the collective migration of differentiated pronephric epithelial cells accounting for the proximal shift in nephron segment boundaries and proximal tubule convolution (Vasilyev *et al.*, 2009). Finally, morpholino-mediated knockdown of the zebrafish orthologues of the human polycystin genes *PKD1 and PKD2*, responsible for autosomal dominant polycystic kidney disease (ADPKD), the most common heritable human disease, resulted in a range of developmental defects, including the formation of pronephric cysts (Mangos *et al.*, 2010). Although the ultrastructural basis of cyst formation was not investigated, the authors showed that the axis curvature phenotype of polycystin zebrafish morphants is linked to increased *col2a1a* expression, and concomitant *col2a1a* knockdown rescued the defects, pointing to a role of polycystins as components of a negative feedback loop to attenuate the expression of collagens and/or ECM/BM maturation (Mangos *et al.*,

2010). Future studies will reveal whether similar alterations in BM integrity may be a primary defect underlying ADPKD tissue pathologies.

E. Central Nervous System

The neuroepithelial BM plays essential roles during various processes of neural development, serving as an anchor for neuroepithelial cells and as a substrate for migrating neurons or axons. In the neural tube, neuroepithelial cells are organized along the apical–basal (medial–lateral) axis of the tube, with cell contacts to the BM on the basal (lateral) sides (Ciruna *et al.*, 2006; Geldmacher-Voss *et al.*, 2003). Time-lapse *in vivo* recordings in zebrafish revealed that during cell division, neuroepithelial cells round up and divide apically along the medial–lateral axis of the neural keel and their daughter cells become incorporated into opposite sides of the neural tube. The more basal daughter cell maintains contact with the BM through a thin cellular process and returns to its original position within the neuroepithelium. In contrast, the more apical daughter cell loses contact with the BM, becomes polarized along the medial–lateral axis, and intercalates across the midline into the contralateral side of the neural keel. Mutant analyses further revealed that proper neuroepithelial cell reorientation and integration after cell division requires components of both the epithelial (apical–basal) (Geldmacher-Voss *et al.*, 2003) and planar (Ciruna *et al.*, 2006) cell polarity systems. In addition, it is very likely, although not directly investigated, that the BM itself is absolutely essential for proper spatial organization of dividing neuroepithelial cells and the neural keel. In addition, *lama1*, *lamb1a*, and *lamc1* are required for later processes of brain morphogenesis, such as the shaping of the midbrain–hindbrain boundary, allowing proper basal constrictions and apical extensions of neuroepithelial cells that drive the inward bending of the neuroepithelium (Gutzman *et al.*, 2008; Lowery *et al.*, 2009). Furthermore, the BM serves as a crucial substrate for migrating neurons and outgrowing axons within the central nervous system, as revealed by studies in *lama1* mutants (Grant and Moens, 2010; Paulus and Halloran, 2006; Sittaramane *et al.*, 2009). Interestingly, in the case of facial branchiomotor neuron (FBMN) migration in the hindbrain, *lama1* displays a genetic interaction with components of the planar cell polarity system (*vangl2*) (Sittaramane *et al.*, 2009) and the epithelial cell polarity system (aPKCλ, aPKCξ, and Pard6gb) (Grant and Moens, 2010), possibly pointing to an instructive role of laminin to allow neural cell migration by regulating cell polarity. In addition, the BM without doubt serves crucial permissive roles as both a substrate and a boundary that constrains FBMNs to the appropriate migratory path. In line with the latter notion, disruption of the PAR–aPKC complex members aPKCλ, aPKCξ, and Pard6gb results in an ectopic ventral migration in which facial FBMNs escape from the hindbrain through holes in the Laminin-containing BM (Grant and Moens, 2010).

Several other reports deal with essential roles of BMs during eye development and retinotectal projections. Several BMs are present in the developing eye, including the lens capsule, the inner limiting membrane, and Bruch's membrane (Lee and Gross,

2007). *lamb1a* and *lamc1* mutants exhibit defects in the lens capsule and the inner limiting membrane, resulting in lens dysplasia and small retinal ectopias that extend from the retina into the interstitial space between the retina and the lens. In contrast, Bruch's membrane is largely unaffected (Lee and Gross, 2007). In addition, *lamb1*, *lamc1*, and, to a lower extent, *lama1* mutants show alterations in ganglion cell layer organization and optic nerve fasciculation, severe shortening of outer photoreceptor segments, irregular synapse formation, and increased cell death (Biehlmaier *et al.*, 2007). Furthermore, retinotectal axon pathfinding is affected, with failed midline crossing of the anterior and postoptic commissures (Karlstrom *et al.*, 1996; Paulus and Halloran, 2006). An essential later role for the final targeting of ingrowing retinal axons to specific tectal layers has been revealed for the a5 chain of type IV collagen, based on elegant work with the *col4a5* mutant *dragnet* that was isolated during a GFP-based forward genetic screen (Xiao and Baier, 2007; Xiao *et al.*, 2005). Col IV is a BM component normally lining the surface of the tectum, in close association with HSPGs. In wild-type zebrafish, axons choose one of four retinorecipient layers on entering the tectum and remain restricted to this layer. In *col4a5* mutants, by contrast, HSPGs are dispersed throughout the tectum, and a large fraction of retinal axons aberrantly trespass between layers (Xiao and Baier, 2007). Similar defects were observed in *extl3* (*boxer*) mutants, which are deficient in HSPG synthesis. Together, this suggests an essential role of the BM and collagen IV to anchor secreted factors at the surface of the tectum, which serve as guidance cues for retinal axons. Mutations in human COL4A5 cause Alport syndrome, which combines BM defects in kidney, ear, and eyes (Barker *et al.*, 1990; Hudson *et al.*, 2003). Lens degeneration is also observed in zebrafish *col4a5* mutants, whereas no pronephric defects have been reported (Xiao and Baier, 2007). The latter might be due to functional redundancy with other *col4a* genes. In contrast, little is known about the cellular basis of the CNS abnormalities described for some individuals with Alport syndrome. Here, the identified role of zebrafish *col4a5* in ordering synapses might be helpful to elucidate these neurological symptoms of human patients (Xiao and Baier, 2007).

F. Skin and Fins

In our own laboratory, we focus predominantly on the BM of the skin, which separates the epidermis from the dermis. The skin of the trunk and the fin are large and easily accessible areas of zebrafish embryos and adults, making them perfect tissues in which to explore BM function (Fig. 1B). During the first 3 weeks of development, the zebrafish epidermis consists of two epithelial cell layers, an outer periderm, and a layer of basal keratinocytes, which are attached to the underlying BM via hemidesmosome-like junctions (Le Guellec *et al.*, 2004; Sonawane *et al.*, 2005). During metamorphosis, the epidermis becomes multilayered (four to six layers on the dorsal side, three to four layers on the ventral side) (Le Guellec *et al.*, 2004). The dermis is initially relatively thin, but becomes progressively thicker. In the trunk, it contains only rather few flat and elongated fibroblast-like

cells, called dermal endothelial cells, which line the BM at the surface of somatic muscle cells, whereas most of the dermal collagen is generated by epithelial cells (Le Guellec *et al.*, 2004). During metamorphosis, when the thickness of the dermis has already increased several-fold, high numbers of fibroblasts invade the dermis and are mainly involved in scale production (Le Guellec *et al.*, 2004; Sire and Akimenko, 2004).

In the developing body fins, development is slightly different, as best investigated in the caudal fin (Dane and Tucker, 1985). At approximately 24 hpf, the six to nine epidermal basal cells at the apical surface of the tail develop a wedge shape and form an apical ectodermal ridge-like structure that detaches from the underlying mesoderm. Later the basal cells at the apical tip of the ridge maintain this wedge shape and are referred to as cleft cells (Dane and Tucker, 1985). The other epidermal cells in the ridge change their shape, becoming rectangular, and form two apposed epidermal walls (Dane and Tucker, 1985). Already at 27 hpf, much earlier than in the trunk, discontinuous BM stretches become morphologically visible via TEM underneath the epidermal sheets, leading to two epidermal sheets almost directly opposed to each other via their BMs that are separated by only a very thin, completely acellular ECM (Dane and Tucker, 1985). In this space, a set of uncharacterized fibers recognized via TEM crosses the basal lamina and directly contacts the cell membrane, possibly accounting for proper attachment and elasticity between the two opposing BMs (Dane and Tucker, 1985). These cross-fiber structures, together with the earlier establishment of the BM, might be special features of the fins to ensure the integrity and rigidity of this tissue, which despite its thinness must remain erect while subject to high mechanical forces. This might also be the reason why already at approximately 48 hpf, much earlier than in the trunk, fin mesenchymal cells, as marked by expression of *hmcn2* (see below), migrate into the space between the two BMs of the fin epithelia (Carney *et al.*, 2010), where they form the actinotrichia and the fin skeleton (Dane and Tucker, 1985).

Not too surprisingly, multiple mutants have been isolated during forward genetic screens that display specific defects in the skin of the fins, whereas the skin in the rest of the larval body appears unaffected. By morphological criteria, these fin mutants can be further subdivided into two phenotypic classes: fin dysmorphogenesis and fin blistering (Carney *et al.*, 2010). The fin dysmorphogenesis in *fransen* and *badfin* mutants is caused by loss-of-function mutations in the genes encoding the lamininα5 and integrinα3 chains, respectively (Carney *et al.*, 2010; Webb *et al.*, 2007). TEM analyses of *lama5* mutants revealed failed epidermal BM formation, pointing to a crucial role of Lama5 and Itga3b in the epidermis–BM junction (Webb *et al.*, 2007), most likely by binding of Laminin 511 from the BM to integrin $\alpha3\beta1$ receptors in basal epidermal cells (Carney *et al.*, 2010). Studies in epithelial cell culture systems have revealed the involvement of integrin $\alpha3$ in intracellular signaling to promote the assembly and maintenance of adherence junctions, thereby enhancing cell–cell adhesion within the epithelium (Chartier *et al.*, 2006). Accordingly, zebrafish *lama5* and *itga3b* mutants display massively compromised epithelial integrity and a disaggregation of the fin epidermis (Carney *et al.*, 2010; Webb *et al.*, 2007).

This is in striking contrast to the fin blistering mutants, in which the fin epidermis and the underlying BM remain largely intact, whereas blistering occurs between the sublamina densa and the underlying dermis (Carney *et al.*, 2010). Positional cloning revealed that three of these blistering mutants, *pinfin*, *blasen*, and *rafels*, are null mutations in the Fraser syndrome genes *fras1*, *frem2a*, and *frem1a*, respectively (Carney *et al.*, 2010; Gautier *et al.*, 2008; Kiyozumi *et al.*, 2006; Petrou *et al.*, 2005, 2008). Fraser syndrome is a recessive, polygenic, congenital human disorder that is now known to be caused by skin fragility during embryonic development, resulting in blister formation on the limbs and developing eyelids. These blisters later heal but result in the characteristic phenotypes observed at birth, namely, syndactyly of the digits and cryptophthalmos (Petrou *et al.*, 2008; Slavotinek and Tifft, 2002). Studies in corresponding mouse mutants revealed that Fras1, Frem1, and Frem2 form a protein complex that is localized in the sublamina densa of some, but not all regions of the developing skin, pointing to a role of the proteins during the establishment of BM–dermis junctions in areas of the embryo that are subject to particular morphogenetic processes.

In addition to *fras1*, *frem1a*, and *frem2a*, other zebrafish mutants with similar fin blistering defects were identified, caused by mutations in Hemicentin1 (Hmcn1; *nagel*), a member of the fibulin family of ECM proteins that has thus far been functionally analyzed only in the nematode *C. elegans*, or fibrillin 2b (Fbn2b; *puff daddy*), a component of microfibrils (see above) (Carney *et al.*, 2010; Gansner *et al.*, 2008b). However, in contrast to Frem2, Hmcn1 is dispensable for Fras1 stability (Carney *et al.*, 2010). This, together with the known role of fibrillins in elastic fibers, and known physical interactions between other fibulin and fibrillin family members, suggests that Hmcn1 and Fibrillin 2 might be involved in the anchorage of the BM to the aforementioned cross-fibers to allow proper attachment between the two opposing epidermal BMs of the fin fold (Carney *et al.*, 2010). Interestingly, fin mesenchymal cells migrating into the space between these two epidermal sheets express *hmcn2*, a paralog of *hmcn1* (Carney *et al.*, 2010). Therefore, we speculate that to break such cross-fibers, invading mesenchymal cells might secrete similar proteins (Hmcn2) that could replace cross-fiber components (Hmcn1). Further experiments will be necessary to test this notion. In addition, it has to be investigated whether mutations in human *HMCN1* or *FBN2* might contribute to thus far unresolved cases of Fraser syndrome.

III. Methodology for Zebrafish Studies of Basement Membrane Composition and Function

In this section, we introduce the main methods used in the study of the zebrafish BM during embryonic development. For the most part, these are well-established techniques in other model systems, which have not been widely described for use in the zebrafish model system. These techniques can also be used to study the BM of

adult zebrafish, a relatively untouched field, to assist in the elucidation of the role of BMs in adult tissue homeostasis and disease.

A. Embedding Samples and Sectioning

The visualization of BM protein distribution following whole-mount staining of zebrafish embryos or larvae can be difficult. For this reason, sectioning of the sample is fundamental. There are several protocols for embedding zebrafish tissue that include the use of various embedding media, the most common being paraffin wax and JB4 (Nüsslein-Volhard and Dahm, 2002). In the case of paraffin wax, the immunostaining or *in situ* hybridization is usually performed after embedding and sectioning the sample. However, if the sectioning can be done following whole-mount immunostaining, then epoxy resin embedding can be considered because it provides very good preservation of the morphology of the tissue.

Epoxy resins were introduced for sectioning and use in electron microscopy in the 1950s specifically because of the fine preservation of cellular and intercellular connections (Glauert *et al.*, 1956). These early protocols were improved some years later (Finck, 1960) and are still popular now for electron microscopy and in cases where the morphological structure of the sample is particularly important. One example is the developmental atlas from the Driever laboratory, available in the Zebrafish Model Organism Database, ZFIN (http://zfin.org). The epoxy resin most commonly used is known as Araldite. It is a medium based on the mixture of Araldite casting resin M, containing dibutyl phthalate as plasticizer, hardener grade 964, and accelerator grade 964 (Glauert *et al.*, 1956). Araldite with these components is also known as Durcupan.

In our laboratory, we routinely use Durcupan embedding and subsequent sectioning of embryos following whole-mount immunostaining. Besides preserving the tissue, Durcupan does not destroy the fluorescent signal, and beautiful pictures of immunofluorescent specimens can be obtained using a fluorescence microscope or laser confocal microscope (Figs. 2C and 4C and D). In the case of *in situ* hybridization labeling followed by immunostaining, the structure of more fragile tissues, such as the fin, is compromised during the *in situ* hybridization procedure. Therefore, sections in Durcupan are not so advantageous in this case (Carney *et al.*, 2010) (Fig. 4A). Below we provide a detailed protocol for Durcupan resin embedding and sectioning.

1. Durcupan Embedding Protocol

Materials

- Acetone
- Ethanol absolute

- Durcupan ACM Fluka cat. no. 44610, one kit, Fluka Chemika
- Flat embedding mold (silicone) (G369) Agar Scientific (made from silicone rubber with 24 numbered cavities 12.5 mm long × 4.5 mm wide × 3 mm deep)
- Slides SuperFrost Plus (Menzel-Gläser)

Protocol

All steps are performed at room temperature unless otherwise stated. Following immunostaining or *in situ* hybridization, the embryos first pass through dehydration steps. If samples have been stored in a viscous solution of glycerol, then they should be washed with 1× phosphate buffered saline (PBS) containing 0.1% Tween 20 overnight before starting the protocol.

- The samples need to be slowly dehydrated. They pass gradually to a more concentrated ethanol solution: 50, 70, and 90% ethanol for 10–15 min at room temperature in each solution. These incubation times are for small samples, such as 1–4 dpf embryos; older or larger specimens will require longer dehydration steps.
- Wash the samples twice in 100% ethanol for 10 min each and then transfer the tissue into acetone. Wash twice in acetone for 15 min each.
- The samples are incubated open overnight in acetone:Durcupan 1:1 under the hood to allow the slow evaporation of the acetone.
- The samples should then be placed in an embedding mold and new Durcupan solution added, orientated, and incubated overnight or longer at 65–70 °C to allow for complete hardening of the Durcupan.
- Sections of 5–8 μm can be done using a rotary microtome. Glass or disposable high-profile blades can be used.

B. Localization of BM Components

To understand the role of BM components, methods to visualize the site of mRNA and/or protein expression can be used. Techniques such as *in situ* hybridization and antibody labeling (Nüsslein-Volhard and Dahm, 2002) are broadly used by the zebrafish community for the visualization of mRNA and protein expression, respectively, and can successfully be used for the localization of BM components (Carney *et al.*, 2010). In the case of *in situ* hybridization, a standard protocol can be used for the localization of BM components. There are well-established protocols available for antibody labeling; however, variations guarantee the success of the localization of a particular protein in a specific tissue and cell region. In this section, some important points of antibody labeling methods used for the localization of BM components are described.

1. Fixation

For the study of BM component localization, special attention should be paid to the choice of fixative agent for your particular tissue. A fixative should preserve cells and tissue structures as close as possible to the biological state. The best fixative choice for a specific sample depends on the purpose of the analysis, for example: mRNA or protein localization, or simple histological analysis. There are several types of commonly used fixative agents and these are discussed below.

Paraformaldehyde (PFA) is normally used in the laboratory as 4% formaldehyde in PBS solution, pH 7. It is a noncoagulant fixative that fixes proteins and does not separate them from the surrounding water (Baker, 1966; Foster *et al.*, 2006). Formaldehyde fixation of the tissue can produce cross-links within and between proteins, which, particularly in the case of extracellular matrix proteins, can mask the antibody epitope preventing antibody binding (Foster *et al.*, 2006; Helander, 1994; Hopwood *et al.*, 1989). If PFA fixation is to be used, it is recommended to fix for the shortest period possible.

Other fixative agents are available that may produce better results for the localization of BM components. In cases where formaldehyde fixation masks the epitope, coagulant fixatives, such as methanol, which do not form cross-links between proteins, can be used (Foster *et al.*, 2006; Hall *et al.*, 2007). Another alternative is Carnoy's fixative, which is an ethanol, chloroform, and acetic acid (6:3:1) treatment that fixes tissue extremely rapidly and without cross-linking (Puchtler *et al.*, 1968; Stickland, 1975). Carnoy's fixative should always be prepared fresh when needed, and the tissue should then be washed directly through absolute ethanol, cleared, and embedded in paraffin.

If immunohistochemical analysis on fixed, paraffin-embedded tissue does not work, it is also possible to cryopreserve zebrafish tissue for cryosections. The cryoembedded tissue only undergoes a brief methanol or ethanol treatment of the cryosection before immunohistochemical analysis; therefore, antibody epitopes should still be available for antibody binding. However, in the majority of cases, tissue preservation of cryoembedded samples is not as satisfactory as Epon, Araldite, or paraffin-embedded tissue. The various embedding techniques used for zebrafish tissue have been described in the section "Embedding Samples and Sectioning".

2. Histological Staining

Histological analysis is the most classical staining method used to assess the structures and properties of cells and the surrounding environment. Histological stains can be used very effectively to study the pathogenesis of human disease and also to help identify the underlying causes of these diseases in animal models. The BM and the zebrafish are no exceptions to this rule. Periodic acid-Schiff (PAS) staining has long been used to visualize glycogen in tissues, staining structures with a high proportion of carbohydrates such as connective tissue, mucous, and the basal lamina (Bancroft and Stevens, 1977; Rambourg and Leblond, 1967; Swift and

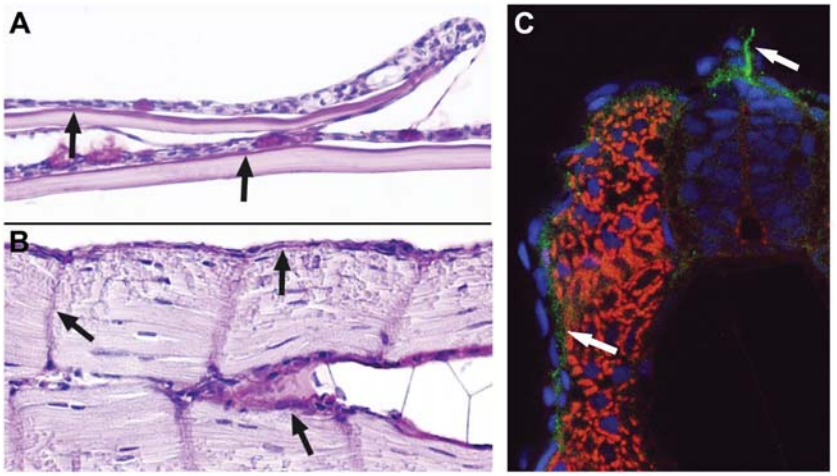

Fig. 2 Analyzing the BM through histological techniques and immunofluorescence. (A and B) PAS staining of larval and adult zebrafish tissues. (A) Adult zebrafish skin consists of a multilayered epidermis covering overlapping scales. The basement membrane appears as a thin magenta line between each scale and the overlying epidermis (arrows). (B) In the 6-day zebrafish larva, longitudinal sections along the trunk reveal PAS staining of the BM surrounding the notochord, underlying the epidermis and surrounding the muscles. (C) Immunofluorescent analysis of BM components in the zebrafish embryo. A transverse section through the trunk of an embryo at 30 hpf embedded in Durcupan. The embryo was stained with laminin to observe the BM (green) (white arrows), phalloidin, staining mainly the somites (red) and DAPI to counterstain the nuclei (blue). (See color plate.)

Saxton, 1967). Using this stain, the BM can be visualized as a magenta line separating two tissues (Fig. 2A and B). We used a PAS staining kit purchased from Merck Chemicals (1.01646 PAS staining kit), and the staining procedure was performed according to the manufacturer's directions. This commonly used histological stain can be used effectively on larval and adult zebrafish, and PFA-fixed and paraffin-embedded tissue (Fig. 2A and B).

3. Antibody Staining

Immunohistochemistry, cytochemistry, or fluorescence analysis is fundamental to the visualization of any protein that is produced by a cell and later exported to the matrix. It indicates where the BM component is assembled and, therefore, active. Extracellular matrix proteins can be transported or diffuse away from the original expressing cell, and therefore localization by antibody binding represents a more accurate method to discover where the protein exerts its function. For example, antibodies against laminin or different collagen chains have been widely used (see Table II and Fig. 2C). Another recent interesting example is the localization of Fras1, a component of the extracellular BM-associated Fraser complex, which, when

Table II
Antibodies used for detection of different zebrafish basement membrane components

Antibody	Tissue	Host species	Company	Reference
Collagen II	Notochord	Mouse	DSHB, II-II6B3	Yamamoto *et al.* (2010)
Collagen IV	Gills Kidney	rabbit	–	MacDonald *et al.* (2006)
	Kidney	Goat	Southern Biotechnology Inc., 1340-01	Majumdar and Drummond (1999)
Collagen XII	Various	Rabbit	–	Bader *et al.* (2009)
		Guinea pig	–	Bader *et al.* (2009)
Collagen XV	Notochord Skeletal muscle	Rabbit	–	Pagnon-Minot *et al.* (2008)
Laminin	Notochord	Rabbit	Sigma, L9393	Hawkins *et al.* (2008), Parsons *et al.* (2002b), Yamamoto *et al.* (2010)
	Skeletal muscle	Rabbit	Sigma, L9393	Hall *et al.* (2007), Jacoby *et al.* (2009), Parsons *et al.* (2002a)
	Ocular vasculature	Rabbit	Sigma, L9393	Skarie and Link (2009)
	Various	Rabbit	Sigma, L9393	Bader *et al.* (2009)
	Midbrain–hindbrain boundary	Rabbit	Sigma, L9393	Gutzman *et al.* (2008)
	Epidermis Fins	Rabbit	Sigma, L9393	Webb *et al.* (2007)
	Eye	Rabbit	Sigma, L9393	Lee and Gross (2007)
	Retinal ganglion cells	Rabbit	Sigma, L9393	Zolessi *et al.* (2006)
	Hindbrain neuroepithelium	Rabbit	Thermo Scientific, RB-082-A	Grant and Moens (2010)
Fras1	Epidermis, intersomitic space	Rabbit	–	Carney *et al.* (2010)
AMACO	Various	Rabbit	–	Gebauer *et al.* (2010)

disrupted, results in blistering of vertebrate embryonic skin and Fraser syndrome in humans (Carney *et al.*, 2010; Petrou *et al.*, 2008; Vrontou *et al.*, 2003). Fras1 protein is produced by epidermal cells, but the Fraser complex, consisting of Fras1 and its associated partners, the Frems, is assembled in the lamina densa of the BM and also in the subepidermal region of the dermal mesenchyme (Kiyozumi *et al.*, 2006; Petrou *et al.*, 2005). Interestingly in zebrafish, Fras1 was detected via antibody labeling close to the expressing cell but also, via unknown mechanisms, far away from this original producing cell (Carney *et al.*, 2010) (Fig. 4A and C).

There are also some adaptations of known protocols for labeling whole-mount embryos to identify proteins located in the BM of the skin. The main adaptation to a standard immunological labeling protocol is the length of time of the permeabilization treatment. Although for the localization of extracellular and BM components, permeabilization of cells should not strictly be required, it can aid antibody binding in whole-mount specimens and is also required for transmembrane proteins. The treatment used and the length of treatment can depend on the tissue, the specific

antibody, and the expected localization of the protein. For example, during embryonic stages, the zebrafish epidermis is composed of just two layers of cells: one layer of basal epidermal cells and an outer layer of peridermal cells. Therefore, permeabilization treatments of the embryos do not need to be harsh to visualize protein localization within this thin epidermis. In our laboratory, we usually employ two different permeabilization techniques: one mild and therefore suitable for analysis of the epidermis, and one harsher, which is better suited for BM labeling of deeper tissues such as around the notochord. For the mild protocol, embryos are washed twice for 10 min in MilliQ water (distilled and deionized water) at room temperature prior to washing in 1× PBS and the start of conventional immunostaining protocols. A harsher permeabilization protocol first requires the dehydration of PFA-fixed embryos into methanol in which they can be stored at −20 °C until required. The embryos are then transferred to ice-cold acetone and incubated at −20 °C for 7 min. The embryos can then be washed in 1× PBS and the immunolabeling protocol continued as normal. Increased permeabilization and improved nonspecific background antibody labeling can also be achieved by addition of 0.5% Triton X-100 or Tween 20, nonionic, nondenaturing detergents, to the 1× PBS used for washing the samples. Immunohistochemical or immunofluorescence analysis of adult zebrafish tissue is usually performed on PFA-fixed paraffin-embedded sections. In our laboratory, we perform antigen retrieval on sections to ensure removal of any PFA cross-links, which might prevent antibody binding. We perform antigen retrieval by incubating tissue sections in prewarmed 10 mM citric acid (pH 6.0) at 70 °C for 1 h. The sections are then allowed to cool to room temperature, washed in 1× PBS, and the immunostaining protocol continued as normal.

C. Transmission Electron Microscopy

To understand BM composition, structure, and, therefore, function fully, it is fundamental to observe its ultrastructure, something best achieved with TEM. The ultrastructure of the BM reveals in more detail how the misassembly of the extracellular matrix could cause a specific phenotype, such as blisters. Although this type of phenotype can be observed macroscopically, it is impossible to distinguish by light microscopy where the rupture between the two tissues occurs, either at the epidermal to BM junction or between the BM and the underlying connective tissue. TEM analysis allows discrimination of the different layers within a BM, as described in more detail for the particularly thick perinotochordal BM (see above). But different layers can be distinguished even in "regular" BMs, which usually consist of the lamina densa and the lamina rara of the basal lamina, and of the underlying lamina reticularis (Vracko, 1974; Yurchenco and Schittny, 1990). The lamina densa consists of a self-assembled rich matrix of collagen IV, separated from epithelial cells by a lighter zone (lamina rara or lucida), which is rich in laminin and integrins. On the opposite side of the lamina densa is a zone named the lamina reticularis, sublamina densa, or subbasal lamina, characterized by large anchoring fibrils and

BM-associated proteins such as collagen VII, fibulins, fibronectin, and fibrillins (Kalluri, 2003; Yurchenco *et al.*, 2004; Yurchenco and Schittny, 1990). In the literature, the basal lamina and the BM are sometimes considered the same structure (Vracko, 1974). However, here we refer to the BM, also called the basement membrane zone (BMZ), as the structure formed by both the basal lamina and the anchoring fibrils or lamina reticularis (Fig. 1A) (Yurchenco and Schittny, 1990).

Electron microscopy has been successfully used to study zebrafish tissues (see Fig. 3 for our own examples). The fixation solution used for samples to be analyzed by electron microscopy usually contains glutaraldehyde (GA) (Bader *et al.*, 2009; Dane and Tucker, 1985; Le Guellec *et al.*, 2004; Parsons *et al.*, 2002b; Slanchev *et al.*, 2009; Sonawane *et al.*, 2005; Webb *et al.*, 2007). This aldehyde, like PFA, forms cross-links but it also fixes tissue very rapidly and so preserves the fine

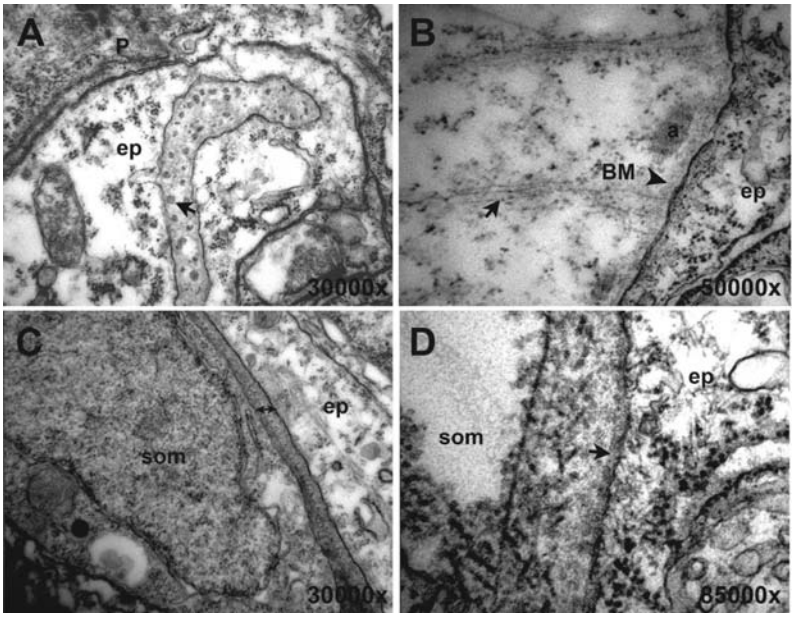

Fig. 3 BM ultrastructure of the fin and trunk at 30 hpf. (A) TEM picture of the most apical part of the fin showing the cleft cell (epidermis) and the extracellular space with assembling actinotrichia (arrow). (B) At higher magnification, the cross-fibers (arrow) are visible. The BM (arrowhead) has a dense appearance and is in close proximity to the actinotrichia. (C and D) Trunk epidermal–somite adhesion. (C) In the trunk at 30 hpf, between the epidermis and the somites, there is a dense matrix (double-headed arrow) but it is difficult to observe the BM. (D) At higher magnification, the BM is visible within this dense matrix (arrow). Collagenous fibers assemble in the extracellular space and assemble separately from the actinotrichia. P, periderm; som, somite; ep, epidermis; BM, basement membrane; a, actinotrichia. Overview at (A and C) 30,000×, (B) 50,000×, and (D) 85,000× magnification.

ultrastructural details of a tissue, making it a valuable addition to any EM fixation protocol. In the case of samples rich in water-soluble ECM components, such as proteoglycans, the samples can be fixed in a solution of aldehydes (2% PFA and 1.5% GA) with different cationic dyes and tannic acid (Dubový and Bednárová, 1999). This treatment allows for more detailed structural analysis, also of soluble molecules. However, some antigens are sensitive to GA fixation, and its concentration should, thus, be decreased or it should be completely removed if immunogold electron microscopy techniques are to be used. The immunogold EM method is used to visualize protein localization on an ultrastructural level via a normal immunolabeling protocol but with specific labeling of the secondary antibody with gold particles (Bader *et al.*, 2009; Nixon *et al.*, 2009). Immunogold EM is the best method available to analyze the ultrastructural localization of a protein. Recently, immunogold EM has also been successfully used on cryosections of zebrafish tissue, reducing the problems caused by cross-linking fixation solutions (Nixon *et al.*, 2009). In addition, immunogold EM has been used for detection of mRNA after *in situ* hybridization, which can be helpful during analyses of the skin, where cells are extremely flat (Le Guellec *et al.*, 2004).

D. Transplantation Experiments

Cell transplantation has been widely used in zebrafish to investigate various aspects of embryo development. It is a well-known technique in the zebrafish community first described in 1990 (Ho and Kane, 1990), and is described in detail in the zebrafish manual edited by Nüsslein-Volhard and Dahm (2002). Labeled cells from transgenic or fluorochrome-injected donor embryos are usually transplanted into unlabeled wild-type host embryos at the late blastula stage (Kimmel *et al.*, 1995). Using this type of experiment, it is possible to test the commitment of cells to their fate in early zebrafish embryos, and to investigate whether a gene product acts in a cell-autonomous fashion, affecting only the cells in which it is generated, or in a non-cell-autonomous fashion, also affecting other cells. It can also nicely be used to label specific cells and to analyze their role in BM formation, function, and BM component production. Recently, using transplantation of wild-type cells into *fras1*$^{-/-}$ mutants, combined with anti-Fras1 immunolabeling, we could show that Fras1 protein, which is produced by epidermal cells but localizes to the BM where it is critical for epidermal adhesion during embryonic stages in human, mouse, and fish, can be deposited in the BM far from the original producing cell (Carney *et al.*, 2010). This might appear surprising, because Fras1 is a transmembrane protein. However, doing the same transplantation experiments with cells from *sturgeon* mutant donors, lacking the proprotein convertase FurinA, we could further show that this localization of Fras1 remote from its site of production requires cell-autonomous furin shedding activity in Fras1-producing cells to enable the release of Fras1 protein from the plasma membrane (Carney *et al.*, 2010) (Fig. 4B–D).

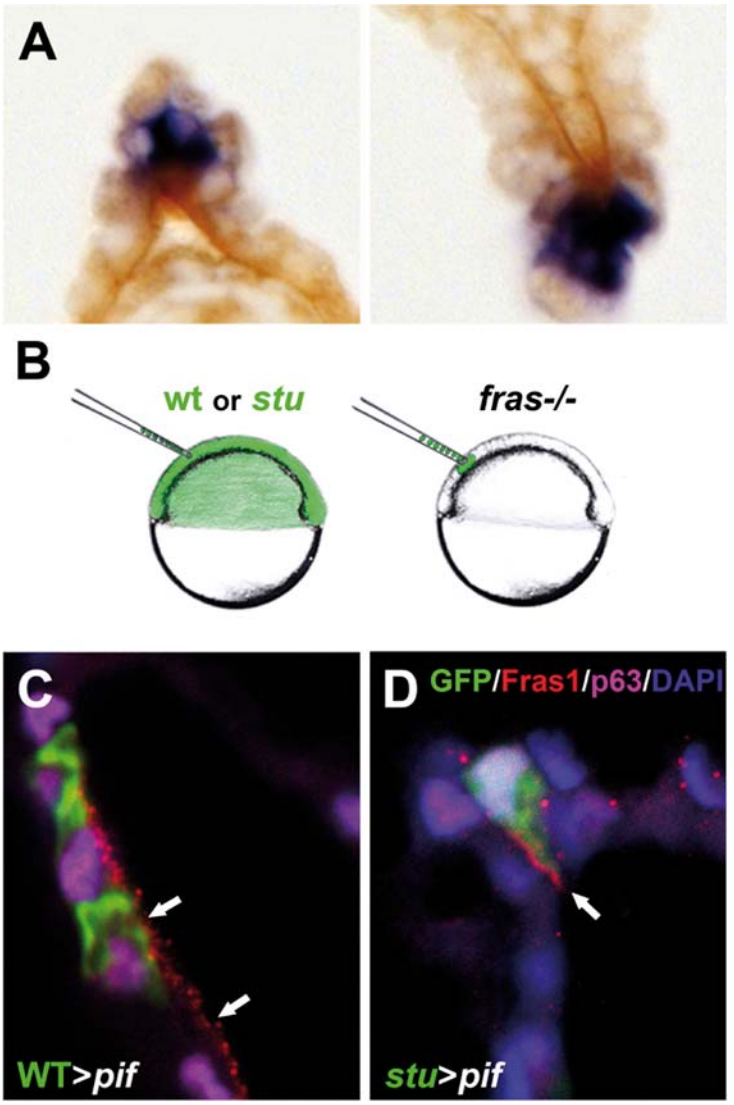

Fig. 4 Transplant techniques can elucidate specific aspects of BM protein deposition. (A) Transverse section through the fin of a wild-type 30 hpf embryo where *fras1* mRNA is localized by *in situ* hybridization (purple) and Fras1 protein distribution is demonstrated using a specific anti-Fras1 antibody (brown). Fras1 protein is localized to a broader region than the mRNA. (B) Diagram depicting an example of a transplant experiment, where GFP-labeled cells (green) are collected from a donor embryo and injected into a host embryo. (C and D) Transverse section through the posterior medial fin of a 30 hpf *fras1*$^{-/-}$ mutant embryo following transplantation of GFP-positive cells from a WT donor (C) or from a *stu* mutant cell (D) at 6 hpf. (C) Fras1 protein from WT cells can be found in the BM several cell diameters proximal of its wild-type source (GFP-positive cells) (white arrows). (D) Interestingly, Fras1 from *stu* mutant cells lacking FurinA remains restricted to the basal surface of the donor cell (white arrow). The embryos were immunolabeled for Fras1 (red), p63 (pink), and GFP (green), and nuclear DNA was counterstained with DAPI (blue). (See color plate.)

E. Forward and Reverse Genetics and Transgenesis

Any disruption to BM structure and stability, for example, the loss of a critical BM component, generally leads to specific and dramatic phenotypes, some of which can be easily analyzed by light microscopy in zebrafish embryos. This, along with the high numbers of zebrafish embryos produced from a single mating, makes the zebrafish an excellent and important tool for forward genetic screens. Although other techniques such as insertional or irradiation-induced mutagenesis are available, forward genetic screening is usually performed by mutagenizing male zebrafish with ethylnitrosourea (ENU), to introduce stable DNA changes throughout the genome, and subsequently screening their F3 progeny for specific phenotypes (Driever *et al.*, 1996; Haffter *et al.*, 1996; Mullins *et al.*, 1994; Solnica-Krezel *et al.*, 1994). BM defects lead to a range of phenotypes, which can be detected using different screening assays. Some phenotypes resulting from mutations in BM component genes can be easily assessed by binocular microscope observation, for example, the fin blistering or fin dysmorphogenesis caused by mutations in the BM components *fras1* and *laminin α5*, respectively (Carney *et al.*, 2010; van Eeden *et al.*, 1996), and the notochord degeneration or muscle detachment and muscular atrophy caused by *laminin α1, α2, β1, β2, or γ1* mutations (Granato *et al.*, 1996; Odenthal *et al.*, 1996; Stemple *et al.*, 1996). In contrast, more subtle phenotypes, for instance, during blood vessel development (Covassin *et al.*, 2009), guidance of neural migrations, retinotectal axonal pathfinding (Grant and Moens, 2010; Karlstrom *et al.*, 1996; Xiao *et al.*, 2005), or BM function in Schwann cell biology and axonal myelination (Pogoda *et al.*, 2006), might be detectable only via more specific and sensitive assays employing transgenic lines or histological techniques to visualize specific cell types. In addition, to search for genes contributing to polygenic or multifactor traits, screens in a mutant background or in combination with environmental insults (such as altered copper concentrations; see above; Gansner *et al.*, 2007) might be feasible.

In addition to forward genetics, zinc finger nuclease (ZNF) technology (Doyon *et al.*, 2008; Meng *et al.*, 2008) and Targeted Induced Local Lesions in Genomes (TILLING) reverse genetic approaches have been established in zebrafish. For TILLING, libraries of ENU-mutagenized F1 genomes are screened for mutations in particular genes via PCR amplification and sequencing (Draper *et al.*, 2004; Wienholds *et al.*, 2003). This technology is offered as a free-of-charge service by various centers in the zebrafish community, in particular the Sanger Center in Cambridge, UK, and similar services are currently being set up for the ZNF technology. In contrast, recombinant gene targeting technology as in the mouse is not available as yet, due to the lack of suitable embryonic stem cell lines (but see Fan *et al.*, 2004).

However, transgenic approaches can be used for spatially and/or temporally controlled overexpression studies, fluorochrome labeling of specific cell types, or specific cell ablations. Depending on the choice of the expression-driving elements, both temporally and spatially controlled overexpression studies are possible. Spatial control is obtained by using *cis*-regulatory elements driving expression in the cell type of interest, very much as is also done in mice. For temporal control, the

inducible and ubiquitously active heat shock protein 70 (hsp70) promoter is widely used, taking advantage of the "cold-blooded" (ectothermic) nature of the zebrafish. Thus, transgenes under the control of this promoter are inactive as long as the fish are kept at normal temperature (28 °C), whereas the transgene can be rapidly activated on transferring of the fish to warmer medium (usually 39 °C). Under some circumstances, it is even possible to activate the hsp70 transgene in individual cells by focusing a sublethal laser microbeam onto them (Halloran *et al.*, 2000). Combined spatial and temporal control of transgene activation can also be obtained via a double transgenic approach, combining, for example, a transgene in which the recombinase Cre is under the control of the hsp70 promoter, with a floxed (Cre-activatable) transgene under the control of a spatially restricted promoter. Alternatively to the *hsp70:Cre* transgene, a ligand-inducible CreER(T2) under the control of any promoter can be used, so that Cre is activated and recombination in the other transgene induced only on administration of the ER-ligand tamoxifen (Hans *et al.*, 2009), comparable to current techniques used in mouse. Such transgene-driven overexpression studies could, for example, be used to verify developmental defects associated with increased production of BM components, as described for the *polycystin* morphants mentioned above (Mangos *et al.*, 2010). They could also be used to address some open questions of human skin pathology. For example, in mouse and human, mutations in the genes encoding laminin $\alpha 3$, $\beta 3$, or $\gamma 3$ chains or the integrin $\alpha 6$ or $\beta 4$ cause epidermolysis bullosa junctionalis, a very severe skin blistering disorder, indicating that laminin 332 and integrin $\alpha 6\beta 4$ are required for anchoring epidermal cells to the underlying BM (Aumailley *et al.*, 2006; Burgeson and Christiano, 1997). However, mutants and patients also show an upregulation of other laminin chains and integrin subunits, and it is currently unclear why these do not compensate for the loss of the missing subunits. According to one hypothesis, such subunits made in excess remain in the endoplasmic reticulum, triggering the unfolded protein response and activating diverse ER stress pathways that could lead to cellular dysfunction and apoptosis. Zebrafish transgenesis could help to elucidate the contribution of such unfolded stress responses to the etiology of epidermolysis. By applying low amounts of tamoxifen, this approach can also be used to generate mosaic animals, in which only a subset of cells expresses the transgene, addressing cell autonomy issues and offering an alternative to transplantation approaches (see above).

A variant of this transgenic approach can also be used for temporally controlled ablation of specific cells, again comparable to a well-established strategy in mouse, where the floxed cDNA encodes a cytotoxin such as the diphtheria toxin A chain. An alternative approach for conditional cell ablation recently established in the zebrafish uses the nitroreductase (NTR) metronidazole (Mtz) system (Curado *et al.*, 2007; Pisharath *et al.*, 2007). Mtz is a predrug, which can be administered to fish at any stage of development and which normally is harmless, unless it is converted to a cytotoxic DNA cross-linking agent in cells expressing the transgene-encoded Mtz enzyme. To increase the effectiveness of cell ablation, a bimodular variant of this system has been invented, in which a spatially restricted promoter drives expression of the yeast Gal4 transcription factor, while within the same cassette, NTR is under

the control of the Gal4-inducible upstream activating sequence (UAS) (Zhao *et al.*, 2009). Such approaches could, for example, be used to study the extent of epithelial versus mesenchymal cell contribution to BM formation and function, a question that in many systems is still a matter of debate.

Transgenic labeling of specific cell types with cytoplasmic, nuclear, or membrane-tagged fluorescent proteins is also widely used for live *in vivo* imaging, another major strength of the zebrafish compared to other vertebrate systems, taking advantage of the transparency of its embryos and larvae, and the availability of mutant lines that are largely transparent even in adulthood (White *et al.*, 2008). In a variant of this approach, histone gene promoters have been used to drive expression of histone–mCherry or histone–GFP fusions, labeling all nuclei or mitotic figures in living fish (McMahon *et al.*, 2009; Pauls *et al.*, 2001). Using a similar approach for a laminin would result in fluorescent labeling of all BMs in live fish, thereby allowing *in vivo* recordings of BM formation and remodeling.

IV. Summary

The BM is a complex, specialized extracellular matrix that is critically important for the development and maintenance of many tissues in the body. BM ultrastructure has been extensively studied in mammalian tissues; however, there remain many questions to be answered particularly related to BM dysfunction in human disease. Several elegant recent studies in the zebrafish, *Danio rerio*, shed important new light on the pathogenesis of human disease in a variety of tissues. These studies, utilizing the techniques for analyzing the BM outlined in this chapter, demonstrate the importance and validity of the zebrafish system for BM research. The conservation of BM components, assembly sites, and function between humans and zebrafish, coupled with the multitude of advantages of this lower vertebrate system, including the ease of transgenesis and transplantation studies as well as the suitability for forward genetic screening, makes the zebrafish a valued addition to the future study of BM function.

Acknowledgments

W.B. thanks Mojgan Ghilav for expert technical assistance during the TEM analyses. Work in M.H.'s laboratory was supported by the Deutsche Forschungsgemeinschaft (SFB 829 and SFB 572), and R.R. by a long-term postdoctoral EMBO fellowship.

References

Alvarez, Y., *et al*. (2010). Predominant cone photoreceptor dysfunction in a hyperglycaemic model of non-proliferative diabetic retinopathy. *Dis. Model Mech.* **3**, 236–245.

Aumailley, M., *et al*. (2005). A simplified laminin nomenclature. *Matrix Biol.* **24**, 326–332.

Aumailley, M., *et al*. (2006). Molecular basis of inherited skin-blistering disorders, and therapeutic implications. *Expert Rev. Mol. Med.* **8**, 1–21.

Aumailley, M., and Krieg, T. (1996). Laminins: a family of diverse multifunctional molecules of basement membranes. *J. Invest. Dermatol.* **106**, 209–214.

Aviezer, D., *et al*. (1994). Perlecan, basal lamina proteoglycan, promotes basic fibroblast growth factor-receptor binding, mitogenesis, and angiogenesis. *Cell* **79**, 1005–1013.

Bader, H. L., *et al*. (2009). Zebrafish collagen XII is present in embryonic connective tissue sheaths (fascia) and basement membranes. *Matrix Biol.* **28**, 32–43.

Baker, J. R. (1966). *Cytological Technique: The Principles Underlying Routine Methods.* Chapman and Hall, London.

Bancroft, J., and Stevens, A. (1977). *Theory and Practice of Histological Techniques.* Churchill Livingstone, Edinburgh, p. 436.

Barker, D. F., *et al*. (1990). Identification of mutations in the COL4A5 collagen gene in Alport syndrome. *Science* **248**, 1224–1227.

Bassett, D. I., *et al*. (2003). Dystrophin is required for the formation of stable muscle attachments in the zebrafish embryo. *Development* **130**, 5851–5860.

Biehlmaier, O., *et al*. (2007). Impaired retinal differentiation and maintenance in zebrafish laminin mutants. *Invest. Ophthalmol. Vis. Sci.* **48**, 2887–2894.

Burgeson, R. E., and Christiano, A. M. (1997). The dermal–epidermal junction. *Curr Opin. Cell Biol.* **9**, 651–658.

Carney, T. J., *et al*. (2010). Genetic analysis of fin development in zebrafish identifies furin and hemicentin1 as potential novel Fraser syndrome disease genes. *PLoS Genet.* **6**, e1000907.

Chartier, N. T., *et al*. (2006). Laminin-5–integrin interaction signals through PI 3-kinase and Rac1b to promote assembly of adherens junctions in HT-29 cells. *J. Cell Sci.* **119**, 31–46.

Chen, E., *et al*. (2006). Functional analysis of zebrafish microfibril-associated glycoprotein-1 (Magp1) *in vivo* reveals roles for microfibrils in vascular development and function. *Blood* **107**, 4364–4374.

Ciruna, B., *et al*. (2006). Planar cell polarity signalling couples cell division and morphogenesis during neurulation. *Nature* **439**, 220–224.

Colognato, H., and Yurchenco, P. D. (2000). Form and function: the laminin family of heterotrimers. *Dev. Dyn.* **218**, 213–234.

Covassin, L. D., *et al*. (2009). A genetic screen for vascular mutants in zebrafish reveals dynamic roles for Vegf/Plcg1 signaling during artery development. *Dev. Biol.* **329**, 212–226.

Curado, S., *et al*. (2007). Conditional targeted cell ablation in zebrafish: a new tool for regeneration studies. *Dev. Dyn.* **236**, 1025–1035.

Dane, P. J., and Tucker, J. B. (1985). Modulation of epidermal cell shaping and extracellular matrix during caudal fin morphogenesis in the zebra fish *Brachydanio rerio*. *J. Embryol. Exp. Morphol.* **87**, 145–161.

De Val, S., *et al*. (2008). Combinatorial regulation of endothelial gene expression by ets and forkhead transcription factors. *Cell* **135**, 1053–1064.

Doyon, Y., *et al*. (2008). Heritable targeted gene disruption in zebrafish using designed zinc-finger nucleases. *Nat. Biotechnol.* **26**, 702–708.

Draper, B. W., *et al*. (2004). A high-throughput method for identifying *N*-ethyl-*N*-nitrosourea (ENU)-induced point mutations in zebrafish. *Methods Cell Biol.* **77**, 91–112.

Driever, W., *et al*. (1996). A genetic screen for mutations affecting embryogenesis in zebrafish. *Development* **123**, 37–46.

Dubový, P., and Bednárová, J. (1999). The extracellular matrix of rat pacinian corpuscles: an analysis of its fine structure. *Anat. Embryol. (Berl.)* **200**, 615–623.

Durbeej, M. (2010). Laminins. *Cell Tissue Res.* **339**, 259–268.

Fan, L., *et al*. (2004). Zebrafish embryo cells remain pluripotent and germ-line competent for multiple passages in culture. *Zebrafish* **1**, 21–26.

Finck, H. (1960). Epoxy resins in electron microscopy. *J. Biophys. Biochem. Cytol.* **7**, 27–30.

Foster, C. S., *et al*. (2006). Primer: tissue fixation and preservation for optimal molecular analysis of urologic tissues. *Nat. Clin. Pract. Urol.* **3**, 268–278.

Gansner, J. M., and Gitlin, J. D. (2008 a). Essential role for the alpha 1 chain of type VIII collagen in zebrafish notochord formation. *Dev. Dyn.* **237**, 3715–3726.

Gansner, J. M., *et al*. (2008 b). Essential role for Fibrillin-2 in zebrafish notochord and vascular morphogenesis. *Dev. Dyn.* **237**, 2844–2861.

Gansner, J. M., *et al*. (2007). Essential role of lysyl oxidases in notochord development. *Dev. Biol.* **307**, 202–213.

Gautier, P., *et al*. (2008). Expression of the fras1/frem gene family during zebrafish development and fin morphogenesis. *Dev. Dyn.* **237**, 3295–3304.

Gebauer, J. M., *et al*. (2010). Expression of the AMACO (VWA2 protein) ortholog in zebrafish. *Gene Expr. Patterns.* **10**, 53–59.

Geldmacher-Voss, B., *et al*. (2003). A 90-degree rotation of the mitotic spindle changes the orientation of mitoses of zebrafish neuroepithelial cells. *Development* **130**, 3767–3780.

Glauert, A. M., *et al*. (1956). A new embedding medium for electron microscopy. *Nature* **178**, 803.

Gohring, W., *et al*. (1998). Mapping of the binding of platelet-derived growth factor to distinct domains of the basement membrane proteins BM-40 and perlecan and distinction from the BM-40 collagen-binding epitope. *Eur. J. Biochem.* **255**, 60–66.

Granato, M., *et al*. (1996). Genes controlling and mediating locomotion behavior of the zebrafish embryo and larva. *Development* **123**, 399–413.

Grant, P. K., and Moens, C. B. (2010). The neuroepithelial basement membrane serves as a boundary and a substrate for neuron migration in the zebrafish hindbrain. *Neural Dev.* **5**, 9.

Gutzman, J. H., *et al*. (2008). Formation of the zebrafish midbrain–hindbrain boundary constriction requires laminin-dependent basal constriction. *Mech. Dev.* **125**, 974–983.

Haffter, P., *et al*. (1996). The identification of genes with unique and essential functions in the development of the zebrafish. *Danio rerio. Development* **123**, 1–36.

Hall, T. E., *et al*. (2007). The zebrafish candyfloss mutant implicates extracellular matrix adhesion failure in laminin alpha2-deficient congenital muscular dystrophy. *Proc. Natl. Acad. Sci. U. S. A.* **104**, 7092–7097.

Hallmann, R., *et al*. (2005). Expression and function of laminins in the embryonic and mature vasculature. *Physiol. Rev.* **85**, 979–1000.

Halloran, M. C., *et al*. (2000). Laser-induced gene expression in specific cells of transgenic zebrafish. *Development* **127**, 1953–1960.

Hans, S., *et al*. (2009). Temporally-controlled site-specific recombination in zebrafish. *PLoS One* **4**, e4640.

Hawkins, T. A., *et al*. (2008). The small molecule Mek1/2 inhibitor U0126 disrupts the chordamesoderm to notochord transition in zebrafish. *BMC Dev. Biol.* **8**, 42.

Helander, K. G. (1994). Kinetic studies of formaldehyde binding in tissue. *Biotech. Histochem.* **69**, 177–179.

Ho, R. K., and Kane, D. A. (1990). Cell-autonomous action of zebrafish spt-1 mutation in specific mesodermal precursors. *Nature* **348**, 728–730.

Hopwood, D., *et al*. (1989). Tissue fixation with phenol-formaldehyde for routine histopathology. *Histochem. J.* **21**, 228–234.

Hubmacher, D., *et al*. (2006). Fibrillins: from biogenesis of microfibrils to signaling functions. *Curr. Top. Dev. Biol.* **75**, 93–123.

Hudson, B. G., *et al*. (1993). Type IV collagen: structure, gene organization, and role in human diseases. Molecular basis of Goodpasture and Alport syndromes and diffuse leiomyomatosis. *J. Biol. Chem.* **268**, 26033–26036.

Hudson, B. G., *et al*. (2003). Alport's syndrome, Goodpasture's syndrome, and type IV collagen. *N. Engl. J. Med.* **348**, 2543–2556.

Hynes, R. O. (2009). The extracellular matrix: not just pretty fibrils. *Science* **326**, 1216–1219.

Iozzo, R. V. (2005). Basement membrane proteoglycans: from cellar to ceiling. *Nat. Rev. Mol. Cell Biol.* **6**, 646–656.

Jacoby, A. S., *et al*. (2009). The zebrafish dystrophic mutant softy maintains muscle fibre viability despite basement membrane rupture and muscle detachment. *Development* **136**, 3367–3376.

Kalluri, R. (2003). Basement membranes: structure, assembly and role in tumour angiogenesis. *Nat. Rev. Cancer* **3**, 422–433.

Karlstrom, R. O., *et al*. (1996). Zebrafish mutations affecting retinotectal axon pathfinding. *Development* **123**, 427–438.

Kimmel, C. B., *et al*. (1995). Stages of embryonic development of the zebrafish. *Dev. Dyn.* **203**, 253–310.

Kiyozumi, D., *et al*. (2006). Breakdown of the reciprocal stabilization of QBRICK/Frem1, Fras1, and Frem2 at the basement membrane provokes Fraser syndrome-like defects. *Proc. Natl. Acad. Sci. U. S. A.* **103**, 11981–11986.

Kleppel, M. M., *et al*. (1989). Human tissue distribution of novel basement membrane collagen. *Am. J. Pathol.* **134**, 813–825.

Knöll, R., *et al*. (2007). Laminin-alpha4 and integrin-linked kinase mutations cause human cardiomyopathy via simultaneous defects in cardiomyocytes and endothelial cells. *Circulation* **116**, 515–525.

Kramer, J. M. (2005). Basement membranes. *WormBook* 1–15.

Kramer-Zucker, A. G., *et al*. (2005). Organization of the pronephric filtration apparatus in zebrafish requires Nephrin, Podocin and the FERM domain protein Mosaic eyes. *Dev. Biol.* **285**, 316–329.

Le Guellec, D., *et al*. (2004). Skin development in bony fish with particular emphasis on collagen deposition in the dermis of the zebrafish (*Danio rerio*). *Int. J. Dev. Biol.* **48**, 217–231.

Lee, J., and Gross, J. M. (2007). Laminin beta1 and gamma1 containing laminins are essential for basement membrane integrity in the zebrafish eye. *Invest. Ophthalmol. Vis. Sci.* **48**, 2483–2490.

Lowery, L. A., *et al*. (2009). Characterization and classification of zebrafish brain morphology mutants. *Anat. Rec. (Hoboken)* **292**, 94–106.

Maatta, M., *et al*. (2004). Differential expression of basement membrane components in lymphatic tissues. *J. Histochem. Cytochem.* **52**, 1073–1081.

MacDonald, B. A., *et al*. (2006). Zebrafish to humans: evolution of the alpha3-chain of type IV collagen and emergence of the autoimmune epitopes associated with Goodpasture syndrome. *Blood* **107**, 1908–1915.

Majumdar, A., and Drummond, I. A. (1999). Podocyte differentiation in the absence of endothelial cells as revealed in the zebrafish avascular mutant, cloche. *Dev. Genet.* **24**, 220–229.

Mangos, S., *et al*. (2010). The ADPKD genes pkd1a/b and pkd2 regulate extracellular matrix formation. *Dis. Model Mech.* **3**, 354–365.

Marinkovich, M. P. (2007). Tumour microenvironment: laminin 332 in squamous-cell carcinoma. *Nat. Rev. Cancer* **7**, 370–380.

Masunaga, T. (2006). Epidermal basement membrane: its molecular organization and blistering disorders. *Connect. Tissue Res.* **47**, 55–66.

McMahon, C., *et al*. (2009). Lmx1b is essential for survival of periocular mesenchymal cells and influences Fgf-mediated retinal patterning in zebrafish. *Dev. Biol.* **332**, 287–298.

Mendelsohn, B. A., *et al*. (2006). Atp7a determines a hierarchy of copper metabolism essential for notochord development. *Cell Metab.* **4**, 155–162.

Meng, X., *et al*. (2008). Targeted gene inactivation in zebrafish using engineered zinc-finger nucleases. *Nat. Biotechnol.* **26**, 695–701.

Mullins, M. C., *et al*. (1994). Large-scale mutagenesis in the zebrafish: in search of genes controlling development in a vertebrate. *Curr. Biol.* **4**, 189–202.

Nakano, K. Y., *et al*. (2001). Loss of alveolar basement membrane type IV collagen alpha3, alpha4, and alpha5 chains in bronchioloalveolar carcinoma of the lung. *J Pathol.* **194**, 420–427.

Nakano, S., *et al*. (1999). Differential tissular expression and localization of type IV collagen alpha1(IV), alpha2(IV), alpha5(IV), and alpha6(IV) chains and their mRNA in normal breast and in benign and malignant breast tumors. *Lab. Invest.* **79**, 281–292.

Ninomiya, Y., *et al*. (1995). Differential expression of two basement membrane collagen genes, COL4A6 and COL4A5, demonstrated by immunofluorescence staining using peptide-specific monoclonal antibodies. *J. Cell Biol.* **130**, 1219–1229.

Nixon, S. J., *et al*. (2009). A single method for cryofixation and correlative light, electron microscopy and tomography of zebrafish embryos. *Traffic* **10**, 131–136.

Nüsslein-Volhard, C., and Dahm, R. (2002). *Zebrafish: A Practical Approach.* Oxford University Press, New York.

Odenthal, J., *et al*. (1996). Mutations affecting the formation of the notochord in the zebrafish. *Danio rerio. Development* **123**, 103–115.

Olasz, E. B., and Yancey, K. B. (2008). Bullous pemphigoid and related subepidermal autoimmune blistering diseases. *Curr. Dir. Autoimmun.* **10**, 141–166.

Pagnon-Minot, A., *et al*. (2008). Collagen XV, a novel factor in zebrafish notochord differentiation and muscle development. *Dev. Biol.* **316**, 21–35.

Parsons, M. J., *et al*. (2002 a). Removal of dystroglycan causes severe muscular dystrophy in zebrafish embryos. *Development* **129**, 3505–3512.

Parsons, M. J., *et al*. (2002 b). Zebrafish mutants identify an essential role for laminins in notochord formation. *Development* **129**, 3137–3146.

Pauls, S., *et al*. (2001). A zebrafish histone variant H2A.F/Z and a transgenic H2A.F/Z:GFP fusion protein for *in vivo* studies of embryonic development. *Dev. Genes Evol.* **211**, 603–610.

Paulsson, M. (1992). Basement membrane proteins: structure, assembly, and cellular interactions. *Crit. Rev. Biochem. Mol. Biol.* **27**, 93–127.

Paulus, J. D., and Halloran, M. C. (2006). Zebrafish bashful/laminin-alpha 1 mutants exhibit multiple axon guidance defects. *Dev. Dyn.* **235**, 213–224.

Petrou, P., *et al*. (2008). The Fras1/Frem family of extracellular matrix proteins: structure, function, and association with Fraser syndrome and the mouse bleb phenotype. *Connect Tissue Res.* **49**, 277–282.

Petrou, P., *et al*. (2005). Basement membrane distortions impair lung lobation and capillary organization in the mouse model for Fraser syndrome. *J. Biol. Chem.* **280**, 10350–10356.

Pisharath, H., *et al*. (2007). Targeted ablation of beta cells in the embryonic zebrafish pancreas using *E. coli* nitroreductase. *Mech. Dev.* **124**, 218–229.

Pogoda, H. M., *et al*. (2006). A genetic screen identifies genes essential for development of myelinated axons in zebrafish. *Dev. Biol.* **298**, 118–131.

Pollard, S. M., *et al*. (2006). Essential and overlapping roles for laminin alpha chains in notochord and blood vessel formation. *Dev. Biol.* **289**, 64–76.

Postel, R., *et al*. (2008). Zebrafish integrin-linked kinase is required in skeletal muscles for strengthening the integrin–ECM adhesion complex. *Dev. Biol.* **318**, 92–101.

Puchtler, H., *et al*. (1968). Carnoy fixation: practical and theoretical considerations. *Histochemie* **16**, 361–371.

Rambourg, A., and Leblond, C. P. (1967). Staining of basement membranes and associated structures by the periodic acid-Schiff and periodic acid-silver methenamine techniques. *J. Ultrastruct. Res.* **20**, 306–309.

Reynaud, C., *et al*. (2008). Morpholino knockdown of lysyl oxidase impairs zebrafish development, and reflects some aspects of copper metabolism disorders. *Matrix Biol.* **27**, 547–560.

Ricard-Blum, S. (2011). The collagen family. *Cold Spring Harb. Perspect. Biol.* 3.

Rowe, R. G., and Weiss, S. J. (2008). Breaching the basement membrane: who, when and how? *Trends Cell Biol.* **18**, 560–574.

Saito, K., *et al*. (2011). Distribution of alpha(IV) collagen chains in the ocular anterior segments of adult mice. *Connect. Tissue Res.* **52**(2), 147–156.

San Antonio, J. D., *et al*. (2009). A key role for the integrin alpha2beta1 in experimental and developmental angiogenesis. *Am. J. Pathol.* **175**, 1338–1347.

Scott, A., and Stemple, D. L. (2005). Zebrafish notochordal basement membrane: signaling and structure. *Curr. Top. Dev. Biol.* **65**, 229–253.

Senger, D. R., *et al*. (1997). Angiogenesis promoted by vascular endothelial growth factor: regulation through alpha1beta1 and alpha2beta1 integrins. *Proc. Natl. Acad. Sci. U. S. A.* **94**, 13612–13617.

Sherwood, D. R. (2006). Cell invasion through basement membranes: an anchor of understanding. *Trends Cell Biol.* **16**, 250–256.

Sire, J. Y., and Akimenko, M. A. (2004). Scale development in fish: a review, with description of sonic hedgehog (shh) expression in the zebrafish (*Danio rerio*). *Int. J. Dev. Biol.* **48**, 233–247.

Sittaramane, V., *et al*. (2009). The cell adhesion molecule Tag1, transmembrane protein Stbm/Vangl2, and Lamininalpha1 exhibit genetic interactions during migration of facial branchiomotor neurons in zebrafish. *Dev. Biol.* **325**, 363–373.

Skarie, J. M., and Link, B. A. (2009). FoxC1 is essential for vascular basement membrane integrity and hyaloid vessel morphogenesis. *Invest. Ophthalmol. Vis. Sci.* **50**, 5026–5034.

Slanchev, K., *et al*. (2009). The epithelial cell adhesion molecule EpCAM is required for epithelial morphogenesis and integrity during zebrafish epiboly and skin development. *PLoS Genet.* **5**, e1000563.

Slavotinek, A. M., and Tifft, C. J. (2002). Fraser syndrome and cryptophthalmos: review of the diagnostic criteria and evidence for phenotypic modules in complex malformation syndromes. *J. Med. Genet.* **39**, 623–633.

Snow, C. J., *et al*. (2008). Time-lapse analysis and mathematical characterization elucidate novel mechanisms underlying muscle morphogenesis. *PLoS Genet.* **4**, e1000219.

Solnica-Krezel, L., *et al*. (1994). Efficient recovery of ENU-induced mutations from the zebrafish germline. *Genetics* **136**, 1401–1420.

Sonawane, M., *et al*. (2005). Zebrafish penner/lethal giant larvae 2 functions in hemidesmosome formation, maintenance of cellular morphology and growth regulation in the developing basal epidermis. *Development* **132**, 3255–3265.

Stemple, D. L. (2005). Structure and function of the notochord: an essential organ for chordate development. *Development* **132**, 2503–2512.

Stemple, D. L., *et al*. (1996). Mutations affecting development of the notochord in zebrafish. *Development* **123**, 117–128.

Stickland, N. C. (1975). A detailed analysis of the effects of various fixatives on animal tissue with particular reference to muscle tissue. *Stain Technol.* **50**, 255–264.

Swift, J. A., and Saxton, C. A. (1967). The ultrastructural location of the periodate-Schiff reactive basement membrane at the dermoepidermal junctions of human scalp and monkey gingiva. *J. Ultrastruct. Res.* **17**, 23–33.

Thornhill, P., *et al*. (2008). Developmental defects in a zebrafish model for muscular dystrophies associated with the loss of fukutin-related protein (FKRP). *Brain* **131**, 1551–1561.

Thyboll, J., *et al*. (2002). Deletion of the laminin alpha4 chain leads to impaired microvessel maturation. *Mol. Cell. Biol.* **22**, 1194–1202.

van Eeden, F. J., *et al*. (1996). Genetic analysis of fin formation in the zebrafish. *Danio rerio. Development* **123**, 255–262.

Vasilyev, A., *et al*. (2009). Collective cell migration drives morphogenesis of the kidney nephron. *PLoS Biol.* **7**, e9.

Vracko, R. (1974). Basal lamina scaffold-anatomy and significance for maintenance of orderly tissue structure. *Am. J. Pathol.* **77**, 314–346.

Vrontou, S., *et al*. (2003). Fras1 deficiency results in cryptophthalmos, renal agenesis and blebbed phenotype in mice. *Nat. Genet.* **34**, 209–214.

Webb, A. E., *et al*. (2007). Laminin alpha5 is essential for the formation of the zebrafish fins. *Dev. Biol.* **311**, 369–382.

White, R. M., *et al*. (2008). Transparent adult zebrafish as a tool for *in vivo* transplantation analysis. *Cell Stem Cell* **2**, 183–189.

Whittaker, C. A., *et al*. (2006). The echinoderm adhesome. *Dev. Biol.* **300**, 252–266.

Wienholds, E., *et al*. (2003). Efficient target-selected mutagenesis in zebrafish. *Genome Res.* **13**, 2700–2707.

Wolff, C., *et al*. (2003). Multiple muscle cell identities induced by distinct levels and timing of hedgehog activity in the zebrafish embryo. *Curr. Biol.* **13**, 1169–1181.

Xiao, T., and Baier, H. (2007). Lamina-specific axonal projections in the zebrafish tectum require the type IV collagen Dragnet. *Nat. Neurosci.* **10**, 1529–1537.

Xiao, T., *et al*. (2005). A GFP-based genetic screen reveals mutations that disrupt the architecture of the zebrafish retinotectal projection. *Development* **132**, 2955–2967.

Yamamoto, M., *et al*. (2010). Mib-Jag1-Notch signalling regulates patterning and structural roles of the notochord by controlling cell-fate decisions. *Development* **137**, 2527–2537.

Yurchenco, P. D., *et al*. (2004). Basement membrane assembly, stability and activities observed through a developmental lens. *Matrix Biol.* **22**, 521–538.

Yurchenco, P. D., and Schittny, J. C. (1990). Molecular architecture of basement membranes. *FASEB J.* **4**, 1577–1590.

Zhao, X. F., *et al*. (2009). Labelling and targeted ablation of specific bipolar cell types in the zebrafish retina. *BMC Neurosci.* **10**, 107.

Zoeller, J. J., *et al*. (2008). A central function for perlecan in skeletal muscle and cardiovascular development. *J. Cell Biol.* **181**, 381–394.

Zoeller, J. J., *et al*. (2009). Perlecan regulates developmental angiogenesis by modulating the VEGF-VEGFR2 axis. *Matrix Biol.* **28**, 284–291.

Zolessi, F. R., *et al*. (2006). Polarization and orientation of retinal ganglion cells *in vivo*. *Neural Dev.* **1**, 2.

CHAPTER 9

Zebrafish Provides a Novel Model for Lymphatic Vascular Research

Terhi Karpanen and Stefan Schulte-Merker

Hubrecht Institute - KNAW and University Medical Center Utrecht, Uppsalalaan 8, Utrecht, The Netherlands

Abstract

The mammalian lymphatic vasculature has an important function in the maintenance of tissue fluid homeostasis, absorption of dietary lipids, and immune surveillance. The lymphatic vessels are also recruited by many tumors as primary routes for metastasis and mediate immune responses in inflammatory diseases, whereas dysfunction of the lymphatic drainage leads to lymphedema. The characterization of a lymphatic vasculature in zebrafish has made the advantages of this small model organism, the suitability for intravital time-lapse imaging of developmental processes and the amenability for chemical and forward genetic screens, available to lymphatic vascular research. Here we review our current understanding of embryonic lymphangiogenesis in zebrafish, its molecular and anatomical similarities to mammalian lymphatic vascular development, and the possibilities zebrafish offers to complement mouse models and cell culture assays in the lymphangiogenesis field.

METHODS IN CELL BIOLOGY, VOL 105

0091-679X/10 $35.00
DOI 10.1016/B978-0-12-381320-6.00009-6

I. Introduction

The lymphatic vascular system is essential in draining interstitial fluid, absorption of long-chain fatty acids in the small intestine, and immune defense. The lymphatic vasculature initiates as a lymphatic capillary network, which uptakes fluid, macromolecules, and immune cells from the tissues. In the small intestine, specialized lymphatic capillaries called lacteals absorb dietary lipids. These are then transported by the precollecting lymphatic vessels to a series of lymph nodes, where antigens are recognized by lymphocytes, and further to the collecting lymphatic vessels, the main one being the thoracic duct (TD), which finally drain the lymph into venous circulation.

The lymphatic vasculature has attracted increasing scientific and clinical interest with the recognition of its central role in several pathological conditions (reviewed in Schulte-Merker *et al.*, 2011). The lymphatic vasculature represents the primary route of metastasis for many solid tumors. Recent experimental findings suggest that lymphatic metastasis might not just be a passive process, but tumors can actively promote lymphangiogenesis and tumor cells can specifically gain access to the lymphatic lumen (reviewed in Achen and Stacker, 2008). Lymphatic vessels are also centrally involved in several inflammatory diseases and autoimmune conditions (reviewed in Angeli and Randolph, 2006). Impaired lymphatic drainage, either as a result of an inherited lymphatic vascular hypoplasia or dysfunction or as a result of an acquired damage to the lymphatic vessels, leads to progressive accumulation of fluid and associated macromolecules in the tissues and swelling of the affected extremities, referred to as lymphedema (reviewed in Rockson, 2008). The recent insights in the molecular regulation of lymphatic vascular development provide a basis for designing targeted anti- and prolymphangiogenic therapies for diseases traditionally lacking specific molecular treatments (reviewed in Nakamura and Rockson, 2008).

Traditionally, the existence of a lymphatic vascular system in teleosts has been somewhat of a debated issue. Rather, a secondary vessel system (SVS), which has connections to arteries and veins but is rarely blood filled, had been described (Vogel, 1985b). It was only in 2006 that a fli1:GFP-positive vessel, which is not filled with blood, but instead structurally, functionally, and in the molecular regulation of its development closely resembles lymphatic vessels, was characterized in zebrafish (Kuchler *et al.*, 2006; Yaniv *et al.*, 2006). The zebrafish TD is found parallel to the dorsal aorta (DA) and the posterior cardinal vein (PCV), in the same anatomical position as the TD in other vertebrates, and has a thin endothelial wall connected with anchoring filaments, a morphological characteristic of lymphatic vessels (Kuchler *et al.*, 2006; Yaniv *et al.*, 2006). The lymphatic vasculature of the zebrafish trunk, which in a 5 days postfertilization (dpf) embryo comprises the TD, the dorsal longitudinal lymphatic vessels (DLLVs), and the intersomitic lymphatic vessels (ISLVs), takes up and transports subcutaneously injected dye (Fig. 1) and thus functionally recapitulates the mammalian lymphatic vascular system (Kuchler *et al.*, 2006; Yaniv *et al.*, 2006). Furthermore, the development of the zebrafish TD was shown to be dependent on the vascular endothelial growth factor (Vegfc)

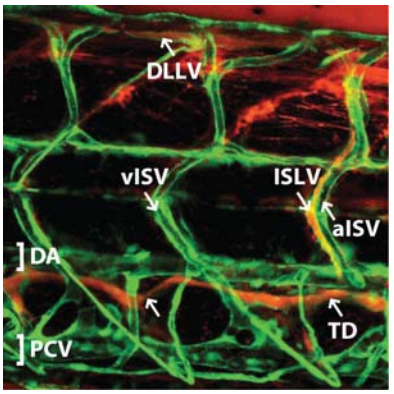

Fig. 1 Lymphangiography indicates that the lymphatic vessels of a 5 dpf zebrafish embryo are functional and uptake subcutaneously injected tracer dyes. Lateral view of a 5 dpf *tg(fli1a:EGFP)*^{y1} embryo that was injected subcutaneously with tetramethylrhodamine dextran (red) into the posterior trunk. Within a few minutes the tracer is taken up by the intersomitic lymphatic vessels (ISLV, arrow), the dorsal longitudinal lymphatic vessel (DLLV, arrow), and the thoracic duct (TD, arrows). No tracer is detected in the intersomitic blood vessels, dorsal aorta (DA), or posterior cardinal vein (PCV) at this time point. aISV, arterial intersomitic vessel; vISV, venous intersomitic vessel. (See color plate.)

receptor 3 (Vegfr3) pathway (Kuchler *et al.*, 2006; Yaniv *et al.*, 2006), which is known to be required for the migration of lymphatic endothelial cells (LECs) in mammalian lymphatic vascular development (Karkkainen *et al.*, 2004). Zebrafish mutants for *ccbe1* (Hogan *et al.*, 2009a) and *vegfr3* (Hogan *et al.*, 2009b), which lack the lymphatic vascular system (Fig. 2), develop edema around the eye and intestine, which we believe is how lymphedema represents itself in zebrafish (Fig. 3). Thus, the genetically modifiable and embryonically transparent zebrafish offers an excellent tool for identification of novel molecular regulators of lymphangiogenesis and *in vivo* visualization of embryonic lymphatic vascular development.

In this chapter, we summarize our current understanding of the embryonic lymphangiogenesis in zebrafish, introduce the prospects zebrafish can offer for lymphatic vascular research, and discuss the possible coexistence of a SVS and lymphatic vasculature in this model organism.

II. Embryonic Lymphangiogenesis in Zebrafish

As in other vertebrates such as mammals and frogs, the zebrafish lymphatic vasculature is derived from venous endothelium. However, in order to fully understand the events leading to the development of embryonic and larval lymphatic vascular structures, it will be necessary to consider not only the venous endothelium of the PCV but also the arterial vessels of the embryonic trunk.

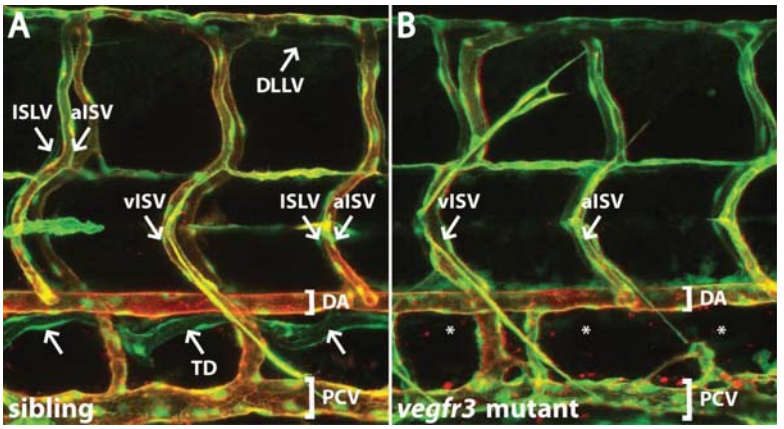

Fig. 2 Wild-type zebrafish embryos present a patent lymphatic vasculature at day 5 postfertilization, whereas mutants for *vegfr3* lack lymphatic vascular structures. Lateral views of a wild-type sibling (A) and a *vegfr3* mutant (B) *tg(fli1a:EGFP)*^{y1}*;tg(kdrl:HsHRAS-mCherry)*^{s916} embryos at 5 dpf. Arrows point to the thoracic duct (TD, green) ventral to the dorsal aorta (DA, yellow), the intersomitic lymphatic vessels (ISLV, green) along arterial intersomitic vessels (aISV, yellow), and the dorsal longitudinal lymphatic vessel (DLLV, green) in the wild-type embryo. Asterisks indicate the absence of a TD in the mutant. PCV, posterior cardinal vein. (See color plate.)

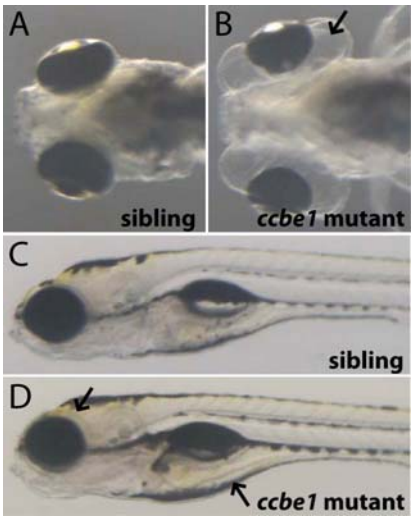

Fig. 3 *ccbe1* mutant zebrafish embryos that lack the lymphatic vasculature display progressive edema around the eye and the intestine starting from day 5 postfertilization. Wild-type sibling (A and C) and *ccbe1* mutant (B and D) embryos at 6 dpf. Arrows indicate the location of edema around the eye (B) and intestine (D) of the mutant embryos. (For color version of this figure, the reader is referred to the web version of this book.)

In zebrafish, vasculogenesis results in the formation of a primitive circulatory loop consisting, at 26 hours postfertilization (hpf), of the DA and the PCV in the trunk. It is from the DA that intersegmental arteries sprout toward the dorsal side of the embryo, in a very stereotypic manner (one pair per segment). These intersegmental vessels consist of three to four cells each, and once the tip cell reaches the dorsal side, it T-branches along the longitudinal axis and individual cells connect with neighboring tip cells (aided by macrophages as was recently shown; Fantin *et al.*, 2010) to form a pair of dorsal longitudinal anastomotic vessels (DLAVs; reviewed in Ellertsdottir *et al.*, 2009). Formally, the intersegmental vessels and DLAVs can be considered arteries at this point, since they emanate from, and are connected to, the DA. Consistent with this notion, both vessels activate the arterial-specific marker flt1^{enh}:RFP (Bussmann *et al.*, 2010).

In a second wave of angiogenesis, sprouts from the PCV start to become visible around 36 hpf (Figs. 4A and 5A). These secondary sprouts follow one of the following two different fates: either they connect with the base of an intersegmental artery, effectively turning it into a vein, or they become migratory and follow a very stereotypic path eventually forming the lymphatic vascular system. In the following, we will consider both possible events individually.

Secondary sprouts that adhere to the former scenario and retain the venous fate grow dorsally from the PCV, past the dorsal aspect of the DA. Here, they make connection with one of the basal stalk cells of a primary intersegmental vessel, and if this connection persists (which it not always does), then a lumen is formed within the venous sprout. For a short period of time, the dorsal part of this intersegmental vessel is connected with both the DA and the PCV. However, the cell that constitutes the connection with the DA soon atrophies, leaving only a lumenized intersegmental vein behind (Isogai *et al.*, 2003). This chain of events transforms roughly one half of all intersegmental arteries into veins by ca. 2.5 dpf (Figs. 4B and 5B; Bussmann *et al.*, 2010; Isogai *et al.*, 2003). The choice of whether an intersegmental vessel stays an artery or turns into a vein seems to be stochastic, even though there is a higher likelihood (71% probability) to find veins and arteries alternating in neighboring segments (Bussmann *et al.*, 2010). The only exceptions are the anterior-most four intersegmental vessels, which invariably follow a vein–artery–vein–vein pattern (Bussmann *et al.*, 2010).

How about those sprouts from the PCV that do not connect to primary intersegmental vessels? Approximately half of the PCV sprouts fall into this class, and, as will be discussed in the following, constitute the future LECs. When sprouting from the PCV, these endothelial cells extend to the midline of the embryo, where they, at approximately 50 hpf, do not migrate further dorsally but rather radially. At this point in time, these cells loose the connection with the PCV, and constitute a string of lymphangioblasts at both sides of the embryo, in the region of the horizontal myoseptum (Figs. 4B and 5B). Previously this string of lymphangioblasts has been mistaken as a blood vessel (the parachordal "vessel"), but it has recently been shown that this is not correct (Hogan *et al.*, 2009a). These cells are called parachordal lymphangioblasts (PLs) to reflect both their position at the time and their fate. The

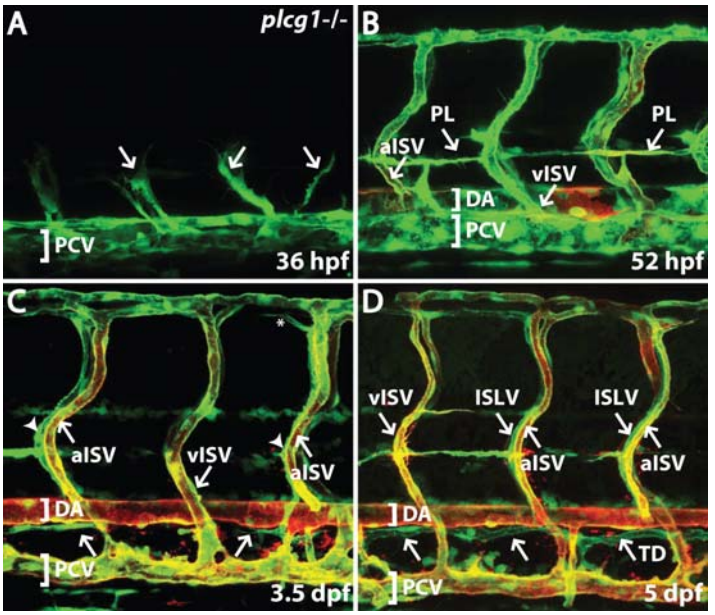

Fig. 4 Embryonic development of the lymphatic vasculature in zebrafish. (A) Secondary sprouts (arrows) from the posterior cardinal vein (PCV), giving rise to the venous connections of the intersomitic vessels and to the parachordal lymphangioblasts (PLs), visualized in *tg(fli1a:EGFP)^{y1};plcg1^{t26480}* mutant background in the absence of primary intersomitic vessels at 36 hpf. (B) At 52 hpf approximately half of the venous sprouts have made a connection with the primary intersomitic vessels turning them into veins (vISV), whereas the other half of the sprouts gives rise to PLs that constitute a string of cells at the horizontal myoseptum region (arrows). (C) The lymphangioblasts (green, arrowheads) migrate dorsally and ventrally along the intersomitic arteries (aISV, yellow) and at 3.5 dpf the first ones have made their way past the ventral aspect of the dorsal aorta (DA, yellow) and extend filopodia to the region where the thoracic duct (TD) starts forming (green, arrows). (D) At 5 dpf a complete TD (green, indicated by arrows) and intersomitic lymphatic vessels (ISLV, green, arrows) are visible in wild-type zebrafish embryos. Lateral views of a *tg(fli1a:EGFP)^{y1};plcg1^{t26480}* mutant (A) and *tg(fli1a:EGFP)^{y1};tg(kdrl:HsHRAS-mCherry)^{s916}* wild-type embryos (B–D); anterior is to the left. In *tg(fli1a:EGFP)^{y1};tg(kdrl:HsHRAS-mCherry)^{s916}* embryos lymphatic endothelial cells are labeled in green, whereas blood endothelial cells express both green and red fluorophores. PLs still contain residual red fluorophore, which disappears by the time lymphatic endothelial cells reach the ventral site of the DA. The steps of lymphatic vascular development in a zebrafish embryo shown in this figure are schematically presented in the corresponding panels of Fig. 5. (See color plate.)

molecular mechanisms guiding cells from the PCV to the horizontal midline are currently incompletely understood, and it is unclear at present whether the future PLs follow an intrinsic program or external cues from the environment. However, both Ccbe1 and the Vegfc/Vegfr3 pathway are essential for the early budding of lymphatic precursor cells from the PCV (Hogan *et al.*, 2009a, 2009b; Karpanen and Schulte-Merker, unpublished). Also, Netrin1 and its receptor Unc5b seem to

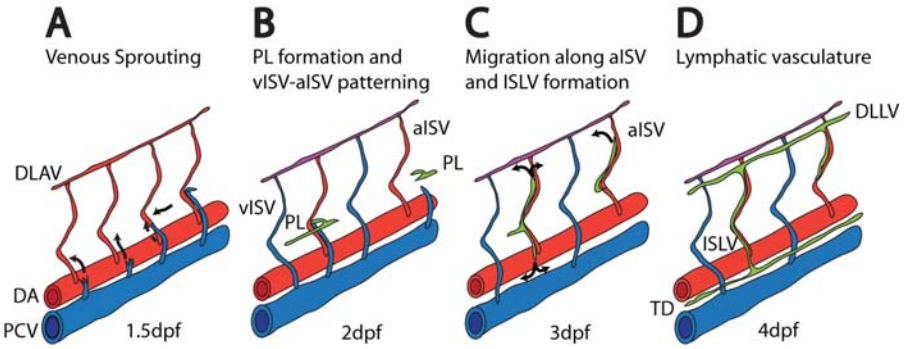

Fig. 5 Schematic presentation of the cellular events that lead to the formation of a fully patent arteriovenous and lymphatic systems in the trunk of an early zebrafish embryo. (A) At 1.5 dpf, after the primary intersomitic vessels (red) and the dorsal longitudinal anastomotic vessel (DLAV) have formed from the primary sprouts of the dorsal aorta (DA), secondary sprouts (blue) appear from the posterior cardinal vein (PCV). (B) By 2 dpf half of the secondary sprouts have fused to the base of the primary intersomitic vessels, which are functionally and molecularly turned into veins (blue, vISV). The other half of the secondary sprouts that does not connect to the intersomitic vessels gives rise to a pool of lymphatic endothelial precursor cells, parachordal lymphangioblasts (PLs, green) that transiently occupy the horizontal myoseptum region. (C) By 3 dpf the PLs (green) have established close contact with the intersomitic arteries (aISV, red) and migrate either dorsally or ventrally along them. (D) At 4 dpf the lymphatic vasculature of a zebrafish embryo consists of the thoracic duct (TD), the intersomitic lymphatic vessels (ISLV), and the dorsal longitudinal lymphatic vessel (DLLV). Figure modified from Bussmann *et al.* (2010). (For interpretation of the references to color in this figure legend, the reader is referred to the web version of this book.)

play a role, as knockdown of Unc5b leads to a failure of PL formation at 48 hpf (Navankasattusas *et al.*, 2008). Netrin, in turn, activates Rac1 through the ELMO1/DOCK180 complex, and both ELMO1 and DOCK180 are also required for accumulation of PLs at the horizontal myoseptum (Epting *et al.*, 2010).

At 60 hpf the PLs start migrating from the horizontal myoseptum along the intersegmental arteries either dorsally or ventrally in a process that leads to the formation of an embryonic lymphatic vasculature consisting of the DLLVs, the ISLVs, and the TD (Figs. 4C and D and 5C and D). When forming the TD, the migrating PLs move ventrally from the horizontal myoseptum, and as soon as they have extended just past the ventral side of the DA, they T-branch and send long filopodia radially, along the DA (see supplementary movie S1 in Kuchler *et al.*, 2006). At those points where filopodia of one cell meet with filopodia of another future TD cell, filopodial connections become stabilized, and, since this process occurs at a number of places along the length of the DA, a continuous string of future TD cells will form. The first time that extending tips of future TD cells can be seen making it past the ventral aspect of the DA is around 3–3.5 dpf, and it takes another 24 h before a continuous TD has been formed.

When PLs migrate dorsally, it is again arteries that are being used as migratory substrates. Once the migratory PLs reach the dorsal side of the embryonic trunk, they T-branch longitudinally in a manner seemingly very similar to the tip cells of

intersegmental vessels, in the process forming the DLLV, which is situated immediately ventral to the DLAV (Hogan *et al.*, 2009a).

When leaving the horizontal myoseptum region, the PLs have a choice and they could theoretically also use intersegmental veins to make their way to the region of the TD or the dorsal side of the embryo. However, as recently shown, PLs prefer arteries in 97% of cases (Bussmann *et al.*, 2010; Geudens *et al.*, 2010). It appears that migrating PLs extend filopodia to make contact with the arterial endothelial cells, and that therefore there is tight physical contact between future lymphatic and arterial endothelial cells at this point. An absence of arteries does not permit the migration of PLs by another route (e.g., along veins). Therefore, arteries must provide – either directly or indirectly by the extracellular matrix they secrete – an essential guidance cue for PLs. There are a number of different experimental settings where this notion has been tested and confirmed. First, in *plcg1*^{t26480} mutants, arterial fates are missing and while sprouting cells from the PCV manage to populate the region of the horizontal myoseptum, PLs cannot migrate any further (Bussmann *et al.*, 2010). In *kdrl*-mutants, intersegmental arteries sprout to the midline, but rarely to the dorsal side of the embryo. Mutant embryos form a TD, since the more ventral aspect of the arterial system is present, but they fail to form a DLLV (Bussmann *et al.*, 2010). Third, in experimental situations where the Notch pathway is blocked (e.g., by DAPT treatment), intersegmental veins are being formed at the expense of intersegmental arteries, and again PLs form but fail to migrate further (Geudens *et al.*, 2010).

In summary, it is a complex chain of events that leads to the formation of a patent embryonic vasculature at 5 days of development (Figs. 4D and 5D). After initial vasculogenesis, the first wave of angiogenesis generates intersegmental arteries and a second wave of venous angiogenesis produces sprouts that either remodel existing arteries into veins or give rise to the PLs that migrate to populate the horizontal myoseptum. From here, PLs migrate dorsally or ventrally to constitute the TD, the DLLV, and the ISLVs. Key questions within further understanding these processes are (1) how venous sprouts make the decision about whether to connect to a primary intersegmental vessel or whether to rather form lymphatic endothelium, (2) what cues are being used by migrating PLs and LECs to follow their route along arteries, and (3) how the initial lymphatic system expands over time within the growing larva.

III. Comparison Between Teleosts and Other Vertebrates

Our level of understanding the early events of lymphangiogenesis is sufficiently advanced by now that a comparison of lymphatic vascular formation in zebrafish and other vertebrates becomes meaningful. As always the case when considering the formation of an organ that is important for the physiology of an organism, one would expect that the similarities outweigh the differences. This indeed seems to be the case for lymphangiogenesis as well, as best evidenced by considering the genes that are essential for the process. In mice, *Prox1*, *Vegfc*, and *Vegfr3* have all been shown to be

essential for lymphangiogenesis to occur and mutants in any of these three genes display severe defects in lymphangiogenesis (Haiko *et al.*, 2008; Karkkainen *et al.*, 2001, 2004; Wigle and Oliver, 1999). For two of these genes, *vegfc* and its receptor *vegfr3*, mutants exist in zebrafish, and also present with a failure in early migration of the lymphatic precursor cells and a lack of lymphatic vessels (Fig. 2; Hogan *et al.*, 2009b; Karpanen and Schulte-Merker, unpublished). Another gene, *Ccbe1*, which has been shown to be essential for venous sprouting and lymphangiogenesis in zebrafish (Hogan *et al.*, 2009a), is also required for lymphangiogenesis in mice (Bos *et al.*, 2011), and (possibly hypomorphic) mutant alleles lead to lymphangiectasias and lymphedema, Hennekam syndrome, in humans (Alders *et al.*, 2009). Therefore, comparing those genes for which mutants exist in zebrafish and mammals, there is an excellent correlation at the functional level. Furthermore, Neuropilin2a knockdown has been shown to induce defects in embryonic lymphangiogenesis both in zebrafish (Hermans *et al.*, 2010) and in mice (Yuan *et al.*, 2002). *Prox1* has two orthologs in zebrafish, *prox1a* and *prox1b*. For both of these genes it has been reported that morpholinos result in loss of TD (Del Giacco *et al.*, 2010; Yaniv *et al.*, 2006), but whether this is a primary failure of cells sprouting from the PCV or whether this constitutes a secondary effect is not entirely clear. Furthermore, an early expression pattern of *prox1a* in endothelial cells has yet to be reported, whereas *prox1b* appears to be expressed in PCV and the sprouts emanating from it (Del Giacco *et al.*, 2010). Another gene, *Sox18*, which functions as an upstream regulator of Prox1 transcription, is dispensable in some genetic contexts in mice (Hosking *et al.*, 2009). In zebrafish, Sox18 has been shown to have a redundant role with Sox7 in arteriovenous specification (Cermenati *et al.*, 2008; Herpers *et al.*, 2008; Pendeville *et al.*, 2008), but its role in zebrafish lymphangiogenesis has not been reported so far. Overall, comparison of mouse and zebrafish mutants would suggest that evolutionary conservation is significant.

IV. The Added Value of Zebrafish

Lymphatic vascular formation and function has been studied for a considerable amount of time in mammals, and in particular in recent years efforts to understand how LECs function in the context of normal and diseased physiology have intensified. Consequently, one might ask what can be learned from fish that is not better studied in mice. There are very instructive, inducible knockout systems that can be employed in mice, and there is a plethora of antibodies that allow monitoring of lymphatic versus blood endothelial cells at the single cell level in fixed samples, including samples from human patients. Furthermore, mammalian LECs can be cultured and manipulated *in vitro*. None of these features is available in zebrafish. However, zebrafish embryos offer the possibility to follow the behavior of individual LECs over time *in vivo*. This can be achieved in transgenic backgrounds that allow to distinguish LECs from endothelial cells of the blood vasculature. Specifically, a combination of two transgenic lines can be used, where kdrl:mcherry labels all blood

endothelial cells in red (Chi *et al.*, 2008; Hogan *et al.*, 2009a), while fli1a:GFP labels all endothelial cells in green (Lawson and Weinstein, 2002). LECs will therefore appear green but not red, while blood endothelial cells will express both fluorophores and can therefore be distinguished from the "green only" LECs (Hogan *et al.*, 2009a; Figs. 2 and 4). Furthermore, YFP expression driven by the Stabilin1 promoter marks predominantly venous endothelial cells, and particularly at later stages (5 dpf and beyond) is a good marker for the PCV, intersegmental veins, the TD, and other lymphatic structures (Hogan *et al.*, 2009a). Finally, a gene trap line (SAGFF27C) exists, which, at least in later stages of development, strongly labels the TD, the ISLVs, and the DLLV. Even though this line needs to be characterized in more detail, it is a useful tool to distinguish lymphatic vessels from arteries and veins (Bussmann *et al.*, 2010).

Another reason to use fish for studying lymphatic vessels is the prospect of gene identification *via* forward genetic screens. Many screens for angiogenesis mutants have been carried out in the past, but since the existence of zebrafish lymphatic vessels has only been reported in 2006, none of these screens have analyzed the lymphatic system. An ENU-based screen using the formation of the TD at 5 dpf as a readout has yielded a number of mutants recently, demonstrating that this approach is useful in zebrafish. Specifically, mutants in *vegfc* (Karpanen and Schulte-Merker, unpublished) and *vegfr3* (Hogan *et al.*, 2009b) have been isolated early in the screen, and present with an absence of the TD due to an early defect in sprouting from the PCV. In addition, a novel gene function was identified through analysis of a mutant in *ccbe1* (Hogan *et al.*, 2009a). Again, mutants in this gene lack the TD, and also other lymphatic structures such as ISLVs and the DLLV. *Ccbe1* encodes a predicted secreted protein with a *c*ollagen-repeat domain and a *c*alcium-*b*inding *E*GF domain. The gene is expressed in a wide variety of tissues in both fish and mice, but appears to be not expressed in blood vascular endothelial cells or LECs in fish, mice, or humans. Rather, the protein is provided to cells of the PCV by other sources, most likely somitic cells. Consistent with this, transplant studies have shown that wild-type muscle cells can partially rescue the lack of a TD in mutant embryos, and TD fragments are of mutant origin in these cases. How precisely future LECs perceive the presence of Ccbe1 protein is presently unclear, but it seems that rather than having an instructive function CCBE1 acts as an essentially required permissive factor (Bos *et al.*, 2011). That notwithstanding, the identification of a novel, essential gene function through forward genetic screens clearly highlights the strength of zebrafish as a model for *in vivo* gene identification. Furthermore, screens using chemical compounds should be informative when using the same or a related readout, and this approach has yielded results in *Xenopus* (Kalin *et al.*, 2009).

Finally, the use of morpholinos allows, in principle, a quick assessment of a given gene function, and can be used in the context of lymphangiogenesis as well. However, even if stringent controls and two separate morpholinos are used (see Eisen and Smith, 2008), one needs to acknowledge that some of the commonly encountered side effects of using morpholinos, in particular cardiac and intestinal edema formation, could be mistaken as a missing or functionally compromised

lymphatic system. From mutant studies (Hogan *et al.*, 2009a, 2009b; Karpanen, van Impel and Schulte-Merker, unpublished), it has become very clear that reduced venous sprouting and a complete lack of lymphatic vessels at 5 dpf allows otherwise normal development to proceed and a swim bladder to be formed. Edema as a consequence of missing lymphatic vessels only starts to develop around 4–5 dpf in the region of the eye and the intestine (Fig. 3; also see Hogan *et al.*, 2009a). Consequently, any edema formation prior to this point is much more likely to represent toxic morpholino side effects rather than being informative about the targeted gene. Similarly, the formation of the TD as a readout is prone to errors due to the developmental delay often introduced by morpholinos. Injecting morpholinos (or applying chemical compounds) and simply scoring for the absence of a TD at 5 dpf will be misleading in many cases, and we ourselves have observed scenarios where two independent morpholinos resulted in such phenotypes, but when a stable mutant line in the respective gene was generated via Targeting Induced Local Lesions in Genomes (TILLING; Wienholds *et al.*, 2002) the mutant embryos were completely unaffected (Karpanen and Schulte-Merker, unpublished). Therefore, it is a much safer approach to not just use TD formation as the only readout, but rather ask where things go wrong in the first place: is secondary sprouting affected at 36–48 hpf, are PLs present at the horizontal myoseptum at 50–60 hpf, and have these cells started to migrate dorsally and ventrally along arterial ISVs at 70 hpf? These stages are well within the range of morpholino efficacy, and are easier to control for in terms of a possible developmental delay. When used with stringent controls, morpholinos can be informative, as exemplified by recent work on the role of the Notch/Delta signaling pathway (Geudens *et al.*, 2010), ELMO1 (Epting *et al.*, 2010), and Claudin-like protein 24 (Saharinen *et al.*, 2010) in the context of lymphangiogenesis.

V. The Secondary Vessel System in Teleosts

The view on lymphatic vessels in fish has been changing through the decades and years. Hewson has described, as early as 1769, vessels that contain no blood but a "milky fluid," and referred to them as the lymphatic vascular system (Hewson, 1769). This account, and later reports such as the ones describing lymphatic vessels in the intestine of rays (Glaser, 1933) or hagfish (Johansen *et al.*, 1962), were challenged to some extent by the important findings of Vogel (1981) who described the existence of an SVS in Actinopterygii, raising the question whether (venous parts of) the SVS had been mistakenly identified as lymphatic vascular structures. The SVS is probably a unique feature of teleosts, and consists of anastomosing connections emanating from systemic arteries that return, through their own capillary network, to the venous system. They can be visualized via dye casts (e.g., Fig. 3 in Vogel, 1985b), and have been studied in some detail in a number of different teleost species, by light and electron microscopy (Lahnsteiner *et al.*, 1990; Skov and Bennett, 2004a), plastic microvascular

casts (Lahnsteiner *et al.*, 1990; Skov and Bennett, 2004b; Vogel, 1981, 1985a), and *in vivo* observation (Dahl Ejby Jensen *et al.*, 2009; Steffensen *et al.*, 1986). The combined picture that emerges from these studies is that a number of small capillary-sized vessels (interarterial anastomoses; Vogel, 1981) originate from larger arteries, and then converge into secondary arteries. These often run next to the primary arteries, which is why the SVS is also referred to as a "parallel vascular system." Secondary capillaries are mainly found on body surfaces (skin, fins, gills, oral and pharyngeal cavity). They connect to secondary veins, which in turn are connected to the main venous system. Where measured, vessels of the SVS often have a very low hematocrit. However, exceptions have been reported, and there is a certain degree of uncertainty whether the low hematocrit could have been caused by stress, or whether a somewhat higher blood content might have been the result of vasodilators used in some studies.

In contrast to lymphatic vessels, components of the SVS always have an arterial connection, while lymphatic vessels never do. Part of the confusion concerning the issue of "true lymphatics" and "SVS" certainly stems from venous components of the SVS that closely resemble lymphatic vessels in that their lumina are often quite large and irregularly outlined, and their endothelial cells are connected to their surroundings with anchoring filaments. As lymphatic capillaries, they also lack a continuous basement membrane and pericytes. Unfortunately, a molecular analysis of the SVS has never been attempted, and it remains to be shown whether ECs of the SVS express markers that are considered to be indicative of the lymphatic system such as Lyve1, Vegfr3, and Podoplanin. Recently an attempt in this direction was made, but the Prox1 antibody used did not highlight the nuclei, which raises questions about the specificity of the staining (Dahl Ejby Jensen *et al.*, 2009).

Importantly, it is obvious that serious attempts to demonstrate the coexistence of an SVS and a lymphatic vascular system within the same species have so far not been undertaken. As noted by Vogel (2010), one can safely assume that zebrafish are unlikely to be an exception within teleosts, where in many species the existence of an SVS can hardly be disputed. On the other hand, in zebrafish embryos there is a TD that (1) is not connected to arteries (a defining element of the SVS), (2) drains interstitial components into the venous system, and (3) shows strong evolutionary conservation with mammalian lymphatic structures based on mutant analysis for *vegfc*, *vegfr3*, and *ccbe1*. A scenario seems most likely where lymphangiogenesis occurs during embryonic and larval stages, and an SVS forms, as it does in other teleosts, at a later stage independently from lymphatic vessels as a separate entity. Whether lymphatic vessels in zebrafish can be blood-perfused under hypoxic conditions as claimed recently (Dahl Ejby Jensen *et al.*, 2009) seems questionable, and in von Hippel–Lindau (*vhl*) mutants this has not been reported (van Rooijen *et al.*, 2010). Rather, Dahl Ejby Jensen *et al.* have likely mistaken the adult SVS as a lymphatic vasculature.

Clearly, this question can only be conclusively resolved by studying both parts of the vasculature within the same species, and zebrafish seem well suited to do this.

VI. Concluding Remarks

Understanding the molecular and cellular mechanisms of lymphangiogenesis is the basis for developing means for diagnosis, prevention, and treatment of the wide variety of pathological conditions with lymphatic vascular involvement. The characterization of the lymphatic vasculature in zebrafish, together with the evolutionary conservation of the origin of the LECs and the molecular regulation of lymphatic vascular development, confirms the applicability of zebrafish to study vertebrate lymphangiogenesis. Thus, the zebrafish, with its amenability for identification of novel gene functions and for *in vivo* imaging of cellular processes during embryonic lymphatic vascular development, provides a powerful system to complement mammalian and *in vitro* models of lymphangiogenesis for acquiring a better understanding of the embryonic development of the lymphatic vasculature, and for revealing potential new targets for anti- and prolymphangiogenic therapy.

VII. Methods

Lymphangiography

In zebrafish embryos, lymphatic vessels start functioning by 5 dpf and can be checked after this developmental stage for their ability to uptake substances from the interstitium (Fig. 1). The method requires a little practice to achieve success rates high enough to allow quantitative analysis, but is otherwise fairly simple:

1. Prepare a solution of 2.5–10 mg/mL fluorophore conjugated dextran in distilled water (we use tetramethylrhodamine-dextran MW 2,000,000; Invitrogen).
2. Anesthetize the embryos at 5–12 dpf in 0.015% MS-222 and immobilize them in 0.5% low-melting-point agarose containing 0.015% MS-222. The agarose solution is kept warm at +42 °C next to the microscope where the embryos are prepared and briefly cooled down to room temperature in continuous mixing before adding it on the embryos. The embryos are aligned laterally in the agarose on a culture dish and the agarose is allowed to become solid.
3. Inject a small bulbous of the tracer subcutaneously into the posterior trunk of the embryo with a fine homemade glass needle (we use filament needles which are identical to the ones we use for injection of nucleic acids) using a conventional microinjection setup. Observe the uptake of the dye into the intersomitic lymphatic vessels and the TD within minutes of the injection under a fluorescent microscope.
4. If desired, the embryos can gently be removed from the agarose, washed, and re-embedded on a culture dish with a coverslip replacing the bottom for imaging on a confocal microscope (Fig. 1).

Acknowledgments

The authors would like to thank members of the lab for discussions, and W.O.P. Vogel for discussions and comments on the manuscript. SSM is supported by the KNAW, and TK by an EMBO LTRF 52-2007 and a VENI grant from NWO.

References

Achen, M. G., and Stacker, S. A. (2008). Molecular control of lymphatic metastasis. *Ann. N. Y. Acad. Sci* **1131**, 225–234.

Alders, M., Hogan, B. M., Gjini, E., Salehi, F., Al-Gazali, L., Hennekam, E. A., Holmberg, E. E., Mannens, M. M., Mulder, M. F., and Offerhaus, G. J., *et al*. (2009). Mutations in CCBE1 cause generalized lymph vessel dysplasia in humans. *Nat. Genet* **41**, 1272–1274.

Angeli, V., and Randolph, G. J. (2006). Inflammation, lymphatic function, and dendritic cell migration. *Lymphat. Res. Biol* **4**, 217–228.

Bos, F. L., Caunt, M., Peterson-Maduro, J., Planas-Paz, L., Kowalski, J., Karpanen, T., van Impel, A., Tong, R., Ernst, J. A., and Korving, J., *et al*. (2011). CCBE1 Is Essential for Mammalian Lymphatic Vascular Development and Enhances the Lymphangiogenic Effect of Vascular Endothelial Growth Factor-C *In Vivo*. *Circ. Res.* published online before print July 21, 2011, doi:10.1161/CIRCRESAHA.111.250738.

Bussmann, J., Bos, F. L., Urasaki, A., Kawakami, K., Duckers, H. J., and Schulte-Merker, S. (2010). Arteries provide essential guidance cues for lymphatic endothelial cells in the zebrafish trunk. *Development* **137**, 2653–2657.

Cermenati, S., Moleri, S., Cimbro, S., Corti, P., Del Giacco, L., Amodeo, R., Dejana, E., Koopman, P., Cotelli, F., and Beltrame, M. (2008). Sox18 and Sox7 play redundant roles in vascular development. *Blood* **111**, 2657–2666.

Chi, N. C., Shaw, R. M., De Val, S., Kang, G., Jan, L. Y., Black, B. L., and Stainier, D. Y. (2008). Foxn4 directly regulates tbx2b expression and atrioventricular canal formation. *Genes Dev* **22**, 734–739.

Dahl Ejby Jensen, L., Cao, R., Hedlund, E. M., Soll, I., Lundberg, J. O., Hauptmann, G., Steffensen, J. F., and Cao, Y. (2009). Nitric oxide permits hypoxia-induced lymphatic perfusion by controlling arterial-lymphatic conduits in zebrafish and glass catfish. *Proc. Natl. Acad. Sci. U. S. A* **106**, 18408–18413.

Del Giacco, L., Pistocchi, A., and Ghilardi, A. (2010). prox1b activity is essential in zebrafish lymphangiogenesis. *PLoS One* **5**, e13170.

Eisen, J. S., and Smith, J. C. (2008). Controlling morpholino experiments: don't stop making antisense. *Development* **135**, 1735–1743.

Ellertsdottir, E., Lenard, A., Blum, Y., Krudewig, A., Herwig, L., Affolter, M., and Belting, H. G. (2009). Vascular morphogenesis in the zebrafish embryo. *Dev. Biol* **341**, 56–65.

Epting, D., Wendik, B., Bennewitz, K., Dietz, C. T., Driever, W., and Kroll, J. (2010). The Rac1 regulator ELMO1 controls vascular morphogenesis in zebrafish. *Circ. Res* **107**, 45–55.

Fantin, A., Vieira, J. M., Gestri, G., Denti, L., Schwarz, Q., Prykhozhij, S., Peri, F., Wilson, S. W., and Ruhrberg, C. (2010). Tissue macrophages act as cellular chaperones for vascular anastomosis downstream of VEGF-mediated endothelial tip cell induction. *Blood* **116**, 829–840.

Geudens, I., Herpers, R., Hermans, K., Segura, I., Ruiz de Almodovar, C., Bussmann, J., De Smet, F., Vandevelde, W., Hogan, B. M., and Siekmann, A., *et al*. (2010). Role of delta-like-4/Notch in the formation and wiring of the lymphatic network in zebrafish. *Arterioscler. Thromb. Vasc. Biol* **30**, 1695–1702.

Glaser, G. (1933). Beiträge zur Kenntnis des Lymphgefässsystems der Fische. *Z. Anat. Entw. Gesch* **100**, 433–511.

Haiko, P., Makinen, T., Keskitalo, S., Taipale, J., Karkkainen, M. J., Baldwin, M. E., Stacker, S. A., Achen, M. G., and Alitalo, K. (2008). Deletion of vascular endothelial growth factor C (VEGF-C) and VEGF-D is not equivalent to VEGF receptor 3 deletion in mouse embryos. *Mol. Cell. Biol* **28**, 4843–4850.

Hermans, K., Claes, F., Vandevelde, W., Zheng, W., Geudens, I., Orsenigo, F., De Smet, F., Gjini, E., Anthonis, K., and Ren, B., *et al*. (2010). Role of synectin in lymphatic development in zebrafish and frogs. *Blood* **116**, 3356–3366.

Herpers, R., van de Kamp, E., Duckers, H. J., and Schulte-Merker, S. (2008). Redundant roles for sox7 and sox18 in arteriovenous specification in zebrafish. *Circ. Res* **102**, 12–15.

Hewson, W. H. W. (1769). An account of the lymphatic system in fish. *Philos. Trans. R. Soc. Lond* **59**, 204–215.

Hogan, B. M., Bos, F. L., Bussmann, J., Witte, M., Chi, N. C., Duckers, H. J., and Schulte-Merker, S. (2009a). Ccbe1 is required for embryonic lymphangiogenesis and venous sprouting. *Nat. Genet* **41**, 396–398.

Hogan, B. M., Herpers, R., Witte, M., Helotera, H., Alitalo, K., Duckers, H. J., and Schulte-Merker, S. (2009b). Vegfc/Flt4 signalling is suppressed by Dll4 in developing zebrafish intersegmental arteries. *Development* **136**, 4001–4009.

Hosking, B., Francois, M., Wilhelm, D., Orsenigo, F., Caprini, A., Svingen, T., Tutt, D., Davidson, T., Browne, C., and Dejana, E., *et al*. (2009). Sox7 and Sox17 are strain-specific modifiers of the lymphangiogenic defects caused by Sox18 dysfunction in mice. *Development* **136**, 2385–2391.

Isogai, S., Lawson, N. D., Torrealday, S., Horiguchi, M., and Weinstein, B. M. (2003). Angiogenic network formation in the developing vertebrate trunk. *Development* **130**, 5281–5290.

Johansen, K., Fange, R., and Johannessen, M. W. (1962). Relations between blood, sinus fluid and lymph in *Myxine glutinosa* L. *Comp. Biochem. Physiol* **7**, 23–28.

Kalin, R. E., Banziger-Tobler, N. E., Detmar, M., and Brandli, A. W. (2009). An *in vivo* chemical library screen in *Xenopus* tadpoles reveals novel pathways involved in angiogenesis and lymphangiogenesis. *Blood* **114**, 1110–1122.

Karkkainen, M. J., Haiko, P., Sainio, K., Partanen, J., Taipale, J., Petrova, T. V., Jeltsch, M., Jackson, D. G., Talikka, M., and Rauvala, H., *et al*. (2004). Vascular endothelial growth factor C is required for sprouting of the first lymphatic vessels from embryonic veins. *Nat. Immunol* **5**, 74–80.

Karkkainen, M. J., Saaristo, A., Jussila, L., Karila, K. A., Lawrence, E. C., Pajusola, K., Bueler, H., Eichmann, A., Kauppinen, R., and Kettunen, M. I., *et al*. (2001). A model for gene therapy of human hereditary lymphedema. *Proc. Natl. Acad. Sci. U. S. A* **98**, 12677–12682.

Kuchler, A. M., Gjini, E., Peterson-Maduro, J., Cancilla, B., Wolburg, H., and Schulte-Merker, S. (2006). Development of the zebrafish lymphatic system requires VEGFC signaling. *Curr. Biol* **16**, 1244–1248.

Lahnsteiner, A., Lametschwandtner, A., and Patzner, R. A. (1990). The secondary blood vessel system of segmental arteries and dorsal aorta in *Blennius pavo* and *Zosterisessor ophiocephalus*. Histology, fine structure and SEM of vascular corrosion casts. *Scanning Microsc* **4**, 111–124.

Lawson, N. D., and Weinstein, B. M. (2002). *In vivo* imaging of embryonic vascular development using transgenic zebrafish. *Dev. Biol* **248**, 307–318.

Nakamura, K., and Rockson, S. G. (2008). Molecular targets for therapeutic lymphangiogenesis in lymphatic dysfunction and disease. *Lymphat. Res. Biol* **6**, 181–189.

Navankasattusas, S., Whitehead, K. J., Suli, A., Sorensen, L. K., Lim, A. H., Zhao, J., Park, K. W., Wythe, J. D., Thomas, K. R., and Chien, C. B., *et al*. (2008). The netrin receptor UNC5B promotes angiogenesis in specific vascular beds. *Development* **135**, 659–667.

Pendeville, H., Winandy, M., Manfroid, I., Nivelles, O., Motte, P., Pasque, V., Peers, B., Struman, I., Martial, J. A., and Voz, M. L. (2008). Zebrafish Sox7 and Sox18 function together to control arterial–venous identity. *Dev. Biol* **317**, 405–416.

Rockson, S. G. (2008). Diagnosis and management of lymphatic vascular disease. *J. Am. Coll. Cardiol* **52**, 799–806.

Saharinen, P., Helotera, H., Miettinen, J., Norrmen, C., D'Amico, G., Jeltsch, M., Langenberg, T., Vandevelde, W., Ny, A., and Dewerchin, M., *et al*. (2010). Claudin-like protein 24 interacts with the VEGFR-2 and VEGFR-3 pathways and regulates lymphatic vessel development. *Genes Dev* **24**, 875–880.

Schulte-Merker, S., Sabine, A., and Petrova, T. V. (2011). Lymphatic vascular morphogenesis in development, physiology, and disease. *J. Cell. Biol* **193**, 607–618.

Skov, P. V., and Bennett, M. B. (2004a). Structural basis for control of secondary vessels in the long-finned eel *Anguilla reinhardtii*. *J. Exp. Biol* **207**, 3339–3348.

Skov, P. V., and Bennett, M. B. (2004b). The secondary vascular system of Actinopterygii: interspecific variation in origins and investment. *Zoomorpholgy* **123**, 55–64.

Steffensen, J. F., Lomholt, J. P., and Vogel, W. O. P. (1986). *In vivo* observations on a specialized microvasculature, the primary and secondary vessels in fishes. *Acta Zool* **67**, 193–200.

van Rooijen, E., Voest, E. E., Logister, I., Bussmann, J., Korving, J., van Eeden, F. J., Giles, R. H., and Schulte-Merker, S. (2010). von Hippel–Lindau tumor suppressor mutants faithfully model pathological hypoxia-driven angiogenesis and vascular retinopathies in zebrafish. *Dis. Model Mech* **3**, 343–353.

Vogel, W. O. P. (1981). Struktur und Organisationsprinzip im Gefässsystem der Knochenfische. *Gegenb. Morph. Jahrb* **127**, 772–784.

Vogel, W. O. P. (1985a). The caudal heart of fish: not a lymph heart. *Acta Anat* **121**, 41–45.

Vogel, W. O. P. (1985b). Systemic vascular anastomoses, primary and secondary vessels in fish, and the phylogeny of lymphatics. *In* "Cardiovascular Shunts" (K. Johansen, and W. W. Burggren, eds.), Alfred Benzon Symposium 21, pp. 143-159. Copenhagen, Minksgaard.

Vogel, W. O. P. (2010). Zebrafish and lymphangiogenesis: a reply. *Anat. Sci. Int* **85**, 118–119.

Wienholds, E., Schulte-Merker, S., Walderich, B., and Plasterk, R. H. (2002). Target-selected inactivation of the zebrafish rag1 gene. *Science* **297**, 99–102.

Wigle, J. T., and Oliver, G. (1999). Prox1 function is required for the development of the murine lymphatic system. *Cell* **98**, 769–778.

Yaniv, K., Isogai, S., Castranova, D., Dye, L., Hitomi, J., and Weinstein, B. M. (2006). Live imaging of lymphatic development in the zebrafish. *Nat. Med* **12**, 711–716.

Yuan, L., Moyon, D., Pardanaud, L., Breant, C., Karkkainen, M. J., Alitalo, K., and Eichmann, A. (2002). Abnormal lymphatic vessel development in neuropilin 2 mutant mice. *Development* **129**, 4797–4806.

CHAPTER 10

Not All Bones are Created Equal – Using Zebrafish and Other Teleost Species in Osteogenesis Research

Alexander Apschner[*], Stefan Schulte-Merker[*,†] and P. Eckhard Witten[‡,§]

[*]Hubrecht Institute-KNAW & UMC Utrecht, Utrecht, The Netherlands

[†]Experimental Zoology Department, WUR, Wageningen, The Netherlands

[‡]Skretting Aquaculture Research Centre, Stavanger, Norway

[§]Biology Department, Ghent University, Ghent, Belgium

Abstract

Developmental osteogenesis and pathologies of mineralized tissues are areas of intense investigations in the mammalian field, but different from other areas of organ formation and developmental biology, zebrafish have been somewhat slow in joining the area of bone research. In recent years, however, genetic screens have provided a number of exciting mutants, and transgenic lines have been developed that permit visualization of osteoblasts and osteoclasts *in vivo*. We here review some of the

METHODS IN CELL BIOLOGY, VOL 105

0091-679X/10 $35.00
DOI 10.1016/B978-0-12-381320-6.00010-2

recent literature and provide examples where insights from studies in zebrafish have complemented the information available from mammalian models or clinical studies. Furthermore, we provide a comparative overview about different forms of bone within the teleost lineage, and between teleosts and mammals.

The vertebrate skeleton serves numerous functions, most notably by providing a stable, but mobile framework against which muscles act. The endoskeleton also has protective functions for the brain and many internal organs, and serves as a store for minerals. The postcranial endoskeleton consists of the axial skeleton, supporting the main body axis, and the appendicular skeleton, supporting the extremities of the body. Bone and cartilage are the main components of the endoskeleton, being produced by osteoblasts and chondrocytes, respectively.

Given the vital roles of the skeleton, it is not surprising that in the human clinic a number of diseases and pathologies affect the skeletal system. They include metabolic bone diseases such as osteoporosis and osteoarthritis as well as birth defects such as cleft palate, congenital vertebral malformations, or skeletal dysplasia (for reviews, see McInnes and O'Dell, 2010; Ralston and Uitterlinden, 2010; Zelzer and Olsen, 2003). Particularly osteoporosis (an increased risk of bone fracture due to a decrease in bone density) and osteoarthritis (a degenerative disease affecting joints) are extremely common, and have an enormous bearing on health care costs in an ever-aging society.

In many areas of cell biology and organogenesis, zebrafish (*Danio rerio*) have provided a plethora of useful models that can be employed to study processes with relevance to human disease. In contrast to mouse and chicken, however, zebrafish has a short history as model for bone disease research, or, for that matter, for studying bone formation from a developmental or cellular point of view. Part of this is certainly due to historic reasons. Initially zebrafish were mainly used to understand early developmental processes, and only gradually the use of the system has been expanded to areas of organogenesis and larval development. Another reason is that there is a diffuse notion about teleost bone being "weird" and different from "normal" (i.e., mammalian) bone. Within the vertebrate phylum, teleost species are by far the most successful (at least in terms of species number), so one could actually argue what "normal" is. However, these discussions are, to a degree, doomed to be pointless in an anthropocentric funding environment.

Despite a slow start, in recent years a steadily raising number of publications prove the zebrafish as a valuable complementation to the traditional model organisms. As so often before, the availability of mutants has been a driving force in the utilization of zebrafish, and forward genetic screens have already yielded hundreds of mutants (reviewed by Spoorendonk *et al.*, 2010). Fortuitously, some zebrafish mutants survive far longer than knockouts in their murine orthologues (see below), allowing to obtain additional information even in cases where mouse mutants had been available for a number of years. An additional and exciting opportunity for studying skeletal formation and osteogenesis in fish is the possibility to observe bone-forming cells (osteoblasts) *in vivo*. Transgenic lines for a number of informative markers have been generated by now in zebrafish and medaka (*Oryzias latipes*) (Renn and

Winkler, 2009; Spoorendonk *et al.*, 2008). This is a key advantage of using zebrafish and medaka as model organisms.

Among the bone and osteogenesis mutants that have been studied in zebrafish are some instructive examples, two of which are discussed in more detail below. Furthermore, with this chapter, we provide an overview about the different types of skeletal tissues that are present in zebrafish, medaka, and other teleost species.

I. Case Studies – Using Zebrafish for Addressing Biomedical Questions

An attractive case for the zebrafish as a bone disease model was recently demonstrated by Clement *et al.* (2008). The authors presented *in vivo* evidence in support of a loss of heterozygosity (LOH) model in osteochondroma formation, which is associated with hereditary, multiple osteochondromas syndrome (MO, also known as hereditary multiple exostoses). Until recently it has been discussed in the field whether LOH or a gene dosage effect due to haploinsufficiency is responsible for osteochondroma formation as LOH could not be detected in all osteochondromas (Bovee *et al.*, 2010).

Particularly, the majority of the patients suffering from MO carry mutations in either of the exostosin genes EXT1 or EXT2 (Jennes *et al.*, 2009), two genes involved in heparan sulfate (HS) biosynthesis. Clement *et al.* (2008) introduced the zebrafish mutant *dackel* (*dak*), harboring a mutation in *Exostin2* as a model with an osteochondroma-like cartilage phenotype: in these mutants, chondrocytes have a round shape and form clusters of cells instead of being flattened and aligned in columns.

Use of the mouse as a model for this disease has turned out to be nontrivial since both $Ext1^{-/-}$ and $Ext2^{-/-}$ mice die during early development (Lin *et al.*, 2000; Stickens *et al.*, 2005), and mice heterozygous for *Ext1* (Hilton *et al.*, 2005) or for *Ext2* (Stickens *et al.*, 2005) do not form osteochondroma-like structures or, respectively, do not form those in long bones as in human patients.

Carrying out transplantation experiments of $dak^{-/-}$ cells into wild-type embryos, Clement *et al.* (2008) were the first to show that in some cases $dak^{-/-}$ cells are not rescued by HS secreted from the surrounding cells and can initiate outgrowths similar to human exostoses. This finding is in support of an LOH model and has recently been independently confirmed by two new mouse models for osteochondromagenesis (Jones *et al.*, 2010; Matsumoto *et al.*, 2010) in which the authors by different strategies generated chondrocytes with a chimeric LOH genotype for *Ext1*.

Apparent advantages in this study were: (1) that zebrafish mutants often survive to stages that allow investigation of bone phenotypes, whereas corresponding murine models die during earlier stages of development, and (2) that transplantation experiments to create mosaic animals can be carried out with relative ease. In addition, by phenotypic comparison of *dak* mutants with mutants isolated from a forward genetic

screen, the authors could introduce 3′-phosphoadenosine 5′-phosphosulfate transporter (*papst1*) as a gene involved in HS synthesis. Thus, *papst1* represents a potential candidate in cases of patients where no mutations in the exostosin genes can be detected. One mechanism by which HSs are thought to act on chondrocytes is by restricting the diffusion of factors such as Hedgehog (Hh) ligands in the growth plate (Koziel *et al.*, 2004). The importance of the Hh pathway is well established for skeletal development and Indian hedgehog (*Ihh*), a member of the Hh family of secreted ligands, is expressed in chondrocytes. There is evidence that *Ihh* controls chondrocyte proliferation and osteoblast differentiation (Lai and Mitchell, 2005; St-Jacques *et al.*, 1999).

However, some details of the Hh pathway and particularly its effect on bone mass after initial stages of development are still not well understood. Recently two studies analyzing bone homeostasis in mice with reduced Hh signaling resulted in contradicting findings. One group (Mak *et al.*, 2008) found that conditional deletion of the Hh receptor Patched1 (*Ptch1*) (deletion of which leads to increased Hh signaling) in mature osteoblasts, using an *Osteocalcin*-Cre line, leads to an overall reduction in bone mass. The authors could relate this to increased osteoclastogenesis, induced via higher *PTHrP* and *RANKL* expression in osteoblasts. Another group (Ohba *et al.*, 2008) investigated a mouse model haploinsufficient for *Ptch1*, which exhibited a high bone mass phenotype. The authors could also measure increased bone mass in patients with nevoid basal cell carcinoma (NBCCS or Gorlin syndrome), a consequence of *Ptch1* haploinsufficiency in humans. These different findings can be attributed to the different experimental setup and to comparing a heterozygous situation to a promoter-induced knockout (Mundy and Yang, 2008).

A recent study in zebrafish (Hammond and Schulte-Merker, 2009) could contribute to a better understanding. The authors made use of a number of zebrafish mutants in the Hh pathway (*ihha, ptc1, ptc2, dre (suppressor of fused)*), which in contrast to mice are viable to a stage that allows investigation of bone development. Furthermore, drugs were employed acting on *smoothened*, a key mediator in the Hh pathway, to either activate or suppress Hh signaling. Using this experimental setup in combination with an *osterix*-reporter line, the authors could show that there are two populations of osteoblasts in zebrafish. One of them, at the edge of the cartilage scaffold of forming bone elements, requires Hh signaling (*ihha*), but is not sensitive to high levels of Hh signaling. A second population of osteoblasts arises within the cartilage template, where cells that have a chondroblast morphology and express *collagen2* start to express *osterix* and contribute to mineralization in situations where Hh signaling is increased. Importantly the latter population could be observed in mutants as well as on titrating smoothened activity with small compounds. Furthermore, the authors showed that increased Hh signaling such as in *ptc2* mutants leads to an earlier onset of osteoclast activity in developing embryos, whereas reduction of Hh signaling (*ihha*) leads to a delay in comparison to wild-type embryos. This, however, seemed to be independent of the number of surrounding osteoblasts or *rankl* expression.

In conclusion, the study could independently and *in vivo* confirm the findings of both groups: increased Hh signaling promotes differentiation of osteoblasts as well

as osteoclasts. However, in concordance with Ohba *et al.* (2008), a net increase in mineralization could be observed in zebrafish. Furthermore, this study also nicely demonstrates the functional conservation of an important pathway in skeletal homeostasis and development between teleosts and mammals.

II. The Evolution of Skeletal Tissues

The skeleton consists of two major subunits that evolved to a large degree independently: the dermal skeleton and the endoskeleton (Smith and Hall, 1990). The basic unit of the ancestral dermal skeleton is the odontode (Huysseune and Sire, 1998; Reif, 2006). Odontodes were already composed from bone, dentin, and a hypermineralized layer. Their development requires epithelial–mesenchymal interaction. According to Huysseune *et al*. (2009, 2010), teeth are homologous to odontodes and evolved when competent ectoderm migrated via the mouth and via the gill slits into the mouth cavity. Extant chondrichthyans (sharks and rays) retain odontode-like placoid scales in their dermal skeleton (Reif, 1982) and serve as examples for illustrating the homology between teeth and odontodes (Hall and Witten, 2007; Huysseune and Sire, 1998). Reviewing properties and modes of development of skeletal tissues in extant and extinct taxa, Hall and Witten (2007) conclude that skeletal tissues reflect the early evolution of highly plastic skeletogenic cells that can modulate their behavior in response to intrinsic and environmental signals.

The first jawless vertebrates had no vertebral bodies. Their skeleton was an odontode-based mineralized dermal skeleton; the vertebral column was only represented by the notochord (Donoghue *et al.*, 2006; Hall and Witten, 2007). An endoskeleton made from "true" *collagen type 2*–based cartilage evolved only after the dermal skeleton (Cole and Hall, 2004; Hall and Witten, 2007). Compared to their common ancestors (basal osteichthyans), the postcranial dermal skeleton has been completely lost in mammals and has been largely reduced in teleost fish. Scales and scale-derived fin rays of teleost fish mainly represent a reduced dentin part of the ancestral odontodes (Sire and Akimenko, 2004).

Given that all basic types of skeletal tissues were already present in early vertebrates (Hall and Witten, 2007), the characters of skeletal tissues are conserved among vertebrates (Witten and Huysseune, 2009). Consequently also transcription factors and signaling molecules that facilitate skeletal cell differentiation, and hormones that regulate the skeletal development, are conserved. Still, differences between the teleost and the mammalian skeleton exist, differences that are significant if teleosts like zebrafish or medaka are used as models in biomedical research. Teleosts evolved into the most successful group of all vertebrates with about 30,000 species. They dominate the aquatic habitats, by far the largest biosphere on the planet. In view of their enormous radiation, it would be false to assume that the mammalian skeleton is advanced and the teleost skeleton is primitive (Metscher and Ahlberg, 1999; Witten and Huysseune, 2009). In fact, many characters of the teleost

skeleton are more advanced and/or elaborated compared to mammals. One example is the teleost skull that contains twice the number of skeletal elements compared to the mammalian skull (Owen, 1845). Differences between the teleost skeleton and the mammalian skeleton may also relate to adaptations to different habitats (aquatic and terrestrial), the truncation of developmental process, and size differences (Witten and Huysseune, 2009). The following section describes similarities and differences between the mammalian and the teleost skeleton.

III. Cartilage and Bone in Teleost Fish

The major categories of skeletal tissues (cartilage, bone, dentine, and enamel/enameloid) and the major categories of skeletal cells (chondroblasts, chondrocytes, osteoblasts, bone lining cells, osteocytes, osteoclasts, odontoblasts, ameloblasts) are present in both teleosts and mammals (Huysseune, 2000; Witten and Huysseune, 2009). Apart from dentine, enamel/enameloid, and bone of attachment, which are restricted to the dermal skeleton, all skeletal tissues and respective cells occur in the teleost dermal and endoskeleton. The first step in the development of "regular" cartilage in teleosts is the condensation of mesenchymal cells (blastema stage) that develop into closely packed prechondroblasts (Huysseune and Sire, 1992a). These cells differentiate into chondroblasts and finally become separated through the secretion of extracellular cartilage matrix. Perichondral bone formation is the basic process of ossification of the cartilaginous preformed teleost endoskeleton. Different from mammals, it is often not linked to endochondral bone formation (Hall, 1998; Huysseune, 2000; Witten and Villwock, 1997) (Fig. 1). Perichondral bone is laid down at the surface of the cartilaginous template by cells that were formerly part of the perichondrium. The cells have now characteristics of osteoblasts and secrete bone matrix or a mixture of cartilage and bone matrix (Huysseune, 2000; Huysseune and Sire, 1992a; Verreijdt *et al.*, 2002). On the beginning of perichondral bone formation, the former perichondrium has become a periosteum and further thickening of the bone is carried out through deposition of bone by the osteogenic cells. A typical element of the teleost endoskeleton consists of a persisting cartilage rod inside a bone tube with cartilage sticking out as a condyle. This applies especially to smaller teleost species, such as medaka and zebrafish where endochondral bone formation is uncommon (but does occur). Cartilage remains inside the bone shaft and if cartilage is removed, it is replaced by adipose tissue (Witten *et al*., 2001; Witten *et al*., 2010) (Fig. 1). Replacement of cartilage by spongiosa (endochondral bone formation) can more readily be observed in larger teleost species such as carp (*Cyprinus carpio*) and salmon (*Salmo salar*).

Bone formation in teleosts can be intramembranous, perichondral, or endochondral. In the endoskeleton membranous apolamellae can form from perichondral bone, a process that resembles intramembranous bone formation (Witten and Huysseune, 2007). The cells involved in bone formation are osteoblasts. They derive

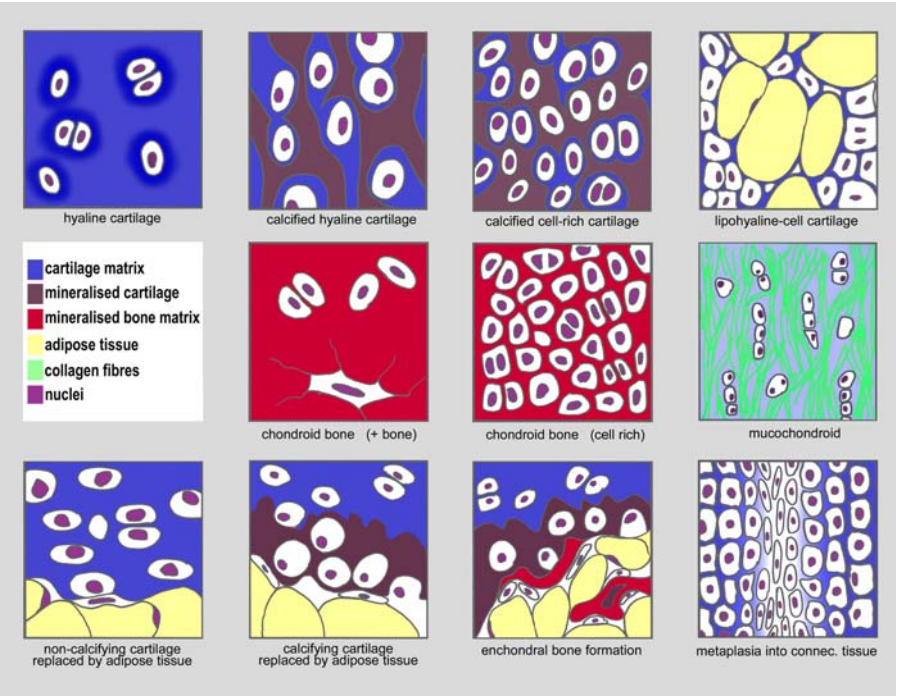

Fig. 1 Hyaline cartilage and different types of tissues that are intermediate between bone and cartilage and between cartilage and connective tissues, which typically occur in teleosts (rows 1 and 2). Different modes of cartilage replacement that typically occur in teleosts (row 3). See Witten *et al.* (2010) for a complete list of cartilage tissues. (See color plate.)

from osteoprogenitor cells, the mesenchymal source of which has not been unequivocally identified in fish. Osteoblasts display various morphologies, depending on their secretory activity and on their position on the bone: they can be pear-shaped, spindle-shaped, or cuboidal with a pseudoepithelial arrangement (Huysseune, 2000; Witten and Hall, 2002). Secretory osteoblasts have a polarized appearance, with a highly basophilic cytoplasm indicative of intensive protein production. Osteoblasts in acellular bone (see definition below) show a polarized secretion of bone matrix, continuously withdraw from the surface, and are thus never incorporated into the matrix (Ekanayake and Hall, 1987, 1988; Huysseune, 2000; Meunier, 1983; Weiss and Watabe, 1979). Structurally, bone tissue in teleost fish develops first as woven bone. Subsequently, parallel-fibered and lamellar bone develops in more mature individuals. In larger individuals lamellar bone can also form osteons (Meunier, 2002; Moss, 1961a; Smith-Vaniz *et al.*, 1995; Witten and Hall, 2002, 2003). As fish have no hematopoietic tissue inside the bone marrow, bone marrow spaces are filled with fat tissue, besides nerves and blood vessels and some connective tissue cells (Huysseune, 2000; Witten *et al.*, 2001).

IV. Intermediate Skeletal Tissues

Compared to mammals, additional skeletal tissue subtypes are recognized in teleost fish as part of the regular (nonpathological, nonregenerating) skeleton (Benjamin, 1988, 1990; Benjamin *et al.*, 1992; Hall and Witten, 2007; Huysseune, 2000; Meunier and Huysseune, 1992; Witten and Huysseune, 2007) (Fig. 1). Benjamin (1990) describes seven categories of cartilage: (a) hyaline cell cartilage, (b) zellknorpel, (c) fibro/cell-rich cartilage, (d) elastic/cell-rich cartilage, (e) cell-rich hyaline cartilage, (f) matrix-rich hyaline cartilage, and (g) scleral cartilage. Secondary cartilage and chondroid cartilaginous tissues also develop on cranial dermal bones (Benjamin, 1989; Beresford, 1993; Gillis *et al.*, 2006; Huysseune, 2000; Witten and Hall, 2002). The best studied teleost "intermediate skeletal" tissue is chondroid bone (Fig. 1). Chondroid bone exhibits characteristics of bone and of cartilage and develops from osteogenic precursors (Huysseune, 1986; Huysseune and Verraes, 1986). This tissue contains chondrocyte-like cells (devoid of cell processes) surrounded by a bone-like matrix (Beresford, 1981; Huysseune and Sire, 1990; Huysseune and Verraes, 1990; Witten and Hall, 2002). Chondroid bone occurs in basal teleosts with osteocyte-containing bone and in advanced teleosts with acellular bone, and must not be confused with cellular bone (Beresford, 1981, 1993; Gillis *et al.*, 2006; Huysseune and Sire, 1990; Huysseune and Verraes, 1990; Meunier and Huysseune, 1992; Witten and Hall, 2002). Chondroid bone can also be remodeled into lamellar bone (Gillis *et al.*, 2006; Witten and Hall, 2002, 2003).

V. Osteocyte-Containing Bone and Acellular Bone

Like mammalian bone, the bone of more basal teleosts such as zebrafish contains osteocytes (Fig. 2). The density of osteocytes in teleost bone can vary considerably, from one species to another and within the skeleton of one species (Moss, 1961b). No data about the number of osteocytes in teleost bone are available, but in mammals, osteocytes represent 95% of all bone cells and cover 96% of all bone surfaces (Franz-Odendaal *et al.*, 2006; Witten and Huysseune, 2010). In contrast, advanced teleosts such as medaka possess acellular or anosteocytic bone, that is, bone that has no enclosed osteocytes (Ekanayake and Hall, 1987; Kölliker, 1859; Meunier and Huysseune, 1992; Moss, 1961b; Witten *et al.*, 2004) (Fig. 2). With few exceptions, the presence or absence of osteocytes is uniform in all elements of the teleost skeleton (for exceptions, see Meunier, 1989; Moss, 1961a). More basal teleosts such as salmonids and cyprinids (the group to which zebrafish belong), with cellular bone in the endoskeleton, have scales and fin rays that are acellular (Meunier, 1989). Different from dentine, no cell processes penetrate acellular bone. This bone bears however resemblance to atubular dentine that typifies the first-generation teeth of teleosts and to acellular mammalian cementum, both of which are also acellular and are not penetrated by cell processes (Ekanayake and Hall, 1987, 1988; Franz-

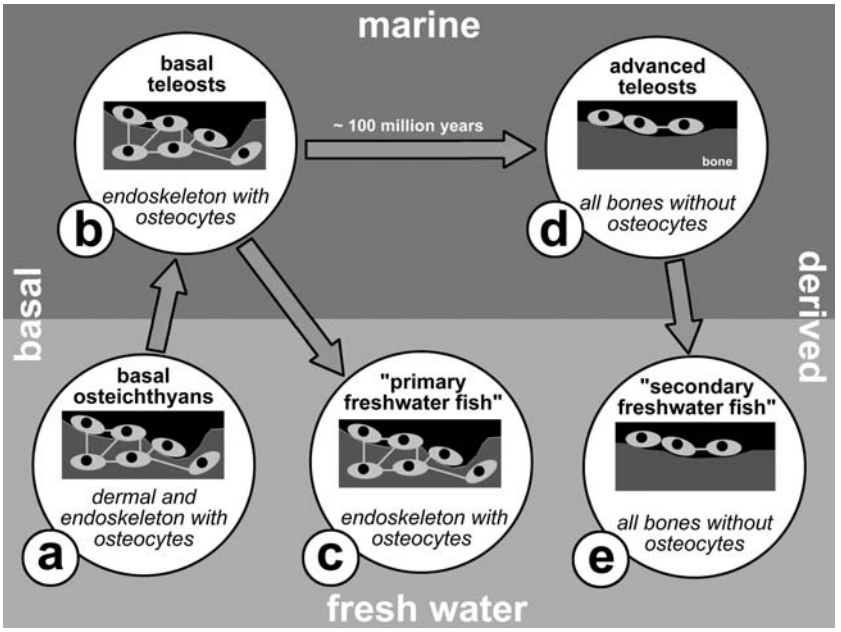

Fig. 2 Relationships between phylogeny, environment, the presence of osteocytes, and the type of osteoclasts in teleost fish such as zebrafish (c) and medaka (e). Basal osteichthyans, which also gave rise to tetrapods, and basal teleosts (a and b) have bone that contains osteocytes, similar to mammalian bone. These fish have mononucleated and many multinucleated osteoclasts. Osteocytes and multinucleated osteoclasts have been preserved during a "first" wave of freshwater reinvasion by teleost fish (e; "primary freshwater fish" such as zebrafish). During a long evolutionary period in the marine environment, osteocytes disappeared (acellular bone) in almost all advanced teleosts (d). The typical osteoclast type of advanced teleosts is mononucleated. This character was maintained when advanced teleosts reinvaded the fresh water (e; "secondary freshwater fish," e.g., medaka). Thus, teleosts that live in fresh water (or in the marine environment) can have different bone types and different types of bone resorbing cells. Modified after Witten and Huysseune (2009).

Odendaal *et al.*, 2006; Meunier, 1989; Sire *et al.*, 2002; Weiss and Watabe, 1979). The formation of acellular bone resembles dentine formation. A polarized secretion of bone matrix ensures that cells never become entrapped in the bone matrix (Huysseune, 2000).

VI. Development of Teleost Vertebral Bodies, A Derived Process

An acellular mineralized tissue particular to all teleosts is the mineralized notochord sheath (Arratia *et al.*, 2001; Bensimon-Brito *et al.*, 2010; Grotmol *et al.*, 2003; Inohaya *et al.*, 2007; Nordvik *et al.*, 2005). Unlike other vertebrates, formation of teleost vertebral bodies does not start with a cartilaginous anlage and

also early bone is lacking. In teleosts, vertebral body development starts with the mineralization of the notochord sheath. The notochord sheath consists of a cartilage-like matrix, rich in proteoglycans and collagen type II, covered by a thin layer of elastin. There is an ongoing debate whether sclerotomal-derived cells from outside or notochord cells from inside facilitate notochord sheath mineralization. Increasing evidence suggests that notochord cells facilitate mineralization of the vertebral body anlagen (Bensimion-Brito *et al.*, 2010; Nordvik *et al.*, 2005). Only the second phase of vertebral body development involves the apposition of bone onto the mineralized notochord sheath, similar to the intramembranous bone formation (Ekanayake and Hall, 1988; Hall and Ekanayake, 1991; Grotmol *et al.*, 2003; Nordvik *et al.*, 2005). Although no cartilage contributes to the initial formation of teleost vertebral bodies (Nordvik *et al.*, 2005; Witten and Villwock, 1997), in larger individuals cartilage at the base of the arches undergoes endochondral ossification and bone that derives from this process becomes part of the vertebral body (Zylberberg and Meunier, 2008). Mineralization of the notochord sheath and the lack of cartilaginous anlagen are derived characters since basal bony fish have, similar to tetrapods (including mammals), cartilaginous vertebral body precursors (Arratia, 1983).

VII. Remodeling of the Teleost Skeleton

The absence of osteocytes in advanced teleosts raises questions about the regulation of bone remodeling, since cell processes from osteocytes and odontoblasts function as stress sensors in other systems. Osteocytes are believed to govern bone remodeling in response to mechanical load (Burger *et al*., 1995; Burger *et al*., 2003). Estimates about the percentage of bone that is resorbed and replaced by new bone in humans range between 4 and 10% per year (Delling and Vogel, 1992; Manolagas, 2000). Such estimates are lacking for teleost fish but a regular resorption and rebuilding of scales and bony skeletal elements is well documented for Atlantic salmon (Kacem *et al.*, 1998; Persson *et al.*, 2000; Witten and Hall, 2002, 2003). While we can expect that the cellular composition of the teleost skeleton affects if and how bone is remodeled, a number of additional factors affect the process. The main characteristics that distinguish teleosts from mammals with respect to skeletal remodeling are as follows (reviewed by Witten and Huysseune, 2009):

(1) In mammals, bone resorbing cells (osteoclasts) originate from hematopoietic tissue located in the bone marrow. The hematopoietic tissue also releases factors that regulate the respective activities of osteoclasts and osteoblasts. Such an intimate spatial relationship between bone resorbing cells and hematopoietic cells does not exist in teleosts as most bone marrow spaces are filled with adipose tissue and hematopoiesis takes place in the head kidney (Field *et al.*, 1995; Song *et al.*, 2004; Witten *et al.*, 2001).

(2) The lack of osteocytes in advanced teleosts coincides with an altered morphology of bone resorbing cells and an alternative mode of bone resorption. Osteoclasts of advanced teleosts are predominately small, mononucleated cells that can perform resorption without generating typical resorption lacunae (Kemp, 2003; Weiss and Watabe, 1979; Witten, 1997; Witten and Huysseune, 2010).

(3) In mammals, endochondral bone formation is a prime cause of skeletal resorption and remodeling. Typical endochondral ossification is, however, often lacking in teleosts, especially in species with small individuals such as medaka and zebrafish. In addition, in all teleosts, vertebral bodies develop (ossify) without cartilaginous precursors and thus initially without remodeling (Arratia *et al.*, 2001; Bensimon-Brito *et al.*, 2010; Grotmol *et al.*, 2003; Inohaya *et al.*, 2007; Nordvik *et al.*, 2005).

(4) Regulation of plasma calcium content is crucial for all terrestrial vertebrates and the skeleton is tightly integrated into the animals' calcium homeostasis. Teleosts have a different approach. They obtain and release calcium from and into the water via their gills and the skeleton is not used as a source or deposit of calcium (Guerreiro *et al.*, 2002; Lall and Lewis-McCrea, 2010; Perry *et al.*, 2003). In particular, resorption of the endoskeleton may be used only as a last mineral resort under extreme conditions (Moss, 1962; Takagi and Yamada, 1991, 1992). When there is a need for skeletal resorption, minerals are first mobilized from the postcranial dermal skeleton (scales) and therefore minerals must not be released from the endoskeleton (Persson *et al*., 1998; Persson *et al*., 1999; Persson *et al*., 2000).

(5) The acellular teleost skeleton responds and adapts to mechanical load (Huysseune *et al.*, 1994; Kranenbarg *et al.*, 2005; Meyer, 1987; Witten *et al.*, 2005a) but the lack of osteocytes in advanced teleosts implies that bone remodeling in response to mechanical load must be triggered by other cell types (Witten and Huysseune, 2009).

(6) Different from sharks, teleosts are capable of repairing their endoskeleton (Ashhurst, 2004; Clement *et al.*, 1992; Moss, 1962, 1977) but the regenerative capacity of elements of the teleost dermal skeleton (fin rays and scales) largely exceeds the regenerative capacity of the endoskeleton (Akimenko and Smith, 2007; Huysseune *et al.*, 2009).

(7) Teleosts replace their teeth throughout life, a process that requires resorption of teeth, tooth attachment bone, and dentigerous bone (Huysseune, 1983, 2000; Huysseune and Sire, 1992b; Huysseune and Witten, 2008; Witten and Huysseune, 2010; Peyer, 1968; Witten *et al.*, 2005b).

(8) Teleosts never stop growing, and certain skeletal elements develop rather late. Thus, growth-related skeletal modeling continues throughout life and should not be mistaken for metabolism-related skeletal remodeling (Kacem *et al.*, 1998; Meunier, 2002; Persson *et al.*, 1998, 1999; Reznick *et al.*, 2002; Smith-Vaniz *et al.*, 1995; Witten and Hall, 2002, 2003).

VIII. Conclusions

The aim of this chapter is to highlight similarities and differences of skeleton formation among teleosts, and between teleosts and mammals. Through the course of evolution different forms of bone have evolved, but all the basic types of skeletal tissues have already been present in ancestral jawless vertebrates. What might appear as significant differences today (e.g., osteocyte-containing bone vs. acellular bone and mononucleated vs. multinucleated osteoclasts) are a variation of a common scheme. Not surprisingly, there is mounting evidence that the genetic control of osteogenesis is conserved and shared among all vertebrates. In other areas, most notable vascular and endothelial cell biology, the close interaction of researchers using the full array of methodologies (from *in vitro* cell culturing systems, morpholino knockdown studies, *in vivo* imaging of cell behavior in zebrafish embryos, inducible knockouts in mice, antibody staining on histological human material) has helped significantly to advance the field as a whole. Comparable progress can be made in the area of osteogenesis if resources are used in a complementing manner.

Acknowledgments

A. Apschner and S. Schulte-Merker would like to thank lab members (past and present) for discussions, in particular C. Hammond, L. Huitema, E. Mackay, I. Logister, J. Peterson-Maduro, and K. Spoorendonk. S.Schulte-Merker is supported by the KNAW and a FP7 Grant (Translation Research in Europe Applied Technologies for Osteoarthritis (TreatOA).

References

Akimenko, M. A., and Smith, A. (2007). Paired fin repair and regeneration. *In* "Fins into Limbs: Evolution, Development, and Transformation," (and B. K. Hall, ed.), pp. 152–162. The University of Chicago Press, Chicago.

Arratia, G. (1983). The caudal skeleton of ostariophysan fishes (Teleostei): intraspecific variation in trichomyteridae (Siluriformes). *J. Morphol.* **177**, 213–229.

Arratia, G., Schultze, H. P., and Casciotta, J. (2001). Vertebral column and associated elements in dipnoans and comparison with other fishes: development and homology. *J. Morphol.* **250**, 101–172.

Ashhurst, D. E. (2004). The cartilaginous skeleton of an elasmobranch fish does not heal. *Matrix Biol.* **23**, 15–22.

Benjamin, M. (1988). Mucochondroid (mucous connective) tissue in the head of teleosts. *Anat. Embryol.* **178**, 461–474.

Benjamin, M. (1989). The development of hyaline-cell cartilage in the head of the black molly, Poecilia sphenops. Evidence for secondary cartilage in a teleost. *J Anat.* **164**, 145–154.

Benjamin, M. (1990). The cranial cartilages of teleosts and their classification. *J. Anat.* **169**, 153–172.

Benjamin, M., Ralphs, J. R., and Eberewariye, O. S. (1992). Cartilage and related tissues in the trunk and fins of teleosts. *J. Anat.* **181**, 113–118.

Bensimon-Brito, A., Cancela, M. L., Huysseune, A., and Witten, P. E. (2010). The zebrafish (*Danio rerio*) caudal complex – a model to study vertebral body fusion. *J. Appl. Ichthyol.* **26**(2), 235–238.

Beresford, W. A. (1981). *Chondroid Bone. Secondary Cartilage and Metaplasia.* Urban & Schwarzenberg, Baltimore-Munich 454 pp.

Beresford, W. A. (1993). Cranial skeletal tissues: diversity and evolutionary trends. *In* "The Skull: Vol. 2. Patterns of Structural and Systematic Diversity," (J. Hanken, and B. K. Hall, eds.), University of Chicago Press, Chicago, pp. 69–130.

Bovee, J. V., Hogendoorn, P. C., Wunder, J. S., and Alman, B. A. (2010). Cartilage tumours and bone development: molecular pathology and possible therapeutic targets. *Nat. Rev. Cancer* **10**, 481–488.

Burger, E. H., Klein-Mullend, J., and Van Der Plas, A. (1995). Function of osteocytes in bone – their role in mechanotransduction. *J. Nutr.* **125**(suppl), 202S–2023S.

Burger, E. H., Klein-Nulend, J., and Smit, T. H. (2003). Strain-derived canalicular fluid flow regulates osteoclast activity in a remodelling osteon – a proposal. *J. Biomech.* **36**, 1453–1459.

Clement, J. G., Officer, R. A., and Dykes, E. (1992). 3-Dimensional reconstruction of shark vertebrae – a technique with applications skeletal remodelling in teleost fish to age and growth-studies. *Aust. J. Mar. Freshwater Res.* **43**, 923–933.

Clement, A., Wiweger, Mvon der Hardt, S., Rusch, M. A., Selleck, S. B., Chien, C. B., and Roehl, H. H. (2008). Regulation of zebrafish skeletogenesis by ext2/dackel and papst1/pinscher. *PLoS Genet.* **4**, e1000136. doi: 10.1371/journal.pgen.1000136.

Cole, A. G., and Hall, B. K. (2004). The nature and significance of invertebrate cartilages revisited: distribution and histology of cartilage and cartilage-like tissues within the Metazoa. *Zoology* **107**(4), 261–273.

Delling, G., and Vogel, M. (1992). Patomorphologie der Osteoporose. *In* "Osteoporose," (H. H. Schild, and M. Heller, eds.), pp. 7–26. Georg Thieme Verlag, Stuttgart.

Donoghue, P. J., Sansom, I., and Downs, J. (2006). Early evolution of vertebrate skeletal tissues and cellular interactions, and the canalization of skeletal development. *J. Exp. Zool. Mol. Dev. Evol.* **306**(3), 278–294.

Ekanayake, S., and Hall, B. K. (1987). The development of the acellularity of the vertebral bone of the Japanese medaka, *Oryzias latipes* (Teleostei; Cyprinidontidae). *J. Morphol.* **193**, 253–261.

Ekanayake, S., and Hall, B. K. (1988). Ultrastructure of the osteogenesis of acellular vertebral bone in the Japanese medaka, *Oryzias latipes* (Teleostei; Cyprinidontidae). *Am. J. Anat.* **182**, 241–249.

Field, M. D. R., Hutchinson, T. H., and Manning, M. J. (1995). Development of adherence techniques for collecting kidney phagocytes from marine fish (*Limanda limanda* L.). *Fish Shellfish Immunol.* **5**, 505–517.

Franz-Odendaal, T., Hall, B. K., and Witten, P. E. (2006). Buried alive: how osteoblasts become osteocytes? *Dev. Dyn.* **235**, 176–190.

Gillis, J. A., Witten, P. E., and Hall, B. K. (2006). Chondroid bone and secondary cartilage contribute to apical dentary growth in juvenile Atlantic salmon. *Salmo salar Linnaeus (1758). J. Fish Biol.* **68**, 1133–1143.

Grotmol, S., Kryvi, H., Nordvik, K., and Totland, G. K. (2003). Notochord segmentation may lay down the pathway for the development of the vertebral bodies in the Atlantic salmon. *Anat. Embryol.* **207**, 263–272.

Guerreiro, P. M., Fuentes, J., Canario, A. V., and Power, D. M. (2002). Calcium balance in sea bream (Sparus aurata): the effect of oestradiol-17ß. *J. Endocrinol.* **173**, 377–385.

Hall, B. K. (1998). *Evolutionary Developmental Biology, 2nd. London, Chapman and Hall.*

Hall, B. K., and Ekanayake, S. (1991). Effects of growth factors on the differentiation of neural crest cells and neural crest cell-derivatives. *Int J Dev Biol.* **35**(4), 367–387.

Hall, B. K., and Witten, P. E. (2007). Plasticity of and transitions between skeletal tissues in vertebrate evolution and development. *In* "Major Transitions in Vertebrate Evolution," (J. S. Anderson, and H. -D. Sues, eds.), pp. 13–56. Bloomington, IN, Indiana University Press.

Hammond, C. L., and Schulte-Merker, S. (2009). Two populations of endochondral osteoblasts with differential sensitivity to Hedgehog signalling. *Development* **136**, 3991–4000.

Hilton, M. J., Gutierrez, L., Martinez, D. A., and Wells, D. E. (2005). EXT1 regulates chondrocyte proliferation and differentiation during endochondral bone development. *Bone* **36**, 379–386.

Huysseune, A. (1983). Observations on tooth development and implantation in the upper pharyngeal jaws in Astatotilapia elegans (Teleostei, Cichlidae). *J. Morphol.* **175**(3), 217–234.

Huysseune, A. (1986). Late skeletal development at the articulation between upper pharyngeal jaws and neurocranial base in the fish, *Astatotilapia elegans*, with the participation of a chondroid form of bone. *Am. J. Anat.* **177**, 119–137.

Huysseune, A. (2000). Skeletal system. *In* "The Laboratory Fish. Part 4 Microscopic Functional Anatomy," (and G. K. Ostrander, ed.), pp. 307–317. Academic Press, San Diego.

Huysseune, A., and Sire, J. Y. (1990). Ultrastructural observations on chondroid bone in the teleost fish *Hemichromis bimaculatus*. *Tissue Cell* **22**, 371–383.

Huysseune, A., and Sire, J. -Y. (1992a). Development of cartilage and bone tissues of the anterior part of the mandible in cichlid fish: a light and TEM study. *Anat. Rec.* **233**, 357–375.

Huysseune, A., and Sire, J. -Y. (1992b). Bone and cartilage resorption in relation to tooth development in the anterior part of the mandible in cichlid fish: a light and TEM study. *Anat. Rec.* **234**, 1–14.

Huysseune, A., Sire, J. Y., and Meunier, F. J. (1994). Comparative study of lower pharyngeal jaw structure in two phenotypes of *Astatoreochromis alluaudi* (Teleostei: Cichlidae). *J. Morphol.* **221**, 25–43.

Huysseune, A., Sire, J. Y., and Witten, P. E. (2009). Evolutionary and developmental origins of the vertebrate dentition. *J Anat.* **214**, 465–476.

Huysseune, A., Sire, J. Y., and Witten, P. E. (2010). A revised hypothesis on the evolutionary origin of the vertebrate dentition. *J. Appl. Ichthyol.* **26**(2), 152–155.

Huysseune, A., and Verraes, W. (1986). Chondroid bone on the upper pharyngeal jaws and neurocranial base in the adult fish *Astatotilapia elegans*. *Am. J. Anat.* **177**, 527–535.

Huysseune, A., and Verraes, W. (1990). Carbohydrate histochemistry of mature chondroid bone in *Astatotilapia elegans* (Teleostei: Cichlidae) with a comparison to acellular bone and cartilage. *Ann. Sci. Nat. B Zool. Biol. Anim.* **11**(1), 29–43.

Huysseune, A., and Witten, P. E. (2008). An evolutionary view on tooth development and replacement in wild Atlantic salmon (*Salmo salar* L). *Evol. Dev.* **10**(1), 6–14.

Inohaya, K., Takano, Y., and Kudo, A. (2007). The teleost intervertebral region acts as a growth centre of the centrum: *in vivo* visualization of osteoblasts and their progenitors in transgenic fish. *Dev. Dyn.* **236**, 3031–3046.

Jennes, I., Pedrini, E., Zuntini, M., Mordenti, M., Balkassmi, S., Asteggiano, C. G., Casey, B., Bakker, B., Sangiorgi, L., and Wuyts, W. (2009). Multiple osteochondromas: mutation update and description of the multiple osteochondromas mutation database (MOdb). *Hum. Mutat.* **30**, 1620–1627.

Jones, K. B., Piombo, V., Searby, C., Kurriger, G., Yang, B., Grabellus, F., Roughley, P. J., Morcuende, J. A., Buckwalter, J. A., and Capecchi, M. R., *et al*. (2010). A mouse model of osteochondromagenesis from clonal inactivation of Ext1 in chondrocytes. *Proc. Natl. Acad. Sci. U. S. A.* **107**, 2054–2059.

Kacem, A., Meunier, F. J., and Baglinière, J. L. (1998). A quantitative study of morphological and histological changes in the skeleton of *Salmo salar* during its anadromous migration. *J. Fish Biol.* **53**, 1096–1109.

Kemp, A. (2003). Ultrastructure of developing tooth plates in the Australian lungfish, *Neoceratodus forsteri* (Osteichthyes: Dipnoi). *Tissue Cell* **35**, 401–426.

Kölliker, A. (1859). On the different types in the microstructure of the skeletons of osseous fish. *Proc. R. Soc. Lond.* **9**, 656–668.

Koziel, L., Kunath, M., Kelly, O. G., and Vortkamp, A. (2004). Ext1-dependent heparan sulfate regulates the range of Ihh signaling during endochondral ossification. *Dev. Cell* **6**, 801–813.

Kranenbarg, S., van Cleynenbreugel, T., Schipper, H., and van Leeuwen, J. (2005). Adaptive bone formation in acellular vertebrae of sea bass (*Dicentrarchus labrax* L). *J. Exp. Biol.* **208**, 3494–3502.

Lai, L. P., and Mitchell, J. (2005). Indian hedgehog: its roles and regulation in endochondral bone development. *J. Cell. Biochem.* **96**, 1163–1173.

Lall, S. P., and Lewis-McCrea, L. M. (2010). Effects of phosphorus and vitamin C deficiency, vitamin A toxicity, and lipid peroxidation on skeletal abnormalities in Atlantic halibut (*Hippoglossus hippoglossus*). *J. Appl. Ichthyol.* **26**(2), 334–343.

Lin, X., Wei, G., Shi, Z., Dryer, L., Esko, J. D., Wells, D. E., and Matzuk, M. M. (2000). Disruption of gastrulation and heparan sulfate biosynthesis in EXT1-deficient mice. *Dev. Biol.* **224**, 299–311.

Mak, K. K., Bi, Y., Wan, C., Chuang, P. T., Clemens, T., Young, M., and Yang, Y. (2008). Hedgehog signaling in mature osteoblasts regulates bone formation and resorption by controlling PTHrP and RANKL expression. *Dev. Cell* **14**, 674–688.

Manolagas, S. C. (2000). Birth and death of bone cells: basic regulatory mechanisms and implications for the pathogenesis and treatment of osteoporosis. *Endocr. Rev.* **21**, 115–137.

Matsumoto, K., Irie, F., Mackem, S., and Yamaguchi, Y. (2010). A mouse model of chondrocyte-specific somatic mutation reveals a role for Ext1 loss of heterozygosity in multiple hereditary exostoses. *Proc. Natl. Acad. Sci. U. S. A.* **107**, 10932–10937.

McInnes, I. B., and O'Dell, J. R. (2010). State-of-the-art: rheumatoid arthritis. *Ann. Rheum. Dis.* **69**, 1898–1906.

Metscher, B. D., and Ahlberg, P. E. (1999). Zebrafish in context: uses of a laboratory model in comparative studies. *Dev. Biol.* **210**, 1–4.

Meunier, F.J. (1983). Les tissus osseux des Osteichthyens. Structure, genèse, croissance et evolution. Archives et Documents, Micro-Edition, Inst. Ethnol., S.N 82-600, 238, 1–200.

Meunier, F. J. (1989). The acellularisation process in osteichthyan bone. *Prog. Zool.* **35**, 443–445.

Meunier, F. J. (2002). Skeleton. *In* "Manual of Fish Sclerochronology," (J. Panfili, H. de Pontual, H. Troadec, and P. J. Wright, eds.), pp. 65–88. Ifremer-IRD coedition, Brest.

Meunier, F. J., and Huysseune, A. (1992). The concept of bone tissue in osteichthyes. *Neth. J. Zool.* **42**, 445–458.

Meyer, A. (1987). Phenotypic plasticity and heterochrony in *Cichlasoma managuense* (Pisces, Cichlidae) and their implications for speciation in cichlid fishes. *Evolution* **41**, 1357–1369.

Moss, M. L. (1961 a). Osteogenesis of acellular teleost fish bone. *Am. J. Anat.* **108**, 99–110.

Moss, M. L. (1961 b). Studies of the acellular bone of teleost fish. 1. Morphological and systematic variations. *Acta Anat.* **46**, 343–462.

Moss, M. L. (1962). Studies of the acellular bone of teleost fish. 2. Response to fracture under normal and acalcemic variations. *Acta Anat.* **48**, 46–60.

Moss, M. L. (1977). Skeletal tissues in sharks. *Am. Zool.* **17**, 335–342.

Mundy, G. R., and Yang, X. (2008). Hedgehog coordination of postnatal osteoclast and osteoblast activities. *Dev. Cell* **14**, 637–638.

Nordvik, K., Kryvi, H., Totland, G. K., and Grotmol, S. (2005). The salmon vertebral body develops through mineralization of two preformed tissues that are encompassed by two layers of bone. *J. Anat.* **206**, 103–114.

Ohba, S., Kawaguchi, H., Kugimiya, F., Ogasawara, T., Kawamura, N., Saito, T., Ikeda, T., Fujii, K., Miyajima, T., and Kuramochi, A., *et al*. (2008). Patched1 haploinsufficiency increases adult bone mass and modulates Gli3 repressor activity. *Dev. Cell* **14**, 689–699.

Owen, R. (1845). *Odontography or, a Treatise on the Comparative Anatomy of the Teeth; Their Physiological Relations, Mode of Development and Microscopic Structure in the Vertebrate Animals, Vol. 2, 35 pages, 168 plates.* Hippolyte Bailierre Publisher, London.

Perry, S. F., Shahsavarani, A., Georgalis, T., Bayaa, M., Furimsky, M., and Thomas, S. L. Y. (2003). Channels, pumps, and exchangers in the gill and kidney of freshwater fishes: their role in ionic and acid–base regulation. *J Exp. Zool.* **300A**, 53–62.

Persson, P., Björnsson, B. T., and Takagi, Y. (1999). Characterisation of morphology and physiological actions of scale osteoclasts in the rainbow trout. *J. Fish Biol.* **54**, 669–684.

Persson, P., Shrimpton, J. M., McCormick, S. D., and Björnsson, B. T. (2000). The presence of high-affinity. low-capacity estradiol-17ß binding in rainbow trout scale indicates a possible endocrine route for the regulation of scale resorption. *Gen. Comp. Endocrinol.* **120**, 35–43.

Persson, P., Sundell, K., Björnsson, B. T., and Lundqvist, H. (1998). Calcium metabolism and osmoregulation during sexual maturation of river running Atlantic salmon. *J. Fish Biol.* **52**, 334–349.

Peyer, B. (1968). *Comparative Odontology.* Chicago and London, The University of Chicago Press.

Ralston, S. H., and Uitterlinden, A. G. (2010). Genetics of osteoporosis. *Endocr. Rev.* **31**, 629–662.

Reif, W. E. (1982). Evolution of dermal skeleton and dentition in vertebrates: the odontode regulation theory. *Evol. Biol.* **15**, 287–368.

Reif, W. E. (2006). Conodonts, odontodes, stem-groups, and the ancestry of enamel genes. *Neues Jahrbuch Geologie Paläontologie Abhandlungen* **241**, 405–439.

Renn, J., and Winkler, C. (2009). Osterix-mCherry transgenic medaka for *in vivo* imaging of bone formation. *Dev. Dyn.* **238**, 241–248.

Reznick, D., Ghalambo, C., and Nunney, L. (2002). The evolution of senescence in fish. *Mech. Ageing Dev.* **123**, 773–789.

Sire, J. Y., and Akimenko, M. A. (2004). Scale development in fish: a review, with description of sonic hedgehog (shh) expression in the zebrafish (*Danio rerio*). *Int. J. Dev. Biol.* **48**, 233–247.

Sire, J. Y., Davit-Beal, T., Delgado, S., Van der heyden, C., and Huysseune, A. (2002). First-generation teeth in non-mammalian lineages: evidence for a conserved ancestral character? *Microsc. Res. Tech.* **59**, 408–434.

Smith, M. M., and Hall, B. K. (1990). Development and evolutionary origins of vertebrate skeletogenic and odontogenic tissues. *Biol. Rev.* **65**, 277–373.

Smith-Vaniz, W. F., Kaufman, L. S., and Glowacki, J. (1995). Species-specific patterns of hyperostosis in marine teleost fishes. *Mar. Biol.* **121**, 573–580.

Song, H. D., Sun, X. J., Deng, M., Zhang, G. W., Zhou, Y., Wu, X. Y., Sheng, Y., Chen, Y., Ruan, Z., Jiang, C. L., Fan, H. Y., Zon, L. I., Kanki, J. P., Liu, T. X., Look, A. T., and Chen, Z. (2004). Hematopoietic gene expression profile in zebrafish kidney marrow. *Proc. Natl. Acad. Sci. U. S. A.* **101**(46), 16240–16245.

Spoorendonk, K. M., Hammond, C. L., Huitema, L. F. A., Vanoevelen, J., and Schulte-Merker, S. (2010). Zebrafish as a unique model system in bone research: the power of genetics and *in vivo* imaging. *J. Appl. Ichthyol.* **26**, 219–224.

Spoorendonk, K. M., Peterson-Maduro, J., Renn, J., Trowe, T., Kranenbarg, S., Winkler, C., and Schulte-Merker, S. (2008). Retinoic acid and Cyp26b1 are critical regulators of osteogenesis in the axial skeleton. *Development* **135**, 3765–3774.

St-Jacques, B., Hammerschmidt, M., and McMahon, A. P. (1999). Indian hedgehog signaling regulates proliferation and differentiation of chondrocytes and is essential for bone formation. *Genes Dev.* **13**, 2072–2086.

Stickens, D., Zak, B. M., Rougier, N., Esko, J. D., and Werb, Z. (2005). Mice deficient in Ext2 lack heparan sulfate and develop exostoses. *Development* **132**, 5055–5068.

Takagi, Y., and Yamada, J. (1991). Effects of calcium and phosphate deficiencies on bone metabolism in a teleost. tilapia (*Oreochromis niloticus*): a histomorphometric study. *In* "Mechanisms and Phylogeny of Mineralization in Biological Systems," (S. Suga, and H. Nakahara, eds.), pp. 187–191. Springer Verlag, Tokyo (517 pp.).

Takagi, Y., and Yamada, J. (1992). Effects of calcium deprivation on the metabolism of acellular bone in tilapia. *Oreochromis niloticus. Comp. Biochem. Physiol.* **102A**, 481–485.

Verreijdt, L., Vandervennet, E., Sire, J. Y., and Huysseune, A. (2002). Developmental differences between cranial bones in the zebrafish (*Danio rerio*): some preliminary light and TEM observations. *Connect. Tissue Res.* **43**, 109–112.

Weiss, R. E., and Watabe, N. (1979). Studies on the biology of fish bone. III. Ultrastructure of osteogenesis and resorption in osteocytic (cellular) and anosteocytic (acellular) bones. *Calcif. Tissue Int.* **28**, 43–56.

Witten, P. E. (1997). Enzyme histochemical characteristics of osteoblasts and mononucleated osteoclasts in a teleost fish with acellular bone (*Oreochromis niloticus Cichlidae*). *Cell Tissue Res.* **287**, 591–599.

Witten, P. E., Gil-Martens, L., Hall, B. K., Huysseune, A., and Obach, A. (2005a). Compressed vertebrae in Atlantic salmon (*Salmo salar*): evidence for metaplastic chondrogenesis as a skeletogenic response late in ontogeny. *Dis. Aquat. Organ.* **64**(3), 237–246.

Witten, P. E., and Hall, B. K. (2002). Differentiation and growth of kype skeletal tissues in anadromous male Atlantic salmon (*Salmo salar*). *Int. J. Dev. Biol.* **46**, 719–730.

Witten, P. E., and Hall, B. K. (2003). Seasonal changes in the lower jaw skeleton in male Atlantic salmon (*Salmo salar* L): remodelling and regression of the kype after spawning. *J. Anat.* **203**, 435–450.

Witten, P. E., Hall, B. K., and Huysseune, A. (2005b). Are breeding teeth in Atlantic salmon a component of the drastic alterations of the oral facial skeleton? *Arch. Oral Biol.* **50**, 213–217.

Witten, P. E., Hansen, A., and Hall, B. K. (2001). Features of mono and multinucleated bone resorbing cells of the zebrafish *Danio rerio* and their contribution to skeletal development, remodelling and growth. *J. Morphol.* **250**, 197–207.

Witten, P. E., and Huysseune, A. (2007). Mechanisms of chondrogenesis and osteogenesis in fins. *In* "Fins into Limbs: Evolution, Development, and Transformation," (and B. K. Hall, ed.), pp. 79–92. Chicago, The University of Chicago Press.

Witten, P. E., and Huysseune, A. (2009). A comparative view on mechanisms and functions of skeletal remodelling in teleost fish, with special emphasis on osteoclasts and their function. *Biol. Rev.* **84**, 315–346.

Witten, P. E., and Huysseune, A. (2010). The unobtrusive majority: mononucleated bone resorbing cells in teleost fish and mammals. *J. Appl. Ichthyol.* **26**(2), 225–229.

Witten, P. E., Huysseune, A., Franz-Odendaal, T., Fedak, T., Vickaryous, M., Cole, A., and Hall, B. K. (2004). Acellular teleost bone: primitive or derived, dead or alive? *Palaeontol. Newslett* **55**, 37–41.

Witten, P. E., Huysseune, A., and Hall, B. K. (2010). A practical approach for the identification of the many cartilaginous tissues in teleost fish. *J. Appl. Ichthyol.* **26**(2), 257–262.

Witten, P. E., and Villwock, W. (1997). Growth requires bone resorption at particular skeletal elements in a teleost fish with acellular bone (*Oreochromis niloticus,* Teleostei: Cichlidae). *J. Appl. Ichthyol.* **13**(4), 149–158.

Zelzer, E., and Olsen, B. R. (2003). The genetic basis for skeletal diseases. *Nature* **423**, 343–348.

Zylberberg, L., and Meunier, F. J. (2008). New data on the structure and the chondrocyte populations of the haemal cartilage of abdominal vertebrae in the adult carp *Cyprinus carpio* (Ostariophysii, Cyprinidae). *Cybium* **32**(3), 225–239.

CHAPTER 11

Zebrafish Assays of Ciliopathies

Norann A. Zaghloul[*] and Nicholas Katsanis[†]

[*]Department of Medicine, Division of Endocrinology, Diabetes and Nutrition, University of Maryland School of Medicine, Baltimore, Maryland, USA

[†]Center for Human Disease Modeling, Departments of Cell Biology and Pediatrics, Duke University Medical Center, Durham, North Carolina, USA

Abstract

In light of the growing list of human disorders associated with their dysfunction, primary cilia have recently come to attention as being important regulators of developmental signaling pathways and downstream processes. These organelles, present on nearly every vertebrate cell type, are highly conserved structures allowing for study across a range of species. Zebrafish, in particular, have emerged as useful organisms in which to explore the consequences of ciliary dysfunction and to model human ciliopathies. Here, we present a range of useful techniques that allow for investigation of various aspects of ciliary function. The described assays capitalize on the hallmark gastrulation defects associated with ciliary defects as well as relative ease of visualization of cilia in whole-mount embryos. Further, we describe our recently developed assay for querying functionality of human gene variants in live developing embryos. Finally, a current catalog of known zebrafish ciliary mutant lines is included. The techniques presented here provide a basic toolkit for *in vivo* investigation of both the biological and genetic mechanisms underlying a growing class of human diseases.

METHODS IN CELL BIOLOGY, VOL 105

0091-679X/10 $35.00
DOI 10.1016/B978-0-12-381320-6.00011-4

I. Introduction

Primary cilia are highly conserved cellular structures, now understood to be present on the surface of most vertebrate cell types, at least during some point of their life cycle. In contrast to the multiciliated nature of cells bearing motile cilia, cells typically bear a solitary primary cilium that extends from the apical cell surface and is made up of a microtubule-based axoneme, anchored at the base by the basal body. Although the functions of the basal body are not fully understood, one of its roles is to regulate trafficking to the cilium (Jin *et al.*, 2010), where proteins undergo transport along the axoneme. This mechanism, termed intraflagellar transport (IFT), is mediated by complexes of IFT and motor proteins that transport proteins between the basal body and the tip of the cilium (Pedersen and Rosenbaum, 2008).

While motile cilia have long been recognized as being of physiological importance in specialized ciliated cell types, such as those lining the lung epithelium, primary cilia (also known as sensory or immotile cilia) have only recently gained prominence as having an important role in the regulation of reception and transduction of cellular signaling (Berbari *et al.*, 2009; Goetz *et al.*, 2009; Satir *et al.*, 2010). Two pathways with major roles in developmental specification, Sonic hedgehog (Shh) and Wnt, require intact functioning cilia for proper transduction (Corbit *et al.*, 2005, 2008; Gerdes *et al.*, 2007; Huangfu *et al.*, 2003). There is some controversy over whether ciliary dysfunction in zebrafish produces defects in Wnt only, Shh only, or both. Although studies have shown Wnt-related defects in basal body suppressed embryos, including convergent extension phenotypes bearing the hallmark of defects in the noncanonical Wnt planar cell polarity (PCP) pathway (Ross *et al.*, 2005) and a concomitant slight upregulation of canonical Wnt targets (Gerdes *et al.*, 2007), a maternal zygotic *ift88* mutant showed no sign of Wnt defects, even in the complete absence of cilia (Huang and Schier, 2009). The latter study showed Shh defects exclusively. A recent study, however, showed no sign of Hedgehog signaling defects in *ift57*, *ift88*, and *ift172* mutants (Lunt *et al.*, 2009). Although the exact role of cilia in *in vivo* regulation of these pathways remains elusive, the zebrafish has emerged as a useful model in which to query signaling defects associated with ciliary dysfunction.

A structure that has made this organism particularly useful in the study of cilia is the highly ciliated Kupffer's vesicle (KV), a transient spherical structure appearing at the 5-somite stage and persisting until Prim-5. KV, which plays a role in patterning akin to the roles of the mammalian node, is comprised of cells bearing cilia that beat to direct fluid flow across the structure and contribute to asymmetrical gene expression. Thus, KV offers a useful tool to investigate the extent of ciliary defects, both in the formation of cilia and in their functionality.

In addition to assays of motile ciliary beat function using KV flow as a model, recent efforts have focused increasingly on the use of this system to assay defects in primary cilia (Jaffe *et al.*, 2010). This has paved the way for the development of the zebrafish as a useful model for many of the disorders associated with ciliary dysfunction, the ciliopathies. The ciliopathies are a group of disorders often characterized by

pleiotropic defects as a result of mutations in genes that affect ciliary function. Diseases of cilia range from relatively rare syndromes, such as Bardet–Biedl syndrome, Meckel–Gruber syndrome, and Joubert syndrome, to more common clinical entities, such as polycystic kidney disease. Although these disorders vary by their combinations of phenotypes, hallmark characteristics of ciliary dysfunction are often observed across them. These include renal dysfunction, retinal degeneration, obesity, mental retardation, and left–right patterning defects (Cardenas-Rodriguez and Badano, 2009). Many of these features, particularly kidney cysts, are found in zebrafish models of ciliopathies and have been used to identify ciliary mutants in forward genetic screens (Sullivan-Brown *et al.*, 2008; Sun *et al.*, 2004).

A useful feature in the development of zebrafish models for these disorders is the significant genetic overlap between ciliopathies, in which multiple disorders can be caused by mutations in the same gene or multiple genes can contribute to the same disorder. For example, the Meckel–Gruber syndrome genes, *MKS1* and *MKS3*, can contribute causative and modifying alleles to Bardet–Biedl syndrome, respectively, as does one of the nephronophthisis genes, *NPHP6/CEP290* (Leitch *et al.*, 2008). These data are likely representative of the mutual contribution of ciliary genes to similar biological processes that underlie overlapping disease phenotypes. As such, zebrafish ciliary mutants and morphants with defects in various genes often display similar phenotypes, such as the cystic kidneys and body curving defects observed in *ift* mutants (Sun *et al.*, 2004) or the gastrulation defects observed in *BBS* and *NPHP* morphants (Gerdes *et al.*, 2007; Leitch *et al.*, 2008; Zhou *et al.*, 2010); consequently, individual lines may serve as models for multiple ciliopathies.

Zebrafish models of human ciliopathies have been established in lines with null mutations in IFT or basal body genes as well as in wild-type embryos by suppressing protein expression of ciliary genes via injection of translation- or splice-blocking antisense morpholinos. For example, several mutant lines and a morpholino have been developed that target the zebrafish polycystic kidney disease ortholog, *polycystin-2* (Sun *et al.*, 2004). Morphant embryos develop pronephric cysts early in development and enlarged pronephric ducts (Obara *et al.*, 2006; Schottenfeld *et al.*, 2007; Sun *et al.*, 2004). Similarly, two lines have been identified through forward genetic screens with mutations in Joubert syndrome genes, *arl13b* and *cc2d2a* (Owens *et al.*, 2008; Sun *et al.*, 2004). These lines provide useful developmental systems in which to investigate phenotypes resulting from the loss of these genes. In addition to ciliary mutants, zebrafish ciliopathy models have been generated using targeted gene knockdown via morpholino injection. Each of the 14 Bardet–Biedl syndrome genes, for example, has been investigated in this way with suppression resulting in early developmental phenotypes, including perturbed gastrulation movements (Gerdes *et al.*, 2007; Zaghloul *et al.*, 2010). In addition to providing insight as to the developmental ramifications of perturbing BBS gene expression, we have recently demonstrated the power of this system to model human BBS gene functionality. Using human BBS mRNA to rescue the morphant phenotypes, this system allows for interrogation of the functional consequences of any introduced variant (Leitch *et al.*, 2008; Zaghloul *et al.*, 2010). This provides a method of "humanizing"

the zebrafish to use it as a model for human disease gene function and variability. The ability of human variants to function in zebrafish represents a tremendous advantage of this system due to the possibility of exploring on a large scale the consequences of gene variation on developmental phenotypes in an *in vivo* vertebrate system with physiological relevance to humans. This method, described below, adds power of the zebrafish model.

II. Methods

A. Visualization of Cilia in Zebrafish Embryos

Visualization of cilia in ciliary morphant or mutant embryos is often a necessary first step in verifying a ciliary defect. Because ciliary structural proteins are highly conserved, reagents developed for use in mammalian systems can be readily applied to zebrafish. This includes common antibodies used for specific labeling of individual cilia.

1. Whole-mount Fluorescence Imaging of Cilia

The following protocol was developed for whole-mount immunostaining of cilia using a mouse anti-acetylated α-tubulin primary antibody (Sigma T6793):

1. Embryos cultured in embryo medium (Westerfield, 2000) should be fixed at the desired embryonic stage. We have found that use of Dent's fixative (80% MeOH, 20% DMSO) is more effective for labeling of cilia compared to 4% paraformaldehyde. Fix embryos at room temperature for 2 h to overnight. To dehydrate, transfer embryos to 100% MeOH for at least 2 h before proceeding and store up to several weeks at -20 °C.
   Rehydrate embryos sequentially for 10 min in each wash: 75% MeOH in PBS, 50% MeOH in PBS, 25% MeOH in PBS, and 100% PBS. Wash once in immunostaining buffer (1× PBS, 0.1% Tween 20, 1% BSA) for 10 min.
2. Transfer embryos to blocking buffer (10% sheep serum, 1% BSA, 1× PBS) for 1 h at room temperature. Incubate embryos in 1° antibody (1:500 in blocking buffer) solution overnight at 4 °C.
3. To remove 1° antibody solution, wash embryos in immunostaining buffer twice, 10 min each. Transfer embryos to 2° antibody solution – goat anti-mouse (Invitrogen A-10667) – at 1:1000 in blocking buffer. Incubate for 1 h at room temperature. Wash embryos in immunostaining buffer twice, 10 min each.
4. Embryos can be incubated in DAPI (1:5000) solution for 10 min, at this point, and then washed twice, 10 min each, in immunostaining buffer.
5. Following the protocol, embryos are stored at 4 °C in immunostaining buffer or 100% MeOH until imaging.
6. For imaging, place individual embryo in a depression slide, covered with Permount. Quickly, place a coverslip over the depression well and slide the

coverslip over embryo until the desired orientation is attained (Fig. 1A). Embryos should be imaged using confocal microscopy (Fig. 1B).

2. Visualization of Kupffer's Vesicle

KV can be visualized in segmentation and early pharyngula stage embryos from five somites until prim-5 (24 hpf). This heavily ciliated spherical structure makes it ideal for visualization of the presence/absence of cilia, ciliary length, and ciliary orientation. KV is best observed by dual antibody staining of both cilia (via anti-acetylated α-tubulin antibody) and the apical surface of epithelial KV cells (via anti-atypical protein kinase C antibody; Amack *et al.*, 2007). This is carried out using the immunostaining protocol described above with two minor adjustments:

1. Include the second, anti-aPKC antibody (Santa Cruz Biotechnology SC-216) in the primary antibody solution for overnight incubation at 4 °C. The final concentration should be 1:100 while the anti-acetylated α-tubulin concentration remains at 1:500.
2. Include a second, goat anti-rabbit (Invitrogen A-11012) antibody in the secondary antibody solution. Both secondary antibodies should be used at 1:1000.

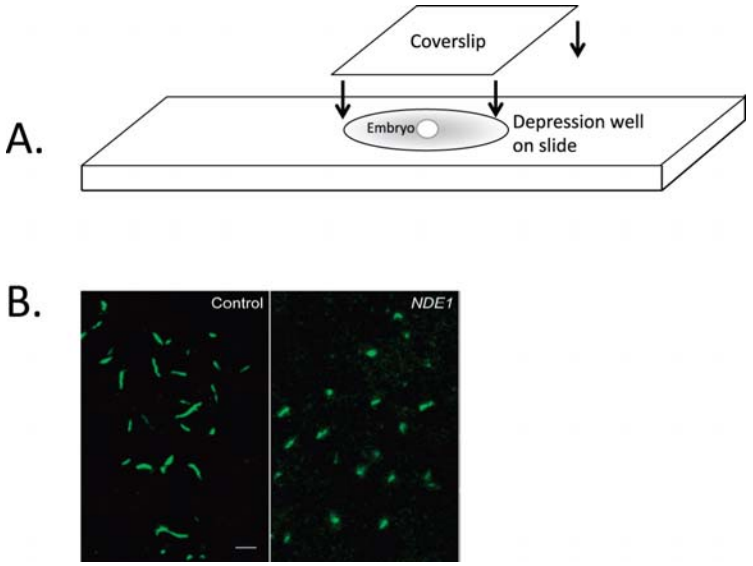

Fig. 1 Visualization of cilia in whole-mount fixed embryos. (A) After immunostaining for acetylated α-tubulin, whole embryos are mounted in depression well slides and covered with a coverslip. Once placed in the well, the embryo is rotated by gentle rotation of the coverslip until the desired orientation for imaging is achieved. (B) Confocal imaging of cilia in Kupffer's vesicle in immunostained, mounted embryos. Cilia conformation and length can be easily observed. In this example, control embryos exhibit normal length cilia, whereas *NDE1*-overexpressing embryos exhibit shorter cilia (modified from Kim *et al.*, 2011). (Permission from Nat. Cell Biol., License #: 2721450638335.) (For color version of this figure, the reader is referred to the web version of this book.)

B. Phenotypic Assays of Ciliary Dysfunction

Though the molecular mechanisms underlying the early developmental steps giving rise to ciliopathy phenotypes have yet to be fully deciphered, assessment of zebrafish embryos early in development provides insight into defects in patterning and specification that may give rise to later organ-specific defects. The most prominent of these early defects are those associated with perturbed PCP signaling and resulting defects in convergent extension movements. Embryos with PCP defects exhibit characteristic phenotypes at the segmentation stages. We have developed a suite of assays to systematically assess these phenotypes to determine the extent of the defect conferred by ciliary dysfunction.

1. Live Embryo Phenotypes

Defective convergent extension, as a result of disrupted PCP signaling, produces aberrant movement of cells during gastrulation. The result is perturbed specification of anatomical structures during segmentation stages, which may give rise to later organogenesis defects. This assay of ciliopathy mutants and morphant phenotypes focuses on phenotypes established in PCP signaling mutants (Sepich *et al.*, 2000).

1. Inject wild-type embryos at the one- to two-cell stage with a morpholino targeting a ciliary gene of interest or, alternatively, collect embryos from matings of a ciliary mutant line.
2. Culture embryos in embryo medium for 11–14 h until the 8–10 somite stage.
3. Embryos can be scored directly in the culture dish, without dechorionation. We have devised a system of scoring and categorization into classes based on the extent and number of defects. Observed convergent extension defects are: shortening of the body axis (from lateral view), reduced head size (lateral view), broadening of the notochord (from dorsal view), kinking of the notochord (dorsal view), wide somites (dorsal view), and thin somites (dorsal view). Embryos considered "Class I" or moderately affected are characterized by the presence of one very severe defect or two moderate defects (Fig. 2). Embryos classed as "Class II" or severely affected are characterized by the presence of three or more defects of moderate or extreme severity (Fig. 2). An additional class, "Class Y," was introduced to denote embryos in which gastrulation epiboly movements were not completed.

2. Measurement of Convergent Extension Defects by ISH

To verify and quantify the extent of the convergent extension defect, we have developed a method by which to measure the most prominent convergent extension defect, shortening of the body axis.

1. Fix morphant or mutant embryos at 8–10 somites in 4% paraformaldehyde overnight at 4 °C. Transfer to 100% MeOH. Store at −20 °C for at least 2 h or as long as several months.

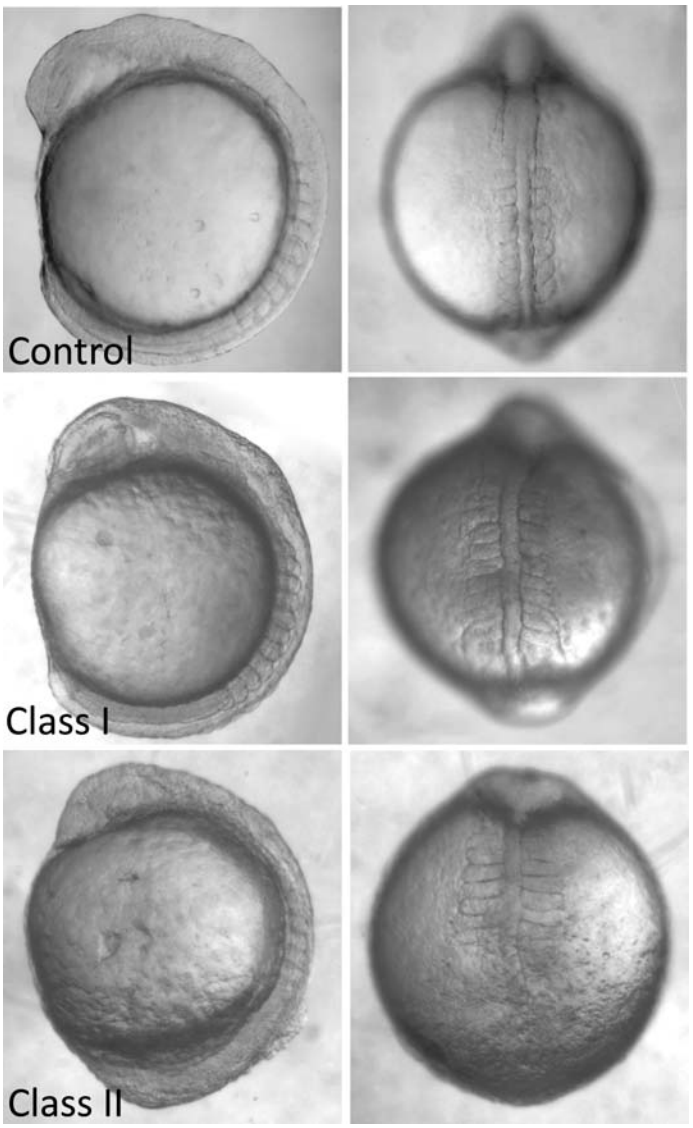

Fig. 2 Gastrulation defect phenotypes associated with ciliary dysfunction. Embryos with disrupted ciliary gene expression (by morpholino suppression in this example) exhibit gastrulation defects that manifest at somitic stages as shortened body axes, widened and kinked notochords, and widened and thinned somites. Embryos can be categorized, based on the extent and severity of the phenotypes, into Class I (moderately affected) and Class II (severely affected).

2. Perform whole-mount *in situ* hybridization according to standard protocol (Thisse and Thisse, 2008) using a riboprobe cocktail of *myoD*, *krox20*, and *pax2* to label adaxial mesodermal cells, somites, anterior neural structures, and pronephric mesoderm, respectively. Individual embryos must be flat-mounted and imaged with consistent magnification across all samples.
3. On each embryo image, measure the distance from the first to the last (anterior to posterior) appreciable somite. Measurements for embryos in each injection or mutant treatment, or controls, are normally distributed when plotted. Each curve can then be compared to others as a means of quantification of the average shortened body axis defect for each group (Fig. 3).

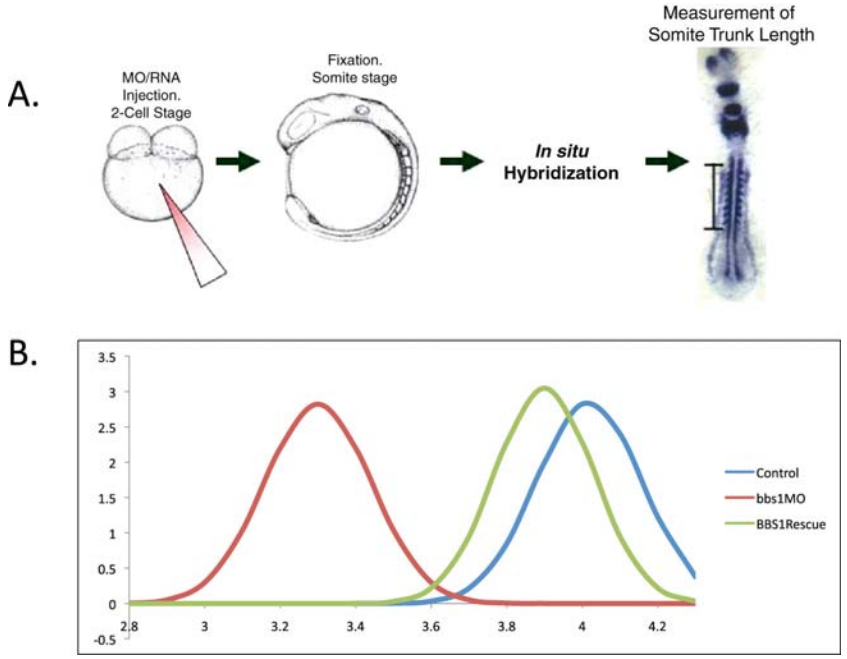

Fig. 3 Measurement of somite-trunk length at somite stages. (A) Shortening of the body axis, the most prominent defect observed in ciliary mutant and morphant embryos at somitic stages, is quantified by labeling of somite stage embryos with markers of somites and notochord, and anterior/posterior markers. Embryo trunk length is measured as the distance from the first to the last somite (bar). (B) *BBS1* morpholino knockdown and rescue by wild-type mRNA. For each injection treatment, the trunk lengths of groups of embryos are measured; the observed lengths are normally distributed. Defects in ciliary function, shown here by treatment with *bbs1* morpholino, produce shorter body axes compared to controls, and the morphant phenotype can be rescued by co-injection of *BBS1* wild-type mRNA. (For color version of this figure, the reader is referred to the web version of this book.)

3. Epiboly Cell Tracking

Convergent extension movements occur during epiboly and are characterized by convergence of cells on the dorsal axis and extension along that axis. We have developed a method to track the movement of cells throughout gastrulation to observe the process of convergence and extension.

1. After injection of morpholinos into 1- or 2-cell stage embryos or collection of mutant embryos, culture embryos in embryo medium until the 16-cell stage. Inject a single marginal blastomere (see Fig. 4A) with 1 nL of 10,000-MW dextran-conjugated fluorescent lineage tracer (Invitrogen D-22910). *Note*: At the 16-cell stage, it is impossible to determine the dorsal from the ventral axis of the embryo. Therefore, only 50% of lineage-tracer-injected embryos will express fluorescence on the dorsal part of the embryo. This is easily determined at epiboly stages when the dorsal axis is easily distinguishable due to formation of the shield.
2. Culture embryos in embryo medium until 30% epiboly (4.67 hpf). Position embryos in embryo medium on an agarose imaging dish (5% agarose with semispherical wells indented in agarose, one per embryo) such that the lateral view of the embryo is facing up.
3. Image embryo using a fluorescence-capable dissecting microscope and camera at 30% epiboly. Without moving the embryo, continue to culture the embryos in the dish until 50% epiboly. Image the embryo again. Repeat at 65 and 75% epiboly (Fig. 4B).
4. On comparison to each other, control embryos at 30, 50, 65, and 75% epiboly will exhibit a distinct migration of fluorescent cells toward the dorsal axis and an elongation along the axis in a narrowing arc. Ciliary morphants and mutants exhibit a defect in this process characterized by a delay or failure of cells to migrate to and along the dorsal axis. This can be easily visualized by the failure of the distinctive fluorescent arc to form by 75% epiboly.

4. Assaying Human Gene Variation in Zebrafish

The zebrafish model has many benefits, particularly in the areas of functional genetics and disease. A considerable advantage is the functionality of exogenous human genes in zebrafish embryos. We have developed a protocol for suppression of endogenous embryonic genes and introduction of the homologous human gene to assay for altered functionality conferred by known variants.

1. Prepare cDNA of the human ciliary gene of interest by subcloning into the pCS2+ vector. For analysis of mutation effect, variants can be introduced by site-directed mutagenesis via PCR (Quick Change, Stratagene). Linearize the cDNA plasmid with the appropriate restriction enzyme and transcribe using SP6 polymerase (mMessage mMachine Kit, Ambion).
2. Prepare a range of concentrations for a ciliary morpholino of interest with known efficacy in zebrafish. It is imperative for a translation-blocking morpholino that a portion of the sequence is 3′ of the ATG start site. Otherwise, the morpholino may bind to and prevent translation of the co-introduced exogenous mRNA as well.

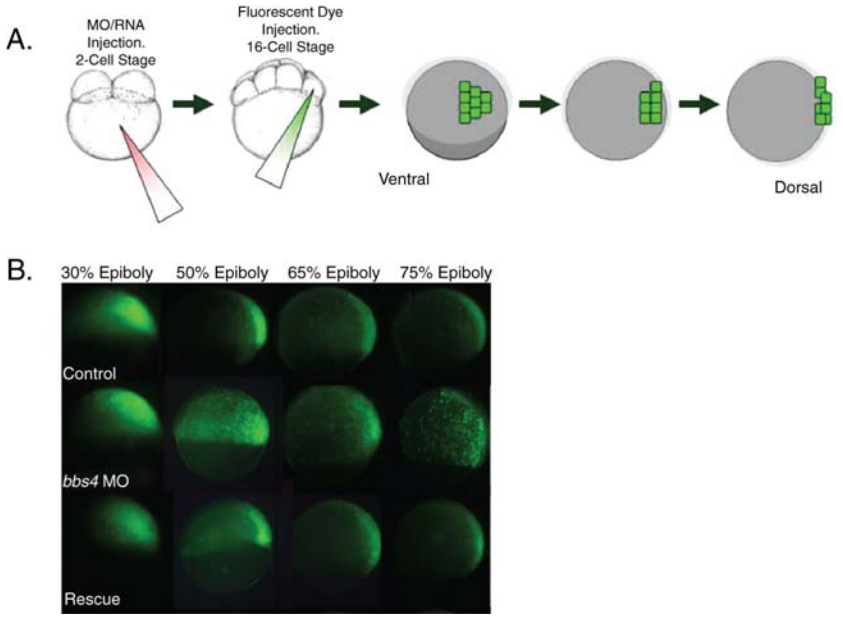

Fig. 4 Labeling of cells and tracking of movements through gastrulation. (A) After embryo treatment with morpholino or RNA injection at the 1- to 2-cell stage, fluorescent dye is injected into a single marginal blastomere at the 16-cell stage. At gastrulation stages, fluorescing cells can be tracked to monitor movement. (B) Ciliary morphant embryos (*bbs4* shown here) exhibit defects in the characteristic movements whereby cells converge on and extend along the dorsal axis. This defect can be rescued by co-injection of wild-type mRNA (modified from Zaghloul *et al.*, 2010). (Permission from Nat. Cell Biol., License #: 2721450638335). (See color plate.)

3. Starting with a morpholino concentration of moderate effect (i.e., approximately 50–60% of embryos exhibiting phenotypes), co-inject morpholino with three different concentrations of wild-type human mRNA (typically, 50, 100, and 125 pg/nL and 1 nL delivered per injection) at the one- to two-cell stage. Culture embryos until desired stage for phenotyping (8–10 somites for PCP phenotypes) in embryo medium. If scoring PCP phenotypes, the proportion of unaffected, Class I, and Class II embryos should be quantified for each injection combination, as well as morpholino alone and uninjected controls. On introduction of wild-type mRNA, a curve of efficacy for the differing mRNA concentrations can be determined based on the proportion of unaffected embryos. An increase in unaffected embryos with co-injection indicates a rescue of the morphant phenotype. Based on this curve, the optimal rescue concentration can be determined using either one of these concentrations or another concentration within this range.
4. Once the concentrations for both morpholino and mRNA have been determined for wild-type rescue, the same concentrations are used for subsequent co-injection of morpholino and mutant mRNA. Inject the morpholino/mRNA cocktail at the

one- to two-cell stage and culture embryos in embryo medium until the desired stage for phenotyping. *Note*: This stage must be exactly the same for mutant mRNA rescue embryos and wild-type rescue embryos. Embryos should be categorized by phenotypic class with quantification of the proportion of unaffected, Class I, and Class II embryos.

5. Compare the quantification of the mutant rescue experiment to the wild-type rescue experiment to determine if mutant mRNA behaves similarly to wild type or causes a perturbed phenotype. Mutant mRNAs that rescue the morphant phenotype in a manner similar to wild type are deemed benign or wild type. Those that do not rescue the morphant phenotype, producing defects similar to morpholino alone, have probably lost all functionality and are, therefore, functionally null. An mRNA that partially rescues the phenotype is likely to be a hypomorphic or partial loss-of-function variant. Finally, those variants that do not rescue the phenotype and produce defects more severe than morpholino alone may be behaving in a dominant negative fashion, a possibility that can be verified by injection of mutant mRNA alone. Categorization of variants in this way can be used to assay a large series of variants and to assign functionality to ambiguous alleles identified in the context of human genetic disease.

III. Zebrafish Ciliary Mutant Lines

Although we lack mutant lines for most ciliary genes, 11 zebrafish lines with mutations in known ciliary genes and 1 transgenic reporter line have been developed. Most of these are readily available via the Zebrafish International Research Center (http://zebrafish.org/zirc/home/guide.php).

1. *oval* and *MZoval* (gene: *ift88*, allele(s): *tz288*): Both the mutant line bearing the point mutation (*ovl*) (Tsujikawa and Malicki, 2004) and the line with the maternal zygotic allele (MZ*ovl*) (Huang and Schier, 2009) display a loss of cilia but have intact basal bodies. The transduction of Shh signaling differs, however, in these lines with the former embryos showing no effect on Shh (Lunt *et al.*, 2009), whereas the maternal zygotic mutant embryos have dampened Shh (Huang and Schier, 2009). Embryos do display morphological defects associated with ciliary dysfunction including degeneration of photoreceptor outer segments (Tsujikawa and Malicki, 2004) and disrupted neural and somite patterning.
2. *fleer* (*ift70*, *m477*): Embryos produced with this point mutation exhibit hallmark pleiotropic features associated with ciliary defects, including kidney cysts, randomized left–right asymmetry, hydrocephalus, and rod outer segment defects (Pathak *et al.*, 2007). Further, this mutant exhibits shortened cilia with reduced beat amplitude, possibly caused by defects in tubulin polyglutamylation. The *fleer* locus is homologous to the *C. elegans* DYF1 gene.

3. *seahorse* (*lrrc6l*, *hi3308/fa20r/tg238a*): Kidney cysts are highly prevalent in these mutants, as well as the characteristic body curvature and left–right patterning defects often seen in ciliary mutants (Kishimoto *et al.*, 2008; Sun *et al.*, 2004). Cilia are present in *seahorse* embryos, although with reduced motility (Serluca *et al.*, 2009), which suggests that this gene is not necessary for ciliogenesis. However, canonical Wnt signaling is suppressed while noncanonical Wnt is upregulated, indicating an important role of the gene in the regulation of this pathway (Kishimoto *et al.*, 2008).
4. *Elipsa* (*traf3ip1*, *m649/tp49d*): *elipsa* embryos exhibit kidney cysts, body axis curving, and defects in retinal development, as well as defects in ciliogenesis (Malicki *et al.*, 1996; Omori *et al.*, 2008). The protein, homologous to the *C. elegans* DYF-11, localizes to basal bodies and axonemes in otic vesicle and olfactory epithelial cells, whereas in retina the protein is only found in basal bodies. The protein plays an important role in linking the IFT particle to the membrane-associated small GTPase Rab8 via its interaction with Rabaptin5 (Omori *et al.*, 2008).
5. *switch hitter* (*lrrc50*, *tm317/hu255*): *swt* mutant embryos develop downward body curving, left–right patterning defects, and severe pronephric cysts (Sullivan-Brown *et al.*, 2008). Although mutants exhibit cilia, *lrrc50* is necessary for ciliary motility in KV and thus gives rise to the patterning defect (van Rooijen *et al.*, 2008). This gene is mutated in primary cilia dyskinesia (PCD) patients (Loges *et al.*, 2009), which suggests the potential of this mutant as a model for the disorder.
6. *qilin* (*qilin*, *hi3959A*): Identified in a forward genetic screen, mutant embryos develop kidney cysts and body curving (Sun *et al.*, 2004). The *C. elegans* ortholog, DYF-3, undergoes IFT, thereby indicating a role for this gene in promoting formation of sensory cilia (Ou *et al.*, 2005).
7. *curly* (*ift57*, *hi3417*): This mutation results in loss of cilia (Lunt *et al.*, 2009) and produces renal cysts and body curving (Sun *et al.*, 2004) as well as shortened photoreceptor outer segments with decreased opsin and retinal degeneration by 5 dpf (Krock and Perkins, 2008). Since no defects in Shh signaling were observed in *ift57* mutants (Lunt *et al.*, 2009), the mutant phenotype is attributed to the role of *ift57* in regulating kinesin-II dissociation from the IFT particle (Krock and Perkins, 2008).
8. *larry* (*ift81*, *hi409Tg*) and *moe* (*ift172*, *hi2211Tg*): Although embryos exhibit kidney cysts and body curvature, neither cilia formation nor Shh signaling is affected (Lunt *et al.*, 2009; Sun *et al.*, 2004) in these mutants. However, outer segments of photoreceptors do not form, giving rise to a severe retinal defect (Sukumaran and Perkins, 2009).
9. *pkd2/curly up* (*polycystin-2*, *hi4166Tg/hu2173/tc321/tg226d/tp85a/ty30*): Although these mutants show body curvature and left–right patterning defects, no kidney cysts develop and ciliogenesis does occur (Sun *et al.*, 2004). However, morpholino suppression of the gene produces cysts and hydrocephalus, which suggests that the gene may also be involved in regulation of these phenotypes (Obara *et al.*, 2006; Schottenfeld *et al.*, 2007; Sun *et al.*, 2004).

10. *scorpion* (*arl13b*, *hi459Tg*): A model for Joubert syndrome, cilia do not develop in mutant embryos, resulting in characteristic ciliary phenotypes including kidney cysts, body curvature, and left–right patterning defects (Sun *et al.*, 2004). The protein localizes to the cilium, a feature that is required for its proper function (Duldulao *et al.*, 2009).
11. *sentinel* (*cc2d2a*, *w38*): Also an ortholog of a Joubert syndrome gene, *sentinel* mutants exhibit pronephric cysts and body curvature defects (Owens *et al.*, 2008). The mammalian ortholog localizes to the basal body and interacts with another ciliopathy-associated protein, CEP290 (Gorden *et al.*, 2008).
12. *Arl13b–GFP transgenic* (*Tg(βact::Arl13b–GFP)*): This line has been developed for visualization of fluorescent cilia in live embryos. Embryos produce an Arl13b–GFP fusion protein under the control of the β-actin promoter, which allows for strong expression across all tissues. GFP-expressing cilia are observed in the axonemes of motile cilia (KV, floor plate) and primary cilia (ectoderm, notochord, somites, and neural tube) (Borovina *et al.*, 2010).

IV. General Considerations/Future Development

Zebrafish have proven to be an extremely useful model for the study of ciliary biology due to the developmental ramifications of ciliary dysfunction. It is important to note that special consideration must be applied when assessing the defects associated with ciliary knockdown. For example, defective gastrulation movements are a hallmark of disrupted ciliary function and have been observed by morpholino-induced knockdown as well as in various mutant strains. However, this is also a common side effect of morpholino-associated toxicity, making imperative the need for verification of knockdown specificity by rescue. The use of gastrulation defects as a phenotypic readout for ciliary gene knockdown highlights the challenges of morpholinos in comparison with genomic manipulation. As more mutant lines become available, the concerns raised with morpholinos will be alleviated although other factors will remain as issues. Masking of a ciliary phenotype due to other genomic factors is a potential problem that may result in milder phenotypes or none at all. Morpholino injection, a more acute treatment, will therefore still remain a useful technique for knockdown as it can circumvent this problem.

As zebrafish tools for the study of ciliary dysfunction, such as mutant lines, antibodies, and cultured cells, continue to be developed, the advantages of this system for analysis of ciliary biology will expand. For example, zebrafish are not inbred strains and therefore exhibit considerable phenotypic variability. Considering the extent of variability across human ciliopathies and the complexity of those disorders, zebrafish present the opportunity to investigate ciliopathies in the context of genomic variability. Further, the continued development of transgenic reporter lines and transient reporter fusion proteins will allow for direct visualization of ciliary processes *in vivo*. This type of manipulation is elegantly demonstrated by the recent observation of centrosomal movement during gastrulation *in vivo* through the use of GFP-labeled centrosomal

proteins (Sepich *et al.*, 2011). Similar studies can track ciliogenesis, ciliary orientation, and movement of ciliary proteins through various stages of development. Detailed cellular studies such as these will capitalize on the many advantages of the zebrafish to make it an indispensable tool in the study of ciliary biology.

Acknowledgment

We thank Iain Drummond for generously sharing his protocol for immunostaining of cilia in zebrafish, from which our own protocol has benefited greatly.

References

Amack, J. D., Wang, X., and Yost, H. J. (2007). Two T-box genes play independent and cooperative roles to regulate morphogenesis of ciliated Kupffer's vesicle in zebrafish. *Dev. Biol.* **310**, 196–210.

Berbari, N. F., O'Connor, A. K., Haycraft, C. J., and Yoder, B. K. (2009). The primary cilium as a complex signaling center. *Curr. Biol.* **19**, R526–R535.

Borovina, A., Superina, S., Voskas, D., and Ciruna, B. (2010). Vangl2 directs the posterior tilting and asymmetric localization of motile primary cilia. *Nat. Cell Biol.* **12**, 407–412.

Cardenas-Rodriguez, M., and Badano, J. L. (2009). Ciliary biology: understanding the cellular and genetic basis of human ciliopathies. *Am. J. Med. Genet. C Semin. Med. Genet.* **151C**, 263–280.

Corbit, K. C., Aanstad, P., Singla, V., Norman, A. R., Stainier, D. Y., and Reiter, J. F. (2005). Vertebrate smoothened functions at the primary cilium. *Nature* **437**, 1018–1021.

Corbit, K. C., Shyer, A. E., Dowdle, W. E., Gaulden, J., Singla, V., Chen, M. H., Chuang, P. T., and Reiter, J. F. (2008). Kif3a constrains beta-catenin-dependent Wnt signalling through dual ciliary and non-ciliary mechanisms. *Nat. Cell Biol.* **10**, 70–76.

Duldulao, N. A., Lee, S., and Sun, Z. (2009). Cilia localization is essential for *in vivo* functions of the Joubert syndrome protein Arl13b/Scorpion. *Development* **136**, 4033–4042.

Gerdes, J. M., Liu, Y., Zaghloul, N. A., Leitch, C. C., Lawson, S. S., Kato, M., Beachy, P. A., Beales, P. L., DeMartino, G. N., and Fisher, S., *et al*. (2007). Disruption of the basal body compromises proteasomal function and perturbs intracellular Wnt response. *Nat. Genet.* **39**, 1350–1360.

Goetz, S. C., Ocbina, P. J., and Anderson, K. V. (2009). The primary cilium as a Hedgehog signal transduction machine. *Methods Cell Biol.* **94**, 199–222.

Gorden, N. T., Arts, H. H., Parisi, M. A., Coene, K. L., Letteboer, S. J., van Beersum, S. E., Mans, D. A., Hikida, A., Eckert, M., and Knutzen, D., *et al*. (2008). CC2D2A is mutated in Joubert syndrome and interacts with the ciliopathy-associated basal body protein CEP290. *Am. J. Hum. Genet.* **83**, 559–571.

Huang, P., and Schier, A. F. (2009). Dampened Hedgehog signaling but normal Wnt signaling in zebrafish without cilia. *Development* **136**, 3089–3098.

Huangfu, D., Liu, A., Rakeman, A. S., Murcia, N. S., Niswander, L., and Anderson, K. V. (2003). Hedgehog signalling in the mouse requires intraflagellar transport proteins. *Nature* **426**, 83–87.

Jaffe, K. M., Thiberge, S. Y., Bisher, M. E., and Burdine, R. D. (2010). Imaging cilia in zebrafish. *Methods Cell Biol.* **97**, 415–435.

Jin, H., White, S. R., Shida, T., Schulz, S., Aguiar, M., Gygi, S. P., Bazan, J. F., and Nachury, M. V. (2010). The conserved Bardet–Biedl syndrome proteins assemble a coat that traffics membrane proteins to cilia. *Cell* **141**, 1208–1219.

Loges, N. T., Olbrich, H., Becker-Heck, A., Häffner, K., Heer, A., Reinhard, C., Schmidts, M., Kispert, A., Zariwala, M. A., Leigh, M. W., Knowles, M. R., Zentgraf, H., Seithe, H., Nurnberg, G., Nunberg, P., Reinhardt, R., and Omran, H. (2009). Deletions and point mutations of *LRRC50* cause primary ciliary dyskinesia due to dynein arm defects. *Am. J. Hum. Genet.* **85**, 883–889.

Kim, S., Zaghloul, N. A., Bubenshchikova, E., Oh, E. C., Rankin, S., Katsanis, N., Obara, T., and Tsiokas, L. (2011). Nde1-mediated inhibition of ciliogenesis affects cell cycle re-entry. *Nat. Cell Biol.* **13**(4), 351–360.

Kishimoto, N., Cao, Y., Park, A., and Sun, Z. (2008). Cystic kidney gene seahorse regulates cilia-mediated processes and Wnt pathways. *Dev. Cell* **14**, 954–961.

Krock, B. L., and Perkins, B. D. (2008). The intraflagellar transport protein IFT57 is required for cilia maintenance and regulates IFT-particle–kinesin-II dissociation in vertebrate photoreceptors. *J. Cell Sci.* **121**, 1907–1915.

Leitch, C. C., Zaghloul, N. A., Davis, E. E., Stoetzel, C., Diaz-Font, A., Rix, S., Alfadhel, M., Lewis, R. A., Eyaid, W., and Banin, E., *et al*. (2008). Hypomorphic mutations in syndromic encephalocele genes are associated with Bardet–Biedl syndrome. *Nat. Genet.* **40**, 443–448.

Lunt, S. C., Haynes, T., and Perkins, B. D. (2009). Zebrafish ift57, ift88, and ift172 intraflagellar transport mutants disrupt cilia but do not affect hedgehog signaling. *Dev. Dyn.* **238**, 1744–1759.

Malicki, J., Neuhauss, S. C., Schier, A. F., Solnica-Krezel, L., Stemple, D. L., Stainier, D. Y., Abdelilah, S., Zwartkruis, F., Rangini, Z., and Driever, W. (1996). Mutations affecting development of the zebrafish retina. *Development* **123**, 263–273.

Obara, T., Mangos, S., Liu, Y., Zhao, J., Wiessner, S., Kramer-Zucker, A. G., Olale, F., Schier, A. F., and Drummond, I. A. (2006). Polycystin-2 immunolocalization and function in zebrafish. *J. Am. Soc. Nephrol.* **17**, 2706–2718.

Omori, Y., Zhao, C., Saras, A., Mukhopadhyay, S., Kim, W., Furukawa, T., Sengupta, P., Veraksa, A., and Malicki, J. (2008). Elipsa is an early determinant of ciliogenesis that links the IFT particle to membrane-associated small GTPase Rab8. *Nat. Cell Biol.* **10**, 437–444.

Ou, G., Qin, H., Rosenbaum, J. L., and Scholey, J. M. (2005). The PKD protein qilin undergoes intraflagellar transport. *Curr. Biol.* **15**, R410–R411.

Owens, K. N., Santos, F., Roberts, B., Linbo, T., Coffin, A. B., Knisely, A. J., Simon, J. A., Rubel, E. W., and Raible, D. W. (2008). Identification of genetic and chemical modulators of zebrafish mechanosensory hair cell death. *PLoS Genet.* **4**, e1000020.

Pathak, N., Obara, T., Mangos, S., Liu, Y., and Drummond, I. A. (2007). The zebrafish fleer gene encodes an essential regulator of cilia tubulin polyglutamylation. *Mol. Biol. Cell* **18**, 4353–4364.

Pedersen, L. B., and Rosenbaum, J. L. (2008). Intraflagellar transport (IFT) role in ciliary assembly, resorption and signalling. *Curr. Top. Dev. Biol.* **85**, 23–61.

Ross, A. J., May-Simera, H., Eichers, E. R., Kai, M., Hill, J., Jagger, D. J., Leitch, C. C., Chapple, J. P., Munro, P. M., and Fisher, S., *et al*. (2005). Disruption of Bardet–Biedl syndrome ciliary proteins perturbs planar cell polarity in vertebrates. *Nat. Genet.* **37**, 1135–1140.

Satir, P., Pedersen, L. B., and Christensen, S. T. (2010). The primary cilium at a glance. *J. Cell Sci.* **123**, 499–503.

Schottenfeld, J., Sullivan-Brown, J., and Burdine, R. D. (2007). Zebrafish curly up encodes a Pkd2 ortholog that restricts left-side-specific expression of southpaw. *Development* **134**, 1605–1615.

Sepich, D. S., Myers, D. C., Short, R., Topczewski, J., Marlow, F., and Solnica-Krezel, L. (2000). Role of the zebrafish trilobite locus in gastrulation movements of convergence and extension. *Genesis* **27**, 159–173.

Sepich, D. S., Usmani, M., Pawlicki, S., and Solnica-Krezel, L. (2011). Wnt/PCP signaling controls intracellular position of MTOCs during gastrulation convergence and extension movements. *Development* **138**, 543–552.

Serluca, F. C., Xu, B., Okabe, N., Baker, K., Lin, S. Y., Sullivan-Brown, J., Konieczkowski, D. J., Jaffe, K. M., Bradner, J. M., and Fishman, M. C., *et al*. (2009). Mutations in zebrafish leucine-rich repeat-containing six-like affect cilia motility and result in pronephric cysts, but have variable effects on left–right patterning. *Development* **136**, 1621–1631.

Sukumaran, S., and Perkins, B. D. (2009). Early defects in photoreceptor outer segment morphogenesis in zebrafish ift57, ift88 and ift172 intraflagellar transport mutants. *Vision Res.* **49**, 479–489.

Sullivan-Brown, J., Schottenfeld, J., Okabe, N., Hostetter, C. L., Serluca, F. C., Thiberge, S. Y., and Burdine, R. D. (2008). Zebrafish mutations affecting cilia motility share similar cystic phenotypes and suggest a mechanism of cyst formation that differs from pkd2 morphants. *Dev. Biol.* **314**, 261–275.

Sun, Z., Amsterdam, A., Pazour, G. J., Cole, D. G., Miller, M. S., and Hopkins, N. (2004). A genetic screen in zebrafish identifies cilia genes as a principal cause of cystic kidney. *Development* **131**, 4085–4093.

Thisse, C., and Thisse, B. (2008). High-resolution in situ hybridization to whole-mount zebrafish embryos. *Nat. Protoc.* **3**, 59–69.

Tsujikawa, M., and Malicki, J. (2004). Intraflagellar transport genes are essential for differentiation and survival of vertebrate sensory neurons. *Neuron* **42**, 703–716.

van Rooijen, E., Giles, R. H., Voest, E. E., van Rooijen, C., Schulte-Merker, S., and van Eeden, F. J. (2008). LRRC50, a conserved ciliary protein implicated in polycystic kidney disease. *J. Am. Soc. Nephrol.* **19**, 1128–1138.

Westerfield, M. (2000). The Zebrafish Book. A Guide for the Laboratory Use of Zebrafish (Danio rerio), 4th ed. University of Oregon Press, Eugene.

Zaghloul, N. A., Liu, Y., Gerdes, J. M., Gascue, C., Oh, E. C., Leitch, C. C., Bromberg, Y., Binkley, J., Leibel, R. L., and Sidow, A., *et al*. (2010). Functional analyses of variants reveal a significant role for dominant negative and common alleles in oligogenic Bardet–Biedl syndrome. *Proc. Natl. Acad. Sci. U. S. A.* **107**, 10602–10607.

Zhou, W., Dai, J., Attanasio, M., and Hildebrandt, F. (2010). Nephrocystin-3 is required for ciliary function in zebrafish embryos. *Am. J. Physiol. Renal Physiol.* **299**, F55–F62.

CHAPTER 12

Infectious Disease Modeling and Innate Immune Function in Zebrafish Embryos

Chao Cui, Erica L. Benard, Zakia Kanwal, Oliver W. Stockhammer, Michiel van der Vaart, Anna Zakrzewska, Herman P. Spaink and Annemarie H. Meijer

Institute of Biology, Leiden University, Leiden, The Netherlands

Abstract

The major cell types of the innate immune system, macrophages and neutrophils, develop during the first two days of zebrafish embryogenesis. The interaction of these immune cells with pathogenic microbes can excellently be traced in the optically transparent zebrafish embryos. Various tools and methods have recently been developed for visualizing and isolating the zebrafish embryonic innate immune

METHODS IN CELL BIOLOGY, VOL 105

0091-679X/10 $35.00
DOI 10.1016/B978-0-12-381320-6.00012-6

cells, for establishing infections by different micro-injection techniques, and for analyzing the host innate immune response following microbial recognition. Here we provide practical guidelines for the application of these methodologies and review the current state of the art in zebrafish infectious disease research.

I. Introduction

Over the recent years, the zebrafish has firmly gained ground as a model for inflammatory and infectious diseases. A rapidly growing list of human pathogens or closely related animal pathogens has been used for experimental infections in zebrafish (Allen and Neely, 2010; Kanther and Rawls, 2010; Lesley and Ramakrishnan, 2008; Meeker and Trede, 2008; Meijer and Spaink, 2011; Sullivan and Kim, 2008). Tuberculosis and other human infectious diseases can be modeled in zebrafish either using adult individuals with a fully developed adaptive immune system or using embryos and larvae that have developed only innate immune cell types. Microarray and deep sequencing technologies have been instrumental to characterize immune responses to different types of infection. These studies have demonstrated the induction of transcriptional regulators and immune effectors that are highly conserved between zebrafish and human (Meijer and Spaink, 2011). In addition, functional studies have shown that central signaling pathways of the innate immune system are already operational during infections in 1-day-old embryos and subsequent larval stages (Aggad *et al.*, 2010; Clay *et al.*, 2008; Stockhammer *et al.*, 2009).

The zebrafish offers significant advantages for studying host–pathogen interactions. First, due to their optical transparency, zebrafish embryos are highly suited for live imaging of chemotaxis, phagocytosis, and pathogenesis. As further discussed below, these studies are greatly facilitated by transgenic reporter lines expressing fluorescent proteins in different immune cell types and by specific immune response assays that can be performed *in vivo*. Second, the large number of offspring, the short generation time, and the high-quality genome sequence of zebrafish enable the rapid accumulation of loss- or gain-of-function mutants using forward or reverse genetic screening approaches (Amacher, 2008; Haffter and Nusslein-Volhard, 1996; Wienholds *et al.*, 2002). Morpholino technology provides an efficient complementary tool for transient gene knockdown in embryos until larval stages (Nasevicius and Ekker, 2000). Finally, a major strength of the zebrafish model has come from the opportunity to study early developmental stages of the innate immune cells, which are barely accessible in classical vertebrate models (Traver *et al.*, 2003; Trede *et al.*, 2004). Because of these special features, the zebrafish model is a valuable addition to mammalian models for vertebrate immunology, and an excellent screening tool to define novel factors that participate in host–pathogen interactions.

The innate immune system, which can be classified into physical barriers, cellular, and humoral components, controls the first line of defense against infections. Functional phagocytes, complement factors, and antimicrobial enzymes are present in the embryo before or soon after hatching (Herbomel *et al.*, 1999; Traver *et al.*,

2003; Trede *et al.*, 2004). Recognition of microbes by the innate immune system is mediated by the germline-encoded pattern recognition receptors (PRRs), which are located on the cell surface, on endosomal compartments, and in the cytosol. PRRs recognize pathogen-associated molecular patterns (PAMPs) and intracellular chemical components released through injury or infection (Mogensen, 2009). The best studied family of PRRs is that of the Toll-like receptors (TLRs) (Coban *et al.*, 2009). Putative orthologs of the mammalian TLRs and many downstream signaling intermediates as well as other PRRs, such as the NOD receptors, have been identified in zebrafish (Jault *et al.*, 2004; Meijer *et al.*, 2004; Stein *et al.*, 2007). Microbe recognition by PRRs directly initiates specific signal transduction cascades that not only activate innate effector mechanisms but also function to alert the adaptive immune system (T- and B-cell-mediated immunity). However, in zebrafish the adaptive immune system is not fully matured until approximately 4 weeks postfertilization (Lam *et al.*, 2004). This temporal separation between the two branches of the immune system makes zebrafish embryos and larvae highly suitable for analyzing the innate host factors involved in the interaction with pathogens.

Several detailed reviews of zebrafish as an experimental infection model have been published in the last few years (Kanther and Rawls, 2010; Lesley and Ramakrishnan, 2008; Meeker and Trede, 2008; Meijer and Spaink, 2011; Sullivan and Kim, 2008). In this chapter, our main goal is to give practical guidelines for infection studies in zebrafish embryos. In the following sections, we provide a brief summary of innate immune cell development in zebrafish, followed by an overview of tools and methods used for visualizing specific immune cell populations in embryos. We then describe various strategies to achieve systemic or local infection of embryos with bacterial pathogens, and we discuss quantification methods to analyze bacterial burden at low- or high-throughput levels. Finally, we provide advice on the use of transcriptomic technologies for characterizing innate immune responses and discuss functional studies of some key factors in the innate immune system. For additional reading, we recommend other highly useful methods papers on the analysis of innate immunity in zebrafish (Hall *et al.*, 2009; Herbomel and Levraud, 2005; Levraud *et al.*, 2008; Mathias *et al.*, 2009).

II. Observation and Isolation of Innate Immune Cells

A. Innate Immune Cell Development in Zebrafish

The majority of innate immune cell types, including the phagocytic cells, belong to the myeloid cell lineage, but natural killer cells, which are of lymphoid origin, also belong to the innate immune system. As in mammals, the development of immune cells during zebrafish embryogenesis occurs in distinct waves of primitive and definitive hematopoiesis (Bertrand and Traver, 2009; Davidson and Zon, 2004). The primitive wave of hematopoiesis begins in the anterior lateral plate mesoderm or rostral blood island, where hemangioblasts differentiate into myeloid cells, and in the posterior lateral plate mesoderm, which gives rise to erythroid cells. A transient

wave of hematopoiesis occurs in the posterior blood island of 1-day-old embryos that contains the first erythromyeloid progenitor cells (EMPs) (Bertrand *et al.*, 2007). The posterior blood island region subsequently expands into the caudal hematopoietic tissue, which forms a transient site of hematopoiesis from where cells further migrate to seed the thymus and pronephros (Murayama *et al.*, 2006). The pronephros develops into the kidney marrow in adult fish and is considered equivalent to mammalian bone marrow (Traver *et al.*, 2003). A final wave of definitive hematopoiesis in the ventral wall of the embryonic dorsal aorta produces cells that have a long-term hematopoietic stem cell potential and that become the founders of the adult hematopoietic system, similar to situation in the mouse embryo (Bertrand *et al.*, 2010; Boisset *et al.*, 2010; Kissa and Herbomel, 2010).

In the zebrafish embryo, the first innate immune cells to differentiate are the primitive macrophages, which migrate to the yolk sac before the onset of blood circulation and subsequently join the blood circulation or invade cephalic mesenchyme, brain, retina, and epidermis (Herbomel *et al.*, 1999, 2001). The next type of immune cells that differentiate are the neutrophils, which have detectable myeloperoxidase (Mpx) enzyme activity and Sudan Black staining cytoplasmic granules by 2 days postfertilization (dpf) (Le Guyader *et al.*, 2008; Lieschke *et al.*, 2001; Willett *et al.*, 1999). As a molecular marker, the enzyme myeloperoxidase (*mpx*) was shown to be expressed only in neutrophils (Bennett *et al.*, 2001; Lieschke *et al.*, 2001). Prior to the maturation of neutrophils, *mpx* messenger RNA is already apparent in a distinct myeloid population at 28 hours postfertilization (hpf) (Zakrzewska *et al.*, 2010). Mast cells, characterized by carboxypeptidase 5 expression, form another myeloid lineage developing from the first day of embryogenesis. Around 60 hpf, macrophages that have previously invaded the brain and retina undergo a phenotypic transition into microglia (Herbomel *et al.*, 2001). Thus, at least four distinct myeloid cell types are present before the first immature lymphocyte precursors appear in the developing thymus around 4 dpf. Two other myeloid cell types have been characterized in adult zebrafish, the eosinophils and a population of antigen-presenting cells similar to the mammalian dendritic cells (Balla *et al.*, 2010; Lugo-Villarino *et al.*, 2010). Based on the expression of characteristic receptor genes, it is presumed that natural killer cells also exist in zebrafish, but these cells remain to be characterized (Yoder *et al.*, 2009). For visualizing different innate immune cell populations during embryonic and larval development, various methods have been established, which will be further described in the following sections.

B. Detection of Immune Cells Using Cell-Specific Markers

1. Colocalization Studies of Immune Cell Markers by *in situ* Hybridization

One of the most basic methods in zebrafish research is the *in situ* study of gene expression patterns in the whole embryo. In whole-mount *in situ* hybridization, gene-specific markers can be used to trace the spatial–temporal distribution of immune cells during their development or in response to infection or wounding. In early zebrafish

embryos, two gene-specific markers have been widely used to distinguish macrophages and neutrophils. The gene *mpx* is currently the most robust marker for detection of neutrophils, whereas the gene encoding colony-stimulating factor 1 receptor (*csf1ra*, previously called *fms*) has been extensively utilized to identify the macrophages (Herbomel *et al.*, 2001; Lieschke *et al.*, 2001). Although the use of *csf1ra* as a macrophage marker has been well documented in previous research, its disadvantage is that it is also expressed in a pigment cell type, the xanthophores. Therefore, the search for marker genes specific only to macrophages has been crucial to facilitate the analysis of macrophage responses to various types of immune system triggers.

Our recent study of early myeloid genes under control of the Spi1 (Pu.1) transcription factor led to the discovery of four novel markers for early zebrafish macrophages, *mfap4*, *mpeg1*, *cxcr3.2*, and *ptpn6* (Zakrzewska *et al.*, 2010). First, to determine that the spatial–temporal expression pattern of these genes resembles that of other myeloid-specific genes such as *lcp1*, *spi1*, and *mpx*, whole-mount *in situ* hybridization with digoxigenin-labeled antisense RNA probes and alkaline phosphatase detection was used. This method has been described in detail elsewhere (Westerfield, 2000). To verify whether these novel marker genes are specifically expressed in macrophages, rather than neutrophils, double fluorescent *in situ* hybridization (FISH) was utilized to determine the overlap with the known marker genes. In the FISH procedure, standard digoxigenin- and fluorescein-labeled probes are combined with tyramide signal amplification (TSA), which increases the signal-to-noise ratio considerably. Horseradish peroxidase (HRP)–conjugated antibodies are used to catalyze the precipitation of the fluorophore-labeled tyramide amplification reagent at the specific sites of mRNA–probe binding. Two variants of the protocol are available (Fig. 1). The one-step procedure utilizes the HRP-conjugated anti-digoxigenin or anti-fluorescein antibodies for detection of the site-specific gene expression. In the two-step procedure, two consecutive antibodies are applied for the detection of each probe, first a sheep anti-digoxigenin or anti-fluorescein antibody and next an HRP-conjugated anti-sheep antibody (Clay and Ramakrishnan, 2005). The one-step procedure is shorter by 2 days than the two-step procedure. However, the two-step procedure appears to be more sensitive due to the additional amplification of the signal by a secondary antibody. TSA amplification systems can be used with Alexa Fluor dyes (Invitrogen) or with Cy dyes and fluorescein (PerkinElmer). We generally use the TSA-Plus systems (PerkinElmer), which provide higher sensitivity than regular TSA, although this also creates higher background, especially in the yolk region. Furthermore, we prefer the combination of a digoxigenin-labeled probe with a red fluorescent dye for the detection of the gene that has the lower expression level of the two genes tested. In these HRP-based double FISH protocols, it is absolutely crucial to inactivate HRP completely using hydrogen peroxide after detection of the first gene. Failure to do so may result in an artifactual overlap of the expression patterns of the two genes tested.

In our study, we performed double FISH on 28 hpf zebrafish embryos, using our genes of interest labeled with digoxigenin and detected with TSA-Plus/Cy3 combined with either *csf1ra* (macrophage marker) or *mpx* (neutrophil marker) labeled

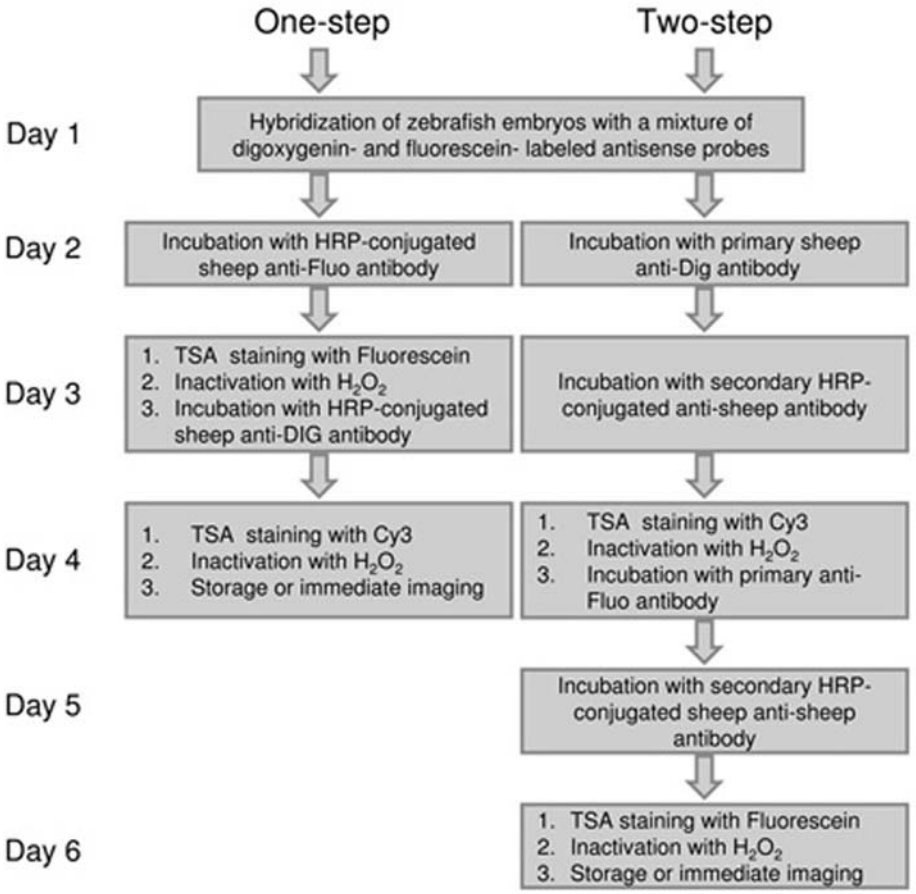

Fig. 1 Schematic representation of the double fluorescent *in situ* hybridization (FISH) protocol. Anti-Dig, anti-digoxigenin; anti-Fluo, anti-fluorescein.

with fluorescein and detected with TSA-Plus/fluorescein. This method allowed us to determine that all four genes identified in this study are expressed specifically in macrophages of 1-day-old embryos and that *mpeg1* and *mfap4* are the most robust and specific markers for detecting macrophages also at later stages of embryonic development. Below we describe the protocols for the one- and two-step double FISH procedures.

Two-Step Double FISH Protocol

Day 1:

1. Fix embryos overnight (O/N) in 4% paraformaldehyde in phosphate buffered saline (PFA–PBS) at 4 °C.

2. Dehydrate embryos using a graded series of PBST/methanol (PBST: 0.1% Tween 20 in PBS) and store in 100% methanol at −20 °C.
3. Rehydrate embryos using a graded series of methanol/PBST solution.
4. Digest embryos in Proteinase K solution (10 μg/mL) in PBST at 37 °C; adjust the time to the embryos' age.
5. Fix embryos in 4% PFA–PBS for 20 min at room temperature (RT) followed by 5 × 5 min washing in PBST at RT.
6. Prehybridize embryos in hybridization mix (HM) buffer (formamide 50%, 5× SSC, Tween 20 – 0.1%, citric acid to pH 6.0) for 2–6 h at 65 °C.
7. Hybridize O/N at 65 °C in HM buffer containing 50 μg/mL heparin (Sigma), 500 μg/mL tRNA (Sigma), and 200 ng of each antisense probe (digoxigenin- and fluorescein-labeled).

Day 2:

8. Remove and store the probe mix in −20 °C for reuse (four to five uses per probe).
9. Wash shortly in prewarmed 100% HM at RT.
10. Wash embryos using a graded series of HM/2× SSCT solutions at 65 °C, 15 min each.
11. Wash embryos 2 × 30 min in 0.2× SSCT at 65 °C.
12. Wash embryos using a graded series of 0.2× SSCT/PBST solution, 10 min each.
13. Block embryos for 2–3 h in blocking buffer (BB, Western Block Reagent, Roche, 1:10 dilution in PBST) at RT.
14. Incubate O/N at 4 °C in a 1/3000 dilution of the sheep anti-digoxigenin antibody (Roche catalog number 11093274910) in BB.

Day 3:

15. Wash 6 × 10 min in PBST at RT.
16. Block embryos for 1 h in BB at RT.
17. Incubate O/N at 4 °C in a 1/200 dilution of HRP-conjugated rabbit anti-sheep antibody (Jackson ImmunoResearch catalog number 313-035-047) in BB.

Day 4:

18. Wash 6 × 10 min in PBST at RT.
19. Incubate embryos in the dark for 20–30 min at RT in a 1/50 dilution of TSA-Plus/Cy3 (PerkinElmer) in the provided amplification buffer.
20. 5× quick rinses in PBST at RT.
21. Incubate for 30 min in 6% H_2O_2 solution at RT.
22. Wash embryos 3 × 10 min in PBST at RT, and check fluorescence.
23. Block embryos for 2–3 h in BB at RT.
24. Incubate embryos O/N at 4 °C in a 1/3000 dilution of sheep anti-fluorescein antibody (Roche catalog number 11426338910) in BB.

Day 5:

25. Wash embryos 6 × 10 min in PBST at RT.
26. Block embryos for 1 h in BB at RT.
27. Incubate O/N at 4 °C in a 1/200 dilution of HRP-conjugated rabbit anti-sheep antibody (Jackson ImmunoResearch catalog number 313-035-047) in BB.

Day 6:

28. Wash embryos 3 × 10 min in PBST at RT.
29. Incubate in the dark for 20–30 min at RT in a 1/50 dilution of TSA-Plus/fluorescein (PerkinElmer) in the provided amplification buffer.
30. Wash embryos 5 × 10 min in PBST at RT.
31. Incubate for 30 min in 6% H_2O_2 solution at RT.
32. Wash embryos 3 × 10 min in PBST at RT and store embryos in fresh PBT at 4 °C or image directly.

One-Step Double FISH Protocol

Refer to the above two-step protocol for the first 11 steps.

12. Incubate O/N at 4 °C in a 1/500 dilution of HRP-conjugated anti-fluorescein POD antibody (Roche catalog number 11426346910).

Day 3:

13. Wash 6 × 10 min in PBST at RT.
14. Incubate embryos in the dark for 30–50 min at RT in a 1/50 dilution of TSA-Plus/fluorescein in the provided amplification buffer.
15. Wash and incubate embryos for 30 min in 6% H_2O_2 solution at RT.
16. Wash embryos 6 × 10 min in PBST at RT.
17. Block embryos for 2 h in BB at RT.
18. Incubate O/N at 4 °C in a 1/500 dilution of HRP-conjugated anti-digoxigenin POD antibody (Roche catalog number 11207733910).

Day 4:

19. Wash embryos 6 × 10 min in PBST at RT.
20. Incubate embryos in the dark for 45–60 min at RT in a 1/50 dilution of TSA-Plus/Cy3 in the provided amplification buffer.
21. Wash embryos 5 × 10 min in PBST at RT.
22. Incubate for 30 min in 6% H_2O_2 solution at RT.
23. Wash embryos 3 × 10 min in PBST at RT and store embryos in fresh PBT at 4 °C or image directly.

2. Identification of Cell Types Using Immunodetection and Histochemical Staining

Antibodies against L-plastin, encoded by the *lcp1* gene, are a useful tool for the rapid detection of all myeloid cell types in the embryo (Mathias *et al.*, 2007). There are also antibodies available for the neutrophil-specific Mpx protein (Mathias *et al.*, 2007), but macrophage-specific antibodies are not yet described. Nevertheless, the combination of L-plastin and Mpx antibodies can be used to distinguish macrophages (L-plastin-positive, Mpx-negative) and neutrophils (L-plastin- and Mpx-positive). Because both of the available antibodies are rabbit polyclonals, this requires that one of the two antibodies is coupled directly to a fluorescent dye, while the second can be detected using a dye-coupled secondary antibody (Mathias *et al.*, 2009). A convenient alternative is to combine L-plastin immunofluorescence staining with a histochemical assay for detection of Mpx activity or with Sudan Black staining for specific detection of neutrophil granules (Le Guyader *et al.*, 2008; Lieschke *et al.*, 2001; Mathias *et al.*, 2009; Fig. 3). A fluorescent detection of Mpx activity can be performed with fluorescein isothiocyanate (FITC)- or Cy3-conjugated tyramide (Le Guyader *et al.*, 2008). Staining for Mpx activity can also be performed using a chromogenic substrate that produces a brown to black precipitate (Lieschke *et al.*, 2001). Due to this dark precipitate in the neutrophils, the immunostaining of the pan-leukocytic L-plastin marker only highlights the macrophage population. Below we provide a protocol for this procedure.

Combined L-Plastin Immunofluorescence and Chromogenic Mpx Activity Detection

Day 1:

1. Fix embryos O/N at 4° C in 4% PFA–PBS.
2. Wash embryos in 1× Trizmal (supplied by Peroxidase (Mpx) Leukocyte Kit, Sigma catalog number 390A) containing 0.01% Tween 20 (TT buffer) for 5 min.
3. Incubate embryos in TT buffer containing 1.5 mg/mL substrate (supplied) and 0.015% H_2O_2 for 5–10 min at 37 °C.
4. Wash embryos 3 × 10 min in PBST (0.1% Tween 20 in PBS), and check Mpx staining.
5. Dehydrate embryos in a graded series of PBST/methanol solution and in 100% methanol O/N at −20 °C.

Day 2:

6. Rehydrate embryos in a graded series of methanol in PBS containing 0.8% Triton X-100 (PBS-TX).
7. Wash 4 × 5 min in PBS-TX.
8. Digest embryos in 10 μg/mL Proteinase K for 10 min at 37 °C followed by quick rinse in PBS-TX.
9. Block embryos with PBS-TX containing 1% BSA for 2 h at RT.
10. Incubate O/N at 4 °C in rabbit anti-L-plastin (Mathias *et al.*, 2007) in BB (1:500 dilution).

Day 3:

11. Quick rinse 3× in PBS-TX followed by 4 × 10 min washes in PBS-TX.
12. Block embryos with PBS-TX containing 1% BSA for 1 h at RT.
13. Incubate for 2 h at RT in Alexa Fluor 488 or 568 goat anti-rabbit (Invitrogen, 1:200).
14. Quick rinse 3× in PBS-TX followed by 3 × 10 min washes in PBS-TX, and store embryos at 4 °C or image directly.

C. Transgenic Reporter Lines for Live Imaging of Immune Cell Behavior

The excellent availability of *in vivo* imaging is one of the biggest advantages of the zebrafish as a vertebrate model to study innate immunity. Transgenic reporter lines expressing fluorescent proteins under the control of leukocyte-specific promoters are ideal tools to study host–pathogen interactions in the zebrafish model. Several valuable transgenic reporter lines are available to visualize immune cells throughout their development (Table I). Myeloid precursor cells can be visualized as early as 1 dpf using GFP expression under control of the *spi1* promoter (Hsu *et al.*, 2004; Ward *et al.*, 2003; Zakrzewska *et al.*, 2010). Early myeloid cells are also labeled in *fli1:EGFP* transgenic fish, in addition to the GFP expression in the vascular system of this line (Redd *et al.*, 2006). Starting at 2 dpf, the *mpx* promoter can be used as a specific marker for neutrophils. Two transgenic lines, produced with different strategies, that use the *mpx* promoter to label the neutrophil population with GFP brightly are available. One of these lines was constructed in the Huttenlocher lab by fusing an 8-kb promoter region to GFP (Mathias *et al.*, 2006). An additional population of low

Table I
Promoter transgenes used for labeling myeloid cells

Promoter	Specificity	Remarks	References
spi1	Early myeloid cells	Visible at 1–2 dpf	Ward *et al.* (2003), Hsu *et al.* (2004)
fli1	Early myeloid cells	Marker for vasculature	Redd *et al.* (2006)
mpx	Neutrophils	Weak fluorescence in macrophages also reported	Mathias *et al.* (2006, 2009), Renshaw *et al.* (2006)
lyz	Neutrophils		Hall *et al.* (2007)
csf1ra	Macrophages	Also labeling xanthophores	Gray *et al.* (2011)
mpeg1	Macrophages		Ellett *et al.* (2010)
cxcr3.2	Macrophages and minor neutrophil subset	Currently under construction	Meijer lab
mych	Subset of neutrophils	YFP enhancer trap line	Meijer *et al.* (2008)
myd88	Subsets of myeloid cells		Hall *et al.* (2009)
apoeb	Microglia		Peri and Nusslein-Volhard (2008)

GFP-expressing cells can be observed in this transgenic line. This population was later characterized as inflammatory macrophages based on morphology, marker gene expression, and behavior (Mathias *et al.*, 2009). The other *mpx:GFP* neutrophil line was created in the Renshaw lab using a BAC recombineering strategy, which replaced the coding sequence of the gene with GFP and therefore maintained the entire promoter region (Renshaw *et al.*, 2006). The Renshaw lab has not reported an additional population of low GFP-expressing inflammatory macrophages in this line. In our laboratory, this line also appears exclusively neutrophil-specific, but others observed a low GFP-expressing macrophage population, suggesting that some differences in expression may have arisen in different offspring from the original line (Ellett *et al.*, 2010). Using promoter fragments of the lysozyme C (*lyz*) gene, *lyz:EGFP/DsRED2* transgenes have been created that display a significant overlap with the *mpx:GFP* transgene expression (Hall *et al.*, 2007). Although originally reported to label a macrophage subset too, *lyz* is thought to drive neutrophil-specific expression, based on several reports (Ellett *et al.*, 2010; Meijer *et al.*, 2008). A transgenic line that specifically labels macrophages has long been awaited. Recently, a BAC recombineering strategy has been used to create a transgenic line for the macrophage-specific marker *csf1ra* (*fms*) (Gray *et al.*, 2011). Despite the fact that it also shows transgene expression in xanthophores, this line has great potential for use, together with the *mpx:GFP* lines, in live imaging studies of macrophage and neutrophil behavior. The zebrafish genes *mfap4*, *mpeg1*, *cxcr3.2*, and *ptpn6* have recently been identified as early macrophage-specific marker genes, not showing the additional xanthophore expression (Zakrzewska *et al.*, 2010). In an independent study, the Lieschke lab used the promoter sequence of the *mpeg1* gene to create the first entirely macrophage-specific transgenic lines (Ellett *et al.*, 2010). In collaboration with the Renshaw lab, we have a *cxcr3.2* reporter line under construction. The preliminary analysis of a BAC recombineering transgene construct shows that it is expressed in macrophages and a small subset of *mpx:GFP*-expressing neutrophils, making it an interesting marker to further investigate various myeloid subsets. Other lines that label subsets of myeloid cells include the *Et(CLG-YFP)smb463* line (CLGY463), which has a YFP enhancer trap insertion close to a member of the *myc* gene family (*mych*) (Meijer *et al.*, 2008), and the *myd88:EGFP* and *myd88:DsRED2* lines, which have fluorescent protein expression driven by the promoter of *myd88*, a key adaptor molecule in TLR signaling (Hall *et al.*, 2009). Introduction of a membrane-bound GFP into the apolipoprotein E (*apoeb*) locus resulted in a transgenic line that labels zebrafish microglia (Peri and Nusslein-Volhard, 2008). Generating transgenic lines not only is useful to visualize subsets of innate immune cells but can also be used to create reporter lines for transcription factors or chemokines that are important in innate immunity, such as NFκB or IL-8 (also known as CXCL8) (Kanther and Rawls, 2010). The creation of such reporter lines will be of great help in studies of the dynamics of the innate immune response.

The Gal4/upstream activating sequence (UAS) two-component system provides a highly versatile toolbox for transgene expression (Halpern *et al.*, 2008). The first component of this system, the so-called transgenic driver line, consists of a cell- or

tissue-specific promoter that drives the expression of the yeast Gal4 transcription factor. The second component is a fish line that contains a transgene under the control of the UAS of Gal4. When these two transgenic fish lines are crossed, the transgene under the control of UAS will be expressed only in those cells where the cell- or tissue-specific promoter that drives Gal4 is active. With this system, it is possible to drive transgene expression in different leukocyte subsets. A large variety of UAS lines is available, which can be used for different purposes. For example, a *UAS:Kaede* line highlights cells by green fluorescence. The green fluorescent Kaede protein can be photoconverted into its red fluorescent form by exposing it to UV light (Halpern *et al.*, 2008). This photoconversion can be used, for example, to visualize the dynamics of arriving and departing leukocytes at a site of infection, by photoconverting the Kaede proteins in cells in that area into their red fluorescent form (Ellett *et al.*, 2010). A second example of the usefulness of this system is the possibility to ablate subsets of cells or entire tissues specifically. This can be done by combining a Gal4 line specific for the target cells with the *UAS:NfsB-mCherry* line, which drives expression of the *E. coli* gene *nitroreductase B* (Halpern *et al.*, 2008). Nitroreductase B is an enzyme that can convert precursor drugs such as metronidazole into toxic cellular metabolites. The cells that are targeted for ablation by nitroreductase B are simultaneously made visible, due to the fusion of nitroreductase B with mCherry protein. This strategy was used to ablate macrophages specifically, without significantly altering neutrophil numbers (Gray *et al.*, 2011). An alternative strategy for cell ablation is light-induced killing using the *UAS:KillerRed* line (Del Bene *et al.*, 2010). Creating Gal4 driver and UAS reporter lines has become more efficient by the introduction of Tol2-based vectors, the use of which leads to high rates of genomic integration when co-injected with Tol transposase mRNA (Suster *et al.*, 2009). A potential problem when using the Gal4/UAS system is that silencing of the UAS sequence might occur over subsequent generations, making it necessary to regenerate UAS lines frequently.

D. Isolation of Immune Cells from Reporter Lines

The zebrafish transgenic lines with fluorescently labeled immune cells can be utilized conveniently for the isolation of specific populations of immune cells based on their fluorescent characteristics. In our recent study of Spi1-dependent genes expressed in early zebrafish myeloid cells, we performed transcriptome profiling of myeloid cells that were obtained from *spi1:GFP* embryos by fluorescence-activated cell sorting (FACS). For preparation of a single-cell suspension for FACS sorting, the embryos were digested with trypsin. The removal of yolk prior to trypsin treatment drastically reduces the amount of debris in the single-cell suspension, therefore providing better resolution and faster sampling during FACS. The number of embryos required for FACS sorting and subsequent applications depends on the expected percentage of fluorescent cells per embryo. In the case of the *spi1:GFP* line used in our study, which shows some additional brain-specific GFP expression, there are on average 1.5% GFP+ (expressing) cells per 28–30 hpf embryo. Approximately

300 embryos gave a standard yield of approximately 2×10^5 GFP+ cells, from which sufficient RNA could be obtained for microarray hybridization using the Ambion RNAqueous Microkit and a single round of RNA amplification. As discussed in the section "Transcriptomic Analysis," it is also possible to use less starting material and an extra round of RNA amplification. Our protocol for obtaining single-cell suspensions and FACS sorting follows here (based on Covassin *et al.*, 2006).

1. Embryo Dissociation for FACS

1. Collect 300–600 embryos at the desired developmental stage (depends on the expected percentage of fluorescent cells per embryo, 300–600 embryos work fine for 1.5% GFP-positive cells).
2. Dechorionate embryos by treatment with freshly prepared 2 mg/mL pronase (Sigma catalog number P5147) in egg water (60 μg/mL sea salts), for 1 min at 28.5 °C.
3. Rinse the embryos in calcium-free Ringer solution for 15 min and pass them several times through a 200-μL pipette tip to remove the yolk.
4. Transfer the embryos into a 35-mm culture dish with 2 mL PBS (PBS, pH 8) containing 0.25% trypsin and 1 mM EDTA.
5. Incubate 90 min at 28.5 °C (depends on the number of embryos, this time works for 300 embryos of 28 hpf); during incubation pass samples through a 200-μL pipette tip every 10 min in order to triturate embryos into a single-cell suspension.
6. Stop the digestion by adding $CaCl_2$ to a final concentration of 1 mM and fetal calf serum to 10%.
7. Centrifuge the cells for 3 min at $1000 \times g$.
8. Rinse the cells with PBS once and repeat centrifugation.
9. Resuspend the cells at $\sim 10^7$ cells/mL in Leibovitz medium L15 without phenol red, 10% fetal calf serum, 0.8 mM $CaCl_2$, penicillin 50 U/mL, and streptomycin 0.05 mg/mL.
10. Immediately proceed with FACS.

2. FACS

1. During FACS, cells are separately collected in L15, 0.8 mM $CaCl_2$, 10% fetal calf serum, 10% zebrafish embryo extract, penicillin 50 U/mL, and streptomycin 0.05 mg/mL.
2. Immediately proceed with RNA extraction.

3. RNA Extraction from FACS-Sorted Cells

1. Pellet the cells by centrifugation at $12{,}000 \times g$ for 4 min.
2. Remove supernatant.
3. Use RNAqueous Microkit (RNAqueous®-Micro Kit, Ambion catalog number AM1931) according to the protocol.

III. Bacterial Infection Methods

A. Routes of Infection

The infection of zebrafish embryos is usually initiated by injecting the infectious agent into the host via different sites, depending on the type of experiment to be performed. Borosilicate glass capillary needles (1 mm O.D. × 0.78 mm I.D.), equivalent to those used for injecting morpholinos, are prepared using a micropipette puller and loaded with the inoculum using a microloader tip. The loaded needle is mounted onto a micromanipulator and positioned under the stereomicroscope. The injection time and pressure are set to obtain the correct injection volume, because these values will differ for each needle used. The diameter for a drop of 1 nL is 0.62 nm ($V = 4/3\pi r^3$). The drop size is adjusted to match the desired diameter with the help of a scale bar on a microscope slide or in the ocular. The micromanipulator with the loaded needle is set into the correct position prior to injections and is only moved up and down to inject. The injection plate containing embryos is moved by hand during injections to orientate the embryos into the preferred position for injection. Except when the yolk is used as the injection site, the embryos are dechorionated prior to injection and kept in a Petri dish filled with egg water (60 μg/mL sea salts) and with a layer of 1% agarose on the bottom to prevent embryos from sticking to the plastic surface. Embryos can be anesthetized with 200 μg/mL buffered 3-aminobenzoic acid (tricaine, Sigma–Aldrich). If required for subsequent imaging, 0.003% 1-phenyl-2-thiourea (PTU, Sigma) can be added to prevent melanization. Below we give guidelines for different injection procedures that we have used to achieve systemic or local infection with bacterial pathogens, but these methods can also be applied for injection of viruses, fungal spores, or protozoan parasites. The best positioning of the injection needle during these procedures is illustrated in Fig. 2. For bacterial injections, we check the amount of colony-forming units (cfu) injected into the embryos, by injecting the same inoculum directly into a sterile PBS drop on growth medium. This drop is then plated out and the bacterial colonies are counted after incubation. Because the immune system becomes increasingly competent during embryo development, the proper staging of embryos is very important to compare results among different infection experiments (Kimmel *et al.*, 1995).

1. Yolk Injection

The yolk is a convenient injection site that can be used to achieve systemic infection with slow-growing bacteria such as *Mycobacterium marinum*, which have a generation time of approximately 6-8 h. However, with other pathogens, for instance, *Salmonella typhimurium*, yolk injection leads to rapid proliferation and early lethality of the embryo. We have found that yolk injection of *M. marinum* during the first hours of embryogenesis, from the 16-cell stage onwards, does not interfere with embryo development. To prevent their immediate diffusion, the bacteria are resuspended in 2% polyvinylpyrrolidone (PVP_{40}) prior to yolk injection. During

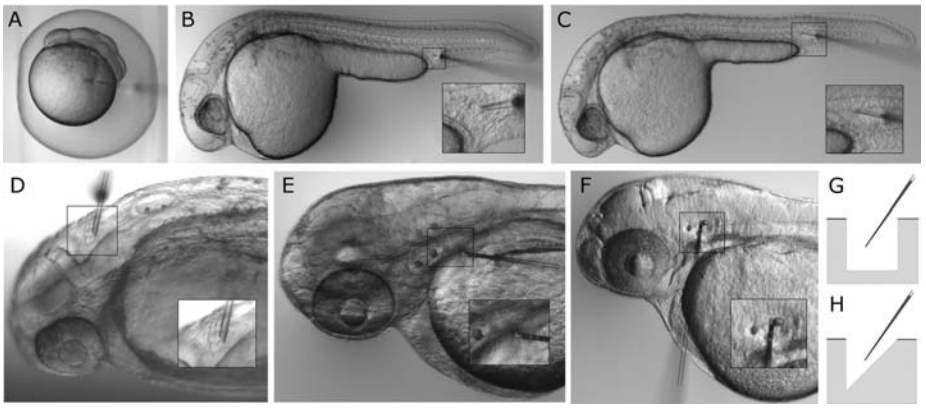

Fig. 2 Injection sites to initiate systemic (A, B, and E) or local (C, D, and F) bacterial infection in the zebrafish embryo. (A) Yolk injection at 16-cell stage. (B) Posterior blood island and (C) tail muscle injection at 28 hpf. (D) Hindbrain ventricle injection at 28 hpf. (E) Duct of Cuvier injection at 54 hpf. (F) Otic vesicle injection at 54 hpf. (G) An agarose plate with rectangular channels can be used for yolk, tail muscle, and otic vesicle injections. (H) An agarose plate with triangular channels can be used for hindbrain injection by positioning the embryo with its ventral side against the vertical wall of the channel and the dorsal side against the slanted wall facing up toward the needle. For the posterior blood island and duct of Cuvier injections, embryos can simply be placed on flat agarose plates.

the first days of embryogenesis, the *M. marinum* bacteria disseminate from the yolk into the tissues, resulting in a similar infection phenotype as on the intravenous route of infection described below (Carvalho *et al*., 2011). In collaboration with the company ZFscreens, our laboratory has developed an automated injection system for yolk injections, which supports high-throughput assays (Carvalho *et al*., 2011).

2. Tail Muscle Injection

To examine immune cell migration toward a local bacterial infection, injection can be conducted in the tail muscle of 1-day-old embryos where macrophages are normally not present. Muscle injections can also be performed at later stages when neutrophils have differentiated. Because the injection location is chosen just above the blood island (or later caudal hematopoietic region) located behind the urogenital opening, it can rapidly induce the migration of innate immune cells. This injection location is also convenient to compare the number of migrated cells relative to the total number of innate immune cells in the tail (Zakrzewska *et al.*, 2010). To perform the injection, the anesthetized embryos are oriented horizontally on a flat 1% agarose plate with the tail pointing toward the needle as shown in Fig. 2C. A volume of 5 nL of bacterial inoculum in PBS can be injected into the muscle above the urogenital opening without causing damage to the notochord and blood vessels. In muscle injections of 28 hpf embryos, we have observed that two distinct myeloid cell populations are attracted to the infection site, one expressing *mpx* and the other

expressing macrophage markers (Zakrzewska *et al.*, 2010). Knockdown of the chemokine receptor *cxcr3.2* specifically reduced migration of the population expressing the macrophage markers (Zakrzewska *et al.*, 2010). Although the injection of PBS buffer alone also attracts some myeloid cells due to muscle tissue damage, the effect of *cxcr3.2* knockdown was specifically related to the migration of macrophages to bacteria.

3. Hindbrain Ventricle Injection

The hindbrain ventricle is a closed cavity of the embryo that contains zero to two macrophages at 30 hpf (Davis *et al.*, 2002; Herbomel *et al.*, 1999). The migration of macrophages following injection of bacteria into this cavity has been documented in several studies (Clay *et al.*, 2007; Davis *et al.*, 2002; Herbomel *et al.*, 1999). For example, injection of 20–100 *M. marinum* bacteria rapidly induced macrophage recruitment into this area (Davis *et al.*, 2002). Because the size of the hindbrain cavity is limited, not more than 0.5–1 nL should be injected. For hindbrain injections, we recommend to line up the anesthetized embryos on a 1% agarose injecting plate with *V*-shaped channels. A description of the plastic mold to make these channels can be found in *The Zebrafish Book* (Westerfield, 2000), also available on the ZFIN website (zfin.org). The embryos are positioned and orientated with their ventral side toward the vertical wall of the channel (Fig. 2D). The needle is inserted into the hindbrain ventricle from an anterior position without touching the underlying neuroepithelium and the bacteria are injected. For practicing the procedure, it is convenient to use a fluorescent dye, which will reveal possible damage of the underlying tissue (Gutzman and Sive, 2009; Levraud *et al.*, 2008).

4. Otic Vesicle Injection

For embryos older than 48 hpf, another suitable body cavity for bacterial injection is the otic vesicle due to its increasing size during development. For otic vesicle injections, anesthetized embryos are positioned laterally on a flat 1% agarose plate with just enough egg water to create surface tension to hold the embryos in place on the agarose layer during injections (Fig. 2F). Puncture of the vesicle has to be conducted with extra care to avoid local tissue rupture, which by itself will result in a massive attraction of immune cells. If carefully performed, PBS injection into the otic vesicle induces no or only minor cell migration, whereas the injection of various bacteria such as *E. coli*, *M. marinum*, and *S. typhimurium* specifically attracts both macrophages and neutrophils (Carvalho *et al.*, 2011; Le Guyader *et al.*, 2008). To avoid wounding effects, the injection volume should be limited to 1 nL (Levraud *et al.*, 2008). We generally use approximately 20 bacteria for injection. We prefer to inject between 2 and 3 dpf, because the epithelium of the otic vesicle becomes more difficult to penetrate at later stages.

5. Systemic Infection via the Blood Island

A systematic infection of 1-day-old embryos can be obtained by injecting bacteria into the blood circulation at the blood island. We usually perform these infections at 28 hpf, shortly after the onset of circulation. The anesthetized embryos are lined up on a flat 1% agarose injecting plate with their tails pointing toward the tip of the needle (Fig. 2B). As mentioned above, only a limited amount of egg water is used to keep the embryos in place on flat agarose plates. The periderm is pierced with the needle tip, and bacteria are injected directly into the caudal vein close to the urogenital opening. The injected volume will always follow the blood flow throughout the caudal vein toward the heart and can be monitored directly after the pulse by the expanding volume within the vascular system (Davis *et al.*, 2002).

6. Infection via Duct of Cuvier

Alternatively to blood island injection, bacteria can also be introduced into the blood circulation via injection at the duct of Cuvier, which is the wide blood circulation valley on the yolk sac connecting the heart to the trunk vasculature. The duct of Cuvier can be used for injections between 1 and 3 dpf. As for blood island injections, the anesthetized embryos are lined up on a flat agarose plate, their tails pointing toward the needle. The needle is inserted into the starting point of the duct of Cuvier just dorsal to the location where the duct starts broadening over the yolk sac (Fig. 2E). This location is the deepest section of the duct and therefore provides the lowest risk of puncturing the yolk sac. The bacterial inoculum will follow the blood flow through the duct of Cuvier over the yolk sac toward the heart and can be monitored directly after the injection by the expanding volume within the duct.

B. Quantification of Bacterial Burden

1. CFU Determination

The most straightforward approach to determine the bacterial burden of infected zebrafish embryos is to quantify the amount of cfu by plating on a suitable growth medium. Commonly, a group of five embryos is triturated by repetitively pipetting the embryos up and down in a volume of 100 μL PBS containing 1% Triton X-100 (van der Sar *et al.*, 2003). Alternatively, embryos can be placed in a 2-mL Eppendorf tube and disrupted by addition of a metal bead (4 mm diameter, Fabory) followed by shaking for 1 min at maximum frequency in a grinder such as the MM 301 mixer mill (Retsch). Subsequently, serial dilutions are cultured on appropriate selection agar plates for cfu assessment. However, a common problem with slow-growing bacteria such as *M. marinum* is the growth competition by the natural microbial flora of the zebrafish embryo. A strategy to overcome this problem in the case of mycobacterial infections is the use of the BBL® MycoPrep™ Kit (BD Biosciences catalog number 240862). After dissociation of embryos in PBS containing 0.1% Triton X-100, the samples are incubated for 9 min in 100 μL MycoPrep reagent and subsequently

plated on selection plates (Clay *et al.*, 2007). Besides being labor intensive, this and other methods for cfu determination will not allow following the progression of bacterial infection of a distinct embryo over time.

2. Pixel Count Analysis Using Fluorescent Images

A convenient alternative to cfu counts is pixel count analysis. Taking advantage of fluorescently labeled bacteria, it is possible to follow the progression of the infection over time. Counting the amount of fluorescent pixels for each embryo, the bacterial burden can be expressed in relative units and different treatment groups can be compared. For example, in *M. marinum* infection experiments, the results of pixel quantification have been shown to correlate well with cfu determination (Tobin *et al.*, 2010). Pixel quantification can be performed with various image analysis software programs, for example, the freeware program ImageJ. A program specially developed for the analysis of zebrafish embryos proved very useful for the batchwise analysis of images of infected embryos in an *M. marinum* mutant screen (Stoop *et al.*, 2011).

3. High-Throughput Quantification Using the COPAS System

High-throughput detection of the bacterial load of single embryos can be carried out by the complex object parametric analyzer and sorter (COPAS). The COPAS™ XL (Union Biometrica) large particle sorter has been designed for the analysis, sorting, and dispensing of objects up to 1.5 mm in diameter based on size, optical density (OD), and fluorescence intensity. It is equipped with 488- and 561-nm solid state lasers. Up to 8000 data points per embryo can be simultaneously detected and analyzed to set sorting parameters based on the fluorescence profiles in two channels. Prior to analysis, embryos older than 24 hpf and younger than 48 hpf need to be removed from the chorion and kept sedated using 0.02% tricaine to prevent attachment of the embryos to the tubing. The parameters for the analysis need to be set depending on the fluorescent label of the bacterial strain used. In a standard analysis using *M. marinum* (Carvalho *et al.*, 2011), time of flight (TOF), indicating the axial length of an embryo, is set against optical extinction (EXT), indicating the size and internal structure of the embryo. This will allow discrimination between live and dead embryos. Simultaneously, the peak width of the green (510/23 band-pass filter) or red (615/24 band-pass filter) channel is set against the peak height of the same channel to determine the population of infected embryos according to the distribution of the fluorescent signal over the embryo. An infection caused by *M. marinum* will lead to spatially restricted sites of bacterial accumulation and infected embryos will therefore show high but narrow peaks. To define the sorting parameters for the first time, it is necessary to run the samples through the system once to create a profile before starting the analysis. After the profile is set, the samples can be analyzed and sorted into 96-microwell plates. A profile of each embryo showing the distribution of the fluorescent signal across the embryo will be created and the

measured values of the fluorescent signal (given in millivolts) are stored in a spreadsheet for subsequent analysis. The COPAS procedure needs to be optimized according to the specific properties of the pathogen, the type of assay that is used, and the information that needs to be gathered. In addition, due to proliferation of the bacteria and size increase of the embryos, a profile needs to be defined for each analysis time point separately.

C. Model Systems for Infectious Diseases

As summarized in recent reviews, the number of zebrafish infection models for bacterial pathogens has rapidly expanded during the recent years (Allen and Neely, 2010; Kanther and Rawls, 2010; Lesley and Ramakrishnan, 2008; Meeker and Trede, 2008; Meijer and Spaink, 2011; Sullivan and Kim, 2008). Bacterial virulence factors and host immune response genes have been the focus of many investigations in these models. Real-time analyses of the interaction between intracellular bacterial pathogens and host phagocytes have demonstrated that hallmarks of different host–pathogen interactions are reproduced in zebrafish embryos (Davis *et al.*, 2002, 2009; Davis and Ramakrishnan, 2009; Levraud *et al.*, 2009; van der Sar *et al.*, 2003; Vergunst *et al.*, 2010). Below we provide guidelines on how to perform infections with *S. typhimurium* and *M. marinum*, as two representative examples of bacterial pathogens that produce acute and chronic infections in zebrafish embryos, respectively.

1. *S. typhimurium* Infections

S. enterica serovar Typhimurium (*S. typhimurium*) is a good model for the study of Gram-negative infections in zebrafish. Two strains of *S. typhimurium* have been studied in detail, the wild-type SL1027 strain and its isogenic derivative SF1592 (Ra), which is defective in the synthesis of the O-antigen side chain of the outer membrane lipopolysaccharide (LPS). Using wild-type and Ra mutant bacteria containing the DsRed expression vector pGMDs3, it was shown that the wild-type strain induces a rapid lethal infection, whereas infection with the Ra strain is transient and nonpathogenic in zebrafish embryos (van der Sar *et al.*, 2003). A time-course transcriptome profiling study of infection of 28 hpf embryos with the wild-type strain showed a gradual increase of the expression levels of innate immune response genes up to 24 h, at which time point this infection becomes lethal. The gene expression profile was consistent with a strong inflammatory response in these embryos, showing high induction levels of genes such as interleukin 1 beta (*il1b*) and matrix metalloproteinase 9 (*mmp9*), as well as other genes. The Ra strain induced a similar but attenuated response during the first 8 h of the infection, with significantly lower induction levels of these inflammatory genes, and a clear decline of the response was observed at 24 h (Stockhammer *et al.*, 2009). This nonpathogenic strain proved useful for demonstrating the immunocompromised phenotype of zebrafish embryos impaired in innate immunity signaling (van der Sar *et al.*, 2006).

In the laboratory, *S. typhimurium* stocks are kept at −80 °C. For injections, bacteria are freshly grown O/N at 37 °C on LB agar plates supplemented with 100 μg/mL carbenicillin to select for the DsRED expression vector. Individual colonies are picked and resuspended in sterile PBS. To avoid clumping of the bacteria, the suspension should be vortexed well before loading into the microcapillary pipettes. Embryos grown at 28.5–31 °C in egg water are dechorionated, staged at 28 hpf according to their morphological criteria (Kimmel *et al.*, 1995), and injected with approximately 250 cfu into the blood island as described above. Due to the relatively large size of *S. typhimurium* bacteria and their bright DsRED fluorescence, individual bacteria can easily be counted with a fluorescence stereomicroscope to set the injection dose. For verification, an injection drop is also spotted onto LB agar plates and incubated at 37 °C O/N for cfu counting. Individual DsRED *S. typhimurium* cells can be observed circulating in the bloodstream directly after injection, and embryos not properly injected are discarded. Injected embryos are transferred into fresh egg water in agarose-coated plates and are incubated at 28 °C. For survival curves or real-time imaging, embryos are monitored every few hours (wild type) and daily (Ra) after infection.

2. *M. marinum* Infections

M. marinum is an excellent model for human tuberculosis research. *M. marinum* and *M. tuberculosis* are genetically closely related species that cause similar pathological hallmarks in their natural hosts, fish and human (Tobin *et al.*, 2010). They both survive within macrophages and induce the formation of granulomas, which are complex structures of immune cells that provide a niche for the long-term persistence of these pathogens inside their respective hosts (Russell, 2007; Tobin and Ramakrishnan, 2008). The structure of *M. marinum*–induced granulomas in adult zebrafish highly resembles that of human tuberculous granulomas (Swaim *et al.*, 2006). Importantly, it has been shown that the context of the innate immune system of zebrafish embryos is sufficient to initiate granuloma formation (Davis *et al.*, 2002). Following infection by *M. marinum* bacteria at 1 dpf, tight aggregates of infected and noninfected macrophages are observed within several days. Furthermore, granuloma-activated genes (*gag* genes) of *M. marinum*, which are genes that are activated only when the bacteria are contained inside a granuloma, are also activated in these embryonic macrophage aggregates (Davis *et al.*, 2002). The process of macrophage aggregation into initial granulomas has been documented in a detailed manner by real-time imaging (Davis and Ramakrishnan, 2009). Wild-type (M-strain) and mutant strains labeled with many useful fluorescent constructs have been produced by the Ramakrishnan laboratory, which has pioneered the use of this model. For example, *M. marinum* bacteria labeled with the photoconvertible Kaede protein were used to trace how secondary granulomas are seeded from a primary granuloma by egression of single infected macrophages (Davis and Ramakrishnan, 2009). A mutant defective in the ESX-1/RD-1 secretion system, which is conserved between *M. marinum* and *M. tuberculosis*, shows a significantly reduced formation of granulomas and is

attenuated compared to wild-type bacteria, indicating that granuloma formation is part of the virulence mechanism (Volkman *et al.*, 2004, 2010). Another attenuated mutant, *erp*, has a cell wall defect that reduces its growth inside macrophages (Cosma *et al.*, 2006). In functional studies of host genes, this mutant is useful to score effects on bacterial burden of individual infected macrophages by fluorescence microscopy, which is not possible using wild-type bacteria due to their rapid growth kinetics (Clay *et al.*, 2008). Other *M. marinum* strains originating from infected humans or fish have been described that showed marked differences in pathogenicity and induced host gene responses, such as the Mma20 and E11 strains (van der Sar *et al.*, 2004, 2009). *M. marinum* strains can be grown either on Middlebrook 7H10 agar (Difco) plates or in Middlebrook 7H9 liquid medium. For infecting zebrafish embryos, we generally use bacteria grown O/N in 7H9 liquid medium supplemented with ADC, 0.05% Tween 80, and antibiotics (50 μg/mL hygromycin or 20 μg/mL kanamycin) dependent on the fluorescent plasmid used. It is not possible to set the injection dose of *M. marinum* bacteria by counting under the fluorescence stereomicroscope like we do for *S. typhimurium*, as described above. Therefore, the injection dose is based on a standard curve of growth. The generation time of *M. marinum* is approximately 12 h, varying according to the strain. The OD of the bacteria is measured at 600 nm. An OD of 1 at 600 nm corresponds to approximately 1×10^8 *M. marinum*/mL (this may vary according to the bacterial strain used). When the bacteria are in logarithmic phase (OD_{600} should not exceed 1.00), they are harvested by centrifugation and washed three times with PBS. The OD_{600} is measured again and the suspension is diluted to the desired concentration of cfu. For injections, we prefer to centrifuge this suspension and resuspend the pellet in 2% PVP_{40}, which we find improves homogeneity of the suspension resulting in more reproducible inocula. The standard route for infecting embryos is blood island injection, as described above. We generally inject a dose of 150–200 cfu in 1 nL. For high-throughput applications such as drug screening, injection of approximately 40 cfu into the yolk around the 16-cell stage or later proved useful (Carvalho *et al.*, 2011). This method results in the formation of granulomas in the head, body, and tail of the larvae, similar as with the conventional blood island infection route.

IV. Analysis of the Innate Immune Response

A. Bioassays for the Innate Immune Response

The production of reactive oxygen and nitrogen species is a major effector mechanism of the innate immune response. The respiratory burst in zebrafish embryos can be determined by an assay that measures the oxidation of the nonfluorescent dye 2′,7′-dihydrodichlorofluorescein diacetate (H2DCFDA) to the fluorescent product dichlorofluorescein (DCF) (Hermann *et al.*, 2004). In addition, nitric oxide production can be visualized in living zebrafish embryos using diaminofluorophore 4-amino-5-methylamino-2′-7′-difluorofluorescein diacetate (DAF-FM-DA) as a cell-permeant probe (Lepiller *et al.*, 2007).

B. Transcriptomic Analysis

Microarray and deep sequencing technologies are powerful tools to obtain insight into the gene expression changes underlying host responses to infectious agents. In several recent studies, these technologies have been used to characterize zebrafish infection models (Encinas *et al.*, 2010; Hegedus *et al.*, 2009; Meijer *et al.*, 2005; Ordas *et al.*, 2010; Stockhammer *et al.*, 2009, 2010; van der Sar *et al.*, 2009; Wu *et al.*, 2010). In the following section, an overview of the available platforms is given, with guidelines for their use and a protocol to isolate high-quality mRNA from zebrafish embryos for transcriptome analysis.

1. Microarray-Based Transcriptome Analysis

Commercial microarray chips for zebrafish are available from Affymetrix, Agilent Technologies, and NimbleGen. The Affymetrix GeneChip® Zebrafish Genome Array allows studying gene expression of over 14,900 zebrafish transcripts. However, the sequence information is derived from databank releases from 2003 and, thus, is not up to date. Agilent offers the Zebrafish (V3) Gene Expression Microarray 4×44K, containing 43,803 probes sourced among others from RefSeq (Release 38, November 2009), Unigene (Release 117, September 2009), and Ensembl (Release 56, September 2009), and, in addition, provides a service to order custom-designed chips. Nimblegen, which also provides custom design, claims the most comprehensive commercial design with its 385k arrays based on the Zv7 genome build. We currently use a 180k custom-made Agilent design containing 133,691 sequences derived from the Zv8 genome build (Ensembl 57, Vega 37) and the RefSeq 39 and UniGene 117 databases (Rauwerda *et al.*, 2010).

Labeling samples with fluorescent dyes can be achieved by either direct or indirect labeling reactions. In the first case, the fluorescent label is directly incorporated during cDNA synthesis and aRNA amplification or in a post-aRNA reverse transcription reaction. Indirect labeling, on the other hand, incorporates a modified nucleotide to which the fluorescent label is later attached. Although direct labeling is faster (one step vs. two steps), it is more expensive and less suited for dye swapping. Furthermore, the use of labeled nucleotides in the direct labeling procedure can lead to variations in the incorporation efficiency of different dyes because Cy-labeled dyes have lower incorporation efficiencies.

Good results were obtained for RNA derived from zebrafish embryos using the Amino Allyl Message Amp™ II aRNA amplification kit (Ambion). Amino allyl UTP is incorporated during the *in vitro* transcription reaction step, resulting in amino allyl aRNA that subsequently can be coupled to either a Cy3 or Cy5 amine-reactive dye. The kit is supplied with material for 20 reactions. However, by using only half of the supplied materials for each reaction, aRNA for up to 40 samples can be sufficiently amplified and labeled. To prevent loss of yield during the cDNA and aRNA cleanup steps, those need to be carried out as recommended by the manufacturer. Routinely, we use 500 ng of high-quality RNA as starting material and perform all

steps of the first- and second-strand cDNA synthesis as well as the aRNA synthesis using only half of the recommended reagents. If necessary, the input amount of RNA can be lowered to 200 ng without requiring an extra round of amplification. When two rounds of amplification are used, the first with UTP and the second with amino allyl UTP, RNA amounts down to 20 ng are sufficient.

The experimental design of microarray studies is very important for data interpretation and should include proper controls for each treatment. For example, in the case of a bacterial infection via injection, zebrafish embryos injected with the carrier (e.g., PBS) alone should be included to control for gene expression changes induced by the wounding response. In the case of combinations with morpholino knockdown, good controls should be included for the morpholino treatment because these could also induce immune-related responses. In our studies, we have used a standard control morpholino supplied by Genetools or mismatch morpholinos as controls (Stockhammer *et al.*, 2010; Zakrzewska *et al.*, 2010). Furthermore, for sufficient statistical power in the data analysis, the experiment should consist of three to five biological replicates, and the treatment order should be randomized. If a two-color platform, such as the Agilent microarray chip, is used, one can choose to compare samples directly to each other (competitive hybridization of two samples) or via a common reference approach (competitive hybridization of the samples vs. the common reference). Choosing a common reference approach avoids the need for a dye swap and gives greater flexibility in the subsequent analysis as all samples can be compared to each other.

2. Next-Generation Sequencing

Next-generation sequencing technologies such as Solexa (Illumina) or SOLID (Applied Biosystems) are powerful alternatives to microarray experiments and have recently been applied for transcriptome profiling studies in zebrafish (Hegedus *et al.*, 2009; Ordas *et al.*, 2010; Stockhammer *et al.*, 2010). Solexa and SOLID are able to sequence in parallel up to tens of millions of DNA molecules derived directly from mRNA (Wang *et al.*, 2009). The direct sequencing yields libraries of short (25–50 nucleotides) sequences that then need to be mapped onto the relevant genome or transcript database. Avoiding the inherent limitations of microarray-based analysis, such as a low dynamic range and a sequence-based design, deep sequencing permits detection and quantification of low-abundance mRNA and transcript isoforms. However, due to considerably lower costs and less complex data analysis, microarrays remain highly useful, especially for the analysis of larger numbers of biological samples.

Two different approaches for deep sequencing of the transcriptome are whole-transcriptome sequencing, known as RNA-Seq, and tag-based sequencing, referred to as Tag-Seq or Digital Gene Expression (DGE). In RNA-Seq methods, RNA is first sheared and converted to cDNA, or cDNA is produced first and then sheared into short fragments. In Tag-Seq or DGE, cDNA is enzymatically digested and the 3′ ends are captured on magnetic beads. Subsequently, a second enzyme is used to cut a short

fragment from the 5′ end of each captured cDNA, thus providing a library of sequence-specific tags that are further processed for sequencing. Both methods proved suitable for quantification of transcriptome changes during infection of zebrafish embryos (Ordas *et al.*, 2010).

3. RNA Isolation Protocol

RNA quality is crucial for transcriptome analysis. A good way to assess RNA quality is Lab-on-Chip analysis (Agilent Technologies). An RNA Integrity Number (RIN, quality measurement from Agilent Technologies) greater or equal to 7 is generally considered sufficient, but we prefer not to use samples with RIN values below 8. Below we provide a protocol that normally generates RNA with an RIN value between 9 and 10.

RNA Isolation Protocol for Pools of 15–20 Embryos

1. Collect embryos in a 2-mL reaction tube; remove remaining water and immediately immerse embryos in 500 μL TRIzol® reagent (Invitrogen). Alternatively, embryos can be immersed in RNA*later*® (Ambion) or snap frozen in liquid nitrogen and stored at 4 or −80 °C, respectively.
2. Homogenize embryos either by passing the embryos repeatedly through an injection needle (21G 2″, 0.8 × 50 mm) or by using a grinder, such as the MM 301 mixer mill (Retsch, 2 × 30 s at maximum frequency). In the latter case, place a metal bead (4 mm diameter, Fabory) in the tube before grinding. Transfer the homogenate sample to a new 1.5-mL tube.
3. Centrifuge for 10 min at 12,000 × *g* (4 °C) and subsequently transfer supernatant to a new tube.
4. Incubate samples for 5 min at RT.
5. Add 0.1 mL chloroform. Cap sample tubes securely and shake vigorously by hand for 15 s.
6. Incubate samples for 2–3 min at RT.
7. Centrifuge for 10 min at full speed (4 °C) in an Eppendorf centrifuge for phase separation. The mixture separates into a lower phenol chloroform phase (red), an interphase (white), and a colorless upper aqueous phase. RNA remains exclusively in the aqueous phase. Transfer the aqueous phase to a new 1.5-mL tube.
8. Add 0.25 mL of isopropyl alcohol and mix by turning the tube upside down for several times.
9. Incubate samples for 10 min at RT.
10. Centrifuge at no more than 12,000 × *g* for 10 min at 4 °C. The RNA will form a gel-like pellet that is sometimes hard to see.
11. Remove the supernatant and wash the pellet once with 0.5–1 mL of 75% ethanol, and centrifuge at 7500 × *g* for 5 min at 4 °C.
12. Remove the supernatant and air-dry the pellet for 5–10 min at RT.

13. To dissolve the RNA, incubate in 100 μL of RNase-free water for 10 min at 55 °C and vortex well.
14. To remove contaminating DNA that might interfere with subsequent applications, treat RNA samples for 20 min at 37 °C with 10 U of RNase-free DNase I (Roche Applied Science).
15. Column-purify the samples using the RNeasy MinElute Cleanup Kit (Qiagen).

Several other commercial kits for RNA isolation will also produce good results. For example, we have had good results with the Ambion RNAqueous Microkit to obtain RNA from FACS-sorted cells (Zakrzewska *et al.*, 2010). If RNA samples will also be used for microRNA analysis, the miRNeasy Mini kit (Qiagen) provides good preservation of small RNA species. For isolating RNA from individual embryos, we use a recently published method that provides sufficient high-quality mRNA for microarray analysis from single embryos (de Jong *et al.*, 2010). This method, using a combination of sample homogenization in liquid nitrogen, RNA extraction with phenol (Qiazol, Qiagen), and column purification (RNeasy MinElute Cleanup Kit, Qiagen), yields approximately 200–500 ng RNA per embryo.

C. Morpholino Knockdown of Innate Immunity Mediators

Morpholinos are the most widely used knockdown tools in zebrafish. Common practices for their use and potential pitfalls of morpholino application have been extensively reviewed (Bill *et al.*, 2009; Eisen and Smith, 2008). Morpholinos can be applied to block translation (AUG MOs) or pre-mRNA splicing (splice MOs). Due to the lack of antibody tools to check efficacy of AUG MOs, it may be preferable to use splice MOs where the effects can be checked by reverse transcription PCR. Injection of morpholinos into zebrafish embryos at the one- to two-cell stage can result in a variable period of transient knockdown. For example, MyD88 and TNFR MOs have been used up to 5–8 days to study gut immune responses and *M. marinum* infection, whereas other MOs are less effective or toxic at higher doses (Bates *et al.*, 2007; Clay *et al.*, 2008).

As shown in Table II, morpholino knockdown of the Spi1/Pu.1 transcription factor has been frequently used for infection studies (Brannon *et al.*, 2009; Clatworthy *et al.*, 2009; Clay *et al.*, 2007; Prajsnar *et al.*, 2008; Wiles *et al.*, 2009; Zakrzewska *et al.*, 2010). Knockdown of this transcription factor results in embryos that lack macrophages and show a major reduction of neutrophils during the first days of development (Fig. 3) (Rhodes *et al.*, 2005; Su *et al.*, 2007). Spi1/Pu.1 morphants showed increased susceptibility to *Pseudomonas aeruginosa* and *Staphylococcus aureus* infections (Brannon *et al.*, 2009; Clatworthy *et al.*, 2009; Prajsnar *et al.*, 2008). In addition, Spi1 knockdown studies demonstrated that macrophages play an essential role in tissue dissemination of *M. marinum* infection (Clay *et al.*, 2007). A dual microarray approach, in which genes downregulated by Spi1/Pu.1 morpholino knockdown were compared with genes enriched in FACS-sorted myeloid cells from *spi1:GFP* transgenic embryos, was used in our laboratory to identify the putative

Table II
Overview of innate immunity mediators studied by morpholino knockdown in zebrafish embryos

Genes	Functions	Conclusion from knockdown experiments	References
crfb family	Cytokine receptor family member b	Different receptor complexes required for signaling of IFN-γ and IFN-φ interferons	Aggad *et al.* (2010)
cftr	Cystic fibrosis transmembrane conductance regulator	Required for control of *Pseudomonas aeruginosa* infection	Phennicie *et al.* (2010)
csf3r	Granulocyte colony-stimulating factor receptor	Required for primitive and definitive myelopoiesis, early myeloid cell migration, and LPS-induced emergency myelopoiesis	Liongue *et al.* (2009)
cxcr3.2	CXCL chemokine receptor, homologous to human CXCR3/CXCR5	Required for macrophage migration to bacterial infection sites	Zakrzewska *et al.* (2010)
duox	Member of the NADPH-oxidase family	Required to control enteric *S. typhimurium* infection	Flores *et al.* (2010)
gprk2	NFκB signaling regulator	Required for *Escherichia coli*–induced *tnfa* and *il1b* expression	Valanne *et al.* (2010)
ifng1-1,1-2	IFN-γ family members	Required for control of *E. coli* and *Yersinia ruckeri* infections Signals through specific crfb receptor complexes	Sieger *et al.* (2009) Aggad *et al.* (2010)
irf8	Interferon regulatory transcription factor 8	Regulation of macrophage versus neutrophil cell fate during primitive myelopoiesis	Li *et al.* (2010)
ita4h	Leukotriene A_4 hydrolase	Required for proinflammatory leukotriene production. Knockdown results in increased anti-inflammatory lipoxin production and susceptibility to *Mycobacterium marinum* infection	Tobin *et al.* (2010)
mmp9	Matrix metalloproteinase family member	Required for recruitment of macrophages during mycobacterial granuloma formation	Volkman *et al.* (2010)
myd88	Adaptor molecule for TLRs and IL1R	Required for control of *S. typhimurium* Ra infection	van der Sar *et al.* (2006)
		Myd88-dependent induction of *il1b*, *mmp9*, and *irak3* during *S. typhimurium* infection	Stockhammer *et al.* (2009), Liu *et al.* (2010)
		Myd88-dependent induction of *il1b* in response to peptidoglycans (PGNs) and lipoteichoic acid (LTA)	Cheesman *et al.* (2010)
		Required for gut responses to endogenous microbiota	Bates *et al.* (2007)

(Continued)

Table II *(Continued)*

Genes	Functions	Conclusion from knockdown experiments	References
pglyrp5	Peptidoglycan recognition protein	Required for defense against *Salmonella enterica* and *Bacillus subtilis* infections	Li *et al.* (2007)
spi1 (*pu.1*)	Hematopoietic transcription factor	Myeloid cell depletion	Rhodes *et al.* (2005), Su *et al.* (2007)
		Required for control of *M. marinum*, *E. coli*, *P. aeruginosa*, *S. typhimurium*, and *Staphylococcus aureus* infections	Clay *et al.* (2007), Prajsnar *et al.* (2008), Brannon *et al.* (2009), Clatworthy *et al.* (2009), Wiles *et al.* (2009)
		Required for expression of a myeloid-specific gene set	Zakrzewska *et al.* (2010)
tlr4a/b	TLR family member, LPS receptor in mammals	Not required for LPS recognition	Sepulcre *et al.* (2009)
tlr5	TLR family member, flagellin receptor in mammals	Required for flagellin-induced *mmp9*, *cxcl-C1c*, *irak3*, *il8*, and *il1b* expression	Stockhammer *et al.* (2009)
tnfrsf1a	Tumor necrosis factor receptor 1	Required for intestinal immune cell homeostasis and intestinal inflammation in response to LPS	Bates *et al.* (2007)
		Required for control of *M. marinum* infection	Clay *et al.* (2008)
traf6	Signaling intermediate in TNFR and TLR signaling	Required for induction and repression of specific sets of immune response genes	Stockhammer *et al.* (2010)

targets of Spi1-directed innate immunity. By morpholino knockdown, one of the Spi1-dependent macrophage markers identified in this approach, the chemokine receptor gene *cxcr3.2*, was shown to be involved in macrophage migration to the site of bacterial infection (Zakrzewska *et al.*, 2010).

MyD88 is a pivotal signaling component of the innate immune response, serving as an adaptor for the interleukin 1 receptor and the majority of TLRs (Takeda and Akira, 2007). The role of MyD88 during bacterial infection in zebrafish embryos has been demonstrated by conducting morpholino knockdown studies with *S. typhimurium* challenge (van der Sar *et al.*, 2003). The induction levels of *mmp9*, *il1b*, and *irak3* expression were significantly reduced in the MyD88 morphants, whereas no changes were observed for *ifnphi1* or *il8* expression, indicating that both MyD88-dependent and MyD88-independent signaling pathways are involved in the innate immune response to *S. typhimurium* infection (Stockhammer *et al.*, 2009). Traf6, which functions downstream of MyD88 and in TNF receptor signaling, was also studied by morpholino knockdown. Although higher concentrations of Traf6 morpholino caused developmental aberrations, the role of Traf6 in the response to *S. typhimurium*

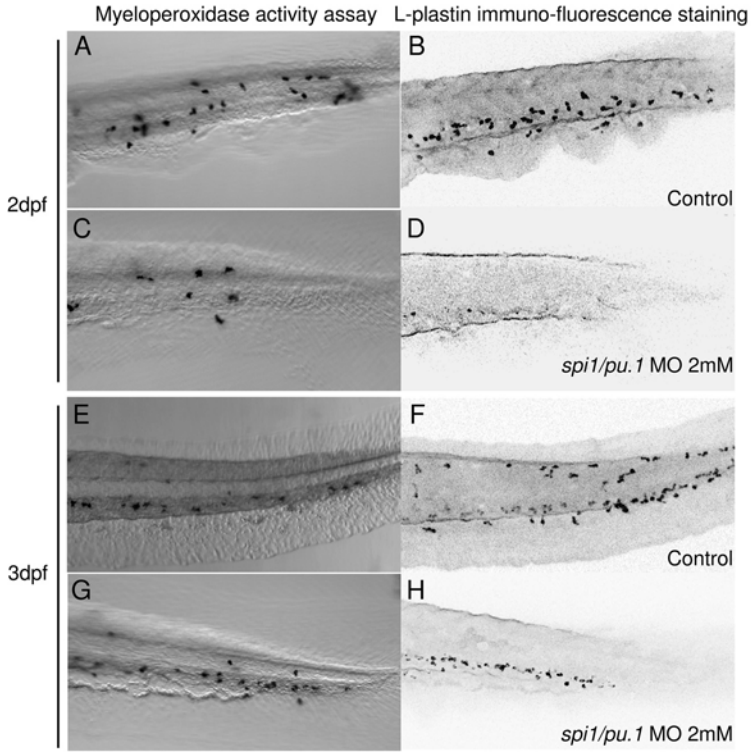

Fig. 3 Reduction of myeloid cell development by knockdown of the Spi1 transcription factor. A combination of myeloperoxidase (Mpx) activity assay and L-plastin immunofluorescence staining is used for the detection of neutrophils and macrophages in *spi1* morpholino-injected (MO) and control embryos. Details of the tail region are shown. (A, C, E, and G) Bright-field images of Mpx-activity stained neutrophils in wild-type embryos (A and E) and spi1 morphants (C and G). (B, D, F, and H) Confocal Z-stack images of L-plastin immunofluorescence staining applied on the same embryos to visualize the macrophage population. L-Plastin staining detected with Alexa 568-conjugated secondary antibody is shown in black. Although L-plastin is also present in neutrophils, the Alexa 568 fluorescence signal is not visible in these cells due to interference of the precipitate of the Mpx staining. Knockdown of spi1/pu.*1* significantly reduced the amount of neutrophils (C) and completely abolished macrophages (D) at 2 dpf. Recovery of the neutrophils was detected at 3 dpf (G). In contrast, the number of macrophages was still significantly reduced (H) and these cells appeared immature in morphology compared to the macrophages in the control (F). The *spi1* MO (Rhodes *et al.*, 2005) can be used at high doses (at least up to 2 mM with injection of 1 nL) without causing any visible developmental defects other than the reduction of myeloid cells. The MO concentration can be titrated to manipulate the ratio between macrophages and neutrophils. At lower doses of MO, neutrophil differentiation is already restored to wild-type levels at 2 dpf, while macrophage development is still strongly reduced.

could be studied by titrating the morpholino. The combined use of microarray analysis and whole-transcriptome deep sequencing demonstrated the dynamic role of Traf6 as a positive and negative regulator in the innate immune response of 1-day-old embryos (Stockhammer *et al.*, 2010). TNF signaling was also shown to play an

important role in the innate immune response of zebrafish embryos (Clay *et al.*, 2008). Morpholino knockdown of the TNF receptor 1 gene, *tnfrsf1a* (*tnfr1*), accelerated intracellular *M. marinum* growth and granuloma formation, followed by necrotic death of macrophages and granuloma breakdown, which provided direct evidence that TNF signaling is protective during the early stages of mycobacterial infection in the absence of adaptive immunity. In a subsequent study, TNF production levels during *M. marinum* infection were shown to depend on the balance between proinflammatory and anti-inflammatory lipid mediators (Tobin *et al.*, 2010).

Morpholino technology was also used to investigate signaling by interferon gamma (IFN-γ) and virus-induced interferons (IFN-φ) (Aggad *et al.*, 2010; Sieger *et al.*, 2009). Partially redundant functions were found for the *ifng1-1* and *ifng1-2* genes in mediating resistance against *E. coli* and *Yersinia ruckeri* infections, whereas raising IFN-γ levels sensitized embryos against bacterial infection, indicating the necessity of a tight control of IFN-γ levels (Sieger *et al.*, 2009). Morpholino knockdown of the NADPH oxidase family member, dual oxidase (*duox*), required for production of reactive oxygen species, led to an impaired capacity of zebrafish larvae to control enteric *S. typhimurium* infection (Flores *et al.*, 2010). Knockdown of the cystic fibrosis transmembrane conductance regulator (*cftr*) gene also dampened the respiratory burst in zebrafish embryos and led to an increased bacterial burden during *P. aeruginosa* infection (Phennicie *et al.*, 2010). A complete overview of innate immune response genes studied by morpholino knockdown in zebrafish embryos is given in Table II.

V. Conclusions

Zebrafish embryos provide an ideal vertebrate model to study infectious diseases due to their optical clarity, large number of embryos, fast development, and high similarity with human immunity counterparts. Many different infection models and techniques have been established to address the functions of key factors and crucial mechanisms in the complex host–pathogen interaction, which has accompanied the entire history of human evolution. In this chapter, we have summarized the current knowledge on zebrafish innate immune cells and described the available assays for observation and isolation of distinct cell populations, and local and systemic infection methods in zebrafish embryos. This overview shows that the zebrafish model is highly suitable to study the many challenging problems in the understanding of the innate immune system. For example, it will be possible to link the great wealth in transcriptomic data obtained from RNA-microarray-based transcriptome profiling and novel deep sequencing approaches with cellular imaging technologies. Such cellular imaging technologies are possible even at the scale of single molecules (Schaaf *et al.*, 2009), and, therefore, this integration can lead to insights into dynamic molecular processes involved in cellular recognition. Furthermore, it will be possible to link these molecular insights to functions in various differentiation processes of immune cells. These differentiation processes that are dependent on highly

dynamic communication between various cell types are currently still poorly understood because they are difficult to study in cell culture models. This means that in future zebrafish research, there will be an increased need to employ methods that are commonly used in cell culture studies, such as high-throughput genetic knockdown studies in combination with pharmaceutical approaches to analyze cell signaling components functionally. For such approaches, an increased availability of antibody tools, knockout lines, and additional transgenic reporters is still needed. These tools can be applied in automated injection and high-throughput detection systems making the zebrafish infection models a powerful tool for large-scale drug screening. This will significantly improve our understanding of infectious diseases in an *in vivo* setting, and by comparisons with data from cell culture and rodent test systems will have many clinical implications. In fact, the approaches described in this chapter are already used for the analysis of other disease models in zebrafish (Mione *et al.*, 2009). Several direct applications of these technologies for analysis of disease processes in which the immune system plays an important role, such as cancer, are currently underway in our department (Snaar-Jagalska, 2009).

Acknowledgments

CC, ELB, and MvdV are supported by the Smart Mix Programme of the Netherlands Ministry of Economic Affairs and the Ministry of Education, Culture and Science. ZK is supported by the Higher Education Commission of Pakistan. OWS is supported by the European Commission 7th framework project ZF-HEALTH (HEALTH-F4-2010-242048). AZ is supported by a Horizon grant of the Netherlands Genomics Initiative. The work in our laboratory was additionally supported by the European Commission 6th framework projects ZF-MODELS (LSHG-CT-2003-503496) and ZF-TOOLS (LSHG-2006-037220).

References

Aggad, D., Stein, C., Sieger, D., Mazel, M., Boudinot, P., Herbomel, P., Levraud, J. P., Lutfalla, G., and Leptin, M. (2010). In vivo analysis of Ifn-{gamma}1 and Ifn-{gamma}2 signaling in zebrafish. *J. Immunol.* **185**, 6774–6782.

Allen, J. P., and Neely, M. N. (2010). Trolling for the ideal model host: zebrafish take the bait. *Future Microbiol.* **5**, 563–569.

Amacher, S. L. (2008). Emerging gene knockout technology in zebrafish: zinc-finger nucleases. *Brief Funct. Genomic Proteomic* **7**, 460–464.

Balla, K. M., Lugo-Villarino, G., Spitsbergen, J. M., Stachura, D. L., Hu, Y., Banuelos, K., Romo-Fewell, O., Aroian, R. V., and Traver, D. (2010). Eosinophils in the zebrafish: prospective isolation, characterization, and eosinophilia induction by helminth determinants. *Blood* **116**, 3944–3954.

Bates, J. M., Akerlund, J., Mittge, E., and Guillemin, K. (2007). Intestinal alkaline phosphatase detoxifies lipopolysaccharide and prevents inflammation in zebrafish in response to the gut microbiota. *Cell Host Microbe* **2**, 371–382.

Bennett, C. M., Kanki, J. P., Rhodes, J., Liu, T. X., Paw, B. H., Kieran, M. W., Langenau, D. M., Delahaye-Brown, A., Zon, L. I., Fleming, M. D., and Look, A. T. (2001). Myelopoiesis in the zebrafish. *Danio rerio. Blood* **98**, 643–651.

Bertrand, J. Y., Cisson, J. L., Stachura, D. L., and Traver, D. (2010). Notch signaling distinguishes 2 waves of definitive hematopoiesis in the zebrafish embryo. *Blood* **115**, 2777–2783.

Bertrand, J. Y., Kim, A. D., Violette, E. P., Stachura, D. L., Cisson, J. L., and Traver, D. (2007). Definitive hematopoiesis initiates through a committed erythromyeloid progenitor in the zebrafish embryo. *Development* **134**, 4147–4156.

Bertrand, J. Y., and Traver, D. (2009). Hematopoietic cell development in the zebrafish embryo. *Curr. Opin. Hematol.* **16**, 243–248.

Bill, B. R., Petzold, A. M., Clark, K. J., Schimmenti, L. A., and Ekker, S. C. (2009). A primer for morpholino use in zebrafish. *Zebrafish* **6**, 69–77.

Boisset, J. C., van Cappellen, W., Andrieu-Soler, C., Galjart, N., Dzierzak, E., and Robin, C. (2010). In vivo imaging of haematopoietic cells emerging from the mouse aortic endothelium. *Nature* **464**, 116–120.

Brannon, M. K., Davis, J. M., Mathias, J. R., Hall, C. J., Emerson, J. C., Crosier, P. S., Huttenlocher, A., Ramakrishnan, L., and Moskowitz, S. M. (2009). Pseudomonas aeruginosa type III secretion system interacts with phagocytes to modulate systemic infection of zebrafish embryos. *Cell. Microbiol* **11**, 755–768.

Carvalho, R., de Sonneville, J., Stockhammer, O. W., Savage, N. D., Veneman, W. J., Ottenhoff, T. H., Dirks, R. P., Meijer, A. H., and Spaink, H. P. (2011). A high-throughput screen for tuberculosis progression. *PLoS One* **6**, e16779.

Cheesman, S. E., Neal, J. T., Mittge, E., Seredick, B. M., and Guillemin, K. (2010). Microbes and Health Sackler Colloquium: epithelial cell proliferation in the developing zebrafish intestine is regulated by the Wnt pathway and microbial signaling via Myd88. *Proc. Natl. Acad. Sci. U.S.A.* **108**(Suppl 1), 4570–4577.

Clatworthy, A. E., Lee, J. S., Leibman, M., Kostun, Z., Davidson, A. J., and Hung, D. T. (2009). *Pseudomonas aeruginosa* infection of zebrafish involves both host and pathogen determinants. *Infect Immun.* **77**, 1293–1303.

Clay, H., Davis, J. M., Beery, D., Huttenlocher, A., Lyons, S. E., and Ramakrishnan, L. (2007). Dichotomous role of the macrophage in early *Mycobacterium marinum* infection of the zebrafish. *Cell Host Microbe* **2**, 29–39.

Clay, H., and Ramakrishnan, L. (2005). Multiplex fluorescent in situ hybridization in zebrafish embryos using tyramide signal amplification. *Zebrafish* **2**, 105–111.

Clay, H., Volkman, H. E., and Ramakrishnan, L. (2008). Tumor necrosis factor signaling mediates resistance to mycobacteria by inhibiting bacterial growth and macrophage death. *Immunity* **29**, 283–294.

Coban, C., Ishii, K. J., and Akira, S. (2009). Immune interventions of human diseases through toll-like receptors. *Adv. Exp. Med. Biol.* **655**, 63–80.

Cosma, C. L., Swaim, L. E., Volkman, H., Ramakrishnan, L., and Davis, J. M. (2006). Zebrafish and frog models of *Mycobacterium marinum* infection. *Curr. Protoc. Microbiol.* Chapter 10, Unit 10B.2.

Covassin, L., Amigo, J. D., Suzuki, K., Teplyuk, V., Straubhaar, J., and Lawson, N. D. (2006). Global analysis of hematopoietic and vascular endothelial gene expression by tissue specific microarray profiling in zebrafish. *Dev. Biol.* **299**, 551–562.

Davidson, A. J., and Zon, L. I. (2004). The 'definitive' (and 'primitive') guide to zebrafish hematopoiesis. *Oncogene* **23**, 7233–7246.

Davis, J. M., Clay, H., Lewis, J. L., Ghori, N., Herbomel, P., and Ramakrishnan, L. (2002). Real-time visualization of mycobacterium–macrophage interactions leading to initiation of granuloma formation in zebrafish embryos. *Immunity* **17**, 693–702.

Davis, J. M., Haake, D. A., and Ramakrishnan, L. (2009). *Leptospira interrogans* stably infects zebrafish embryos, altering phagocyte behavior and homing to specific tissues. *PLoS Negl. Trop. Dis.* **3**, e463.

Davis, J. M., and Ramakrishnan, L. (2009). The role of the granuloma in expansion and dissemination of early tuberculous infection. *Cell* **136**, 37–49.

de Jong, J. L., Davidson, A. J., Wang, Y., Palis, J., Opara, P., Pugach, E., Daley, G. Q., and Zon, L. I. (2010). Interaction of retinoic acid and scl controls primitive blood development. *Blood* **116**, 201–209.

Del Bene, F., Wyart, C., Robles, E., Tran, A., Looger, L., Scott, E. K., Isacoff, E. Y., and Baier, H. (2010). Filtering of visual information in the tectum by an identified neural circuit. *Science* **330**, 669–673.

Eisen, J. S., and Smith, J. C. (2008). Controlling morpholino experiments: don't stop making antisense. *Development* **135**, 1735–1743.

Ellett, F., Pase, L., Hayman, J. W., Andrianopoulos, A., and Lieschke, G. J. (2010). mpeg1 promoter transgenes direct macrophage-lineage expression in zebrafish. *Blood* **117**, e49–e56.

Encinas, P., Rodriguez-Milla, M. A., Novoa, B., Estepa, A., Figueras, A., and Coll, J. (2010). Zebrafish fin immune responses during high mortality infections with viral haemorrhagic septicemia rhabdovirus. A proteomic and transcriptomic approach. *BMC Genomics* **11**, 518.

Flores, M. V., Crawford, K. C., Pullin, L. M., Hall, C. J., Crosier, K. E., and Crosier, P. S. (2010). Dual oxidase in the intestinal epithelium of zebrafish larvae has anti-bacterial properties. *Biochem. Biophys. Res. Commun.* **400**, 164–168.

Gray, C., Loynes, C. A., Whyte, M. K., Crossman, D. C., Renshaw, S. A., and Chico, T. J. (2011). Simultaneous intravital imaging of macrophage and neutrophil behaviour during inflammation using a novel transgenic zebrafish. *Thromb. Haemost* **105**, 811–819.

Gutzman, J. H., and Sive, H. (2009). Zebrafish brain ventricle injection. *J. Vis. Exp.* **26**, http://www.jove.com/details.php?id=1218, doi: 10.3791/1218.

Haffter, P., and Nusslein-Volhard, C. (1996). Large scale genetics in a small vertebrate, the zebrafish. *Int. J. Dev. Biol.* **40**, 221–227.

Hall, C., Flores, M. V., Crosier, K., and Crosier, P. (2009). Live cell imaging of zebrafish leukocytes. *Methods Mol. Biol.* **546**, 255–271.

Hall, C., Flores, M. V., Storm, T., Crosier, K., and Crosier, P. (2007). The zebrafish lysozyme C promoter drives myeloid-specific expression in transgenic fish. *BMC Dev. Biol.* **7**, 42.

Halpern, M. E., Rhee, J., Goll, M. G., Akitake, C. M., Parsons, M., and Leach, S. D. (2008). Gal4/UAS transgenic tools and their application to zebrafish. *Zebrafish* **5**, 97–110.

Hegedus, Z., Zakrzewska, A., Agoston, V. C., Ordas, A., Racz, P., Mink, M., Spaink, H. P., and Meijer, A. H. (2009). Deep sequencing of the zebrafish transcriptome response to mycobacterium infection. *Mol. Immunol.* **46**, 2918–2930.

Herbomel, P., and Levraud, J. P. (2005). Imaging early macrophage differentiation, migration, and behaviors in live zebrafish embryos. *Methods Mol. Med.* **105**, 199–214.

Herbomel, P., Thisse, B., and Thisse, C. (1999). Ontogeny and behaviour of early macrophages in the zebrafish embryo. *Development* **126**, 3735–3745.

Herbomel, P., Thisse, B., and Thisse, C. (2001). Zebrafish early macrophages colonize cephalic mesenchyme and developing brain, retina, and epidermis through a M-CSF receptor-dependent invasive process. *Dev. Biol.* **238**, 274–288.

Hermann, A. C., Millard, P. J., Blake, S. L., and Kim, C. H. (2004). Development of a respiratory burst assay using zebrafish kidneys and embryos. *J. Immunol. Methods* **292**, 119–129.

Hsu, K., Traver, D., Kutok, J. L., Hagen, A., Liu, T. X., Paw, B. H., Rhodes, J., Berman, J. N., Zon, L. I., Kanki, J. P., and Look, A. T. (2004). The pu.1 promoter drives myeloid gene expression in zebrafish. *Blood* **104**, 1291–1297.

Jault, C., Pichon, L., and Chluba, J. (2004). Toll-like receptor gene family and TIR-domain adapters in *Danio rerio*. *Mol. Immunol.* **40**, 759–771.

Kanther, M., and Rawls, J. F. (2010). Host–microbe interactions in the developing zebrafish. *Curr. Opin. Immunol.* **22**, 10–19.

Kimmel, C. B., Ballard, W. W., Kimmel, S. R., Ullmann, B., and Schilling, T. F. (1995). Stages of embryonic development of the zebrafish. *Dev. Dyn.* **203**, 253–310.

Kissa, K., and Herbomel, P. (2010). Blood stem cells emerge from aortic endothelium by a novel type of cell transition. *Nature* **464**, 112–115.

Lam, S. H., Chua, H. L., Gong, Z., Lam, T. J., and Sin, Y. M. (2004). Development and maturation of the immune system in zebrafish, *Danio rerio*: a gene expression profiling, in situ hybridization and immunological study. *Dev. Comp. Immunol.* **28**, 9–28.

Le Guyader, D., Redd, M. J., Colucci-Guyon, E., Murayama, E., Kissa, K., Briolat, V., Mordelet, E., Zapata, A., Shinomiya, H., and Herbomel, P. (2008). Origins and unconventional behavior of neutrophils in developing zebrafish. *Blood* **111**, 132–141.

Lepiller, S., Laurens, V., Bouchot, A., Herbomel, P., Solary, E., and Chluba, J. (2007). Imaging of nitric oxide in a living vertebrate using a diamino-fluorescein probe. *Free Radic. Biol. Med.* **43**, 619–627.

Lesley, R., and Ramakrishnan, L. (2008). Insights into early mycobacterial pathogenesis from the zebrafish. *Curr. Opin. Microbiol.* **11**, 277–283.

Levraud, J. P., Colucci-Guyon, E., Redd, M. J., Lutfalla, G., and Herbomel, P. (2008). In vivo analysis of zebrafish innate immunity. *Methods Mol. Biol.* **415**, 337–363.

Levraud, J. P., Disson, O., Kissa, K., Bonne, I., Cossart, P., Herbomel, P., and Lecuit, M. (2009). Real-time observation of *Listeria monocytogenes*–phagocyte interactions in living zebrafish larvae. *Infect Immun.* **77**, 3651–3660.

Li, L., Jin, H., Xu, J., Shi, Y., and Wen, Z. (2010). Irf8 regulates macrophage versus neutrophil fate during zebrafish primitive myelopoiesis. *Blood* **117**, 1359–1369.

Li, X., Wang, S., Qi, J., Echtenkamp, S. F., Chatterjee, R., Wang, M., Boons, G. J., Dziarski, R., and Gupta, D. (2007). Zebrafish peptidoglycan recognition proteins are bactericidal amidases essential for defense against bacterial infections. *Immunity* **27**, 518–529.

Lieschke, G. J., Oates, A. C., Crowhurst, M. O., Ward, A. C., and Layton, J. E. (2001). Morphologic and functional characterization of granulocytes and macrophages in embryonic and adult zebrafish. *Blood* **98**, 3087–3096.

Liongue, C., Hall, C. J., O'Connell, B. A., Crosier, P., and Ward, A. C. (2009). Zebrafish granulocyte colony-stimulating factor receptor signaling promotes myelopoiesis and myeloid cell migration. *Blood* **113**, 2535–2546.

Liu, Y., Li, M., Fan, S., Lin, Y., Lin, B., Luo, F., Zhang, C., Chen, S., Li, Y., and Xu, A. (2010). A unique feature of Toll/IL-1 receptor domain-containing adaptor protein is partially responsible for lipopolysaccharide insensitivity in zebrafish with a highly conserved function of Myd88. *J. Immunol.* **185**, 3391–3400.

Lugo-Villarino, G., Balla, K. M., Stachura, D. L., Banuelos, K., Werneck, M. B., and Traver, D. (2010). Identification of dendritic antigen-presenting cells in the zebrafish. *Proc. Natl. Acad. Sci. U. S. A.* **107**, 15850–15855.

Mathias, J. R., Dodd, M. E., Walters, K. B., Rhodes, J., Kanki, J. P., Look, A. T., and Huttenlocher, A. (2007). Live imaging of chronic inflammation caused by mutation of zebrafish Hai1. *J. Cell Sci.* **120**, 3372–3383.

Mathias, J. R., Perrin, B. J., Liu, T. X., Kanki, J., Look, A. T., and Huttenlocher, A. (2006). Resolution of inflammation by retrograde chemotaxis of neutrophils in transgenic zebrafish. *J. Leukoc. Biol.* **80**, 1281–1288.

Mathias, J. R., Walters, K. B., and Huttenlocher, A. (2009). Neutrophil motility in vivo using zebrafish. *Methods Mol. Biol.* **571**, 151–166.

Meeker, N. D., and Trede, N. S. (2008). Immunology and zebrafish: spawning new models of human disease. *Dev. Comp. Immunol.* **32**, 745–757.

Meijer, A. H., Gabby Krens, S. F., Medina Rodriguez, I. A., He, S., Bitter, W., Ewa Snaar-Jagalska, B., and Spaink, H. P. (2004). Expression analysis of the Toll-like receptor and TIR domain adaptor families of zebrafish. *Mol. Immunol.* **40**, 773–783.

Meijer, A. H., and Spaink, H. P. (2011). Host–pathogen interactions made transparent with the zebrafish model. *Curr Drug Targets.* **12**, 1000–1017.

Meijer, A. H., van der Sar, A. M., Cunha, C., Lamers, G. E., Laplante, M. A., Kikuta, H., Bitter, W., Becker, T. S., and Spaink, H. P. (2008). Identification and real-time imaging of a myc-expressing neutrophil population involved in inflammation and mycobacterial granuloma formation in zebrafish. *Dev. Comp. Immunol.* **32**, 36–49.

Meijer, A. H., Verbeek, F. J., Salas-Vidal, E., Corredor-Adamez, M., Bussman, J., van der Sar, A. M., Otto, G. W., Geisler, R., and Spaink, H. P. (2005). Transcriptome profiling of adult zebrafish at the late stage of chronic tuberculosis due to *Mycobacterium marinum* infection. *Mol. Immunol.* **42**, 1185–1203.

Mione, M., Meijer, A. H., Snaar-Jagalska, B. E., Spaink, H. P., and Trede, N. S. (2009). Disease modeling in zebrafish: cancer and immune responses – a report on a workshop held in Spoleto, Italy, July 20-22, 2009. *Zebrafish* **6**, 445–451.

Mogensen, T. H. (2009). Pathogen recognition and inflammatory signaling in innate immune defenses. *Clin. Microbiol. Rev.* **22**, 240–273 (Table of Contents).

Murayama, E., Kissa, K., Zapata, A., Mordelet, E., Briolat, V., Lin, H. F., Handin, R. I., and Herbomel, P. (2006). Tracing hematopoietic precursor migration to successive hematopoietic organs during zebrafish development. *Immunity* **25**, 963–975.

Nasevicius, A., and Ekker, S. C. (2000). Effective targeted gene 'knockdown' in zebrafish. *Nat. Genet.* **26**, 216–220.

Ordas, A., Hegedus, Z., Henkel, C. V., Stockhammer, O. W., Butler, D., Jansen, H. J., Racz, P., Mink, M., Spaink, H. P., and Meijer, A. H. (2010). Deep sequencing of the innate immune transcriptomic response of zebrafish embryos to *Salmonella* infection. *Fish Shellfish Immunol.* , Sep. 8. [Epub ahead of print] doi:10.1016/j.fsi.2010.08.022.

Peri, F., and Nusslein-Volhard, C. (2008). Live imaging of neuronal degradation by microglia reveals a role for v0-ATPase a1 in phagosomal fusion in vivo. *Cell* **133**, 916–927.

Phennicie, R. T., Sullivan, M. J., Singer, J. T., Yoder, J. A., and Kim, C. H. (2010). Specific resistance to *Pseudomonas aeruginosa* infection in zebrafish is mediated by the cystic fibrosis transmembrane conductance regulator. *Infect. Immun.* **78**, 4542–4550.

Prajsnar, T. K., Cunliffe, V. T., Foster, S. J., and Renshaw, S. A. (2008). A novel vertebrate model of *Staphylococcus aureus* infection reveals phagocyte-dependent resistance of zebrafish to non-host specialized pathogens. *Cell. Microbiol.* **10**, 2312–2325.

Rauwerda, H., de Jong, M., de Leeuw, W. C., Spaink, H. P., and Breit, T. M. (2010). Integrating heterogeneous sequence information for transcriptome-wide microarray design; a zebrafish example. *BMC Res. Notes* **3**, 192.

Redd, M. J., Kelly, G., Dunn, G., Way, M., and Martin, P. (2006). Imaging macrophage chemotaxis in vivo: studies of microtubule function in zebrafish wound inflammation. *Cell Motil. Cytoskeleton* **63**, 415–422.

Renshaw, S. A., Loynes, C. A., Trushell, D. M., Elworthy, S., Ingham, P. W., and Whyte, M. K. (2006). A transgenic zebrafish model of neutrophilic inflammation. *Blood* **108**, 3976–3978.

Rhodes, J., Hagen, A., Hsu, K., Deng, M., Liu, T. X., Look, A. T., and Kanki, J. P. (2005). Interplay of pu.1 and gata1 determines myelo-erythroid progenitor cell fate in zebrafish. *Dev. Cell* **8**, 97–108.

Russell, D. G. (2007). Who puts the tubercle in tuberculosis? *Nat. Rev. Microbiol.* **5**, 39–47.

Schaaf, M. J., Koopmans, W. J., Meckel, T., van Noort, J., Snaar-Jagalska, B. E., Schmidt, T. S., and Spaink, H. P. (2009). Single-molecule microscopy reveals membrane microdomain organization of cells in a living vertebrate. *Biophys. J.* **97**, 1206–1214.

Sepulcre, M. P., Alcaraz-Perez, F., Lopez-Munoz, A., Roca, F. J., Meseguer, J., Cayuela, M. L., and Mulero, V. (2009). Evolution of lipopolysaccharide (LPS) recognition and signaling: fish TLR4 does not recognize LPS and negatively regulates NF-kappaB activation. *J. Immunol.* **182**, 1836–1845.

Sieger, D., Stein, C., Neifer, D., van der Sar, A. M., and Leptin, M. (2009). The role of gamma interferon in innate immunity in the zebrafish embryo. *Dis. Model Mech.* **2**, 571–581.

Snaar-Jagalska, B. E. (2009). ZF-CANCER: developing high-throughput bioassays for human cancers in zebrafish. *Zebrafish* **6**, 441–443.

Stein, C., Caccamo, M., Laird, G., and Leptin, M. (2007). Conservation and divergence of gene families encoding components of innate immune response systems in zebrafish. *Genome Biol.* **8**, R251.

Stockhammer, O. W., Rauwerda, H., Wittink, F. R., Breit, T. M., Meijer, A. H., and Spaink, H. P. (2010). Transcriptome analysis of Traf6 function in the innate immune response of zebrafish embryos. *Mol. Immunol.* **48**, 179–190.

Stockhammer, O. W., Zakrzewska, A., Hegedus, Z., Spaink, H. P., and Meijer, A. H. (2009). Transcriptome profiling and functional analyses of the zebrafish embryonic innate immune response to *Salmonella* infection. *J. Immunol.* **182**, 5641–5653.

Stoop, E. M., Schipper, T., Huber, S. R., Nezhinsky, A. E., Verbeek, F. J., Gurcha, S. S., Besra, G. S., Vandenbroucke-Grauls, C. M., Bitter, W., and van der Sar, A. M. (2011). Zebrafish embryo screen for mycobacterial genes involved in granuloma formation reveals a novel ESX-1 component. *Dis. Model Mech.* **4**, 526–536.

Su, F., Juarez, M. A., Cooke, C. L., Lapointe, L., Shavit, J. A., Yamaoka, J. S., and Lyons, S. E. (2007). Differential regulation of primitive myelopoiesis in the zebrafish by Spi-1/Pu.1 and C/ebp1. *Zebrafish* **4**, 187–199.

Sullivan, C., and Kim, C. H. (2008). Zebrafish as a model for infectious disease and immune function. *Fish Shellfish Immunol.* **25**, 341–350.

Suster, M. L., Kikuta, H., Urasaki, A., Asakawa, K., and Kawakami, K. (2009). Transgenesis in zebrafish with the tol2 transposon system. *Methods Mol. Biol.* **561**, 41–63.

Swaim, L. E., Connolly, L. E., Volkman, H. E., Humbert, O., Born, D. E., and Ramakrishnan, L. (2006). *Mycobacterium marinum* infection of adult zebrafish causes caseating granulomatous tuberculosis and is moderated by adaptive immunity. *Infect Immun.* **74**, 6108–6117.

Takeda, K., and Akira, S. (2007). Toll-like receptors. *Curr. Protoc. Immunol.* Chapter 14, Unit 14.12.

Tobin, D. M., and Ramakrishnan, L. (2008). Comparative pathogenesis of *Mycobacterium marinum* and *Mycobacterium tuberculosis*. *Cell. Microbiol* **10**, 1027–1039.

Tobin, D. M., Vary Jr., J. C., Ray, J. P., Walsh, G. S., Dunstan, S. J., Bang, N. D., Hagge, D. A., Khadge, S., King, M. C., Hawn, T. R., Moens, C. B., and Ramakrishnan, L. (2010). The lta4h locus modulates susceptibility to mycobacterial infection in zebrafish and humans. *Cell* **140**, 717–730.

Traver, D., Herbomel, P., Patton, E. E., Murphey, R. D., Yoder, J. A., Litman, G. W., Catic, A., Amemiya, C. T., Zon, L. I., and Trede, N. S. (2003). The zebrafish as a model organism to study development of the immune system. *Adv. Immunol.* **81**, 253–330.

Trede, N. S., Langenau, D. M., Traver, D., Look, A. T., and Zon, L. I. (2004). The use of zebrafish to understand immunity. *Immunity* **20**, 367–379.

Valanne, S., Myllymaki, H., Kallio, J., Schmid, M. R., Kleino, A., Murumagi, A., Airaksinen, L., Kotipelto, T., Kaustio, M., Ulvila, J., Esfahani, S. S., Engstrom, Y., Silvennoinen, O., Hultmark, D., Parikka, M., and Ramet, M. (2010). Genome-wide RNA interference in *Drosophila* cells identifies G protein-coupled receptor kinase 2 as a conserved regulator of NF-kappaB signaling. *J. Immunol.* **184**, 6188–6198.

van der Sar, A. M., Abdallah, A. M., Sparrius, M., Reinders, E., Vandenbroucke-Grauls, C. M., and Bitter, W. (2004). *Mycobacterium marinum* strains can be divided into two distinct types based on genetic diversity and virulence. *Infect Immun.* **72**, 6306–6312.

van der Sar, A. M., Musters, R. J., van Eeden, F. J., Appelmelk, B. J., Vandenbroucke-Grauls, C. M., and Bitter, W. (2003). Zebrafish embryos as a model host for the real time analysis of *Salmonella typhimurium* infections. *Cell. Microbiol.* **5**, 601–611.

van der Sar, A. M., Spaink, H. P., Zakrzewska, A., Bitter, W., and Meijer, A. H. (2009). Specificity of the zebrafish host transcriptome response to acute and chronic mycobacterial infection and the role of innate and adaptive immune components. *Mol. Immunol.* **46**, 2317–2332.

van der Sar, A. M., Stockhammer, O. W., van der Laan, C., Spaink, H. P., Bitter, W., and Meijer, A. H. (2006). MyD88 innate immune function in a zebrafish embryo infection model. *Infect Immun.* **74**, 2436–2441.

Vergunst, A. C., Meijer, A. H., Renshaw, S. A., and O'Callaghan, D. (2010). *Burkholderia cenocepacia* creates an intramacrophage replication niche in zebrafish embryos, followed by bacterial dissemination and establishment of systemic infection. *Infect Immun.* **78**, 1495–1508.

Volkman, H. E., Clay, H., Beery, D., Chang, J. C., Sherman, D. R., and Ramakrishnan, L. (2004). Tuberculous granuloma formation is enhanced by a mycobacterium virulence determinant. *PLoS Biol.* **2**, e367.

Volkman, H. E., Pozos, T. C., Zheng, J., Davis, J. M., Rawls, J. F., and Ramakrishnan, L. (2010). Tuberculous granuloma induction via interaction of a bacterial secreted protein with host epithelium. *Science* **327**, 466–469.

Wang, Z., Gerstein, M., and Snyder, M. (2009). RNA-Seq: a revolutionary tool for transcriptomics. *Nat. Rev. Genet.* **10**, 57–63.

Ward, A. C., McPhee, D. O., Condron, M. M., Varma, S., Cody, S. H., Onnebo, S. M., Paw, B. H., Zon, L. I., and Lieschke, G. J. (2003). The zebrafish spi1 promoter drives myeloid-specific expression in stable transgenic fish. *Blood* **102**, 3238–3240.

Westerfield, M. (2000). *The Zebrafish Book: A Guide for the Laboratory Use of Zebrafish (Danio rerio), 4th ed. University of Oregon Press, Eugene, OR.*

Wienholds, E., Schulte-Merker, S., Walderich, B., and Plasterk, R. H. (2002). Target-selected inactivation of the zebrafish rag1 gene. *Science* **297**, 99–102.

Wiles, T. J., Bower, J. M., Redd, M. J., and Mulvey, M. A. (2009). Use of zebrafish to probe the divergent virulence potentials and toxin requirements of extraintestinal pathogenic *Escherichia coli*. *PLoS Pathog.* **5**, e1000697.

Willett, C. E., Cortes, A., Zuasti, A., and Zapata, A. G. (1999). Early hematopoiesis and developing lymphoid organs in the zebrafish. *Dev. Dyn.* **214**, 323–336.

Wu, Z., Zhang, W., Lu, Y., and Lu, C. (2010). Transcriptome profiling of zebrafish infected with *Streptococcus suis*. *Microb. Pathog.* **48**, 178–187.

Yoder, J. A., Turner, P. M., Wright, P. D., Wittamer, V., Bertrand, J. Y., Traver, D., and Litman, G. W. (2009). Developmental and tissue-specific expression of NITRs. *Immunogenetics* **62**, 117–122.

Zakrzewska, A., Cui, C., Stockhammer, O. W., Benard, E. L., Spaink, H. P., and Meijer, A. H. (2010). Macrophage-specific gene functions in Spi1-directed innate immunity. *Blood* **116**, e1–e11.

CHAPTER 13

Zebrafish as a Model for the Study of Human Cancer

Julia Etchin, John P. Kanki and A. Thomas Look

Department of Pediatric Oncology, Dana-Farber Cancer Institute and Children's Hospital, Boston, Massachusetts, USA

Abstract

Zebrafish provide an exciting animal model system for the study of human cancers. During the last few years many zebrafish models of cancer have been generated that recapitulate human hematologic malignancies and solid tumors. Concurrent technological advances have significantly improved the genetic

METHODS IN CELL BIOLOGY, VOL 105

0091-679X/10 $35.00
DOI 10.1016/B978-0-12-381320-6.00013-8

tractability and unique advantage of *in vivo* imaging in zebrafish, providing a means to dissect the molecular pathways underlying tumor initiation, progression and metastasis. Comparisons of cancer-associated gene expression profiles have demonstrated a high degree of similarity in the gene signatures of specific types of tumor cells in fish and humans, indicating that the contributing genetic pathways leading to cancer are evolutionarily conserved. Furthermore, the high fecundity, optical clarity and small embryo size of zebrafish continue to make it particularly amenable to performing whole-organism small molecule screens to identify targets for therapeutic development. This chapter reviews a wide array of these zebrafish cancer models and illustrates the advantages of the zebrafish system for exploring the molecular mechanisms governing cancer-related cellular processes.

I. Introduction: Zebrafish as a Cancer Model

The zebrafish has recently emerged as an invaluable model system for the study of human cancers. Distinct advantages of the zebrafish arise from the evolutionary conservation of genetic pathways implicated in cancer that are shared between fish and humans coupled to the unique attributes of zebrafish as a tool for modeling human disease and analyzing the underlying cellular processes. Over the past few years, a wide spectrum of zebrafish models of human cancer has been developed largely through well-established transgenic methodologies and the identification of lines with gene-specific mutations. These include models that recapitulate human hematologic malignancies, melanoma, rhabdomyosarcoma, and other solid tumors. This chapter will present a subset of the currently published zebrafish cancer models and highlight several that demonstrate recent advances. Table I provides reference information covering a wide array of zebrafish transgenic lines that have been developed for the study of human cancers.

The transparency of the zebrafish embryos and the recent development of the pigment-deficient "Casper" zebrafish line give one the valuable capacity to observe directly cancer formation and progression in the living animal (White *et al.*, 2008). The optical clarity of zebrafish can be exploited further by the use of fluorescent tags to label specific cell lineages to visualize tumor processes including initiation, progression, and regression. Recently, the power of zebrafish has been underscored by the remarkable progress and utility of tumor transplantation methodologies performed in this model organism. The zebrafish is experimentally amenable to transplantation assays that test the serial passage and malignant potential of fluorescently labeled tumor cells as well as their capacity to disseminate and/or metastasize. Several groups have also applied xenotransplantation methods to zebrafish for the study of the human cancer cell malignancy within the context of the whole organism. The experimental repertoire of the zebrafish allows unprecedented inquiry into the *in vivo* processes involved in the pathogenesis of malignancy (Fig. 1).

Importantly, comparisons of cancer-associated gene expression profiles between zebrafish and human cancers reveal a high degree of similarity in gene signatures. In

Table I
Overview of zebrafish cancer models

Cancer type	Genetic basis	Methodology	Onset (months)	Advantages/significance	References
AML	*TEL-JAK2*	Transient transgenesis	Embryo	Myeloid oncogenesis	Onnebo *et al.* (2005)
AML	*MYST3/NCOA2*	Stable transgenesis	14	Oncogenic potency of MYST3/NCOA2	Zhuravleva *et al.* (2008)
B-ALL	*TEL-AML1*	Stable transgenesis	8–12	Mimics childhood $CD10^{+}$ pre-B ALL	Sabaawy *et al.* (2006)
T-ALL	*c-Myc*	Stable/conditional transgenesis	2/4	Characterizes molecular basis underlying T-LBL progression to T-ALL	Feng *et al.* (2007, 2010), Langenau *et al.* (2003)
T-ALL	*NOTCH1*	Transient/stable transgenesis	5/11	Synergy between NOTCH and bcl2	Chen *et al.* (2007)
T-ALL	Heritable models	ENU mutagenesis	3–8	Identify multiple heritable T-LBL and T-ALL fish lines	Frazer *et al.* (2009)
RMS	*KRASV12*	Stable/conditional transgenesis	2/1	Identify conserved gene signatures in RMS Discover that RAS activation is common in human RMS	Langenau *et al.* (2007), Le *et al.* (2007)
Melanoma	$BRAF^{V600}$ (in $tp53^{-/-}$ line) HRASV12 NRASQ61K (in $tp53^{-/-}$ line)	Stable transgenesis	1–6	Both early and late-onset models are available Direct role of PI3K signaling in melanoma progression	Anelli *et al.* (2009), Dovey, White, and Zon (2009), Michailidou *et al.* (2009), Patton *et al.* (2005)
Neural tumor	*fbxw4* (Hagoromo)	Insertional mutagenesis	24	Misregulation of fgf8 leads to neural tumors	Amsterdam *et al.* (2009)

(Continued)

Table I *(Continued)*

Cancer type	Genetic basis	Methodology	Onset (months)	Advantages/significance	References
Pancreatic neuroendocrine carcinoma	*MYCN*	Transient transgenesis	5	Tumors are driven by *myoD* promoter Tumors resemble malignant lesions	Yang *et al.* (2004)
Exocrine pancreatic carcinoma	*KRASV12*	Stable transgenesis	6	Reveal tumor-initiating effects of oncogenic KRAS	Park *et al.* (2008)
Liver carcinoma		Carcinogenesis	3	Conserved gene expression signatures of liver tumors	Lam *et al.* (2006)
Liver, intestinal, pancreatic cancer	*apc*	TILLING		Characterization of molecular pathways that underlie apc-induced differentiation and proliferation defects	Haramis *et al.* (2006), Phelps *et al.* (2009)
Testicular cancer		ENU mutagenesis	7	Highly penetrant germ cell tumors	Neumann *et al.* (2009)
MPNST	*tp53*/ribosomal proteins/ *mlh1*, *msh2*, *msh6*	TILLING/insertional mutagenesis		Tumor suppressors and mismatch repair genes in MPNST	Amsterdam *et al.* (2004), Berghmans *et al.* (2005), Feitsma *et al.* (2008)
Li–Fraumeni syndrome/ sarcoma	*tp53*	ENU		Highly penetrant tumorigenesis	Parant *et al.* (2010)

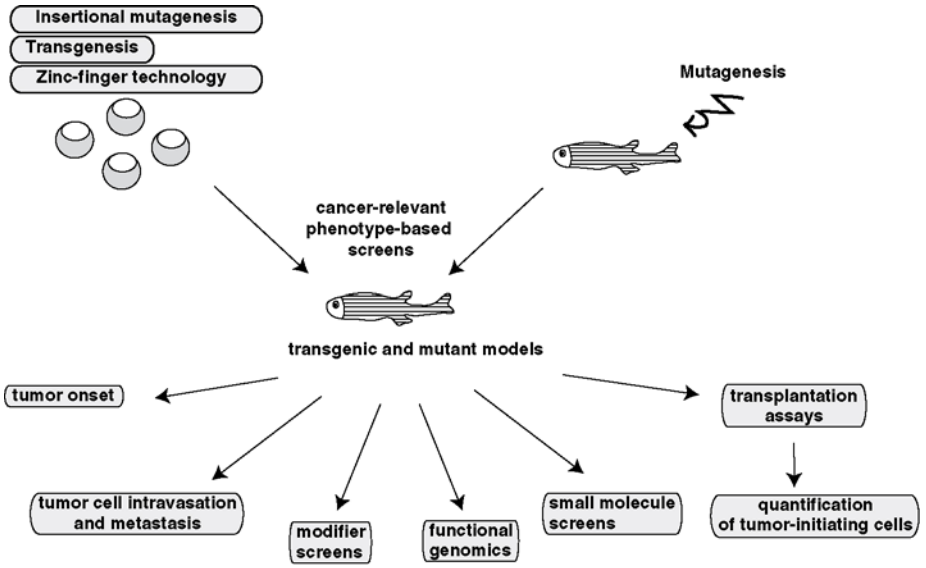

Fig. 1 The diverse utility of zebrafish models of human cancer.

fact, the genetics of human cancer have been recapitulated in zebrafish transgenic lines through the overexpression of human wild-type or mutant oncogenes and through the isolation of mutant lines harboring inactivating mutations in orthologous tumor suppressor genes. In addition, the resultant tumor histopathologies in these animals are strikingly similar to the human diseases, further emphasizing the suitability of zebrafish for dissecting the molecular mechanisms that underlie pathogenesis. Relevant pathways include those aberrantly affecting the cell cycle, genomic stability, apoptosis, or normal development and differentiation. The zebrafish models of cancer established to date have been highly informative with respect to the molecular basis of human tumorigenesis and progression.

Due to its fecundity and the optical clarity during embryonic development, the zebrafish has also proven to be an excellent *in vivo* model system for high-throughput drug screening, because it allows the visual assessment of both drug efficacy and toxicity. Adult fish are also suitable for testing drugs that are administered as water-soluble compounds, by simply adding them directly to the water for treatment. Taken together, zebrafish represent a powerful vertebrate animal model for both dissecting the molecular pathways underlying human cancer and chemical screening for anti-cancer drug development.

II. The Genetically Tractable Zebrafish

In addition to the zebrafish being amenable to experimental manipulation, it also benefits from having a short generation time, large number of offspring, and external embryonic development. These make the zebrafish an attractive system

for genetic manipulation for generating transgenic models of oncogenesis and mutant tumor suppressor lines that recapitulate the genetic aberrations of many human cancers.

A. Transgenesis

The methodologies for the creation of novel transgenic lines have become well established in the recent years. The two most common transgenesis strategies for stable incorporation of gene of interest within zebrafish genome are (i) I-SceI meganuclease-mediated and (ii) transposon-mediated transgenic technologies (Grabher and Wittbrodt, 2008). The method employing I-SceI meganuclease is based on the cleavage of injected DNA to promote the efficient integration of transgenes into the genome. The microinjection of plasmid DNA in the presence of I-SceI greatly enhances the frequency of transgenesis when compared to injections without I-SceI. The formation of tandem transgene arrays via I-SceI-mediated transgenesis allows one to detect transgene integration through coinjection and cointegration with a fluorescent marker gene and to express multiple transgenes of interest that are cointegrated and segregate together in subsequent generations.

The Tol2 transposon-mediated system has been adopted for enhancer and gene trapping experiments due to the capability to remobilize the transposon DNA insertions by crossing the transposon-carrying line to one that expresses transposase (Balciunas and Ekker, 2005). The Tol2-mediated transgenic strategy allows a high frequency of transgenesis and its widespread use among zebrafish geneticists resulted in the generation of multiple Tol2 vectors with convenient Gateway cloning sites, which greatly simplifies the preparation of new transgene constructs (Kwan *et al.*, 2007; Suster *et al.*, 2009). Importantly, the significant increase in the rates of transgene genomic integration attained by using either the I-SceI- or Tol2-mediated methodologies has accelerated progress in this research. Furthermore, the development of conditional transgenic systems, such as Cre/Lox-regulated fish lines, permits regulated transgene expression to provide flexibility in the timing of transgene induction and to facilitate propagation of the lines expressing transgenes that affect zebrafish reproduction.

B. Mutagenesis

Due to the advantages of fecundity, small size, short generation time, and the ease of visualization, zebrafish provide an ideal vertebrate experimental system to perform forward genetic screens. Forward genetic screens in zebrafish have contributed greatly to the discovery of cancer-relevant genes and to the subsequent generation of zebrafish models of a variety of human cancers. The methodology for conducting forward genetic screens in fish has been based on mutagenesis via chemical treatment, for example, with the alkylating mutagen *N*-ethyl-*N*-nitrosourea (ENU) and retroviral or transposon insertions (Amatruda and Patton, 2008; Amsterdam *et al.*,

1999; Amsterdam and Hopkins, 1999; Feitsma and Cuppen, 2008; Mullins *et al.*, 1994). After mutagenesis, phenotype-based screens allow the identification of cancer phenotypes followed by positional cloning strategies to identify the underlying genomic alterations. The unbiased nature of forward genetic screens provides the opportunity to uncover "novel" genes, whose relevance and implication to cancer has not been previously established.

Although reverse genetics in the zebrafish system has previously been limited by the lack of targeted gene knockout strategies, recent studies have yielded major advances in this area. The two principal methods currently used are the (i) Targeting Induced Local Lesions in Genomes (TILLING) and (ii) zinc finger nuclease (ZFN) strategies (Doyon *et al.*, 2008; Meng *et al.*, 2008; Wienholds *et al.*, 2003). TILLING permits the isolation of loss-of-function mutants through target gene sequencing and the identification of target-selected mutations in genes corresponding to disease-causing alleles. ZFN strategies target specific gene sequences and elicit double-strand breaks that can generate loss-of-function mutations through errors in the DNA repair process. Taken together, forward and reverse genetic methodologies have resulted in the generation of several zebrafish lines carrying inactivating mutations in tumor suppressor genes.

Furthermore, the possibility to induce gene knockdown using morpholino antisense oligonucleotides, a well-established transient gene inactivation technique in fish, allows rapid epistasis analyses and further emphasizes the power of zebrafish as a tool for loss-of-function genetic analysis to elucidate critical pathways. "Caged" morpholinos have the added benefit of being able to knock down genes at selected times during early development. Recent progress in microRNA-based shRNA technologies for lineage-specific gene knockdown in fish may provide an invaluable novel tool for assessing the gene dosage effects on the pathogenesis of human malignant disorders (Dong *et al.*, 2009).

III. Transgenic Models of Oncogenesis

The ease of introducing foreign DNA into the zebrafish genome at the single-cell stage resulted in the development of a variety of tumor models, including models of leukemia and solid cancers. In general, transgenic lines are generated by the stable integration of a mammalian oncogene into the zebrafish genome driven by a zebrafish tissue-specific promoter. This section highlights the attributes of several of the zebrafish cancer models and their contributions to understanding the molecular basis underlying human malignant disorders.

A. Zebrafish Models of Leukemia

T-cell acute lymphoblastic leukemia (T-ALL) was the first cancer to be modeled in zebrafish, and this transgenic model was created in our laboratory by expressing mouse *c-Myc* (*mMyc*) or the chimeric enhanced green fluorescent

protein (*EGFP*)-*mMyc* fusion protein under the lymphocyte-specific *rag2* promoter (Langenau *et al.*, 2003). In this system, the EGFP-labeled lymphocytes were followed by fluorescence microscopy to monitor leukemogenic thymic expansion and the infiltration of transformed lymphocytes into surrounding skeletal muscle and other organs, a characteristic of human leukemia. Analyses of gene expression profiles revealed that the leukemic cells isolated from the transgenic zebrafish arise from T-lymphocyte precursors that express zebrafish orthologs of the human T-ALL oncogenes, *TAL1/SCL* and *LMO2*, which genetically recapitulates the most prevalent and treatment-resistant subgroup of human T-ALL. Langenau *et al.* also demonstrated the ability to propagate tumors by transplanting mMyc-expressing leukemic cells into wild-type hosts and thus verifying their malignant potential.

Due to the rapid induction of leukemia in *EGFP-mMyc* transgenic fish, they die prior to reaching reproductive maturity and this line had to be maintained by *in vitro* fertilization techniques. To circumvent this problem, the Cre/Lox-mediated system was used to express *EGFP-mMyc* conditionally on excision of an upstream *LoxP-dsRED2-LoxP* cassette by either Cre RNA injections or heat-shock induction (Feng *et al.*, 2007; Langenau *et al.*, 2005). The development of this conditionally expressed *EGFP-mMyc* line demonstrated the feasibility of Cre/Lox regulation in fish and allowed the zebrafish T-ALL model to be propagated easily and used effectively in subsequent studies of Myc-induced leukemia, as well as genetic and chemical screens (Fig. 2).

Recently our laboratory used this model to explore the molecular and cellular basis of T-lymphoblastic leukemia (T-LBL) progression to T-ALL (Feng *et al.*, 2010). T-LBL cases often present with a localized mediastinal mass that can progress to T-ALL where thymocytes aggressively disseminate into the bone marrow and peripheral blood. Clinically, T-LBL and T-ALL are not considered distinct hematologic malignancies because they share similarities in morphology and genotypic features, but recent gene expression profiling of T-LBL versus T-ALL showed differences between the two disorders (Raetz *et al.*, 2006). Feng *et al.* (2010) used the zebrafish model to explore the molecular basis for the distinct clinical presentations of T-LBL and T-ALL, by addressing the contributing role of the antiapoptotic protein, Bcl2. To do this, the compound transgenic *rag2:LDL-EGFP-mMyc;rag2:EGFP-bcl2 (Myc;bcl2)* fish were crossed to the zebrafish expressing *Cre* under the heat-shock promoter. As might be predicted based on the antiapoptotic role of Bcl2, the *Myc;Cre;bcl2* transgenic fish displayed an accelerated onset of T-LBL compared to the *Myc;Cre* line; however, lymphomas in the *Myc;Cre;bcl2* fish were also profoundly inhibited in their progression of T-LBL to T-ALL. Immunohistochemical analyses and *in vivo* imaging of transplanted Bcl2-overexpressing lymphoma cells within the context of the *fli:EGFP* transgenic line in the "Casper" pigment-deficient (White *et al.*, 2008) background to visualize the vasculature revealed impaired intravasation of the T-LBL cells (Fig. 3). T-LBL cells isolated from *Myc;Cre;bcl2* transgenic fish were also shown to undergo autophagy, presumably due to their inability to disseminate from the thymic

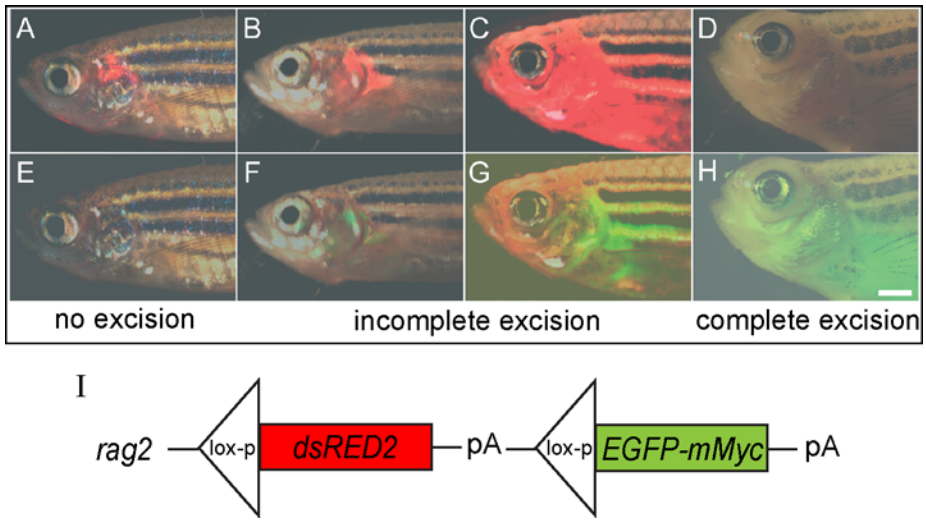

Fig. 2 Zebrafish model of heat-shock-induced T-cell lymphoma/leukemia. (A-H) Overlay of bright-field and fluorescence images (A-D: *dsRED2*; E-H: *EGFP*) of T cells expressing *dsRED2* and/or *EGFP-mMyc.* Control fish carrying the *rag2:Loxp-dsRED2-Loxp (LDL)* transgene harbors normal thymocytes expressing only dsRED2 (A) and not EGFP-mMyc (E). The *rag2:LDL-EGFP-mMyc*;*hsp70-Cre* compound transgenic fish (B-H) express both dsRED2 (B-C) and EGFP-mMyc (F-G) because of incomplete excision of the LDL cassette by Cre. The EGFP- and dsRED2-labelled T-lymphoblasts are either locally invasive (B, F) or disseminated (C, G). Upon complete excision of the *LDL* cassette in double-transgenic fish only EGFP-mMyc-labeled lymphoblasts are detected (D; H). I. Diagram of the *rag2:loxP-dsRED2-loxP-EGFP-mMyc* construct. Modified with permission from (Feng *et al.*, 2007). (See color plate.)

region via the blood. Feng *et al.* (2010) demonstrated that activated AKT could overcome this block to promote T-LBL cell dissemination and progression to T-ALL. Consistent with the findings in the zebrafish model, BCL2 levels were found to be higher in human T-LBL when compared with those in T-ALL, and human T-LBL cells also displayed autophagy.

Feng *et al.* showed that these cellular phenotypes arose due to elevated levels of S1P1 and its downstream target, ICAM1, which drives homotypic intercellular adhesion and inhibits intravasation. Moreover, using *Myc;Cre;bcl2* zebrafish, the increased aggregation of Bcl2-overexpressing T-LBL cells could be overcome by S1P1 inhibition or expression of constitutively active murine Akt2, suggesting potential pathways to target therapeutically to prevent the progression of T-LBL to T-ALL. This study clearly emphasizes the powerful strategy of using the zebrafish system together with the detailed analysis of human tumor cells to dissect the molecular mechanisms underlying human malignancies.

One of the most common molecular abnormalities in T-ALL is aberrant activation of Notch signaling arising from gain-of-function deletions or mutations within the *NOTCH1* locus, or a rare t(7;9)(q34;34.3) chromosomal translocation, in which the intracellular domain of human NOTCH1 (ICN1) is juxtaposed to the T-cell receptor-β

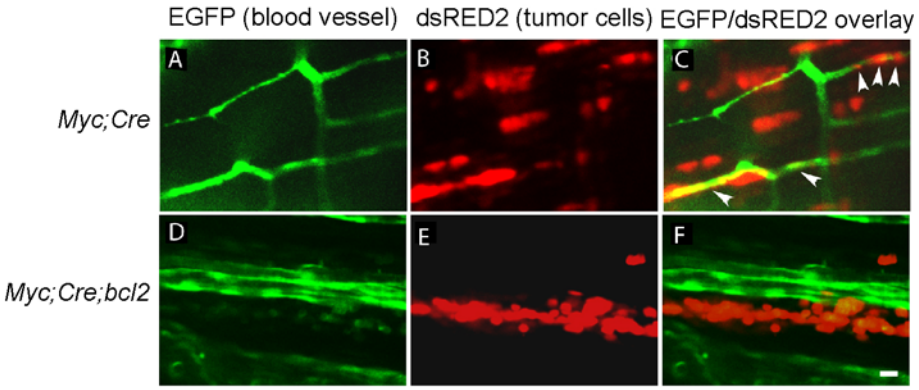

Fig. 3 Zebrafish T-lymphoblasts overexpressing *bcl2* fail to intravasate into blood vasculature. (A, B, and C) dsRED2-expressing lymphoma cells (B) isolated from the *Myc;Cre* fish intravasate into EGFP-labeled vasculature (A) of the *fli1:EGFP* by 6 days posttransplantation (see arrowheads in C). (D, E, and F) By contrast, dsRED2-expressing lymphoma cells (E) from the *Myc;Cre;bcl2* fish fail to intravasate vasculature (D) of the *fli1:EGFP* hosts by 6 days post-transplantation (compare F with C). (A)–(E). Modified with permission from (Feng *et al.*, 2007). (See color plate.)

gene. To investigate the molecular mechanisms underlying NOTCH1-driven tumorigenesis, our laboratory generated a transgenic zebrafish expressing the *ICN1-EGFP* fusion protein under the control of the *rag2* promoter (Chen *et al.*, 2007). Both F0 mosaic fish and the stable transgenic *rag2:ICN1-EGFP* fish developed aggressive oligoclonal and transplantable leukemia, albeit the stable line exhibited longer latency for disease onset (11 months as compared to 5 months for the mosaic fish). The NOTCH1-transformed T cells exhibited high expression levels of NOTCH target genes, including *her6* and *her9*.

To address the cooperativity between NOTCH1 and Bcl2 pathways, the researchers crossed the *rag2:ICN1-EGFP* transgenic line with *rag2:bcl2* fish. Although *rag2:bcl2* fish do not develop leukemia independently, the double transgenic *rag2:ICN1-EGFP; rag2:bcl2* fish demonstrated a significant acceleration of T-ALL onset (40 days postfertilization) as compared to *rag2:ICN1-EGFP* line, demonstrating the synergistic interaction between NOTCH1 signaling and the Bcl2-driven antiapoptotic pathway. The findings by Chen *et al.* establish a zebrafish model that recapitulates NOTCH1-induced T-ALL and provides the opportunity for performing genetic and chemical modifier screens to identify genes and small molecules that suppress or enhance the NOTCH1-associated malignant phenotype.

A zebrafish model of precursor-B (pre-B) ALL has been developed to recapitulate human *ETV6-RUNX1*-induced leukemia (Sabaawy *et al.*, 2006). *ETV6-RUNX1*-driven leukemia, found in 25% of children with pre-B ALL, arises as a result of a genetic rearrangement, which leads to the formation of the chimeric *ETV6-RUNX1* (also known as *TEL-AML1*) protein. To establish a zebrafish model of *ETV6-RUNX1*-induced early B-ALL, Sabaawy *et al.* generated a stable zebrafish transgenic line that

expressed *ETV6-RUNX1* under both a ubiquitous (*XlEef1a1*) and a lymphoid lineage-restricted (*rag2*) promoter. The ubiquitous expression of *ETV6-RUNX1* induced the development of leukemia in 3% of transgenic fish. This low penetrance suggests the requirement for the acquisition of additional mutations in the preleukemic cells that ultimately lead to the development of the leukemia. Histological analysis showed B-cell differentiation arrest in the leukemic cells of *TEL-AML1* transgenic zebrafish, resembling TEL-AML1-induced human pre-B ALL, supporting the use of this model for defining the additional molecular pathways underlying this human disease.

The zebrafish system has also been used in studies of RUNX1-RUNX1T1 (AML1-ETO)–induced acute myeloid leukemia (AML). Transient expression of RUNX1-RUNX1T1 led to disrupted hematopoiesis and cellular dysplasia (Kalev-Zylinska *et al.*, 2002). Subsequent studies utilized a stable inducible *AML1-ETO*-transgenic line to demonstrate that AML1-ETO promotes hematopoietic cell fate changes, redirecting erythropoiesis to granulopoiesis in the myeloerythroid progenitor cells mediated via the downregulation of *tal1* expression (Yeh *et al.*, 2008). Importantly, the *AML1-ETO* transgenic model was utilized in small-molecule chemical screens, which led to the identification of cyclooxygenase inhibitors as a class of compounds capable of interfering with AML1-ETO activity (Dayyani *et al.*, 2008; Yeh *et al.*, 2009).

B. Pancreatic Cancer Models

The first model of pancreatic neuroendocrine carcinoma was developed in our laboratory by the targeted expression of the human *MYCN* oncogene (Yang *et al.*, 2004). To generate *MYCN* transgenic zebrafish, Yang *et al.* (2004) microinjected zebrafish embryos with a construct carrying the *MYCN* oncogene under the control of both zebrafish *myod1* and human–zebrafish hybrid *MyoD* promoter sequences. Expression of MYCN was detected in muscle, hindbrain, spinal cord, and ectopically in pancreatic islet cells. The effect of increasing the levels of MYCN in these pancreatic islet cells promoted the development of pancreatic neuroendocrine carcinoma. Importantly, transmission electron microscopy illustrated the presence of cytoplasmic dense core granules resembling those observed in human neuroendocrine carcinoma (Yang *et al.*, 2004). Upregulated MYCN levels have been correlated with early events in human β-cell tumor progression (Pavelic *et al.*, 1995, 1996).

Human exocrine pancreatic cancer has been linked to oncogenic mutations in KRAS during early stages of tumorigenesis (Hruban *et al.*, 1993, 2000). To create a zebrafish model of exocrine pancreatic cancer, the Leach group used BAC recombineering technology to establish transgenic lines that carried a fusion of the ptf1a locus to either EGFP or EGFP-KRAS^{G12V} (Park *et al.*, 2008). As visualized by transcutaneous GFP fluorescence, the targeted expression of EGFP-KRAS^{G12V} promoted the development of pancreatic tumors. The histological analysis of the pancreatic tumors isolated from affected EGFP-KRAS^{G12V} transgenic zebrafish pointed to the similarity of features found in exocrine pancreatic tumors of fish and humans. The study also demonstrated that oncogenic KRAS expression blocks

cell differentiation in EGFP-KRAS^{G12V}-expressing pancreatic progenitor cells. Zebrafish pancreatic carcinoma displays active hedgehog signaling, another hallmark of invasive human pancreatic cancer (Park *et al.*, 2008; Thayer *et al.*, 2003).

C. Melanoma Models

Because the process of melanocyte differentiation from the neural crest is evolutionarily conserved among vertebrates, the zebrafish has proven to be a valuable system for the study of melanoma. Similar to the human disease, melanoma in zebrafish arises from the malignant transformation of melanocytes. Most human melanomas present with activating mutations in the serine/threonine kinase BRAF, which transduces signals from RAS kinases to MEK kinases as part of the RAS-RAF-MEK-MAPK cascade (Davies *et al.*, 2002). To test the direct effect of activating BRAF mutations on the development of melanoma, Patton *et al.* (2005) created zebrafish transgenic lines expressing human BRAF or activated BRAF^{V600E} under the melanocyte-specific *mitfa* promoter. The overexpression of BRAF^{V600E} led to development of ectopic melanocytes and induced the formation of patches of ectopic melanocytes, termed fish (f)-nevi (Fig. 4A and B), and malignant tumors arose when BRAF^{V600E} was expressed in the p53-deficient background (Fig. 4C), pointing to a synergistic interaction between the BRAF and p53 pathways in the development of melanoma. Histological analysis provided evidence for similarities between human and zebrafish melanomas (Patton *et al.*, 2005).

NRAS- and *HRAS*-driven zebrafish models have also been created to recapitulate human melanoma that arises due to the oncogenic mutations in *NRAS* and *HRAS*, respectively (Anelli *et al.*, 2009; Dovey *et al.*, 2009; Michailidou *et al.*, 2009). Activating mutations in *RAS* occur in a significant proportion of human primary and metastatic melanomas (Papp *et al.*, 1999). In the study by Dovey *et al.* (2009), the

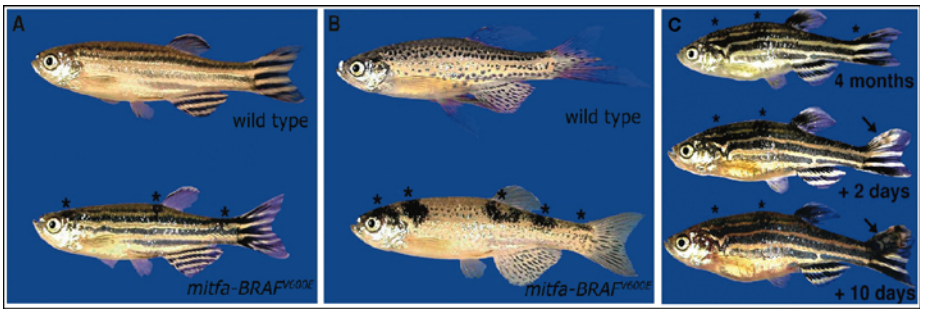

Fig. 4 Zebrafish melanoma model. (A-B). BRAF^{V600E} promotes ectopic f-nevi in adult zebrafish in wild-type (A) and leopard (B) genetic backgrounds. Wild-type fish with normal pigmentation (top) and BRAF^{V600E} –injected siblings (bottom). (C) BRAF^{V600E} –induced F nevi are observed on the tail, body, and dorsal fin of the 4 month-old *tp53*-deficient fish (asterisks, top). Local pigmentation patterns change at the f-nevus of the tail by 2 days (middle) and a large tumor mass appears within 10 days (arrow, bottom). Modified with permission from (Patton *et al.*, 2005).

expression of $NRAS^{Q61K}$ oncogenic mutation under the control of the melanocyte-specific *mitfa* promoter caused severe disruptions in the patterning of pigment cells and promoted the development of low-grade melanoma. An acceleration in disease incidence and onset occurred with p53 loss, confirming the synergistic effect of NRAS and p53 in melanoma. The observed molecular similarities between human and zebrafish tumors further confirmed the suitability of NRAS-driven models as a basis of mechanistic studies of human melanoma. In $HRAS^{V12}$ zebrafish models, expression of $HRAS^{V12}$, driven by the *mitfa* or *kita* promoter, causes ectopic melanocytes during early embryogenesis and rapid progression to melanoma (Anelli *et al.*, 2009; Michailidou *et al.*, 2009; Patton *et al.*, 2010). $HRAS^{V12}$-driven melanoma models share histopathological and epigenomic features with human melanoma (Anelli *et al.*, 2009). Using the $HRAS^{V12}$ model, Michailidou *et al.* (2009) demonstrated the direct role of PI3K-Akt signaling in melanoma progression, illustrating the potential therapeutic advantage of targeting PI3K signaling for melanoma treatment.

D. Embryonic Rhabdomyosarcoma Model

Embryonic rhabdomyosarcoma (ERMS) is the most common subtype of the pediatric soft-tissue sarcoma. Langenau *et al.* (2007) established an RAS-induced ERMS model in fish that exhibits the morphologic and molecular features of the human disease, as shown by microarray profiling and gene set enrichment analysis. Importantly, this study uncovered a previously unknown RAS-induced molecular signature present in ERMS, which is shared with pancreatic adenocarcinoma. By using cell transplantation assays and a novel fluorescent transgenic methodology, they were able to identify cancer stem cells in the zebrafish ERMS model (Ignatius and Langenau, 2009; Langenau *et al.*, 2007).

IV. Modeling the Loss of Tumor Suppression

The ability to perform large-scale forward genetic screens in the zebrafish led to the isolation of several mutant lines that carry complete and partial loss-of-function alleles of known human tumor suppressors. In addition, these screens have contributed to the identification of previously undefined tumor suppressor genes.

A. *tp53*

The use of the target-selected TILLING mutagenesis strategy led to the recovery of missense mutations within the zebrafish *tp53* gene, the ortholog of the human tumor suppressor gene *TP53*, which is mutated in 50% of human cancers (Berghmans *et al.*, 2005). The mutations found in *tp53* corresponded to the ones most often detected in human cancers ($Tp53^{N168K}$ and $Tp53^{M214K}$), and homozygous $Tp53^{M214K}$ embryos suppressed apoptosis and failed to arrest at the G1/S cell

cycle checkpoint in response to γ radiation. The tumor spectrum of adult $Tp53^{M214K}$ homozygous fish differs from humans in that zebrafish primarily develop malignant peripheral nerve sheath tumors (MPNST; Fig. 5). The performance of the chemical and genetic modifier screens directed at uncovering genetic mutations and small-molecule compounds that influence TP53 and parallel signaling pathways can be exceptionally valuable given the prevalent role of TP53 in cancers.

Our laboratory used the $Tp53^{M214K}$ zebrafish as a sensitized background in a morpholino screen for suppressors of $Tp53^{M214K}$-associated radioresistance (Sidi *et al.*, 2008). The screen led to the identification of DNA-damage-response kinase, *chek1*, as a loss-of-function suppressor of $Tp53^{M214K}$-based radioresistance. The molecular dissection of the Chek1-apoptotic pathway through *in vivo* epistasis analyses revealed that knockdown of Chek1 promotes ATM/ATR-caspase-2 signaling that circumvents the mitochondrial and death receptor apoptotic pathways. Interestingly, this ATM/ATR-caspase-2 is evolutionary conserved, and is being triggered in multiple human cancer cell lines in response to γ radiation in both the presence and absence of Tp53, suggesting that this is an alternative DNA-damage-induced, p53-independent pathway. The findings in this study demonstrate that Chek1 inhibition sensitizes $Tp53^{M214K}$ zebrafish to IR-induced apoptosis, pointing to the promising therapeutic potential of Chek1 inhibitors in cancers with TP53 loss. Furthermore, the study illustrates that ATM/ATR-caspase-2 signaling is also insensitive to BCL2/BCL-XL gain, another common antiapoptotic feature in human cancers, indicating the possibility of using Chek1 inhibitors in combinatorial therapies to treat human cancers that overexpress BCL2 family members.

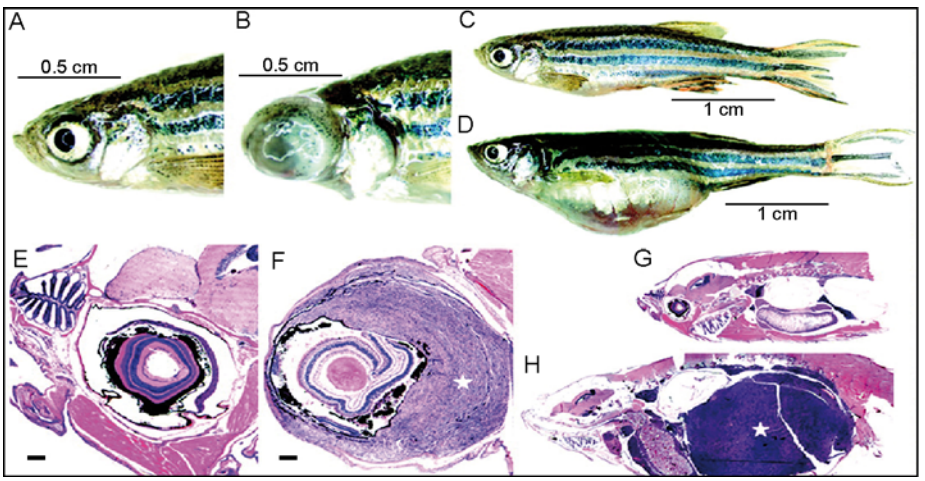

Fig. 5 MPNST in *tp53* mutant zebrafish. (A and C) Wild-type fish. External appearance of an ocular (B) and abdominal tumor (D) in *tp53* mutant zebrafish. (E-H) Histopathology staining with hematoxylin/eosin shows MPNST in the eye (F) and abdominal cavity (H) when compared with controls (E and G). Modified with permission from (Berghmans *et al*., 2005). (See color plate.)

B. *rp*

By screening an insertional mutagenesis library, the Hopkins group identified 11 ribosomal protein (*rp*) genes that predispose zebrafish to several tumor types, with an increased proportion of MPNSTs (Amsterdam *et al.*, 2004). The findings suggest a tumor suppressor role for the *rp* genes in fish with reduced *rp* gene expression being responsible for cancer predisposition. Interestingly, loss-of-function mutations in the *rp* genes and in the *tp53* gene predispose to the development of MPNSTs in zebrafish. To address the possible link between the deficiency in ribosomal proteins and the Tp53 pathway, the Lees group investigated the status of Tp53 in MPNSTs isolated from heterozygous *rp* mutant zebrafish (MacInnes *et al.*, 2008). Their findings show that haploinsufficiency for several *rp* proteins results in decreased Tp53 synthesis that contributes to tumor development. Recent studies by the Hopkins group have utilized the *rp* and *tp53* zebrafish lines to test for the presence of gross chromosomal abnormalities in cancer genomes (Zhang *et al.*, 2010). Their work supports the findings that MPNSTs exhibit aneuploidy with preferential whole-chromosome changes and, along with studies from our laboratory (Rhodes *et al.*, 2009), point to the suitability of the zebrafish model for the study of chromosomal aberrations in human cancers.

C. *apc*

Screening by TILLING of ENU-mutagenized fish also led to identification of zebrafish carrying truncating mutations within the tumor suppressor gene, *adenomatous polyposis coli* (*apc*) (Haramis *et al.*, 2006; Hurlstone *et al.*, 2003). Mutated *APC* has been found in multiple colorectal cancers and familial adenomatous polyposis (FAP) syndrome. Haramis *et al.* demonstrate that *apc* mutant zebrafish undergo spontaneous development of intestinal, hepatic, and pancreatic tumors that exhibit the morphology and histopathological features of human gastrointestinal tumors. Furthermore, the loss of *apc* in zebrafish results in the constitutive activation of the Wnt/β-catenin pathway (Bienz and Clevers, 2000), and the accumulation of β-catenin and the expression of downstream Wnt target genes has been demonstrated in neoplasias of the *apc* mutant zebrafish.

apc mutant fish have also been utilized for determining the functional connection between mutated *apc* and the increased expression of cyclooxygenase-2 (COX-2), which is often upregulated in human colorectal cancers. Specifically, Eisinger *et al.* (2006) show that mutations in *apc* upregulate levels of COX-2 via deficiency in retinoic acid biosynthesis.

Using both human colon cancer cell lines and the mutant *apc* zebrafish model, Phelps *et al.* demonstrate that the transcriptional corepressor *C-terminal binding protein-1* (*CtBP1*) contributes to defects in intestinal differentiation and the development of APC-induced adenoma. Both *APC* loss and *KRAS* or *RAF1* mutations are essential for promoting nuclear localization and oncogenic activity of β-catenin for carcinoma progression (Phelps *et al.*, 2009). Recently, the Jones group used the *apc*

mutant zebrafish and mutant *APC* human cell lines to elucidate the regulation of the DNA demethylase pathway by APC. Their findings show that inactivation of APC suppresses retinoic acid biosynthesis via Ctbp1, LSD1, Groucho2, CoRest, and Lef1, which in turn derepresses Pouf5f1 and Cebpβ to promote DNA demethylation. The increased activity of DNA demethylase in intestinal cells maintains a hypomethylated state that inhibits their differentiation following APC loss (Rai *et al.*, 2010).

D. *pten*

Phosphatase and tensin homolog on chromosome 10 (*PTEN*) is a tumor suppressor gene that is found mutated in a broad range of human cancers (Stokoe, 2001). *PTEN* encodes a protein tyrosine phosphatase that acts as a negative regulator of the PI-3 kinase/Akt/PKB pathway to modulate cell cycle progression, cell proliferation, and survival (Sun *et al.*, 1999). Target-selected gene inactivation strategies led to the identification of nonsense mutations in *ptena* and *ptenb*, zebrafish orthologs of human PTEN (Faucherre *et al.*, 2008). The presence of two zebrafish genes that correspond to a single human ortholog is not uncommon as a result of a genome duplication event during teleost evolution. Using *in vitro* assays, Faucherre *et al.* showed that recombinant Ptena and Ptenb exhibit selective lipid phosphatase activity, identical to human PTEN, and that this catabolic activity is lacking in $ptena^{-/-}$; $ptenb^{-/-}$ mutants. In addition, the study illustrates that $ptena^{-/-}$;$ptenb^{-/-}$ zebrafish embryos exhibit a severe hyperplastic–dysplastic phenotype that occurs due to aberrant cellular proliferation and survival (Faucherre *et al.*, 2008). Interestingly, although Ptena and Ptenb are functionally redundant in embryonic development, only deficiency in Ptenb promotes tumorigenesis in eyes of adult fish. Importantly, a PI-3 kinase inhibitor rescued the embryonic phenotype of the *ptena;ptenb* mutant fish, providing further support for the use of *pten* mutant fish in genetic and chemical screens to isolate suppressors of Pten loss of function (Faucherre *et al.*, 2008).

E. *mybl2*

A cell-proliferation forward genetic screen by Shepard *et al.* (2005), designed to assay cell cycle defects and cancer predisposition, uncovered the *crash&burn* (*crb*) mutant that carries a loss-of-function mutation in the transcriptional regulator, *mybl2* (previously called *bmyb*). *crb* mutant embryos exhibit defects in spindle formation that affect mitotic progression and genomic stability. The researchers also observed increased cancer susceptibility in *crb* heterozygote adults, and gene profiling experiments revealed similarities in gene expression signatures between *crb* zebrafish and human tumor samples. The *crb* mutant was subsequently used in a small-molecule chemical suppressor screen by Stern *et al.* (2005) that led to the identification of suppressors of *mybl2*-dependent mitotic defects.

F. *hlk*, *srk*, and *otg* mutants

The Trede group performed a forward genetic screen in search of T-cell malignancy-prone mutants and identified the *hlk*, *srk*, and *otg* genes as novel genes that contribute to a predisposition to T-cell leukemia (Frazer *et al.*, 2009). In their experiments, the use of transgenic fish that express EGFP under the control of the native T-cell-specific *lck* gene promoter allowed the identification of mutant lines based on abnormal GFP expression phenotypes. These three mutant lines develop T-ALL malignancies that phenotypically and histologically resemble oncogene-induced leukemia (Frazer *et al.*, 2009).

V. Modeling Tumor Cell Intravasation and Metastasis

The optical clarity of zebrafish embryos coupled to the development of the transparent "Casper" fish coupled to the advances in transplantation methodologies (described below) makes zebrafish a unique system for high-resolution imaging of tumor vascularization and metastasis (Sahai, 2007; Stoletov and Klemke, 2008). Importantly, accumulating evidence supports the evolutionary conservation of the vascular biology shared between humans and zebrafish (Isogai *et al.*, 2003). Hence, zebrafish can provide an ideal model for *in vivo* chemical screening for therapeutic agents that inhibit the angiogenic response to tumor formation.

The generation of transgenic zebrafish that express GFP in vascular endothelial cells under the control of the zebrafish *fli1* or murine *Tie2* promoters and the use of real-time imaging methodologies provide unprecedented high-resolution imaging of complex and dynamic vascular intravasation processes (Lawson and Weinstein, 2002; Motoike *et al.*, 2000). Stoletov *et al.* (2007) used the transgenic *fli1:EGFP* zebrafish and high-resolution confocal microscopy to interrogate the role of RhoC and VEGF in mediating tumor cell intravasation. In their study, fluorescently labeled human MDA-435 breast adenocarcinoma (MDA-435) cells were injected into the peritoneal cavity of *fli1:EGFP* fish where microtumor formation, vessel remodeling, and angiogenesis could be visualized (Stoletov *et al.*, 2007). Intravital real-time imaging in conjunction with optical sectioning and 3D reconstruction of the neovasculature showed that VEGF is responsible for the rapid formation of a network of vessels with distended vessel lumens and increased permeability (Fig. 6). RhoC mediates intravasation by promoting the formation of invadopodia that protrude into the vessel lumen. In a subsequent study, Stoletov *et al.* (2010) showed that the intravascular migration of transplanted MDA-435 cells caused endothelial cells to cluster around the MDA-435 cells and that endothelial cell junction remodeling was mediated in part by the prometastatic *Twist* gene.

van Rooijen *et al.* (2010) recently utilized the zebrafish system to analyze the role of the tumor suppressor von Hippel–Lindau (*vhl*) and the VEGF signaling pathway

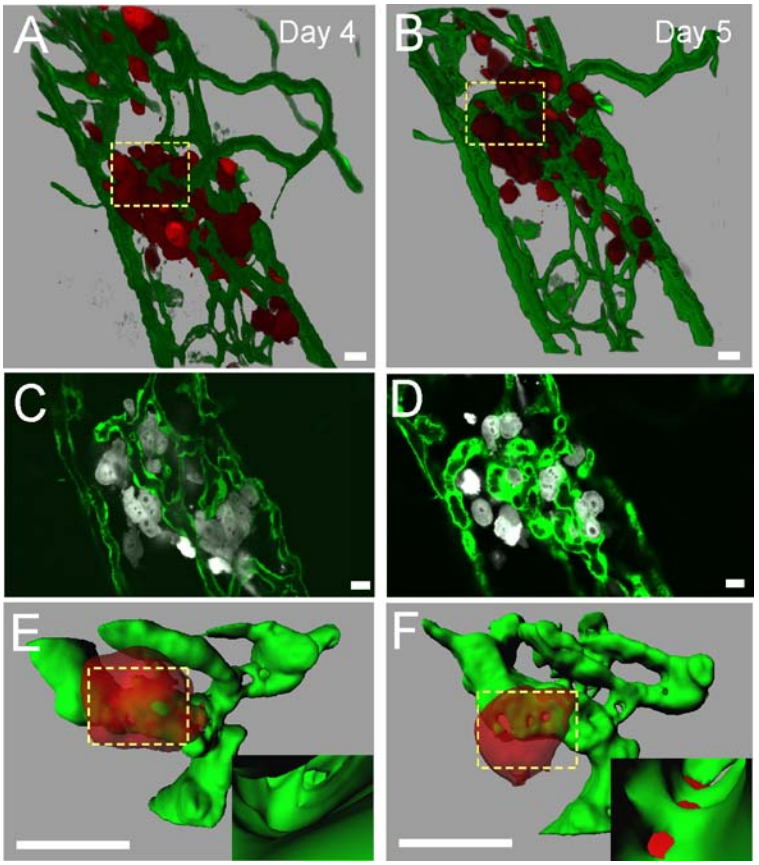

Fig. 6 Visualization of human tumor-induced angiogenesis. (A, B) Three-dimensional (3D) confocal reconstructions of VEGF-secreting MDA-435 tumor cells in the body wall of *fli1:EGFP* zebrafish, 4 (A), and 5 (B) days post injection. (C, D) Single confocal optical sections (1 μm) of microtumor in (A) and (B). (E, F) 3D reconstructions of digitally isolated tumor cells in contact with host blood vessels from A and B. Dotted squares indicate insets showing magnified views of the interior vessel surface at sites of vessel openings and tumor cell membrane insertion. Modified with permission from (Stoletov *et al*., 2007). (See color plate.)

in vasculature formation. vhl syndrome is characterized by an elevated predisposition to blood vessel neoplasms that affect several organ systems (Park *et al.*, 2007). van Rooijen *et al.* showed that aberrant neovascularization observed in the brain, retina, and trunk of $vhl^{-/-}$ embryos led to macular edema, retinal detachment, and vascular leakage in the retina. The authors showed that this pathological angiogenesis correlated with elevated levels of Vegf ligands and could be significantly reduced in response to Vegf receptor tyrosine kinase inhibitors (van Rooijen *et al.*, 2010).

Vlecken and Bagowski (2009) employed the zebrafish system to study the role of the PDZ/LIM family of kinases, LIMK1 and LIMK2, in the progression of pancreatic cancer metastases. Pancreatic cancer cell lines treated with siRNAs against LIMK1 and LIMK2 were injected into zebrafish embryos and assays of angiogenesis and metastases were conducted to analyze neovascularization and cell migration using real-time confocal microscopy. These studies provide evidence for both LIMK1 and LIMK2 having prominent roles in angiogenesis and the metastatic behavior of pancreatic cancer cells.

As discussed above, Feng *et al.* (2010) in our laboratory utilized the *fli1:EGFP* translucent fish and transplantation assays with *in vivo* confocal imaging in critical studies to show that elevated levels of Bcl2 inhibit the progression of T-LBL to T-ALL by blocking T-LBL cell intravasation into the microvasculature and that this inhibition could be overcome by S1P1 antagonists. Together, these studies clearly highlight the unique attributes of the zebrafish model system for unraveling mechanisms that underlie invasive properties of tumorigenic cells.

Zebrafish-based screens for agents that exhibit antivascular activity have led to the identification of several new lead compounds with therapeutic potential. Murphy *et al.* (2010) utilized transgenic *fli1:EGFP* zebrafish in conjunction with cell-based assays to screen for antivascular activities of selected kinase inhibitors. The screen led to the identification of an orally active small-molecule compound that inhibits B-RAF and PDGFRβ, and is able to suppress kidney and pancreatic tumors in murine models (Murphy *et al.*, 2010). Chemical screens using translucent *fli1:EGFP* zebrafish transgenic have also led to the identification of the antiangiogenic compound rosuvastatin, which has antiangiogenic and tumor-suppressive properties, as shown by prostate tumor xenograft studies in mice (Wang *et al.*, 2010). Interestingly, the fruit of *Alpinia oxyphylla* and indirubin, commonly used as East Asian herbal medicines for the treatment of cancer and chronic myelocytic leukemia (CML), respectively, have also been shown to demonstrate antiangiogenic properties using transgenic zebrafish embryo-based assays (Alex *et al.*, 2010; He *et al.*, 2010).

VI. Tumor-Initiating Cells

Zebrafish have recently been used to study the process of cellular self-renewal in cancer. The small size and fecundity of the fish make it possible to carry out large-scale cell transplantation experiments required to study the self-renewal potential of tumor cells. The development of the "Casper" zebrafish, the line that promotes the visualization of fluorescent markers (White *et al.*, 2008), together with recent advances in transplantation methods, permits the zebrafish to be used as a model for the assessment of cancer cell self-renewal (Taylor and Zon, 2009). Zebrafish transplantation assays have been used successfully to demonstrate the malignant potential of several cancers, including leukemias, myeloproliferative neoplasias, and solid tumors. Specifically, lymphoblasts isolated from zebrafish with Myc-induced

T-ALL and transplanted into wild-type zebrafish recipients were shown to home to the thymus, whereas leukemic kidney marrow cells isolated from TEL-AML1-induced B-ALL transgenic animals and melanoma cells from $BRAF^{V600E}$ expressing $tp53^{-/-}$ fish demonstrated the capacity for the serial propagation of tumors (Langenau *et al.*, 2003; Patton *et al.*, 2005; Sabaawy *et al.*, 2006). In recent years, zebrafish have also emerged as an *in vivo* model for investigating human tumor cell behavior and understanding the underlying mechanisms of cancer progression. The malignant potential of cancer cells derived from varying tissue origin, including adenocarcinoma, fibrosarcoma, and melanoma, has been assessed using transplantation strategies in larval (2–5 days old) and juvenile (30-day-old) zebrafish (Haldi *et al.*, 2006; Ignatius and Langenau, 2009; Nicoli *et al.*, 2007; Topczewska *et al.*, 2006).

Zebrafish allow one to perform transplantation assays efficiently with low numbers of tumor cells for the study of cancer self-renewal and to address the effects of clonal evolution on tumor-initiating potential (Ignatius and Langenau, 2009). Frazer *et al.* took advantage of the transplantability of GFP-labeled malignant thymocytes isolated from *srk*, *hlk*, or *otg* mutant fish lines that display heritable T-cell malignancies. Fluorescent malignant cells from the three mutant lines demonstrated engraftment, tumor progression, and dissemination, as they were tracked *in vivo*. In particular, by the serial passage of tumor cells, the researchers determined that tumor cells were capable of increasing their malignant potential and were able to quantify the tumor-initiating cells from these T-cell malignancies (Frazer *et al.*, 2009).

Langenau *et al.* utilized novel targeting and multifluorescent labeling strategies to identify and analyze distinct subpopulations of tumor cells from zebrafish ERMS based on the differentiation status of muscle cells (Fig. 7). Using FACS analysis, cell transplantation, and limiting dilution assays, cancer stem cells were studied in zebrafish ERMS (Langenau *et al.*, 2007, 2008). Specifically, Langenau *et al.* (2007) showed that in kRASG12D-driven ERMS, RAS is capable of tumor induction and that tumor cells accumulate additional defects that lead to differentiation arrest, contributing a greater tumor-initiating potential among less-differentiated muscle cells (Merlino and Khanna, 2007).

The development of syngenic, clonal zebrafish has greatly empowered the use of zebrafish as a cancer self-renewal model (Mizgireuv and Revskoy, 2006). Using these fish in cell transplantation assays, the Langenau group demonstrated the abundance of tumor-initiating cells in zebrafish T-ALLs (Smith *et al.*, 2010). These experiments also provided evidence for a single cell's ability to give rise to T-ALL and show the variability of tumor-initiating potential among T-ALLs. Furthermore, the Langenau group established a high-throughput fluorescent imaging method to score T-ALL engraftment in recipient host animals (Smith *et al.*, 2010). However, although zebrafish transplantation models have been very informative, the generation of new surface antibodies or additional transgenic fluorescent lines for distinguishing subpopulations of tumor cells will greatly enhance the use of zebrafish for the study of tumor cell self-renewal (Ignatius and Langenau, 2009).

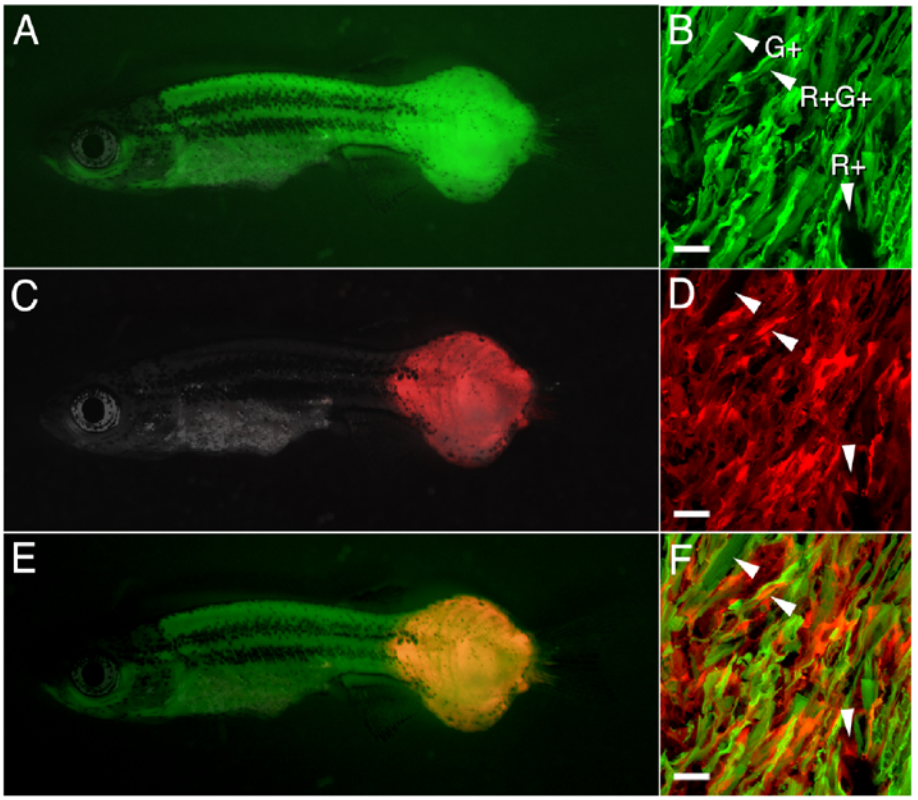

Fig. 7 Coinjection approaches for labeling distinct cell populations within zebrafish rhabdomyosarcoma (RMS). (A) GFP fluorescent image of RMS developing in a *rag2:dsRED2*$^{+}$*;rag2:kRASG12D*; *α-actin:GFP*$^{+}$ co-injected fish. (B) GFP fluorescence in frozen section. (C) dsRED2 fluorescence image of fish shown in A. (D) dsRED2 fluorescence in a frozen section. (E,F) Merged image of fish in A and C. Arrowheads in B, D, and F show cells that express GFP (G^{+}), dsRED2^{+} (R^{+}), or both ($R^{+}G^{+}$) within the zebrafish RMS. Modified with permission from (Langenau *et al*., 2007). (See color plate.)

VII. *In vivo* Small-Molecule Screens and Drug Discovery

Because of the many attributes of the zebrafish, including high fecundity, small size, being amenable to experimental manipulation, and ease of visualization due to transparency, the zebrafish system is uniquely suited for the performance of whole-animal phenotype-based small-molecule screens (Fig. 8). Together with its genetic tractability that contributes to the ease of generating cancer models, these attributes promote the use of the zebrafish as an important tool for the identification of lead compounds for the development of novel therapeutic strategies to treat human cancer. Specifically, large numbers of zebrafish embryos or larvae can be assessed

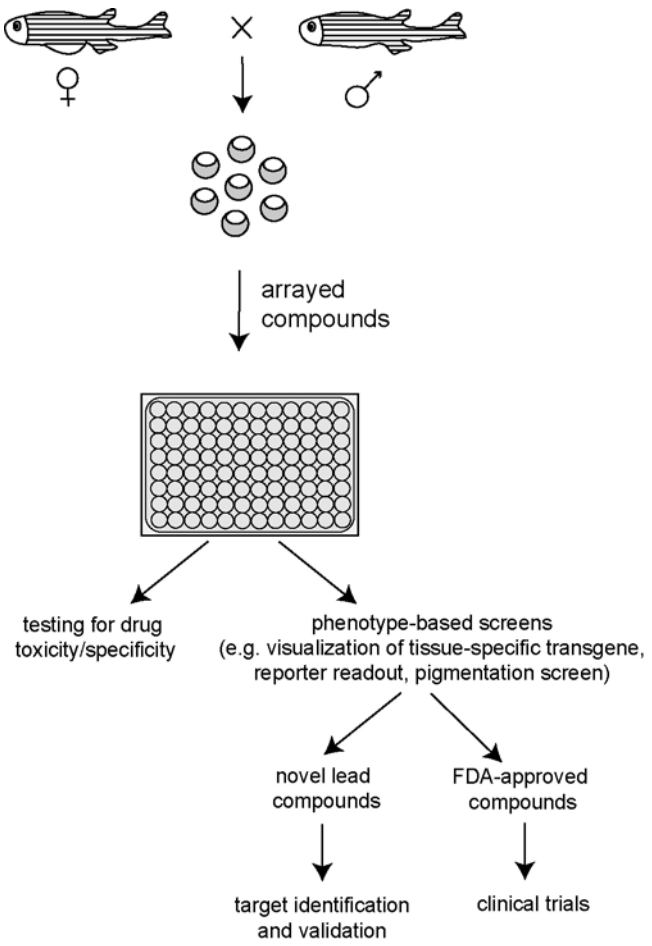

Fig. 8 Schematic for performing small-molecule screens and assessing drug toxicity in zebrafish.

quickly for cancer-relevant phenotypic alterations based on direct microscopic visualization, *in situ* hybridization or immunohistochemical assays, or reporter readouts (Wheeler and Brandli, 2009). Furthermore, drug screening of chemical libraries is facilitated by the administration of compounds by their simple addition to the fish water of embryos or larvae that are arrayed in microwell plates, thus requiring small amounts of drug. While the use of zebrafish for drug discovery compliments *in vitro* cell culture–based drug screens, the zebrafish allows the important analysis of drug efficacy in the context of the whole organism. Zebrafish also represent a "nontransformed" system that is not subject to the accumulation of, and selection for, additional mutations carried by immortalized cell lines.

In vivo animal models for small-molecule screening allow the assessment of drug absorption, distribution, metabolism, excretion, and toxicity (ADMET) at the initial stages of the drug development pipeline (Bowman and Zon, 2010). However, it is important to note that due to the incomplete understanding of physiological and pharmacological drug responses in humans and fish, ADMET in zebrafish may not be fully predictive of these parameters in humans. For this reason, researchers often consider the use of chemical compound libraries of FDA-approved drugs where these parameters in humans are already described. Aside from circumventing the species differences in ADMET, the use of FDA-approved drugs promotes discovery of an alternative therapeutic potential for the known drug and, therefore, greatly shortens the time required to get to human clinical trials (Bowman and Zon, 2010).

In recent years, chemical screens using zebrafish embryos have uncovered a wide range of putative chemotherapeutic agents. Since oncogenes found in leukemia cause both uncontrolled proliferation and arrested differentiation, chemical screens directed at the identification of compounds that may inhibit differentiation will complement the traditional chemotherapies that target cellular proliferation pathways. In AML, the oncogenic *AML1-ETO* rearrangement reprograms cells from an erythrocyte fate to a granulocytic blast cell fate. In an attempt to identify chemical modifiers of oncogenic *AML1-ETO*-driven cell fate changes, Yeh *et al.* (2009) screened a library of 2000 bioactive compounds using a conditional *hsp70:AML1-ETO* transgenic fish. The screen resulted in the identification of a COX-2 inhibitor as an antagonist of AML1-ETO-driven cell fate changes as detected by the appearance of the hematopoietic erythrocyte lineage marker gata1 that is normally absent in heat-shock-induced AML1-ETO-expressing cells. In another study, Hao *et al.* (2010) performed a structure–activity relationship (SAR) screen and revealed a previously unknown antiangiogenic property (VEGF inhibitor) of dorsomorphin, a small-molecule inhibitor of bone morphogenetic protein (BMP) signaling. This work emphasizes the relevance of the SAR approach in isolating effective and specific small-molecule modifiers of signaling pathways that have the potential to be developed further into chemotherapeutics (Hao *et al.*, 2010).

In vivo chemical screening in search of bioactive tools that affect cell cycle progression have led to the identification of several previously unknown compounds. For example, the small-molecule screen on *crb* mutant embryos by Stern *et al.* led to the isolation of a suppressor of the cell cycle pathway in these *mybl2* loss-of function mutants. The *crb* suppressors were identified by reduced antiphosphorylated histone H3 labeling, indicating a reduction in aberrantly proliferating cells in the *crb* mutants. Persynthamide (psy), the chemical suppressor isolated using this screening strategy, causes S-phase delay via an ATR-dependent checkpoint and promotes an accumulation of *cyclin B1*, which is known to be deficient in both zebrafish *crb* mutants and B-MYB-deficient human cells (Stern *et al.*, 2005; Taylor *et al.*, 2010). The small-molecule study by Murphey *et al.* identified compounds affecting cell cycle progression in zebrafish and emphasized the importance of combining *in vivo* and *in vitro* screens Murphey *et al.* (2006). The screen resulted in the identification of novel inhibitors of mitosis that were previously missed in cell

culture–based screenings. Furthermore, several known cell cycle compounds isolated from mammalian cell line screens were also active in fish embryos.

The strategies outlined for the performance of drug screens on zebrafish embryos can be adapted to include drug testing on adult fish. Small-molecule screens in adult fish are feasible because adult fish can be exposed easily to chemical compounds by administering drugs to the fish water.

VIII. Conclusions

Zebrafish presents an exciting whole-organism system that is suitable both for assessing signaling pathways in malignancy and as a platform for the development of novel therapeutic strategies. It already plays an important role in cancer research and the system is constantly evolving to encompass novel experimental strategies that further empower its use for the study of carcinogenesis. For example, there have been major recent advances in the development of transplantation techniques. These transplantation strategies exploit the unique capability of zebrafish for *in vivo* imaging to address cancer cell intravasation and metastasis, self-renewal, and host–tumor cell interactions using both zebrafish and human cancer cells. Recent advances in zebrafish genetics further expand the cancer research tool box in this model organism. The establishment of mosaic analysis in zebrafish (MAZe) technique, which permits clonal analysis of gene function and cell-lineage tracing via *in vivo* live imaging, introduces a valuable approach in zebrafish genetics that can be utilized for the study of oncogene-expressing cells in the wild-type environment (Blackburn and Langenau, 2010; Collins *et al.*, 2010). The zebrafish is also emerging as a powerful system for exploring the function of short noncoding RNAs (microRNAs), a new class of elegant molecular regulators, in cancer-relevant cellular processes. Understanding the specific regulatory mechanisms of signaling pathways dysregulated in cancer by microRNAs may provide further important insights into the molecular basis of cancer initiation and progression.

References

Alex, D., Lam, I. K., Lin, Z., and Lee, S. M. (2010). Indirubin shows anti-angiogenic activity in an *in vivo* zebrafish model and an *in vitro* HUVEC model. *J. Ethnopharmacol.* **131**, 242–247.

Amatruda, J. F., and Patton, E. E. (2008). Genetic models of cancer in zebrafish. *Int. Rev. Cell Mol. Biol.* **271**, 1–34.

Amsterdam, A., Burgess, S., Golling, G., Chen, W., Sun, Z., Townsend, K., Farrington, S., Haldi, M., and Hopkins, N. (1999). A large-scale insertional mutagenesis screen in zebrafish. *Genes Dev.* **13**, 2713–2724.

Amsterdam, A., and Hopkins, N. (1999). Retrovirus-mediated insertional mutagenesis in zebrafish. *Methods Cell Biol.* **60**, 87–98.

Amsterdam, A., Lai, K., Komisarczuk, A. Z., Becker, T. S., Bronson, R. T., Hopkins, N., and Lees, J. A. (2009). Zebrafish Hagoromo mutants up-regulate fgf8 postembryonically and develop neuroblastoma. *Mol. Cancer Res.* **7**, 841–850.

Amsterdam, A., Sadler, K. C., Lai, K., Farrington, S., Bronson, R. T., Lees, J. A., and Hopkins, N. (2004). Many ribosomal protein genes are cancer genes in zebrafish. *PLoS Biol.* **2**, E139.

Anelli, V., Santoriello, C., Distel, M., Koster, R. W., Ciccarelli, F. D., and Mione, M. (2009). Global repression of cancer gene expression in a zebrafish model of melanoma is linked to epigenetic regulation. *Zebrafish* **6**, 417–424.

Balciunas, D., and Ekker, S. C. (2005). Trapping fish genes with transposons. *Zebrafish* **1**, 335–341.

Berghmans, S., Murphey, R. D., Wienholds, E., Neuberg, D., Kutok, J. L., Fletcher, C. D., Morris, J. P., Liu, T. X., Schulte-Merker, S., and Kanki, J. P., *et al*. (2005). tp53 mutant zebrafish develop malignant peripheral nerve sheath tumors. *Proc. Natl. Acad. Sci. U.S.A.* **102**, 407–412.

Bienz, M., and Clevers, H. (2000). Linking colorectal cancer to Wnt signaling. *Cell* **103**, 311–320.

Blackburn, J. S., and Langenau, D. M. (2010). aMAZe-ing tools for mosaic analysis in zebrafish. *Nat. Methods* **7**, 188–190.

Bowman, T. V., and Zon, L. I. (2010). Swimming into the future of drug discovery: *in vivo* chemical screens in zebrafish. *ACS Chem. Biol.* **5**, 159–161.

Chen, J., Jette, C., Kanki, J. P., Aster, J. C., Look, A. T., and Griffin, J. D. (2007). NOTCH1-induced T-cell leukemia in transgenic zebrafish. *Leukemia* **21**, 462–471.

Collins, R. T., Linker, C., and Lewis, J. (2010). MAZe: a tool for mosaic analysis of gene function in zebrafish. *Nat. Methods* **7**, 219–223.

Davies, H., Bignell, G. R., Cox, C., Stephens, P., Edkins, S., Clegg, S., Teague, J., Woffendin, H., Garnett, M. J., and Bottomley, W., *et al*. (2002). Mutations of the BRAF gene in human cancer. *Nature* **417**, 949–954.

Dayyani, F., Wang, J., Yeh, J. R., Ahn, E. Y., Tobey, E., Zhang, D. E., Bernstein, I. D., Peterson, R. T., and Sweetser, D. A. (2008). Loss of TLE1 and TLE4 from the del(9q) commonly deleted region in AML cooperates with AML1-ETO to affect myeloid cell proliferation and survival. *Blood* **111**, 4338–4347.

Dong, M., Fu, Y. F., Du, T. T., Jing, C. B., Fu, C. T., Chen, Y., Jin, Y., Deng, M., and Liu, T. X. (2009). Heritable and lineage-specific gene knockdown in zebrafish embryo. *PLoS One* **4**, e6125.

Dovey, M., White, R. M., and Zon, L. I. (2009). Oncogenic NRAS cooperates with p53 loss to generate melanoma in zebrafish. *Zebrafish* **6**, 397–404.

Doyon, Y., McCammon, J. M., Miller, J. C., Faraji, F., Ngo, C., Katibah, G. E., Amora, R., Hocking, T. D., Zhang, L., and Rebar, E. J., *et al*. (2008). Heritable targeted gene disruption in zebrafish using designed zinc-finger nucleases. *Nat. Biotechnol* **26**, 702–708.

Eisinger, A. L., Nadauld, L. D., Shelton, D. N., Peterson, P. W., Phelps, R. A., Chidester, S., Stafforini, D. M., Prescott, S. M., and Jones, D. A. (2006). The adenomatous polyposis coli tumor suppressor gene regulates expression of cyclooxygenase-2 by a mechanism that involves retinoic acid. *J. Biol. Chem.* **281**, 20474–20482.

Faucherre, A., Taylor, G. S., Overvoorde, J., Dixon, J. E., and Hertog, J. (2008). Zebrafish pten genes have overlapping and non-redundant functions in tumorigenesis and embryonic development. *Oncogene* **27**, 1079–1086.

Feitsma, H., and Cuppen, E. (2008). Zebrafish as a cancer model. *Mol. Cancer Res.* **6**, 685–694.

Feitsma, H., Kuiper, R. V., Korving, J., Nijman, I. J., and Cuppen, E. (2008). Zebrafish with mutations in mismatch repair genes develop neurofibromas and other tumors. *Cancer Res.* **68**, 5059–5066.

Feng, H., Langenau, D. M., Madge, J. A., Quinkertz, A., Gutierrez, A., Neuberg, D. S., Kanki, J. P., and Look, A. T. (2007). Heat-shock induction of T-cell lymphoma/leukaemia in conditional Cre/lox-regulated transgenic zebrafish. *Br. J. Haematol.* **138**, 169–175.

Feng, H., Stachura, D. L., White, R. M., Gutierrez, A., Zhang, L., Sanda, T., Jette, C. A., Testa, J. R., Neuberg, D. S., and Langenau, D. M., *et al*. (2010). T-lymphoblastic lymphoma cells express high levels of BCL2, S1P1, and ICAM1, leading to a blockade of tumor cell intravasation. *Cancer Cell* **18**, 353–366.

Frazer, J. K., Meeker, N. D., Rudner, L., Bradley, D. F., Smith, A. C., Demarest, B., Joshi, D., Locke, E. E., Hutchinson, S. A., and Tripp, S., *et al*. (2009). Heritable T-cell malignancy models established in a zebrafish phenotypic screen. *Leukemia* **23**, 1825–1835.

Grabher, C., and Wittbrodt, J. (2008). Recent advances in meganuclease-and transposon-mediated transgenesis of medaka and zebrafish. *Methods Mol. Biol.* **461**, 521–539.

Haldi, M., Ton, C., Seng, W. L., and McGrath, P. (2006). Human melanoma cells transplanted into zebrafish proliferate, migrate, produce melanin, form masses and stimulate angiogenesis in zebrafish. *Angiogenesis* **9**, 139–151.

Hao, J., Ho, J. N., Lewis, J. A., Karim, K. A., Daniels, R. N., Gentry, P. R., Hopkins, C. R., Lindsley, C. W., and Hong, C. C. (2010). *In vivo* structure–activity relationship study of dorsomorphin analogues identifies selective VEGF and BMP inhibitors. *ACS Chem. Biol.* **5**, 245–253.

Haramis, A. P., Hurlstone, A., van der Velden, Y., Begthel, H., van den Born, M., Offerhaus, G. J., and Clevers, H. C. (2006). Adenomatous polyposis coli-deficient zebrafish are susceptible to digestive tract neoplasia. *EMBO Rep.* **7**, 444–449.

He, Z. H., Ge, W., Yue, G. G., Lau, C. B., He, M. F., and But, P. P. (2010). Anti-angiogenic effects of the fruit of Alpinia oxyphylla. *J. Ethnopharmacol* **132**(2), 443–449.

Hruban, R. H., van Mansfeld, A. D., Offerhaus, G. J., van Weering, D. H., Allison, D. C., Goodman, S. N., Kensler, T. W., Bose, K. K., Cameron, J. L., and Bos, J. L. (1993). K-ras oncogene activation in adenocarcinoma of the human pancreas. A study of 82 carcinomas using a combination of mutant-enriched polymerase chain reaction analysis and allele-specific oligonucleotide hybridization. *Am. J. Pathol.* **143**, 545–554.

Hruban, R. H., Wilentz, R. E., and Kern, S. E. (2000). Genetic progression in the pancreatic ducts. *Am. J. Pathol.* **156**, 1821–1825.

Hurlstone, A. F., Haramis, A. P., Wienholds, E., Begthel, H., Korving, J., Van Eeden, F., Cuppen, E., Zivkovic, D., Plasterk, R. H., and Clevers, H. (2003). The Wnt/beta-catenin pathway regulates cardiac valve formation. *Nature* **425**, 633–637.

Ignatius, M. S., and Langenau, D. M. (2009). Zebrafish as a model for cancer self-renewal. *Zebrafish* **6**, 377–387.

Isogai, S., Lawson, N. D., Torrealday, S., Horiguchi, M., and Weinstein, B. M. (2003). Angiogenic network formation in the developing vertebrate trunk. *Development* **130**, 5281–5290.

Kalev-Zylinska, M. L., Horsfield, J. A., Flores, M. V., Postlethwait, J. H., Vitas, M. R., Baas, A. M., Crosier, P. S., and Crosier, K. E. (2002). Runx1 is required for zebrafish blood and vessel development and expression of a human RUNX1-CBF2T1 transgene advances a model for studies of leukemogenesis. *Development* **129**, 2015–2030.

Kwan, K. M., Fujimoto, E., Grabher, C., Mangum, B. D., Hardy, M. E., Campbell, D. S., Parant, J. M., Yost, H. J., Kanki, J. P., and Chien, C. B. (2007). The Tol2kit: a multisite gateway-based construction kit for Tol2 transposon transgenesis constructs. *Dev. Dyn.* **236**, 3088–3099.

Lam, S. H., Wu, Y. L., Vega, V. B., Miller, L. D., Spitsbergen, J., Tong, Y., Zhan, H., Govindarajan, K. R., Lee, S., and Mathavan, S., *et al*. (2006). Conservation of gene expression signatures between zebrafish and human liver tumors and tumor progression. *Nat. Biotechnol.* **24**, 73–75.

Langenau, D. M., Feng, H., Berghmans, S., Kanki, J. P., Kutok, J. L., and Look, A. T. (2005). Cre/lox-regulated transgenic zebrafish model with conditional myc-induced T cell acute lymphoblastic leukemia. *Proc. Natl. Acad. Sci. U.S.A.* **102**, 6068–6073.

Langenau, D. M., Keefe, M. D., Storer, N. Y., Guyon, J. R., Kutok, J. L., Le, X., Goessling, W., Neuberg, D. S., Kunkel, L. M., and Zon, L. I. (2007). Effects of RAS on the genesis of embryonal rhabdomyosarcoma. *Genes Dev.* **21**, 1382–1395.

Langenau, D. M., Keefe, M. D., Storer, N. Y., Jette, C. A., Smith, A. C., Ceol, C. J., Bourque, C., Look, A. T., and Zon, L. I. (2008). Co-injection strategies to modify radiation sensitivity and tumor initiation in transgenic zebrafish. *Oncogene* **27**, 4242–4248.

Langenau, D. M., Traver, D., Ferrando, A. A., Kutok, J. L., Aster, J. C., Kanki, J. P., Lin, S., Prochownik, E., Trede, N. S., Zon, L. I., and Look, A. T. (2003). Myc-induced T cell leukemia in transgenic zebrafish. *Science* **299**, 887–890.

Lawson, N. D., and Weinstein, B. M. (2002). *In vivo* imaging of embryonic vascular development using transgenic zebrafish. *Dev. Biol.* **248**, 307–318.

Le, X., Langenau, D. M., Keefe, M. D., Kutok, J. L., Neuberg, D. S., and Zon, L. I. (2007). Heat shock-inducible Cre/Lox approaches to induce diverse types of tumors and hyperplasia in transgenic zebrafish. *Proc. Natl. Acad. Sci. U.S.A.* **104**, 9410–9415.

MacInnes, A. W., Amsterdam, A., Whittaker, C. A., Hopkins, N., and Lees, J. A. (2008). Loss of p53 synthesis in zebrafish tumors with ribosomal protein gene mutations. *Proc. Natl. Acad. Sci. U.S.A.* **105**, 10408–10413.

Meng, X., Noyes, M. B., Zhu, L. J., Lawson, N. D., and Wolfe, S. A. (2008). Targeted gene inactivation in zebrafish using engineered zinc-finger nucleases. *Nat. Biotechnol.* **26**, 695–701.

Merlino, G., and Khanna, C. (2007). Fishing for the origins of cancer. *Genes Dev.* **21**, 1275–1279.

Michailidou, C., Jones, M., Walker, P., Kamarashev, J., Kelly, A., and Hurlstone, A. F. (2009). Dissecting the roles of Raf- and PI3K-signalling pathways in melanoma formation and progression in a zebrafish model. *Dis. Model Mech* **2**, 399–411.

Mizgireuv, I. V., and Revskoy, S. Y. (2006). Transplantable tumor lines generated in clonal zebrafish. *Cancer Res.* **66**, 3120–3125.

Motoike, T., Loughna, S., Perens, E., Roman, B. L., Liao, W., Chau, T. C., Richardson, C. D., Kawate, T., Kuno, J., and Weinstein, B. M., *et al*. (2000). Universal GFP reporter for the study of vascular development. *Genesis* **28**, 75–81.

Mullins, M. C., Hammerschmidt, M., Haffter, P., and Nusslein-Volhard, C. (1994). Large-scale mutagenesis in the zebrafish: in search of genes controlling development in a vertebrate. *Curr. Biol.* **4**, 189–202.

Murphey, R. D., Stern, H. M., Straub, C. T., and Zon, L. I. (2006). A chemical genetic screen for cell cycle inhibitors in zebrafish embryos. *Chem. Biol. Drug Des.* **68**, 213–219.

Murphy, E. A., Shields, D. J., Stoletov, K., Dneprovskaia, E., McElroy, M., Greenberg, J. I., Lindquist, J., Acevedo, L. M., Anand, S., and Majeti, B. K., *et al*. (2010). Disruption of angiogenesis and tumor growth with an orally active drug that stabilizes the inactive state of PDGFRbeta/B-RAF. *Proc. Natl. Acad. Sci. U.S.A.* **107**, 4299–4304.

Neumann, J. C., Dovey, J. S., Chandler, G. L., Carbajal, L., and Amatruda, J. F. (2009). Identification of a heritable model of testicular germ cell tumor in the zebrafish. *Zebrafish* **6**, 319–327.

Nicoli, S., Ribatti, D., Cotelli, F., and Presta, M. (2007). Mammalian tumor xenografts induce neovascularization in zebrafish embryos. *Cancer Res.* **67**, 2927–2931.

Onnebo, S. M., Condron, M. M., McPhee, D. O., Lieschke, G. J., and Ward, A. C. (2005). Hematopoietic perturbation in zebrafish expressing a tel-jak2a fusion. *Exp. Hematol.* **33**, 182–188.

Papp, T., Pemsel, H., Zimmermann, R., Bastrop, R., Weiss, D. G., and Schiffmann, D. (1999). Mutational analysis of the N-ras, p53, p16INK4a, CDK4, and MC1R genes in human congenital melanocytic naevi. *J. Med. Genet.* **36**, 610–614.

Parant, J. M., George, S. A., Holden, J. A., and Yost, H. J. (2010). Genetic modeling of Li–Fraumeni syndrome in zebrafish. *Dis. Model Mech.* **3**, 45–56.

Park, S. W., Davison, J. M., Rhee, J., Hruban, R. H., Maitra, A., and Leach, S. D. (2008). Oncogenic KRAS induces progenitor cell expansion and malignant transformation in zebrafish exocrine pancreas. *Gastroenterology* **134**, 2080–2090.

Park, D. M., Zhuang, Z., Chen, L., Szerlip, N., Maric, I., Li, J., Sohn, T., Kim, S. H., Lubensky, I. A., and Vortmeyer, A. O., *et al*. (2007). von Hippel–Lindau disease-associated hemangioblastomas are derived from embryologic multipotent cells. *PLoS Med.* **4**, e60.

Patton, E. E., Mitchell, D. L., and Nairn, R. S. (2010). Genetic and environmental melanoma models in fish. *Pigment Cell Melanoma Res.* **23**, 314–337.

Patton, E. E., Widlund, H. R., Kutok, J. L., Kopani, K. R., Amatruda, J. F., Murphey, R. D., Berghmans, S., Mayhall, E. A., Traver, D., and Fletcher, C. D., *et al*. (2005). BRAF mutations are sufficient to promote nevi formation and cooperate with p53 in the genesis of melanoma. *Curr. Biol.* **15**, 249–254.

Pavelic, K., Hrascan, R., Kapitanovic, S., Karapandza, N., Vranes, Z., Belicza, M., Kruslin, B., and Cabrijan, T. (1995). Multiple genetic alterations in malignant metastatic insulinomas. *J. Pathol.* **177**, 395–400.

Pavelic, K., Hrascan, R., Kapitanovic, S., Vranes, Z., Cabrijan, T., Spaventi, S., Korsic, M., Krizanac, S., Li, Y. Q., and Stambrook, P., *et al*. (1996). Molecular genetics of malignant insulinoma. *Anticancer Res.* **16**, 1707–1717.

Phelps, R. A., Chidester, S., Dehghanizadeh, S., Phelps, J., Sandoval, I. T., Rai, K., Broadbent, T., Sarkar, S., Burt, R. W., and Jones, D. A. (2009). A two-step model for colon adenoma initiation and progression caused by APC loss. *Cell* **137**, 623–634.

Raetz, E. A., Perkins, S. L., Bhojwani, D., Smock, K., Philip, M., Carroll, W. L., and Min, D. J. (2006). Gene expression profiling reveals intrinsic differences between T-cell acute lymphoblastic leukemia and T-cell lymphoblastic lymphoma. *Pediatr. Blood Cancer* **47**, 130–140.

Rai, K., Sarkar, S., Broadbent, T. J., Voas, M., Grossmann, K. F., Nadauld, L. D., Dehghanizadeh, S., Hagos, F. T., Li, Y., and Toth, R. K., *et al*. (2010). DNA demethylase activity maintains intestinal cells in an undifferentiated state following loss of APC. *Cell* **142**, 930–942.

Rhodes, J., Amsterdam, A., Sanda, T., Moreau, L. A., McKenna, K., Heinrichs, S., Ganem, N. J., Ho, K. W., Neuberg, D. S., and Johnston, A., *et al*. (2009). Emi1 maintains genomic integrity during zebrafish embryogenesis and cooperates with p53 in tumor suppression. *Mol. Cell. Biol.* **29**, 5911–5922.

Sabaawy, H. E., Azuma, M., Embree, L. J., Tsai, H. J., Starost, M. F., and Hickstein, D. D. (2006). TEL-AML1 transgenic zebrafish model of precursor B cell acute lymphoblastic leukemia. *Proc. Natl. Acad. Sci. U. S. A.* **103**, 15166–15171.

Sahai, E. (2007). Illuminating the metastatic process. *Nat. Rev. Cancer* **7**, 737–749.

Shepard, J. L., Amatruda, J. F., Stern, H. M., Subramanian, A., Finkelstein, D., Ziai, J., Finley, K. R., Pfaff, K. L., Hersey, C., and Zhou, Y., *et al*. (2005). A zebrafish bmyb mutation causes genome instability and increased cancer susceptibility. *Proc. Natl. Acad. Sci. U. S. A.* **102**, 13194–13199.

Sidi, S., Sanda, T., Kennedy, R. D., Hagen, A. T., Jette, C. A., Hoffmans, R., Pascual, J., Imamura, S., Kishi, S., and Amatruda, J. F., *et al*. (2008). Chk1 suppresses a caspase-2 apoptotic response to DNA damage that bypasses p53, Bcl-2, and caspase-3. *Cell* **133**, 864–877.

Smith, A. C., Raimondi, A. R., Salthouse, C. D., Ignatius, M. S., Blackburn, J. S., Mizgirev, I. V., Storer, N. Y., de Jong, J. L., Chen, A. T., and Zhou, Y., *et al*. (2010). High-throughput cell transplantation establishes that tumor-initiating cells are abundant in zebrafish T-cell acute lymphoblastic leukemia. *Blood* **115**, 3296–3303.

Stern, H. M., Murphey, R. D., Shepard, J. L., Amatruda, J. F., Straub, C. T., Pfaff, K. L., Weber, G., Tallarico, J. A., King, R. W., and Zon, L. I. (2005). Small molecules that delay S phase suppress a zebrafish bmyb mutant. *Nat. Chem. Biol.* **1**, 366–370.

Stokoe, D. (2001). Pten. *Curr. Biol.* **11**, R502.

Stoletov, K., Kato, H., Zardouzian, E., Kelber, J., Yang, J., Shattil, S., and Klemke, R. (2010). Visualizing extravasation dynamics of metastatic tumor cells. *J. Cell Sci.* **123**, 2332–2341.

Stoletov, K., and Klemke, R. (2008). Catch of the day: zebrafish as a human cancer model. *Oncogene* **27**, 4509–4520.

Stoletov, K., Montel, V., Lester, R. D., Gonias, S. L., and Klemke, R. (2007). High-resolution imaging of the dynamic tumor cell vascular interface in transparent zebrafish. *Proc. Natl. Acad. Sci. U. S. A.* **104**, 17406–17411.

Sun, H., Lesche, R., Li, D. M., Liliental, J., Zhang, H., Gao, J., Gavrilova, N., Mueller, B., Liu, X., and Wu, H. (1999). PTEN modulates cell cycle progression and cell survival by regulating phosphatidylinositol 3,4,5-trisphosphate and Akt/protein kinase B signaling pathway. *Proc. Natl. Acad. Sci. U. S. A.* **96**, 6199–6204.

Suster, M. L., Kikuta, H., Urasaki, A., Asakawa, K., and Kawakami, K. (2009). Transgenesis in zebrafish with the tol2 transposon system. *Methods Mol. Biol.* **561**, 41–63.

Taylor, K. L., Grant, N. J., Temperley, N. D., and Patton, E. E. (2010). Small molecule screening in zebrafish: an *in vivo* approach to identifying new chemical tools and drug leads. *Cell Commun. Signal.* **8**, 11.

Taylor, A. M., and Zon, L. I. (2009). Zebrafish tumor assays: the state of transplantation. *Zebrafish* **6**, 339–346.

Thayer, S. P., di Magliano, M. P., Heiser, P. W., Nielsen, C. M., Roberts, D. J., Lauwers, G. Y., Qi, Y. P., Gysin, S., Fernandez-del Castillo, C., and Yajnik, V., *et al*. (2003). Hedgehog is an early and late mediator of pancreatic cancer tumorigenesis. *Nature* **425**, 851–856.

Topczewska, J. M., Postovit, L. M., Margaryan, N. V., Sam, A., Hess, A. R., Wheaton, W. W., Nickoloff, B. J., Topczewski, J., and Hendrix, M. J. (2006). Embryonic and tumorigenic pathways converge via Nodal signaling: role in melanoma aggressiveness. *Nat. Med.* **12**, 925–932.

van Rooijen, E., Voest, E. E., Logister, I., Bussmann, J., Korving, J., van Eeden, F. J., Giles, R. H., and Schulte-Merker, S. (2010). von Hippel–Lindau tumor suppressor mutants faithfully model pathological hypoxia-driven angiogenesis and vascular retinopathies in zebrafish. *Dis. Model Mech.* **3**, 343–353.

Vlecken, D. H., and Bagowski, C. P. (2009). LIMK1 and LIMK2 are important for metastatic behavior and tumor cell-induced angiogenesis of pancreatic cancer cells. *Zebrafish* **6**, 433–439.

Wang, C., Tao, W., Wang, Y., Bikow, J., Lu, B., Keating, A., Verma, S., Parker, T. G., Han, R., and Wen, X. Y. (2010). Rosuvastatin, identified from a zebrafish chemical genetic screen for antiangiogenic compounds, suppresses the growth of prostate cancer. *Eur. Urol.* **58**, 418–426.

Wheeler, G. N., and Brandli, A. W. (2009). Simple vertebrate models for chemical genetics and drug discovery screens: lessons from zebrafish and *Xenopus*. *Dev. Dyn.* **238**, 1287–1308.

White, R. M., Sessa, A., Burke, C., Bowman, T., LeBlanc, J., Ceol, C., Bourque, C., Dovey, M., Goessling, W., Burns, C. E., and Zon, L. I. (2008). Transparent adult zebrafish as a tool for *in vivo* transplantation analysis. *Cell Stem Cell* **2**, 183–189.

Wienholds, E., van Eeden, F., Kosters, M., Mudde, J., Plasterk, R. H., and Cuppen, E. (2003). Efficient target-selected mutagenesis in zebrafish. *Genome Res.* **13**, 2700–2707.

Yang, H. W., Kutok, J. L., Lee, N. H., Piao, H. Y., Fletcher, C. D., Kanki, J. P., and Look, A. T. (2004). Targeted expression of human MYCN selectively causes pancreatic neuroendocrine tumors in transgenic zebrafish. *Cancer Res.* **64**, 7256–7262.

Yeh, J. R., Munson, K. M., Chao, Y. L., Peterson, Q. P., Macrae, C. A., and Peterson, R. T. (2008). AML1-ETO reprograms hematopoietic cell fate by downregulating scl expression. *Development* **135**, 401–410.

Yeh, J. R., Munson, K. M., Elagib, K. E., Goldfarb, A. N., Sweetser, D. A., and Peterson, R. T. (2009). Discovering chemical modifiers of oncogene-regulated hematopoietic differentiation. *Nat. Chem. Biol.* **5**, 236–243.

Zhang, G., Hoersch, S., Amsterdam, A., Whittaker, C. A., Lees, J. A., and Hopkins, N. (2010). Highly aneuploid zebrafish malignant peripheral nerve sheath tumors have genetic alterations similar to human cancers. *Proc. Natl. Acad. Sci. U. S. A.* **107**, 16940–16945.

Zhuravleva, J., Paggetti, J., Martin, L., Hammann, A., Solary, E., Bastie, J. N., and Delva, L. (2008). MOZ/TIF2-induced acute myeloid leukaemia in transgenic fish. *Br. J. Haematol.* **143**, 378–382.

CHAPTER 14

Generating and Analyzing Fish Models of Melanoma

E. Elizabeth Patton[*], Marie E. Mathers[†] and Manfred Schartl[‡]

[*]MRC Human Genetics Unit & Edinburgh Cancer Research Centre, The University of Edinburgh, Edinburgh, EH4 2XR, Scotland, UK

[†]Department of Pathology, Western General Hospital, Edinburgh, EH4 2XU, Scotland, UK

[‡]University of Würzburg, Physiological Chemistry I, Biocenter, Am Hubland, Würzburg 97074, Germany

METHODS IN CELL BIOLOGY, VOL 105

0091-679X/10 $35.00
DOI 10.1016/B978-0-12-381320-6.00014-X

Abstract

Melanoma is the most deadly form of skin cancer and incidence continues to rise rapidly (Gray-Schopfer *et al*., 2007). Melanoma develops from melanocytes, the pigmented cells that color our skin, hair, and eyes. Fish also have melanocytes, among other pigment cell types, and the fish and human developmental programme are highly conserved (Kelsh, 2004). The first fish models of melanoma were established in *Xiphophorus*, and more recently, transgenic melanoma models in zebrafish and medaka have been developed (Meierjohann and Schartl, 2006; Patton *et al*., 2010; Schartl *et al*., 2010). In this Chapter, we describe the basic techniques to generate genetic, environmental, and transgenic models of melanoma, discuss diagnoses, and describe standard molecular analysis techniques.

I. Introduction

A. Melanoma

Melanoma is a cancer of melanocytes, the pigment producing cells that determine the color of our hair, skin, and eyes. It is the deadliest form of skin cancer, and people diagnosed with metastatic melanoma have an average life expectancy of less than 1 year (Ko and Fisher, 2011). UV exposure is the greatest risk factor for melanoma for people with fair skin, and sun bed use has propelled melanoma incidence to one of the fastest growing cancers in fair skinned young women (Garibyan and Fisher, 2010).

Melanoma is characteristically highly invasive and resistant to standard chemotherapeutics. Recently, inhibitors of the mutated form of BRAF have been developed and have led to the greatest advance in the history of metastatic melanoma therapy (Flaherty *et al*., 2010, 2011). Despite this advance, melanomas have already shown resistance to BRAF inhibitors and identifying other targets of melanoma remains critical (Johannessen *et al*., 2010; Ko and Fisher, 2011; Little *et al*., 2011).

Melanoma is histopathologically characterized by a series of steps, from proliferation of normal melanocytes to metastatic tumors. Activation of MAPK-signaling has a central role in melanocyte proliferation: 15–20% of nevi (commonly known as moles) and melanoma carry N-RAS mutations and 50–80% carry BRAF mutations (Gray-Schopfer *et al*., 2007). Most nevi remain static for decades, and the similar incidence of BRAF mutations in nevi and in melanoma suggest that additional molecular changes are required for melanoma development. The ARF-MDM2-p53 pathway is frequently altered by loss of CDKN2A, a single locus encoding the cell cycle regulators INK4A and ARF (Chin *et al*., 2006). Loss of CDKN2A is frequently found in melanoma prone families, highlighting the importance of the ARF-MDM2-p53 and INK4A-CDK4/6-RB pathways in melanoma. Other

important genetic alterations in melanoma progression include loss of the tumor suppressor PTEN that modulates PI3K-AKT survival signaling (Dankort *et al*., 2009); amplification and mutation of the lineage survival gene, MITF (Cronin *et al*., 2009; Garraway *et al*., 2005); changes in cell adhesion molecules, including amplification of NEDD9 to promote cell invasion and metastasis (Kim *et al*., 2006); and dependence on protein trafficking genes TBC1D16 and RAB27A (Akavia *et al*., 2010; Johannessen *et al*., 2010; Little *et al*., 2011).

B. Melanoma Genetics in Fish

Like other vertebrates, fish develop benign and malignant tumors, with similar histological, molecular, and pathological features to human cancers (Amatruda *et al*., 2002; Spitsbergen *et al*., 2000a, 2000b). Histopathological analysis indicates that fish tumors share many salient features with the cancers derived from the analogous tissue in humans (see below). These features are further mirrored in their shared molecular features. For example, the molecular signatures of the progressive stages of liver neoplasia – from adenoma to carcinoma – are shared between zebrafish and human (Lam *et al*., 2006).

A detailed knowledge of the cellular, molecular, and genetic events during melanoma progression is highly relevant to both diagnosis and the development of new therapies. Because of the similarities between humans and fish, melanoma progression models in fish can be viewed as a starting point for identifying novel genes, environmental conditions, and therapeutic compounds that affect melanoma progression, and is a major justification for using animals in this research (Table I).

1. Xiphophorus

The *Xiphophorus* model offers the opportunity to study spontaneous as well as UV- and carcinogen-induced melanoma in the natural genetic context (Meierjohann and Schartl, 2006) (Fig. 1A,B). However, due to the fact that these fish are livebearing, transgenic technologies are not developed. Nevertheless, this model is quite useful because it provides clear-cut genetics in the context of hereditary melanoma development that enabled the isolation of a melanoma oncogene termed *xmrk* (for Xiphophorus melanoma receptor kinase). This gene is a mutant version of the epidermal growth factor receptor, which is constitutively active. In wild-type fish, *xmrk* is under the control of a tumor suppressor locus, termed *R* or *Diff* (whose molecular identity is still unknown) (Adam *et al*., 1993; Wittbrodt *et al*., 1989, Table I). In this situation the repressed action of *xmrk* leads only to nevus like pigment spots. As *xmrk* and *R* are located on different chromosomes, they can be separated by simple breeding crosses utilizing fish of related species. In the heterozygous condition, *xmrk* can induce benign melanocytic lesions or hyperpigmentation. In the absence of *R*, *xmrk* is overexpressed in melanocytes and triggers the

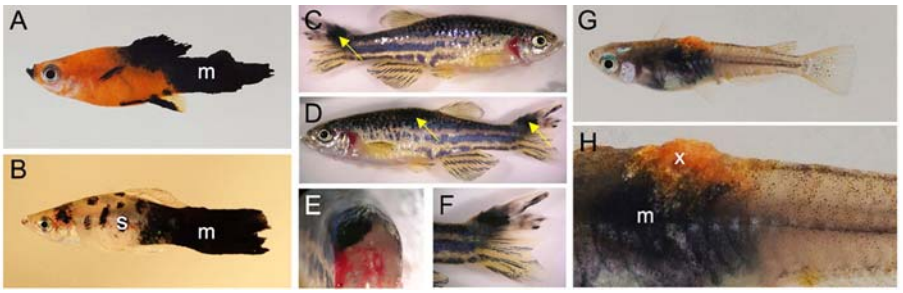

Fig. 1 Laboratory fish with melanoma. Examples of *Xiphophorus*, zebrafish, and medaka melanoma models. (A) *Xiphophorus* backcross hybrid from the classical cross with darkly pigmented, spontaneous malignant melanoma (B) *Xiphophorus* backcross hybrid (hybrid 1 cross) with UV-induced melanoma. Note, this fish has both benign spots (s) and melanoma (m). (C–F) Zebrafish $BRAF^{V600E}$ transgenic fish develop melanoma in the *p53* mutant background. Both (E) endophytic melanoma in the body and (F) exophytic melanoma on the tail are present. (G, H) Medaka expressing the *xmrk* transgene with both black (invasive) melanoma (m) and orange (exophytic) xanthoerythrophoroma (x). (See color plate.)

development of highly malignant melanoma. In certain *Xiphophorus* crosses, fish that would otherwise not develop melanoma spontaneously do so when irradiated with UV as newborns. Similarly some hybrid genotypes show a high susceptibility for carcinogen-induced melanoma, while in others melanoma induction is more rare (Patton *et al*., 2010).

Analyzing the oncogenic signal transduction elicited by the pigment cell specific overexpression of Xmrk has uncovered common pathways of mammalian and fish melanoma cell development (some even detected first in the fish model). Notably, this model illustrates how a single activated oncogene can trigger all the changes necessary for the transformation of a normal melanocyte to a fully malignant melanoma cell (Meierjohann and Schartl, 2006). It should be noted that this progress was only possible because initial findings from the *Xiphophorus* fish system were further elaborated in defined mouse and human cell culture systems expressing the fish oncogene. Subsequently, these findings obtained in the *in vitro* systems were evaluated in the *in vivo Xiphophorus* melanoma fish (Meierjohann *et al*., 2006; Morcinek *et al*., 2002; Teutschbein *et al*., 2010; Wellbrock *et al*., 2002).

2. Zebrafish

As with *Xiphophorus* and medaka, an advantage of the zebrafish system is that large numbers of zebrafish can be grown within the laboratory at relatively low cost. Zebrafish fertilize their eggs externally, and hundreds of single-cell embryos can be collected each week from a pair of fish. The embryos are transparent, and key aspects of embryogenesis – from the first cell division to organogenesis to melanocyte pigmentation – can be viewed under the light microscope. The zebrafish genome is sequenced, and importantly, cancer and tumor suppressor genes are conserved

between fish and humans, as are key signaling, DNA damage, apoptosis, and senescence pathways.

A model for melanoma progression has been developed in zebrafish based on the most frequently mutated human gene in melanoma, BRAF (Patton *et al*., 2005, Table I). Expression of $BRAF^{V600E}$ in melanocytes causes the development of nevi that are stable and do not become malignant but have the potential for recurrence from undifferentiated precursor cells (Richardson *et al*., 2011). These $BRAF^{V600E}$ nevi develop into melanoma when expressed in a *p53* mutant line (Fig. 1C–F) (Patton *et al*., 2005). This model has contributed an important insight into the genetics of nevi and melanoma development by demonstrating the causal effect of the $BRAF^{V600E}$ mutation, first identified by the sequencing efforts of the Cancer Genome Project (Davies *et al*., 2002). Recently, the histone methyltransferase SETDB1 was found to be amplified in human melanoma, and shown to accelerate $BRAF^{V600E}$*p53* mutant zebrafish melanoma progression (Ceol *et al*., 2011, Table I). In addition, small molecule screens in $BRAF^{V600E}$ zebrafish have identified chemical inhibitors of dihydroorotate dehydrogenase that can prevent neural crest development and are active against human melanoma cells (White *et al*., 2011).

RAS is also an important oncogene in melanoma, and expression of RAS mutations in zebrafish can promote melanoma development (Dovey *et al*., 2009; Michailidou *et al*., 2009; Santoriello *et al*., 2009, 2010, Table I). RAS melanomas develop from undifferentiated precursor populations and transgenic fluorescent reporter lines allow for visualization of developing cancerous cells, and individual cancer cells interacting with the immune system (Feng *et al*., 2011). Finally, while beyond the scope of this chapter, transplantations of mammalian melanoma cells into zebrafish larvae and adults (White *et al*., 2008) is providing a novel platform for melanoma gene discovery, cancer biology, and small molecule screening (Patton *et al*., 2010).

3. Medaka

Medaka have similar features and comparable advantages for melanoma research as zebrafish. Notably, in the medaka system, a number of highly inbred lines of different geographic or genetic origin are available. So far, only one melanoma model has been developed in this fish (Fig. 1G,H). The melanoma oncogene of *Xiphophorus*, *xmrk*, was placed under the pigment cell specific promoter from the *mitfa* gene of medaka (Schartl *et al*., 2010, Table I). Remarkably, this is the only fish oncogene used so far and the only fish sequence to drive tumor formation, because all other transgenic models use the human oncogenes. The transgenic medaka developed various types of pigment cell tumors, including melanoma of the skin and at extracutaneous sites (e.g., the uvea or the meninx of the spinal cord), and xanthoerythrophoromas of the skin. The melanomas were usually more aggressive than the xanthoerythrophoromas and showed a greater invasiveness and metastatic progression.

When the *xmrk* transgene was introduced into several of the medaka inbred lines it revealed that the types of tumors that develop strongly depend on the genetic background. Although the *xmrk* tumors in medaka are not dependent on the absence of p53, when expressed in a *p53-/-* background additional focal, more rapidly growing and more aggressive tumors developed. On the molecular level the medaka tumors showed the expected upregulation of several signaling pathways known to be activated by Xmrk and to be relevant for bringing about the full neoplastic phenotype of malignant cells, for example AKT, Stat5, and enhanced Mitf protein. These studies demonstrate how the genetic context and background can shape the tumor spectrum and the pathology. This medaka *xmrk* model provides a framework for future genetic and chemical screens to identify the modifiers of melanoma pathology (Patton and Nairn, 2010).

C. Rationale

Fish provide a number of advantages for functional studies and high throughput approaches, including drug screens (Taylor *et al*., 2010; White *et al*., 2011). For studying melanoma, fish models have an additional relevance for studying the processes in primary tumor development and disease progression. In rodents, unlike in humans, the melanocytes are locally restricted to the hair follicle and not distributed throughout the epidermis (Kelsh *et al*., 2009). Due to this position, murine melanocytes are sheltered from the carcinogenic action of UV. Mice, with the exception of some specifically engineered transgenic models, are thus refractory to UV melanoma induction and spontaneous melanoma in rodents is relatively unknown. Fish, on the other hand, share the human skin architecture for melanocyte localization and spontaneous and UV melanoma formation occur in multiple fish species.

This Chapter aims to provide the interested researcher with an overview of the existing melanoma models in zebrafish, medaka, and *Xiphophorus* allowing the right model to be chosen for specific questions and experimental studies. Those who want to create their own model will find some guidelines for generating the corresponding transgenic lines. UV is considered to be the major risk factor for human melanoma, and therefore UV irradiation of fish is also described in this Chapter. We present the basis of melanoma diagnosis and key pathological features based on routine experience with fish melanoma in our laboratories. The heavy pigment content of melanoma cells sometimes can interfere with immunohistochemical and biochemical procedures for characterizing and analyzing fish melanoma and needs to be considered. On the other hand, the black pigmentation together with their location in the skin makes the tumors easily detectable at the earliest stage of development without the need for sacrificing the fish or using complicated bioimaging approaches and instrumental setups.

Table I
Examples of transgenes and genetic crosses used to study melanoma in laboratory fish

Species	Diagnosis	Gene/ transgene	Co-operating genes	Environment	Reference (example)
Xiphophorus	Nevi/spotted	*Xmrk*	R or *Diff*		(Adam *et al*., 1993; Wittbrodt *et al*., 1989)
Xiphophorus	Melanoma	*Xmrk*			(Adam *et al*., 1993; Wittbrodt *et al*., 1989)
Xiphophorus	Melanoma	*Xmrk*	R or *Diff*	UV exposure	(Setlow *et al*., 1989) (Setlow *et al*., 1993) (Nairn *et al*., 1996) (Mitchell *et al*., 2010)
Zebrafish	Nevi	$BRAF^{V600E}$			(Patton *et al*., 2005)
Zebrafish	Melanoma	$BRAF^{V600E}$	*p53* loss of function		(Patton *et al*., 2005)
Zebrafish	Nevi	$NRAS^{Q61K}$			(Dovey *et al*., 2009)
Zebrafish	Melanoma	$NRAS^{Q61K}$	*p53* loss of function		(Dovey *et al*., 2009)
Zebrafish	Melanoma	$HRAS^{G12V}$			(Michailidou *et al*., 2009; Santoriello *et al*., 2009; Santoriello *et al*., 2010)
Zebrafish	Melanoma	$BRAF^{V600E}$	*p53* loss of function SETDB1 over-expression		(Ceol *et al*., 2011)
Zebrafish	DNA damage			UV exposure	(Zeng *et al*., 2009)
Medaka	Nevi	*Xmrk*			(Schartl *et al*., 2010)
Medaka	Melanoma	*Xmrk*	*p53* loss of function		(Schartl *et al*., 2010)
Medaka	Melanoma	*Xmrk*	*Backgrounds*		(Schartl *et al*., 2010)

II. Transgenic Melanoma Lines in Zebrafish and Medaka

Generating transgenic animals in zebrafish for cancer studies uses the same basic techniques as generating other zebrafish transgenic lines, and generating transgenic medaka follows the principles established for zebrafish (Nusslein-Volhard C, 2002).

There are a few points, however, that need to be considered, which are unique to medaka:

1. The chorion of medaka is much harder, but can be penetrated with glass injection needles (Fig. 2). This requires strong needles (prepared from Borosilicate glass capillaries, 1.0 – 1.2 mm diameter) of similar shape as used for zebrafish, however, the tip should be shorter (see Fig. 2) and not flexible. More force to penetrate the chorion than for zebrafish is necessary, but with some practice, microinjection of freshly fertilized medaka eggs becomes simple and routine.

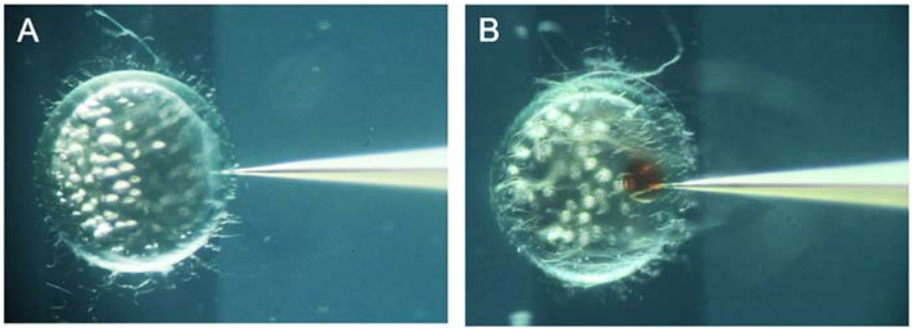

Fig. 2 Medaka transgenic microinjection equipment and procedure. Microinjection into the cytoplasm of a one-cell-stage embryo of medaka. (A) Position of the tip of the injection needle in the cytoplasm after penetration of the chorion and cell membrane before applying injection pressure. (B) Injected cell just before retraction of the needle. The red droplet of injection fluid has reached a size that does not interfere with further development (Photograph: Peter Fischer, Würzburg). (For color version of this figure, the reader is referred to the web version of this book.)

Thereafter, the chorion hardens considerably during the first hours of development and is not suited for microinjection anymore.

2. The maximum concentration for DNA injection into medaka embryos is less than 50 ng/μl, which is lower than what can be used in zebrafish. Nevertheless, the transgenic rates are comparable.
3. As for zebrafish, it is mandatory to inject the one cell stage embryo, because transgenic rates decrease considerably by the 2-cell stage and get close to zero after this stage. To have enough embryos suitable for microinjection it is possible to store the freshly laid and just fertilized eggs at 4 °C in embryo rearing medium (ERM) for up to 2 h and use them as needed. Alternatively, mating pairs can be reunited at different intervals, up to 6 h after the light turned on, without apparent negative effects on the microinjection procedure.
4. Microinjection has to be done directly into the cytoplasm of the cell; thus the fertilized egg is positioned to the injection needle so that the cell faces the needle (Fig. 2). Injection through the yolk is inefficient and not recommended.
5. Vector systems, plasmids, and BAC transgenesis can be used, essentially as described for zebrafish. For plasmids, the meganuclease technology (Grabher and Wittbrodt, 2008) has shown an advantage for obtaining higher rates of stable transgenic lines. The Tol2 system cannot be used in medaka for making transgenic lines, as Tol2 is an active DNA-based transposable element in the medaka and due to its endogenous activity is not suitable as a vector integration tool. Other transposon-based strategies, however, work in medaka like in zebrafish, for example the Sleeping Beauty system. Besides stable transgenesis, for analytical purposes microinjection of capped mRNAs and morpholinos can be performed in medaka similar as in zebrafish. Due to the longer embryonic development of medaka it should be considered that morpholinos will be effective only up to a

few days after hatching but efficiency decreases strongly 5 to 6 days post injection.

All medaka strains can be used as recipient lines for transgenic experiments, but unexperienced experimenters might consider the more hardy outbred lines, like Cab or HdrR, for their first attempts. Medaka strains are provided by the medaka stock center of the NRBB at Okazaki (Japan). For further information see: http://www.shigen.nig.ac.jp/medaka/

For melanocyte specific expression of oncogenes in medaka, so far, only the mitfa promoter from medaka has been used. 1057 bp upstream of the sequence of this gene (ENSORLG00000003123) are sufficient to drive transgene expression specifically in the pigment cell lineage. This promoter in medaka is not only active in melanocytes but also in the yellow xanthophores and the red erythrophores. Thus, an oncogene driven by this promoter led to tumors of the black and the red/yellow cell lineage; this is different from analogous constructs in zebrafish (Schartl *et al*., 2010).

A. Medaka Microinjection Protocol

The instrumentation needed for microinjection of medaka fertilized eggs is identical to that used for zebrafish (Nusslein-Volhard C, 2002). Researchers with no previous experience in raising medaka and handling medaka embryos are, however, advised to consult additional literature, for example the medaka handbook (Kinoshita *et al.*, 2009).

1. Separate males and females the evening before the microinjection day. Make sure to use only females that had eggs the same day, as they are most likely to easily spawn again the next day. After onset of light, put mating pairs together immediately before injection. Do not disturb fish while mating. Collect the egg clutch from the female and transfer to a petri dish with ERM. Remove hairs by gently rolling the egg clutch over the bottom of the dish until all eggs are singularized. Alternatively, the hairs can be removed with fine forceps. Transfer to a new dish with ERM.
2. Place fertilized eggs to a channel of the agar egg holder (filled with ERM) and orientate so that the cell is on top and faces the injection needle.
3. Have the microinjection apparatus prepared and the microinjection needle filled bubble-free with 3 – 5 μl of DNA solution (containing 0.1% phenol red). Dip the needle tip into ERM. Apply pressure ("inject"), break the needle, for example by touching the envelope surface of an egg and then sliding the egg holder back and forwards. Red outflow confirms that the tip is open. If this does not work, use fine forceps for opening the needle (carefully!).
4. Adjust injection pressure to 500 – 1250 hPa and compensation pressure to 50 – 200 hPa (to avoid strong outflow of injection fluid). Put to compensation pressure.

5. Start microinjection by positioning the next egg. Approach the egg gently until the tip touches the chorion and makes a visible indent. Push the tip through the chorion and then through the cell membrane into the cytoplasm and apply injection pressure. Red injection fluid starts to flow when the cytoplasm is reached. Avoid pushing the needle too deeply, because then injection fluid will leak out into the yolk. When the red droplet in the cytoplasm has reached the desired volume (up to half of the cell volume, see Fig. 2B), gently retract the needle.
6. Stop applying pressure. Re-adjust injection and compensation pressures, if necessary, before injecting the next egg.
7. Collect injected eggs, transfer to Petri dish with fresh ERM and incubate at 25 °C.
8. Inspect daily and remove dead embryos. Embryos damaged by the microinjection procedure will disintegrate and turn blue within 1 day. Death or abortive development due to overdose of the injected DNA, RNA, or morpholino can occur up to several days after injection.

Medaka ERM:

100 × stock: 50 g NaCl, 1.5 g KCl, 2 g $CaCl_2 \times 2H_2O$, 8 g $MgSO_4 \times 7H_2O$ in 500 ml distilled water. Alternatively, 0.33 × Danieau's solution or distilled water can be used. To limit bacterial growth, add 0.0001% methyleneblue to the embryo medium. The additional advantage of methyleneblue is that it stains dead embryos dark blue, so that they can be easily removed immediately. A disadvantage is that embryos take up some of the dye in the yolk, which then gives rise to strong autofluorescence that disturbs for instance observation of GFP or other fluorescence.

1. Crossing Procedures for Obtaining *Xiphophorus* Tumors

Large nevi, benign tumors, pre-malignant lesions, and spontaneous and UV-induced malignant melanoma are obtained from hybrid *Xiphophorus* genotypes. Parental strains are available from the *Xiphophorus* stock center at San Marcos (Texas) and listed in the stock center manual (http://www.xiphophorus.txstate.edu/). Researchers inexperienced with maintaining and propagating *Xiphophorus* fish will find there detailed information as well as in Kallman (1975) in Handbook of Genetics (King, ed).

Spontaneous Melanoma and Pigment Lesions

For spontaneous malignant melanoma and benign pigment lesions, the classical Gordon-Kosswig-Anders cross (hybrid 1 cross) is recommended because of its clear genetics and large amounts of information on the molecular and biochemical processes underlying neoplastic transformation. For the parental cross use virgin females of *Xiphophorus hellerii*, strain Rio Lancetilla, Db-, and male *Xiphophorus maculatus*, strain Jp163A.

Note: This is an interspecific cross, which needs artificial insemination, because these fish do not mate naturally. Artificial insemination is described in detail at http://www.xiphophorus.txstate.edu/research.html. F1 fish show many aspects of

hybrid vigor, including larger size than the parentals. This is also true for the F1 embryos, which are especially large. Thus, only the larger of the two parental species, *X. hellerii,* should be used as the maternal fish. *X. maculatus* females may suffer and sometimes die from the enormous growing hybrid embryos.

F1 fish are born 3 weeks after artificial insemination, but it can take up to 6 weeks for broods to come to term. Due to sex chromosome linkage of two different melanoma pre-disposing loci (X-chromosome: spotted dorsal pattern (Sd) = $mdl^{Sd}xmrk^{B}$; Y-chromosome: striped pattern (Sr) = $mdl^{Sr}xmrk^{A}$) the F1 fish will segregate in Sd fish with large nevi over the whole dorsal fin, which mostly will become female, and Sr fish with a only slightly enhanced striped pattern on the flanks. Use the Sd females for setting up crosses with *X. hellerii* males to produce a backcross generation. These will mate unassisted and no artificial insemination is necessary anymore.

Backcross fish will segregate phenotypically: 50% of fish will be whole-body gray and look like *X. hellerii*; 25% will have giant nevi over the whole dorsal fin, occasionally with some large spots around the base of the dorsal fin, the dorsal midline and the tail fin; and 25% will have malignant melanoma (Fig. 1A). The classes with the two types of pigment cell lesions are often not clearly separated and there is a phenotypic continuum of some fish with very heavy hyperpigmentation and some signs of invasiveness from the giant nevi, to fish with only mildly malignant tumors (the fish even reach a normal age). These borderline phenotypes should not be used for comparative studies of malignant versus benign lesions. Backcross fish can be genotyped (for instance for presence of the *R/Diff* locus) using microsatellite markers (Kazianis *et al*. (1998); Kazianis *et al*. (2004)).

UV-induced Melanoma Crosses

For UV induction of melanoma, different crosses (hybrid1 and hybrid7 crosses) are used. A similar crossing procedure as above is followed, however, this time with a male from the *X. maculatus* strain Jp163B (X-chromosome: spotted pattern (Sp) = $mdl^{Sp}xmrk^{B}$; Y-chromosome: striped pattern (Sr) = $mdl^{Sr}xmrk^{A}$). Only the Sp females of the F1 generation are used for backcross to *X. hellerii*. The backcross segregates into 50% gray *X. hellerii*-type fish and 50% that have inherited the Sp locus. These will segregate in half of the fish with prominent spotting and half that will develop more severe hyperpigmentation with some signs of progression to malignancy. UV will induce highly malignant melanoma in both classes (Fig. 1B). Alternatively, instead of *X. hellerii* another species, *X. couchianus,* can be used as the recurrent parent for the backcross. This has the advantage that no strong hybrid vigor and oversized embryos are produced, so females of *X. maculatus* Jp163B can be used and all F1 fish can be mated for producing offspring. In addition, these two species mate if put together in a tank and no artificial insemination is necessary (however, make sure that the parental fish do not see conspecifics through the glass in a neighboring aquarium). The Sp carrying backcross segregants show light and heavy pigmented patterns, both of which can be used for UV-induction of melanoma.

III. Ultra-violet Irradiation Treatments

Ultra-violet light is an established risk factor for melanoma (Garibyan and Fisher, 2010; Mitchell and Fernandez, 2011). Sun exposure, especially exposure that leads to burning, and sun-bed use significantly enhance melanoma risk. There is a strong correlation between skin pigmentation, UV-exposure, and melanoma risk. Recent analysis of the melanoma genome reveals that UV-induced DNA damage plays a significant role in altering the genome (Pleasance *et al*., 2010). UV also induces DNA damage in fish, and plays a critical role in promoting melanoma in *Xiphophorus* (Mitchell and Nairn, 2006). Laboratory fish can be exposed to UV light while in the water and without anesthetic, limiting the amount of stress experienced by the fish. Of note, unlike humans, fish have a photoactivated UV damage repair system (Mitchell *et al*., 2009) and so it is important for the fish to be in the dark before and after UV treatment.

Here we describe the set-up of a UV-irradiation box for treating laboratory fish based on the design by David Mitchell (University of Texas, MD Anderson Cancer Centre). Details of the UV irradiation box are shown in Fig. 3. The UVB source is four UVB lamps emitting 311 – 312 nm light (TL 20W/01, Philips). UVB was quantified with a UVB detector (SEL005/WBS320/TD, International Light) coupled to a radiometer (ILT1400A, International Light).

For the induction of melanoma in *Xiphophorus* hybrids details on treatment protocols and dosage can be found in Mitchell *et al*. (2010).

A. Protocol for UVB Treatment of Laboratory Fish

Day 1: Twenty-four hours prior to irradiation, fish were moved to a dark room to prevent exposure to visible light.
Day 2:

1. In the dark room equipped with a yellow light lamp, turn on and warm up the UVB lamps for 10 min prior to irradiation.
2. Transfer fish to the irradiation box for immediate UVB exposure. The irradiation, chamber is filled with fish water, so that the fish swim freely during the, course of the experiment. The duration of UVB exposure depends on the, developmental stage and body size of fish. For example, to induce melanoma, in Xiphophorus, the dose is usually near to or less than half of LD50 (e.g. 6.4 kJ/m^2 at 12.2 J/m^2/sec each day; total dose = 32 kJ/m^2 using TL01 Philips narrow band UVB lamp). Xiphophorus are exposed daily at this dose for 5 days beginning at 5 days after live birth. To induce DNA damage in zebrafish skin we exposed adult fish to a UVB dose rate, from both sides at 6 J/M^2/s, for 0.36 kJ/m^2 or 60 s for 6-day-old larvae and 1.08 kJ/m^2 or 180 s for 6-week-old young adult fish (Zeng *et al*., 2009).
3. After UVB exposure, fish are returned to fish tanks and remain in the dark room for the first 24 h to avoid light-dependent PER.

Day 3: Return fish to the aquarium.

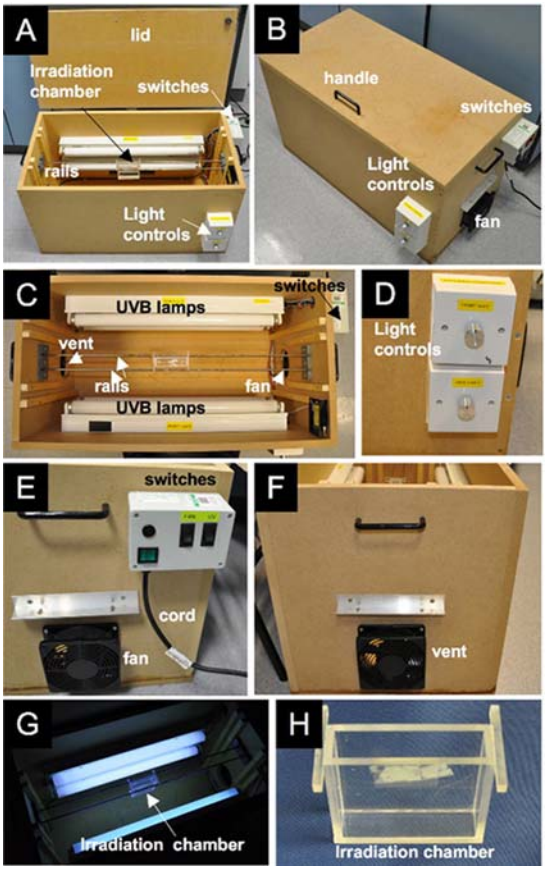

Fig. 3 UV-irradiation box for laboratory fish. (A) The irradiation box is approximately 1 m wide. Two UVB lamps are attached to each side of the box, and are controlled by light controls on the outside of the box. Two parallel rails extend horizontally along the middle of the box, and hold the UV permeable irradiation chamber. (B) View of the irradiation box with a closed lid. Note, in this example a safety switch has been engineered so that the UV lights can only be turned on when the lid is closed. The fan is visible on one end, as are the switches that turn on/off the fan and UV bulbs. (C) An inside view shows the irradiation chamber poised equal distance between the UV bulb banks. The vent is indicated. (D) Light controls allow for control of the intensity of UV light. (E, F) Due to the heat from the UV bulbs, it can be necessary to use the fan to blow cool air through the box, and through the exit vent. (G) Photograph of the fish in the irradiation chamber with UV bulbs turned on. (H) The irradiation chamber (Photographs: Zhiqiang Zeng). (For color version of this figure, the reader is referred to the web version of this book.)

IV. Basic Melanoma Pathology

Histological evaluation of fish melanomas requires a systematic approach, with careful analysis of the tumors at various magnifications. Here, we aim to provide a basic introduction to melanoma pathology. This method allows observation of a large number of tumor characteristics. Ideally, the tumors will be assessed by a histopathologist who is familiar with routine diagnostic reporting of human

melanomas. In addition, familiarity with normal microanatomical structures is key to the interpretation of tumors in fish models.

Fish nevi are typically recognized by abnormalities in the quantity and distribution of melanin pigmentation, using a combination of naked eye macroscopic assessment supported by histological analysis (Fig. 4). These nevi differ significantly from those observed in human tissues, where a cellular proliferation of melanocytes is typically seen at the dermo-epidermal junction or in the superficial dermis. However, in both species nevi can be distinguished from malignant melanoma by assessing a combination of architectural and cytological features. In fish, melanomas are typically more cellular than nevi, and may show characteristic cytological features of malignancy such as nuclear pleomorphism and mitotic activity (see below). Invasive growth into underlying tissues such as skeletal muscle is considered to be diagnostic of malignancy.

We have designed a series of questions to assist in the basic description and diagnosis of fish melanomas, and aim to provide helpful examples in Figs. 4 and 5.

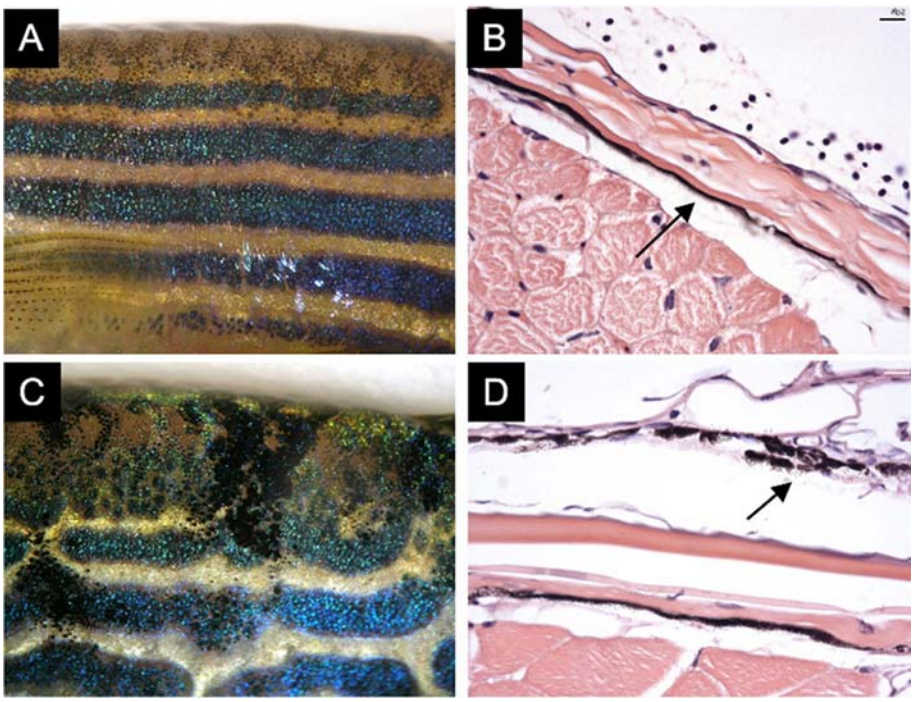

Fig. 4 Macroscopic and microscopic features of nevi in zebrafish. Normal patterns of melanin pigmentation in wild-type zebrafish. (A) Lateral view of the stripe pattern on a wild type zebrafish. (B) An H&E section of a transverse section of the wild type zebrafish in A; melanin pigment indicated with an arrow. (C) Following induction of nevi, abnormalities in pigmentation can be seen macroscopically. Lateral view of the $BRAF^{V600E}$ nevus on a wild-type zebrafish. (D) Nevi are recognized by an excess of melanin pigmentation (arrow), which is distributed abnormally. Individual melanocytes are not easily visualized (Photographs: Jennifer Richardson). (See color plate.)

A. Morphological Assessment of Tumors

Low power examination of a well-stained hematoxylin and eosin section at x20 or x40 magnification gives an overall impression of the growth pattern of the nevus or melanoma. Observations made at this magnification may closely reflect initial impressions formed at the time of macroscopic examination of the whole fish.

A checklist of features to consider includes:

- Does the tumor have a predominantly endophytic (growing inward) or exophytic (growing outward) growth pattern (Fig. 5A,B)?
- Is there an area of superficial growth along the surface of the fish (Fig. 5B)?
- What normal microanatomical structures does the tumor invade and/or distort (Fig. 5)?

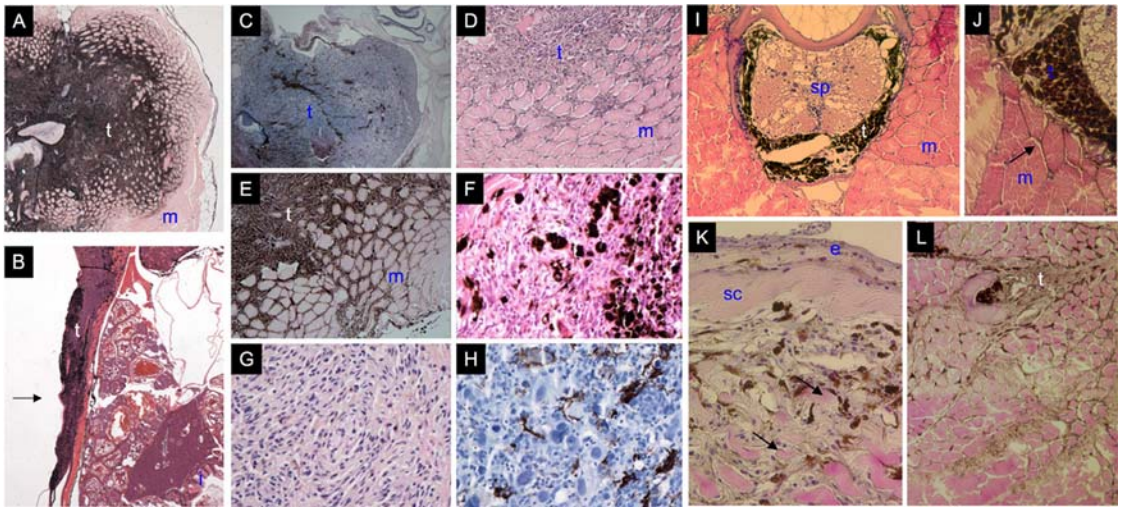

Fig. 5 Pathological features of fish melanomas. A spectrum of pathological characteristics of zebrafish $BRAF^{V600E}$ (A–H), medaka *xmrk* (I, J), and *Xiphophorus xmrk* melanomas (K, L). (A) This transverse section shows an entirely endophytic pattern of tumor growth, with little distortion of the external contour of the fish. (B) In this example, some of the tumor bulges from the external surface of the fish (exophytic growth). This image also shows an example of superficial tumor growth over the surface of the fish (arrow). (C) An example of a melanoma with a pushing, well-circumscribed invasive edge, whilst (D) shows a tumor with a highly infiltrative edge extending around individual skeletal muscle myocytes. (E) A heavily pigmented tumor, where melanin pigment is contained within the melanoma tumor cells. (F) A heavily pigmented tumor where melanin pigment may be predominantly contained within tumor infiltrating melanophages, which are of macrophage lineage. (G) This melanoma is composed predominantly of spindle-shaped melanocytes, which show minimal nuclear pleomorphism. (H) An example of a predominantly epithelioid melanoma, showing marked nuclear pleomorphism. (I) This is a perineural melanoma that develops from the meninx of the spinal cord (sp). It is a common site for extracutaneous melanoma in medaka. (J) This tumor grows for some time only inside the vertebrae, but then breaks through and invades the muscle bundles (arrow). (K, L) Heavily pigmented and highly invasive melanoma in *Xiphophorus* hybrids. In this example, the melanoma has infiltrated the muscle bundles and has led to their degeneration (arrows). The epidermis with scattered melanocytes is separated from the deeper layers by a massive connective tissue layer (stratum compactum, sc) that is still intact here, but is penetrated by melanoma cells at other sites, from which the body musculature is invaded. m: muscle; t: tumor. (See color plate.)

At intermediate magnification, a closer inspection of the invasive edge of the tumor can be made. It is also possible to start assessing the cellularity and degree of melanin pigmentation at this stage. Note that for heavily pigmented tumors, a melanin bleached section may be required to allow the tumor to be visualized.

- Is the invasive edge of the tumor relatively well-circumscribed and pushing, or is it irregular and highly infiltrative (Fig. 5C,D)? An infiltrative growth pattern, such as in Fig. 5D, is likely to imply more aggressive tumor behavior.
- What is the degree of melanin pigmentation? Melanin may be contained either within melanoma cells themselves, or within tumor infiltrating melanophages (Fig. 5E,F).

High power magnifications (x200, x400 or higher) allow assessment of tumor cell morphology. At these magnifications mitotic figures may be visualized, giving some impression of the rate of tumor proliferation. Useful questions include:

- Are the tumor cells mainly spindle-shaped, epithelioid, or a mixture of the two (Fig. 5G,H)? Some authors have reported prognostic differences between these two cell types in certain categories of human melanoma (Spatz *et al*., 1998).
- What is the degree of nuclear pleomorphism – are the nuclei relatively regular and monotonous in size and shape, or is there marked variation (Fig. 5G,H)? In human melanoma, marked nuclear pleomorphism typically correlates with more aggressive tumor behavior.
- Can any mitotic figures be seen? If these are present, it may be of value to quantify the mitotic rate using the standard methodology for routine diagnostic assessment of human melanomas. Using this method, the mitotic rate should be expressed as the number of mitoses per mm^2, in the area of the tumor where the most mitotic activity is observed (see below) (Edge *et al*., 2009).

Many of these features are routinely assessed in the diagnosis and histopathological reporting of human melanomas, and are used to determine the further management of the patient (Broekaert *et al*., 2010). Many of these features have been shown to be of prognostic value in the clinical setting, and may in turn yield valuable information about the behavior of melanomas in experimental models. In our different genetic models of melanoma in $BRAF^{V600E}$ zebrafish, we have observed characteristic and distinct differences in tumor growth pattern, pigmentation, and cellular morphology (M.E.M., J. Richardson, J. den Hertog, J. Lister, E.E.P, *unpublished data*). Observation of these differences in morphology in different genetic backgrounds may allow us to make some early comparisons with recognized growth phases and sub-types of human melanoma (Broekaert *et al*., 2010).

V. Histology

A. From the Tank to the Slide: Tissue Preparation and Sectioning

To prepare fish for histology, zebrafish are killed by immersion in an anesthetic, such as tricaine (Sigma–Aldrich). Zebrafish are dissected in half transversely to

increase fixative penetration, fish are fixed in 4% PFA (Electron Microscopy Sciences) for 3 days at 4 °C, washed once in PBS and decalcified in 0.5 M EDTA pH 8 for 5 days at 4 °C. Tissue samples are perfused with paraffin wax using a Tissue Processor Leica ASP3005 using the following cycles: Alcohol 50% – 1.5 h – 35 °C; Alcohol 80% – 1.5 h – 35 °C; Alcohol 95% – 1.5 h – 35 °C; Alcohol 100% – 2 × 1.5 h, 2 × 2 h– 35 °C; Xylene 100% – 2 × 1.5 h – 1 × 2 h – 35 °C; Paraffin wax – 3 × 1.5 h, 1 × 2 h – 60 °C.

Tissue samples are oriented and embedded in paraffin wax blocks, and sectioned at 5 μm thickness onto Superfrost Plus slides (VWR International).

B. Hematoxylin and Eosin (H&E) Staining

Hematoxylin and eosin (H&E) are common stains to examine the cells and tissues of a melanoma sample. They stain basophilic cellular structures blue (such as nuclei) and eosinophilic structures shades of red, pink, and orange. The method described below relies on over-staining the hematoxylin, and differentiating slightly in acid alcohol; alternatively the time in hematoxylin can be reduced (e.g., 10 s), without the need to dedifferentiate the stain. Sometimes, the black–brown pigment melanin obscures cellular detail, and an optional bleaching step is required. In this case, following rehydration and washing in water, sections are bleached in a solution of 1% potassium hydroxide and 3% hydrogen peroxide for 15 min, or for heavily melanized sections up to 30 min.

a. Deparaffinate the sample slide

1. 3 × 5 min washes in xylene
2. 3 × 5 min washes in absolute Ethanol
3. 2 min in 90% EtOH
4. 2 min in 70% EtOH
5. 2 min in 50% EtOH
6. 2 min in 50% EtOH
7. Wash in running tap water for 1 min

b. Stain the sample

1. 4 min in Hematoxylin (ensure it is filtered prior to use, it will get an oxidized film on top)
2. Wash in running tap water
3. Quick immersion in acid alcohol (1% hydrochloric acid in 70% alcohol i.e., 700 ml alcohol + 10 ml acid + 290 ml distilled water)
4. Wash in running tap water
5. Quick immersion in lithium carbonate (to make Hematoxylin blue)
6. Wash in running tap water
7. 2 min in eosin
8. Wash in running tap water

c. **Wash the sample and mount**

1. Quick immersion in absolute ethanol
2. 4 × 1 min washes in absolute ethanol
3. 3 × 5 min washes in xylene

d. **Mounting the sample**

Following dehydration of the sections, slides are mounted using DPX mounting medium (BDH, available via VWR International) and the appropriately sized cover glass.

VI. Molecular Analysis

Immunohistochemical examination may be a useful adjunct to the morphological assessment of melanomas by H&E stain alone. Immunohistochemistry is useful in establishing the nature of cell types present within tumor tissue, and may also be a semi-quantitative tool in the study of proliferation and the cell cycle. In our experience, many of the antibodies that have been optimized for use in human tissues work very well in our fish models.

A. Immunohistochemistry Protocol

a. **Deparaffinate the sample slide**

1. Incubate 2 × 5 min washes in xylene
2. 99% ethanol 2 × 5 min washes
3. 90% ethanol 1 × 5 min wash
4. 70% ethanol 1 × 5 min wash
5. Wash in dH_2O 2 × 5 min
6. Bleach in 3% H_2O_2 and 1% KOH (15–30 min depending on need)
7. Wash in dH_2O 3 × 5 min

b. **Antigen Retrieval**

Antigens need to be unmasked prior to antibody staining. We use two different buffers, critrate or EDTA-based unmasking, and each new antibody is tested with both approaches. For example, successful staining with Melan A (DAKO) (1:75 dilution) requires an EDTA-based buffer, while anti-phospho Histone H3 (1:2000) requires a citrate buffer.

Citrate antigen retrieval (make 1 L)
0.01 M Citrate buffer pH 6
18 ml 0.1 M Citric acid
82 ml 0.1 M Sodium citrate
900 ml H_2O

EDTA pH 8 (make 1 L)
10 mM, Dissolve 3.72 g in 1 L of dH_2O and pH to 8.0

Place samples within a pressure cooker and add the 1 L of antigen retrieval solution (above)

1. Place 1 L of buffer into pressure cooker without lid. Put on at full power until solution is at a boil.
2. Ensure solution is boiling, and immediately place in slides
3. Cover with lid and pressure weight
4. Microwave on high setting for up to 2 min to bring the pressure cooker to full pressure. Once at full pressure, microwave on high for another 5 min
5. *Put on face shield and gloves*, remove from microwave
6. Vent gas, and once fully vented, remove lid
7. Cool slides on bench for 20 min

c. **Staining the sample**

1. Wash in dH_2O 3 × 5 min
2. Incubate in 3% H_2O_2 for 10 min
3. Wash in dH_2O 2 × 5 min
4. Wash in wash buffer (1x TBS) for 5 min
5. Block in DAKO serum free protein block solution for 30 min at room temp
6. Pour off block solution add primary antibody (diluted in DAKO antibody diluent)
7. Incubate overnight at 4 °C
8. Remove primary antibody
9. Wash in TBS 3 × 5 min
10. Add secondary antibody (in DAKO EnVison kit) incubate at room temperature for 30 min
11. Wash in TBS 2 × 5 min
12. Visualize with DAB (20 μl DAB chromogen per 1 ml of DAB substrate, DAKO EnVison kit). Incubate 10 min at room temperature
13. Wash in dH_2O 2 × 5 min
14. Counterstain with hematoxylin for 10 s
15. Wash in running tap water
16. Wash in running tap water
17. Blue up in Lithium chloride
18. Wash in running tap water
19. Dehydrate: 1 min washes in 70, 90, 99, and 99% alcohol
20. 2 × 2 min washes in xylene
21. Mount with DPex

B. Pigmentation

A recurring problem in the use of immunohistochemistry to study fish melanomas is the marked degree of melanin pigmentation that is seen in many of the tumors. The

melanin pigment obscures the tumor cells, and makes it very difficult to appreciate cytological detail. In addition, the brown melanin pigment leads to confusion in interpreting sections stained using the standard D.A.B. (Diaminobenzidine) method, which results in a brown product. One approach to this problem is to subject the tissue sections to melanin bleaching (1% potassium hydroxide and 3% hydrogen peroxide) before any immunohistochemical staining is carried out, and we have used this technique on many of our heavily pigmented tumors. The use of alkaline phosphatase as a marker enzyme may also be useful when conducting immunohistochemistry on melanotic tumors, as this method results in a red labeling product (see Fig. 6A). All these problems may be circumvented when the experimental set-up and the scientific questions allow the use of albino fish for the induction of melanoma.

C. Melanocytic Markers

Melan-A (also known as MART-1, Melanoma Antigen Recognized by T-cells) is a melanosomal differentiation antigen that is recognized by cytotoxic T-cells. Two monoclonal antibodies are available for use in paraffin-embedded, formalin fixed tissue – A103 and M2-7C10 (Busam and Jungbluth, 1999). These antibodies are regularly used in the routine diagnostic assessment of human melanomas, either to confirm the melanocytic nature of a tumor, or to highlight important architectural features of a melanocytic lesion. The Melan-A antigen is expressed by normal melanocytes, benign nevi, and melanomas, and is thus a marker of histogenesis rather than an indicator of malignancy. The only other tissue types which are known to stain with these antibodies are relatively uncommon perivascular epithelioid cell tumors and, in the case of A103 only, steroid hormone producing tissues such as the adrenal cortex and Leydig cells of the testis. Thus, this is a relatively specific marker for the study of melanocytes and melanocytic lesions.

A number of other melanocytic markers are used in routine diagnostic practice, and may also be helpful in the study of fish melanomas. These include S-100 and

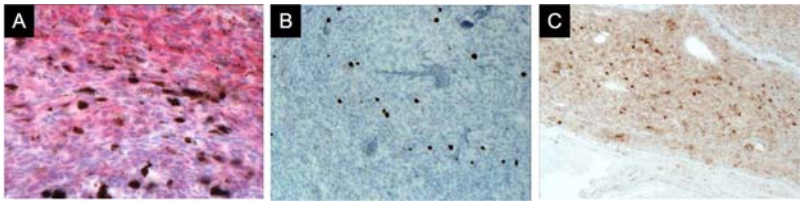

Fig. 6 Examples of basic immunohistochemistry stains for zebrafish melanoma. (A) An example of Melan-A staining using the alkaline phosphatase method. The cytoplasm of the tumoral melanocytes stains red, in contrast to the black–brown melanin pigment contained in tumor infiltrating melanophages. (B) Phospho-histone H3 stains the nuclei of actively proliferating cells. Counting of positive nuclei as a percentage of the total nuclei present gives a quantitative assessment of the tumor proliferation rate. (C) Phospho-H2AX immunohistochemistry highlights DNA damage within melanoma cells. (See color plate.)

HMB-45. S-100 is known to be the most sensitive melanocytic marker, although it is less specific than Melan-A as it also stains a number of other tissues including nerves. HMB-45 has been shown to be the least sensitive of the routinely used markers (Orchard, 2000).

Figure 6A shows an example of Melan-A staining in a $BRAF^{V600E}$ zebrafish melanoma. We have found this stain to be useful in confirming the melanocytic nature of the tumors generated in these fish models. In addition, this staining can help to delineate the architectural features of a particular tumor, highlighting the growth pattern and any invasion into internal organs.

D. Histogenetic Markers for Other Cell Types

Detailed microscopic examination of melanomas will reveal a number of other cell types admixed with the melanoma cells, including inflammatory cells, endothelial cells, and stromal cells. The admixture of cell types within a tumor may lead to confusion, and a number of immunohistochemical stains are available to highlight the different populations. A list of cell types and corresponding antibodies that may be useful are given in Table II.

E. Markers of Proliferation and Cell Cycle Activity

Immunohistochemical markers of proliferation and cell cycle activity are sometimes helpful in the routine diagnostic assessment of human melanomas. Selected markers may help to determine the biological nature of a melanocytic lesion (i.e., benign or malignant), if interpreted carefully in the context of the morphological appearance on an H&E stain. Some markers have also been shown to be of prognostic significance in selected groups of tumors. Study of these markers may also give us helpful information about melanoma behavior in the experimental setting.

A useful panel of immunohistochemical markers for proliferative activity includes:

- Ki-67 (MIB-1 antibody): Ki-67 is a cell cycle associated antigen, which is a useful marker of cellular proliferation. This antigen is present at all stages of the cell cycle, except for G_0 and early G_1 phases (Gerdes *et al*., 1984). MIB-1/Ki-67 immunoreactivity has been shown to be of diagnostic utility in distinguishing benign nevi from melanomas (Li *et al*., 2000), and has also emerged as a prognostic factor in certain categories of melanoma (Ramsay *et al*., 1995).
- Phospho-histone H3: This is an alternative marker for quantitative assessment of proliferative activity within tumors (see below). An example of phospho-histone H3 staining of a zebrafish melanoma is given in Fig. 6B. During the late G2-phase and early M-phase, Histone H3 is phosphorylated on serine 10. Using antibodies that detect phosphorylation of histone H3 (p-H3) at serine 10 can assist in the characterization of how rapidly a melanoma is proliferating (Fig. 6B). Following

Table II
Non-melanocytic cell types that may be present in melanocytic tumors, and suggested immunohistochemical markers

Cell type	Immunohistochemical marker
Macrophages	CD68
Lymphocytes	CD45 (leukocyte common antigen)
T cells	CD3
B cells	CD20
Endothelial cells of blood vessels	Factor VIII, CD31, CD34
Stromal cells (fibroblasts)	CD34
Nerves	S100 protein

p-H3 antibody staining, 40X magnification fields of view are randomly selected and image captured. Images are printed using a color printer and the total number of cells in each field of view is manually counted, as well as the number of positively stained cells, in order to calculate the percentage of p-H3 positively stained cells. Between three and six randomly selected fields of view are imaged, based on the size of the tumor, and an average percentage of proliferating cells is calculated.

- Cyclins and cyclin dependent kinases (CDKs): Study of these cell cycle regulators has proven diagnostically useful in some settings. Some authors have demonstrated a correlation between expression of certain cyclins/CDKs and both tumor stage and histological subtype (Georgieva *et al.*, 2001).
- phospho-H2AX: This is a marker which highlights the DNA damage response within tumor cells and works well in zebrafish (Zeng *et al.*, 2010). Figure 6C shows an example of H2AX staining.

VII. RNA and Protein Isolation From Adult Fish Tumors

A. RNA Isolation From Melanoma

RNA from tumor tissue is prepared using a standard commercial RNA purification kit (Qiagen RNeasy Mini Kit).

1. The tissue is excised from the animal, snap frozen, and stored at −80 °C.
2. To prepare RNA the frozen tumor tissue is placed in liquid nitrogen and disrupted using a mortar and pestle. The tissue is homogenized by adding a lysis buffer and passing the sample through a needle and syringe. Ethanol is added to the lysate to promote selective binding of RNA to the column membrane.
3. The sample is added to a column allowing binding of total RNA to the membrane, contaminants are washed away and high-quality RNA is eluted in RNase-free water. Binding, washing, and elution protocol steps are carried out by centrifugation.

4. The final RNA concentration is determined using a NanoDrop and total RNA prepared is stored at −80 °C.

B. Preparation of Protein Lysate From Fish Tissue

Preparing protein extracts from fish melanoma samples (e.g., for western blotting) can be done with standard protein extraction protocols. Below, we present a protocol that we find consistently successful to analyze proteins in embryonic and adult zebrafish. A similar protocol is also used for *Xiphophorus* and medaka tissues, using a HEPES based buffer (below).

1. Remove tumor tissue (store at −80 °C or proceed immediately to lysis). For embryos, dechorionate (if required) and transfer to a clean 1.5 ml microcentrifuge tube. Remove all water or medium, and immediately store at -80 °C or proceed immediately to lysis.
2. Add 40 μl enhanced RIPA buffer (+++) to each sample and pipette up and down until the sample is homogenised. Alternatively, for tissues that do not disaggregate easily, ribolyse the tissue after adding glass beads (e.g., 20–50 μl) and 40 μl RIPA (+++) buffer. Keep the ribolysed samples on ice for 15 min before proceeding.
3. Centrifuge the samples at maximum speed on a table-top centrifuge for 15 min at 4 °C. Transfer the supernatant into a new 1.5 ml microcentrifuge tube.
4. Quantify the protein concentration (e.g., Bradford assay or Nanodrop) using RIPA (+++) buffer as blank.

RIPA buffer (10 ml) (Aliquots can be stored at −20 °C)

2 M Tris HCl pH 7.5	250 μl
5 M NaCl	300 μl
1% NP40	100 μl
Na deoxycholate	0.05 g
10% SDS	100 μl
ddH_2O	up to 10 ml

RIPA (+++) buffer (Make fresh before lysis and keep on ice)

RIPA buffer	1 ml
NaF	10 μl
25 × Protease inhibitor mix (Roche)	40 μl

HEPES NP40-Lysis buffer

20 mM HEPES pH 7.8 (NaOH)
500 mM NaCl
5 mM $MgCl_2$

5 mM KCl
After autoclaving, add: 0.5% NP40, 0.1% deoxycholate (filter sterilize; Sigma D-5670-25G).
Store at 4 °C.

Add protease inhibitors before use

10 μg/ml Leupeptin
10 μg/ml Aprotinin
1 mM PMSF
100 μM Na_3VO_4
0.1 M NaF

VIII. Conclusions

Multiple scientific approaches are needed to understand melanoma development and identify targetable pathways. Laboratory fish provide a relevant and tractable model to study the genetics and environmental risk factors that contribute to melanoma development. The similarity of melanocyte development in mammals and fish has already led to valuable results, which help shape and direct human studies. The three main melanoma fish models each have characteristics that make them well-suited to specific scientific questions, while also sharing many properties and rendering them amenable to most techniques discussed here. Human melanoma is a complex disease with many subtypes, each with a different prognosis, and varied genetic and environmental factors that contribute to its origin. The rich biodiversity in the fish melanoma models provides an important foundation to approach this problem. However, the pathological and etiological variety is limited in the existing melanoma models and thus there continues to be a need to develop new melanoma models using defined transgenic, genetic, and environmental strategies. Large-scale genomic efforts in human and animal models of melanoma are already proving fruitful, and fish models can play an important role in identifying and validating new melanoma mutations. Finally, these small aquarium fish with their stereotypic melanocyte and melanoma development are ideal for performing high throughput drug screens that will be of considerable value for melanoma research.

Acknowledgments

We are grateful to Jennifer Richardson, Peter Fischer, Daniel Liedtke, Dr. Zhiqiang Zeng, Corina Anastaski and Amy Capper for assistance with protocols and photographs, and Professor David Mitchell (MD Anderson Cancer Center, USA) for helpful comments and Dr. John Bartlet for help with protocols. EEP is supported by the Medical Research Council, Medical Research Scotland, and the FP7 Framework ZF-CANCER project. MS is supported by the Deutsche Forschungsgemeinschaft and the German Melanoma Network of the Deutsche Krebshilfe.

References

Adam, D., Dimitrijevic, N., and Schartl, M. (1993). Tumor suppression in Xiphophorus by an accidentally acquired promoter. *Science* **259**, 816–819.

Akavia, U. D., Litvin, O., Kim, J., Sanchez-Garcia, F., Kotliar, D., Causton, H. C., Pochanard, P., Mozes, E., Garraway, L. A., and Pe'er, D. (2010). An integrated approach to uncover drivers of cancer. *Cell* **143**, 1005–1017.

Amatruda, J. F., Shepard, J. L., Stern, H. M., and Zon, L. I. (2002). Zebrafish as a cancer model system. *Cancer Cell* **1**, 229–231.

Broekaert, S. M., Roy, R., Okamoto, I., van den Oord, J., Bauer, J., Garbe, C., Barnhill, R. L., Busam, K. J., Cochran, A. J., Cook, M. G., Elder, D. E., McCarthy, S. W., Mihm, M. C., Schadendorf, D., Scolyer, R. A., Spatz, A., and Bastian, B. C. (2010). Genetic and morphologic features for melanoma classification. *Pigment Cell Melanoma. Res.* **23**, 763–770.

Busam, K. J., and Jungbluth, A. A. (1999). Melan-A, a new melanocytic differentiation marker. *Adv. Anat. Pathol.* **6**, 12–18.

Ceol, C. J., Houvras, Y., Jane-Valbuena, J., Bilodeau, S., Orlando, D. A., Battisti, V., Fritsch, L., Lin, W. M., Hollmann, T. J., Ferre, F., Bourque, C., Burke, C. J., Turner, L., Uong, A., Johnson, L. A., Beroukhim, R., Mermel, C. H., Loda, M., Ait-Si-Ali, S., Garraway, L. A., Young, R. A., and Zon, L. I. (2011). The histone methyltransferase SETDB1 is recurrently amplified in melanoma and accelerates its onset. *Nature* **471**, 513–517.

Chin, L., Garraway, L. A., and Fisher, D. E. (2006). Malignant melanoma: genetics and therapeutics in the genomic era. *Genes Dev.* **20**, 2149–2182.

Cronin, J. C., Wunderlich, J., Loftus, S. K., Prickett, T. D., Wei, X., Ridd, K., Vemula, S., Burrell, A. S., Agrawal, N. S., Lin, J. C., Banister, C. E., Buckhaults, P., Rosenberg, S. A., Bastian, B. C., Pavan, W. J., and Samuels, Y. (2009). Frequent mutations in the MITF pathway in melanoma. *Pigment Cell Melanoma Res.* **22**, 435–444.

Dankort, D., Curley, D. P., Cartlidge, R. A., Nelson, B., Karnezis, A. N., Damsky Jr., W. E., You, M. J., DePinho, R. A., McMahon, M., and Bosenberg, M. (2009). Braf(V600E) cooperates with Pten loss to induce metastatic melanoma. *Nat. Genet.* **41**, 544–552.

Davies, H., Bignell, G. R., Cox, C., Stephens, P., Edkins, S., Clegg, S., Teague, J., Woffendin, H., Garnett, M. J., Bottomley, W., Davis, N., Dicks, E., Ewing, R., Floyd, Y., Gray, K., Hall, S., Hawes, R., Hughes, J., Kosmidou, V., Menzies, A., Mould, C., Parker, A., Stevens, C., Watt, S., Hooper, S., Wilson, R., Jayatilake, H., Gusterson, B. A., Cooper, C., Shipley, J., Hargrave, D., Pritchard-Jones, K., Maitland, N., Chenevix-Trench, G., Riggins, G. J., Bigner, D. D., Palmieri, G., Cossu, A., Flanagan, A., Nicholson, A., Ho, J. W., Leung, S. Y., Yuen, S. T., Weber, B. L., Seigler, H. F., Darrow, T. L., Paterson, H., Marais, R., Marshall, C. J., Wooster, R., Stratton, M. R., and Futreal, P. A. (2002). Mutations of the BRAF gene in human cancer. *Nature* **417**, 949–954.

Dovey, M., White, R. M., and Zon, L. I. (2009). Oncogenic NRAS cooperates with p53 loss to generate melanoma in zebrafish. *Zebrafish* **6**, 397–404.

Edge, S. B., Byrd, D. R., Compton, C. C., Fritz, A. G., Greene, F. L., and Trotti, A. (eds.). (2009). Melanoma of the skin. AJCC Cancer Staging Manual. Springer, New York, NY.

Feng, Y., Santoriello, C., Mione, M., Hurlstone, A., and Martin, P. (2011). Live imaging of innate immune cell sensing of transformed cells in zebrafish larvae: parallels between tumor initiation and wound inflammation. *PLoS Biol.* **8**, e1000562.

Flaherty, K. T., Hodi, F. S., and Bastian, B. C. (2010). Mutation-driven drug development in melanoma. *Curr. Opin. Oncol.* **22**, 178–183.

Flaherty, K. T., Puzanov, I., Kim, K. B., Ribas, A., McArthur, G. A., Sosman, J. A., O'Dwyer, P. J., Lee, R. J., Grippo, J. F., Nolop, K., and Chapman, P. B. (2011). Inhibition of mutated, activated BRAF in metastatic melanoma. *N. Engl. J. Med.* **363**, 809–819.

Garibyan, L., and Fisher, D. E. (2010). How sunlight causes melanoma. *Curr. Oncol. Rep.* **12**, 319–326.

Garraway, L. A., Widlund, H. R., Rubin, M. A., Getz, G., Berger, A. J., Ramaswamy, S., Beroukhim, R., Milner, D. A., Granter, S. R., Du, J., Lee, C., Wagner, S. N., Li, C., Golub, T. R., Rimm, D. L., Meyerson,

M. L., Fisher, D. E., and Sellers, W. R. (2005). Integrative genomic analyses identify MITF as a lineage survival oncogene amplified in malignant melanoma. *Nature* **436**, 117–122.

Georgieva, J., Sinha, P., and Schadendorf, D. (2001). Expression of cyclins and cyclin dependent kinases in human benign and malignant melanocytic lesions. *J. Clin. Pathol.* **54**, 229–235.

Gerdes, J., Lemke, H., Baisch, H., Wacker, H. H., Schwab, U., and Stein, H. (1984). Cell cycle analysis of a cell proliferation-associated human nuclear antigen defined by the monoclonal antibody Ki-67. *J. Immunol.* **133**, 1710–1715.

Grabher, C., and Wittbrodt, J. (2008). Recent advances in meganuclease-and transposon-mediated transgenesis of medaka and zebrafish. *Methods Mol. Biol.* **461**, 521–539.

Gray-Schopfer, V., Wellbrock, C., and Marais, R. (2007). Melanoma biology and new targeted therapy. *Nature* **445**, 851–857.

Johannessen, C. M., Boehm, J. S., Kim, S. Y., Thomas, S. R., Wardwell, L., Johnson, L. A., Emery, C. M., Stransky, N., Cogdill, A. P., Barretina, J., Caponigro, G., Hieronymus, H., Murray, R. R., Salehi-Ashtiani, K., Hill, D. E., Vidal, M., Zhao, J. J., Yang, X., Alkan, O., Kim, S., Harris, J. L., Wilson, C. J., Myer, V. E., Finan, P. M., Root, D. E., Roberts, T. M., Golub, T., Flaherty, K. T., Dummer, R., Weber, B. L., Sellers, W. R., Schlegel, R., Wargo, J. A., Hahn, W. C., and Garraway, L. A. (2010). COT drives resistance to RAF inhibition through MAP kinase pathway reactivation. *Nature* **468**, 968–972.

Kelsh, R. N. (2004). Genetics and evolution of pigment patterns in fish. *Pigment Cell Res.* **17**, 326–336.

Kelsh, R. N., Harris, M. L., Colanesi, S., and Erickson, C. A. (2009). Stripes and belly-spots – a review of pigment cell morphogenesis in vertebrates. *Semin. Cell Dev. Biol.* **20**, 90–104.

Kim, M., Gans, J. D., Nogueira, C., Wang, A., Paik, J. H., Feng, B., Brennan, C., Hahn, W. C., Cordon-Cardo, C., Wagner, S. N., Flotte, T. J., Duncan, L. M., Granter, S. R., and Chin, L. (2006). Comparative oncogenomics identifies NEDD9 as a melanoma metastasis gene. *Cell* **125**, 1269–1281.

Kinoshita, M., Murata, K., Naruse, K., and Tanaka, M. (2009). *Medaka: Biology, Management, and Experimental Protocols.* Wiley-Blackwell.

Ko, J. M., and Fisher, D. E. (2011). A new era: melanoma genetics and therapeutics. *J. Pathol.* **223**, 241–250.

Lam, S. H., Wu, Y. L., Vega, V. B., Miller, L. D., Spitsbergen, J., Tong, Y., Zhan, H., Govindarajan, K. R., Lee, S., Mathavan, S., Murthy, K. R., Buhler, D. R., Liu, E. T., and Gong, Z. (2006). Conservation of gene expression signatures between zebrafish and human liver tumors and tumor progression. *Nat. Biotechnol.* **24**, 73–75.

Li, L. X., Crotty, K. A., McCarthy, S. W., Palmer, A. A., and Kril, J. J. (2000). A zonal comparison of MIB1-Ki67 immunoreactivity in benign and malignant melanocytic lesions. *Am. J. Dermatopathol.* **22**, 489–495.

Little, A. S., Balmanno, K., Sale, M. J., Newman, S., Dry, J. R., Hampson, M., Edwards, P. A., Smith, P. D., and Cook, S. J. (2011). Amplification of the driving oncogene, KRAS or BRAF, underpins acquired resistance to MEK1/2 inhibitors in colorectal cancer cells. *Sci. Signal.* **4**, ra17.

Meierjohann, S., and Schartl, M. (2006). From Mendelian to molecular genetics: the Xiphophorus melanoma model. *Trends Genet.* **22**, 654–661.

Meierjohann, S., Wende, E., Kraiss, A., Wellbrock, C., and Schartl, M. (2006). The oncogenic epidermal growth factor receptor variant Xiphophorus melanoma receptor kinase induces motility in melanocytes by modulation of focal adhesions. *Cancer Res.* **66**, 3145–3152.

Michailidou, C., Jones, M., Walker, P., Kamarashev, J., Kelly, A., and Hurlstone, A. F. (2009). Dissecting the roles of Raf- and PI3K-signalling pathways in melanoma formation and progression in a zebrafish model. *Dis. Model Mech.* **2**, 399–411.

Mitchell, D. L., and Fernandez, A. A. (2011). Different types of DNA damage play different roles in the etiology of sunlight-induced melanoma. *Pigment Cell Melanoma Res.* **24**, 119–124.

Mitchell, D. L., Fernandez, A. A., Nairn, R. S., Garcia, R., Paniker, L., Trono, D., Thames, H. D., and Gimenez-Conti, I. (2010). Ultraviolet A does not induce melanomas in a Xiphophorus hybrid fish model. *Proc. Natl. Acad. Sci. U. S. A.* **107**, 9329–9334.

Mitchell, D. L., and Nairn, R. S. (2006). Photocarcinogenesis in Xiphophorus hybrid models. *Zebrafish* **3**, 311–323.

Mitchell, D. L., Paniker, L., and Douki, T. (2009). DNA damage, repair and photoadaptation in a Xiphophorus fish hybrid. *Photochem. Photobiol.* **85**, 1384–1390.

Morcinek, J. C., Weisser, C., Geissinger, E., Schartl, M., and Wellbrock, C. (2002). Activation of STAT5 triggers proliferation and contributes to anti-apoptotic signalling mediated by the oncogenic Xmrk kinase. *Oncogene* **21**, 1668–1678.

Nairn, R. S., Kazianis, S., McEntire, B. B., Della Coletta, L., Walter, R. B., and Morizot, D. C. (1996). A CDKN2-like polymorphism in Xiphophorus LG V is associated with UV-B-induced melanoma formation in platyfish-swordtail hybrids. *Proc. Natl. Acad. Sci. U. S. A.* **93**, 13042–13047.

Nusslein-Volhard C, D. R. (2002). Zebrafish, Practical Approach Series 261.

Orchard, G. E. (2000). Comparison of immunohistochemical labelling of melanocyte differentiation antibodies melan-A, tyrosinase and HMB 45 with NKIC3 and S100 protein in the evaluation of benign naevi and malignant melanoma. *Histochem J.* **32**, 475–481.

Patton, E. E., Mitchell, D. L., and Nairn, R. S. (2010). Genetic and environmental melanoma models in fish. *Pigment Cell Melanoma Res.* **23**, 314–337.

Patton, E. E., and Nairn, R. S. (2010). Xmrk in medaka: a new genetic melanoma model. *J. Invest. Dermatol.* **130**, 14–17.

Patton, E. E., Widlund, H. R., Kutok, J. L., Kopani, K. R., Amatruda, J. F., Murphey, R. D., Berghmans, S., Mayhall, E. A., Traver, D., Fletcher, C. D., Aster, J. C., Granter, S. R., Look, A. T., Lee, C., Fisher, D. E., and Zon, L. I. (2005). BRAF mutations are sufficient to promote nevi formation and cooperate with p53 in the genesis of melanoma. *Curr. Biol.* **15**, 249–254.

Pleasance, E. D., Cheetham, R. K., Stephens, P. J., McBride, D. J., Humphray, S. J., Greenman, C. D., Varela, I., Lin, M. L., Ordonez, G. R., Bignell, G. R., Ye, K., Alipaz, J., Bauer, M. J., Beare, D., Butler, A., Carter, R. J., Chen, L., Cox, A. J., Edkins, S., Kokko-Gonzales, P. I., Gormley, N. A., Grocock, R. J., Haudenschild, C. D., Hims, M. M., James, T., Jia, M., Kingsbury, Z., Leroy, C., Marshall, J., Menzies, A., Mudie, L. J., Ning, Z., Royce, T., Schulz-Trieglaff, O. B., Spiridou, A., Stebbings, L. A., Szajkowski, L., Teague, J., Williamson, D., Chin, L., Ross, M. T., Campbell, P. J., Bentley, D. R., Futreal, P. A., and Stratton, M. R. (2010). A comprehensive catalogue of somatic mutations from a human cancer genome. *Nature* **463**, 191–196.

Ramsay, J. A., From, L., Iscoe, N. A., and Kahn, H. J. (1995). MIB-1 proliferative activity is a significant prognostic factor in primary thick cutaneous melanomas. *J. Invest. Dermatol.* **105**, 22–26.

Richardson, J., Zeng, Z., Ceol, C., Mione, M., Jackson, I. J., and Patton, E. E. (2011). A zebrafish model for nevus regeneration. *Pigment Cell Melanoma Res.* **24**, 378–381.

Santoriello, C., Deflorian, G., Pezzimenti, F., Kawakami, K., Lanfrancone, L., d'Adda di Fagagna, F., and Mione, M. (2009). Expression of H-RASV12 in a zebrafish model of Costello syndrome causes cellular senescence in adult proliferating cells. *Dis Model Mech.* **2**, 56–67.

Santoriello, C., Gennaro, E., Anelli, V., Distel, M., Kelly, A., Koster, R. W., Hurlstone, A., and Mione, M. (2010). Kita driven expression of oncogenic HRAS leads to early onset and highly penetrant melanoma in zebrafish. *PLoS One* **5**, e15170.

Schartl, M., Wilde, B., Laisney, J. A., Taniguchi, Y., Takeda, S., and Meierjohann, S. (2010). A mutated EGFR is sufficient to induce malignant melanoma with genetic background-dependent histopathologies. *J. Invest. Dermatol.* **130**, 249–258.

Setlow, R. B., Grist, E., Thompson, K., and Woodhead, A. D. (1993). Wavelengths effective in induction of malignant melanoma. *Proc. Natl. Acad. Sci. U. S. A.* **90**, 6666–6670.

Setlow, R. B., Woodhead, A. D., and Grist, E. (1989). Animal model for ultraviolet radiation-induced melanoma: platyfish-swordtail hybrid. *Proc. Natl. Acad. Sci. U. S. A.* **86**, 8922–8926.

Spatz, A., Shaw, H. M., Crotty, K. A., Thompson, J. F., and McCarthy, S. W. (1998). Analysis of histopathological factors associated with prolonged survival of 10 years or more for patients with thick melanomas (> 5 mm). *Histopathology* **33**, 406–413.

Spitsbergen, J. M., Tsai, H. W., Reddy, A., Miller, T., Arbogast, D., Hendricks, J. D., and Bailey, G. S. (2000a). Neoplasia in zebrafish (Danio rerio) treated with 7,12-dimethylbenz[a]anthracene by two exposure routes at different developmental stages. *Toxicol. Pathol* **28**, 705–715.

Spitsbergen, J. M., Tsai, H. W., Reddy, A., Miller, T., Arbogast, D., Hendricks, J. D., and Bailey, G. S. (2000b). Neoplasia in zebrafish (Danio rerio) treated with N-methyl-N'-nitro-N-nitrosoguanidine by three exposure routes at different developmental stages. *Toxicol. Pathol* **28**, 716–725.

Taylor, K. L., Grant, N. J., Temperley, N. D., and Patton, E. E. (2010). Small molecule screening in zebrafish: an *in vivo* approach to identifying new chemical tools and drug leads. *Cell Commun. Signal.* **8**, 11.

Teutschbein, J., Haydn, J. M., Samans, B., Krause, M., Eilers, M., Schartl, M., and Meierjohann, S. (2010). Gene expression analysis after receptor tyrosine kinase activation reveals new potential melanoma proteins. *BMC Cancer* **10**, 386.

Wellbrock, C., Weisser, C., Geissinger, E., Troppmair, J., and Schartl, M. (2002). Activation of p59(Fyn) leads to melanocyte dedifferentiation by influencing MKP-1-regulated mitogen-activated protein kinase signaling. *J. Biol. Chem.* **277**, 6443–6454.

White, R. M., Cech, J., Ratanasirintrawoot, S., Lin, C. Y., Rahl, P. B., Burke, C. J., Langdon, E., Tomlinson, M. L., Mosher, J., Kaufman, C., Chen, F., Long, H. K., Kramer, M., Datta, S., Neuberg, D., Granter, S., Young, R. A., Morrison, S., Wheeler, G. N., and Zon, L. I. (2011). DHODH modulates transcriptional elongation in the neural crest and melanoma. *Nature* **471**, 518–522.

White, R. M., Sessa, A., Burke, C., Bowman, T., LeBlanc, J., Ceol, C., Bourque, C., Dovey, M., Goessling, W., Burns, C. E., and Zon, L. I. (2008). Transparent adult zebrafish as a tool for *in vivo* transplantation analysis. *Cell Stem Cell* **2**, 183–189.

Wittbrodt, J., Adam, D., Malitschek, B., Maueler, W., Raulf, F., Telling, A., Robertson, S. M., and Schartl, M. (1989). Novel putative receptor tyrosine kinase encoded by the melanoma-inducing Tu locus in Xiphophorus. *Nature* **341**, 415–421.

Zeng, Z., Richardson, J., Verduzco, D., Mitchell, D. L., and Patton, E. E. (2009). Zebrafish have a competent p53-dependent nucleotide excision repair pathway to resolve ultraviolet B-induced DNA damage in the skin. *Zebrafish* **6**, 405–415.

CHAPTER 15

Screening Pancreatic Oncogenes in Zebrafish Using the Gal4/UAS System

Shu Liu and Steven D. Leach

Department of Surgery and the McKusick-Nathans Institute of Genetic Medicine, Johns Hopkins University School of Medicine, Maryland, Baltimore

Abstract

Pancreatic cancer is a genetic disease in which somatic mutations in the *KRAS* proto-oncogene are detected in a majority of tumors. *KRAS* mutations represent an early event during pancreatic tumorigenesis, crucial for cancer initiation and progression. Recent studies, including comprehensive sequencing of the pancreatic cancer exome, have implicated the involvement of a number of additional core

METHODS IN CELL BIOLOGY, VOL 105

0091-679X/10 $35.00
DOI 10.1016/B978-0-12-381320-6.00015-1

signaling pathways during pancreatic tumorigenesis. Improving our understanding of genetic interactions between KRAS and these additional pathways represents a critical challenge, as these interactions may provide novel opportunities for diagnosis and treatment. However, studying these interactions requires the expression of multiple transgenes in relevant cell types, an effort that has proven very difficult to achieve using gene targeted mice and is also technically challenging in zebrafish. Based on the ability of the Gal4 transcriptional activator to drive the expression of multiple transgenes under regulation of UAS (upstream activator sequence) regulatory elements, the Gal4/UAS system represents an attractive strategy for the study of genetic interactions. In this chapter, we review our experience using the Gal4/UAS system to model KRAS-initiated pancreatic cancer in zebrafish, as well as our early efforts using this system to study the influence of other cooperating oncogenes. We also describe techniques used to identify and characterize pancreatic tumors in adult transgenic fish.

I. Introduction

Pancreatic cancer is a deadly disease, with a predicted 43,140 new cases and 36,800 deaths occurring in US in 2010 (Jemal *et al*., 2010). The 5-year survival rate for this type of cancer remains around 5% (Altekruse *et al*., 2010). The poor outcome of the disease is largely due to the lack of effective early-stage diagnostic tools as well as intrinsic resistance to current therapeutic modalities.

The vast majority of pancreatic cancers are categorized as pancreatic ductal adenocarcinomas (PDACs). Over 90% of PDACs carry point mutations in the *KRAS* gene, resulting in constitutive activation of the KRAS protein and enhanced activity of downstream signaling cascades, including MAPK, PI3K/AKT, and PLCε/PKC pathways. Abnormal *KRAS* activation represents an early event during pancreatic tumorigenesis, as *KRAS* mutations have been detected in pancreatic intraepithelial neoplasia (PanIN), a common PDAC precursor. Evidence from mouse models indicates that mutant KRAS plays a critical role in the initiation of PDAC. (Reviewed in (Karreth and Tuveson, 2009)).

In addition to *KRAS* mutations, recent advances in genome sequencing have documented a complex picture of genetic interactions in the initiation and progression of pancreatic cancer (Jones *et al*., 2008). This analysis has demonstrated frequent genetic alterations in a wide variety of core signaling pathways, including TGFβ, Wnt, Notch, and Hedgehog. While these core pathways were altered in the majority of analyzed tumors, the specific pathway components found to be mutated in any individual tumor varied widely, and the functional significance of the many identified mutations remains unclear. Further understanding of these changes at a functional level, especially related to genetic interactions between mutant *KRAS* and other observed mutations, will doubtlessly be important in the identification of new genetic targets for both early diagnosis and more effective treatment.

The zebrafish pancreas shares significant anatomical similarity with its mammalian counterparts. More importantly, the underlying regulatory molecular mechanisms for pancreas development are well-conserved between zebrafish and mammals (Reviewed in (Kinkel and Prince, 2009; Tiso *et al*., 2009)). To study KRAS-initiated pancreatic tumorigenesis, our lab generated a transgenic zebrafish model that specifically expresses the human $KRAS^{G12V}$ mutant fused with an N-terminal eGFP tag in the exocrine pancreas (Park *et al*., 2008). The transgene was placed under control of zebrafish *ptf1a* regulatory elements through BAC recombineering. Ptf1a (pancreas specific transcription factor 1 a) is a basic-helix-basic transcription factor that plays a crucial role in pancreas development both in mammals and zebrafish (Kawaguchi *et al*., 2002; Lin *et al*., 2004; Zecchin *et al*., 2004). In the mouse model, constitutive activation of a mutant human KRAS protein in Ptf1a-expressing cells led to the development of PanIN and eventual PDAC, fully recapitulating the progression sequence observed in humans (Hingorani *et al*., 2003). ptf1a:eGFP-$KRAS^{G12V}$ transgenic fish developed pancreatic tumors that displayed some histological resemblance to human pancreatic cancer, albeit with a strong bias towards acinar cell carcinomas as opposed to classical PDAC (Park *et al*., 2008). Further analysis of the tumors also showed abnormal activation of Hedgehog signaling pathway, a trait commonly observed in human tumors.

These results indicated that the zebrafish indeed represents a potentially useful organism for studying the biology of KRAS-initiated pancreatic cancer. Furthermore, based on the relative low cost associated with zebrafish transgenesis, the fish may represent the most attractive platform for functionally annotating the emerging pancreatic cancer genome, especially the evaluation of novel dominant candidate oncogenes. However, the generation of multiple BAC transgenic lines in which candidate oncogenes are expressed under the control of *ptf1a* regulatory elements represents a daunting task, which led us to develop a novel Gal4/UAS approach that allows the simultaneous expression of multiple candidate oncogenes in ptf1a-expressing pancreatic cell types.

A. Rationale

In this chapter, we describe the utility of a dyad Gal4/UAS system for establishing either stable or transient transgenic models that consistently produce tumors in adult fish. The Gal4/UAS system has been successfully adapted to zebrafish, thus providing precise temporal and spatial control of transgene expression (Reviewed in (Halpern *et al*., 2008)). In the absence of a Gal4 driver gene, transgenes placed downstream of UAS (upstream activator sequence) elements are typically not expressed, thus avoiding the possible toxic effect of oncogene overexpression that can hinder generation of stable transgenic models.

The Gal4/UAS system allows quick and effective generation of transgenic models that can be used to interrogate interactions among multiple genes of interest in a tissue-specific manner. Multiple transgenes can be easily cloned downstream of UAS elements in *Tol2*-based vectors via conventional cloning methods and then

co-injected into an established Gal4 driver line to generate simultaneous transient and/or stable expression of the transgenes within the same tissue. Utilization of *Tol2* transposon-mediated transgenesis thereby provides the simultaneous advantages of both high frequency somatic expression as well as high germline transmission efficiency, especially when compared to the lower efficiency associated with BAC transgenesis.

We also describe techniques used to identify and characterize pancreatic tumors in adult transgenic fish. To study the molecular mechanism underlying pancreatic tumorigenesis, it is essential to be able to detect and document distinct histologic features as well as associated molecular changes during cancer initiation and progression.

II. Transgenic Zebrafish with Gal4/UAS-Mediated eGFP-KRAS^{G12V} Expression in the Exocrine Pancreas

A. Generation of UAS Regulated eGFP-KRAS^{G12V} Transgene

The fusion eGFP-KRAS^{G12V} transgene was cloned downstream of a 14xUAS element in a *Tol2*-based vector backbone (Davison *et al*., 2007). A single amino acid change at codon 12 of human KRAS protein, from glycine to valine, leads to membrane localization and constitutive activation of the mutant protein. To avoid the insertion site position effects observed commonly among UAS transgenes, multiple founders need to be identified and examined for phenotypes (Urasaki and Kawakami, 2009).

The UAS construct was co-injected with *Tol2* transposase into wildtype AB zebrafish embryos at the one- to two-cell stage. To identify fish carrying the UAS transgene, we routinely genotype fish when they reach reproductive maturation. The *Tol2*-mediated microinjection protocol and purification of genomic DNA for genotyping PCR have been described elsewhere (Fisher *et al*., 2006; Westfield, 2007).

Mosaicism and silencing of transgene expression are two major issues commonly encountered when using the Gal4/UAS system (Davison *et al*., 2007; Halpern *et al*., 2008). In the case of functional analysis of candidate oncogenes, mosaic transgene expression may be advantageous, because the cells not expressing the oncogene can be used as neighboring controls for comparative analysis against oncogene-expressing cells. However, the silencing issue, together with oncogene toxicity, does present an obstacle to establishing stable transgenic models that provide consistent tumor formation across multiple generations. In our experience, maintaining UAS transgenic fish in the absence of a Gal4-VP16 driver seems to minimize these issues.

B. Gal4/UAS-Mediated Expression of eGFP-KRAS^{G12V} Transgene in the Exocrine Pancreas

The UAS:eGFP-KRAS^{G12V} transgenic fish are crossed to the ptf1a:Gal4-VP16 transgenic fish, to direct eGFP-KRAS^{G12V} expression in the exocrine pancreas (Fig. 1) (Halpern *et al*., 2008; Pisharath and Parsons, 2009). In zebrafish, the

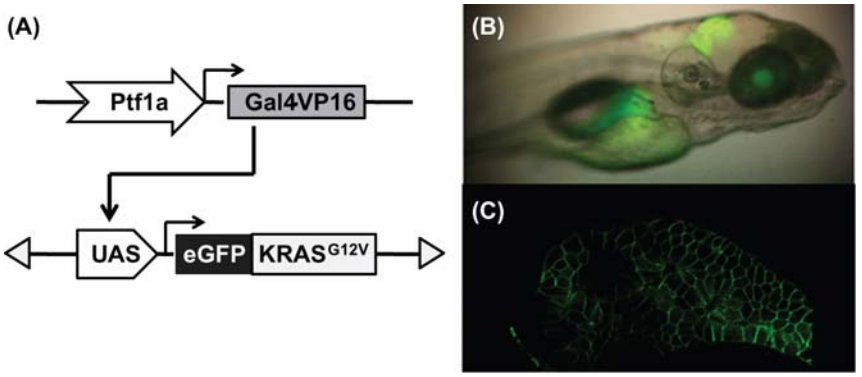

Fig. 1 Targeted expression of eGFP-KRAS^{G12V} transgene in zebrafish pancreas. (A) Schematic drawing of the dyad Gal4/UAS system used to drive eGFP-KRAS^{G12V} transgene expression in the Ptf1a domain. (B) Lateral view under transmitted and fluorescent illumination of a larval fish at 5 days post fertilization (dpf), showing expression pattern of eGFP-KRAS^{G12V} transgene in the Ptf1a domain, including the retina, the hindbrain, and the exocrine pancreas. (C) Two-photon confocal image of the pancreas from a live 5 dpf larval fish, revealing the membrane localization of eGFP-KRAS^{G12V} protein. (For color version of this figure, the reader is referred to the web version of this book.)

earliest ptf1a-driven expression is observed in the hindbrain at 22 hpf (Lin *et al*., 2004). The expression in the exocrine pancreas begins around 34 hpf, and continues through adulthood. The embryos are cultured in embryo medium (Westfield, 2007) containing 0.003% phenylthiourea, and screened for pancreatic expression based on eGFP fluorescence (Fig. 1B). The eGFP-KRAS^{G12V} protein displays a membrane-bound subcellular localization, as expected based upon normal activated KRAS localization (Fig. 1C).

In our previous model, where the eGFP-KRAS^{G12V} transgene was placed directly under *ptf1a* regulatory elements through BAC recombineering, exocrine pancreatic progenitor cells expressing eGFP-KRAS^{G12V} failed to undergo primary exocrine differentiation, leading to an accumulation of undifferentiated progenitor cells expressing oncogenic KRAS (Park *et al*., 2008). This embryonic phenotype was associated with eventual loss of eGFP fluorescence as early as 96 hpf. The Gal4/UAS-mediated model does not display this type of embryonic phenotype – transgene expression of eGFP-kRAS^{G12V} was observed uninterrupted from larval stages through adulthood. We suspect that the difference observed between the two models may be explained by the levels and timing of Gal4 onset, as delayed Gal4 onset in early developmental stages has been observed by others (Zhan and Gong, 2010).

III. Identification and Characterization of Pancreatic Tumors

Tagging the oncogenic KRAS mutant with eGFP allows tracking of pancreatic tumor formation by monitoring visceral expression of GFP fluorescence in transgenic fish (Fig. 2A.B). Tumors developing in transgenic fish can be easily

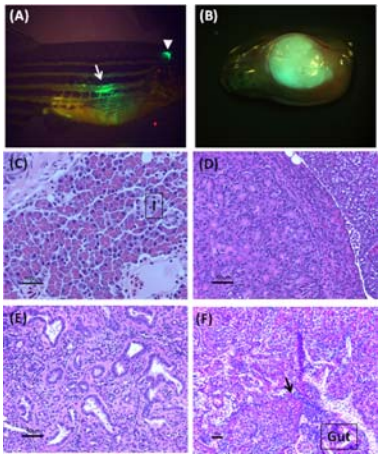

Fig. 2 Identification and histological evaluation of KRAS-initiated pancreatic tumors in transgenic zebrafish. (A) Lateral view under transmitted and fluorescent illumination of an adult transgenic fish carrying a tumor in the pancreas. Expression of eGFP-KRAS^{G12V} transgene remains strong in the cerebellum (white arrowhead) of the adult fish. Formation of a tumor is indicated by the presence of intense eGFP fluorescence (white arrow) detected transcutaneously. (B) Lateral view under transmitted and fluorescent illumination, of an entire viscera with an eGFP-positive tumor. (C) Normal zebrafish adult pancreas, showing well-organized acinar cells in the exocrine pancreas (I: islet). (D) A tumor with acinar cell differentiation. The periphery of acinar cell carcinoma is generally circumscribed with minimal stroma within the tumor. Acinar cell differentiation of the tumor can be further confirmed by the presence of pancreatic exocrine enzymes, such as trypsin and elastase. (E) Part of a tumor showing ductal differentiation. The haphazard growth pattern of the ducts associated with stromal desmoplastia is a prominent histological feature of tumors with ductal differentiation. (F) A malignant tumor invading neighboring intestinal tube (gut). Infiltrating tumor cells (black arrow) disrupt normal borders between pancreas and adjacent organs. (See color plate.)

distinguished from normal adult pancreas histologically, based upon their size, distribution, and disrupted pattern of epithelial organization. Typically, 50% of ptf1a:Gal4-VP16; UAS:eGFP-KRAS^{G12V} fish are found to develop pancreatic tumors by 5 months of age, with detection of tumors as early as 2 months. These tumors display features of acinar cell and/or ductal cell differentiation and invasion into neighboring organs, all demonstrating significant similarity to the human disease (Fig. 2C–F) (Hruban *et al*., 2007). Transient expression of eGFP-KRAS^{G12V}, through injection of the *Tol2*-based UAS:eGFP-KRAS^{G12V} construct into ptf1a:Gal4-VP16 embryos, displayed a mosaic transgene expression pattern in ptf1a domains and did not result in tumor formation in adult fish. Functional analysis of potential oncogenes can thus be carried out in both stable and transient models to address their role in both cancer initiation and/or progression. The stable model of ptf1a:Gal4-VP16; UAS:eGFP-KRAS^{G12V} may be more suitable for the analysis of oncogene interactions during cancer progression, whereas the transient approach may be more informative for studies of tumor initiation.

In both BAC and Gal4/UAS transgenic models, expression of the eGFP-KRAS^{G12V} transgene in the hindbrain is observed during embryonic stages and later restricted to the cerebellum in adult fish (Fig. 1B, 2A). We have not identified any

tumor developing in the hindbrain/cerebellum region of transgenic fish expressing eGFP-KRAS^{G12V}. However, when overexpression of mutant KRAS is combined with transient expression of an additional oncogene – for example, a constitutively active mutant form of human YAP1 protein – rapid formation of tumors was observed in the hindbrain/cerebellum region by 1 month of age. Many oncogenes are involved in tumorigenesis only in selected tissues, thus the hindbrain/cerebellum region presents an additional organ site for evaluating a target gene's oncogenic function.

To best preserve anatomical details of tumors and surrounding organs, we embed tissues in paraffin and then evaluate tumor histology after hematoxylin and eosin staining. Immunohistochemical and immunofluorescent staining are performed on paraffin-embedded and/or frozen sections to further confirm eGFP-KRAS^{G12V} transgene expression and to determine the expression patterns of other genes that may be involved in pancreatic tumorigenesis. Together, these techniques allow the initial detection and characterization of oncogene-initiated pancreatic cancer in zebrafish.

A. Identifying Pancreatic Tumors Expressing eGFP-KRAS^{G12V} in Living Fish

In adult zebrafish, the anatomical structure of the pancreas evolves from the distinct head–neck–tail morphology observed during larval and early juvenile stages to organization of four linked lobes surrounding the intestinal tube (Chen *et al.*, 2007). Prior to tumor formation, diffuse pancreatic eGFP expression in ptf1a:Gal4-VP16; UAS:eGFP-KRAS^{G12V} transgenic fish is indistinguishable from autofluorescence from the intestinal tube when the whole fish is visualized under a fluorescent dissecting microscope. In contrast, when tumors arise in the pancreas, the intensity of the eGFP expression from most of the tumor mass is usually strong enough to be detected transcutaneously, except in the few cases where very small tumor masses are nested in between folds of intestinal tube.

To check for pancreatic tumor formation in ptf1a:Gal4-VP16; UAS:eGFP-KRAS^{G12V} transgenic fish, anesthetize fish in a 250 ml beaker containing 100 ml of system water and 4–5 ml of 400 mg/ml tricaine stock solution prepared with dH_2O. Lay fish sideways on a petri dish lid. Confirm transgene expression by viewing eGFP fluorescence in the cerebellum with a fluorescence dissecting microscope (Fig. 2A). Then look for discernible eGFP expression in the abdominal area (Fig. 2A). After examination, return fish promptly to fresh system water for recovery.

B. Dissection and Fixation of Transgenic Fish Bearing KRAS-Initiated Pancreatic Tumors

1. Dissection of Visceral Organs

A major concern when obtaining pancreatic tumor samples from transgenic fish is the prevention of autolysis, because pancreatic tissue carries high levels of both protease and ribonuclease activity. To minimize degradation of tissues during the process, we recommend using a rapid cooling method for euthanasia (Wilson *et al.*,

2009). Dissection should be carried out as soon as fish are euthanized. Normal adult pancreas is heavily infiltrated with fatty tissues, giving an opaque "slimy" appearance when visualized under brightfield illumination. Tumors are densely packed and present themselves as solid white masses under brightfield with detectable eGFP fluorescence (Fig. 2B).

a. Place euthanized fish on a petri dish lid, with right side of the fish facing up. Use microdissection scissors to make an incision near the cloaca, and gently open up the right abdominal wall from posterior to anterior, to expose internal organs.
b. Under a dissecting microscope, use sharp tipped forceps to separate the skin from the viscera. Once separated, cut the skin with scissors to remove the right abdominal wall in its entirety.
c. Confirm tumor location via bright field and/or fluorescence microscopy.
d. Remove the two swim bladders with forceps. Make a final cut right below the heart to dissect out the entire viscera. Segments of tumor can be removed with scissors at this stage if further RNA/protein purification is desired. Rinse the remaining tissue briefly in PBS. Blot dry tissue and proceed to fixation.

2. Fixation

Fixation solutions should be at least 10 times the volume of tissue.

a. Fixation for paraffin-embedded sections: Incubate dissected tissue in 10% buffered formalin solution at room temperature overnight. If sample will be used solely for paraffin-embedded sections, whole fish can be fixed prior to dissection. The fixation hardens tissue and facilitates organ separation during dissection. For whole-fish fixation, first inject 100–200 μl of 10% buffered formalin intraperitonially into euthanized fish with a 1-ml syringe fitted with a 26-gauge needle. This step helps to minimize autolysis of the pancreas during fixation process. The whole fish can then be incubated in 10% buffered formalin at room temperature overnight.
b. Fixation for frozen sections: Incubate dissected tissue in 4% paraformaldehyde (PFA) prepared in PBS overnight at 4 °C. Our experience suggests that frozen sections are not suitable with whole fish.

C. Preparing Paraffin-Embedded Sections of Tumors

Paraffin-embedded sections best preserve the overall structure of tumors and their surrounding organs and therefore are optimal for evaluating tumor histology. However, paraffin-embedded sections are not compatible for labeling with certain antibodies and are especially problematic when observed by immunofluorescence microscopy.

1. Decalcification (optional)

Decalcification is recommended if an entire adult fish is embedded in paraffin.

a. Incubate fish in 0.5 M EDTA, pH 7.8, for 7 days at room temperature.
b. Wash three times with dH2O for 20 min each.

2. Preliminary Embedding in Agar (Optional)

Embedding tissues in agar prior to paraffin embedding is very beneficial when working with small and friable samples (Lund *et al*., 1961). It minimizes the loss of tissue during vigorous processing procedures, allows placement of multiple small tissues within one block, and provides orientation for sectioning.

a. Prepare agar solution per manufacturer's instruction. Sterilize agar solution and let cool to ~50 °C.
b. Blot dry tissues briefly. Arrange tissues on a glass slide, with the region of interest in contact with the slide surface.
c. Slowly drip agar solution on top of tissues. Let solidify. If the tissue does not stay flat on its own, use forceps to hold the tissue in place during agar solidification.
d. Use a razor blade to trim agar block to desired size for paraffin embedding.

3. Paraffin Embedding and Sectioning

Place tissue in an embedding cassette (FisherScientific, 22-272-417). Use working solution at least 10 times the volume of tissue embedded for each step. When processing small sized tissue samples, the length of incubation time in the initial dehydration steps may be shortened to avoid over-drying of samples and resulting tissue tearing during sectioning.

a. Incubate tissue in two washes of 70% ethanol for 15 min each at room temperature with gentle agitation.
b. Incubate tissue in 85% ethanol for 30 min at room temperature with gentle agitation.
c. Incubate tissue in 95% ethanol for 30 min at room temperature with gentle agitation.
d. Incubate tissue in two washes of 100% ethanol for 30 min each at room temperature with gentle agitation.
e. Incubate tissue in Histoclear (National Diagnostics: HS-200) for 15–30 min at room temperature with gentle agitation.
f. Incubate tissue in Histoclear for 15–30 min at 60 °C.
g. Incubate tissue in Histoclear/paraffin (V/V = 1:1) for 30 min at 60 °C.
h. Incubate tissue in two washes of paraffin for 30–60 min each at 60 °C.
i. Incubate tissue in paraffin for 30–60 min at 60 °C. Alternatively, tissue can be left in paraffin overnight at 60 °C.

j. Fill the bottom of a stainless steel base mold (Sakura Finetek, 4163) with paraffin at 60 °C. If tissues have been embedded in agar, place the agar block in the middle of the mold, then proceed to STEP k. If tissue has not been preliminarily embedded in agar, place tissue in the middle of mold, with region of interest facing down, then place the mold on cold plate briefly to immobilize tissue in the mold while leaving most of the paraffin in liquid form.
k. Fill the mold with paraffin at 60 °C. Leave mold on cold plate until paraffin solidifies.
l. Process paraffin blocks on Leica RM2135 microtome or equivalent. Sections are cut at 5 μm thickness and then placed on superfrost plus-charged microscope slides (FisherScientific, 12-550-15). Microtome sectioning techniques will not be discussed here.
m. Heat slides at 60 °C for 20 min, or at 42 °C overnight, to ensure complete dehydration and flattening of the paraffin. The slides can then be stored at room temperature away from light.

D. Preparing Frozen Sections of Dissected Tumors

Although some histologic detail is lost with frozen sections, this is typically the embedding method of choice for immunofluorescent labeling due to better epitope preservation. In addition, native eGFP fluorescence expressed from the transgene is preserved when tissue is fixed in 4% PFA and embedded in O.C.T. compound. This allows rapid assessment of transgene expression in frozen sections.

1. Sucrose Treatment

a. Rinse PFA fixed tissue twice with PBS. Blot dry tissue.
b. Incubate tissue in 30% sucrose prepared in PBS at 4 °C overnight.

2. O.C.T Compound Treatment

a. Place a plastic cryomold (Sakura Finetek, 4557) on dry ice. Cover bottom of the cryomold with a layer of O.C.T. Compound (Sakura Finetek, 4583). Let the compound freeze.
b. Rinse tissue briefly in PBS. Blot dry the tissue, place on top of the layer of O.C.T. compound, and orient the tissue for sectioning.
c. Add O.C.T. compound to cover tissue in the cryomold. Allow compound to freeze at −80 °C (dry ice) or by placing in liquid nitrogen. Store frozen block at −80 °C.

3. Sectioning

Frozen blocks are sectioned using a Leica CM1850 cryostat or equivalent. Sections are cut at 5–10 μm thickness and then placed on superfrost plus charged microscope slides. Air dry slides briefly and store slides at −80 °C.

4. Rapid Evaluation of eGFP-KRAS^{G12V} Expression

a. Wash slides three times in PBS for 5 min each.
b. Remove excess PBS from slides. Add Vectashield mounting media (Vector Laboratories, H-1200) to slides for fluorescence microscopy. Gently place coverslip on slides to avoid air bubbles. Slides can be sealed with nail polish around coverslip edges.
c. Check slides for eGFP expression under an inverted fluorescence microscope.

E. Hematoxylin and Eosin (H&E) Staining

H&E staining provides optimal histologic detail for characterizing tumor differentiation, invasion, and/or metastatic behavior. Staining of paraffin-embedded sections requires deparaffinization/rehydration. For frozen sections, thaw slides to room temperature and start from STEP 2.

1. Deparaffinization/Rehydration

a. Deparaffinize slides in two washes of Histoclear for 5 min each.
b. Hydrate slides by two washes of 100% ethanol for 2 min each, then two washes of 95% ethanol for 2 min each.
c. Wash slides twice in dH_2O for 5 min each.

2. H&E staining

The intensity of H&E staining can be modified by adjusting the incubation time in hematoxylin and/or eosin solution.

a. Incubate slides in Harris hematoxylin staining solution (Sigma–Aldrich, HHS16) for 30 s to 2 min.
b. Rinse in running tap water for 5 min.
c. Incubate slides in 95% ethanol for 1 min.
d. Incubate in eosin Y solution (Sigma–Aldrich, HT1101128), prepared per manufacturer's instruction, for 15 s to 2 min.
e. Dehydrate slides in 95% ethanol for 2 min then wash twice with 100% ethanol (2 min each).
f. Air dry slides briefly.
g. Add Histomount (Invitrogen, 00-8030) to cover sections. Gently place coverslip on slides to avoid air bubbles.

F. Immunohistochemical (IHC) Staining for Paraffin-Embedded Sections

We usually test new antibodies using the following protocol as starting point. All steps are performed at room temperature unless specified.

1. Deparaffinize and Rehydrate Sections as Described in Section II.E.
2. Antigen Unmasking (Optional)

Our lab routinely uses the sodium citrate buffer method for antigen unmasking. For most antibodies we tested, the addition of this step prior to staining leads to more intense signals. However, there are cases where antigen unmasking does not help or actually weakens staining signals.

a. Place the slides in a slide rack and immerse them in a plastic staining dish with 250 ml of antigen unmasking solution (Vector Laboratories, H-3300). Bring solution to boiling in water bath or microwave. Maintain temperature at 95–99 °C for 10 min.
b. Place the plastic staining dish with solution and slides on ice. Allow slides to cool for 30 min.
c. Wash slides three times in dH_2O for 5 min each.

1. IHC Staining Using ABC Avidin/Biotin Method

a. Quench endogenous peroxidase activity by incubating slides in 3% hydrogen peroxide diluted in dH_2O for 10 min.
b. Wash slides twice in dH_2O for 5 min each.
c. Incubate slides in blocking buffer (PBS-0.1%Tween-20 (PBST) containing 10% normal serum from the same species as the secondary antibody) for 60 min.
d. Prepare primary antibody dilution in blocking buffer. Remove blocking buffer from slides. Add antibody solution to slides, and incubate overnight at 4 °C.
e. Wash slides three times in PBST for 5 min each.
f. Incubate slides in biotinylated secondary antibody diluted in blocking buffer for 1 h.
g. Wash slides three times with PBST for 5 min each.
h. During STEPs f and g, prepare ABC reagent (Vector Laboratories, PK-6100) per manufacturer's instructions and incubate solution for 30 min.
i. Add ACB reagent to cover sections and incubate for 30 min.
j. Wash slides three times with PBST for 5 min each.
k. Add DAB substrate (Vector Laboratories, SK-4100) to each section. Monitor the sections develop staining. When the staining reaches desired intensity, immerse slides immediately into dH_2O.
l. Follow Section II.E.2a to counterstain slides in hematoxylin (Optional).
m. Wash slides twice with dH_2O for 5 min each.
n. Dehydrate slides.
o. Incubate slides in 95% ethanol for 2 min, then in two washes of 100% ethanol for 2 min each, and finally in two washes of Histoclear for 2 min each.
p. Add Histomount to slides. Gently place coverslip on slides to avoid air bubbles. Slides should be stored away from light at room temperature.

G. Immunofluorescent (IF) Staining

IF staining can be performed on paraffin-embedded or frozen sections depending on the characteristics of the antibody tested. IF staining allows detection of multiple antigens on the same slide. However, the utility of this method is limited by the availability and quality of antibodies.

Paraffin-embedded sections require deparaffinization/rehydration and antigen unmasking (optional) described in Sections II.E and II.F prior to the IF staining procedure. All steps are performed at room temperature unless specified. Place slides in a humidified chamber during the procedure to prevent drying.

1. Blocking

a. Rinse slides in PBS for 5 min.
b. Incubate slides in blocking buffer (PBST containing 5% normal serum from the same species as the secondary antibody) for 60 min.

2. Incubation in Primary Antibody

a. Prepare primary antibody dilution in blocking buffer.
b. Remove blocking buffer. Add primary antibody solution to slides, and incubate overnight at 4 °C.
c. Wash slides three times in PBST for 5 min each.

3. Detection

a. Prepare fluorochrome-conjugated secondary antibody dilution in PBST.
b. Incubate slides in secondary antibody solution for 1–2 h in dark.
c. Wash slides three times in PBST for 5 min each.
d. Add Vectashield mounting media to slides. Gently place coverslip on slides to avoid air bubbles. Slides can be sealed with nail polish around coverslip edges. IF stained slides should be stored flat at 4 °C in dark.

IV. Conclusions

The Gal4/UASA-mediated zebrafish pancreatic cancer model is a useful tool for examining the biology of KRAS-initiated pancreatic neoplasia, especially for delineating crosstalk between KRAS and other signaling pathways involved in the initiation and progression of pancreatic tumor formation. The techniques reviewed in this chapter are suitable for generating and characterizing any transgenic zebrafish cancer model involving tissue-specific single or multiple candidate oncogenes.

Acknowledgments

We thank Michael J. Parsons for providing ptf1a:Gal4-VP16 transgenic zebrafish for the study. This work is supported by NIH Grant P01 CA134292 (to SDL).

References

In "SEER Cancer Statistics Review, 1975–2007," (S. F. Altekruse, C. L. Kosary, M. Krapcho, N. Neyman, R. Aminou, W. Waldron, J. Ruhl, N. Howlader, Z. Tatalovich, H. Cho, A. Mariotto, M. P. Eisner, D. R. Lewis, K. Cronin, H. S. Chen, E. J. Feuer, D. G. Stinchcomb, and B. K. Edwards, eds.), National Cancer Institute, Bethesda, MD http://seer.cancer.gov/csr/1975_2007/, based on November 2009 SEER data submission, posted to the SEER web site, 2010.

Chen, S., Li, C., Yuan, G., and Xie, F. (2007). Anatomical and histological observation on the pancreas in adult zebrafish. *Pancreas* **34**, 120–125.

Davison, J. M., Akitake, C. M., Goll, M. G., Rhee, J. M., Gosse, N., Baier, H., Halpern, M. E., Leach, S. D., and Parsons, M. J. (2007). Transactivation from Gal4-VP16 transgenic insertions for tissue-specific cell labeling and ablation in zebrafish. *Dev. Biol.* **304**, 811–824.

Fisher, S., Grice, E. A., Vinton, R. M., Bessling, S. L., Urasaki, A., Kawakami, K., and McCallion, A. S. (2006). Evaluating the biological relevance of putative enhancers using Tol2 transposon-mediated transgenesis in zebrafish. *Nat. Protoc.* **1**, 1297–1305.

Halpern, M. E., Rhee, J., Goll, M. G., Akitake, C. M., Parsons, M., and Leach, S. D. (2008). Gal4/UAS transgenic tools and their application to zebrafish. *Zebrafish* **5**, 97–110.

Hingorani, S. R., Petricoin, E. F., Maitra, A., Rajapakse, V., King, C., Jacobetz, M. A., Ross, S., Conrads, T. P., Veenstra, T. D., and Hitt, B. A., *et al*. (2003). Preinvasive and invasive ductal pancreatic cancer and its early detection in the mouse. *Cancer Cell* **4**, 437–450.

Hruban, R. H., Pitman, M. B., and Klimstra, D. S. (2007). *AFIP Atlas of Tumor Pathology. Tumors of the pancreas.* American Registry of Pathology Press, Washington, DC.

Jemal, A., Siegel, R., Xu, J., and Ward, E. (2010). Cancer statistics, 2010. *CA Cancer J. Clin.* **60**, 277–300.

Jones, S., Zhang, X., Parsons, D. W., Lin, J. C., Leary, R. J., Angenendt, P., Mankoo, P., Carter, H., Kamiyama, H., and Jimeno, A., *et al*. (2008). Core signaling pathways in human pancreatic cancers revealed by global genomic analyses. *Science* **321**, 1801–1806.

Karreth, F. A., and Tuveson, D. A. (2009). Modelling oncogenic Ras/Raf signalling in the mouse. *Curr. Opin. Genet. Dev.* **19**, 4–11.

Kawaguchi, Y., Cooper, B., Gannon, M., Ray, M., MacDonald, R. J., and Wright, C. V. (2002). The role of the transcriptional regulator Ptf1a in converting intestinal to pancreatic progenitors. *Nat. Genet.* **32**, 128–134.

Kinkel, M. D., and Prince, V. E. (2009). On the diabetic menu: zebrafish as a model for pancreas development and function. *Bioessays* **31**, 139–152.

Lin, J. W., Biankin, A. V., Horb, M. E., Ghosh, B., Prasad, N. B., Yee, N. S., Pack, M. A., and Leach, S. D. (2004). Differential requirement for ptf1a in endocrine and exocrine lineages of developing zebrafish pancreas. *Dev. Biol.* **270**, 474–486.

Lund, H. Z., Forrest, W. W., Harris, J. R., and Brown, E. H. (1961). Preliminary embedding in agar-agar. Its value in the processing of multiple separately identified specimens, and in the orientation of small biopsy specimens. *Tech. Bull. Regist. Med. Technol.* **31**, 192–194.

Park, S. W., Davison, J. M., Rhee, J., Hruban, R. H., Maitra, A., and Leach, S. D. (2008). Oncogenic KRAS induces progenitor cell expansion and malignant transformation in zebrafish exocrine pancreas. *Gastroenterology* **134**, 2080–2090.

Pisharath, H., and Parsons, M. J. (2009). Nitroreductase-mediated cell ablation in transgenic zebrafish embryos. *Methods Mol. Biol.* **546**, 133–143.

Tiso, N., Moro, E., and Argenton, F. (2009). Zebrafish pancreas development. *Mol. Cell Endocrinol.* **312**, 24–30.

Urasaki, A., and Kawakami, K. (2009). Analysis of genes and genome by the tol2-mediated gene and enhancer trap methods. *Methods Mol. Biol.* **546**, 85–102.

Westfield, M. (2007). *The Zebrafish Book. A guide for the Laboratory Use of Zebrafish (Danio rerio). University of Oregon Press, Eugene.*

Wilson, J. M., Bunte, R. M., and Carty, A. J. (2009). Evaluation of rapid cooling and tricaine methanesulfonate (MS222) as methods of euthanasia in zebrafish (Danio rerio). *J. Am. Assoc. Lab. Anim. Sci.* **48**, 785–789.

Zecchin, E., Mavropoulos, A., Devos, N., Filippi, A., Tiso, N., Meyer, D., Peers, B., Bortolussi, M., and Argenton, F. (2004). Evolutionary conserved role of ptf1a in the specification of exocrine pancreatic fates. *Dev. Biol.* **268**, 174–184.

Zhan, H., and Gong, Z. (2010). Delayed and restricted expression of UAS-regulated GFP gene in early transgenic zebrafish embryos by using the GAL4/UAS system. *Mar. Biotechnol. (NY)* **12**, 1–7.

CHAPTER 16

Zebrafish Models of Rhabdomyosarcoma

Eleanor Y. Chen[*,†] **and David M. Langenau**[*,‡,§]

[*]Molecular Pathology Unit, Massachusetts General Hospital, Charlestown, MA, USA

[†]Department of Pathology, Brigham and Women's Hospital, Harvard Medical School, Boston, MA, USA

[‡]Center of Cancer Research, Massachusetts General Hospital, Charlestown, MA, USA

[§]Harvard Stem Cell Institute, Boston, MA, USA

Abstract

Rhabdomyosarcoma (RMS), an aggressive malignant neoplasm that shows features of skeletal muscle, is the most common soft tissue tumor of childhood. In children, the major subtypes are embryonal and alveolar. Although localized disease responds to a multimodal treatment, the prognosis for patients with high-risk features and metastasis remains dismal. Several *in vivo* models of RMS have been developed in mouse, human xenografts, zebrafish, and *Drosophila* to better understand the underlying mechanisms governing malignancy. The findings so far have indicated the potential role of skeletal muscle precursor cells in malignant transformation. To better understand histogenesis and different aspects of tumorigenesis in RMS, we have previously developed a robust zebrafish model of kRAS-induced

METHODS IN CELL BIOLOGY, VOL 105

0091-679X/10 $35.00
DOI 10.1016/B978-0-12-381320-6.00016-3

RMS, which shares morphologic and immunophenotypic features with the human counterpart. Cross-species mircroarray comparisons confirm that conserved genetic pathways drive RMS growth. The ease for *ex vivo* manipulation allows the development of different transgenic and co-injection strategies to induce tumor formation in zebrafish. In contrast to other vertebrate model systems, the tumor onset in zebrafish is short, allowing for efficient study of different tumor processes including tumor growth, self-renewal, and maintenance.

I. Introduction

Rhabdomyosarcoma (RMS) is the most common soft tissue tumor in the pediatric population and displays phenotypic and biological features of embryonic skeletal muscle. RMS occurs in 4.6/million U.S. children under 15 years of age (Gurney *et al*., 1996). It falls into two major groups in children–embryonal and alveolar. Embryonal rhabdomyosarcoma (ERMS) constitutes the most common subtype, accounting for about 60% of childhood cases. Treatment for RMS is multimodal including surgical re-section, chemotherapy, and radiation. Alveolar rhabdomyosarcoma (ARMS) is often more aggressive than the embryonal subtype; however, the prognosis for patients with high-risk features or metastasis remains dismal regardless of subtypes.

ARMS is characterized by a (2; 13) translocation in the majority of cases and a (1; 13) translocation in a smaller subset of cases. These translocations juxtapose the 5' DNA-binding domains of PAX3 or PAX7 genes on chromosomes 2 and 1, respectively, with the transactivation domain at the 3' portion of FKHR gene on chromosome 13. Translocations generate chimeric PAX3/FKHR and PAX7/FKHR fusion genes that act as novel oncogenic transcription factors (Barr *et al*., 1992, 1993; Galili *et al*., 1993; Davis *et al*., 1994). Fusion gene-negative ARMS comprise approximately 15% of the ARMS subtype and are clinically and molecular indistinguishable from ERMS (Williamson *et al*., 2010). ERMS has frequent allelic loss in chromosomal region 11p15 (Koufos *et al*., 1985; Scrable *et al*., 1987), with this genetic interval harboring a number of imprinted genes implicated in oncogenesis, such H19, IGF2, and p57 ^{kip2}. Activating mutations of RAS genes are common in ERMS with ~25% of patients harboring activating point mutations in H-RAS, K-RAS, or N-RAS (Chen *et al*., 2006; Stratton *et al*., 1989). Moreover, cross-species comparisons of human and RAS-induced ERMS in zebrafish revealed that the RAS pathways is active in a majority of human ERMS, but the mechanism leading to constitutive RAS signaling has yet to be elucidated (Langenau *et al*., 2007). Activated RAS signaling has also been shown to block myogenic differentiation through down regulation of myogenic factors such as MyoD and myogenin (Konieczny *et al*., 1989; Lassar *et al*., 1989). Identification of germ-line mutations of H-RAS in Costello syndrome, a genetic disorder that pre-disposes affected individuals to embryonic tumors including ERMS further supports the role of H-RAS in the pathogenesis of RMS. Other significant genetic alterations identified in both

embryonal and ARMS include p53 mutations and *N*-myc amplification (Felix *et al*., 1992; Mulligan *et al*., 1990; Stratton *et al*., 1990). Taken together, it is clear that RAS pathway activation is important for tumor onset in ERMS while other genetic pathways likely aid in the multi-step progression to full malignancy.

Several murine models of RMS have been reported in the literature (Table I). In one murine model, a combination of Her2/neu oncogene activation and p53 inactivation leads to the development of ERMS (Nanni *et al*., 2003). In another murine model, simultaneous loss of Ink4a/Arf function and activation of c-Met signaling in mice transgenic for hepatocyte growth factor/scatter factor (HGF/SF) induces ERMS (Sharp *et al*., 2002). Keller *et al*. (2004) used the conditional knock-in strategy to generate a murine alveolar RMS model, by inducing expression of PAX3-FKHR gene in the skeletal muscle using a Myf6-Cre mouse line. However, the expression of PAX3-FKHR alone did not induce malignancy, and additional inactivation of the Ink4a/Arf and Trp53 pathways was necessary to induce ARMS. These models indicate that functional impairment of p53 is essential for the development of RMS because Arf acts via p53, although additional genetic hits are necessary for tumorigenesis. Tsumura *et al*. (2006) generated a knock-in mouse line with oncogenic K-ras, conditionally activated by Cre/LoxP system in either heterozygous or homozygous for p53 knockout animals. Electroporation of Cre expression vector in skeletal muscle resulted in the generation of RMS in adults with tumor incidences of 100% at 10 weeks and 40% at 15 weeks, in p53 -/- and p53 -/+ backgrounds, respectively. The tumor has the morphologic features of pleomorphic RMS with haphazardly arranged large, round, and pleomorphic cells and positive expression of myogenic markers on immunohistochemistry. Thus, K-ras and p53 deficiency cooperate to induce the development of pleomorphic RMS when targeted to late stage myoblast populations. Finally, the Hedgehog/Patched signaling pathway has also been shown to play a role in the pathogenesis of RMS. RMS has been shown to develop in a subset of Pathced1 (Ptch) heterozygous mutant mice (Calzada-Wack *et al*., 2002). The study by Kappler *et al*. (2004) showed that RMS developed in Ptch1 heterozygous mutant mice are less aggressive and more differentiated than when compared to RMS developing from p53 heterozygous mutant mice. In addition, cDNA microarray analysis revealed distinct expression profiles in two groups of tumors, indicating that different causative mutations can lead to distinct gene expressions correlating with morphologic variations in RMS. In addition, it has also been shown that heterozygous Ptch1 mutation and p53 deficiency collaborate to hasten the onset to RMS formation in mice (Lee *et al*., 2007).

Linardic *et al*. (2005) generated a genetic model of human RMS. Two types of primary human skeletal muscle cells, primitive fetal skeletal muscle precursors (SkMC) and human postnatal skeletal myoblasts (HSMM), were transformed with defined genetic elements to deregulate the p53, Rb, Myc, telomerase, and Ras pathways. The study showed that SkMC-derived tumors showed a range of phenotypes with most developing sarcomas having unclassified morphology based on H&E analysis with some evidence of skeletal muscle differentiation based on positive expression of myogenic markers. In contrast, HSMM-derived tumors showed

Table I
Animal models of rhabdomyosarcoma

Species	Approach	Histologic subtype	Tumor onset	References
Zebrafish	Mosaic Transgenic Approach *(rag2-kRASG12D* injection at one-cell stage)	Embryonal	10 days post-fertilization	Langenau *et al*., 2007
Zebrafish	Heat shock-inducible Cre-Lox approach {*β-actin-ioxP*-EGFP-pA-LoxP-*kRASGUD* line x *hsp70-Cre* line)	Embryonal	Heat shocked: Average 35 days Non Heat shocked: Average 65 days	Le *et al*., 2008
Zebrafish	Tol2 gene trap system with transgene expressing constitutively active human H-RASV12	Costello syndrome	60–365 days	Santoriello *et al*., 2009
Mouse	Conditional Pax3: Fkhr knock-in/Myf6-specific Cre driver (Pax3: Fkhr heterozygous lines)	Alveolar	383 days	Keller *et al*., 2004
	Pax3: Fkhr homozygous lines			
	× Trp53 −/+	. . . . . →	202 days	
	× Trp53 −/−	. . . . . →	75–91 days	
	× lnk4a/Arf −/−	. . . . . →	56–89 days	
Mouse	HGF/SF-transgenic ×Ink4a/Arf −/−	Embryonal	∼90 days	Sharp *et al*., 2002
Mouse	Cre-Loxp conditional krasG12V knock in × p53 −/−	Pleomorphic	∼30–70 days	Tsumura *et al*., 2006
Human Tumor Xenografts in Mice	Cell lines derived from normal human skeletal muscle precursor cells (SkMCs) or human myoblasts (HSMM) stably expressing SV40 T/t-Ag (T), hTERT, H-Ras (V12G); transformed tumor cells were applied to xenograft assays	Embryonal	SkMC: -30–77 days (SQ injection) HSMM: 14 days (SQ); 56 days (SQ)	Linardic *et al*., 2005
Mouse	Conditionally regulated expression of an activated allele (Smoothened (R26-SMOM2))xCre transgene (CAGGS-CreER) induced by tamoxifen	Embryonal	35 days	Mao *et al*., 2006

morphologic and immunophenotypic features resembling the embryonal-type RMS. Electron microscopy also demonstrated evidence of skeletal muscle differentiation with formation of myofilaments. The study further showed the invasive and metastatic nature of the tumor. These data suggest that ERMS requires multiple genetic pathways to be disrupted to convert normal muscle into RMS including those regulating the p53, RB, Myc, telomerase, and Ras pathways. HSMMs can be induced to undergo malignant transformation into RMS, supporting the utility of this genetic model in dissecting the molecular mechanisms underlying human disease.

Generation of murine models is expensive, time consuming, requires complex breeding schemes requiring multiple generations to develop reproducible models of RMS, multiple genetic perturbations are often required, and RMS commonly develops only after a long latency (Table I). In contrast, zebrafish are amenable to large-scale genetic screens due to their fecundity, easy *ex vivo* manipulation from embryonic stage to adulthood, short latency for tumor development, and biological and pathologic similarity to human malignancies. We have developed a robust zebrafish transgenic model of kRAS-induced RMS (Langenau *et al*., 2007). Morphologically, zebrafish RMS resembles features of the human counterpart, showing spindle cell morphology and occasional nests of primitive round blue cells, recapitulating different stages of embryonic muscle development. The presence of cross striations in some tumor cells further supports that ERMS cells are blocked in myogenic differentiation. Similar to human RMS, zebrafish tumors express myogenic markers that are commonly used in to diagnose human disease including desmin, myoD, and myogenin. This chapter gives an overview of different approaches utilized to induce zebrafish RMS, to identify tumor-propagating ERMS cell subpopulations, and to uncover conserved pathways in cancer using genomic resources and bioinformatics approaches.

II. Rationale

As in most types of human sarcomas, the cell of origin remains to be determined in RMS. As animal models have indicated that cells involved in skeletal muscle development play a role in the pathogenesis of RMS, the advantages of the zebrafish models of RMS can be utilized to investigate the histogenesis and molecular mechanisms underlying the disease. This chapter gives an overview of different approaches to generate RMS. Zebrafish RMS is highly similar to human ERMS and using fluorescent transgenic approaches, we can visualize tumor onset, image tumor growth over time, and study the tumor self-renewal processes.

III. Material and Methods

A. Generation of Zebrafish Rhabdomyosarcoma Mosaic Transgenic Approach

The *rag2* promoter is expressed in T- and B-lymphoid progenitor cells, olfactory rosettes, and sperm (Jessen *et al*., 2001; Langenau *et al*., 2003). A transgenic model

using the *rag2* promoter to drive expression of the *mouse c-Myc* gene results in the development of T-cell acute lymphoblastic leukemia (Langenau *et al*., 2003). We have subsequently shown that *rag2* is also expressed in the mononuclear component of the skeletal muscle, which is composed of satellite cells and early myoblasts (Langenau *et al*., 2007). The *rag2* promoter is not active in terminally differentiated multinucleated muscle fibers.

Mosaic transgenic zebrafish that are pre-disposed to developing RAS-induced ERMS can be created using the following method. First, the human *kRASG12D* is amplified by PCR and cloned into the *rag2-GFP* vector (Jessen *et al*., 2001; Langenau *et al*., 2003). The *rag2-kRASG12D* construct was linearized, phenol/chloroform extracted, and ethanol precipitated. The DNA was re-suspended in 0.5x Tris-EDTA buffer + 100 mM KCl and was injected into wild-type embryos (i.e., AB-strain) at the one-cell stage of development. For most applications, 60–120 ng/µl of DNA can be microinjected. Animals were monitored for tumor onset beginning at 10 days of life and a subset of mosaic zebrafish containing the *rag2-kRASG12D* transgene develop externally visible tumors (Fig. 1A). In our experience, animals begin to develop ERMS by 10 days post-fertilization (dpf, Fig. 1B) and nearly 40% of mosaic transgenic zebrafish develop tumors by 80 dpf (dpf). ERMS can also be labeled with green fluorescence by coinjection of *rag2-kRASG12D* and *rag2-GFP.* In this instance, the two transgenes co-segregate and co-express in the developing tumor; allowing ERMS cells to be tracked by fluorescent imaging using a

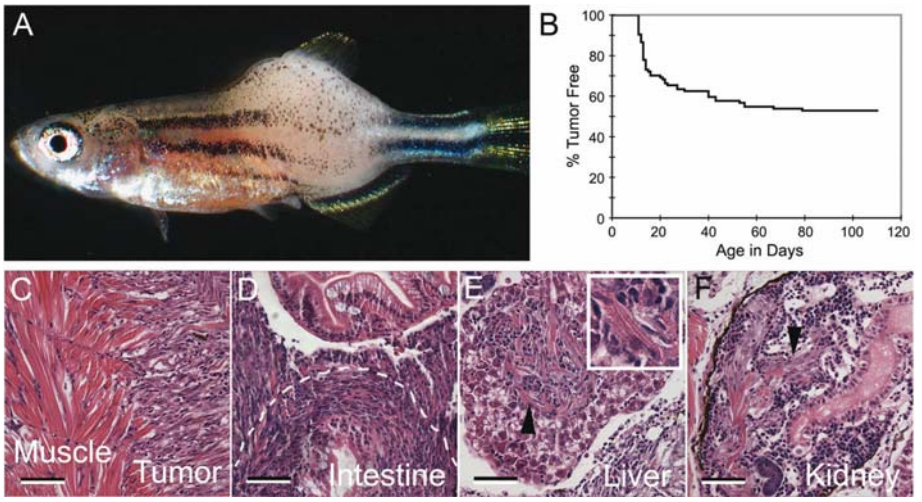

Fig. 1 Mosaic transgenic approaches to develop RAS-induced embryonal rhabdomyosarcoma. *rag2-kRASG12D* was microinjected into one-cell stage fish and animals were monitored for tumor onset over time. (A) Bright-field image of a 30-day-old zebrafish with ERMS. (B) Tumor onset in AB strain fish injected with *rag2-kRASG12D.* (C–F) ERMS cells invade into adjacent muscle (C), intestine (D), liver (E), and kidney (F). Scale bars are 50 microns. (See color plate.)

dissecting microscope (Fig. 1). Finally, ERMS is the major type of tumor detected in mosaic transgenic animals. Only one mosaic animal has been identified that developed a lymphoid hyperplasia/leukemia following injection of *rag2-kRASG12D* into one-cell stage animals, with >500 animals analyzed to date.

1. Generation of Stable Transgenic Lines

Costello syndrome is caused by germ-line mutations in the H-Ras gene and is characterized by craniofacial dysmorphology, cardiac defects, and tendency to develop various types of neoplasia, including RMS and neuroblastoma. To model Costello syndrome in zebrafish, Santoriello *et al*. (2009) utilized the Tol2 gene trap system (Kawakami *et al*., 2000) to generate a stable transgenic line carrying a constitutively active form of human Ras, HRASV12, tagged with GFP. The authors observed that fish carrying the integrated transgene showed several features of Costello syndrome including craniofacial dysmorphology, short stature, and development of tumor. In older fish (5–12 months old), the transgenic group showed a higher frequency of tumor formation (n = 12/200) compared with the wild-type controls (1 in 500). Tumor types observed include RMS (n = 1), hepatocellular carcinoma (n = 2), metastatic melanoma (n = 2), and gut carcinoma (n = 1). Taken together, this zebrafish model of Costello syndrome is powerful tool for studying the constellation of abnormities associated with this syndrome. However, as other tumor types can develop in this model and that RMS develops only after a long-latency with low penetrance, it may be difficult to discover RMS-specific pathways associated with tumor onset using these transgenic lines.

2. Heat Shock-Inducible Cre-Lox Approaches to Induce Rhabdomyosarcoma in Zebrafish

Le *et al*. (2007) developed a heat shock-inducible Cre-Lox approach to conditionally induce the expression of activated human kRASG12D. Briefly, to express activated human kRASG12D in various tissue types, a zebrafish β-actin promoter was used to drive the expression of a floxed transgene containing enhanced green fluorescent protein (EGFP) cassette that is followed by a transcriptional stop signal and located upstream of the constitutively active human *kRASG12D. B-actin-LoxP-EGFP-pA-LoxP-kRASG12D* stable transgenic lines were bred to the heat shock inducible Cre *(hsp70-Cre)* line. Because the *hsp70* promoter is leaky during early larval development, a portion of cells recombine the locus and of those that develop tumors, ~40% develop ERMS while numerous other lesions are also seen. By contrast, embryos heat shocked at 37 °C from 4 to 5 hpf or 24–25 hpf exhibited high levels of *Cre* expression without compromising embryonic development and genomic recombination was significantly enhanced when compared to non-heat shocked sibling controls. Eighty per cent tumor-bearing animals developed RMS in the heat-shocked cohort. Overall, the heat-shocked group showed increased tumor incidence and earlier tumor onset compared to the non-heat shocked group. Although this model provides a nice methodology to rapidly induce RMS in stable

transgenic animals, these tumors do not morphologically resemble human RMS, nor have detailed analysis been undertaken to assess the molecular similarity to human disease. Moreover, other tumor cell types are evident in double transgenic animals potentially confounding analysis of RMS in these animals.

B. Identification of Genetic Modifiers of Cancer Initiation and Maintenance

P53 pathway disruption is common in ERMS. To determine whether disruption of this genetic pathway can affect tumor initiation, *p53-/+* heterozygous mutant zebrafish were incrossed (Berghmans *et al*., 2005) and the resulting one-cell stage animals injected with *rag2-kRASG12D* (Langenau *et al*., 2007). Animals were monitored for externally visible tumor masses beginning at day 10 of life and a subset of animals were sacrificed, fixed, and sectioned to confirm tumor morphology. All animals were genotyped at the end of the experiment using an allele specific genomic PCR assay (Berghmans *et al*., 2005) and time to tumor onset was plotted by the method of Kaplan-Meier. Heterozygous and homozygous p53 loss-of-function fish displayed a marked increase in tumor incidence compared with wild-type injected siblings (Fig. 2A). In addition, homozygous p53 loss-of-function

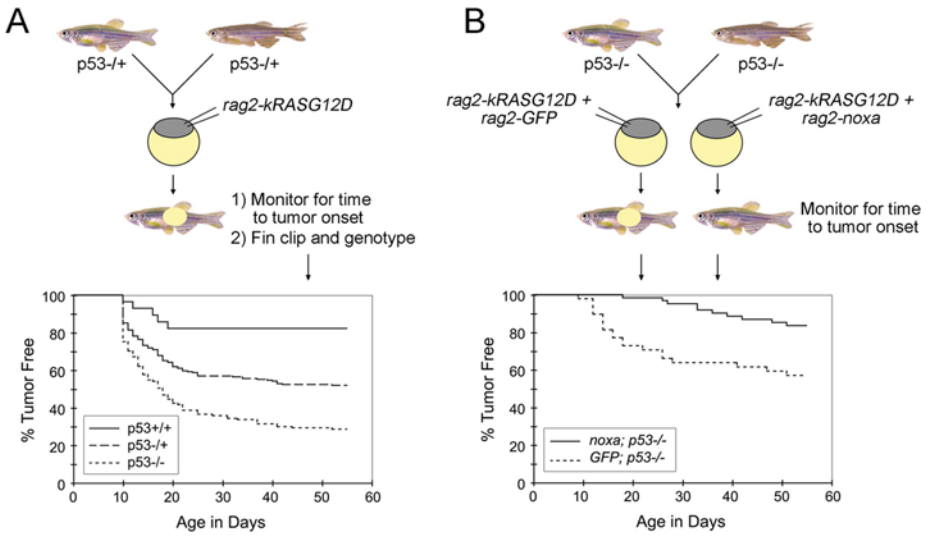

Fig. 2 Assessing collaborating genetic events that modify time to ERMS onset in mosaic transgenic zebrafish. (A) Schematic demonstrating injection of oncogenic *rag2-kRASG12D* into embryos with p53 alterations. P53 loss accelerates time to tumor onset and overall numbers of animals that develop ERMS. (B) Schematic demonstrating injection strategy to determine the effect of noxa on p53 pathway in kRAS-induced zebrafish rhabdomyosarcoma. In these experiments, tumor onset is assessed by the development of externally visible tumors and then animals from each genotype are compared by Kaplan-Meier survival analysis (bottom). Noxa suppresses tumor onset in p53-deficient animals. (For color version of this figure, the reader is referred to the web version of this book.)

animals developed more tumors compared with heterozygous p53 siblings. These findings indicate that p53 loss-of-function collaborates with kRASG12D to induce RMS and establishes that co-injection approaches can be used to rapidly identify tumor-modifying events that are relevant to human disease. Importantly, these methods do not require multiple generations to introduce your transgenic model into a various genetic backgrounds, but instead the modifying gene effects can be assessed directly by microinjection into various mutant lines.

The co-injection technique can also be utilized to identify genetic modifiers of tumor initiation. Langenau *et al*. (2008) previously showed that noxa, a pro-apoptotic BH3-only protein and a direct transcriptional target of p53, is a potent suppressor of tumor initiation. Specifically, wild-type AB-strain animals injected with *rag2-kRASG12D* and *rag2-noxa* showed longer latency in tumor onset compared to animals injected with *rag2-kRASG12D* and *rag2-dsRED2.* Tumor onset was also assessed in p53-LOF animals co-injected with *rag2-kRASG12D* and either *rag2-noxa* or *rag2-GFP.* Again, noxa functioned as a potent genetic suppressor as tumor onset was more delayed in the group co-injected with *rag2-kRASG12D* and *rag2-noxa* compared to the group co-injected with *rag2-kRASG12D* and *rag2-GFP* (Fig. 2B). This transgenic co-injection methodology establishes a rapid assay to identify enhancers and suppressors of tumor initiation and growth.

The co-injection strategy may also prove useful for assessing pathways required for tumor maintenance (Fig. 3). For example, co-injection of *rag2-kRASG12D + rag2-GFP + heat shock-inducible-dsRED (hsp70-dsREDexpress)* into one-cell stage animals led to the development of GFP+/red-negative tumors. Following heat shock at 37 °C for 45 min, ERMS become dsRED-labeled 2 days latter and persisted until 10 days. Engineering heat shock–inducible constructs that de-regulate pathways in established cancers will likely provide a unique and rapid assay for identifying pathways required for tumor maintenance and stopping tumor growth.

C. Co-Injection Strategies to Label ERMS Cell Subpopulations

Co-injection of two constructs into one-cell stage embryos leads to co-segregation and co-expression of multiple transgenes within developing ERMS and T-cell leukemia (Langenau *et al*., 2008). In order to differentially label ERMS cells based on differentiation status, the *rag2-kRASG12D* transgenic construct was co-injected with *rag2-dsRED* into *α-actin-GFP* transgenic fish (Fig. 4A). *rag2-dsRED* is expressed in satellite cells and early myoblasts while *α-actin-GFP* is expressed in more mature muscle cells. To verify that heterogeneous ERMS cell populations could be differentially labeled with fluorescent proteins, ERMS was isolated from zebrafish by surgical resection and minced in 5 ml of 0.9X PBS/5% FBS (fetal bovine serum). To facilitate dissociation of tumor cells, the minced contents can be repeated pipetted up and down using a 10 ml pipette. Samples were filtered through a 40 ump cell strainer (#352340, BD Falcon), centrifuged at 1000 g for 5–10 min and re-suspended in

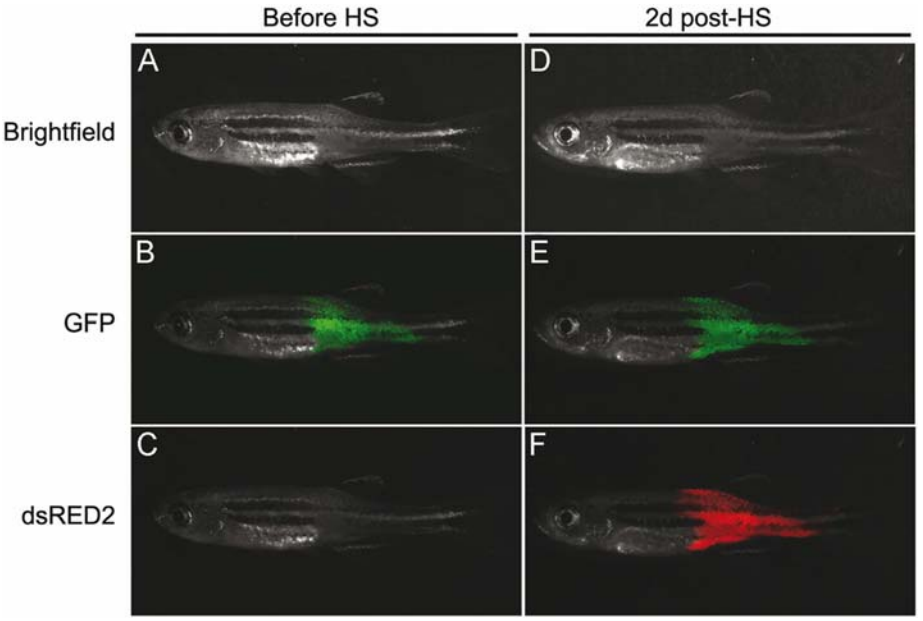

Fig. 3 Co-injection approaches to selectively induce gene expression in RAS-induced ERMS. The *rag2-kRASG12D* transgene was co-injected with *rag2-GFP* and *hsp70-dsRED2* into AB-strain embryos at one-cell stage. Animals develop GFP-labeled tumors that do not express high levels of dsRED2 (A-C, Before HS). ERMS-effected animals were heat shocked at 37 °C for 45 min. Two days post-heat-shock (2 d post-HS), ERMS express both GFP and dsRED2 in surviving animals (D–F). Bright field (A and D), GFP (B and E), and dsRED2 (C and F). (See color plate.)

500 µl of 0.9x PBS x 5% FBS containing propidium iodide at a concentration of 1 µg/ml to exclude dead cells or debris. Fluorescence activated cell sorting (FACS) was performed based on forward and side scatter, green and dsRed fluorescence using FACSVantage flow cytometer (Beckton Dickinson). FACS analysis confirmed that the mononuclear component of the tumor was composed of four populations of cells (double negative, GFP+/dsRED-, dsRED+/GFP-, and double positive, Fig. 4C). Sorted cell populations were FACS sorted twice to optimize cell purity and assessed for morphology and gene expression. All four populations expressed human *kRASG12D,* while the R+ population expressed satellite cell marker expression *(cMet+, m-cadherin+, and myf5+)* and lower or undetectable levels of myoblast and mature muscle markers *(myod, myogenin, muscle creatine kinase andmyosin light chain-2 (mylz2))* when compared with R+G+ and G+ populations. Microarray profiling confirmed that these cell populations were molecularly distinct. Taken together, our data showed that co-injection strategies can be a powerful tool to label tumor cell populations within the tumor and may be amenable to other zebrafish tumor models.

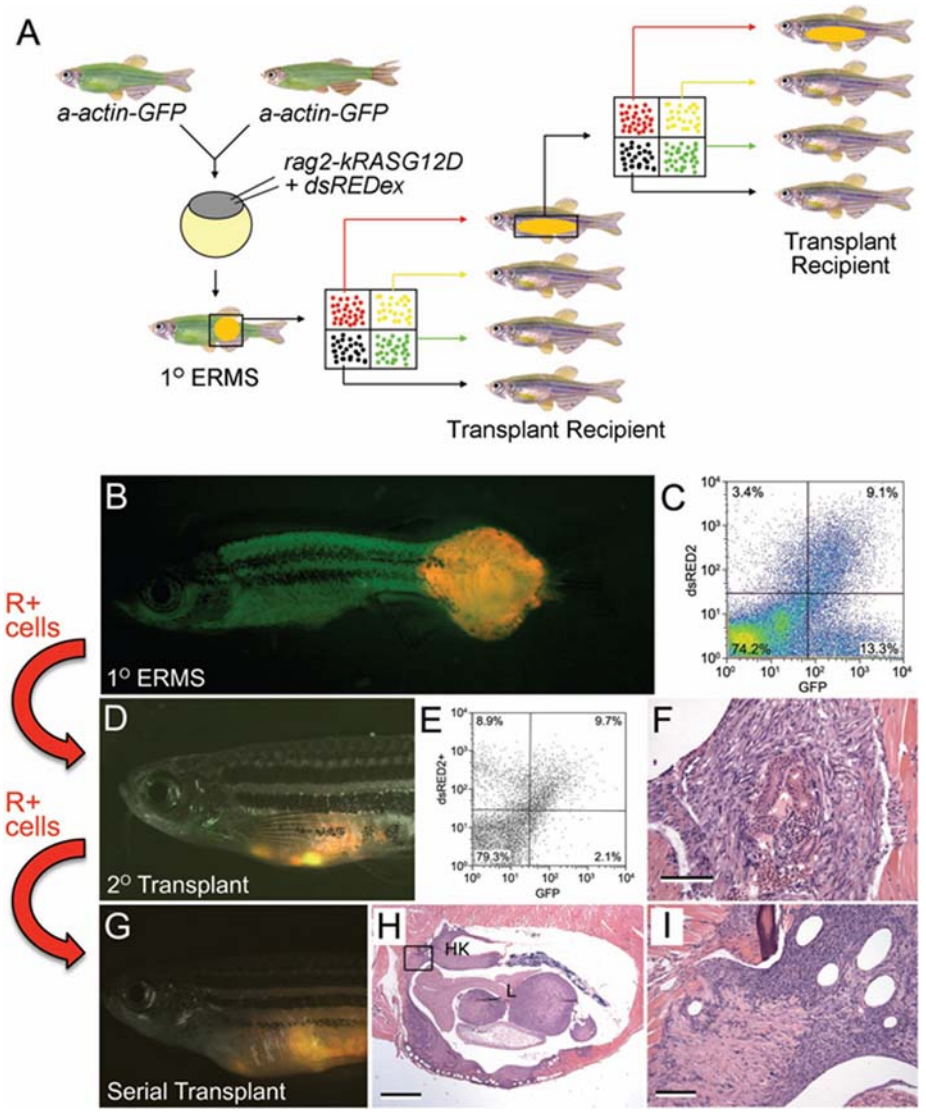

Fig. 4 Mosaic transgenic approaches to identify distinct cell populations within zebrafish ERMS and cell transplantation approaches to identify tumor-propagating cell populations. (A) Schematic: *rag2-kRASG12D* and *rag2-dsREDex* are co-injected into one-cell stage *α-actin-GFP* stable transgenic animals. The primary ERMS was subjected to FACS to sort out distinct populations of fluorescent tumor cells. Each population of cells was transplanted into recipient animals. For subsequent serial transplantation, each round of transplantation was preceded by FACS-based cell sorting. (B) Merged image from dsREDex fluorescence image and GFP fluorescence image of a primary ERMS. (C) FACS profile of *α–actin-GFP* transgenic animals injected at the one-cell stage with *rag2-dsRED2* and *rag2-G12D.* (D) Merged image of GFP fluorescent, dsRED2 fluorescent, and bright field images of primary transplanted

D. Identifying the Serially Transplantable ERMS-Propagating Cell Population

1. Short-Term Irradiation Assay

The ability to remake tumor in transplant animals is a hallmark of cancer. To establish that ERMS are fully malignant, ERMS cells were transplanted into irradiated recipients. Wild-type recipients were subjected to sublethal radiation at 20–25 Gy, 2 days before transplant and transplanted with unsorted primary ERMS by intraperitoneally injection (2×10^4 cells/animal). Small bundles of fluorescent tumor cells were detected as early as 7 days post-transplant using a fluorescence dissecting microscope and large tumor masses developed near the site of injection by 14 days post-transplant.

To define the population of cells that contains the transplantable ERMS cell population, FACS-sorted cells are obtained from primary rag2-dsRED+/α-actin-GFP+ ERMS and injected into irradiated recipient fish at limiting dilution (2×10^A4, 4×10^A3, 200, 50, and 10 cells). Specifically, 5 μl of cell suspension was injected into the peritoneal cavity of irradiated AB strain adult animals using a Hamilton syringe (#701, Fisher Scientific). Each labeled cell population was transplanted from lowest to highest concentration and the syringe was cleaned when a different subtraction of cells was injected into recipient animals. Cleaning of the syringe was completed by pipetting and aspirating 10 washes in 10% bleach in dH_2O, 10 washes in 100% ethanol, and 20 washes in 0.9X PBS. Following cell transplant of ERMS cells into recipient zebrafish, animals were analyzed for engraftment based on dsRED2 and GFP fluorescence at 7, 11, 14, and 18 days post-injection (Fig. 4D–F). To confirm that R+ cell subpopulation contained the long-term self-renewing ERMS cell, FACS-sorted populations from serially transplanted tumors were also assessed for engraftment potential. Specifically, ERMS cells were isolated from animals engrafted with ERMS from the R+ cell subpopulation and re-introduced into recipient animals by intraperitoneal injection (Fig. 4G–I). These experiments confirmed that rag2-dsRED +/α-actin-GFP-negative cell population was better at engrafting ERMS than other tumor subpopulations and was serially transplantable – a hallmark of self-renewing cells. Serial transplantation at limiting dilution showed that as few as 10 R+ cells were required for transplantation while other tumor subpopulations required a much higher number of cells to transplant and engraft. A subset of transplant fish were sacrificed in order to verify that fluorescence

---

Fig. 4 ***(Continued)*** tumors from *α–actin-GFP+/rag2-dsRED2+* zebrafish (primary recipient). (E) FACS analysis of primary recipient with engrafted ERMS. (F) Morphology of the tumor from the primary recipient, showing mostly fascicles of spindle cells and rare nests of round, hyperchromatic round cells. (G) Merged image of GFP fluorescent, dsRED2 fluorescent, and bright field images of 5° recipient. (H) Hematoxylin and eosin-stained section showing engrafted tumor at low power, showing infiltration of kidney and liver. (I) High-power magnification of (H) showing tumor infiltration of the liver. (See color plate.)

corresponded to areas of tumor formation, that heterogeneity of tumor cell types was similar between passage, and that fish scored negative for tumor by fluorescent microscopy were indeed negative for tumor. Fluorescence imaging and histological analysis of tumors yielded similar total numbers of engrafted animals and confirmed that the rag2-dsRED+/α-acting-negative cells are the tumor-propagating cancer stem cells in ERMS. The limiting dilution assay allows us to identify the transplantable population of cells in ERMS. Monitoring and tracking this population facilitates the investigation of self-renewal mechanisms in ERMS.

2. Transplanting into Clonally Syngeneic Fish

One issue with transplanting tumor cells into an irradiated non-immune-matched host is that immune suppression is temporary, and tumor can regress as the immune system recovers. The previous study by Smith *et al*. (2010) took advantage of the clonal syngeneic CG1 strain animals and compared the transplantation efficiency of T-cell acute lymphoblastic leukemia (T-ALL) cells to irradiated wild-type AB-strain animals. Leukemias were generated by co-injecting *rag2-mouse-cMyc* and *rag2-dsRED* express, *rag2-zsYellow* or *rag2-Amcyan* into one-cell stage CG1-strain embryos. Fluorescence-labeled T-ALL developed in a subset of animals and fluorescent blasts were isolated from primary leukemic fish by FACS and transplanted into non-irradiated CG1-strain animals, non-irradiated AB-strain animals, and irradiated AB-strain animals (AB+IR). Compared to CG1 recipients, AB+IR recipients had fewer engrafted animals at 10 and 20 days post-transplant. In addition, irradiation also increased death rate in AB recipients. Most T-ALLs arising in AB+IR recipients regressed by 30 days post-transplant. However, tumors in CG1 recipients continued to grow. Limiting dilution analysis revealed that transplantation into AB+IR recipients underestimated the number of leukemia-initiating cells by 20–33-fold, secondary to inefficient ablation of the immune system and increased lethality from irradiation. The same study also showed that T-ALLs can also be transplanted into CG1 outcrossed animals. By third outcross to CG1 most tumors engrafted tumors arising in CG1 animals.

Our group has also shown that ERMS tumor cells derived from co-injection of CG1 strain animals with *rag2-dsREDexpress* and *rag2-kRASG12D* can engraft successfully into CG1 recipient animals. Moreover, a subset of RMS from AB strain animals that have been serially outcrossed to CG1 strain fish can be transplanted into CG1 recipient animals, suggesting that immune matching has occurred in a subset of animals. Serial transplantation in either experiment nicely demonstrated the existence of tumor-propagating cell population in ERMS. Although, the CG1 strain zebrafish have yet to be used in limiting dilution cell transplantation experiments in ERMS, our results from Myc-induced T-ALL models suggest that these experiments will identify long-term re-populating cell types in ERMS capable of remaking tumor.

E. Bioinformatics Approaches to Identify Conserved Pathways in Zebrafish and Human ERMS

1. Microarray Analysis and Gene Set Enrichment Analysis (GSEA)

Gene Set Enrichment Analysis (GSEA) is a computational method that determines whether an *a priori* defined set of genes shows statistically significant, concordant differences between two biological states (e.g., phenotypes). This method has been used in mouse and human to identify gene signatures associated with cancer and also in zebrafish to classify different types of tumor (Lam *et al*., 2006, Langenau *et al*., 2007; Ramaswamy *et al*., 2001; Sweet-Cordero *et al*., 2005). The study by Langenau *et al*. (2007) used GSEA to identify conserved pathways in both zebrafish and human RMS. The gene sets were determined by microarray analysis comparing zebrafish RAS-induced RMS ($n = 8$) to normal control muscle ($n = 8$) from AB-strain fish at 30 dpf. Several fold changes cut-offs were used in the GSEA analysis to verify that differences between disease and normal states were reproducible and not due to arbitrary assignment of gene lists. In the study, the zebrafish up-regulated gene sets were significantly associated with the human embryonal RMS data set at all fivefold changes but never with the ARMS data set (Fig. 5A–C). Unexpectedly, zebrafish ERMS up-regulated gene set was significantly associated with the human pancreatic adenocarcinoma. To test that the up-regulated zebrafish gene set comprised a RAS-specific signature, human mammary epithelial cells (HMECs) infected with activated RAS, MYC, SRC, B-CATENIN, or E2F3 were compared with cells infected with GFP using GSEA and the zebrafish ERM gene set. The upregulated zERMS gene set was determined to be significantly associated with RAS status. Further analysis of the gene set revealed several known transcriptional targets of RAS.

To identify a set of genes involved in tumor-specific and tissue-restricted pathways associated with embryonal RMS, a subset of zebrafish ERMS up-regulated genes was further refined to include only genes that contribute maximally to the GSEA score in human ERMS but not pancreatic adenocarcinoma or HMECs transduced with RAS (Global Cancer Map data set from Ramaswamy *et al*., 2001). Specifically, a Venn diagram was used to identify the overlapping genes found in each of these human data sets (Fig. 5D). Most genes are coordinately regulated in pancreatic adenocarcinoma or HMECs transduced with RAS, suggesting that these genes comprise a RAS specific signature. Twenty four genes including *Muscle Regulatory Factor 5 (MYF5)* were contained within only the human ERMS unregulated data set, identifying a tumor-specific and tissue-restricted signature associated with the ERMS phenotype. *Myf5* is a myogenic transcription factor that is expressed in activated satellite cells (Cornelison and Wold, 1997; McKinnell *et al*., 2008) and is required along with MyoD to specify muscle in early embryogenesis (Berkes and Tapscott, 2005; Kablar *et al*., 2003; Weintraub *et al*., 1991). The presence of *MYF5* expression in the ERMS-specific gene signature suggests that the gene likely participates in the lineage and stage-specific stage of ERMS cells.

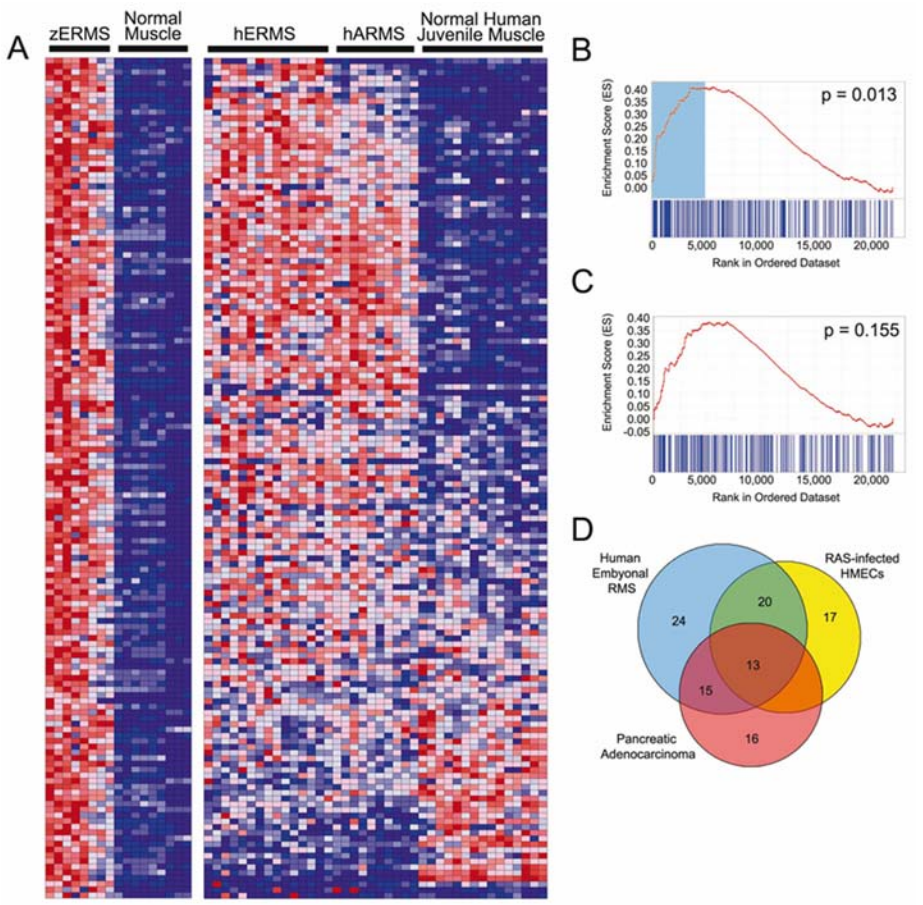

Fig. 5 Gene Set Enrichment Analysis (GSEA) identifies a conserved gene signature in both zebrafish and human ERMS. (A) Heat map showing genes up-regulated in zebrafish ERMS when compared with normal muscle at 2.25-fold change (left) and juxtaposed to the corresponding human orthodox in ERMS, ARMS, and normal juvenile muscle (right). Graphical representation of the rank-ordered gene lists found when comparing human ERMS (B) or translocation+ ARMS (C) to normal muscle. The up-regulated gene set identified in zebrafish ERMS is significantly enriched in human ERMS (B, $p = 0.013$). (D) A Venn diagram illustrating the genes from the up-regulated zebrafish ERMS gene set that contribute maximally to the GSEA score in the pancreatic adenocarcinoma, human ERMS, and RAS-infected human mammary epithelial cells (HMECs). Genes found in the non-overlapping blue portion are ERMS-specific and comprise the *MYF5* transcription factor. By contrast, the other genes are likely RAS-targets and are found to be coordinately regulated in zebrafish RAS-induced ERMS and either RAS-infected human mammary epithelial cells or human pancreatic adenocarcinoma, of which >90% have activating mutations in kRAS. (See color plate.)

2. Array CGH Approach

Comparative Genomic Hybridization (CGH) measures DNA copy number differences between a test and reference genome. This technology scans the entire genome for variations in DNA copy number, hence can be applied to detect genetic imbalances present in a disease model. Array-based CGH is a high-resolution platform constructed from DNA fragments, PCR products, or oligonucleotides that are mapped to the genome sequence. Array CGH has been an important tool in detecting genetic imbalances in human cancers and has also be utilized in various cancer models in other species such as the rodents, canines, and even nematodes.

Freeman *et al*. (2009) recently developed the first array CGH platform for use in zebrafish utilizing large genomic DNA fragments from zebrafish that were inserted into bacterial artificial chromosomes (BAC) (Freeman *et al*., 2009). Three hundred fifty-seven BAC clones were selected based on containing anthologies to human oncogenes from the CHORI-211 (zC), Danio Key (zK), and CHORI-73 (zH) genomic DNA libraries. BAC clones were selected based on containing orthologues to human oncogenes and tumor suppressor genes. Each clone was also assigned a precise cytogenetic location by fluorescent in situ hybridization.

The BAC array CGH was applied to three transgenic zebrafish cancer models: RMS, T-ALL, and melanoma (Freeman *et al*., 2009). For assessing chromosome alterations in ERMS, mosaic transgenic RAS-induced RMSs were created by co-injection of *rag2-kRASG12D* and *rag2-GFP* into AB strain wild-type animals. GFP+ tumor tissue was identified using a fluorescent dissecting microscope and adjacent unlabeled normal tissue was used as the reference sample. Total genomic DNA was isolated from the test and the reference samples using the Gentra Puregene Genomic DNA Purification Kit (Qiagen) and differentially labeled with fluorescent molecules (e.g., Cy3, Cy5). Labeled DNA was competitively hybridized to the BAC array. A two-color scan of the arrays was conducted using the GenePix 4000B Scanner (Molecular Devices, Union City, CA) at a 5 urn resolution and the fluorescent intensities of Cy3 and Cy5 was quantified for each DNA spot. For a given genomic segment, gains or losses in copy number were detected based on deviation of Cy3 to Cy5 ratio from 1 to 1. Seven RMS specimens were analyzed on the custom zebrafish BAC-based array and observed to have 6–14 significant genomic imbalances per sample. Gains of multiple BAC clones were cytogenetically mapped to various regions on zebrafish chromosomes, indicating the presence of several genetic imbalances in zebrafish embryonal RMS. While zebrafish BAC-based array CGH has lower resolution compared to oligonucleotide array CGH platforms from other species, these experiments provide a nice proof-of-concept that initial genome-wide identification of chromosomal imbalances can be assessed by array CGH in zebrafish models of cancer. As the annotation of zebrafish genomic sequences nears completion, higher resolution platforms will be a useful resource for exploring changes in the zebrafish genome related to RMS.

IV. Discussion

Studies have shown that only a limited number of cancer cells within the tumor mass have the ability for self-renewal and hence cause tumor formation (Reya *et al*., 2001). The same population of cells has also been implicated in treatment-refractory relapse. The tumor initiating cells or cancer stem cells have been characterized in some solid tumors such as brain, breast, colon, and skin cancer (Alcantara Llaguno *et al*., 2009; Banerjee and Eyden, 2008; Charafe-Jauffret *et al*., 2009; Todaro *et al*., 2010). However, for most malignancies including soft tissue sarcomas such as RMS, the mechanisms for self-renewal remain to be elucidated. We have shown that kRAS-induced zebrafish RMS resembles human ERMS. The discovery of a self-renewal population of tumor initiating cells in the zebrafish model of RMS opens the door for further investigation into the mechanism driving tumor self renewal. In addition, therapeutic targets aimed at genes involved in self-renewal also promise better clinical management of cancer patients suffering from treatment refractory.

Zebrafish as a model for the study of human disease and development serves many advantages. The feasibility for large-screen genetic screens (forward or reverse) allows for rapid identification of essential genes in various biological and disease processes. The ability to identify genetically modifying events using approaches such as heat shock-inducible Cre-Lox transgenics and co-injection of transgenes also facilitates the understanding of pathways essential for different processes involved in tumorigenesis. Gene sets ("signatures") identified from microarrays and GSEA will refine the conserved pathways in cancer and provide a tremendous opportunity for targeted therapy.

Acknowledgments

Eleanor Chen is supported by a T32 Training grant through Brigham and Woman's Hospital (T32 HL007627). David Langenau is supported by NIH grants K01AR05562190-01 A1 and K01AR05562190-S1, a new investigator grant from Alex Lemonade Stand, the Sarcoma Foundation of America, the Leukemia Research Foundation, and a seed grant from the Harvard Stem Cell Institute.

References

Alcantara Llaguno, S., Chen, J., Kwon, C. H., Jackson, E. L., Li, Y., Burns, D. K., Alvarez-Buylla, A., and Parada, L. F. (2009). Malignant astrocytomas originate from neural stem/progenitor cells in a somatic tumor suppressor mouse model. *Cancer Cell* **15**(1), 45–56.

Banerjee, S. S., and Eyden, B. (2008). Divergent differentiation in malignant melanomas: a review. *Histopathology* **52**(2), 119–129.

Barr, F. G., Galili, N., Holick, J., Biegel, J. A., Rovera, G., and Emanuel, B. S. (1993). Rearrangement of the PAX3 paired box gene in the paediatric solid tumour alveolar rhabdomyosarcoma. *Nat Genet* **3**(2), 113–117.

Barr, F. G., Holick, J., Nycum, L., Biegel, J. A., and Emanuel, B. S. (1992). Localization of the t(2;13) breakpoint of alveolar rhabdomyosarcoma on a physical map of chromosome 2. *Genomics* **13**(4), 1150–1156.

Berghmans, S., Murphey, R. D., Wienholds, E., Neuberg, D., Kutok, J. L., Fletcher, C. D., Morris, J. P., Liu, T. X., Schulte-Merker, S., Kanki, J. P., Plasterk, R., Zon, L. I., and Look, A. T. (2005). tp53 mutant zebrafish develop malignant peripheral nerve sheath tumors. *Proc Natl Acad Sci U S A* **102**(2), 407–412.

Berkes, C. A., and Tapscott, S. J. (2005). MyoD and the transcriptional control of myogenesis. *Semin. Cell Dev. Biol.* **16**(4–5), 585–595.

Calzada-Wack, J., Kappler, R., Schnitzbauer, U., Richter, T., Nathrath, M., Rosemann, M., Wagner, S. N., Hein, R., and Hahn, H. (2002). Unbalanced overexpression of the mutant allele in murine Patched mutants. *Carcinogenesis* **23**(5), 727–733.

Charafe-Jauffret, E., Ginestier, C., and Birnbaum, D. (2009). Breast cancer stem cells: tools and models to rely on. *BMC Cancer* **9**, 202.

Chen, Y., Takita, J., Hiwatari, M., Igarashi, T., Hanada, R., Kikuchi, A., Hongo, T., Taki, T., Ogasawara, M., Shimada, A., and Hayashi, Y. (2006). Mutations of the PTPN11 and RAS genes in rhabdomyosarcoma and pediatric hematological malignancies. *Genes Chromosomes Cancer* **45**(6), 583–591.

Cornelison, D. D., and Wold, B. J. (1997). Single-cell analysis of regulatory gene expression in quiescent and activated mouse skeletal muscle satellite cells. *Dev. Biol.* **191**(2), 270–283.

Davis, R. J., D'Cruz, C. M., Lovell, M. A., Biegel, J. A., and Barr, F. G. (1994). Fusion of PAX7 to FKHR by the variant t(1;13)(p36;q14) translocation in alveolar rhabdomyosarcoma. *Cancer Res* **54**(11), 2869–2872.

Felix, C. A., D'Amico, D., Mitsudomi, T., Nau, M. M., Li, F. P., Fraumeni Jr., J. F., Cole, D. E., McCalla, J., Reaman, G. H., and Whang-Peng, J., *et al*. (1992). Absence of hereditary p53 mutations in 10 familial leukemia pedigrees. *J Clin Invest* **90**(2), 653–658.

Freeman, J. L., Ceol, C., Feng, H., Langenau, D. M., Belair, C., Stern, H. M., Song, A., Paw, B. H., Look, A. T., Zhou, Y., Zon, L. I., and Lee, C. (2009). Construction and application of a zebrafish array comparative genomic hybridization platform. *Genes Chromosomes Cancer* **48**(2), 155–170.

Galili, N., Davis, R. J., Fredericks, W. J., Mukhopadhyay, S., Rauscher 3rd, F. J., Emanuel, B. S., Rovera, G., and Barr, F. G. (1993). Fusion of a fork head domain gene to PAX3 in the solid tumour alveolar rhabdomyosarcoma. *Nat Genet* **5**(3), 230–235.

Gurney, J. G., Davis, S., Severson, R. K., Fang, J. Y., Ross, J. A., and Robison, L. L. (1996). Trends in cancer incidence among children in the U.S. *Cancer* **78**(3), 532–541.

Jessen, J. R., Jessen, T. N., Vogel, S. S., and Lin, S. (2001). Concurrent expression of recombination activating genes 1 and 2 in zebrafish olfactory sensory neurons. *Genesis* **29**(4), 156–162.

Kablar, B., Krastel, K., Tajbakhsh, S., and Rudnicki, M. A. (2003). Myf5 and MyoD activation define independent myogenic compartments during embryonic development. *Dev Biol* **258**(2), 307–318.

Kappler, R., Bauer, R., Calzada-Wack, J., Rosemann, M., Hemmerlein, B., and Hahn, H. (2004). Profiling the molecular difference between Patched- and p53-dependent rhabdomyosarcoma. *Oncogene* **23**(54), 8785–8795.

Kawakami, K., Shima, A., and Kawakami, N. (2000). Identification of a functional transposase of the Tol2 element, an Ac-like element from the Japanese medaka fish, and its transposition in the zebrafish germ lineage. *Proc Natl Acad Sci U S A* **97**(21), 11403–11408.

Keller, C., Arenkiel, B. R., Coffin, C. M., El-Bardeesy, N., DePinho, R. A., and Capecchi, M. R. (2004). Alveolar rhabdomyosarcomas in conditional Pax3: Fkhr mice: cooperativity of Ink4a/ARF and Trp53 loss of function. *Genes Dev* **18**(21), 2614–2626.

Konieczny, S. F., Drobes, B. L., Menke, S. L., and Taparowsky, E. J. (1989). Inhibition of myogenic differentiation by the H-ras oncogene is associated with the down regulation of the MyoD1 gene. *Oncogene* **4**(4), 473–481.

Koufos, A., Hansen, M. F., Copeland, N. G., Jenkins, N. A., Lampkin, B. C., and Cavenee, W. K. (1985). Loss of heterozygosity in three embryonal tumours suggests a common pathogenetic mechanism. *Nature* **316**(6026), 330–334.

Lam, S. H., Wu, Y. L., Vega, V. B., Miller, L. D., Spitsbergen, J., Tong, Y., Zhan, H., Govindarajan, K. R., Lee, S., Mathavan, S., Murthy, K. R., Buhler, D. R., Liu, E. T., and Gong, Z. (2006). Conservation of gene expression signatures between zebrafish and human liver tumors and tumor progression. *Nat Biotechnol* **24**(1), 73–75.

Langenau, D. M., and Keefe, M. D., *et al*. (2007). Effects of RAS on the genesis of embryonal rhabdomyosarcoma. *Genes Dev.* **21**(11), 1382–1395.

Langenau, D. M., Keefe, M. D., Storer, N. Y., Jette, C. A., Smith, A. C., Ceol, C. J., Bourque, C., Look, A. T., and Zon, L. I. (2008). Co-injection strategies to modify radiation sensitivity and tumor initiation in transgenic Zebrafish. *Oncogene* **27**(30), 4242–4248.

Langenau, D. M., Traver, D., Ferrando, A. A., Kutok, J. L., Aster, J. C., Kanki, J. P., Lin, S., Prochownik, E., Trede, N. S., Zon, L. I., and Look, A. T. (2003). Myc-induced T cell leukemia in transgenic zebrafish. *Science* **299**(5608), 887–890.

Lassar, A. B., Thayer, M. J., Overell, R. W., and Weintraub, H. (1989). Transformation by activated ras or fos prevents myogenesis by inhibiting expression of MyoD1. *Cell* **58**(4), 659–667.

Le, X., Langenau, D. M., Keefe, M. D., Kutok, J. L., Neuberg, D. S., and Zon, L. I. (2007). Heat shock-inducible Cre/Lox approaches to induce diverse types of tumors and hyperplasia in transgenic zebrafish. *Proc Natl Acad Sci U S A* **104**(22), 9410–9415.

Lee, Y., Kawagoe, R., Sasai, K., Li, Y., Russell, H. R., Curran, T., and McKinnon, P. J. (2007). Loss of suppressor-of-fused function promotes tumorigenesis. *Oncogene* **26**(44), 6442–6447.

Linardic, C. M., Downie, D. L., Qualman, S., Bentley, R. C., and Counter, C. M. (2005). Genetic modeling of human rhabdomyosarcoma. *Cancer Res* **65**(11), 4490–4495.

Mao, J., Ligon, K. L., Rakhlin, E. Y., Thayer, S. P., Bronson, R. T., Rowitch, D., and McMahon, A. P. (2006). A novel somatic mouse model to survey tumorigenic potential applied to the Hedgehog pathway. *Cancer Res* **66**(20), 10171–10178.

McKinnell, I. W., Ishibashi, J., Le Grand, F., Punch, V. G., Addicks, G. C., Greenblatt, J. F., Dilworth, F. J., and Rudnicki, M. A. (2008). Pax7 activates myogenic genes by recruitment of a histone methyltransferase complex. *Nat Cell Biol* **10**(1), 77–84.

Mulligan, L. M., Matlashewski, G. J., Scrable, H. J., and Cavenee, W. K. (1990). Mechanisms of p53 loss in human sarcomas. *Proc Natl Acad Sci U S A* **87**(15), 5863–5867.

Nanni, P., Nicoletti, G., De Giovanni, C., Croci, S., Astolfi, A., Landuzzi, L., Di Carlo, E., Iezzi, M., Musiani, P., and Lollini, P. L. (2003). Development of rhabdomyosarcoma in HER-2/neu transgenic p53 mutant mice. *Cancer Res* **63**(11), 2728–2732.

Ramaswamy, S., Tamayo, P., Rifkin, R., Mukherjee, S., Yeang, C. H., Angelo, M., Ladd, C., Reich, M., Latulippe, E., Mesirov, J. P., Poggio, T., Gerald, W., Loda, M., Lander, E. S., and Golub, T. R. (2001). Multiclass cancer diagnosis using tumor gene expression signatures. *Proc Natl Acad Sci U S A* **98**(26), 15149–15154.

Reya, T., Morrison, S. J., Clarke, M. F., and Weissman, I. L. (2001). Stem cells, cancer, and cancer stem cells. *Nature* **414**(6859), 105–111.

Santoriello, C., Deflorian, G., Pezzimenti, F., Kawakami, K., Lanfrancone, L., d'Adda di Fagagna, F., and Mione, M. (2009). Expression of H-RASV12 in a zebrafish model of Costello syndrome causes cellular senescence in adult proliferating cells. *Dis Model Mech* **2**(1–2), 56–67.

Scrable, H. J., Witte, D. P., Lampkin, B. C., and Cavenee, W. K. (1987). Chromosomal localization of the human rhabdomyosarcoma locus by mitotic recombination mapping. *Nature* **329**(6140), 645–647.

Sharp, R., Recio, J. A., Jhappan, C., Otsuka, T., Liu, S., Yu, Y., Liu, W., Anver, M., Navid, F., Helman, L. J., DePinho, R. A., and Merlino, G. (2002). Synergism between INK4a/ARF inactivation and aberrant HGF/SF signaling in rhabdomyosarcomagenesis. *Nat Med* **8**(11), 1276–1280.

Smith, A. C., Raimondi, A. R., Salthouse, C. D., Ignatius, M. S., Blackburn, J. S., Mizgirev, I. V., Storer, N. Y., de Jong, J. L., Chen, A. T., Zhou, Y., Revskoy, S., Zon, L. I., and Langenau, D. M. (2010). High-throughput cell transplantation establishes that tumor-initiating cells are abundant in zebrafish T-cell acute lymphoblastic leukemia. *Blood* **115**(16), 3296–3303.

Stratton, M. R., Fisher, C., Gusterson, B. A., and Cooper, C. S. (1989). Detection of point mutations in N-ras and K-ras genes of human embryonal rhabdomyosarcomas using oligonucleotide probes and the polymerase chain reaction. *Cancer Res* **49**(22), 6324–6327.

Stratton, M. R., Moss, S., Warren, W., Patterson, H., Clark, J., Fisher, C., Fletcher, C. D., Ball, A., Thomas, M., and Gusterson, B. A., *et al*. (1990). Mutation of the p53 gene in human soft tissue sarcomas: association with abnormalities of the RB1 gene. *Oncogene* **5**(9), 1297–1301.

Sweet-Cordero, A., Mukherjee, S., Subramanian, A., You, H., Roix, J. J., Ladd-Acosta, C., Mesirov, J., Golub, T. R., and Jacks, T. (2005). An oncogenic KRAS2 expression signature identified by cross-species gene-expression analysis. *Nat Genet* **37**(1), 48–55.

Todaro, M., Francipane, M. G., Medema, J. P., and Stassi, G. (2010). Colon cancer stem cells: promise of targeted therapy. *Gastroenterology* **138**(6), 2151–2162.

Tsumura, H., Yoshida, T., Saito, H., Imanaka-Yoshida, K., and Suzuki, N. (2006). Cooperation of oncogenic K-ras and p53 deficiency in pleomorphic rhabdomyosarcoma development in adult mice. *Oncogene* **25**(59), 7673–7679.

Weintraub, H., Dwarki, V. J., Verma, I., Davis, R., Hollenberg, S., Snider, L., Lassar, A., and Tapscott, S. J. (1991). Muscle-specific transcriptional activation by MyoD. *Genes Dev* **5**(8), 1377–1386.

Williamson, D., Missiaglia, E., de Reynies, A., Pierron, G., Thuille, B., Palenzuela, G., Thway, K., Orbach, D., Lae, M., Freneaux, P., Pritchard-Jones, K., Oberlin, O., Shipley, J., and Delattre, O. (2010). Fusion gene-negative alveolar rhabdomyosarcoma is clinically and molecularly indistinguishable from embryonal rhabdomyosarcoma. *J Clin Oncol* **28**(13), 2151–2158.